AD

USAAVLABS TECHNICAL REPORT 69-56

PRESSURE RECOVERY PERFORMANCE OF STRAIGHT-CHANNEL, SINGLE-PLANE DIVERGENCE DIFFUSERS AT HIGH MACH NUMBERS

By

Peter W. Runstadler, Jr.

October 1969

U. S. ARMY AVIATION MATERIEL LABORATORIES
FORT EUSTIS, VIRGINIA

CONTRACT DAAJ02-67-C-0106
CREARE INCORPORATED
HANOVER, NEW HAMPSHIRE

DISCLAIMERS

The findings in this report are not to be construed as an official Department of the Army position unless so designated by other authorized documents.

When Government drawings, specifications, or other data are used for any purpose other than in connection with a definitely related Government procurement operation, the United States Government thereby incurs no responsibility nor any obligation whatsoever; and the fact that the Government may have formulated furnished or in any way supplied the said d drawings, specifications, or other data is not to be regarded by implication or otherwise as in any manner licensing the holder or any other person or corporation, or conveying any rights or permission, to manufacture, use, or sell any patented invention that may in any way be related thereto.

Trade names cited in this report do not constitute an official endorsement or approval of the use of such commercial hardware or software.

DISPOSITION INSTRUCTIONS

Destroy this report when no longer needed. Do not return it to the originator.

DEPARTMENT OF THE ARMY
HEADQUARTERS US ARMY AVIATION MATERIEL LABORATORIES
FORT EUSTIS, VIRGINIA 23604

The objective of the work performed during this program was to generate straight-channel diffuser data to provide the design engineer with the information required to design centrifugal compressor diffusers.

This report was prepared by Creare, Incorporated, under the terms of Contract DAAJ02-67-C-0106. It describes the diffuser test rig constructed as a vehicle to provide diffuser data, the experimental procedure used, and the results of the testing performed. The data are analyzed and presented in forms convenient to the designer; in addition, a general approach to the design of a centrifugal compressor diffuser has been devised.

The investigation shows that knowledge in this area is still incomplete in certain respects. The results do provide valuable and useful information to the diffuser designer.

This report has been reviewed by technical personnel of this Command. The conclusions contained herein are concurred in by this Command and will be considered in any future centrifugal compressor programs.

Task 1G162203D14413
Contract DAAJ02-67-C-0106
USAAVLABS Technical Report 69-56
October 1969

PRESSURE RECOVERY PERFORMANCE OF STRAIGHT-CHANNEL, SINGLE-PLANE DIVERGENCE DIFFUSERS AT HIGH MACH NUMBERS

Final Report

Creare Technical Note No. N-88

by
Peter W. Runstadler, Jr.

Prepared by

Creare Incorporated
Hanover, New Hampshire

for

U.S. ARMY AVIATION MATERIEL LABORATORIES
FORT EUSTIS, VIRGINIA

ABSTRACT

Measurements have been made of the pressure recovery of straight-channel, symmetric, single-plane divergence diffusers with inlet Mach numbers between 0.2 and choking ($0.2 \leqq M_t \leqq 1.0$).

Three aspect ratios, AS = 0.25, 1.0, and 5.0, have been studied for a range of length-to-throat width ratios L/W_1 and divergence angles 2θ of diffuser geometries near peak recovery.

Diffuser performance maps are given that show pressure recovery C_p as a function of diffuser geometry for fixed values of throat Mach number M_t, throat blockage B, and aspect ratio AS for the range of variables tested. Of significant importance to the designer is the alteration in the shape of the pressure recovery contours on the performance maps with variations in M_t, B, and AS.

Four subprograms have measured the effect of changes in diffuser inlet Reynolds number, nearness of the inlet boundary layer to separation, asymmetric distribution of inlet blockage around the throat periphery, and the influence of rounded throat corners on the pressure recovery behavior of the straight-channel diffuser. These subprograms have underscored the necessity of understanding cumulative effects of a number of secondary parameters on pressure recovery.

The importance to the designer of a knowledge of how diffuser performance depends upon the diffuser geometric and inlet parameters is discussed. The application of channel diffuser performance data to the design of centrifugal compressor diffusers is described.

The channel diffuser performance measured in the present study is compared with recovery performance of the channel diffusers in centrifugal compressors.

FOREWORD

The author acknowledges the support of the following people who have contributed significantly to this investigation:

Dr. R. C. Dean, Jr., for his theoretical and practical understanding of the diffuser behavior investigated in these studies.

Mr. Frank R. LeBlanc, Jr., for his tireless effort to the acquisition of experimental data. The accuracy and quality of much of the information gained on these studies is attributable to his work.

Dr. Charles J. Sagi and Mr. David D. Wright for their contributions to the design of the experimental apparatus, experimental design, and much of the data reduction.

The author especially acknowledges the interest and support of Mr. R. A. Langworthy and Mr. H. L. Morrow of the U. S. Army Aviation Materiel Laboratories. Their knowledge and appreciation of the information to be gained from these studies was in large part responsible for the information that has been gathered.

TABLE OF CONTENTS

LIST OF ILLUSTRATIONS

LIST OF TABLES

LIST OF SYMBOLS

A	cross-section area (in.^{2})
A_e	effective channel flow throat area
AR	area ratio = $(bW)_2/(bW)_1$
AS	aspect ratio = b/W_1
A_{flow}, $A_{effective}$	"one-dimensional" cross-sectional flow area (in.^{2})
$A_{geometrical}$	geometric throat cross-sectional area (in.^{2})
a	local speed of sound (ft/sec)
B	throat blockage = $1 - \frac{A_{effective}}{A_{geometric}}$
b	diffuser depth (in.)
C_D	discharge coefficient of flow nozzle
C_p	pressure recovery coefficient = $p_e - p_t \,/\, p_{o_t} - p_t$, also specific heat at constant pressure
C_p^*	diffuser's optimum pressure recovery line at constant length-to-throat-width ratio
C_p^{**}	diffuser's optimum pressure recovery line at constant area ratio
C_{p_i}	ideal pressure recovery
$C_{p_{peak}}$	peak pressure recovery
C_v	specific heat at constant volume

D	hydraulic diameter (in.)
H	boundary layer shape factor = δ^*/θ
k	ratio of specific heats = C_p/C_v
L	diffuser length measured along centerline (in.)
M	Mach number
M_t	throat Mach number
M_x	Mach number ahead of shock
M_y	Mach number behind shock
m_i	"ideal" mass flow (lb mass/sec)
m_m	measured mass flow (lb mass/sec)
N	centerline length or number of diffuser vanes
p	static pressure (psia)
p_e	diffuser exit (collector) static pressure (psia)
p_o	stagnation pressure (psia)
p_{o_t}	throat stagnation pressure (psia)
p_t	throat static pressure (psia)
Q	flow rate (ft^3/sec)
R	gas constant
R_D	Reynolds number based on hydraulic diameter and flow velocity
R_e	Reynolds number based on impeller exit depth

r	radius
T_o	total temperature (°R)
T_{o_t}	throat total temperature (°R)
T_t	throat static temperature (°R)
U_∞	core flow velocity (ft/sec)
V	throat centerline "core" velocity (ft/sec)
$\bar{V}$	bulk mean velocity
v_o	wall suction velocity (ft/sec)
W	diffuser width (in.)
x	axial distance along diffuser centerline (in.)
Δp_{o_r}	flow nozzle pressure differential (psia)
δ^*	boundary layer displacement thickness (in.)
ε	effectiveness = C_p/C_{p_i}
θ	boundary layer momentum thickness (in.)
2θ	diffuser divergence angle
ν	fluid kinematic viscosity (ft^2/sec)
ρ	fluid density (lb mass/ft^3)

Subscripts

1	diffuser entrance (start of divergence)
2	diffuser exit (end of divergence) or impeller exit

c	collector
i	ideal
o	stagnation, wall
t	throat
v	diffuser vane leading edge

Superscript

*	after impeller exit mixing process

1.0 INTRODUCTION

The diffusing passage is a key element of many fluid machines and fluid dynamic systems. The ability to recover pressure and/or the ability to establish a stable flow or a flow of low distortion is critical to the behavior of many devices and systems which incorporate a fluid dynamic diffuser. The optimum performance and the proper design of diffusing passages for many devices, e.g., in turbomachines, aircraft inlets, carburetors, flowmeters, noise suppressors, etc., depend upon an understanding of the important flow parameters governing the performance of the fluid dynamic diffuser.

The diffuser is of particular importance to the performance of the centrifugal compressor. The centrifugal compressor achieves its effect by accelerating the fluid, in order to add energy, and then diffusing this fluid to convert the kinetic energy into an increase in static pressure. The purpose of the diffuser of a centrifugal compressor is to convert the flow kinetic energy leaving the impeller into a maximum rise in static pressure. In a single-stage machine, the residual kinetic energy after the diffuser is usually dumped into a collector. It is thus the static pressure recovery in the diffuser that is of significance to the compressor performance.

The effectiveness with which the diffusion can be accomplished plays a large part in determining the efficiency of the compressor. In present state-of-the-art centrifugal compressors, the diffuser is often responsible for more than half of the fluid dynamic losses. The pressure recovery and/or the stability of the diffuser flow is also believed to be instrumental in establishing the range and surge behavior of the compressor. The design of optimum diffuser systems will be essential to the further development of advanced technology centrifugal compressors of high pressure ratio, long range, and good efficiency.

1.1 BACKGROUND

The centrifugal compressor diffuser may be either a vaneless or a vaned diffuser or a combination of the two.

Vaneless Diffusers

When vaneless diffusers are used, they are selected primarily because of the large range they provide (on the order of

40 to 60% of the design flow). However, the vaneless diffuser has considerably poorer efficiency than the vane type. Cases have been frequently encountered in high pressure ratio centrifugal compressors where the boundary layer in the vaneless diffuser stalls (by the limiting wall streamlines turning completely to the tangential direction). A backflow of boundary layer fluid then usually occurs, this fluid sometimes even flowing back into the impeller. This has severe consequences for overall compressor performance because the impeller must reenergize this fluid before it is ejected again into the diffuser.

From empirical evidence, it appears clear that except for the possibility of the use of a rotating-wall, vaneless diffuser (where either the shrouds of the impeller are extended or the vaneless diffuser walls are rotated independently), the losses occurred in high pressure ratio, purely vaneless diffusers cause too severe a penalty on centrifugal compressor performance to make them attractive in comparison with the vaned diffuser.

Vaned Diffusers

The use of a vaned diffuser for the centrifugal compressor offers the opportunity to obtain a high pressure recovery, although this is usually gained at the expense of range.

Vaned diffusers may be categorized by two types of blading: the vane-island or wedge diffuser and the cascade diffuser.

1. Vane-Island or Wedge Diffuser

The vane-island or wedge diffuser may be regarded as a cascade of blades with blunt trailing edges. When considered as a "cascade" of blades, the blades may be said to have a very low aspect ratio. A diagramatic sketch of the vane-island diffuser is shown in Figure 1. Depending upon the shape of the "vane" and the control of the depth between the sidewalls, the flow passage between the vane suction and pressure surfaces describes a diffusing passage of a particular geometric configuration. A common design used in practice is to keep the depth between the sidewalls constant and to diverge the pressure and suction surfaces. In this case, the resulting flow passage

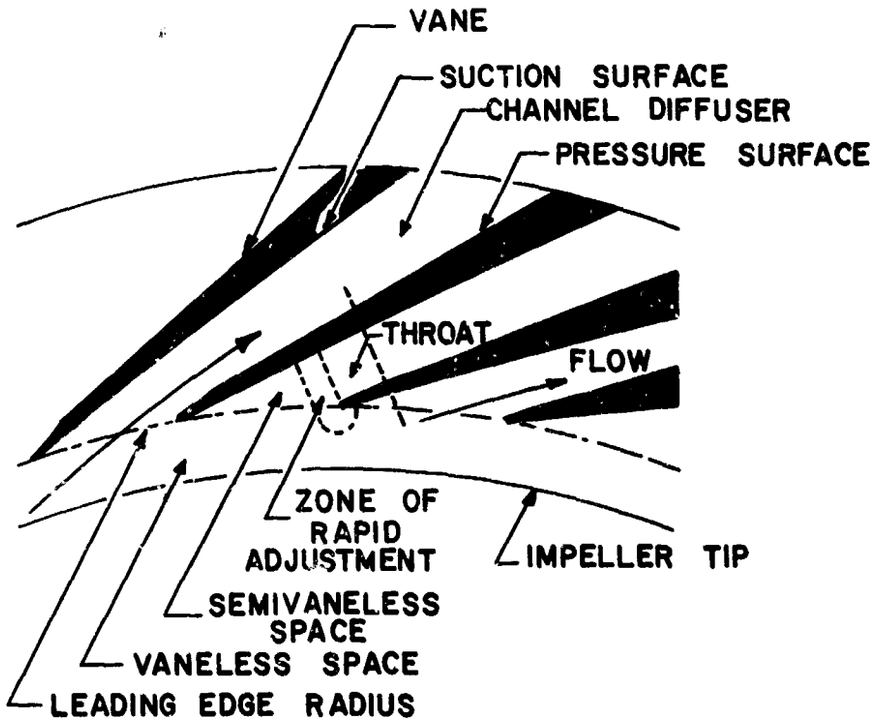

Figure 1. Vane-Island and Cascade Diffuser Geometry.

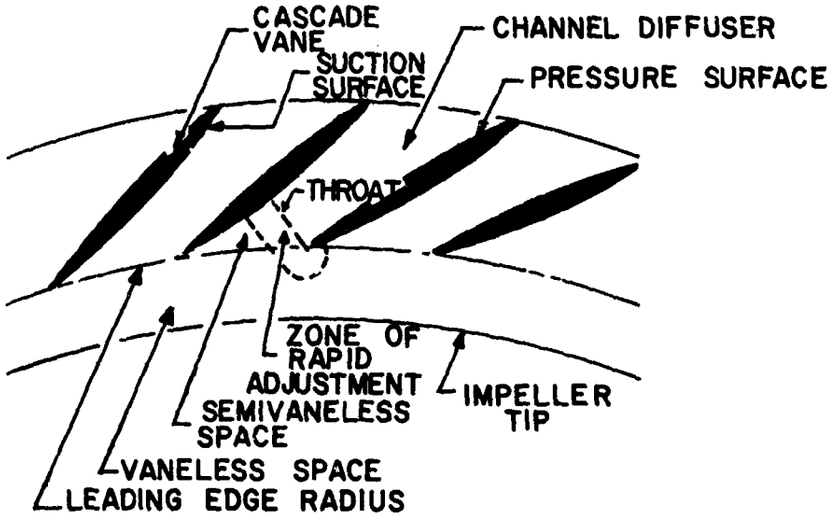

CASCADE DIFFUSER GEOMETRY

Figure 1 Continued.

forms a channel diverging in a single plane and having straight walls. However, other configurations have been used in practice. In some cases, the sidewalls have also been diverged, forming a double-divergence, straight-wall diffuser. Often the divergence is made symmetric; in other cases, an asymmetric divergence has been used. Kenny (1968) has reported a novel vane-island diffuser which lends itself to easy manufacture. In this case, the diffusing channel forms a conical instead of a rectangular diffuser.

In the vane-island diffuser, mixing losses occasioned by the blunt trailing edges are of no real importance since the discharge kinetic energy is not conserved. The designer is given some geometric freedom in designing the diffuser when he does not have to close the trailing edge of the blade, as is the case of the cascade geometry. Also, the channel diffuser divergence angle is not tied to the vane number as it is with the cascade design.

2. Cascade Diffusers

The cascade diffuser is made with multiple rows of thin blades. The length-over-width ratios of the passages between the blades are commonly between 1 and 3.

The flow between the blades has often been treated by methods typical of those used for axial compressors. However, the low aspect ratio of the blading used in centrifugal cascade diffusers, and which is not found in axial machines, cautions against the indiscriminate use of common axial design practice.

In some cases, multiple rows of cascade blading have been used; in other cases, single rows of larger chord blades have been used. For the thin blades in common use in cascade designs, the divergence angle between the blading is intimately linked to the number of blades used in the cascade.

Vaned diffusers generally employ a vaneless space preceding the vane-island or cascade set of vanes. The vaneless space commonly employs a radius ratio, between the tip of the

impeller and the leading edge of the diffuser vanes, between 1.03 and 1.3.

Centrifugal Compressor Diffuser Optimization

The centrifugal compressor vaned diffuser extends from the impeller exit through (1) the vaneless space, (2) the semi-vaneless space, and (3) the channel diffuser to the collector.

In high-pressure-ratio, high-performance compressors, the conventional idea has been to bring the vane leading edge Mach number below some subsonic Mach number limit using the vaneless diffuser. This has been to avoid severe shock effects around the vane leading edges. Recent studies, Welliver and Acurio (1967), have demonstrated that immediately ahead of the vane diffuser leading edge, the flow rapidly adjusts itself to produce a rather uniform flow entering the channel diffuser. Even though these studies were limited to the vane-island geometry, the results indicate that the same type of behavior probably also occurs ahead of the vane leading edge in the cascade diffuser.

The work of Welliver and Acurio (1967) also demonstrated that laboratory tests on channel diffuser geometries having the same configuration as those used in the centrifugal vane-island diffuser produced the same channel diffuser pressure recovery as that obtained in the actual compressor. It was necessary, however, to maintain the same inlet conditions for the laboratory diffusers as those occurring in the compressor channel diffuser inlets.

If the overall diffuser flow from the impeller exit to the collector -- the flow through the vaneless and semivaneless spaces plus the flow through the channel diffuser -- is considered as a series combination of flow elements, the designer is in a position to determine optimum diffuser performance. If the flow can be properly modeled in the vaneless and semivaneless spaces and sufficient data on channel diffuser performance are available, this can be combined with knowledge of impeller performance to optimize the overall centrifugal diffuser and hence compressor performance.

A critical element in this design procedure is knowledge of channel diffuser behavior. Despite the fact that the diffuser is a very simple flow element, its pressure recovery and stability characteristics are not sufficiently understood for the prediction of high-performance, high-pressure-ratio centrifugal compressor diffuser design. The designer is plagued by his inability to predict adequately the performance characteristics of channel diffusers of varying geometries operating over a wide range of inlet flow conditions.

There are basic fundamental reasons for this deficiency related to the details of the internal diffuser flow. Practical diffusing passages are often of small aspect ratio, are three-dimensional in shape, contain boundary layer fluid over a significant portion of the cross-section area, and often operate under inlet flow conditions having large distortions in velocity profile and/or high turbulence levels. Today the designer cannot analyze even the simplest two-dimensional diffuser near peak performance; the reason for this is that the geometry and the viscous behavior of the fluid lead to corner effects, separation, backflow, and unsteady flow behavior which cannot be adequately handled with our present analytical understanding.

Although efforts will continue to advance our analytic ability to predict the behavior of diffusing passages operating under arbitrary conditions, the complexity of the fluid dynamics does not hold promise for a marked improvement in predicting diffuser performance. In the absence of an ability to analyze the flow in arbitrary passages, the designer must of necessity revert to a semiempirical understanding of the flow element. In order to make an optimum design, the designer needs data showing channel diffuser performance as a function of the important design variables. Some of these variables, such as those defining the diffuser geometry, are under the designer's direct control; other variables are set by the upstream and downstream flow elements.

To properly optimize the design of a channel diffuser for the centrifugal compressor, the designer must have a knowledge of the effect of these parameters on the pressure recovery performance of the channel diffuser so that he may couple the channel diffuser performance to the fluid dynamic flow in the vaneless and semivaneless passages.

The designer needs maps similar to those of Reneau et al (1964), examples of which are shown in Figure 2, which have been obtained for the low subsonic Mach number (incompressible flow), straight-channel, single-plane divergence diffuser. When such maps include all of the important design variables, they indicate to the designer the strategy for achieving best diffuser performance in terms of pressure recovery.

Maps are also available for the low-Mach-number diffuser that show the unsteady behavior of the diffuser flow as a function of the geometric and inlet flow variables. In most cases, the diffuser flow has only been qualitatively characterized by its unsteady characteristics in terms of flow regimes. An example of a flow regime performance map for the incompressible flow, straight-channel, single-plane divergence diffuser is shown in Figure 3 from the data of Fox and Kline (1962).

Such maps have not existed for the transonic (high subsonic) Mach number diffuser. Van DeWoestine and Fox (1966) have studied the pressure recovery performance and flow regime behavior of conical diffusers at high subsonic inlet Mach numbers at low inlet boundary layer blockage. However, performance data at high subsonic inlet Mach numbers for straight-channel, two-dimensional, single divergence channel diffusers have not been available.

An empirical program to describe channel diffuser recovery performance as a function of the many inlet and geometric parameters is a large undertaking. Fortunately, data on the pressure recovery performance of straight wall diffusers under incompressible inlet flow conditions have pointed to the importance of flow inlet blockage B as the dominant inlet flow parameter. This information has been most clearly presented by Sovran and Klomp (1965). They showed that in many cases the complex inlet situation could be largely correlated on the basis of the simple blockage parameter B. The data obtained by Welliver and Acurio (1967) appear to confirm that flow blockage B is also the dominant parameter at high inlet Mach numbers.

1.2 PROJECT OBJECTIVES

To supply performance data needed by the designer, an experimental program has been completed to measure channel diffuser

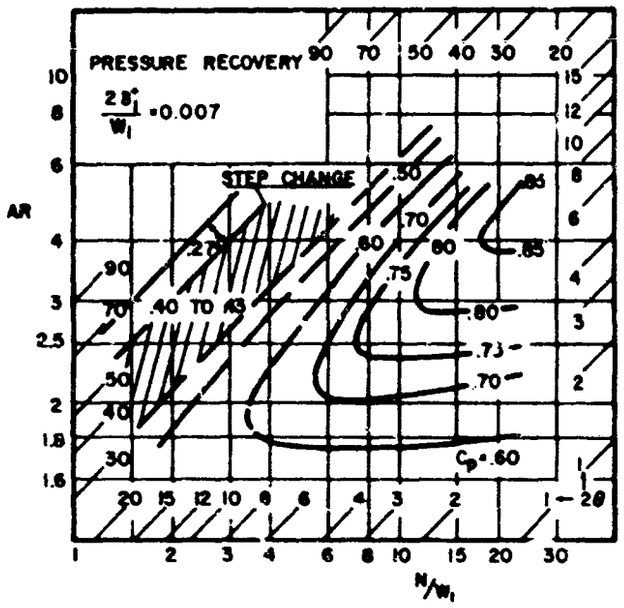

WHERE:

δ_1^* = BOUNDARY LAYER DISPLACEMENT THICKNESS ON DIVERGING WALLS AT ENTRANCE

W_1 = THROAT WIDTH AT ENTRANCE

N = CENTERLINE LENGTH

AR = AREA RATIO

2θ = DIVERGENCE ANGLE

$C_p = (P_2 - P_1) / \rho \frac{\bar{V}_1^2}{2g_o}$

$\bar{V}_1$ = BULK MEAN ENTRANCE VELOCITY

ρ = DENSITY

P = STATIC PRESSURE

1 = ENTRANCE

2 = DISCHARGE

a. $\frac{2\delta_1^*}{W_1} = 0.007$

Figure 2. Incompressible Straight-Channel Diffuser Performance Map (Reneau, et al, 1967).

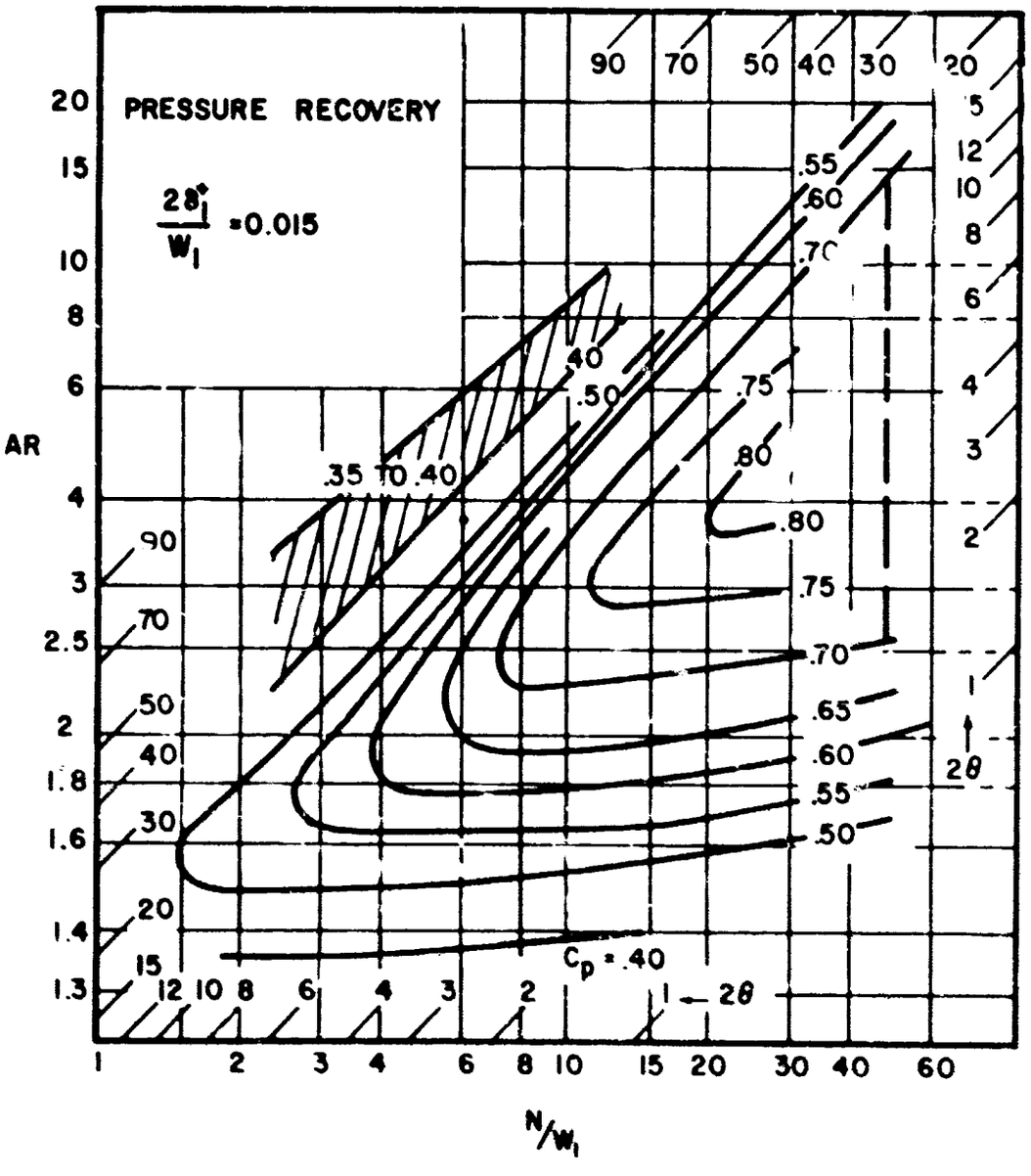

b. $\frac{2\delta_1^*}{W_1} = 0.015$

Figure 2 Continued.

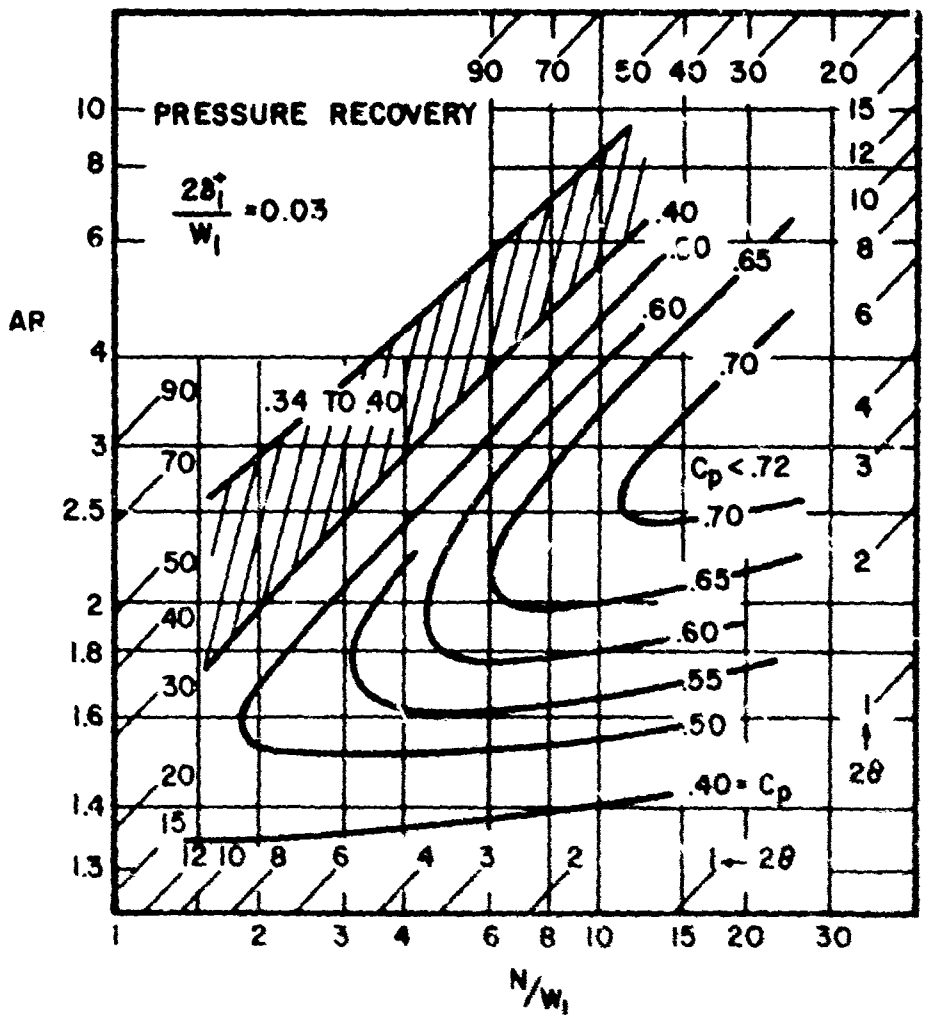

c. $\frac{2\delta_1^*}{W_1} = 0.03$

Figure 2 Continued.

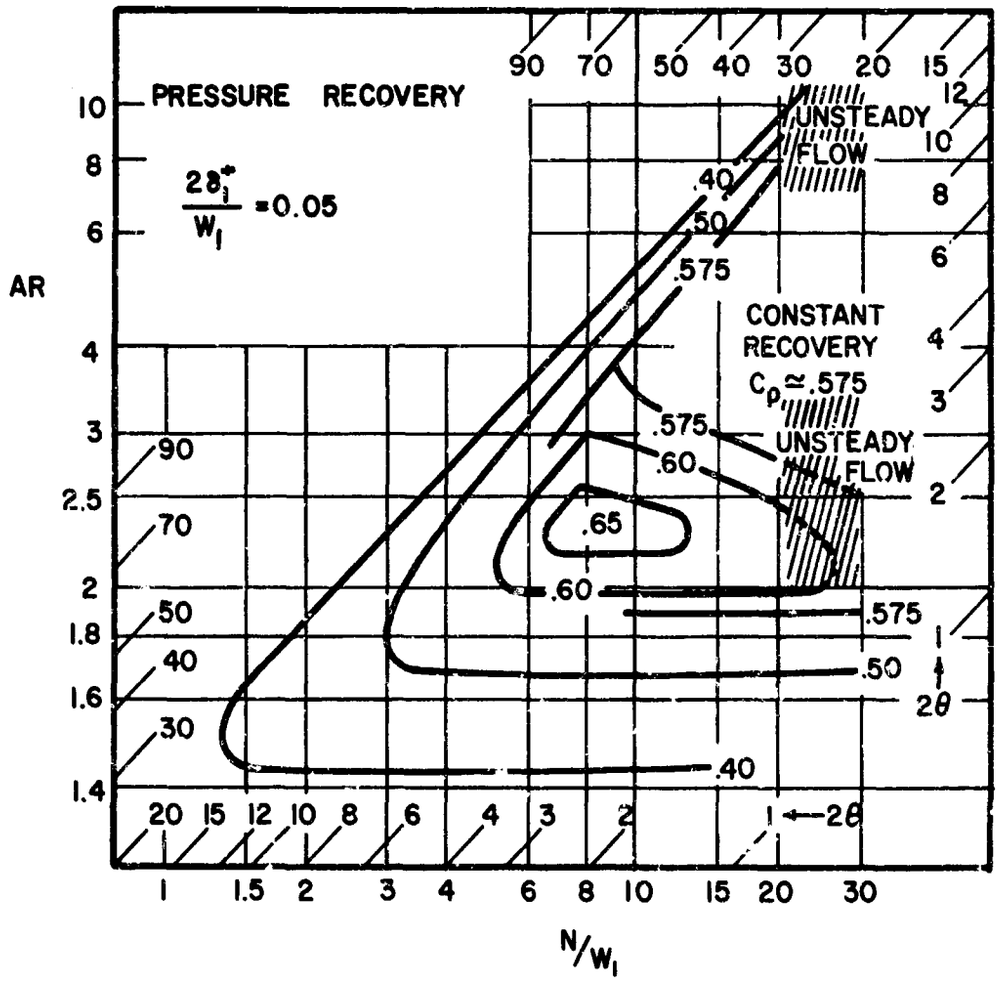

d. $\frac{2\delta_1^+}{W_1} = 0.05$

Figure 2 Concluded.

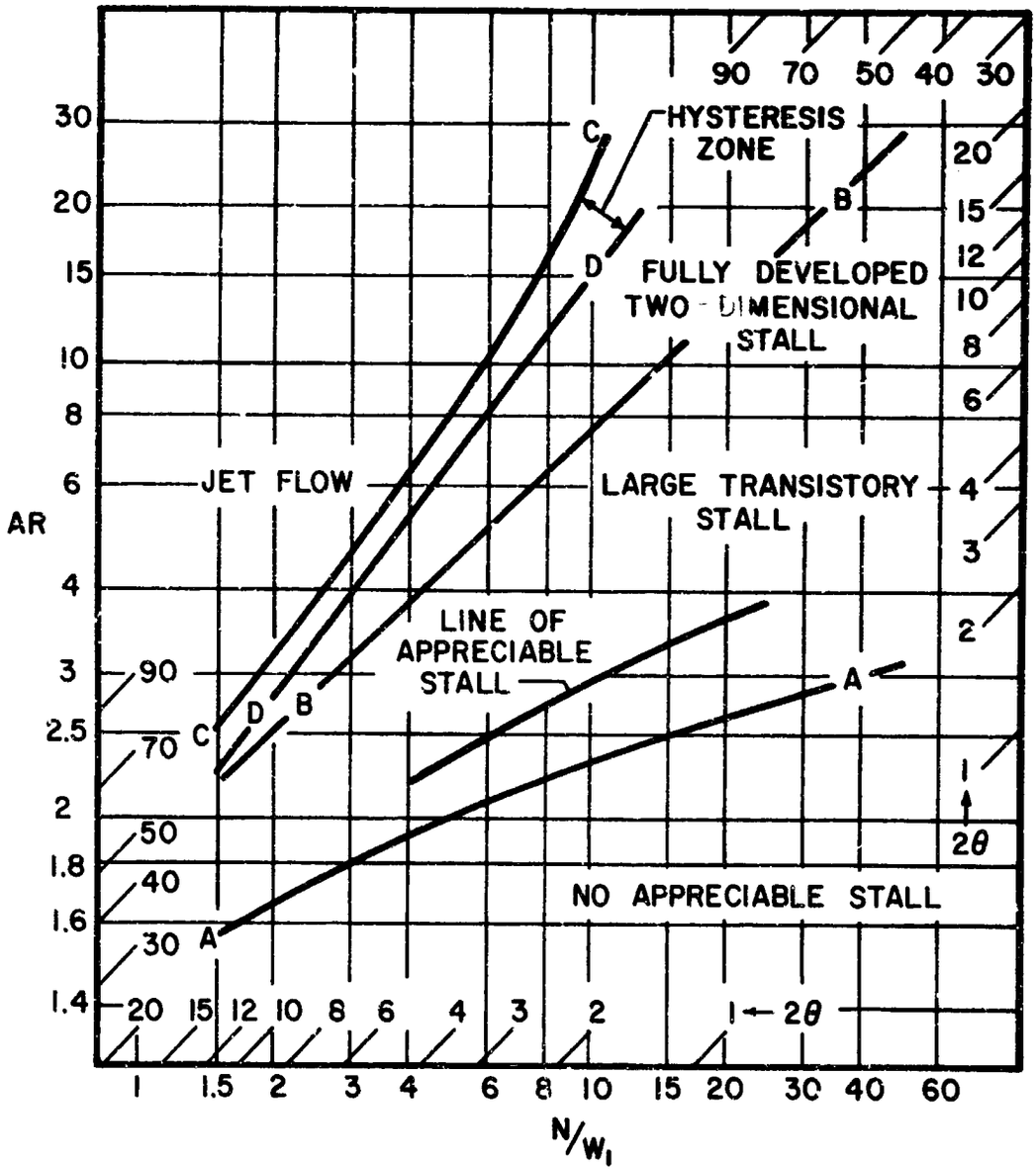

Figure 3. Incompressible Straight-Channel Diffuser Flow Regime Map (Fox and Kline, 1962).

recovery of the commonly used straight-channel, single-plane, symmetric divergence diffuser.

The geometries and inlet flow conditions studied are those found in centrifugal compressor diffuser practice. The studies were designed to include those geometries for which maximum diffuser performance is obtained. Performance maps have been prepared for those geometries of use to the designer. These performance maps have as input flow parameters the inlet blockage B and the inlet Mach number M_t.

These studies have also briefly surveyed the effect of some inlet flow conditions believed to exist in many centrifugal compressor diffuser designs but which have not been specifically included in the broader survey from which the performance maps have been obtained. The additional studies include a survey of the influence of inlet Reynolds number R_D, the effect of an asymmetric distribution of throat blockage B around the inlet throat periphery, the effect of shock boundary layer interaction immediately upstream of the diffuser throat on overall diffuser performance, and a survey of pressure recovery performance over a small range of diffuser geometries having rounded instead of sharp corners at the throat of the diffuser passage.

Table I presents the variation in geometric and inlet parameters studied in this program.

A final objective of this program has been to present the diffuser performance in a form useful to the designer and to describe how channel diffuser performance data can be applied to the optimization of centrifugal compressor performance.

1.3 SUMMARY

Past experimental work on centrifugal compressor diffusers has demonstrated the practicality of treating the diffuser as a series of component flow elements. Flow in each of these elements can be described independently, and the total fluid dynamic behavior of the overall diffuser can be described in terms of matching the inlet and exit conditions of each of the elements.

A key element is the pressure recovery performance of the channel diffuser passage formed by the vanes of a vaned diffuser. The pressure recovery of the channel diffuser will

TABLE I. LISTING OF TEST GEOMETRY, INLET CONDITIONS, AND DIFFUSER DIMENSIONS

Aspect Ratio AS	Throat Blockage B	Stagnation Pressure (psi)	Length-to-Width Ratio L/W	Divergence Angle 2θ	Inlet Length (in.)	Mach Number
0.25	.02-.12	60	7	8	0	.2 .4 .6 .8 1.0 - 1.35 -
"	"	60	7	8	3	.2 .4 .6 .8 1.0 - 1.35 -
"	"	60	7	8	6	.2 .4 .6 .8 1.0 - 1.35 -
"	"	60	7	10	0	.2 .4 .6 .8 1.0 - 1.35 -
"	"	60	7	10	3	.2 .4 .6 .8 1.0 - 1.35 -
"	"	60	7	10	6	.2 .4 .6 .8 1.0 - 1.35 -
"	"	60	7	12	0	.2 .4 .6 .8 1.0 - 1.35 -
"	"	60	7	12	3	.2 .4 .6 .8 1.0 - 1.35 -
"	"	60	7	12	6	.2 .4 .6 .8 1.0 - 1.35 -
"	"	60	7	14	0	.2 .4 .6 .8 1.0 - 1.35 -
"	"	60	7	14	3	.2 .4 .6 .8 1.0 - 1.35 -
"	"	60	7	14	6	.2 .4 .6 .8 1.0 - 1.35 -
"	"	60	7	16	0	.2 .4 .6 .8 1.0 1.2 1.35 -
"	"	60	7	16	3	.2 .4 .6 .8 1.0 1.2 1.35 -
"	"	60	7	16	6	.2 .4 .6 .8 1.0 1.2 1.35 -
"	"	60	10	8	0	.2 .4 .6 .8 1.0 - 1.35 -
"	"	60	10	8	3	.2 .4 .6 .8 1.0 - 1.35 -
"	"	60	10	8	6	.2 .4 .6 .8 1.0 - 1.35 -
"	"	60	10	10	0	.2 .4 .6 .8 1.0 - 1.35 -
"	"	60	10	10	3	.2 .4 .6 .8 1.0 - 1.35 -
"	"	60	10	10	6	.2 .4 .6 .8 1.0 - 1.35 -
"	"	60	10	12	0	.2 .4 .6 .8 1.0 - 1.35 -

TABLE I - Continued

Aspect Ratio AS	Throat Blockage B	Stagnation Pressure (psi)	Length-to Width Ratio L/W	Diver-gence Angle 2θ	Inlet Length (in.)	Mach Number
0.25	.02-.12	60	10	12	3	.2 .4 .6 .8 1.0 - 1.35 -
"	"	60	10	12	6	.2 .4 .6 .8 1.0 - 1.35 -
"	"	60	10	13	0	.2 .4 .6 .8 1.0 1.2 1.35 -
"	"	60	10	13	3	.2 .4 .6 .8 1.0 1.2 1.35 -
"	"	60	10	13	6	.2 .4 .6 .8 1.0 1.2 1.35 -
"	"	60	10	14	0	.2 .4 .6 .8 1.0 - 1.35 -
"	"	60	10	14	3	.2 .4 .6 .8 1.0 - 1.35 -
"	"	60	10	14	6	.2 .4 .6 .8 1.0 - 1.35 -
"	"	60	10	16	0	.2 .4 .6 .8 1.0 1.2 1.35 -
"	"	60	10	16	3	.2 .4 .6 .8 1.0 1.2 1.35 -
"	"	60	10	16	6	.2 .4 .6 .8 1.0 1.2 1.35 -
"	"	60	12	8	0	.2 .4 .6 .8 1.0 1.2 - -
"	"	60	12	8	3	.2 .4 .6 .8 1.0 1.2 - -
"	"	60	12	8	6	.2 .4 .6 .8 1.0 1.2 - -
"	"	60	12	8	9	.2 .4 .6 .8 1.0 1.2 - -
"	"	60	12	10	0	.2 .4 .6 .8 1.0 1.2 - -
"	"	60	12	10	3	.2 .4 .6 .8 1.0 - 1.35 -
"	"	60	12	10	6	.2 .4 .6 .8 1.0 - - 1.4
"	"	60	12	10	9	.2 .4 .6 .8 1.0 1.2 - 1.4
"	"	60	12	12	0	.2 .4 .6 .8 1.0 - 1.35 -
"	"	60	12	12	3	.2 .4 .6 .8 1.0 - 1.35 -
"	"	60	12	12	6	.2 .4 .6 .8 1.0 - - 1.4
"	"	60	12	12	9	.2 .4 .6 .8 1.0 - 1.35 -

TABLE I - Continued

Aspect Ratio AS	Throat Blockage B	Stagnation Pressure (psi)	Length-to-Width Ratio L/W	Divergence Angle 2θ	Inlet Length (in.)	Mach Number
0.25	.02-.12	60	12	13	0	.2 .4 .6 .8 1.0 1.2 1.35 -
"	"	60	12	13	3	.2 .4 .6 .8 1.0 1.2 1.35 -
"	"	60	12	13	6	.2 .4 .6 .8 1.0 1.2 1.35 -
"	"	60	12	14	0	.2 .4 .6 .8 1.0 - 1.35 -
"	"	60	12	14	3	.2 .4 .6 .8 1.0 - 1.35 -
"	"	60	12	14	6	.2 .4 .6 .8 1.0 - 1.35 -
"	"	60	12	16	0	.2 .4 .6 .8 1.0 1.2 1.35 -
"	"	60	12	16	3	.2 .4 .6 .8 1.0 1.2 1.35 -
"	"	60	12	16	6	.2 .4 .6 .8 1.0 1.2 1.35 -
"	"	60	15.2	10	0	.2 .4 .6 .8 1.0 1.2 1.35 -
"	"	60	15.2	10	3	.2 .4 .6 .8 1.0 1.2 1.35 -
"	"	60	15.2	10	6	.2 .4 .6 .8 1.0 1.2 1.35 -
"	"	60	15.2	12	0	.2 .4 .6 .8 1.0 1.2 1.35 -
"	"	60	15.2	12	3	.2 .4 .6 .8 1.0 1.2 1.35 -
"	"	60	15.2	12	6	.2 .4 .6 .8 1.0 1.2 1.35 -
"	"	60	15.2	13	0	.2 .4 .6 .8 1.0 1.2 1.35 -
"	"	60	15.2	13	3	.2 .4 .6 .8 1.0 1.2 1.35 -
"	"	60	15.2	13	6	.2 .4 .6 .8 1.0 1.2 1.35 -
"	"	60	15.2	14	0	.2 .4 .6 .8 1.0 1.2 1.35 -
"	"	60	15.2	14	3	.2 .4 .6 .8 1.0 1.2 1.35 -
"	"	60	15.2	14	6	.2 .4 .6 .8 1.0 1.2 1.35 -
"	"	20	7	16	0	.2 .4 .6 .8 1.0 1.2 1.35 -
"	"	20	7	16	3	.2 .4 .6 .8 1.0 1.2 1.35 -

TABLE I - Continued

Aspect Ratio AS	Throat Blockage B	Stagnation Pressure (psi)	Length-to-Width Ratio L/W	Divergence Angle 2θ	Inlet Length (in.)	Mach Number
0.25	.02-.12	20	7	16	6	.2 .4 .6 .8 1.0 1.2 1.35 -
"	"	20	10	13	0	.2 .4 .6 .8 1.0 1.2 1.35 -
"	"	20	10	13	3	.2 .4 .6 .8 1.0 1.2 1.35 -
"	"	20	10	13	6	.2 .4 .6 .8 1.0 1.2 1.35 -
"	"	20	12	8	0	.2 .4 .6 .8 1.0 - 1.35 -
"	"	20	12	8	3	.2 .4 .6 .8 1.0 - 1.35 -
"	"	20	12	8	6	.2 .4 .6 .8 1.0 - 1.35 -
"	"	20	12	8	9	.2 .4 .6 .8 1.0 1.2 - -
"	"	20	12	10	0	.2 .4 .6 .8 1.0 - - -
"	"	20	12	10	3	.2 .4 .6 .8 1.0 - 1.35 -
"	"	20	12	10	6	.2 .4 .6 .8 1.0 - - 1.4
"	"	20	12	10	9	.2 .4 .6 .8 1.0 - 1.35 -
"	"	20	12	12	0	.2 .4 .6 .8 1.0 - 1.35 -
"	"	20	12	12	0	.2 .4 .6 .8 1.0 - 1.35 -
"	"	20	12	12	3	.2 .4 .6 .8 1.0 - 1.35 -
"	"	20	12	12	3	.2 .4 .6 .8 1.0 - 1.35 -
"	"	20	12	12	6	.2 .4 .6 .8 1.0 - 1.35 -
"	"	20	12	12	9	.2 .4 .6 .8 1.0 - 1.35 -
"	"	20	12	13	0	.2 .4 .6 .8 1.0 1.2 1.35 -
"	"	20	12	13	3	.2 .4 .6 .8 1.0 1.2 1.35 -
"	"	20	12	13	6	.2 .4 .6 .8 1.0 1.2 1.35 -
"	"	20	15.2	13	0	.2 .4 .6 .8 1.0 1.2 1.35 -
"	"	20	15.2	13	3	.2 .4 .6 .8 1.0 1.2 1.35 -

TABLE I - Continued

Aspect Ratio AS	Throat Blockage B	Stagnation Pressure (psi)	Length-to-Width Ratio L/W	Divergence Angle 2θ	Inlet Length (in.)	Mach Number
0.25	.02-.12	20	15.2	13	6	.2 .4 .6 .8 1.0 1.2 1.35 -
"	"	20	15.2	14	0	.2 .4 .6 .8 1.0 1.2 1.35 -
"	"	20	15.2	14	3	.2 .4 .6 .8 1.0 1.2 1.35 -
"	"	20	15.2	14	6	.2 .4 .6 .8 1.0 1.2 1.35 -
1.0	"	60	10	6	0	.2 .4 .6 .8 1.0 - 1.2 1.35
"	"	60	10	6	6	.2 .4 .6 .8 1.0 - 1.2 1.35
"	"	60	10	6	9	.2 .4 .6 .8 1.0 - 1.2 1.35
"	"	60	10	8	0	.2 .4 .6 .8 1.0 1.1 1.2 1.35
"	"	60	10	8	6	.2 .4 .6 .8 1.0 - 1.2 1.35
"	"	60	10	8	9	.2 .4 .6 .8 1.0 1.1 1.2 1.35
"	"	60	10	10	0	.2 .4 .6 .8 1.0 1.1 1.2 1.35
"	"	60	10	10	6	.2 .4 .6 .8 1.0 1.1 1.2 1.35
"	"	60	10	10	9	.2 .4 .6 .8 1.0 1.1 1.2 1.35
"	"	60	10	12	0	.2 .4 .6 .8 1.0 1.1 - 1.35
"	"	60	10	12	6	.2 .4 .6 .8 1.0 - 1.2 1.35
"	"	60	10	12	9	.2 .4 .6 .8 1.0 - 1.2 1.35
"	"	60	12	6	0	.2 .4 .6 .8 1.0 1.1 1.2 1.35
"	"	60	12	6	6	.2 .4 .6 .8 1.0 1.1 1.2 1.35
"	"	60	12	6	9	.2 .4 .6 .8 1.0 1.1 1.2 1.35
"	"	60	12	8	0	.2 .4 .6 .8 1.0 1.1 1.2 1.35
"	"	60	12	8	6	.2 .4 .6 .8 1.0 1.1 1.2 1.35

TABLE I - Continued

Aspect Ratio AS	Throat Blockage B	Stagnation Pressure (psi)	Length to-Width Ratio L/W	Diver-gence Angle 2θ	Inlet Length (in.)	Mach Number
1.0	.02-.12	60	12	8	9	.2 .4 .6 .8 1.0 1.1 1.2 1.35
"	"	60	12	10	0	.2 .4 .6 .8 1.0 1.1 1.2 1.35
"	"	60	12	10	6	.2 .4 .6 .8 1.0 1.1 1.2 1.35
"	"	60	12	10	9	.2 .4 .6 .8 1.0 1.1 1.2 1.35
"	"	60	12	12	0	.2 .4 .6 .8 1.0 1.1 - 1.35
"	"	60	12	12	6	.2 .4 .6 .8 1.0 - 1.2 1.35
"	"	60	12	12	9	.2 .4 .6 .8 1.0 - 1.2 1.35
"	"	60	15.2	6	0	.2 .4 .6 .8 1.0 1.1 1.2 1.35
"	"	60	15.2	6	6	.2 .4 .6 .8 1.0 1.1 1.2 1.35
"	"	60	15.2	6	9	.2 .4 .6 .8 1.0 1.1 1.2 1.35
"	"	60	15.2	6	9	.2 .4 .6 .8 1.0 1.1 1.2 1.35
"	"	60	15.2	8	0	.2 .4 .6 .8 1.0 1.1 1.2 1.35
"	"	60	15.2	8	3	.2 .4 .6 .8 1.0 1.1 1.2 1.35
"	"	60	15.2	8	6	.2 .4 .6 .8 1.0 1.1 1.2 1.35
"	"	60	15.2	8	9	.2 .4 .6 .8 1.0 1.1 1.2 1.35
"	"	60	15.2	10	0	.2 .4 .6 .8 1.0 1.1 1.2 1.35
"	"	60	15.2	10	3	.2 .4 .6 .8 1.0 1.1 1.2 1.35
"	"	60	15.2	10	6	.2 .4 .6 .8 1.0 1.1 1.2 1.35
"	"	60	15.2	10	9	.2 .4 .6 .8 1.0 1.1 1.2 1.35
"	"	60	15.2	12	0	.2 .4 .6 .8 1.0 1.1 1.2 1.35
"	"	60	15.2	12	6	.2 .4 .6 .8 1.0 1.1 1.2 1.35
"	"	60	15.2	12	9	.2 .4 .6 .8 1.0 1.1 1.2 1.35
"	"	60	18.25	6	0	.2 .4 .6 .8 1.0 - 1.2 1.35

TABLE I - Continued

Aspect Ratio AS	Throat Blockage B	Stagnation Pressure (psi)	Length-to-Width Ratio L/W	Divergence Angle 2θ	Inlet Length (in.)	Mach Number
1.0	.02-.12	60	18.25	6	6	.2 .4 .6 .8 1.0 - 1.2 1.35
"	"	60	18.25	6	9	.2 .4 .6 .8 1.0 - 1.2 1.35
"	"	60	18.25	8	0	.2 .4 .6 .8 1.0 - 1.2 1.35
"	"	60	18.25	8	6	.2 .4 .6 .8 1.0 - 1.2 1.35
"	"	60	18.25	8	9	.2 .4 .6 .8 1.0 - 1.2 1.35
"	"	60	18.25	10	0	.2 .4 .6 .8 1.0 - 1.2 1.35
"	"	60	18.25	10	6	.2 .4 .6 .8 1.0 - 1.2 1.35
"	"	60	18.25	10	9	.2 .4 .6 .8 1.0 - 1.2 1.35
"	"	60	18.25	12	0	.2 .4 .6 .8 1.0 - 1.2 1.35
"	"	60	18.25	12	6	.2 .4 .6 .8 1.0 - 1.2 1.35
"	"	60	18.25	12	9	.2 .4 .6 .8 1.0 - 1.2 1.35
5.0	"	60	7	6	0	.2 .4 .6 .8 1.0 1.2 1.35
"	"	60	7	6	3	.2 .4 .6 .8 1.0 1.2 1.35
"	"	60	7	6	6	.2 .4 .6 .8 1.0 1.2 1.35
"	"	60	7	8	0	.2 .4 .6 .8 1.0 1.2 1.35
"	"	60	7	8	3	.2 .4 .6 .8 1.0 1.2 1.35
"	"	60	7	8	6	.2 .4 .6 .8 1.0 1.2 1.35
"	"	60	7	10	0	.2 .4 .6 .8 1.0 1.2 1.35
"	"	60	7	10	3	.2 .4 .6 .8 1.0 1.2 1.35
"	"	60	7	10	6	.2 .4 .6 .8 1.0 1.2 1.35
"	"	60	10	6	0	.2 .4 .6 .8 1.0 1.2 1.35

TABLE I - Continued

Aspect Ratio AS	Throat Blockage B	Stagnation Pressure (psi)	Length-to-Width Ratio L/W	Divergence Angle 2θ	Inlet Length (in.)	Mach Number
5.0	.02-.12	60	10	6	3	.2 .4 .6 .8 1.0 1.2 1.35
"	"	60	10	6	6	.2 .4 .6 .8 1.0 1.2 1.35
"	"	60	10	8	0	.2 .4 .6 .8 1.0 1.2 1.35
"	"	60	10	8	3	.2 .4 .6 .8 1.0 1.2 1.35
"	"	60	10	8	6	.2 .4 .6 .8 1.0 1.2 1.35
"	"	60	10	10	0	.2 .4 .6 .8 1.0 1.2 1.35
"	"	60	10	10	3	.2 .4 .6 .8 1.0 1.2 1.35
"	"	60	10	10	6	.2 .4 .6 .8 1.0 1.2 1.35
"	"	60	12	6	0	.2 .4 .6 .8 1.0 1.2 1.35
"	"	60	12	6	3	.2 .4 .6 .8 1.0 1.2 1.35
"	"	60	12	6	6	.2 .4 .6 .8 1.0 1.2 1.35
"	"	60	12	8	0	.2 .4 .6 .8 1.0 1.2 1.35
"	"	60	12	8	0	.2 .4 .6 .8 1.0 1.2 1.35
"	"	60	12	8	3	.2 .4 .6 .8 1.0 1.2 1.35
"	"	60	12	8	6	.2 .4 .6 .8 1.0 1.2 1.35
"	"	60	12	10	0	.2 .4 .6 .8 1.0 1.2 1.35
"	"	60	12	10	3	.2 .4 .6 .8 1.0 1.2 1.35
"	"	60	12	10	6	.2 .4 .6 .8 1.0 1.2 1.35
"	"	60	15.2	4	0	.2 .4 .6 .8 1.0 1.2 1.35
"	"	60	15.2	4	3	.2 .4 .6 .8 1.0 1.2 1.35
"	"	60	15.2	6	0	.2 .4 .6 .8 1.0 1.2 1.35
"	"	60	15.2	6	3	.2 .4 .6 .8 1.0 1.2 1.35
"	"	60	15.2	6	6	.2 .4 .6 .8 1.0 1.2 1.35
"	"	60	15.2	8	0	.2 .4 .6 .8 1.0 1.2 1.35

TABLE I - Continued

Aspect Ratio AS	Throat Blockage B	Stagnation Pressure (psi)	Length-to-Width Ratio L/W	Divergence Angle 2θ	Inlet Length (in.)	Mach Number
5.0	.02-.12	60	15.2	8	3	.2 .4 .6 .8 1.0 1.2 1.35
"	"	60	15.2	8	6	.2 .4 .6 .8 1.0 1.2 1.35
"	"	60	15.2	10	0	.2 .4 .6 .8 1.0 1.2 1.35
"	"	60	15.2	10	3	.2 .4 .6 .8 1.0 1.2 1.35
"	"	60	15.2	10	6	.2 .4 .6 .8 1.0 1.2 1.35
"	"	20	7	8	0	.2 .4 .6 .8 1.0 1.2 1.35
"	"	20	7	8	3	.2 .4 .6 .8 1.0 1.2 1.35
"	"	20	7	8	6	.2 .4 .6 .8 1.0 1.2 1.35
"	"	20	10	8	0	.2 .4 .6 .8 1.0 1.2 1.35
"	"	20	10	8	3	.2 .4 .6 .8 1.0 1.2 1.35
"	"	20	10	8	6	.2 .4 .6 .8 1.0 1.2 1.35
"	"	20	12	8	0	.2 .4 .6 .8 1.0 1.2 1.35
"	"	20	12	8	3	.2 .4 .6 .8 1.0 1.2 1.35
"	"	20	12	8	6	.2 .4 .6 .8 1.0 1.2 1.35
"	"	20	15.2	6	0	.2 .4 .6 .8 1.0 1.2 1.35
"	"	20	15.2	6	3	.2 .4 .6 .8 1.0 1.2 1.35
"	"	20	15.2	6	6	.2 .4 .6 .8 1.0 1.2 1.35
"	"	20	15.2	8	0	.2 .4 .6 .8 1.0 1.2 1.35
"	"	20	15.2	8	3	.2 .4 .6 .8 1.0 1.2 1.35
"	"	20	15.2	8	6	.2 .4 .6 .8 1.0 1.2 1.35
"	"	20	15.2	10	0	.2 .4 .6 .8 1.0 1.2 1.35
"	"	20	15.2	10	3	.2 .4 .6 .8 1.0 1.2 1.35
"	"	20	15.2	10	6	.2 .4 .6 .8 1.0 1.2 1.35

TABLE I - Continued

Aspect Ratio AS	Throat Blockage B	Stagnation Pressure (psi)	Length-to-Width Ratio L/W	Divergence Angle 2θ	Inlet Length (in.)	Mach Number
8.0	.02-.1[illegible]	60	15	4	0	.2 .4 .6 .8 1.0 1.2 1.35
"	"	60	15	4	3	.2 .4 .6 .8 1.0 1.2 1.35
"	"	60	15	10	0	.2 .4 .6 .8 1.0 1.2 1.35
"	"	60	15	10	3	.2 .4 - - - - -
"	"	60	15	10	3	.2 .4 - - - - -
"	"	60	15	10	3	.2 .4 .6 .8 1.0 1.2 1.35

DIFFUSER DIMENSIONS

AS	b (in.)	W_1 (in.)	2θ degrees	L/W_1 (in.)	Inlet Length Blocks (in.)	D (in.)
0.25	0.233	0.932	8 to 14	7 to 12	0, 3, 6	-
1.0	0.616	0.616	6 to 12	10 to 18	0, 3, 6	-
5.0	1.393	0.278	4 to 12	10 to 15	0, 3, 6	.465

be a function of the geometric parameters and the fluid dynamic inlet conditions.

The designer needs information from which to optimize the channel diffuser in terms of these geometric and flow inlet conditions. The straight-channel, two-dimensional, single-plane-divergence diffuser has been selected as a common diffuser geometry employed in vaned diffusers (either vane-island or cascade-type diffusers). An experimental program to determine the general performance behavior in terms of pressure recovery for this diffuser has been undertaken, covering the range of geometric and inlet variables found in current diffuser practice. A primary objective has been to relate this performance information to the needs of the designer.

2.0 DIFFUSER CHARACTERISTICS

Diffuser characteristics fall into two categories: (1) the diffuser static pressure recovery and (2) the stability and/or unsteady flow behavior in the diffuser.

The experimental studies reported here have measured only the static pressure recovery.

2.1 DIFFUSER PRESSURE RECOVERY

Diffuser static pressure recovery C_p is the ratio of the pressure rise between the inlet and the exit of the diffusing passage to the ideal pressure rise that would be obtained in a one-dimensional, isentropic flow through a diffuser of infinite area ratio. The ideal one-dimensional flow has the same throat centerline conditions as the actual inlet flow.

Pressure recovery is defined as

$$C_p = \frac{p_e - p_t}{p_{o_t} - p_t} \tag{1}$$

or

$$C_p = \frac{p_e/p_{o_t} - p_t/p_{o_t}}{1 - p_t/p_{o_t}} \tag{2}$$

If the fluid is a perfect gas, the pressure recovery coefficient can be written

$$C_p = \frac{p_e/p_{o_t} - F(M_t)}{1 - F(M_t)} \tag{3}$$

$$F(M_t) = \left(1 + \frac{k-1}{2} M_t^2\right)^{\frac{-k}{(k-1)}} \tag{4}$$

where

p_e = exit static pressure

p_t = throat centerline static pressure

p_{o_t} = throat centerline stagnation pressure

k = ratio of specific heats

M_t = throat Mach number based on centerline velocity at the cross section of minimum pressure

For the ideal pressure rise, i.e. for the one-dimensional isentropic flow, the amount of diffusion between the inlet and exit is dependent only upon the area change and the value of the inlet Mach number. Since the area ratio is independent of the geometry of the diffuser (independent of whether the diffuser is a straight-channel, single-divergence, double-divergence, or conical or annular diffuser, etc.), the ideal one-dimensional pressure rise is the maximum possible recovery that can be obtained for all diffuser shapes having the ideal one-dimensional flow. This ideal pressure recovery as a function of Mach number and area ratio is shown in Figure 4.

A diffuser does not actually achieve this optimum, one-dimensional isentropic recovery. Distorted inlet flow and real fluid effects lead to shear forces in the flow, causing boundary layer growth on the diffuser walls and leading to consequent large changes in flow regime behavior. Losses result from viscous shearing and mixing. Whereas the ideal pressure recovery is a function only of inlet Mach number and area ratio as shown in Figure 4, the actual pressure recovery depends upon additional geometric and inlet parameters that determine the importance of viscous effects and consequent shearing and mixing losses within the diffuser.

2.2 DIFFUSER EFFECTIVENESS

Diffuser pressure recovery is sometimes compared with the ideal pressure recovery coefficient that would be obtained with a one-dimensional, isentropic flow through the same diffuser. The effectiveness is defined as

$$\varepsilon = \frac{C_p}{C_{p_i}} \tag{5}$$

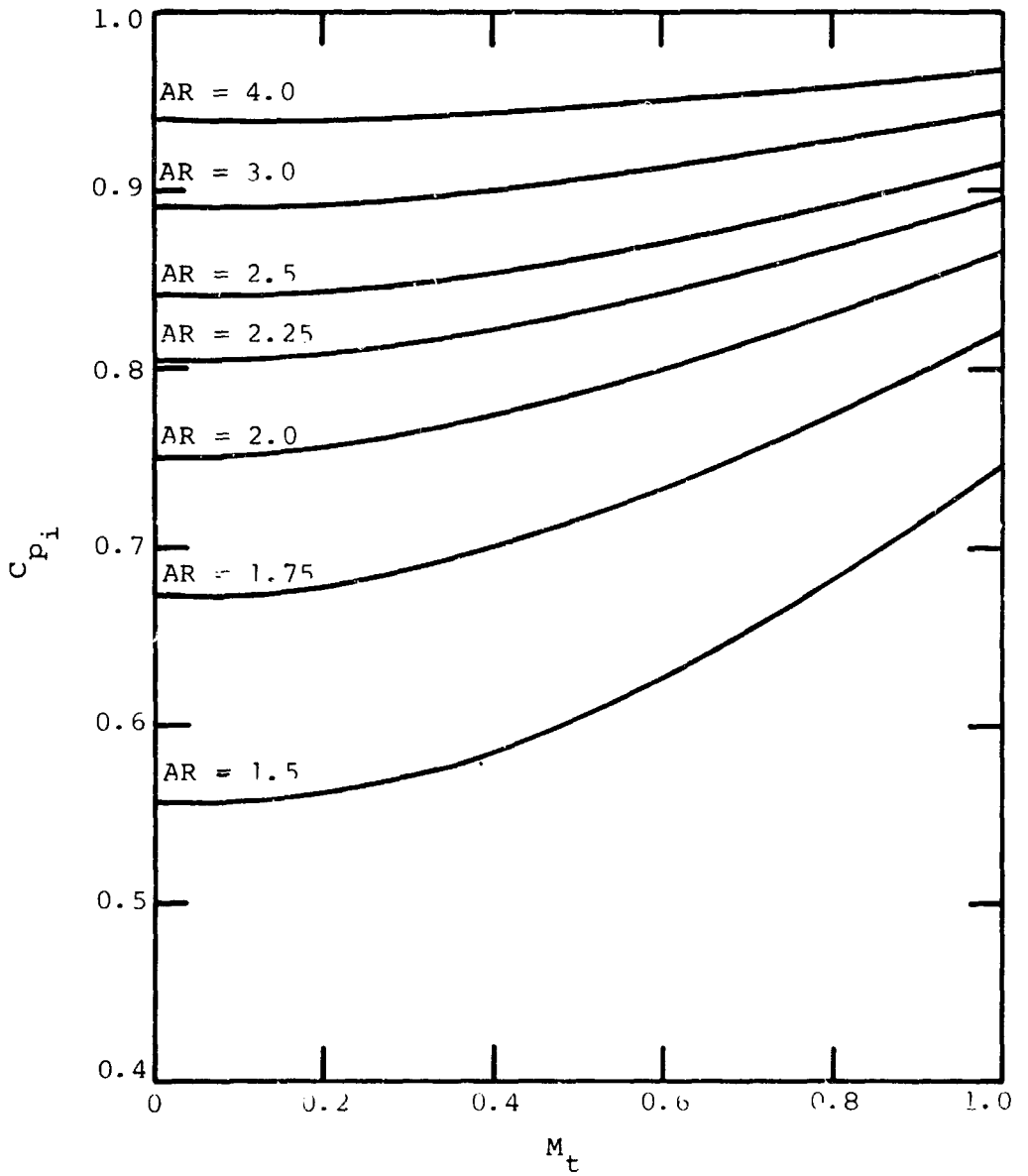

Figure 4. Ideal Pressure Recovery Versus Throat Mach Number.

where

C_p = actual diffuser pressure recovery

C_{p_i} = ideal pressure recovery

The effectiveness is thus the ratio of the actual pressure recovery for a given diffuser at a given throat inlet Mach number M_t to the ideal pressure recovery for the same area ratio diffuser and inlet Mach number (C_{p_i} is given in Figure 4). The effectiveness is a measure of the efficiency of a diffuser in attaining the ideal pressure rise.

2.3 DIFFUSER GEOMETRIC PARAMETERS

Figure 5 defines the diffuser geometry for the straight-channel, single-plane, symmetric divergence diffuser. For this geometry, the geometric variables which define the diffuser shape are:

L = diffuser length (measured along diffuser centerline)
W = diffuser width (at entrance or discharge)
b = diffuser depth (constant)
2θ = divergence angle

Three nondimensional parameters define completely the diffuser geometry:

L/W_1 = length-to-throat width angle
2θ = divergence angle
AS = b/W_1 = throat aspect ratio

A fourth nondimensional parameter is often used:

AR = area ratio

Only three of these four nondimensional parameters are necessary to define completely the single-plane divergence, straight-channel diffuser geometry. The following relation exists among the area ratio AR, length-to-throat width ratio L/W_1, and divergence angle 2θ:

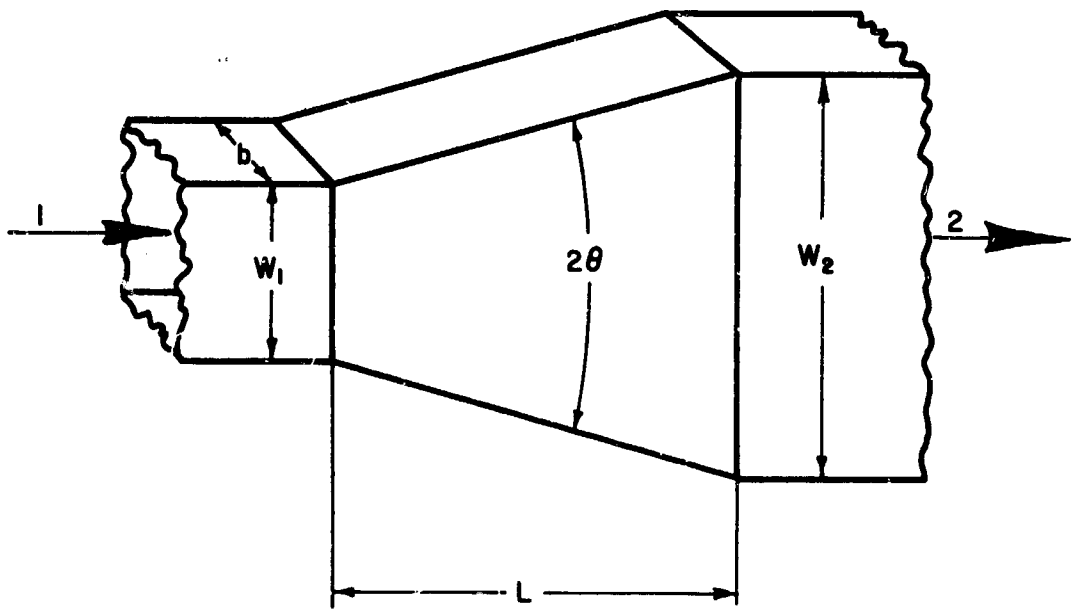

L = DIFFUSER LENGTH (MEASURED ALONG DIFFUSER CENTERLINE)

W = DIFFUSER WIDTH

b = DIFFUSER DEPTH

2θ = DIVERGENCE ANGLE

AS = b/W_1 = ASPECT RATIO

AR = EXIT AREA / INLET AREA = W_2/W_1 = AREA RATIO

1 = ENTRANCE

2 = DISCHARGE

Figure 5. Single-Plane, Symmetric Divergence, Straight-Channel Diffuser Geometry.

$$AR = 1 + 2\ (L/W_1)\ \tan\ (\theta) \qquad (6)$$

For other diffuser channel geometries, i.e., double divergence, conical, etc., other geometric parameters are needed to describe the diffuser shape completely.

2.4 CHANNEL DIFFUSER INLET PARAMETERS

We have already considered throat Mach number M_t and the geometric parameters that influence the pressure recovery of the diffuser. The inlet and geometric parameters controlling diffuser behavior can be grouped as follows:

Group I

(1) M_t = throat Mach number

(2) AR = area ratio

These two parameters are sufficient to determine the ideal pressure recovery and are important parameters for any diffuser.

Group II

The second group describes the variables defining the details of the diffuser geometry and diffuser inlet conditions.

(1) $AS = b/W_1$ = throat aspect ratio

(2) L/W_1 = length-to-throat width ratio or 2θ = diffuser divergence angle

(3) B = throat inlet blockage

(4) R_D = inlet flow Reynolds number. Reynolds number is based on the flow core velocity, the fluid kinematic viscosity, and the throat hydraulic diameter

(5) distribution of displacement thickness δ^*, and hence blockage B, around the throat periphery

(6) inlet velocity profile in terms of the nearness of the boundary layer to separation

(7) inlet potential core flow characteristics (e.g., non-uniform velocity profile in the potential core flow entering the diffuser and the turbulence level in the inlet core flow)

(8) corner geometry at the junction of the diffuser entrance channel and the diverging diffuser walls

(9) cross-section shape of the entrance and diffuser flow channels

(10) skewed inlet boundary layer flow

This is not necessarily a complete list of all possible inlet flow parameters. However, it includes the most important inlet flow conditions affecting diffuser performance.

Throat Inlet Mach Number

With an increase in inlet Mach number, the ideal pressure recovery increases, as presented in Figure 4. Previous experimental work available on pressure recovery performance at high inlet Mach numbers indicated a possibility of a sudden and precipitous drop in diffuser pressure recovery performance as Mach number approached sonic conditions at the throat. In fact, some practitioners in the centrifugal compressor diffuser design field have followed a traditional belief that high inlet Mach numbers should be avoided because pressure recovery in the diffuser would decrease rapidly above some "critical" subsonic Mach number (less than 1.0).

Typical performance variations observed by a number of workers measuring diffuser recovery are shown in Figure 6, taken from an extensive survey of high-subsonic-Mach-number, straight-channel diffuser literature made by Halleen and Johnston (1966). Halleen and Johnston selected 15 papers as the best work then available. On the basis of these studies, they had to conclude that high subsonic Mach number diffuser performance fell into one of three categories; these categories showed performance typified by the three curves labeled A, B, and C in Figure 6. The sort of behavior that would be observed in practice depended upon where the diffuser design lay relative to the flow regime's boundaries obtained for incompressible flow diffusers, shown in Figure 3. In all cases, the diffusers having

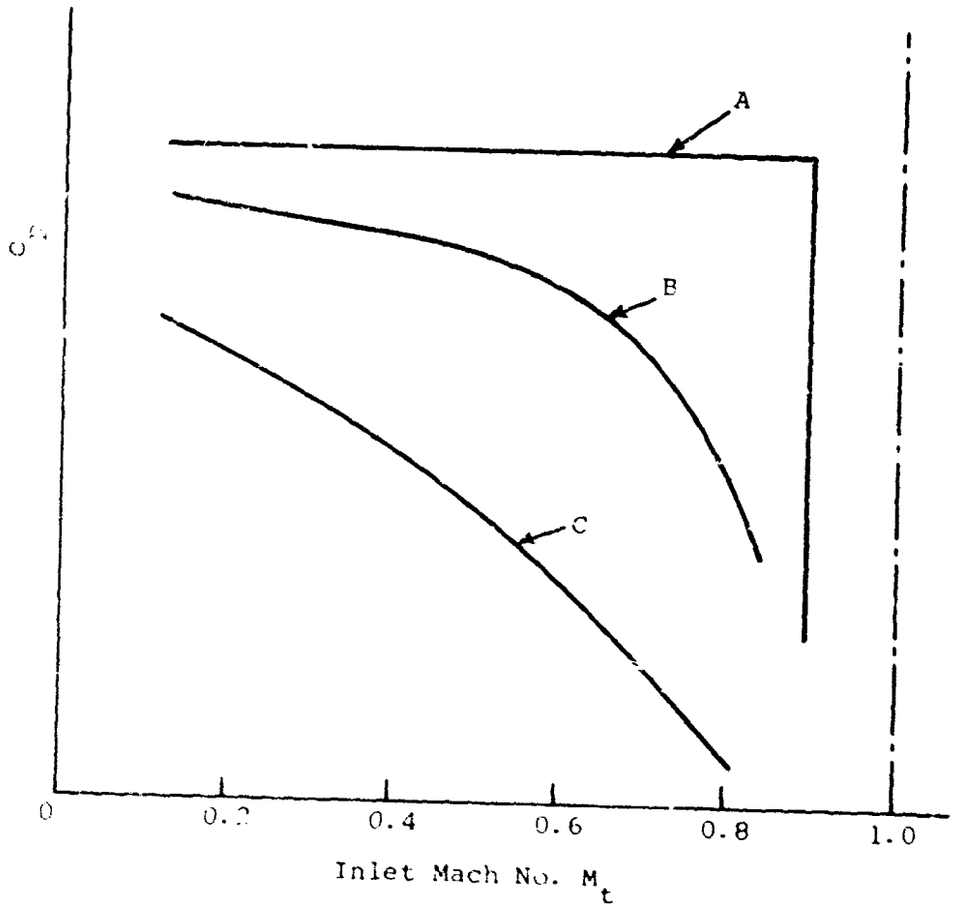

Figure 6. Pressure Recovery Versus Inlet Mach Number - Characteristic Grouping of Data at Fixed Geometry (Halleen and Johnston, 1966).

best recovery at high subsonic Mach numbers displayed Group A behavior. However, in all cases a "critical" Mach number (less than 1.0) was observed, and the drop in performance at this critical Mach number was precipitous.

From the literature that was then available, Halleen and Johnston found that it was possible to correlate the Mach number at which this drop occurred for the Group A diffusers with certain of the diffuser parameters. They found that throat inlet boundary layer blockage had the greatest influence of all, and they were able to derive a very consistent correlation as shown in Figure 7. The Group A diffusers were those having geometries closest to the optimum diffusers on the performance maps. The curve shows that a throat Mach number over 0.8 cannot be allowed, for instance, if the boundary layer blockage in the throat is greater than 3.8%. Note, however, that this level of blockage and higher is common to diffusers of centrifugal compressor stages (and indeed many other systems).

If the results found in the literature were correct, it was difficult to explain how vaned diffusers of high-pressure-ratio centrifugal compressors could produce any significant pressure recovery. In contrast to the predictions from the diffuser literature of the type just discussed, good centrifugal compressor diffuser performance has often been obtained well above the correlation curve shown in Figure 7. Thus the channel part of the diffuser apparently achieves good recovery in the centrifugal compressor diffuser for inlet Mach numbers well above the supposed critical limit found in the literature.

In spite of the evidence from the many diffuser studies in the literature (see Halleen and Johnston, 1966) which appeared to correlate well with the critical Mach number concept as shown in Figure 6, centrifugal diffuser experience indicated that, at least in some instances, good performance with inlet Mach numbers up to choked conditions was possible.

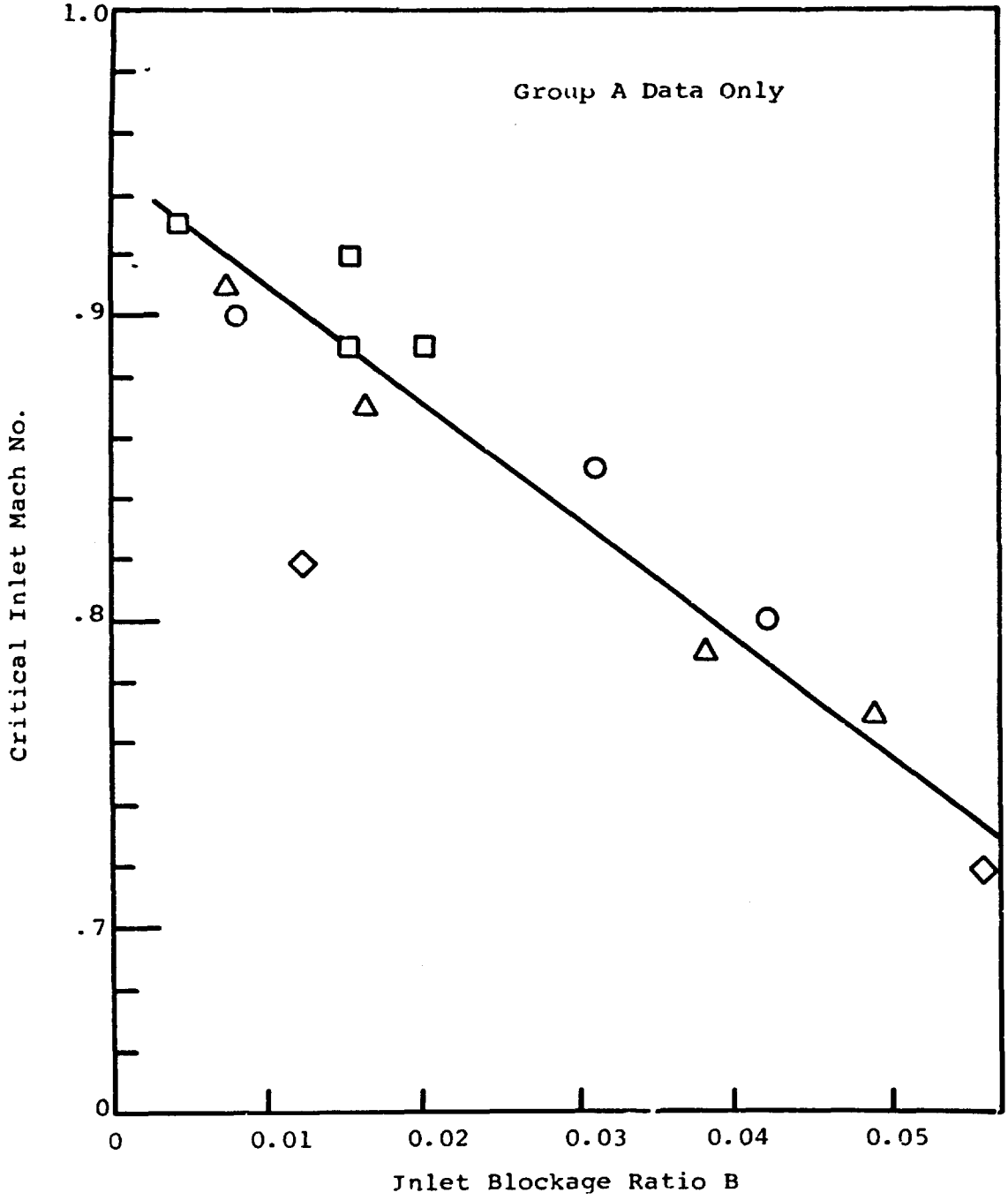

Figure 7. Critical Inlet Mach Number Versus Blockage Ratio (Halleen and Johnston, 1966).

The present studies have obtained data for the straight-channel, single-divergence diffuser which has clarified the critical Mach number limit discussed above. Diffusers do achieve good performance up to and beyond choked conditions at the throat. In some cases, fair recovery is obtained for choked and superchoking conditions. We shall use "superchoking" to indicate choked flow, M_t = 1.0, at the throat with a shock located in the diffusing passage. The Mach number immediately ahead of the shock in the diffusing passage will be designated by M_x. Inlet Mach number behavior will be discussed in detail in Section 4.0.

Aspect Ratio

The present program has obtained diffuser pressure recovery performance for aspect ratio = 0.25, 1.0, and 5.0. These studies will be presented in detail in Section 4.0.

The results of these studies have shown that the optimum recovery as a function of diffuser aspect ratio varies appreciably with aspect ratio. Overall compressor design strategy will be strongly influenced by this recovery-versus-aspect-ratio behavior because the impeller exit depth is strongly coupled geometrically and the fluid dynamically to the diffuser's aspect ratio. Because the diffuser inlet boundary layer thickness in a centrifugal compressor will change only slightly with a small change in diffuser depth, blockage can be expected to change appreciably as aspect ratio is altered. For these reasons, it is imperative in design that good information be available on the variation of pressure recovery with both blockage and aspect ratio.

Throat Inlet Blockage

Many channel diffusers operate where the throat consists of a potential "core" flow surrounded by viscous boundary layers. The boundary layer characteristics of such a flow may be partially described by the "throat" blockage. The throat blockage is defined in terms of the actual geometric throat flow area and an equivalent one-dimensional flow area. This one-dimensional

effective flow area is that required to pass a one-dimensional flow (having a mass flow equal to the actual mass flow through the channel diffuser throat) and having the measured values of throat centerline stagnation pressure and temperature. The throat blockage B is defined as

$$B = 1 - \frac{A_{effective}}{A_{geometrical}} \qquad (7)$$

where

$A_{geometrical}$ = actual diffuser throat area

$A_{effective}$ = the equivalent one-dimensional flow area

The throat blockage B has been described in terms of a potential "core" type flow. However, the same throat blockage can be used for fully developed flow.

Throat blockage B and inlet Mach number M_t are the two primary inlet flow parameters investigated in these studies.

Inlet Reynolds Number

The boundary layer behavior characteristics entering the diffuser will depend upon Reynolds number of the inlet flow. The characteristics may vary sufficiently to affect diffuser performance if the range of inlet Reynolds numbers is large. The present studies have surveyed the influence of inlet Reynolds number by varying inlet Reynolds number by a factor of 3. The results of these experiments will be discussed in Section 4.0.

Nonuniform Distribution of Throat Blockage

The channel diffuser inlet boundary layer is developed on the sidewalls and the suction and pressure surfaces of the centrifugal compressor diffuser in the vaneless

and semivaneless space. These boundary layers are subject to a radial pressure gradient which produces a secondary flow component in the boundary layers on the sidewalls of the diffuser. The amount of secondary flow produced will depend upon the magnitude of the radial pressure gradient and the streamline direction of the flow through the vaneless and semivaneless spaces. If this secondary flow effect is pronounced, it results in a bleeding of the sidewall and suction surface boundary layers into the core flow ahead of the channel diffuser throat. Because of this, the boundary layer flow entering the channel diffuser throat may be quite unevenly distributed around the throat periphery. The small amount of growth on the vane surface immediately ahead of the channel diffuser throat accentuates this effect. This variation in boundary layer thickness reflects an equivalent variation in throat blockage B around the throat periphery.

Diffusers with asymmetric distribution of blockage might have a poorer diffuser performance compared to identical diffuser geometries with the same but uniformly distributed throat blockage. An asymmetric distribution of blockage might produce an unfavorable boundary layer situation on those walls with the large blockage. This would lead to an early separation of the diffuser and a change in optimum recovery as a function of diffuser geometry.

A set of studies has been made to look at this effect. The detailed results are presented in Section 4.0.

Nearness of Inlet Velocity Profile to Separation

The history of the boundary layer flow approaching the channel diffuser throat is important, since it determines the boundary layer velocity profile and the nearness of the boundary layer to separation. Nearness to separation is usually specified either by the approach of the local skin friction coefficient toward zero or by the specification of a velocity profile shape factor for a particular class of boundary layers. It is usually expected that the closer the boundary layer is to separation, the poorer will be the performance of the diffuser.

In high-pressure-ratio centrifugal compressors, the flow leaving the impeller is supersonic relative to the diffuser. From the work of Welliver and Acurio (1967), it appears that the optimum procedure is to diffuse the supersonic flow to Mach numbers less than 1.2 ahead of the vane leading edges, whereupon the flow is caused to shock before entering the diffuser channel. The imprint of the resulting shock upon the boundary layer produces a shock-boundary layer interaction process that may distort the boundary layer characteristics. The resulting boundary layer flow emerging from under the shock and entering the diffuser may be near separation. Although the shock-interaction process is not really well understood, it has been generally assumed that such a shock-boundary layer interaction immediately ahead of the channel diffuser throat will produce a poorer diffuser recovery than that indicated by the dependence of C_p on inlet blockage B alone.

The effect of shock-inlet boundary layer interaction ahead of the diffuser throat has been studied and is discussed in Section 4.0.

Wall Contour Near Diffuser Throat

Diffusers having sharp corners are often found in centrifugal compressor channel diffuser designs. The shape of the corner at the throat of the diffuser may have an important influence on the growth of boundary layer on the diverging walls and hence the pressure recovery of the diffuser. For example, a reduction in the adverse pressure gradient imposed on the boundary layer on the diverging walls near the throat will be obtained if a rounded corner is used instead of a sharp corner. A local dip in static pressure occurs near the throat because of the acceleration of the flow around the corner. This local dip in static pressure will be decreased with a rounded corner, thus lowering the pressure rise imposed upon the boundary layer immediately downstream of the diffuser throat.

Experiments have been run in these studies to measure the influence of rounding the sharp corners of the throat over a small range of geometries. The results of

these studies as they affect diffuser performance are discussed in Section 4.0.

Inlet Potential Core Flow Characteristics*

It is the mixed out flow from the impeller that arrives at the channel diffuser throat. This flow obviously has a high turbulence level. It may also have velocity distortions caused by shedding from separated flow regions in the flow elements ahead of the channel throat, or if the flow is not thoroughly mixed out before it enters the channel diffuser, remnants of the jet and wake portions of the flow off the impeller will be present. However, the small relative velocity between wake and jet and the high passing blade frequency of the impeller blading should make such fluctuations appear as rather high frequency turbulent fluctuations.

Mixing calculations and empirical measurements appear to confirm that the impeller flow is well mixed out prior to entering the channel diffuser. In general, it is expected that the amplitude-frequency spectrum of velocity fluctuations at the inlet flow should be sufficient to describe the inlet unsteady flow behavior.

Inlet and Diffuser Cross-Section Shape

The inlet and diffuser passages are rectangular for the diffuser studies in the present investigation. It is probable that passage cross-section shape has a noticeable effect on the flow development through both the inlet and the diffuser because of three-dimensional and/or wall corner effects.

The addition of fillets in the corners of a basic rectangular cross-section passage represents a simple and practical alteration of geometry. Because separation first occurs in the corners of rectangular diffusers, the

---

*These inlet characteristics and the two remaining effects discussed in this section -- "Inlet and Diffuser Cross Section Shape" and "Skewed Inlet Boundary Layers" -- have not been examined experimentally in any detail in these present studies.

addition of fillets may significantly change boundary layer growth and/or the amount of separation and mixing. Diffuser recovery maps might be significantly altered, and some improvement in peak recovery might be gained by such a geometry change.

Another example of a simple alteration in diffuser geometry is divergence in two directions (double divergence diffusers). Tandem divergence diffusers are another simple geometric modification. In this case, the diffuser diverges at a fixed angle for a given length of the diffuser passage and then diverges at a different angle to produce the required overall area ratio. There is some evidence available that double divergence and tandem divergence diffusers can achieve improved performance in terms of pressure recovery over that obtained by single divergence diffusers with the same overall length-to-width ratio, area ratio, and inlet blockage.

Skewed Inlet Boundary Layers

The boundary layer off the impeller moves onto a surface with a component of motion transverse to the direction of the boundary layer flow. This effect produces a skewed boundary layer velocity profile; the viscous flow near the surface distorts the velocity profile into a three-dimensional pattern [see Johnston (1960)].

The extent to which this effect influences the boundary layer growth and its characteristics in the vaneless and semivainless spaces is not known. However, the skewed boundary layer behavior characteristics may be retained up to the channel diffuser throat and affect the pressure recovery performance thereof.

The secondary flow behavior described previously will also produce skewed boundary layer flow at the diffuser throat. The growth and development of the boundary layer in the diffuser should be somewhat different from the unskewed boundary layers studied in the present program. Such effects may have a direct influence on pressure recovery because of changes in boundary layer development in the diffuser.

2.5 OPTIMUM PRESSURE RECOVERY

A convenient presentation of diffuser pressure recovery performance as a function of the important parameters is the pressure recovery performance map. Such maps are contour plots of pressure recovery as a function of the geometric variables for the straight-channel, single-symmetric divergence diffuser for fixed values of the fluid dynamic inlet variables. At low Mach numbers, maps have been obtained as displayed in Figure 2.

It is convenient to consider the diffuser performance maps as "contour" maps; these maps give contours of constant pressure recovery which describe contours of constant "elevation". Thus, the highest contours of pressure recovery define the "peaks" of the pressure recovery "hills"

For some diffuser applications, geometric restrictions permit only a given area ratio diffuser to be used. In such cases, the diffuser length-to-width ratio L/W_1 and the divergence angle 2θ can be adjusted to obtain the prescribed area ratio. In other applications, the maximum diffuser length-to-width ratio L/W_1 may be prescribed, in which case the diffuser geometry may be varied between limits on 2θ and the area ratio AR to remain under the limitation on length-to-width ratio.

In the literature, these two particular applications have been discussed as defining two ridges of "optimum" performance in terms of the diffuser pressure recovery performance map.

Optimum Diffuser Performance at Constant Area Ratio

Referring to Figure 2, when area ratio is prescribed, there is a given optimum performance available in terms of pressure recovery for each area ratio. These are obtained by following lines of constant area ratio and by determining the value of L/W_1 on the performance map "hill" for which the highest performance is obtained. The locus of these points describes the diffuser nondimensional length-to-width ratio producing a maximum pressure recovery for a prescribed area ratio. Such a line has been called C_p^{**} in the literature [Sovran and Klomp (1965)]. A sketch of a typical diffuser performance map and the line C_p^{**} are shown in Figure 8.

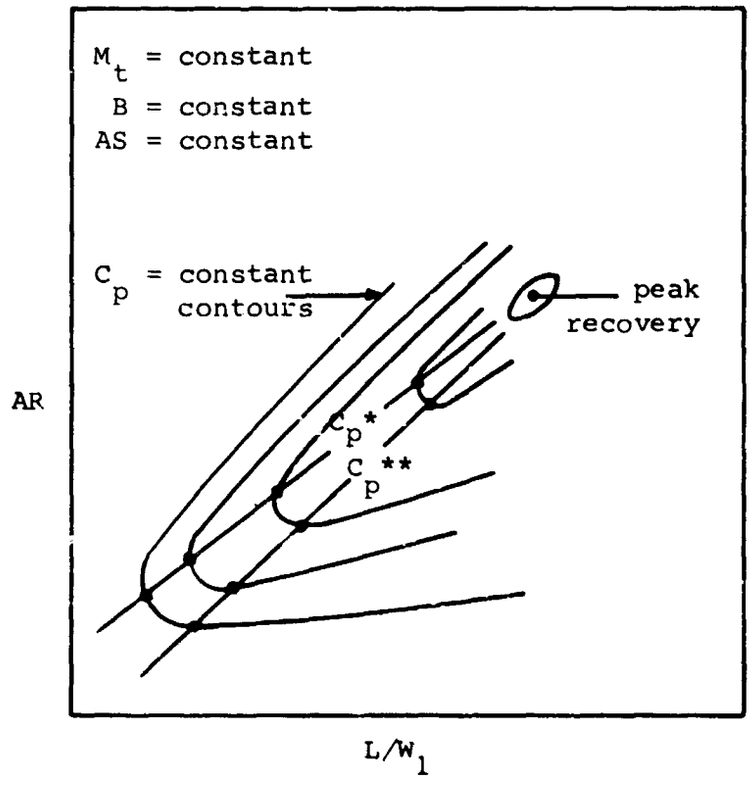

Figure 8. Optimum Pressure Recovery Lines C_p^* and C_p^{**}.

Optimum Diffuser Performance at Constant Length-to-Width Ratio

A second line C_p*, Sovran and Klomp (1965), is the locus of points describing the maxima in diffuser pressure recovery and corresponding values of area ratio AR for constant values of length-to-width ratio L/W_1. The line C_p* is also shown on Figure 8. The line C_p* is always higher in diffuser divergence angle than the line C_p**.

The term "peak" recovery is used here to define the "peak" of the pressure recovery "hill" for a given performance map. Nomenclature in the past has referred to peak recovery as the maximum in pressure recovery at constant L/W_1; the top of the pressure recovery "hill" has been referred to as a maximum in pressure recovery. Throughout the remainder of this report, we shall refer to the peak of pressure recovery as the highest recovery on a given performance map. The lines C_p* and C_p** will be referred to as the ridges of pressure recovery.

The performance behavior of diffusers has been discussed extensively in a number of references within the previous literature, at least for low Mach numbers. The reader is referred in particular to the references Reneau et al (1964) and Sovran and Klomp (1965) for a discussion of the various diffuser optima.

3.0 EXPERIMENTAL PROCEDURE

To provide a variation in Reynolds number and to simulate Reynolds number conditions found in diffuser practice, the experiments have been run in a closed-loop wind tunnel. The closed-loop tunnel permits variable density operation and carefully controlled cleanliness and humidity conditions.

3.1 WIND TUNNEL

A schematic diagram of the diffuser wind tunnel is shown in Figure 9.

The pressure level control equipment provides a variation in operating pressure level from 10 to 100 psia. During the testing program, all studies were run at either 20 or 60 psia nominal pressure A small pump-up compressor charges the main test loop to set the operating pressure level and to supply makeup air to compensate for small leaks in the loop. The pump-up compressor is rated at 10 cfm at 100 pounds per square inch gauge. The pump-up compressor was used in conjunction with a regulator to maintain system pressure during flow operation. The pressure level control unit is designed for dry, oil-free air and has suitable aftercoolers to insure an adequate air supply through the main test loop at ambient temperature. The oil and water desiccators were rated to remove all oil to a concentration of less than two parts per million and water to a dew point of -45°F.

Air Supply

Air is circulated through the test loop by two compressors connected in series. The compressors are specified for constant-displacement, oil-free operation. To run in a closed-loop configuration, special shaft seals are required to prevent oil leakage through the main compressor seals. To help prevent leakage of oil into the air flow system, an air ejector was attached to the compressor oil sumps, keeping them considerably below the compressor inlet pressure.

The compressors are of the rotary screw type and produce large fluctuations in pressure at the compressor outlet. To isolate the pressure fluctuations from the test section, a 50-gallon tank was placed at the entrance of the main compressor

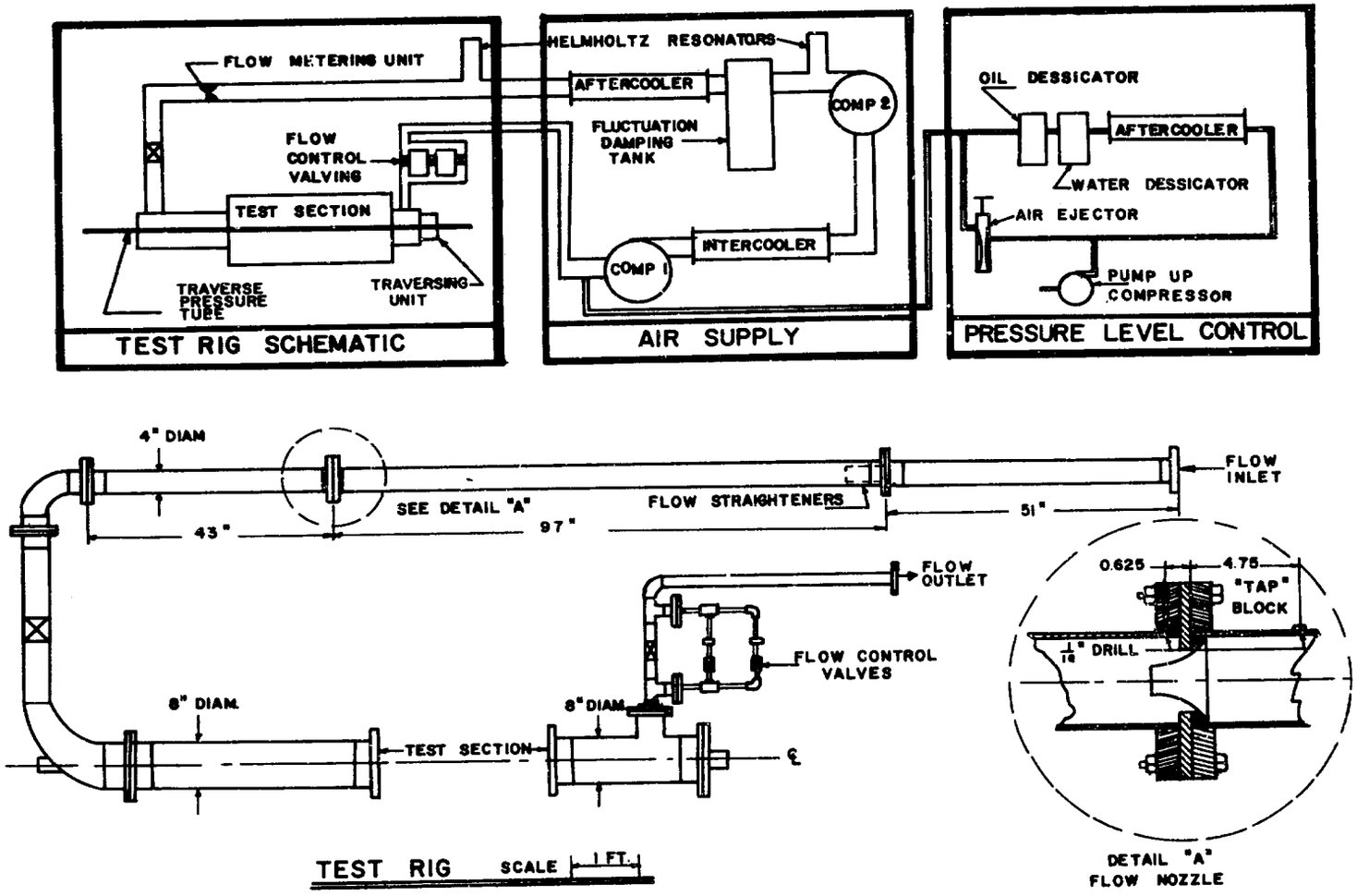

Figure 9. Diagram of Test Section and Wind Tunnel Loop.

aftercooler and filled with low-porosity, flexible foam filtration material. Helmholtz resonators were also installed at two locations in the piping These resonators were tuned to produce an out-of-phase standing wave for the fundamental and first-harmonic frequency of the compressor's pressure fluctuations. The section of piping immediately upstream of the flowmetering unit was filled with porous material to further damp the pressure fluctuations immediately upstream of the test rig. Although the fluctuations were never entirely eliminated, they were reduced to a very small level. A quantitative discussion of the magnitude of the pressure fluctuations is presented in Section 4.0.

Test Rig

The test rig comprises the flowmetering unit, flowmetering valves, and test section. The flow enters through a 51" length of 4" pipe in which the pressure fluctuation material discussed in the foregoing section is mounted ahead of the entry to the flowmetering unit.

Flowmetering Unit

The flowmetering unit comprises the horizontal run of 4" pipe upstream of the test section. The flowmeter is a 1-1/4" Cox flow nozzle assembled in the 4" pipe as shown in detail A of Figure 9. The length of pipe upstream and downstream of the flow nozzle unit meets standard ASME flow nozzle recommendations. The pipe's length-to-diameter ratio is 10 downstream of the flow nozzle and 22 upstream. Recommended ASME-type flow straighteners were provided at the extreme upstream end of the flowmetering unit. The straighteners were 8"-long steel tubes with 3/8" O.D. and 1/16" walls. These were brazed into place in the 4" pipe section. Secondary flow and turbulence were further reduced by the pressure damping porous material immediately ahead of the flow straighteners.

The flowmeter unit was arc welded into the 4" pipe; care was taken to insure alignment and to insure that the weld bead did not extend inside the pipe. After initial alignment of the centerline of the flow nozzle with the centerline of the 4" pipe (concentricity estimated to be $\pm$.002"), the entire assembly was dowel-pinned to insure correct repositioning if the unit were ever disassembled after calibration had been made.

The flowmeter unit (flowmeter and upstream and downstream piping) was assembled at Creare and calibrated at the Colorado Engineering and Experimental Station, Incorporated, a nonprofit corporation providing flowmetering calibration.

The calibration for the Cox flow nozzle unit is shown in Figure 10. The calibration medium was air between 63°F and 76°F. The calibration is given in terms of the discharge coefficient for the flow nozzle C_D as a function of the Reynolds number R_D. Over the range of calibration from Reynolds numbers of approximately 3×10^4 to 1×10^6, the data scatter around the mean calibration curve with a standard deviation of 0.263%. Calibration standards for the flow nozzle calibration are traceable to the Nation Bureau of Standards.

Flow Control Valving

The bypass valving provided control of the back pressure downstream of the diffuser exit. A very fine control is necessary to control the Mach number to high precision. The valves vary in adjustment from coarse to very fine.

Test Section

The schematic diagram of Figure 11 shows the "sandwich" arrangement of the various pieces of the test section. The "block" pieces go together to define the channel of the inlet passage and the diffuser and are "sandwiched" between a top and bottom cover. This sandwich arrangement provides easy access for making changes in the test geometries; however, it does provide some difficulties in sealing.

To provide adjustment in the width of the diffuser channel (W_1), each of the blocks that go together to provide the flow channel contour are individually adjustable in their distance from the centerline of the flow channel. This is accomplished by positioning screws, permitting accurate positioning and clamping of the various insert blocks. During assembly, gauge blocks are used to accurately adjust the flow channel width.

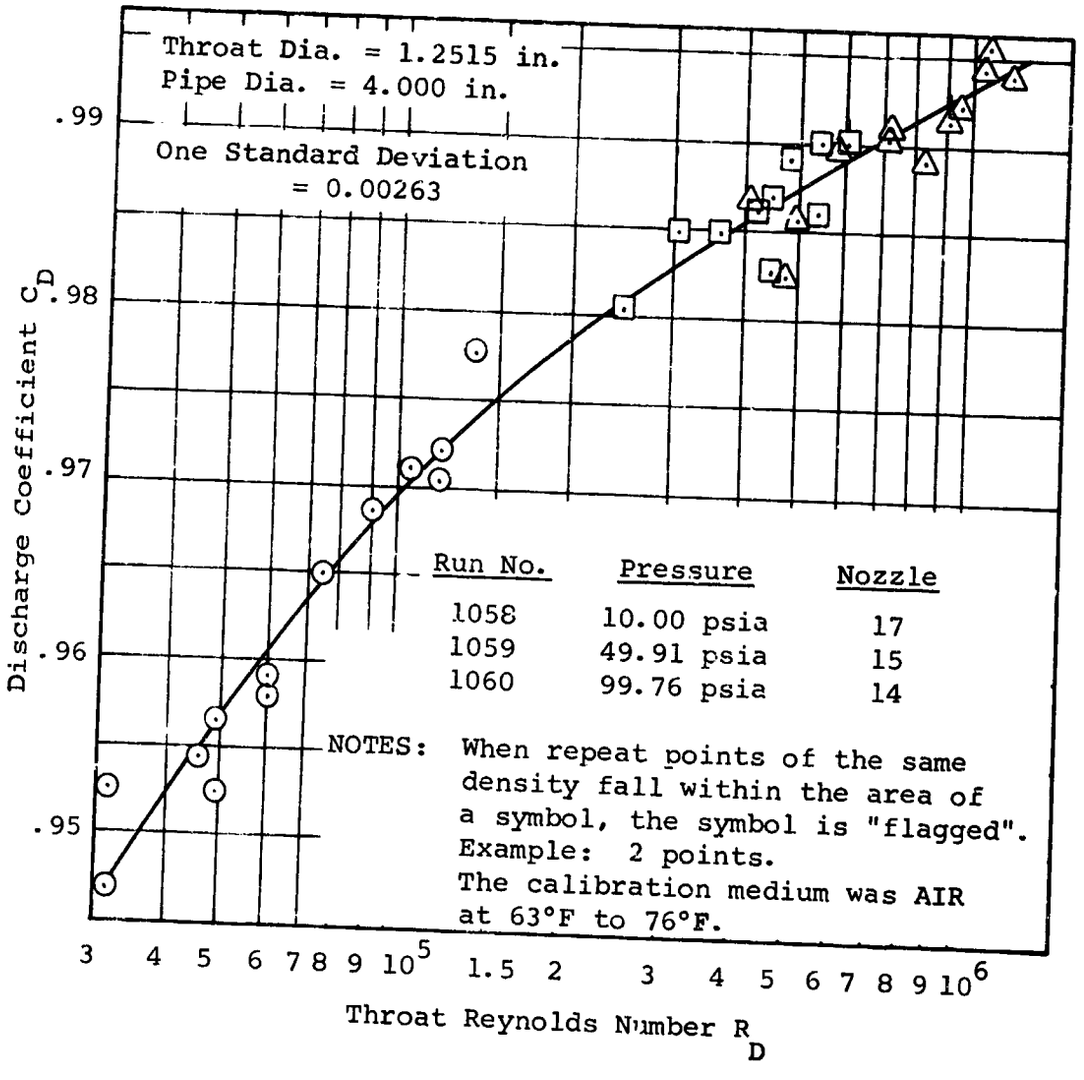

Figure 10. Flowmeter Unit Calibration.

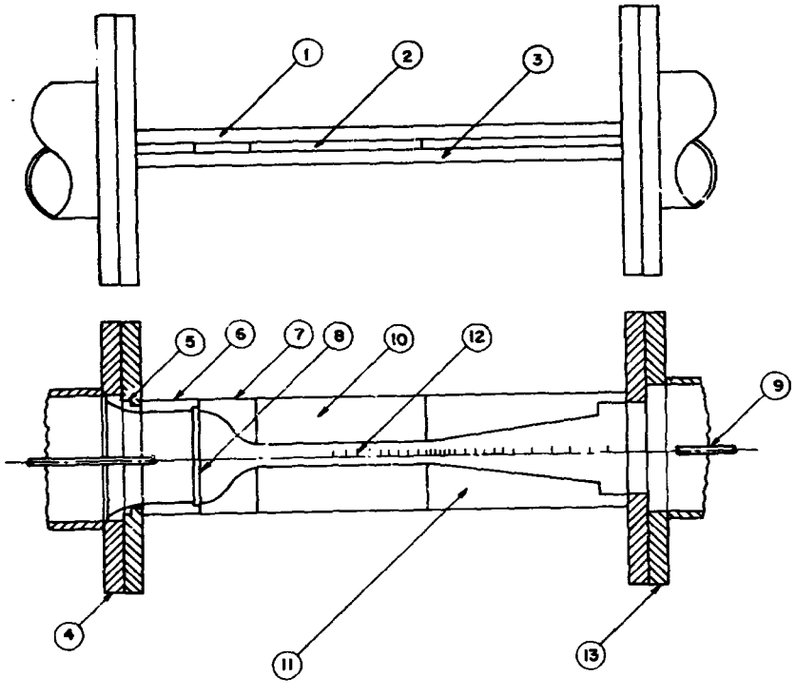

NO.	DESCRIPTION
1	TOP PLATE
2	CHANNEL FORMING BLOCKS
3	BOTTOM PLATE – 3/4" ALUMINUM
4	INLET 8" PIPE
5	INLET DOUBLE CONVERGENCE NOZZLE
6	INLET CHANNEL WALL
7	SINE BLOCKS
8	BOUNDARY LAYER TRIP SLOT
9	STATIC PRESSURE TUBE - 0.050" O. D.
10	CHANNEL WALLS FOR BOUNDARY LAYER GROWTH
11	DIFFUSER BLOCKS
12	STATIC PRESSURE TAPS IN BOTTOM PLATE
13	EXIT 8" PIPE

Figure 11. Diffuser Test Section.

The entire sandwich arrangement is bolted together along the edges. Clearance holes for the bolts in the insert blocks are drilled .098" oversize to allow for variable positioning of the test section blocks. This arrangement provides sufficient flexibility to allow accurate alignment in conjunction with the gauge blocks.

The test section sandwich assembly is bolted to upstream and downstream flange sections. The entire test section assembly then bolts directly to the flanges on the 8" diameter upstream and downstream flow piping shown in Figure 11. The flange bolted to the upstream end of the sandwich assembly has an inlet nozzle for the flow from the 8" diameter upstream pipe. The width of the inlet channel blocks can be adjusted to maintain a flush, continuous surface from the contour of the inlet nozzle to the flow passage in the test assembly.

The sketch of Figure 11 and photographs of Figure 12 show the test section sandwich assembly (minus the top cover) and describe the shape of the flow channel from the 8" upstream pipe diameter through the test section to the 8" diameter downstream plenum. The depth b of the diffuser geometry is governed by the thickness of the insert blocks. All surfaces of the test section pieces were surface-ground (to a surface finish of approximately 10 microinches RMS) to maintain a constant thickness throughout the flow channel.

The insert blocks occur in the following order, from upstream to the exit of the test section:

(1) The inlet nozzle, indicated as (5) in Figure 11, converges the flow from the 8" upstream pipe plenum to the rectangular flow channel formed in the test section.

(2) The flow channel "width" in the upstream section of the test section is formed by the inlet channel blocks (6). These blocks are 3" long. A 1/8" wide by 0.050" deep boundary layer trip slot is machined in the surfaces of the top and bottom covers and the downstream end of the inlet channel blocks (6). The boundary layer trip slot completely encloses the flow channel and induces transition from a laminar to a turbulent boundary layer in those cases where transition from laminar to turbulent boundary layer

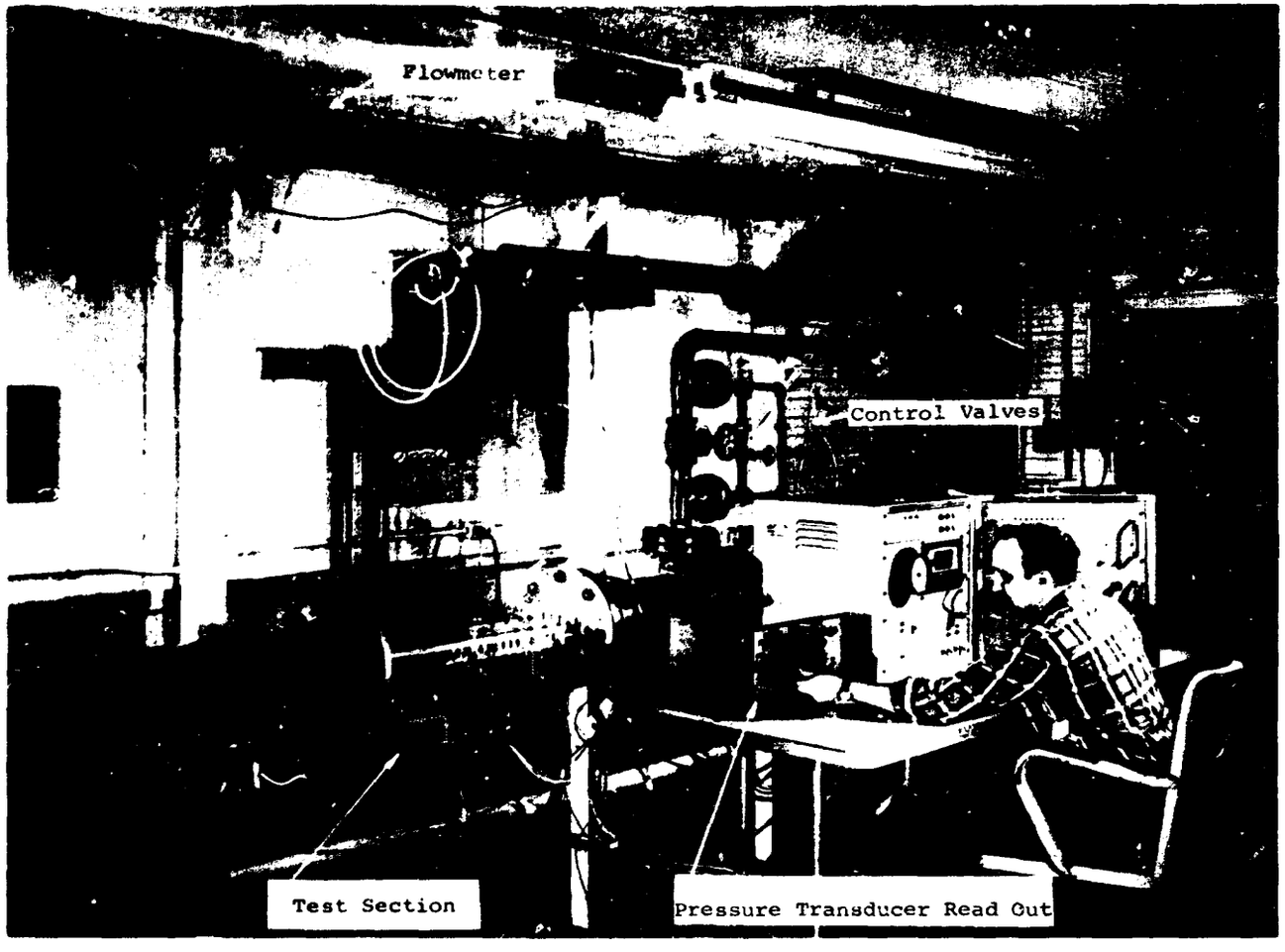

Figure 12a. Test Section.

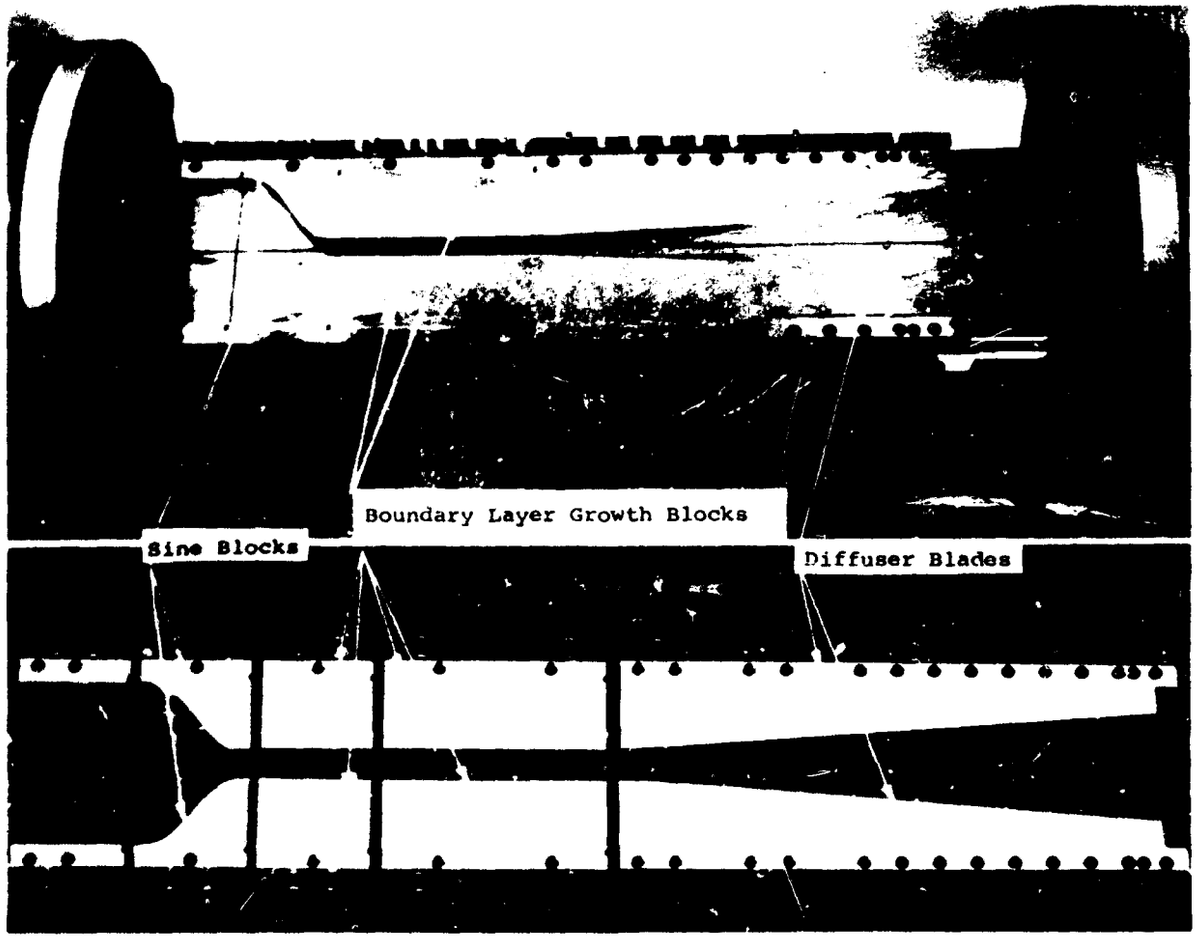

Figure 12b. Test Section.

flow would not have otherwise occurred by this streamwise location. The trip slot was designed using the roughness element criteria described in Schlichting (1964).

(3) The flow channel is next contracted in width by the sine blocks (7). These sine blocks are contoured according to the equation

$$y = \frac{x}{\ell} h - \frac{h}{2\pi} \sin\left(\frac{2\pi x}{\ell}\right) \qquad (8)$$

The terms in the equation are identified in Figure 13.

This equation has its first and second derivatives at the upstream and downstream ends of the sine blocks equal to zero. This provides an impulse-free acceleration of the flow through the sine block contraction. The same equation has been used for all three aspect ratios.

The sine blocks were contour-milled to within .010" of the final shape. The blocks were finished by hand. The final hand-finishing and polishing was carefully done to insure that the edges of the nozzles were not rounded and that the profile was not skewed from side to side.

(4) The next set of blocks (10) are channel wall inlet blocks, providing boundary layer growth ahead of the diffuser. These blocks are of various lengths to provide the required range of throat blockage.

(5) The flow then enters the diffuser blocks (11). The actual divergence of the diffuser starts 1/2" downstream of the junction between the inlet and diffuser blocks. Any deleterious effects on the flow of the joint between the diffuser and inlet blocks tend to be smoothed out before the flow enters the diffuser. During the polishing of the diffuser blocks, a considerable effort was made to keep the divergence corner of the diffuser blocks sharp.

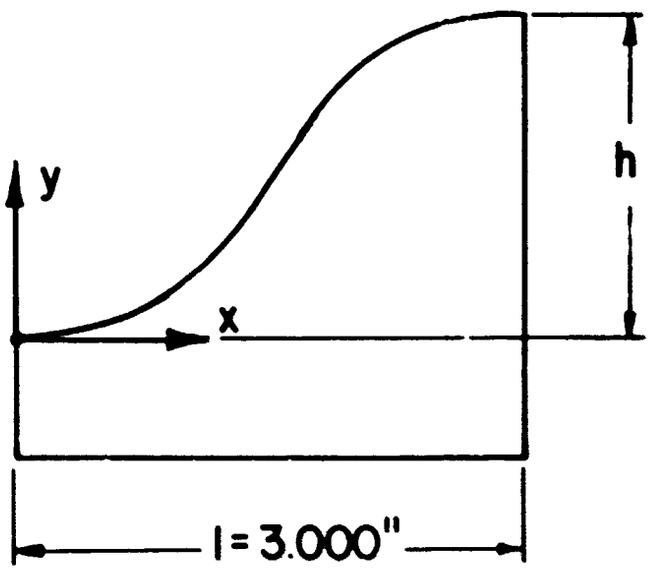

$$y = \frac{x}{l} h - \frac{h}{2\pi} \sin\left(\frac{2\pi x}{l}\right)$$

Figure 13. Sine Block Channel Contour.

At the exit of the diffuser (11), the test section channel enlarges to the same width that it has at the upstream end of the test assembly, i.e., the inlet channel formed by the blocks (6).

In those cases where the diffuser blocks must be moved upstream (because of the use of short inlet channel blocks for boundary layer growth), a filler block is used between the end of the diffuser block and the downstream flange. The filler block is shown in Figure 12. Behind this length adjustment block is a 1" thick aluminum flange that abuts the flange attached to the downstream plenum (13). The flow passage through this flange is somewhat larger than the slot formed by the exit channel in the test assembly; an exit expansion of about 2% is encountered before the flow discharges into the 8"-diameter plenum.

The flow passage downstream of the "exit" of the channel diffuser passage is thus a series of small expansions and then a large expansion to the downstream plenum. Note that the geometry of these expansions changes with the length of inlet and diffuser blocks used. Thus, the downstream geometry is slightly altered from test to test where blockage or diffuser length has been changed.

The setup of the sandwich assembly and the adjustment of the test section blocks are done very carefully with gauge blocks to insure that the flow boundaries of the channel are continuous and that the wall sections of the inlet channel are parallel. Two gauge blocks are used. One is a 5" gauge block for gauging the constant-area section ahead of the sine blocks and downstream of the diffuser. The other is used to gauge the throat width W_1. The gauge block slides between the walls of the constant-area section, giving a uniform "feel" fit in setting up the test section. The repeatability of alignment from setup to setup has been measured and is repeatable to within 0.0005". The accurate repeatability of geometries from setup to setup is important to the overall consistency and accuracy in the test performance data.

Sealing Arrangement

The sealing of the test section "sandwich" assembly is designed around the use of running O-ring seals. Because of the complexity of the assembly, some "butt" sealing points are required. A combination of running O-rings, butt O-rings, and sealing between insert blocks using RTV (room temperature vulcanizing rubber) sealant has been used. Separate in-house tests were run to determine the tolerances that must be used on butt O-ring seals to maintain effective sealing. Good seals require good dimensional control of the length of the O-rings and the use of a slight amount of vacuum grease to allow O-ring movement.

There are a number of critical sealing areas in the test assembly. Particular care has to be taken when O-ring seals are made around corners. In these cases, extra material (epoxy resin) had been added and carefully shaped to prevent the O-rings from withdrawing into the slots at the corners. In particular, the front and bottom covers required considerable handworking to establish the geometric configuration of the O-ring grooves in the initial setup. However, once initial precautions to insure good seals were made, these setups could be easily and quickly repeated. The sealing of the test section in all cases was reliable and excellent.

Pressure Tap Locations

The bottom cover plate has a series of static pressure taps located in the flow direction along the centerline of the flow passage. These are indicated in Figure 11. The pressure tap holes are 0.013" in diameter. The axial location of these holes is given in Table II.

Traversing Pressure Tube Unit

The schematic diagram of Figure 9 indicates a traversing pressure tube indicating unit attached to the test section. This is a 0.050" O.D. traverse tube containing a static pressure hole which can be moved axially down the centerline of the test section flow passage to measure static pressure.

TABLE II. STATIC PRESSURE TAP LOCATIONS

Tap Number	Location Measured From Boundary Layer Trip Slot (in.)
1	.50
2	1.00
3	1.50
4	2.00
5	2.50
6	3.00
7	3.50
8	4.00
9	4.50
10	5.00
11	5.50
12	6.00
13	6.50
14	7.00
15	7.50
16	8.00
17	9.00
18	9.50
19	10.00
20	10.50
21	11.00
22	11.50
23	12.00
24	12.50
25	12.65
26	12.80
27	12.95
28	13.10
29	13.25
30	13.50
31	13.75
32	14.00
33	14.25
34	14.50

TABLE II - Continued

Tap Number	Location Measured From Boundary Layer Trip Slot (in.)
35	15.00
36	15.50
37	16.00
38	16.50
39	17.50
40	18.50
41	19.50
42	20.50
43	21.50
44	22.50
45	23.50
Pressure Transducer	6.50

The 0.050" O.D. tube is attached to 7/32" O.D. support tubing located in the upstream and downstream plenums. The 0.0135"-diameter static pressure hole is drilled through one side of the tubing. The traversing length does not allow the 7/32" tubing to enter the test section.

The 7/32" tubing is mounted in brass bushings aligned by thin spiders in the 8"-diameter upstream and downstream plenum pipe. The tube exits through bushings shown on the scale drawing of the test loop in Figure 9. Sealing between the test rig and traverse tube is made by O-rings placed where the 7/32" tube passes out of the closed loop. The 0.050" tube passes through the 7/32" tube, and a pneumatic line is attached between the tube and pressure transducers.

Steel cables attached to the ends of the traverse tubing outside of the flow loop pass-over pulley connections and are attached to 60-pound weights. The 60-pound tensile force on the static tube results in a vertical static deflection of approximately 0.0018". The static deflection is small enough that the probe is assumed to lie in the center of the throat passage.

Vibration of the tubing in the test section during flow conditions was never measured directly. However, indirect measurements of the effect of any tube vibration on pressure measurements were made during initial testing by varying the tension on the tube between 0 and 60 pounds. The static pressure in the throat of the diffuser was measured as the tension was changed; no change in the pressure indication was observed. Either the tube was not vibrating significantly or vibration does not influence the static pressure measurement. Some tests were run without the static pressure probe to compare the static wall tap pressure readings with and without the presence of the traverse pressure tube. It was concluded that the traverse pressure tube is not affected by tube vibration, and it correctly measures the static pressure throughout the test section.

The traverse tube is manipulated by an actuator and control unit. The traverse motion of the probe can be controlled up to 10" with a position accuracy of .001" in the traverse mode. The control unit (consisting of a potentiometer and associated servo drive) can be manually set to locate and measure the position of the traverse tube.

Some problems were encountered throughout the testing program in maintaining the traversing mechanism in smooth and reliable operation. The traversing unit tends to overshoot a location and has considerable backlash when changing direction of motion. By traversing in one direction only and by taking great care in setting the axial location, a position accuracy to within ±.001" can be maintained.

A second traversing probe configuration was used during some of the preliminary testing. This configuration consists of a second tube attached to the traverse tube to provide a total pressure probe. The configuration is detailed in Figure 14.

3.2 INSTRUMENTATION

Various instrumentation has been used to obtain the necessary data to evaluate diffuser performance. Other instrumentation was used throughout the testing program to check and control conditions under which the data were taken. This section discusses the specifications, characteristics, and experimental uncertainty of each of the instruments used.

All instrument accuracies will be quoted at 20:1 odds; see Kline and McClintock (1953).

Temperature Measurements

All temperature measurements were made with insertion, bulb type thermometers.

The upstream stagnation temperature was measured by a remote-reading insertion bulb thermometer located in the 8"-diameter plenum upstream of the test section. The readout gauge was mounted at the instrument console. All temperature measurements were repeatable to ±3°F. This is typical of the type of thermometer used. The thermometers were checked from time to time with a secondary standard mercury thermometer and were always found to be within ±1°F of the correct temperature.

Pressure Measurements

Two types of pressure transducers were used in the actual recording of performance data. Additional transducers were used in the evaluation and/or calibration of the pressure readout equipment.

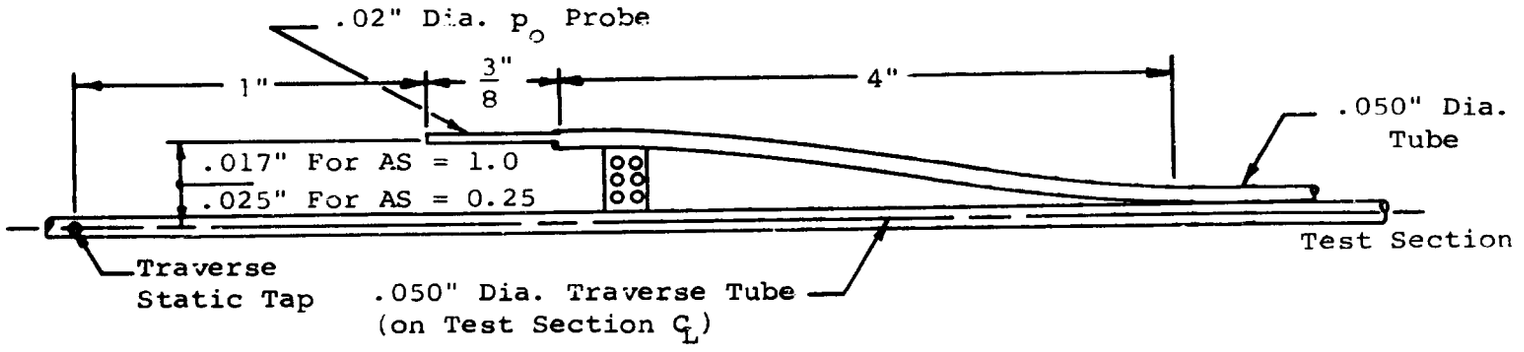

Figure 14. Traverse Stagnation Pressure Probe.

The types of pressure transducers used are:

(1) Mercury barometer -- this barometer was used to record atmospheric pressure data as a reference for base data on diffuser performance and as a reference for calibration purposes.

(2) Differential strain gauge transducers -- a set of three strain gauge transducers was the principal pressure measuring instrument.

(3) Piezoelectric pressure transducer -- this transducer was used to measure pressure fluctuation levels throughout the test section.

(4) 30" to 50" vertical manometers, three manometers containing distilled water, kerosene (specific gravity = .7909 at 50°F), and mercury respectively. Each of the manometers has an inside bore of 0.22".

(5) Two 3" pressure gauges, range 0 to 100 psig -- these gauges were used only for reference and were not used for any final data recording.

(6) Miscellaneous pressure gauges and regulators were used to maintain proper operating pressure ratios across the air supply compressors and to keep the closed-loop pressure level at a constant value.

Barometer

The barometer has a vernier scale and should measure the barometric pressure to an accuracy of $\pm$.010". This instrument has been checked against an equivalent barometer at the Physics Department of Dartmouth College in Hanover, New Hampshire. The barometer reads the same pressure when a suitable correction for altitude differences is made.

Pressure Transducer

The pressure transducer is a high-response transducer for measuring pressure level fluctuations. The specifications

and response information for this transducer are shown in Figure 15. The transducer was used for measuring pressure level fluctuations in the upstream 8"-diameter plenum ahead of the test section, near the throat of the diffuser geometry in the test section, and in the 8"-diameter downstream plenum. The exact location of the hole in the top cover of the test section in which the transducer was located at the diffuser throat can be found from Table II. When the transducer was not used in the test section, a brass plug was inserted into the transducer hole. The depression on the inside of the top cover was filled with epoxy resin and hand-worked until smooth and flat.

The following instrumentation was used with the transducer: a charge amplifier, an oscilloscope, and a camera for recording data.

The strain gauge transducers are part of a transducer recording system used to scan and read pressures throughout the test section. Figure 16 is a schematic diagram of the pressure measuring system showing the electrical and pneumatic connections.

The readings of the strain gauge transducers were the only data needed to evaluate pressure recovery performance with the exception of the measurement of stagnation temperature and atmospheric pressure.

The specifications for each of the strain gauge transducers are:

A. Differential Pressure Diaphragm Actuated Strain Gauge Pressure Transducers

1) Low Range ± 2.5 psid
0.01%/° F thermal shift of sensitivity
0.01%/° F thermal shift in transducer zero (percent of full scale)
0.5% nonlinearity and hysteresis (percent of full scale)
excitation, 10 volts
input resistance, 370.9 ohms (DC)
output resistance, 355.2 ohms (DC)

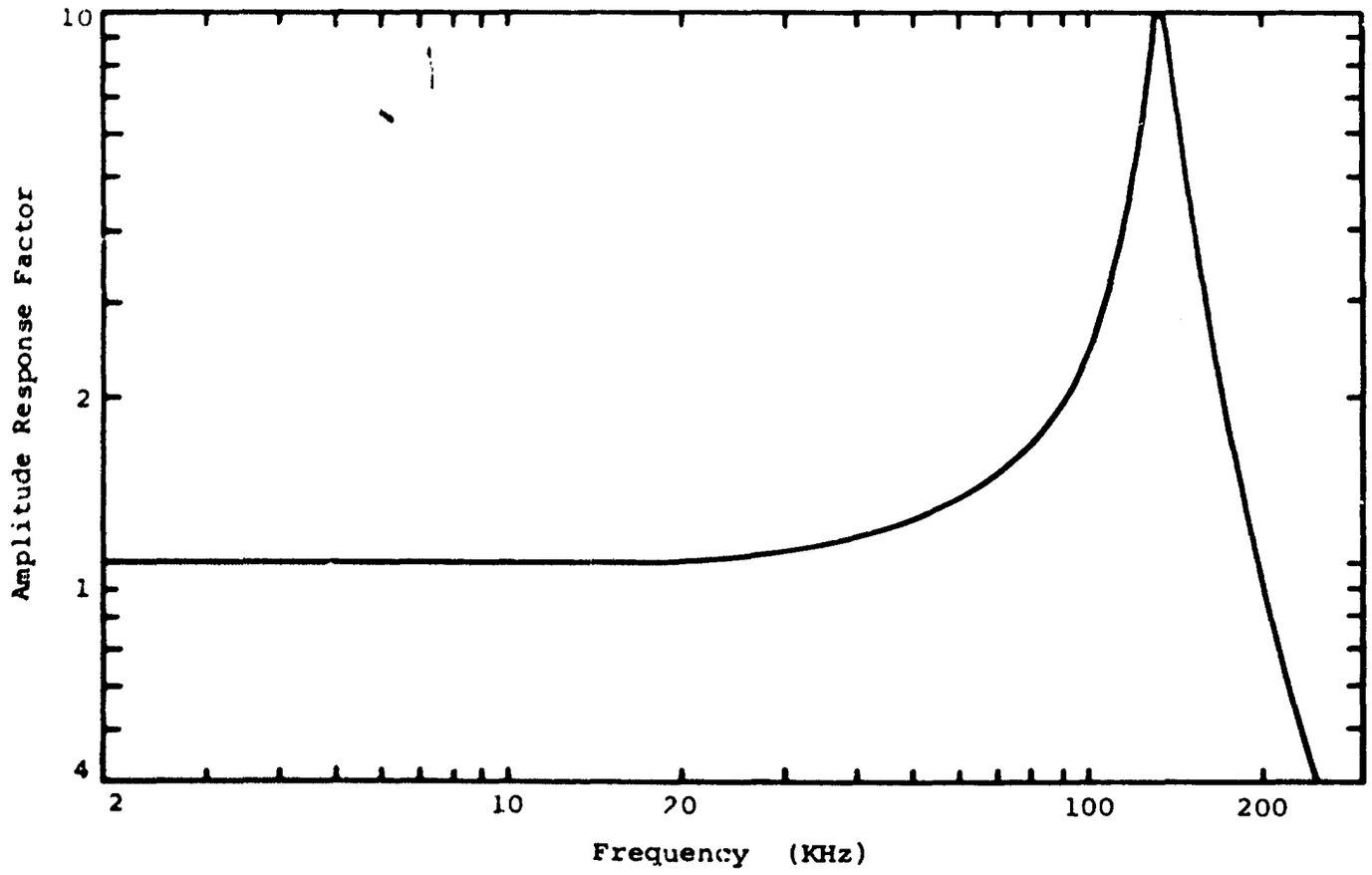

Figure 15. Pressure Transducer Frequency Response.

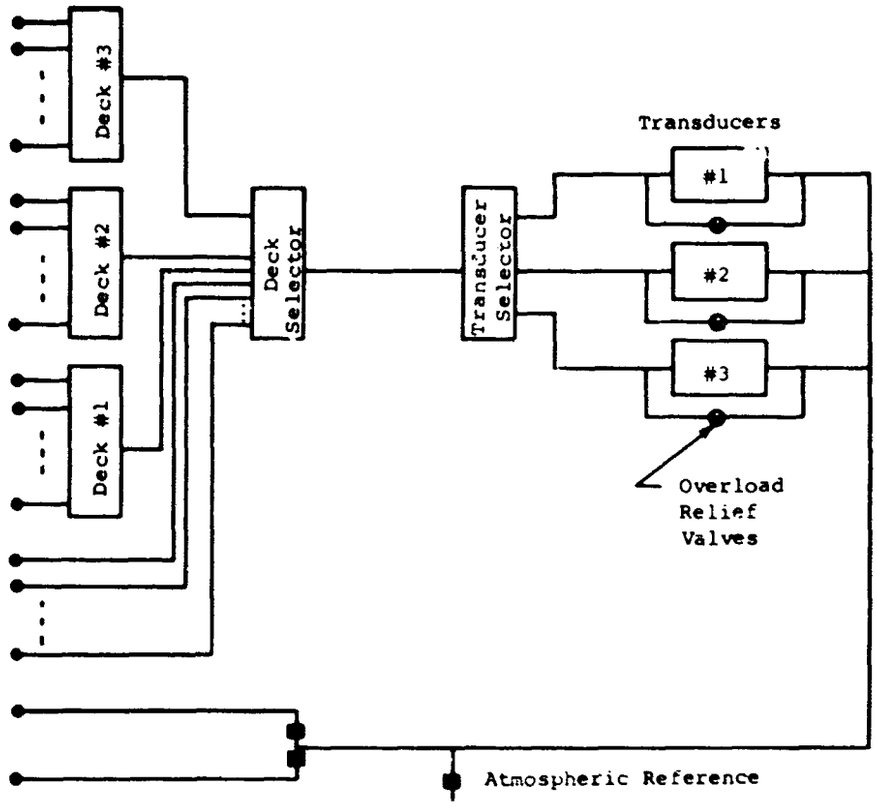

PNEUMATIC DIAGRAM

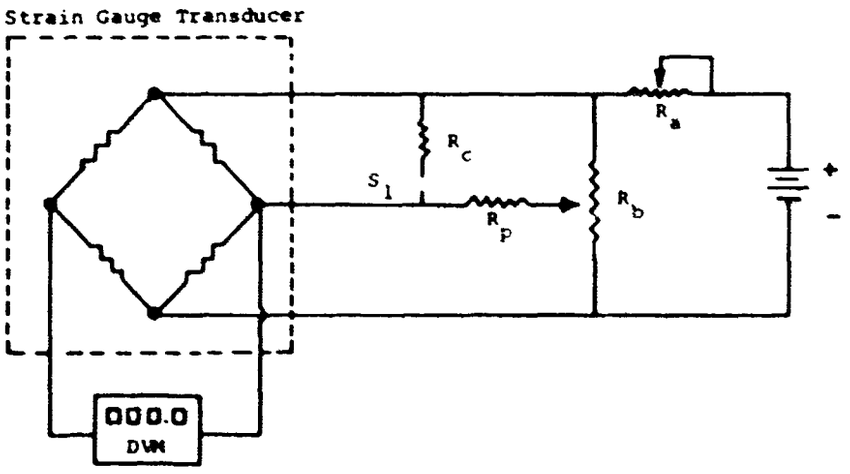

ELECTRICAL DIAGRAM

Figure 16. Electrical and Pneumatic Circuits for Pressure Measuring Instrumentation.

calibration factor, 1.754 mv/volt psi
calibration resistor, 21K ± 1%

2) Medium Range ±25 psid
same nominal ratings as (1) above
input resistance, 355.1 ohms (DC)
output resistance, 339.3 ohms (DC)
calibration factor, 0.1897 mv/volt psi
calibration resistor, 20K ±1%

3) High Range 0 to 100 psid
0.01%/°F thermal shift of sensitivity and of zero (percent of full scale)
5,000 psia maximum line pressure
1% nonlinearity and hysteresis (percent of full scale)
excitation, 5 volts
input resistance, 246 ohms (DC)
output resistance, 345 ohms (DC)
calibration factor, mv/volt psi
calibration resistor, 10K ±1%

The specifications for the remaining elements of the transducer system are:

B. Other Elements of the Transducer System

1) Digital Voltmeter ±100 mv DC with diode reference (zero mechanism)
0.05% linearity, 60°-115°F ambient
0.1% accuracy ± one digit
500K maximum source impedance for rated accuracy
repeatability (estimate) ±.01 mv
uncertainty in setting the zero: +0.03 mv, i.e., stable zero at +0.03 mv

2) Power Supply 0-.750A, 12 volts, 0.75 amps, output regulation ±0.05 volts

3) Bypass Relief Valve 5 to 20 psi adj. for low range and 15 to 60 psi, adj., for medium range

4) Scanivalve Wafer Switches, Scanivalve 0-50 psi wafer switches

5) Scanivalve Pneumatic Connectors and related hardware

6) Precision Potentiometers

Low Range

Zero	30K Resistance ±5% Tolerance ±.25% Linearity
Calibrate	100 ohm Resistance ±5% Tolerance ±.50% Linearity

Medium Range

Zero	30K Resistance ±5% Tolerance ±.25% Linearity
Calibrate	100 ohm Resistance ±5% Tolerance ±50% Linearity

High Range

Zero	30K Resistance ±5% Tolerance ±.25% Linearity
Calibrate	1K Resistance ±5% Tolerance ±.25% Linearity

Except for the power supply, the above components were inspected on a regular basis for proper operation and cleaning. The pressure transducers and pneumatic wafer switches were particularly sensitive to corrosion and wear. These were cleaned on a regular, 6-month basis. Near the beginning of the experimental program, the test loop was run open to ambient air. During this time, high humidity conditions produced water condensation in the wind tunnel loop; water collected below the flowmeter nozzle and in the pressure transducer pneumatic line.

Also at this time a water manometer was "blown", thereby permitting water to enter the transducer strain gauges. The transducer system was completely disassembled, cleaned, reassembled, and recalibrated.

3.3 PRESSURE TRANSDUCER SYSTEM CALIBRATION

The complete pressure transducer system (in which the input is the pneumatic signal to the pressure side of transducers and the output is the digital reading of the digital voltmeter) was calibrated a number of times during the experimental program. All pressure recovery performance data depends upon the readings of the pressure transducer system; it was thus essential to insure that the operation of the transducer system was following the assumed calibration.

There were two types of calibration tests. The first consisted of the connection of pressures simultaneously to both ports of the differential strain gauge transducers. This technique determined variations in transducer performance with changes in pressure level. The second set of tests applied a differential pressure to the transducer while one side of the transducer system was kept at a fixed reference level (atmospheric pressure). Calibration points were obtained throughout the pressure transducer system range to determine effects of both nonlinearities and hysteresis.

The equipment used in the calibrations are listed below with their probable uncertainties at 20:1 odds. The vertical manometers and the barometers are considered to be secondary standards.

	Instrument	Uncertainty (20:1 odds)
1)	0-50" Mercury Manometer	±0.075"
2)	0-50" H_2O Manometer	±0.190"
3)	0-50" Kerosene Manometer	±0.050"
4)	Barometer	±0.010"

The calibrations indicated that the pressure measuring system was considerably more accurate than the manufacturing specifications. More accurate standards should be used to adequately define the transducer system's uncertainties. The

uncertainties are interpreted as the probable maximum uncertainty intervals of the pressure measuring system. The uncertainties in the pressure measuring system at 20:1 odds are given in Table III.

TABLE III. PRESSURE MEASURING SYSTEM UNCERTAINTY

Transducer	Range	Uncertainty	Uncertainty as Percent of Full Scale (20:1)
Low Range	0-2.5 psid (0-45 mv) approx.	±.09 mv	±.2%
Medium Range	1-25 psid (2-45 mv) approx.	±.09 mv	±.2%
High Range	2-100 psid (0-45 mv) approx.	±.1 mv	±.22%

The results of the calibrations are shown in Figure 17 for all three transducers. The uncertainty interval from a statistical analysis of the data is shown as a function of the scale reading in millivolts. These curves have been used for the uncertainty calculations.

3.4 PNEUMATIC CONNECTIONS AND PRESSURE MEASURING LOCATIONS

The locations of the pressure taps on the bottom plate of the diffuser test section are given in Table II. The static pressure tap data were not used in evaluating recovery performance but were used to provide a monitor on operation and to obtain detailed pressure gradient information in addition to the diffuser performance pressure recovery.

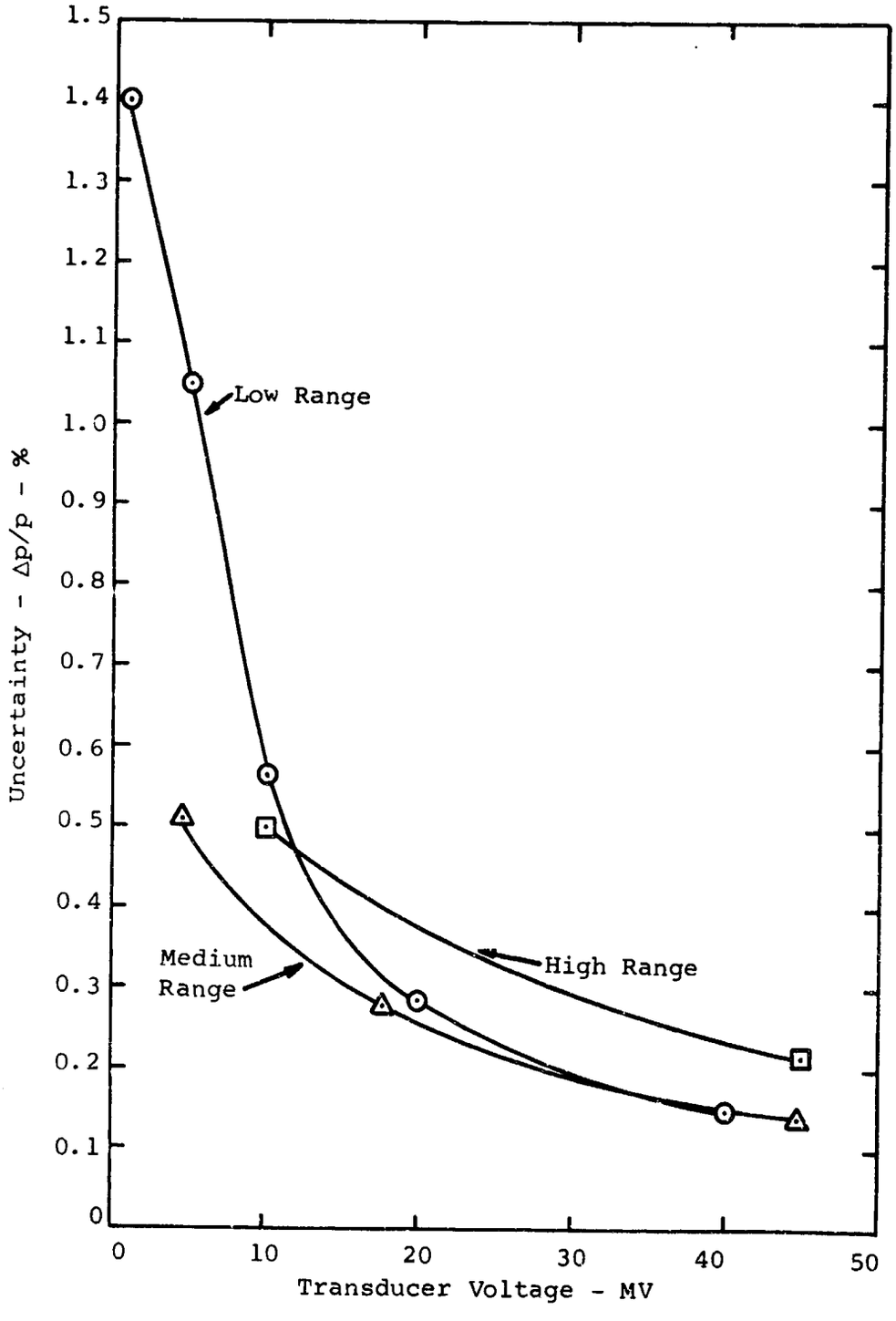

Figure 17. Pressure Transducer System Calibration.

For measurement of pressure recovery, the following pressure data were required: the flowmeter differential pressure, the upstream stagnation pressure measured in the 8"-diameter upstream plenum, the exit plenum pressure measured downstream of the diffuser test section in the 8"-diameter downstream plenum, and the throat static pressure measured with the traverse pressure probe.

All pressure leads were made with nylon tubing from the pressure tap locations to the pressure transducer equipment and were scanned using Scanivalve pressure selection switches. Prior to every run, the entire pressure system was checked for leaks at the elevated upstream stagnation pressure (usually 60 psig); all connections were thus operating against external atmospheric pressure, and any differential pressure indicating a leak could be detected on the low range transducer.

3.5 EXPERIMENTAL TECHNIQUE

The experimental techniques and data reduction procedures required to obtain diffuser performance are now described.

During a test, the operator measured pressure recovery performance for a fixed-geometry diffuser at a prescribed throat inlet Mach number using one of three approach inlet blocks (to produce the desired value of inlet throat blockage). The operator recorded upstream stagnation pressure and temperature, mass flow, barometric pressure, and temperature data, as well as static pressure and total pressure measurements in the test section. These measurements are sufficient to define the throat inlet Mach number M_t, blockage B, Reynolds number R_D, and pressure recovery C_p.

Throat Inlet Blockage

Throat inlet blockage is calculated using the measured mass flow rate and the calculated theoretical, one-dimensional mass flow rate as determined from the diffuser inlet area $A_{geometrical}$, throat stagnation temperature T_{o_t}, throat static pressure p_t, and throat stagnation pressure p_{o_t}.

The mass flow rate passing through the diffuser is measured by the flowmeter unit located upstream of the diffuser test section. Extreme care was maintained to insure that there was no flow leakage between the flow measuring nozzle and the throat of the diffuser; even a small amount of leakage from the test loop between the flowmetering nozzle and the test section at the throat will produce serious errors in the calculation of throat inlet blockage.

The theoretical mass flow rate is calculated as follows (for a one-dimensional flow through the diffuser throat):

$$\text{mass flow}_{\text{ideal}} = \sqrt{\frac{k}{R}} \frac{p_{o_t}}{\sqrt{T_{o_t}}} f(M_t)\, A_{\text{flow}} \tag{9}$$

where T_{o_t} = throat centerline stagnation temperature

$$f(M_t) = M_t \left(1 + \frac{k-1}{2} M_t^2\right)^{\frac{-1-k}{2(k-1)}} \tag{10}$$

A_{flow} = one dimensional cross-sectional flow area

R = gas constant

The ratio of the measured mass flow to the above ideal, theoretical, one-dimensional, mass flow is equal to the ratio of the effective throat area to the geometrical throat area:

$$\frac{\text{mass flow}_{\text{measured}}}{\text{mass flow}_{\text{ideal}}} = \frac{\sqrt{\frac{k}{R}} \frac{p_{o_t}}{\sqrt{T_{o_t}}} f(M_t)\, A_{\text{effective}}}{\sqrt{\frac{k}{R}} \frac{p_{o_t}}{\sqrt{T_{o_t}}} f(M_t)\, A_{\text{geometrical}}} =$$

$$\frac{A_{\text{effective}}}{A_{\text{geometrical}}} \tag{11}$$

The throat blockage B, defined from Equation 7, is

$$B = 1 - \frac{\text{mass flow}_{\text{measured}}}{\text{mass flow}_{\text{ideal}}} \tag{12}$$

Throat Inlet Reynolds Number

The throat inlet Reynolds number is defined by

$$R_D = \frac{VD}{\nu} \tag{13}$$

where V = throat, centerline "core" velocity
ν = fluid kinematic viscosity
D = throat hydraulic diameter

The throat centerline "core" velocity is calculated from the measured throat static pressure, stagnation pressure, and stagnation temperature, assuming isentropic flow from the measured upstream stagnation conditions to the measured static pressure level at the throat, i.e., from the inlet Mach number M_t.

$$V = a\, M_t \tag{14}$$

where a = local speed of sound = $\sqrt{kRT_t}$ (15)

$$T_t = T_{o_t}/(1 + \frac{k-1}{2} M_t^2) \tag{16}$$

Inlet Mach Number

The inlet Mach number was calculated from the measured upstream stagnation pressure and measured throat static pressure assuming one-dimensional, variable-area, isentropic flow from the upstream plenum to the diffuser throat in the "core" flow.

$$\frac{P_{o_t}}{P_t} = (1 + \frac{k-1}{2} M_t^2)^{\frac{k}{k-1}} \tag{17}$$

In all cases, the diffuser "throat" location has been defined as the point of minimum pressure in the region of the geometric throat as determined from the traverse pressure probe measurements. This holds when the ratio of indicated throat static pressure to the upstream stagnation pressure is equal to or greater than 0.528. Whenever this ratio is less than 0.528, the throat location is assumed to correspond to the axial location where the pressure ratio is 0.528 and supersonic flow is assumed to occur downstream of this throat location. Under these conditions, a shock is assumed to exist in the diffuser. The minimum pressure measured in the diffuser is assumed to be equal to the pressure immediately upstream of the assumed one-dimensional shock. Cases in which a shock exists in the diffuser are called "superchoking" flow. For superchoking flow cases, the pertinent Mach number reported is the Mach number ahead of the shock M_x. Whenever M_t is listed as greater than unity, $M_t = M_x$.

Static Pressure Recovery

The static pressure recovery is calculated using Equation 3.

$$C_p = \frac{p_e/p_{o_t} - F(M_t)}{1 - F(M_t)} \qquad (3)$$

p_t is the measured throat centerline minimum static pressure as determined from the traverse probe measurements. p_{o_t} is the throat stagnation pressure as measured in the upstream plenum chamber. p_e, the exit pressure, is measured in the downstream plenum. Note that p_e is not the static pressure in the exit plane of the diffuser. Thus, for most of the data reported, the exit pressure includes a "dump" pressure rise from the diffuser exit area A_2 ($A_2 = bW_2$) to the 8"-diameter downstream pipe plenum area.

The exit dump pressure is analogous to the collector pressure in centrifugal compressor diffusers where the diffuser passages "dump" to a collector scroll or plenum.

Static Pressure Distribution Measurements

Static pressure distribution measurements were made using the traverse tube; they include measurements from the most upstream portion of the test section diffuser geometry through the inlet passage and partially into the diffuser. Static pressure measurements using wall static pressure taps were measured for most of the tests. Interpolated values of diffuser exit pressure at the exit plane of the diffuser geometry can be found from this data from which values of the diffuser pressure recovery coefficient based on diffuser exit plane pressure may be calculated. The area ratios that have been used in these studies, in general, are large, particularly around peak recovery, and the exit plane pressure is usually close to the downstream plenum pressure. A comparison of static pressure recovery coefficients using both pressures shows less than a 3% difference (less than 1.5% near peak recovery) for the geometries studied.

Test Procedure

In measuring pressure recovery for a given divergence angle diffuser, the largest length-to-width ratio L/W_1 to be used with that divergence angle and aspect ratio was tested first. For later tests, the same diffuser blocks were cut to shorter lengths to produce the required L/W_1 values.

Standard operator procedure is to install the diffuser blocks and the inlet blocks to produce the required blockage. After sealing the test section, the operator pressurizes the entire test loop to stagnation pressure (either 60 psia or 20 psia) and checks for leak tightness of the entire loop between the flowmetering valve and the downstream exit plenum.

The operator measures pressure recovery and blockage data for each such setup over the subsonic Mach number range at selected throat Mach number values of M_t = 0.2, 0.4, 0.6, 0.8, and 1.0. Several superchoking flow Mach numbers are also observed, and pressure recovery is measured. These usually correspond to nominal Mach numbers ahead of the shock in the diffuser M_x = 1.1, 1.2, and 1.35.

When 60 psia and 20 psia data were to be obtained for the same diffuser geometry, the test section was not disassembled between data runs for each stagnation pressure.

For each run, throat Mach number M_t is set by adjusting the downstream control valves to supply the appropriate diffuser back pressure and throat Mach number. The traverse static pressure probe is traversed in the vicinity of the diffuser throat to locate the point of minimum pressure. In the case of the supercritical Mach number runs, the traverse static pressure probe is moved into the diverging passage to locate the minimum pressure prior to the pressure rise through the shock in the diffuser. Adjustments of the traverse tube and downstream control valving are continued until the required nominal throat Mach number is achieved. The operator records the position of the minimum throat pressure with respect to the geometric throat location.

Usually, all other static pressure measurements in the diffuser and inlet flow channel are made with the wall static pressure taps. For some studies, however, the static traverse tube was used to measure pressure distributions in the inlet and diffuser portions of the test section.

In most cases, all diffuser angle blocks for a given inlet length at the prescribed aspect ratio were run before inlet length blocks were changed.

3.6 DATA PROCESSING

A very large amount of data was accumulated in the course of these studies and it was necessary to establish a routine procedure for processing, checking, and analyzing the data.

A high-speed digital computer was used to reduce the data from the "raw" form taken by the test operator to the final reduced form which could be used for data plotting and analysis. The steps involved in this chain of data processing are the following:

(1) Record "raw" data by test operator at nominal Mach numbers M_t = 0.2, 0.4, 0.6, 0.8, 1.0, 1.1, 1.2, and 1.35.

(2) A punched paper tape is made for each run of data as input to the digital computer. The punched tape corresponds to 8 level ASCII code.

(3) The data tape is input to the computer. The computer reduces the data as prescribed by a data reduction program. The digital computer prints out the calculated performance in a standard format.

The data reduction program performs the complete calculation of the output parameters required for each run. The printed output from the digital computer provides a summary page giving:

(1) actual mass flow rate
(2) theoretical mass flow rate
(3) run Mach number
(4) run blockage factor
(5) run pressure recovery
(6) run Reynolds number

An example of the computer printout is given in Figure 18.

Data Reduction Program

The data reduction program reduces the experimental data to yield the required diffuser performance information. Table IV is the computer printout of the data reduction program. Explanatory comments are interspersed throughout this program to make the program completely self-explanatory and self-contained. The data reduction computer program is written in BASIC computer program language. This program:

(1) calculates the actual mass flow rate iteratively from a linear interpolation of the discharge coefficient of the flowmeter versus the Reynolds number through the flowmeter using the calibration presented in Figure 10.

(2) calculates the theoretical mass flow rate from the geometric flow area minus the cross-sectional area of the static pressure traverse tube.

AVIATION MATERIEL LABORATORIES — FEBRUARY 17 1969
DIFFUSER TESTS — PAGE 1
ROUNDED CORNER EXPERIMENTS

SUMMARY PAGE

I. DATA REDUCTION CONSTANTS
1) PRESSURE TRANSDUCERS: 5.70125 E-2 .527148 2.05381
2) TEMPERATURE TRANSDUCERS: !
3) BAROMETRIC PRESSURE = 14.3946 PSI - (X .4913)

II. GEOMETRY
1) DIFFUSER DOUBLE ANGLE = 10
2) L/W RATIO = 15
3) ASPECT RATIO = 1
4) BLOCKAGE LENGTH = 0
5) AREA RATIO = 3.624

III. SUMMARY TABLE OF REDUCED DATA

RUN NO.S		$\dot{M}_A$	$\dot{M}_T$	MACH NO.	BLOCK	C-P	REY NO
101510	20060	.174	.177	.2	.022	.836	81000
101510	40060	.325	.33	.398	.015	.848	532000
101510	60060	.432	.436	.583	.011	.854	725000
101510	80060	.502	.508	.797	.011	.859	864000
101510	100060	.52	.526	1.011	.013	.869	967000
101510	130060	.52	.526	1.365	.012	.855	983000

Figure 18. Sample - Data Reduction Summary Page.

TABLE IV. COMPUTER DATA REDUCTION PROGRAM

```
50  THE SPECIFIC DETAILS OF THE DATA REDUCTION PROGRAM
60  ARE EXPLAINED IN COMMENTS LIKE THIS WHICH ARE
70  PLACED AT PERTINENT PLACES IN THE PROGRAM. THESE
80  COMMENTS ARE NOT ACTUALLY PART OF THE PROGRAM BUT ARE
90  FOR CLARIFICATION OF THE DETAILS.
99  LINE 100 DEFINES A ROUND OFF FUNCTION FOR THE OUTPUT PRINTING
100DEFFNA(X)=INT(1000*X+.5)/1000
110DIMR(23),C(23),P(40),X(40),S(50),Y(50)
120 AFTER THE ABOVE DIMENSIONS ARE DEFINED, THE FLOWMETER
121 CALIBRATION DATA IS READ AND STORED AS REY.NO. VS C-D.
130FORI=1TO22
140READR(I),C(I)
150NEXTI
240DATA3E4,.9458,4E4,.9521,5E4,.957,6E4,.9605,7E4,.9632
245DATA8E4,.9656,9E4,.9676,10E4,.9694,12E4,.9722
250DATA15E4,.9752,20E4,.9786,25E4,.981,30E4,.9828
260DATA40E4,.9853,50E4,.9873,60E4,.9888,70E4,.9905
265DATA80E4,.99135,90E4,.9923,100E4,.9931
270DATA120E4,.9945,150E4,.9963
450 THE K(I) BELOW IS THE PRESSURE TRANSDUCER DATA. K4 AND K5
451 ARE (UNUSED) THERMISTOR CONSTANTS, R AND K ARE GAS CONSTANTS.
452 THE DATA READ THUS FAR HAS NEVER BEEN CHANGED IN THE PROGRAM.
460 READ K(1),K(2),K(3),K4,K5,R,K
470DATA.0570125,.527148,2.05381,1.1,53.3,1.4
500 THE PERFORMANCE DATA IS NOW READ. THE VARIABLES ARE:
501 D =DAY OF THE MONTH (1-31)
502 I1= NO. OF RUNS
503 G9 = BAROMETER, CORRECTED FOR TEMPERATURE
504 R8,R9 = RUN NUMBERS
505 L1,P2,P1 = TRANSDUCER INDEX (1-3), P0 AT ORIFICE, P IN PLENUM
506 THESE ARE REFERENCED TO ATMOSPHERE.
507 L2,P0 = TRANSDUCER INDEX, STAGNATION PRES. AT DIFFUSER THROAT
508 REFERENCED TO UPSTREAM PLENUM
509 L3,P3 = TRANSDUCER INDEX, PRESSURE IN DOWNSTREAM PLENUM
510 REFERENCED TO UPSTREAM PLENUM
512 L4,D2 = TRANSDUCER INDEX, DIFFERENTIAL PRESSURE ACROSS NOZZLE
513 T0,T1 = TEMPERATURE IN UPSTREAM PLENUM, TEMPERATURE AT FLOW
514 NOZZLE. NOTE- BOTH ARE IDENTICAL FOR ALL TESTS RUN
515 L5,S(1) = TRANSDUCER INDEX, MINIMUM THROAT PRESSURE REFERENCED
516 TO UPSTREAM PLENUM
517 Y(1) = LOCATION OF MINIMUM PRESSURE (NOT USED OR PRINTED)
600 READ D,I1,G9
610LETG9=G9*.4913
615LETN8=1
619 THE PERFORMANCE IS CALCULATED FROM HERE TO 2490 FOR "I1" RUNS
620FORI4=1TOI1
630 READ R8,R9
```

TABLE IV - Continued

```
660 READ L1,P2,P1,L2,P0,L3,P3,L4,D2
670 READ T0,T1
800 READ L5,S(1),Y(1)
801 THE PRESSURES ARE CONVERTED TO PSI.
810 LET S(1)=K(L5)*S(1)
880 LET P2=K(L1)*P2+G9
890 LET P1=K(L1)*P1+G9
970 LET P0=P1-P0*K(L2)
1030 LET P3=P1-P3*K(L3)
1090 LET D2=D2*K(L4)
1100 THE RUN NUMBERS, R8 AND R9 ARE "DECODED"
1160LETJ1=INT(R8/10000)
1170LETJ2=INT((R8-J1*10000)/100)
1180LETJ3=INT(R8-J1*10000-J2*100)
1190LETJ4=INT(R9/10000)
1200LETJ5=INT((R9-J4*10000)/100)
1210LETJ6=INT(R9-J4*10000-J5*100)
1300 CONSTANTS K0 = K/(1-K) AND U1 = VISCOSITY OF AIR
1340LETK0=K/(1-K)
1350LETU1=(T1/540)↑1.5*738/(T1+198)*1.036E-6
1355 FROM HERE TO 1470 CALCULATES THE ACTUAL MASS FLOW, W1
1360 LET R4=P2*144/(R*T1)
1370 LET R5=1-D2/P2
1380 LET B4=(1.2515/4.026)↑4
1390LETY1=SQR(R5↑(2/K)*K0*(1-R5↑(1/K0))/(1-R5)*(1-B4)/(1-B4*R5↑(2/K)))
1400 LET D2=D2/.03607
1410 LET W1=.0997*Y1*(1.2515)↑2*SQR(R4*D2/(1-B4))
1420 LET R2=4*W1/(3.1415926*1.2515*U1)
1430LETR3=R2
1440 GOSUB2862
1450 LET R3=C*R2
1452GOSUB2862
1454LETR3=C*R2
1456GOSUB2862
1458LETR3=C*R2
1460 LET C8=C
1470LETW1=C8*W1
1500 FROM HERE TO 1720 CALCULATES MACH NO. IN THE "THROAT"
1501 THROAT IS IN QUOTES BECAUSE M7 MAYBE > 1.
1520 LET S(1)=(P1-S(1))/P0
1540 LET M7=1
1590 LETM6=1
1640 LET X7=1
1680 LET M7=S(1)
1710LETM3=1/M7
1720LETM7=SQR(2*(M3↑(1-1/K)-1)/(K-1))
```

TABLE IV - Continued

```
2401 CONVENIENT FORM
2490NEXTI4
2491IFINT(I1/2)=I1/2THEN2494
2492LETH2=49-H3-ABS(N9-N7)
2493GOTO2495
2494LETH2=33-2*(H3+ABS(N7-N9))
2495FORI=1TOH2
2496PRINT
2497NEXTI
2498GOSUB2870
2500FORI=1TO4
2510PRINT
2520NEXTI
2530GOSUB2880
2550PRINT
2560PRINT"                              SUMMARY PAGE"
2570PRINT"                              ------- ----"
2580PRINT
2590PRINT"I. DATA REDUCTION CONSTANTS"
2600PRINT"         1) PRESSURE TRANSDUCERS:"K(1);K(2);K(3)
2610PRINT"         2) TEMPERATURE TRANSDUCERS:"K4,K5
2620PRINT"         3) BAROMETRIC PRESSURE ="G$;"PSI - (X .4913)"
2630PRINT
2640PRINT"II. GEOMETRY"
2650PRINT"         1) DIFFUSER DOUBLE ANGLE ="J1
2660PRINT"         2) L/W RATIO ="J2
2670PRINT"         3) ASPECT RATIO ="J3
2680PRINT"         4) BLOCKAGE LENGTH ="J5
2690PRINT"         5) AREA RATIO ="INT(1000*(2*TAN(J1/114.6)*J2+1)+.5)/100
2700PRINT
2710PRINT"III. SUMMARY TABLE OF REDUCED DATA"
2720PRINT
2730GOSUB2870
2735PRINT"                          .        ."
2740PRINT"   RUN NO.S              M        M      MACH NO.   BLOCK    C-P";
2755PRINT"     REY NO"
2756PRINT"                           A        T"
2760GOSUB2870
2770PRINT
2780FORI=1TOI1
2790PRINTH(I);I(I);G(I);D(I);A(I);B(I);F(I);E(I)
2810PRINT
2820NEXTI
2830FORI=1TO36-2*I1
```

TABLE IV - Continued

```
1725 FROM HERE TO 1860 SETS THE APPLICABLE GEOMETRIC
1726 THROAT AREA AND HYDRAULIC DIAMETER
1730 IF J3=10 THEN 1800
1732 IFJ3=25THEN1750
1734 IFJ3=50THEN1850
1750LETA1=.233*.932-3.14159/4*(.05)↑2
1760LETI8=2*A1/(.233+.932)
1770 LET J3=2.5
1780GOTO1880
1800LETA1=.377506
1810LETI8=2*A1/(.624+.624)
1830GOTO1880
1850LETA1=.279*1.3935-3.141593/4*.0025
1860LETI8=2*A1/(.279+1.3935)
1870 FROM HERE TO 1894 CALCULATES THE ONE DIMENSIONAL
1871 MASS FLOW
1880LETJ9=SQR(32.174*K/(R*T0))
1885 LETJ3=J3/10
1890LETW=J9*P0*M7/((1+(K-1)/2*M7↑2)↑((K+1)/(2*K-2)))*A1
1892IFM7<1THEN1900
1894LETW=.532*P0*A1/SQR(T0)
1899 B = THROAT BLOCKAGE
1900LETB=1-W1/W
1905LETJ=1
1907 C1 = PRESSURE RECOVERY
1910 LET C1=(P3/P0-1/M3)/(1-1/M3)
1920 IF 1/M3>.528 THEN 1945
1925LETJ=2
1930 LET C1=(P3/P0-.528)/.472
1940 FROM HERE TO 2047 CALCULATES REY. NO. AND STORES
1941 THE DESIRED QUANTITIES AFTER FORMING INTERGER VALUES
1945LETA(I4)=FNA(M7)
1950LETB(I4)=FNA(B)
1960LETG(I4)=FNA(W1)
1980LETI5=T0/(1+(K-1)/2*M7↑2)
1990LETU1=(I5/540)↑1.5*738/(I5+198)*1.036E-6
2000LETI6=P0*144/(R*T0*(1+(K-1)/2*M7↑2)↑(1/(K-1)))
2010LETI7=M7*SQR(K*R*32.174*I5)
2020LETH1=I6*I7*I8/(144*U1)
2025LETE(I4)=INT(H1/1000+.5)*1000
2030LETD(I4)=FNA(W)
2040LETF(I4)=FNA(C1)
2044LETH(I4)=R8
2047LETI(I4)=R9
2400 FROM 2491 TO 2895 PRINTS THE OUTPUT IN
```

TABLE IV - Continued

```
2840PRINT
2850NEXTI
2860GOSUB2870
2861GOTO9999
2862 FOR I=1 TO 22
2863 IF R3>R(I) THEN 2866
2864 LET M9=I-1
2865 LET I=22
2866 NEXT I
2867 LET C=C(M9)+(C(M9+1)-C(M9))*(R3-R(M9))/(R(M9+1)-R(M9))
2868 RETURN
2870REM
2871PRINT"-------------------------------------------------------------------"
2874RETURN
2880PRINT"AVIATION MATERIEL LABORATORIES                    FEBRUARY"D$"1969
2890PRINT"DIFFUSER TESTS                                      PAGE"N8
2892PRINT"ROUNDED CORNER EXPERIMENTS"
2895RETURN
3000 FROM HERE TO 9999 IS THE DATA FOR A TYPICAL
3001 RUN. EIGHT LEVEL PAPER TAPES WERE MADE FOR ALL OF
3002 DATA. THESE ARE STORED AT CREARE.
9999END
```

Data Cross-Plotting

Except for the static pressure and traverse data taken through the inlet and diffuser of the test section, all data appears in the data output form shown in Figure 10. This computer output data have been further treated by graphing and cross-plotting in the following manner:

(1) Plots of pressure recovery C_p vs. throat Mach number M_t and throat blockage B vs. throat Mach number M_t are made from the output data. It is at this point that the data are checked to see that it is reasonable and that no obvious experimental errors exist.

(2) Pressure recovery values C_p at Mach number M_t = 0.2, 0.4, 0.6, 0.8, 1.0, and 1.2 are recorded on data tables from the C_p vs. M_t graphs. Blockage B at the same throat Mach numbers are also recorded from the B vs. M_t plots for all data.

(3) Cross-plot curves of pressure recovery C_p vs. throat blockage B are made from the foregoing tabulation of data. From the C_p vs. B curves, C_p values are read off and tabulated for blockage factors B = 0.02, 0.04, 0.06, 0.08, 0.10, and 0.12. This tabulation provides values of pressure recovery C_p as a function of throat blockage B and throat Mach number M_t for a given geometry.

(4) The C_p vs. M_t, B tabulation provides data for cross-plots of pressure recovery C_p vs. length-to-width ratio L/W_1 and pressure recovery C_p vs. double divergence angle 2θ for fixed values of Mach number and for fixed values of constant 2θ and L/W_1 respectively. These C_p vs. L/W_1 and C_p vs. 2θ plots show a series of curves for different values of throat blockage B.

(5) The C_p vs. L/W_1 and C_p vs. 2θ plots for fixed aspect ratio AS, blockage B, and Mach number M_t are used to prepare performance maps showing contours of constant pressure recovery C_p as a function of diffuser geometry. Each of these contour plots thus has fixed values of throat Mach number M_t, throat blockage B, diffuser aspect ratio AS, and throat Reynolds number R_D.

(6) For each diffuser geometry at a given inlet Mach number M_t, a fixed value of ideal pressure recovery C_{p_i} exists. From the tabulated data giving C_p as a function of B and M_t, values of effectiveness $\varepsilon = C_p/C_{p_i}$ are tabulated. From the data, plots of effectiveness ε vs. throat Mach number M_t are made. These ε vs. M_t plots are prepared for fixed diffuser geometry and show curves for values of blockage B = 0.02, 0.04, 0.06, 0.08, 0.10, and 0.12.

(7) All other plots of data such as static pressure distribution curves through the test section, curves of stagnation pressure distribution, etc., have been made directly from the "raw" data.

3.7 EXPERIMENTAL ACCURACY

An important factor in the design of the experiments has been to maintain a low level of experimental uncertainty in the final derived diffuser performance parameters. The derived quantities of interest are the static pressure recovery C_p, throat blockage B, throat Mach number M_t, inlet Reynolds number R_D, and the parameters describing the diffuser geometry -- aspect ratio AS, throat length-to-width ratio L/W_1, and total divergence angle 2θ.

The level of uncertainty must be defined for all of the data accumulated under the present studies. To do this, it is necessary to define the level of uncertainty in each of the

primary quantities that are used to evaluate the derived quantities. It is also necessary to describe the manner in which the uncertainties in the primary measurements determine the final uncertainty in the derived quantities.

Following the analysis of Kline and McClintock (1953), practically all experiments conducted in these studies can be described as "single sample" experiments and analyzed by the techniques presented in their paper.* We will, however, use a statistical analysis of the throat blockage data in order to evaluate an appropriate mean value to be used in cross-plotting, although the level of uncertainty in the blockage data itself is still assumed to be given by analysis appropriate to the single sample type experiment.

Definition of Uncertainty

We assume that we can evaluate and prescribe the level of uncertainty in all of the primary quantities which have been used in the data analysis. This assumes that all fixed errors are known and have been eliminated; the only errors remaining are those due to random errors.

Random errors represent "noise". The source of this "noise" is usually operator error or physical errors due to thermal effects, friction, response time, etc. These errors appear in the final results as scatter in the data. If these errors are truly randomly distributed, a 20-to-1 odds interval (the odds interval represents the experimenter's level of certainty that the uncertainty in the quantity under consideration is as prescribed) is equal to twice the standard deviation 2σ. Kline and McClintock (1953) have shown that this same criterion is applicable when the form of the distribution of the errors is not known.

Let A = a quantity to be calculated from a group of X_i primary quantities that are obtained as measurements. It can be

---

*The reason is that, though there are a number of observations for each type of data, the number of observations is not necessarily "statistically significant". Pearson (1902) showed that in some cases observations by a single observer (even based on samples of 20 or 30 readings) could have a mean value significantly different from the true mean value.

proven rigorously that if the quantity A is linear in each X_i and all the X_i's are independent, the uncertainty in the result A is given precisely by the expression

$$\Delta A = \left[\left(\frac{\partial A}{\partial X_1}\,\Delta X_1\right)^2 + \left(\frac{\partial A}{\partial X_2}\,\Delta X_2\right)^2 + \ldots\right]^{1/2}$$

if the X_i's are normally distributed.

We can normalize the above equation by dividing through by A. We then have

$$\frac{\Delta A}{A} = \left[\left(\frac{X_1}{A}\,\frac{\partial A}{\partial X_1}\,\frac{\Delta X_1}{X_1}\right)^2 + \left(\frac{X_2}{A}\,\frac{\partial A}{\partial X_2}\,\frac{\Delta X_2}{X_2}\right)^2 + \ldots\right]^{1/2} \qquad (18)$$

Kline and McClintock (1953), in investigating distributions other than the normal distribution, concluded that the above expression, Equation 18, gives very reasonable results when other than normal distributions of random errors exist. Kline and McClintock concluded that the inaccuracies due to using Equation 18 for other than a normal distribution are much smaller than the usual inaccuracies that occur in assigning uncertainty values to the primary physical quantities.

Uncertainty in Pressure Recovery

From the definitions of each of the derived quantities, the uncertainty in each quantity can be derived based on the uncertainties in the primary measurements that have been made.

The pressure recovery C_p is defined as

$$C_p = \frac{p_e - p_t}{p_{o_t} - p_t} = \frac{(p_o - p_t) - (p_o - p_e)}{(p_o - p_t) - (p_o - p_{o_t})} = \frac{A-B}{A-C} \qquad (19)$$

where $A = p_o - p_t$

$B = p_o - p_e$

$C = p_o - p_{o_t} = \Delta p_o$

Since $$\frac{A}{C_p}\frac{\partial C_p}{\partial A} = \left(\frac{A-C}{A-B}\right)\left[\left(\frac{1}{A-C}\right) - (A-B)\left(\frac{1}{A-C}\right)^2\right]A \qquad (20)$$

$$\frac{B}{C_p}\frac{\partial C_p}{\partial B} = \left(\frac{A-C}{A-B}\right)\left(\frac{1}{A-C}\right)(-1)\quad B \qquad (21)$$

$$\frac{C}{C_p}\frac{\partial C_p}{\partial C} = \left(\frac{A-C}{A-B}\right)\quad (A-B)\left(\frac{1}{A-C}\right)^2\quad (C) \qquad (22)$$

then

$$\left(\frac{\Delta C_p}{C_p}\right) = \Bigg\{\left[\left(\frac{A}{A-B}\right) - \left(\frac{A}{A-C}\right)\right]^2\left(\frac{\Delta A}{A}\right)^2$$

$$+\left[\left(\frac{B}{A-B}\right)\left(\frac{\Delta B}{B}\right)\right]^2 + \left[\left(\frac{C}{A-C}\right)\left(\frac{\Delta C}{C}\right)\right]^2\Bigg\}^{1/2} \qquad (23)$$

Throat Blockage Uncertainty

The throat blockage B is defined as

$$B = 1 - \frac{m_m}{m_i} = \frac{m_i - m_m}{m_i} \qquad (24)$$

where m_m = mass flow$_{measured}$

m_i = mass flow$_{ideal}$

Since $$\frac{m_i}{B}\frac{\partial B}{\partial m_i} = +m_m\left(\frac{1}{m_i}\right)^2\left(\frac{m_i}{m_i - m_m}\right)m_i \qquad (25)$$

$$\frac{m_m}{B}\frac{\partial B}{\partial m_m} = -\frac{1}{m_i}\left(\frac{m_i}{m_i - m_m}\right)m_m \qquad (26)$$

then $$\frac{\Delta B}{B} = \frac{m_m}{m_i}\frac{1}{B}\left[\left(\frac{\Delta m_m}{m_m}\right)^2 + \left(\frac{\Delta m_i}{m_i}\right)^2\right]^{1/2} \qquad (27)$$

Uncertainty in Ideal Mass Flow Rate

The ideal mass flow rate is defined by the equation

$$m_i = \sqrt{\frac{k}{R}} \frac{p_{o_t} A_t}{\sqrt{T_{o_t}}} \left[\frac{M_t}{\left(1 + \frac{k-1}{2} M_t^2\right)^{\frac{k+1}{2(k-1)}}} \right] \tag{28}$$

where $p_{o_t} = p_o - (p_o - p_{o_t}) = p_o - C$

Thus

$$\frac{\Delta m_i}{m_i} = \left\{ \left[\frac{p_o}{p_o - C} \frac{\Delta p_o}{p_o} \right]^2 + \left[\frac{C}{p_o - C} \frac{\Delta C}{C} \right]^2 + \left[\frac{\Delta A_t}{A_t} \right]^2 \right. \tag{29}$$

$$\left. + \left[\frac{1}{2} \frac{\Delta T}{T} \right]^2 + \left[\frac{(1 - M_t^2)}{\left(1 + \frac{k-1}{2} M_t^2\right)} \left(\frac{\Delta M_t}{M_t} \right) \right]^2 \right\}^{1/2} \tag{30}$$

Uncertainty in Actual Mass Flow Rate

The actual mass flow rate is determined from the flowmeter calibration by the following equation:

$$m_m = C_D \left[\frac{p_{or}}{T} \Delta p_{o_r} \right]^{1/2} \tag{31}$$

where C_D = orifice coefficient

p_{or} = orifice upstream static pressure

T_{or} = orifice upstream temperature

Δp_{or} = pressure drop across orifice

Thus

$$\frac{\Delta m_m}{m_m} = \left[\frac{\Delta C_D}{C_D} \right]^2 + \left[\frac{1}{2} \frac{\Delta p_{or}}{p_{or}} \right]^2 + \left[\frac{1}{2} \frac{\Delta \Delta p_{or}}{\Delta p_{or}} \right]^2 + \left[\frac{1}{2} \frac{\Delta T_{or}}{T_{or}} \right]^2 \Bigg]^{1/2} \tag{32}$$

Uncertainty in Throat Mach Number

The Mach number is calculated from the throat total pressure and the throat static pressure. The uncertainty in Mach number is given by

$$\frac{\Delta M_t}{M_t} = \frac{1}{kM_t^2} \left(\frac{p_{o_t}}{p_t}\right)^{(1 - 1/k)} \frac{\Delta(p_{o_t}/p_t)}{p_{o_t}/p_t} \qquad (33)$$

Uncertainty in Throat Total Pressure to Static Pressure Ratio

The throat total pressure to static pressure ratio can be written

$$\frac{p_{o_t}}{p_t} = \frac{p_o - (p_o - p_{o_t})}{p_o - (p_o - p_t)} = \frac{p_o - C}{p_o - A} \qquad (34)$$

Thus
$$\frac{\Delta(p_{o_t}/p_t)}{p_{o_t}/p_t} = \left\{ \left[\frac{p_o}{p_o - C} - \frac{p_o}{p_o - A}\right]^2 \left(\frac{\Delta p_o}{p_o}\right)^2 + \left[\left(\frac{C}{p_o - C}\right)\left(\frac{\Delta C}{C}\right)\right]^2 + \left[\left(\frac{A}{p_o - A}\right)\left(\frac{\Delta A}{A}\right)\right]^2 \right\}^{1/2} \qquad (35)$$

3.8 EVALUATION OF EXPERIMENTAL UNCERTAINTY FOR TYPICAL CASES

Using the equations derived in the preceding section, the uncertainty in blockage and in pressure recovery coefficient has been evaluated using the best estimates of the uncertainty in the primary quantities. Most of these uncertainty estimates are based upon the calibration data discussed in Section 3.3.

Table V provides a listing of the uncertainty in C_p, B, and M_t for selected values of aspect ratio, inlet length, and Mach number.

3.9 SPECIAL TREATMENT OF BLOCKAGE DATA

Because the pressure recovery coefficient C_p is a strong function of throat inlet blockage, it is extremely important that the magnitude of the throat inlet blockage for each test be known as accurately as possible. As can be seen from

TABLE V. UNCERTAINTY IN PRESSURE RECOVERY AND THROAT BLOCKAGE FOR REPRESENTATIVE RUNS

Aspect Ratio AS	Stagnation Pressure p_o (psia)	2θ	L/W_1	Inlet Length (in)	Mach Number M_t	Pressure Recovery C_p	$\Delta C_p/C_p$ (%)	Throat Blockage B	$\Delta B/B$ (%)
5.0	60	6°	7	0	.4	.60	.93	.02	110.9
5.0	60	6°	7	0	1.0	.69	1.10	.02	28.9
5.0	60	6°	7	3	.4	.51	1.13	.08	32.9
5.0	60	6°	7	3	1.0	.57	1.23	.07	9.0
5.0	60	6°	7	6	.4	.46	1.24	.12	20.9
5.0	60	6°	7	6	1.0	.51	1.34	.10	6.2
5.0	60	10°	7	0	.4	.68	.86	.03	96.3
5.0	60	10°	7	0	1.0	.63	1.16	.04	18.5
5.0	60	10°	7	3	.4	.54	1.07	.09	31.2
5.0	60	10°	7	3	1.0	.56	1.26	.08	8.7
5.0	60	10°	7	6	.4	.49	1.17	.13	20.6
5.0	60	10°	7	6	1.0	.49	1.37	.11	5.8
5.0	60	4°	15	0	.4	.66	.88	.02	131.8
5.0	60	4°	15	0	1.0	.74	1.06	.02	34.8
5.0	60	4°	15	3	.4	.58	1.02	.08	33.2
5.0	60	4°	15	3	1.0	.65	1.14	.07	9.4
5.0	60	10°	15	6	.4	.80	.80	.03	103.4
5.0	60	10°	15	0	1.0	.72	1.07	.03	22.2
5.0	60	10°	15	3	.4	.64	.93	.09	31.0
5.0	60	10°	15	3	1.0	.64	1.15	.08	8.2
5.0	60	10°	15	6	.4	.58	1.02	.12	21.0
5.0	60	10°	15	6	1.0	.58	1.23	.10	6.2

TABLE V - Continued

Aspect Ratio AS	Stagnation Pressure P_o (psia)	2θ	L/W_1	Inlet Length (in)	Mach Number M_t	Pressure Recovery C_p	$\Delta C_p/C_p$ (%)	Throat Blockage B	$\Delta B/B$ (%)
1.0	60	12°	10	0	.4	.81	.78	.01	194.7
1.0	60	12°	10	0	1.0	.81	1.00	.01	53.9
1.0	60	12°	10	6	.4	.61	.97	.09	31.4
1.0	60	12°	10	6	1.0	.59	1.21	.08	8.7
1.0	60	12°	10	9	.4	.56	1.05	.12	22.4
1.0	60	12°	10	9	1.0	.57	1.24	.10	6.6
1.0	60	12°	18	0	.4	.85	.76	.02	171.5
1.0	60	12°	18	0	1.0	.83	.99	.01	46.8
1.0	60	12°	18	6	.4	.65	.93	.09	29.7
1.0	60	12°	18	6	1.0	.63	1.16	.07	8.8
1.0	60	12°	18	9	.4	.60	.98	.12	22.6
1.0	60	12°	18	9	1.0	.59	1.21	.10	6.7
0.25	20	16°	7	0	.4	.70	.49	.02	147.8
0.25	20	16°	7	0	1.0	.73	.67	.02	36.7
0.25	20	16°	7	3	.4	.56	.56	.12	22.5
0.25	20	16°	7	3	1.0	.48	.96	.09	9.1
0.25	20	16°	7	6	.4	.48	.63	.13	19.3
0.25	20	16°	7	6	1.0	.44	1.04	.13	6.6
0.25	20	13°	15	0	.4	.70	.50	-.004	-771.1
0.25	20	13°	15	0	1.0	.75	.66	.02	54.4
0.25	20	13°	15	3	.4	.60	.54	.07	38.5
0.25	20	13°	15	3	1.0	.64	.77	.08	11.1
0.25	20	13°	15	6	.4	.52	.60	.13	19.9
0.25	20	13°	15	6	1.0	.56	.85	.13	6.5

TABLE V - Continued

Aspect Ratio AS	Stagnation Pressure p_o (psia)	2θ	L/W_1	Inlet Length (in)	Mach Number M_∞	Pressure Recovery C_p	$\Delta C_p/C_p$ (%)	Throat Blockage B	$\Delta B/B$ (%)
0.25	60	10°	15	0	.4	.71	.84	.03	94.1
0.25	60	10°	15	0	1.0	.77	1.02	.02	31.7
0.25	60	10°	15	3	.4	.62	.92	.09	31.3
0.25	60	10°	15	3	1.0	.68	1.11	.08	9.8
0.25	60	10°	15	6	.4	.55	1.19	.13	31.5
0.25	60	10°	15	6	1.0	.62	1.17	.12	6.4
0.25	60	14°	15	0	.4	.74	.82	.02	185.4
0.25	60	14°	15	0	1.0	.75	1.05	.02	33.0
0.25	60	14°	15	3	.4	.65	.88	.09	31.1
0.25	60	14°	15	3	1.0	.67	1.12	.07	10.5
0.25	60	14°	15	6	.4	.58	1.02	.13	20.1
0.25	60	14°	15	6	1.0	.62	1.16	.12	6.3
0.25	60	8°	7	0	.4	.60	.99	.02	165.2
0.25	60	8°	7	0	1.0	.70	1.09	.02	31.6
0.25	60	16°	7	0	.4	.74	.82	.03	81.9
0.25	60	16°	7	0	1.0	.70	1.09	.03	29.2
0.25	60	8°	7	3	.4	.52	1.10	.09	31.4
0.25	60	8°	7	3	1.0	.61	1.18	.08	9.5
0.25	60	8°	7	6	.4	.46	1.23	.13	20.2
0.25	60	8°	7	6	1.0	.56	1.26	.11	6.5
0.25	60	16°	7	3	.4	.64	.90	.09	30.5
0.25	60	16°	7	3	1.0	.55	1.27	.08	8.0
0.25	60	16°	7	6	.4	.55	1.06	.13	20.3
0.25	60	16°	7	6	1.0	.49	1.36	.12	6.4

TABLE V - Continued

Aspect Ratio AS	Stagnation Pressure p_o (psia)	2θ	L/W_1	Inlet Length (in)	Mach Number M_t	Pressure Recovery C_p	$\Delta C_p/C_p$ (%)	Throat Blockage B	$\Delta B/B$ (%)
5.0	20	8°	7	0	.4	.66	.51	.03	98.1
5.0	20	8°	7	0	1.0	.65	.75	.03	22.6
5.0	20	8°	7	3	.4	.52	.59	.08	36.0
5.0	20	8°	7	3	1.0	.52	.90	.08	9.8
5.0	20	8°	7	6	.4	.47	.63	.13	20.1
5.0	20	8°	7	6	1.0	.48	.97	.11	6.3
5.0	20	10°	15	0	.4	.80	.46	.03	94.4
5.0	20	10°	15	0	1.0	.72	.70	.03	28.5
5.0	20	10°	15	3	.4	.63	.53	.07	40.5
5.0	20	10°	15	3	1.0	.59	.82	.08	9.8
5.0	20	10°	15	6	.4	.56	.56	.13	20.1
5.0	20	10°	15	6	1.0	.55	.87	.11	6.8
1.0	60	6°	10	0	.4	.69	.86	.01	194.8
1.0	60	6°	10	0	1.0	.77	1.02	.02	70.3
1.0	60	6°	10	6	.4	.57	1.03	.09	30.9
1.0	60	6°	10	6	1.0	.65	1.14	.07	8.9
1.0	60	6°	10	9	.4	.54	1.07	.12	22.1
1.0	60	6°	10	9	1.0	.61	1.18	.10	6.4
1.0	60	6°	18	0	.4	.77	.80	.02	153.5
1.0	60	6°	18	0	1.0	.82	.99	.02	41.1
1.0	60	6°	18	6	.4	.66	.88	.09	31.1
1.0	60	6°	18	6	1.0	.71	1.08	.07	9.3
1.0	60	6°	18	9	.4	.61	.98	.12	22.5
1.0	60	6°	18	9	1.0	.66	1.12	.10	6.7

Table V, the uncertainty in the blockage factor B (particularly at low Mach numbers and at low values of blockage factor B) is quite large. The most severe difficulty with blockage uncertainty is found in the aspect ratio AS = 0.25 data, since the throat geometric area is the smallest of the three aspect ratios studied. It is difficult to make meaningful cross-plots unless the uncertainty in the blockage factor B is reduced.

Blockage, however, is a very strong function of inlet channel length and a very weak function of downstream diffuser geometry. Although the diffuser tests should properly be treated as single sample experiments, if all diffuser tests having the same inlet lengths and same aspect ratio are treated as producing the equivalent values of throat blockage B, enough data are available to attempt a statistical analysis. This has been done for all blockage data by evaluating the mean blockage factor for each inlet length (for fixed aspect ratio) and by evaluating the standard deviation of the blockage data around this mean. Because our estimate of experimental uncertainty (based on 20 to 1 odds) is equivalent to twice the standard deviation, we have a statistical evaluation of our estimate of experimental uncertainty. Our estimate and the statistical evaluation have been found to agree.

In data reduction and cross-plotting beyond the "raw" data form presented in the pressure recovery C_p vs. M_t and B vs. M_t plots, the statistically evaluated mean value of the blockage factor B for each pressure, diffuser aspect ratio, inlet length, and Mach number M_t has been used.

4.0 TEST RESULTS

This section contains the experimental results from the measurement of pressure recovery performance. Results are given for each of the three aspect ratio diffuser geometries and for each of the subprograms carried out on this contract. These subprograms have studied the effect of throat inlet Reynolds number, boundary layer shape factor, asymmetric throat blockage distribution, and the influence of rounding the throat corners of some selected diffuser geometries.

Before presenting these results, several factors which bear upon the results obtained will be discussed. These factors relate to the evaluation of throat stagnation pressure and the level of throat static pressure fluctuations.

Early in the experimental program, experiments were made to verify that the core flow stagnation pressure at the throat inlet was the same as the upstream stagnation pressure. It was assumed that the developing flow in the inlet maintains a potential nonviscous core flow through the inlet passage. In performing these measurements, two disturbing effects were encountered. Both were of principal concern to the measurement of diffuser performance.

The first effect was an indicated throat stagnation pressure drop between the approach plenum chamber and the throat. This indicated that stagnation pressure loss was small and almost negligible for the shorter inlet length geometries. However, the indicated loss became appreciable for the longer throat inlet lengths required to obtain high values of throat blockage. The throat stagnation pressure enters into the calculation of both the diffuser pressure recovery coefficient C_p and the throat blockage B.

The second disturbing effect was the presence of rather large static pressure fluctuations at the diffuser throat location. The appearance of these large pressure fluctuations at the diffuser throat caused concern on two accounts: (1) they might be the cause of the indicated stagnation pressure loss because of a nonlinear amplification of the probe stagnation pressure signal at the diffuser throat, and (2) the high level of static pressure fluctuations might produce a pronounced effect upon the static pressure recovery of the diffuser configurations.

The stagnation pressure measurements will be discussed first.

4.1 THROAT STAGNATION PRESSURE

The propagation of experimental uncertainty into each of the derived quantities C_p and B due to propagation of an uncertainty in each of the primary basic quantities, such as throat stagnation pressure p_{o_t}, has been discussed in Section 3.0.

A major effort was expended early in the research program to determine the magnitude and cause of the indicated inlet stagnation pressure loss over the range of inlet conditions to be used and to discover the reasons why this loss occurred.

At aspect ratio = 0.25, measurements were made of stagnation pressure loss over the complete set of inlet geometries for both the favorable and the adverse pressure gradients. In all of these preliminary studies, the diffuser throat (the start of the diverging portion of the diffuser test block) was located a constant distance downstream of the location of the boundary layer trip slot. The geometry for these studies and their relation to the inlet of the test section and the transition slot are shown in Figure 19.

Our concern with the data from stagnation pressure loss measurements was that, although the measurements themselves qualitatively followed trends logically expected from boundary layer behavior in the inlet section, the actual magnitude of stagnation pressure loss was larger than expected. The results of these measurements are shown in Figure 20.

If the boundary layers on the walls of the inlet merge upstream of the diffuser throat, a stagnation pressure loss will occur in the center of the inlet channel. This loss is a result of viscous mixing in the merged outer portions of the turbulent boundary layer. A low-unit Reynolds number and a long length will promote a thick boundary layer growth.

For the case of zero inlet length (see Figure 19 where the inlet sine blocks are immediately adjacent to the diffuser blocks), the boundary layer will be thick in the low-velocity portion of the inlet (upstream of the sine blocks), since the boundary layer here has a low velocity (low unit Reynolds number) and a long length in which to grow. However, if

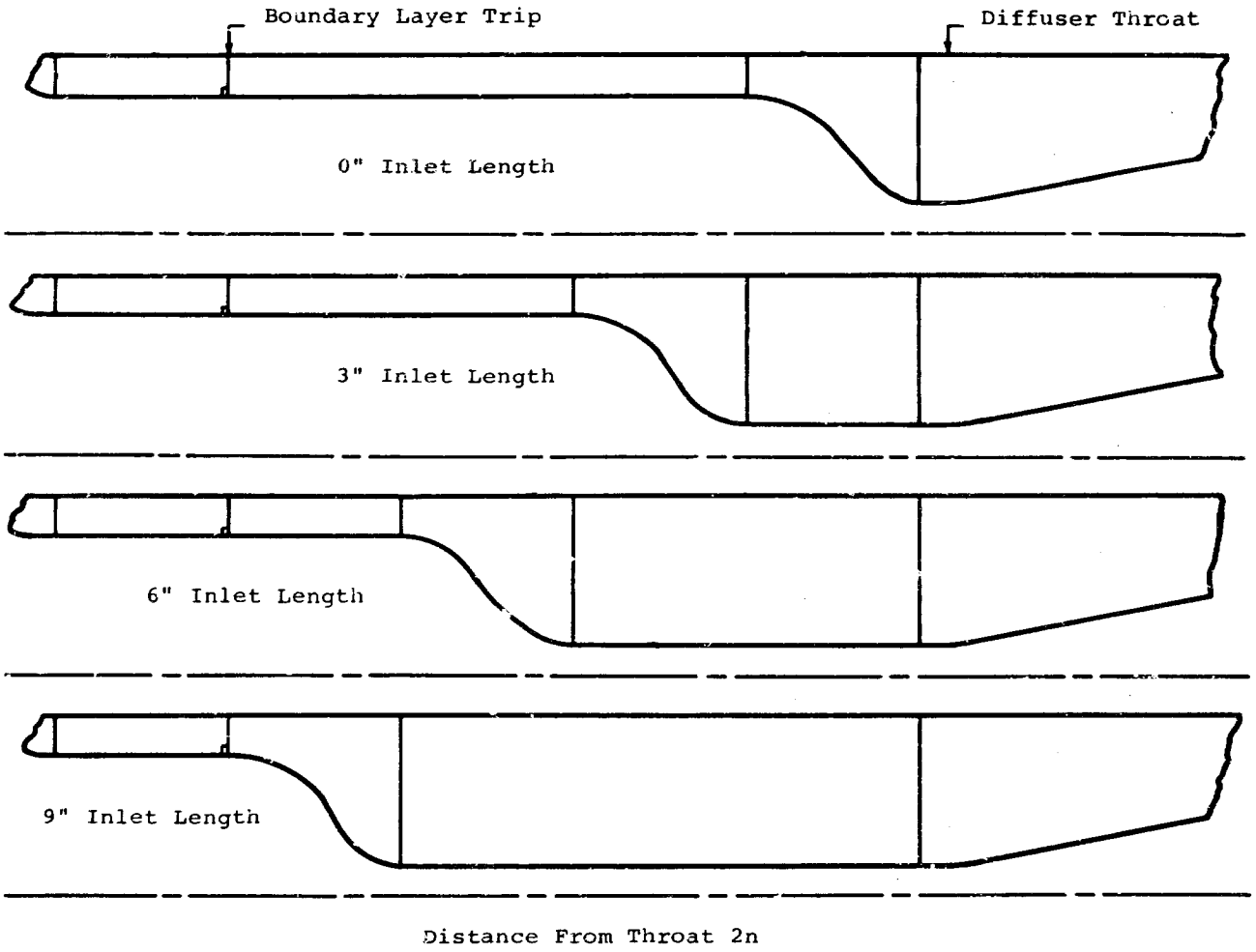

Figure 19. Inlet Geometry for Stagnation Pressure Measurements.

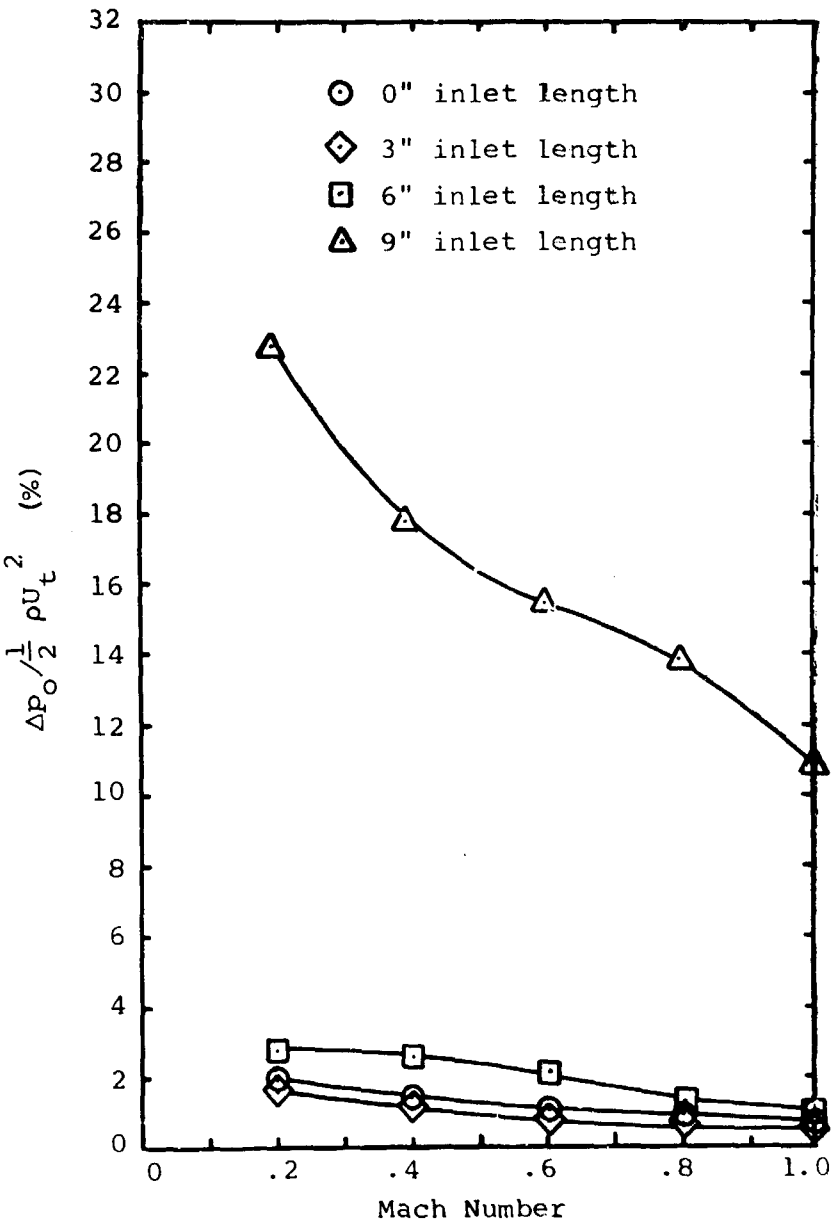

Figure 20. Stagnation Pressure "Loss" Measurements (60 psia).

boundary layer merger occurs ahead of the sine blocks, the stagnation pressure loss in the center of the channel in this region should be small, since mixing occurs under low dynamic head conditions (i.e., under the low velocity present in the relatively large cross section of the inlet channel).

By increasing the length of the inlet between the sine blocks and the diffuser blocks, an increase in stagnation pressure loss, if boundary layer merger occurs, may be expected. For example, if we take the 9" inlet section geometry of Figure 19, the length of the low-velocity region for boundary layer growth is considerably shortened, and the low-velocity boundary layer does not have sufficient length in which to grow and meet in the centerline of the inlet channel; instead, the low-velocity flow is immediately accelerated to a high velocity downstream as the flow passes through the sine blocks. Now the boundary layer can grow and merge in the center of the channel within the 9-1/2" of narrow inlet length. Because the boundary layer is growing under high-velocity conditions over most of the inlet wall length (compared to the low-velocity boundary layer growth in the case of the zero-inlet-length geometry), the point where the boundary layers merge in the center of the channel can be expected to be farther downstream than was the case for the zero-inlet-length geometry. When boundary layer merger does occur, however, the stagnation pressure loss in the center of the channel will be significantly higher per unit length in the flow direction because of the much higher dynamic pressure associated with the mixing process occurring along the channel centerline.

In summary, based on the above qualitative arguments, it is not unreasonable to expect a stagnation pressure loss at the centerline location at the throat. For a fixed throat Mach number, this loss is expected to be higher, the longer the length of inlet between the sine blocks and the diffuser blocks, because of more vigorous mixing once boundary layer merger does occur. The measurements of Figure 20 qualitatively confirm these arguments.

In experiments where the upstream plenum stagnation pressure is low (20 psia compared to 60 psia), the unit length Reynolds number in the inlets will be lower than for corresponding geometries with the high plenum stagnation pressure; for the 20 psia data, the boundary layer growth can be expected to be

more rapid. For identical inlet geometries and throat Mach number, the boundary layers for the 20 psia data will merge sooner and have a higher stagnation pressure loss in the inlet compared to the 60 psia data. As can be seen from Figures 20 and 21, this is what is qualitatively observed to occur.

Although a very detailed analysis of the developing inlet flow was not attempted, boundary layer calculations for the various inlet geometries were made. Figure 22 illustrates the results of boundary layer calculations using compressible boundary layer theory for the 6" inlet geometry at 60 psia upstream stagnation pressure conditions and a throat Mach number = 1.0. The calculation is an iterative process since the freestream conditions through the inlet channel are dependent on the boundary layer growth. These calculations are not assumed to be exact since there are many assumptions in the analysis which do not hold true in the inlet flow. The calculation neglects actual effects such as stream convergence, corner effects in the inlet channel, three-dimensional boundary layer behavior, etc., as well as the inherent inaccuracy of the basic two-dimensional boundary layer prediction method. Nevertheless, the calculations probably give a reasonable approximation to the boundary layer development. Note that the accelerating flow through the sine blocks produces an extreme thinning of the boundary layer and a virtually new development of the flow through the straight inlet block section of the channel. These calculations have also been made for other throat Mach numbers.

The boundary layer calculations show that for the aspect ratio = 0.25 geometries of Figure 19, boundary layer merger probably occurs in the inlets only for the 9" inlet length. Figure 20 for the 60 psia data shows the stagnation pressure loss estimated for an equivalent fully developed channel flow for the calculated merged portion of the 9" inlet boundary layers. The observed centerline stagnation pressure loss appears to be too high relative to this equivalent fully developed flow stagnation pressure loss.

A number of additional experiments were undertaken to attempt to determine if the measured stagnation pressure losses were indeed correct.

A traverse stagnation pressure survey was made to measure the magnitude of stagnation pressure loss as a function of axial distance through the inlet. Such measurements should provide

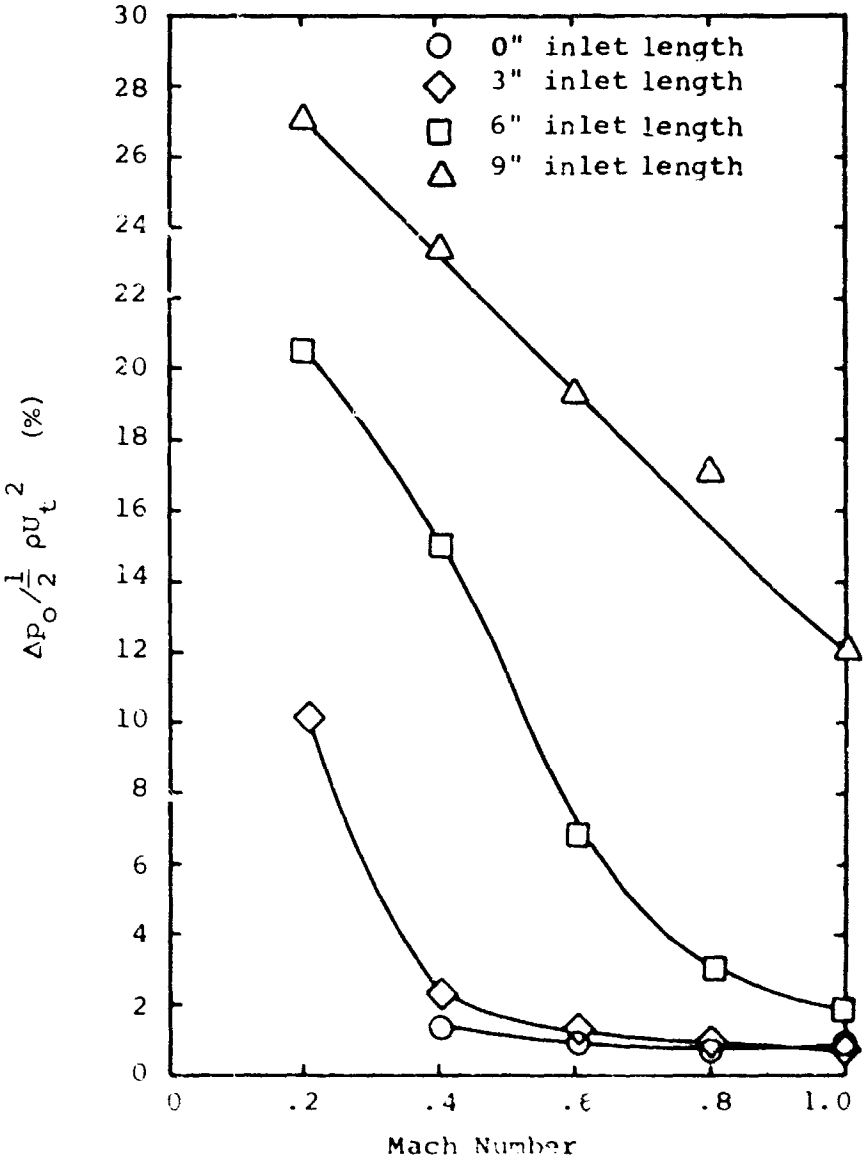

Figure 21. Stagnation Pressure "Loss" Measurements (20 psia).

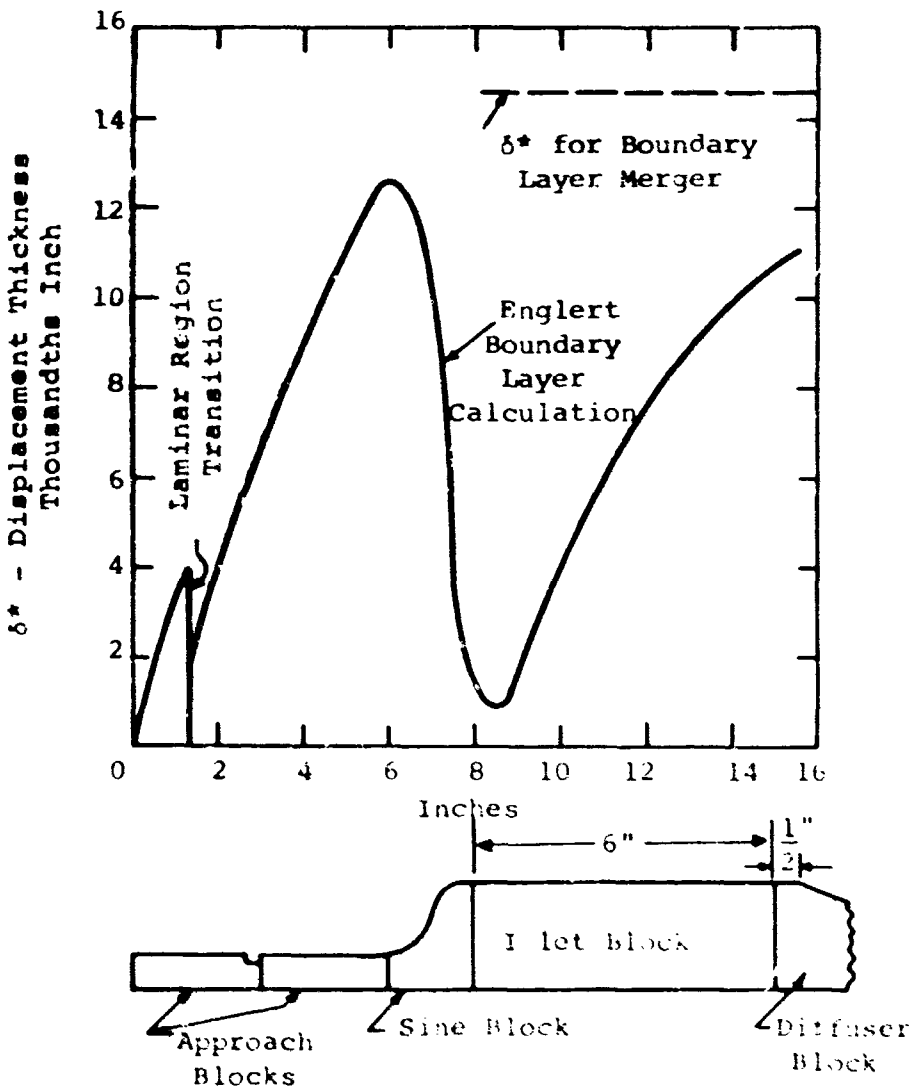

Figure 22. Compressible Boundary Layer Calculations. Aspect Ratio = 0.25, Stagnation Pressure = 60 psia, Inlet Length = 6 Inches.

an indication of the point of boundary layer merger and the amount of stagnation pressure loss after such merger occurred. These experiments involved a change in the diffuser geometry to establish conditions where boundary layer merger should definitely not occur. This was accomplished by changing the aspect ratio of the diffuser to AS = 1.0. For the aspect ratio = 1.0 geometry, the boundary layers in the inlet should not merge in the center of the passage, and the stagnation pressure loss between the upstream plenum and the throat should be zero.

The stagnation pressure distribution measurements were made with a traverse stagnation tube. A drawing of the tube geometry is given in Figure 14. Contrary to the expected inlet flow behavior, these measurements showed a measurable loss starting ahead of the sire blocks, whereas the boundary layer predictions indicated no merger of the boundary layers in the inlet.

These peculiar results of the aspect ratio = 1.0 data led to the conclusion that other effects are probably producing an indicated stagnation pressure loss. It was suspected that such losses might be associated with secondary flow and a resulting eddy mixing in the center of the channel. A square channel geometry of the type under study here is quite prone to producing secondary flow effects in the channel corners. If the boundary layer flow in the corners or along one of the sidewalls is caused to be moved into the center of the flow, this low velocity, stagnation-pressure-deficient fluid could impact on the stagnation pressure measuring probe and "indicate" a stagnation pressure loss in the core flow along the channel centerline.

Experiments to measure the stagnation pressure loss under conditions in which the inlet geometry was significantly altered from the previous geometries were made. While running the 3" inlet block geometry, the diffuser blocks were moved upstream of their previous location. This alteration in geometry is shown in Figure 23. The effect is to move the location of the diffuser throat so that the boundary layer in the inlet has a much shorter development length. This geometry change should show no boundary layer merger and hence no stagnation pressure loss. The stagnation pressure measurements did, however, indicate a loss in stagnation pressure. In

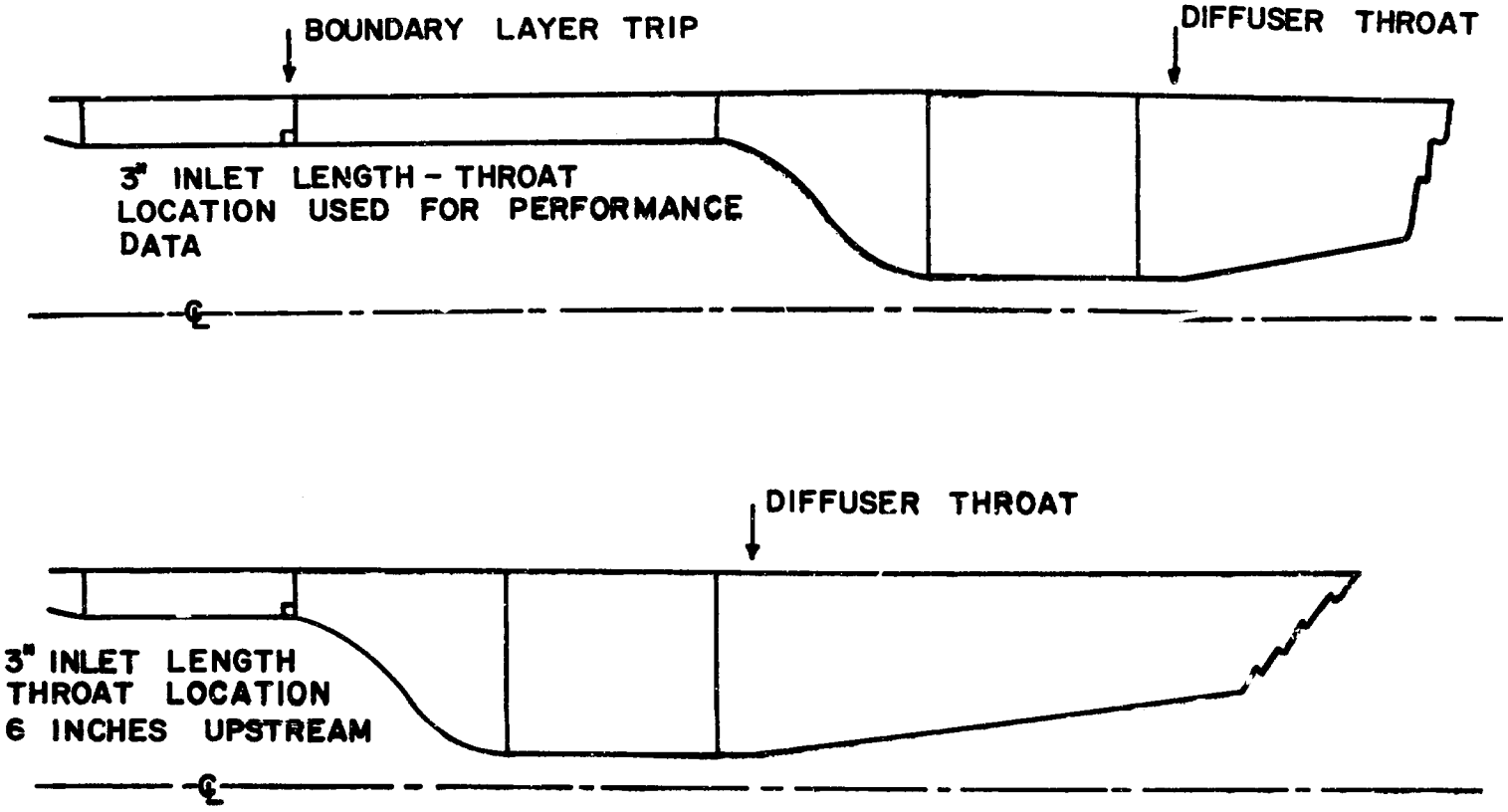

Figure 23. "Base" Data Test Section Geometry.

particular, the measurements of throat stagnation pressure for the upstream location of the diffuser throat show a higher stagnation pressure loss than those for the downstream throat location. This is contradictory to trends in stagnation pressure loss expected from a consideration of possible boundary layer merger effects. The results strengthened the suspicion that secondary flow was responsible for the indicated stagnation pressure loss since the upstream throat location could measure low stagnation pressure fluid dumped into the core flow while downstream throat stagnation pressure measurements could measure a mixed-out and hence higher stagnation pressure.

At this point, it was felt that the possibility could not be overlooked that static pressure fluctuations at the throat could be producing erroneous readings of the total pressure probes even though pressure fluctuations in the upstream plenum had been reduced to a low level.

4.2 THROAT STATIC PRESSURE FLUCTUATIONS

Prior to the stagnation pressure loss measurements, considerable effort had been devoted to reducing the level of pressure fluctuations existing in the test loop. Particular effort had been given to reducing pressure fluctuations in the upstream plenum ahead of the test section.

The original test loop configuration, in which no acoustic damping was provided, had produced static pressure fluctuations of ± 1 psi in the upstream plenum chamber at the 60 psia stagnation pressure conditions. These pressure fluctuation measurements were made with a dynamic pressure transducer capable of resolving the pressure fluctuations over the complete range of frequencies and amplitudes of interest.

Because such levels of pressure fluctuation might affect the accuracy of measurements in the test section and of the pressure differential measured across the flowmeter nozzle, steps were taken to damp these fluctuations. Helmholtz branch resonators and acoustic filtering were installed in the piping test loop. This reduced the amplitude of pressure fluctuations by approximately a factor of 30 from ± 1 psi to approximately $\pm .03$ psi. It was anticipated that this low level of pressure fluctuations would cause little problem in static pressure readings and flow rate measurements.

To check the test section conditions, a high-response pressure transducer was mounted at the throat location. A 1/4" hole was drilled through the test section's top plate at the location of the diffuser throat for the throat geometry of Figure 23. The transducer was sealed into the top plate with the transducer element mounted flush with the inner surface, as shown in Figure 24.

Measurements with this transducer showed large static pressure fluctuations. Figure 25 shows oscilloscope recordings of the transducer output at the throat near choke conditions and also the same type of recording at the upstream and downstream plenum chambers. Some throat fluctuations as large as 3.5 psi peak to peak are present at a throat Mach number 0.98 compared to the average peak-to-peak fluctuation in the upstream plenum of approximately 0.03 psi. Such large pressure fluctuations enforced the suspicion that perhaps a nonlinear response of the total pressure probe to these fluctuations might be responsible for the stagnation pressure loss indicated at the throat. More importantly, however, the measurement of such large fluctuations in static pressure at the throat caused considerable concern as to their influence on the pressure recovery performance of the diffuser geometries. The large throat static pressure fluctuations might by themselves produce a basic change in the fluid dynamic behavior of the diffuser and hence be an important factor in correlating diffuser static pressure recovery. It was felt necessary to pursue additional experiments to determine the influence of the amplitude of the static pressure fluctuations at the throat on both the measured throat stagnation pressure and the diffuser pressure recovery.

To verify that the throat pressure fluctuations were not produced by oscillations of the traverse tube, measurements were repeated with the traverse tube removed. In spite of the removal of the traverse probe, the pressure fluctuations still existed at the throat. It was observed, however, that when the flow choked in the throat of the diffuser, i.e., so that supersonic flow was present downstream of the throat, the level of pressure fluctuations was reduced an order of magnitude below those at a slightly lower Mach number. It appeared that the establishment of supersonic flow in the diffuser throat either was blocking propagation of pressure disturbances from the downstream plenum or was significantly altering any resonance conditions that might be established in the diffuser geometry.

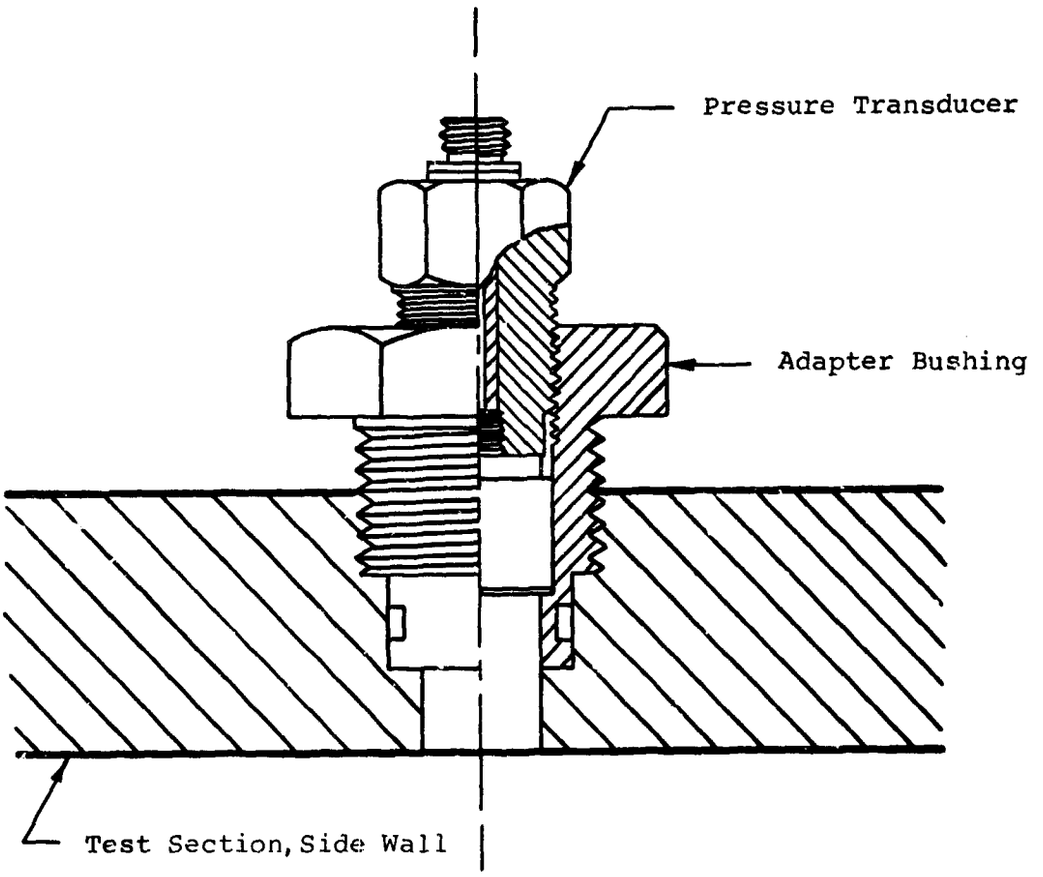

Figure 24. Pressure Transducer Mounting for Pressure Fluctuation Measuremerts.

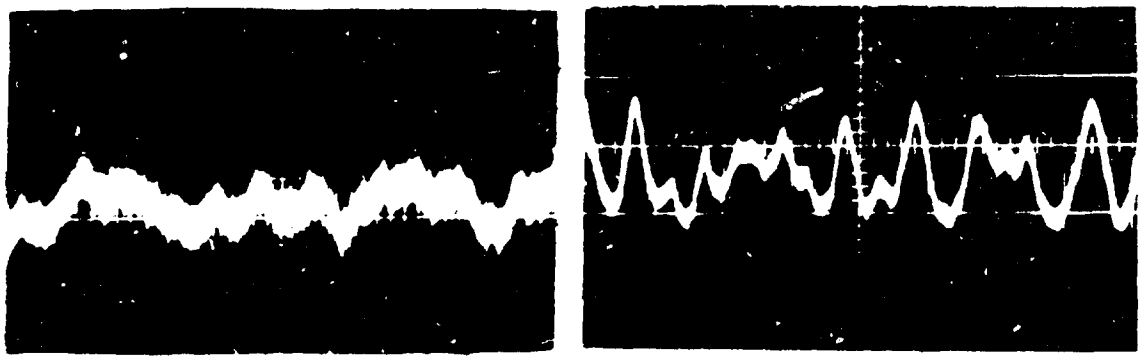

a. UPSTREAM PLENUM M ≅ 0.98
T-Scale 5 Millisec/cm
P-Scale .029 psi/cm

b. THROAT M≅ 0.98
T-Scale 5 Millisec/cm
P-Scale 1.45 psi/cm

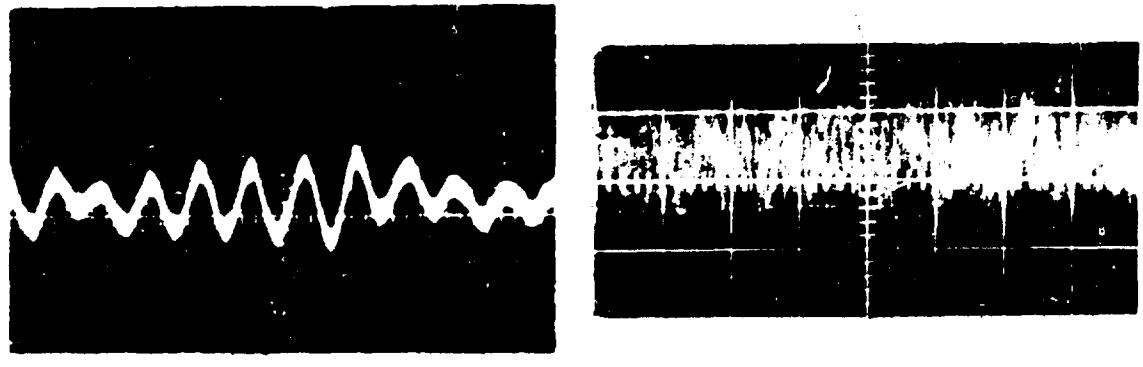

c. DOWNSTREAM PLENUM M ≅ 0.98
T-Scale 5 Millisec/cm
P-Scale .145 psi/cm

d. THROAT M ≅ 1.2
T-Scale 5 Millisec/cm
P-Scale .145 psi/cm

OSCILLOSCOPE PICTURES OF PRESSURE FLUCTUATIONS
MADE WITH PRESSURE TRANSDUCER
NO RESONATOR ON FIRST-STAGE COMPRESSOR P_o = 60 psia

Figure 25. Pressure Fluctuation Measurements in Test Section. Mach Number = 1.0.

A predominant frequency is observed in all the oscilloscope traces. This is about 280 cycles per second, corresponding to the fundamental frequency of pressure fluctuation emanating from the screw-type compressors.

Experiments were run with the downstream piping decoupled from the flow loop, thereby exhausting the test section directly to atmospheric pressure through the plenum pipe. If a standing wave were produced in the downstream plenum pipe, opening the end of the downstream plenum to atmospheric pressure would eliminate the resonance condition or change the frequency for which a resonance condition could occur. Previous to these tests, all attempts at reducing fluctuations in the downstream plenum by muffling the downstream pressure piping system with acoustic damping, using Helmholtz branch resonators, and putting acoustic baffles in the plenum had produced little reduction in the amplitude of fluctuations and no change in the predominant frequency.

With the back flange plate of the downstream plenum chamber removed, the upstream stagnation pressure depended upon the Mach number at the throat since the downstream control valving could not now be used. Flow control through the diffuser test section was obtained by adjusting the upstream gate valve and the bypass valves between the compressor and the diffuser test section.

Comparison tests were run at the same upstream stagnation pressure with the system in both a closed and open configuration. No significant change was observed in the level of throat pressure fluctuations with the system in either the open or closed configuration.

Pressure measurements were made with the transducer traversed throughout the downstream plenum to insure that the plenum was still not producing a resonant condition even though the downstream end of the plenum was open to atmospheric pressure. Surveys of the entire downstream plenum with the transducer showed that the level of pressure fluctuations was virtually indistinguishable from the noise level of the transducer. This was true whether the transducer was located at the end of the downstream plenum or was held directly in the separated region underneath the jet issuing from the test section.

The experiments showed that there was little if any effect of the downstream piping system on the level of oscillations in pressure observed within the test section.

After much experimentation, a means was finally found to reduce the level of fluctuations at the throat. This was accomplished by installing a perforated metal screen (1/16" thick steel sheet with 1/4" diameter holes) over the exit slot of the test section. The screen was quite effective in reducing the level of fluctuations. Comparative measurements of the throat pressure fluctuations at a Mach number $M_t = 0.8$ with and without perforated metal "screen" in place are shown in Figure 26. The amplitude of pressure fluctuations is reduced by approximately a factor of 3.5 with the screen in place for otherwise identical flow conditions.

Comparative tests were then undertaken to determine the effect of the reduction in amplitude of pressure fluctuations at the throat on diffuser performance and throat stagnation pressure.

Figure 27 shows comparative measurements of stagnation pressure drop between the upstream plenum and the diffuser throat; Figure 28 gives comparative data for throat blockage B and pressure recovery C_p for a diffuser geometry of $2\theta = 8°$, $L/W_1 = 12$, AS = 0.25, with upstream stagnation pressure of 60 psia.

Although there is some indication in Figure 27 that the stagnation pressure loss is altered slightly with the reduction in static pressure fluctuations at the throat (screen in place), this change is very small and lies within the uncertainty in measuring the stagnation pressure loss.

From Figure 28, it is strikingly evident that both flow blockage and pressure recovery do not change with the quite substantial reduction in throat static pressure fluctuations.

Several other tests were performed to try to locate the source of throat pressure fluctuations and to determine the effect of diffuser geometry on the measured total pressure drop at the throat.

The placement of the "screen" over the downstream test section exit slot, which partially blocked the flow into the downstream plenum, could be expected to alter separation effects that would otherwise occur at the slot exit without the screen in

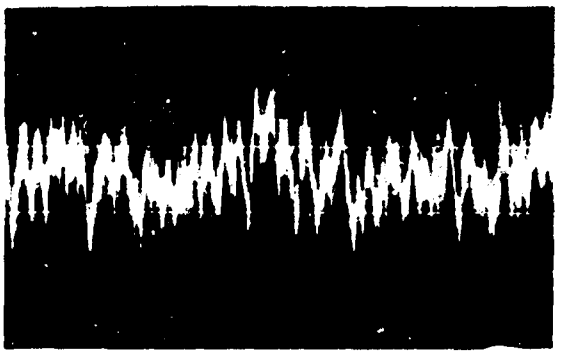

a. CLOSED SYSTEM - THROAT $M_t \cong 0.8$

WITH PERFORATED PLATE IN PLENUM ENTRANCE

T-Scale 10 Millisec/cm P-Scale 0.29 psi/cm

b. CLOSED SYSTEM - THROAT $M_t \cong 0.8$

T-Scale 10 Millisec/cm T-Scale 0.58 psi/cm

OSCILLOGRAPHS OF PRESSURE FLUCTUATIONS MEASURED WITH PRESSURE TRANSDUCER $P_o \cong 60$ psia

Figure 26. Pressure Fluctuation Measurements With and Without Pressure Damping Screen.

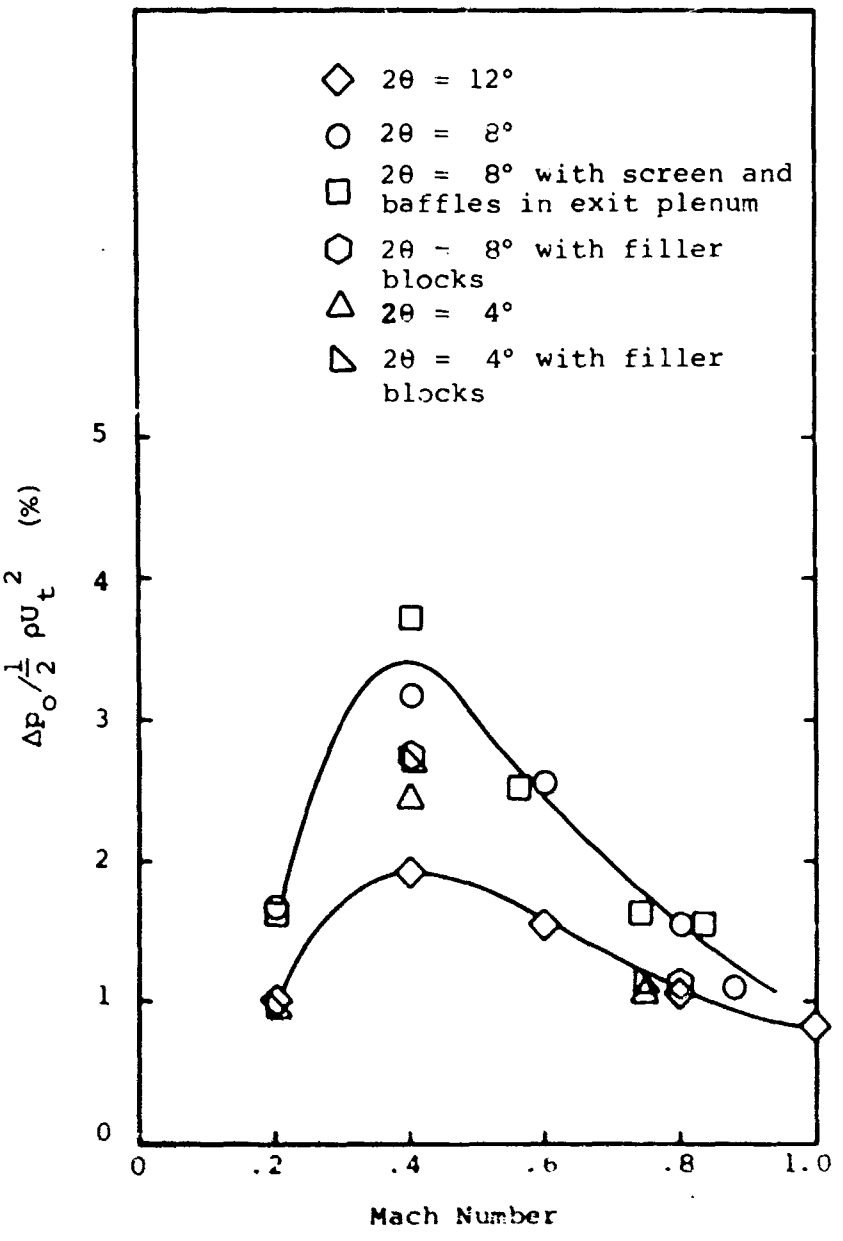

Figure 27. Stagnation Pressure "Loss" Measurements With and Without Pressure Damping Screen.

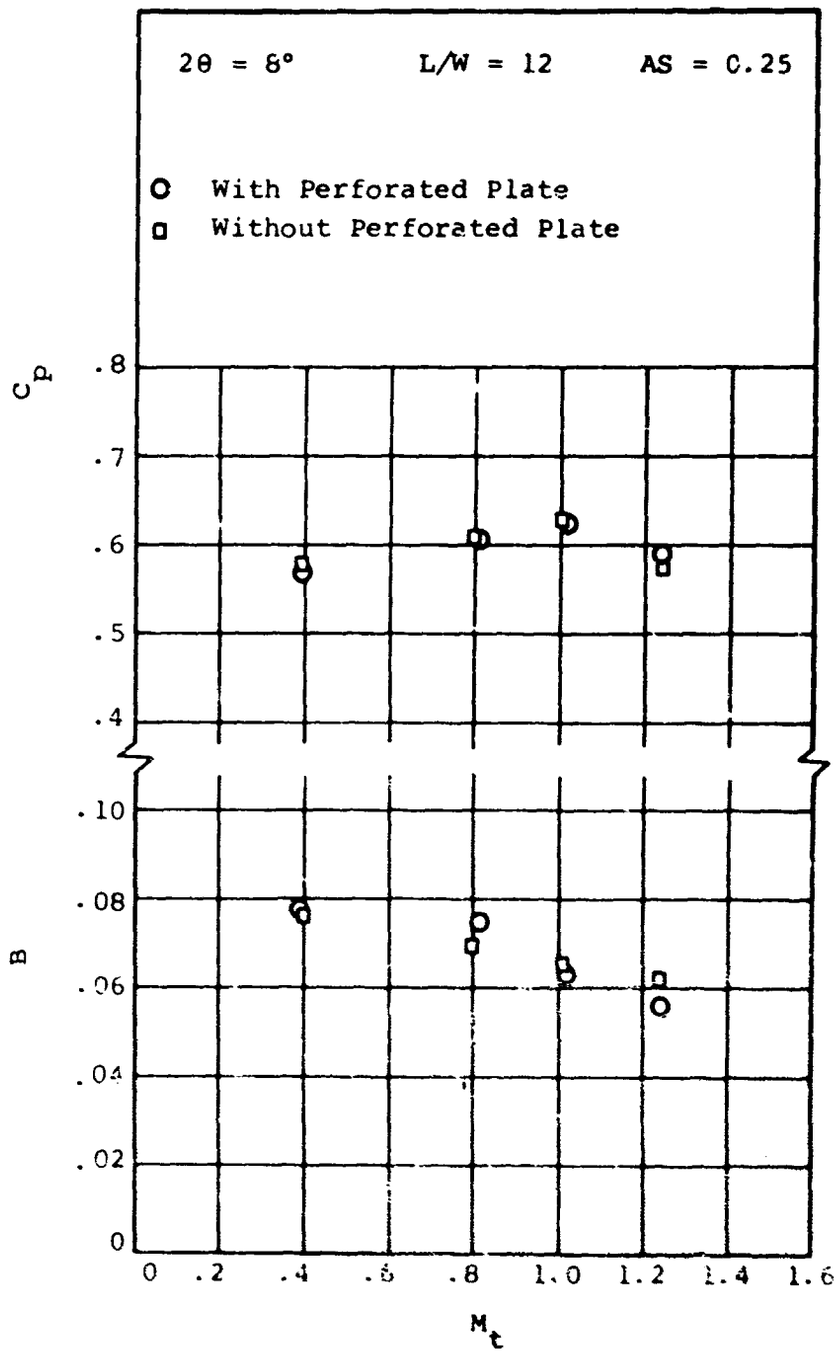

Figure 28. Pressure Recovery and Throat Blockage Versus Mach Number, With and Without Pressure Damping Screen.

place. However, blockage from the perforated screen was also expected to influence the flow downstream of the diffuser exit before the flow exited into the plenum; thus the nature of the separation in the diffuser exit corners might be altered. It was felt that the pressure oscillations at the throat might be the result of periodic shedding phenomena at the sudden expansion steps in the diffuser geometry at the diffuser exit. Possibly, other sources could promote shedding within the diffuser itself or as the flow jets into the downstream plenum.

A separate check on the influence of separation in the downstream corner regions of the test section geometry was made with "filler blocks" inserted downstream of the diffuser exit. These blocks extend the diffuser exit area to the plenum exit slot. A sketch of this geometry is shown in Figure 29. With the filler blocks in place, the level of pressure fluctuations was reduced, although not as much as by the use of the perforated metal "screen". Again, however, measurements of the throat total pressure loss were unchanged. Pressure recovery performance was not measured.

To check the influence of separated flow in the diffuser itself, a diffuser geometry with divergence angle $2\theta = 4°$ was tested. Such a small divergence angle would not cause separation within the diffuser. Again, the throat static pressure fluctuations were reduced, but little change was observed in the stagnation pressure drop measurements.

However, these series of experiments did show that there was a pronounced upstream effect of diffuser geometry on diffuser inlet flow. In Figure 27, only changes in diffuser geometry, not inlet geometry, differentiate the curves; each curve has the same inlet configuration.

4.3 SUMMARY OF THROAT PRESSURE FLUCTUATION AND STAGNATION PRESSURE MEASUREMENTS

In summary, the stagnation pressure loss measurements show:

(1) The downstream diffuser geometry affects stagnation pressure loss for a fixed upstream configuration,

(2) The upstream inlet geometry affects stagnation pressure loss in a manner not always explained by

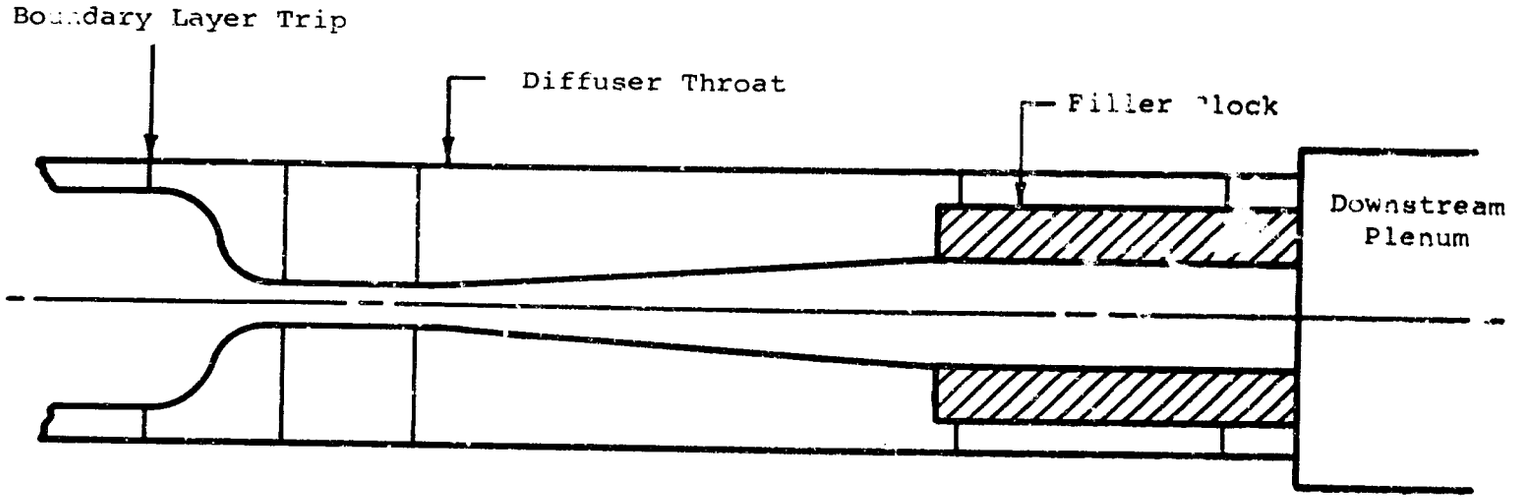

Figure 29. "Filler" Block Geometry Used for Pressure Fluctuation Test Performance.

simple arguments about inlet boundary layer merger.

(3) The indicated stagnation pressure losses are larger for the aspect ratio = 0.25 geometry than for the aspect ratio = 1.0 geometry.

It appears that whatever the mechanism causing an indicated throat stagnation pressure loss, it is a complicated situation and not easily explained, even by the rather extensive set of experiments that were undertaken. The most likely explanation appears to be secondary flow shedding of total pressure deficient fluid from the wall regions into the core flow upstream of the diffuser throat. If stagnation-pressure-deficient fluid is in the core flow at the throat, it is there because of boundary layer behavior on the sidewalls and not because of a stagnation pressure loss in the core flow. For purposes of correlating diffuser behavior, it does not seem appropriate to treat low-stagnation-pressure fluid introduced into the core flow by possible secondary flow motions as representative of a decrease in inlet stagnation pressure of the "core" flow. If stagnation-pressure-deficient fluid is put into the core flow, it comes from the wall regions, and its effect should be correlated through the throat inlet blockage B.

The diffuser recovery data indicate that the stagnation pressure loss should not be treated as a "core" stagnation pressure loss. Sets of data have been reduced to calculate pressure recovery C_p and throat blockage B with and without using the indicated stagnation pressure loss between the plenum and throat shown in Figure 20. The reduction of a large amount of such data has clearly indicated that a consistent variation in pressure recovery and throat blockage with throat Mach number M_t is obtained when no stagnation pressure loss is assumed. When the indicated stagnation pressure loss is included to correct the throat stagnation pressure, the variations in C_p and B with M_t produce a much greater scatter and inconsistency in the trends of the data. An example of the change in pressure recovery is shown in Figure 30.

The relatively large amplitude pressure fluctuations in the diffuser do not affect the basic fluid dynamic performance, at least when reduced by a factor of 3.5, as far as the pressure recovery is concerned. While it may not be safe to

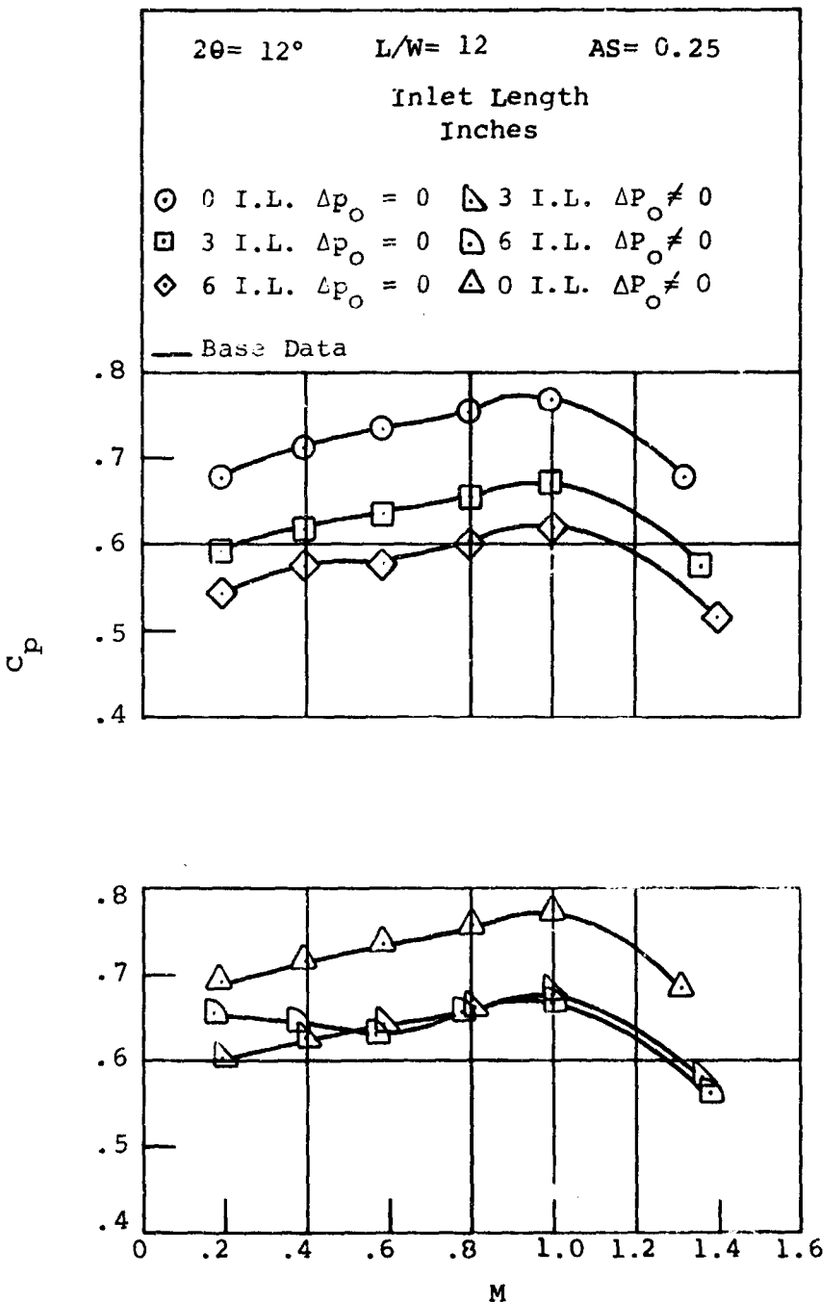

Figure 30. Pressure Recovery Versus Mach Number, With and Without Stagnation Pressure "Loss" Included.

conclude that the same results will hold for all geometries studied, it is difficult to see why these results should differ for geometries other than the $2\theta = 8°$ tested.

The source of the throat pressure fluctuations is not known. It is suspected that the fluctuations arise either from a fluid dynamic shedding phenomena within the diffuser geometry itself or by amplification of pressure fluctuations present in the test loop and originating in the test loop compressors. The second cause appears to be more likely, since the primary frequency of throat fluctuations is the same as that originating from the wind tunnel compressors.

The pressure fluctuation phenomenon observed in these experiments has not been extensively reported in the literature, although similar conditions have probably existed in many experiments. The only analogous situation of which we are aware is in the measurement of flow rate in gas pipeline systems. Here a restriction in the pipeline flow area, for example, a flow measurement orifice, can apparently cause an acoustical impedance mismatch between the upstream and downstream elements of the piping system. It has been reported in the literature [see Sparks (1961)] that this has led to a severe resonance in pressure fluctuations at the orifice meter; only a very small change in the level and nature of the velocity fluctuations in the upstream piping system caused an extremely large increase in the indicated pressure differential across the orifice meter. Even an indication of reversed flow in piping systems has been obtained when reversed flow has been known not to occur. Even more striking effects have been observed in metering sections in blocked branches of gas pipelines; an indication of through flow has been recorded when obviously no flow could exist in the blocked branch line.

It is interesting to conjecture what happens in an actual centrifugal compressor channel diffuser when large pressure fluctuations exist upstream of the diffuser geometry at a frequency caused by the blade-to-blade pressure oscillations produced by the rotating impeller wheel.

4.4 BASE DATA

The diffuser pressure recovery C_p and throat blockage B have been measured for three aspect ratios over the range of

subsonic inlet Mach numbers for a fixed value of upstream stagnation pressure. These data will be referred to as the "base" data.

Range of Parameters

The range of parameters covered in these studies are:

AS = throat aspect ratio = 0.25, 1.0, and 5.0
L/W_1 = length-to-throat width ratio = between 7 and 18
2θ = double divergence angle = 8 to 16°
B = boundary layer blockage at throat = between 0.02 and 0.12 (approximately)
M_t = throat Mach number = low subsonic to superchoking
R_D = throat Reynolds number $\tilde{=}$ 10^6 (throat stagnation pressure = 60 psia)

The experiments to obtain these data have involved more than 2,000 tests. Specifications of the test conditions for these base data studies have been given in Table I.

"Raw" Data and Cross-Plotted Data

The data obtained directly from the tests (after data reduction) will be termed the "raw" data. These data have been plotted in the form of pressure recovery C_p and throat inlet blockage B as a function of throat inlet Mach number M_t for fixed diffuser geometries. Selected examples for the three aspect ratio geometries are shown in Figures 31 through 36. In the case of the throat blockage data, a mean value for the data has been obtained by statistical analysis. For the pressure recovery data, the lines have been drawn through the experimental points.

From this "raw" data, a wide variety of cross-plots are possible. The base data have been cross-plotted for all geometries in the following form:

(1) Pressure recovery C_p vs. throat blockage B. In this case, throat Mach number M_t is a parameter.

(2) Pressure recovery C_p vs. divergence angle 2θ. Throat blockage B is treated as a variable.

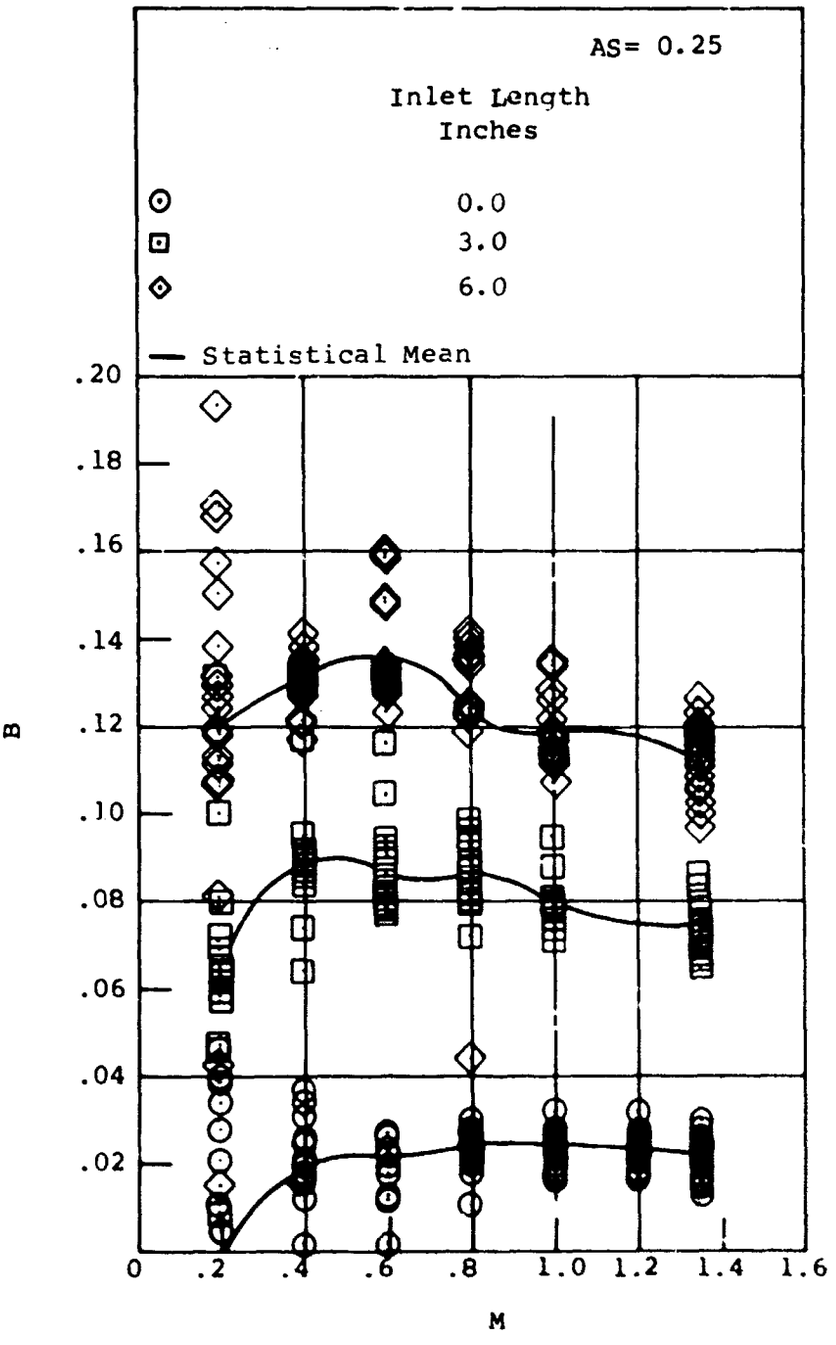

Figure 31. Blockage Versus Mach Number. Aspect Ratio = 0.25.

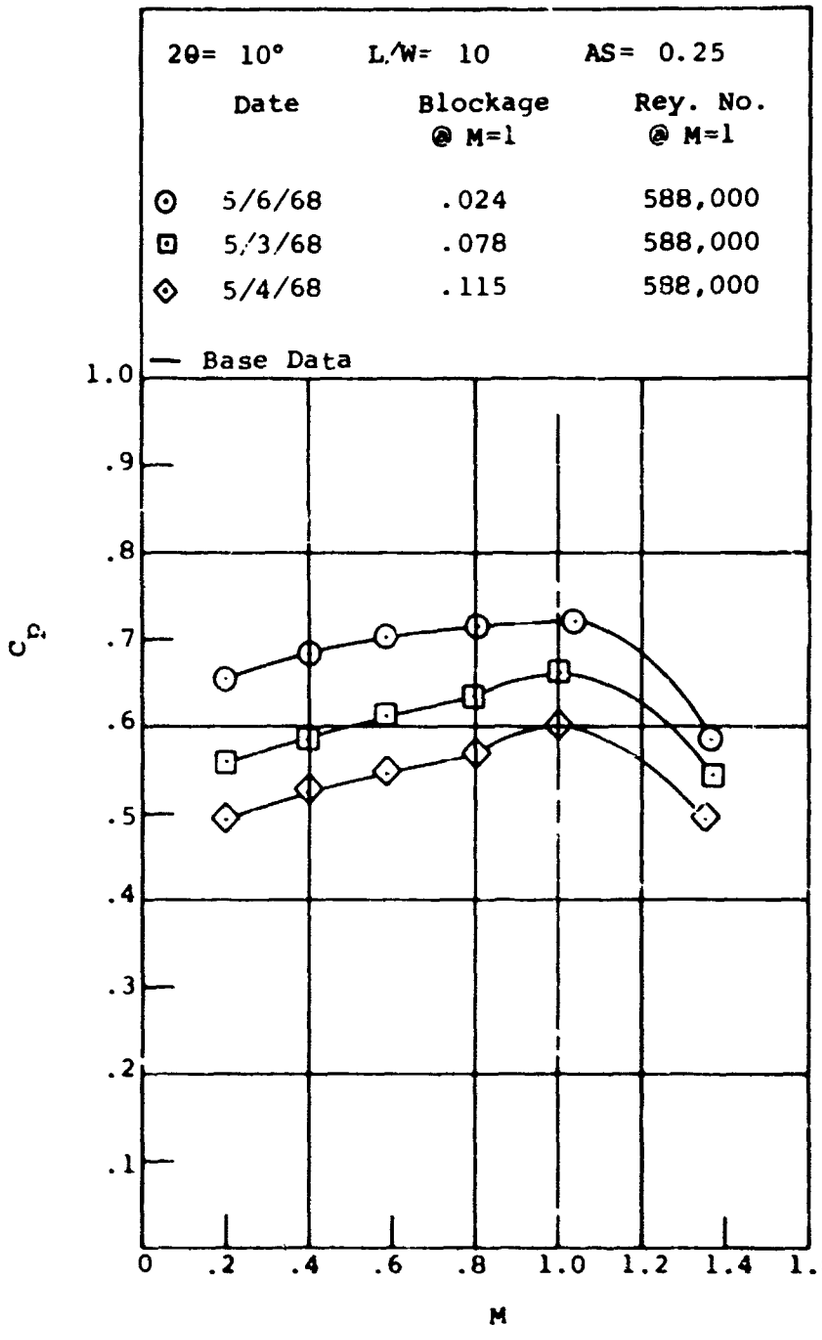

Figure 32. Pressure Recovery Versus Mach Number. Aspect Ratio = 0.25.

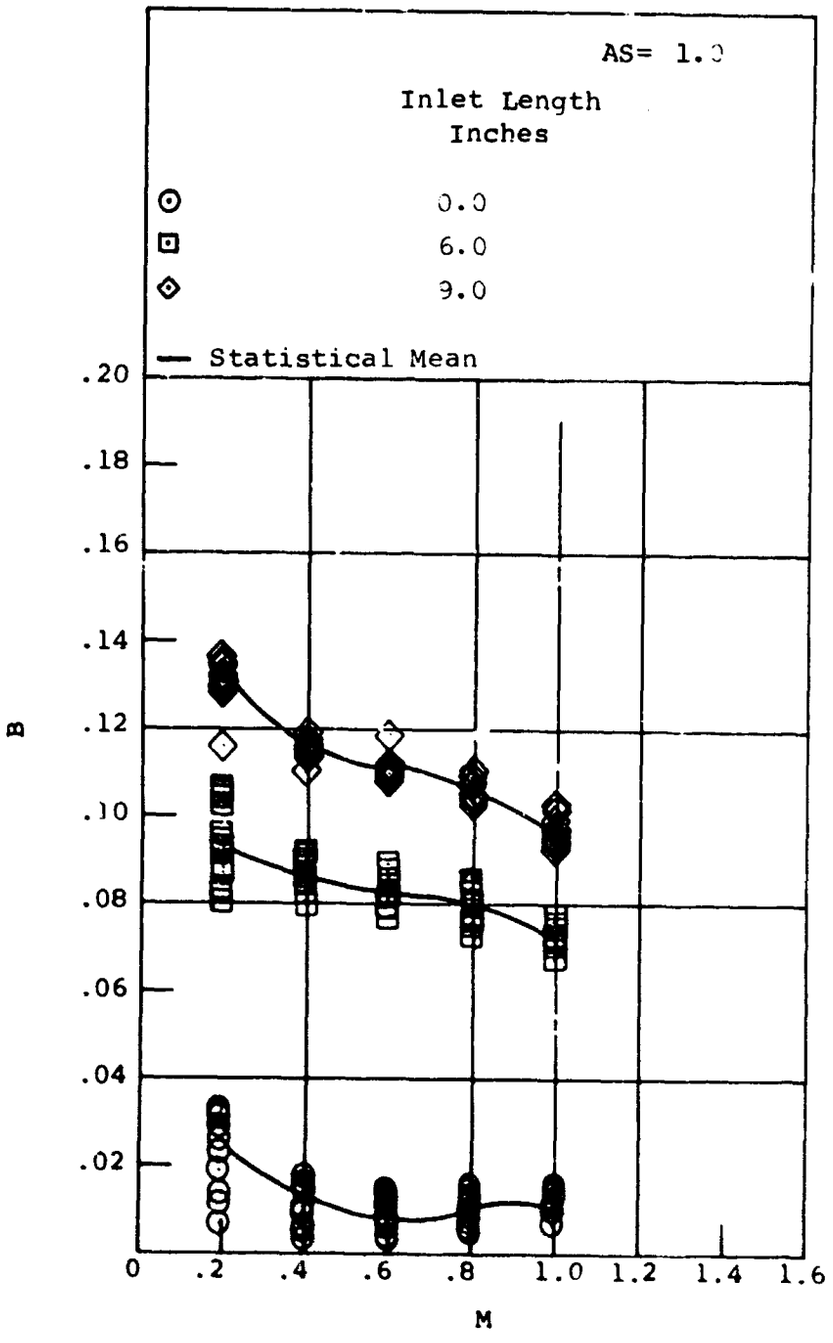

Figure 33. Blockage Versus Mach Number. Aspect Ratio = 1.0.

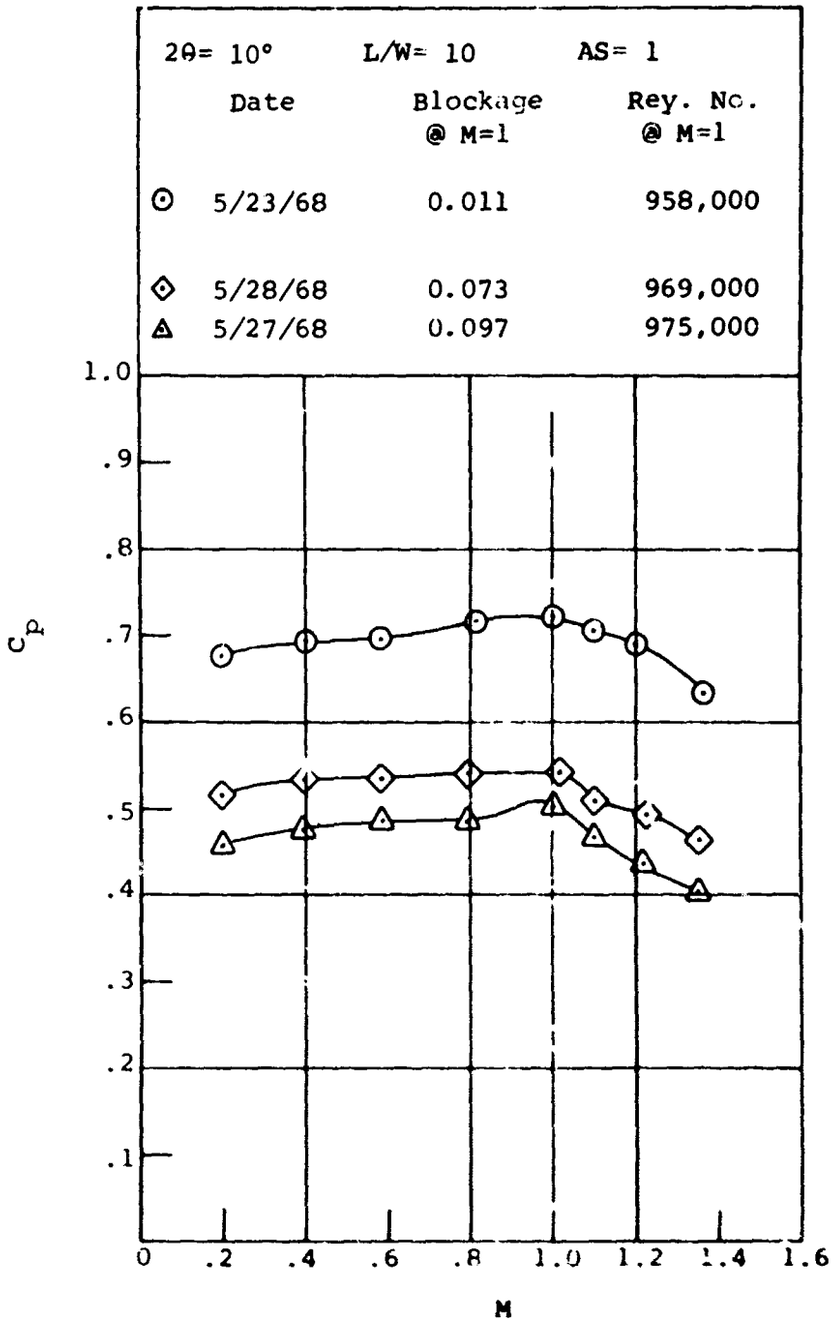

Figure 34. Pressure Recovery Versus Mach Number. Aspect Ratio = 1.0.

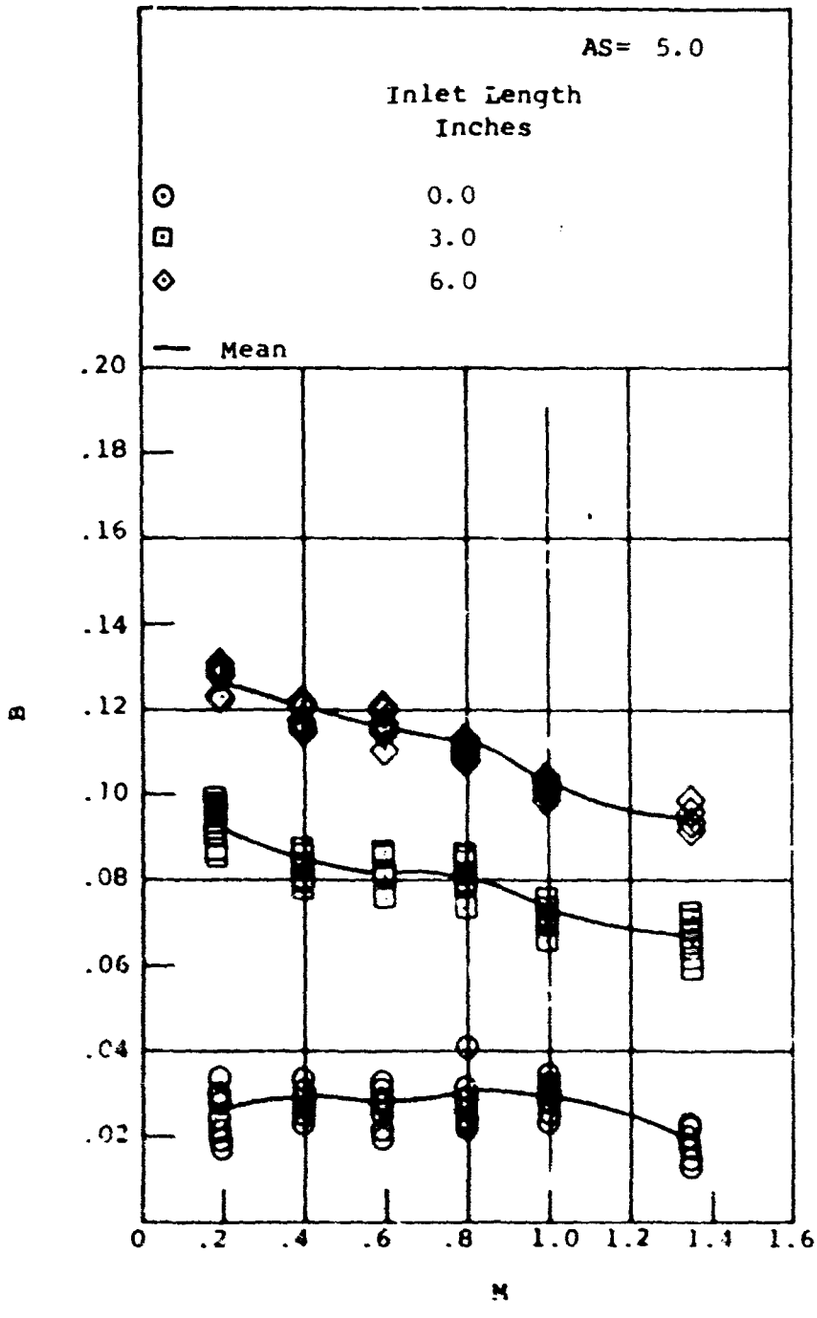

Figure 35. Blockage Versus Mach Number. Aspect Ratio = 5.0.

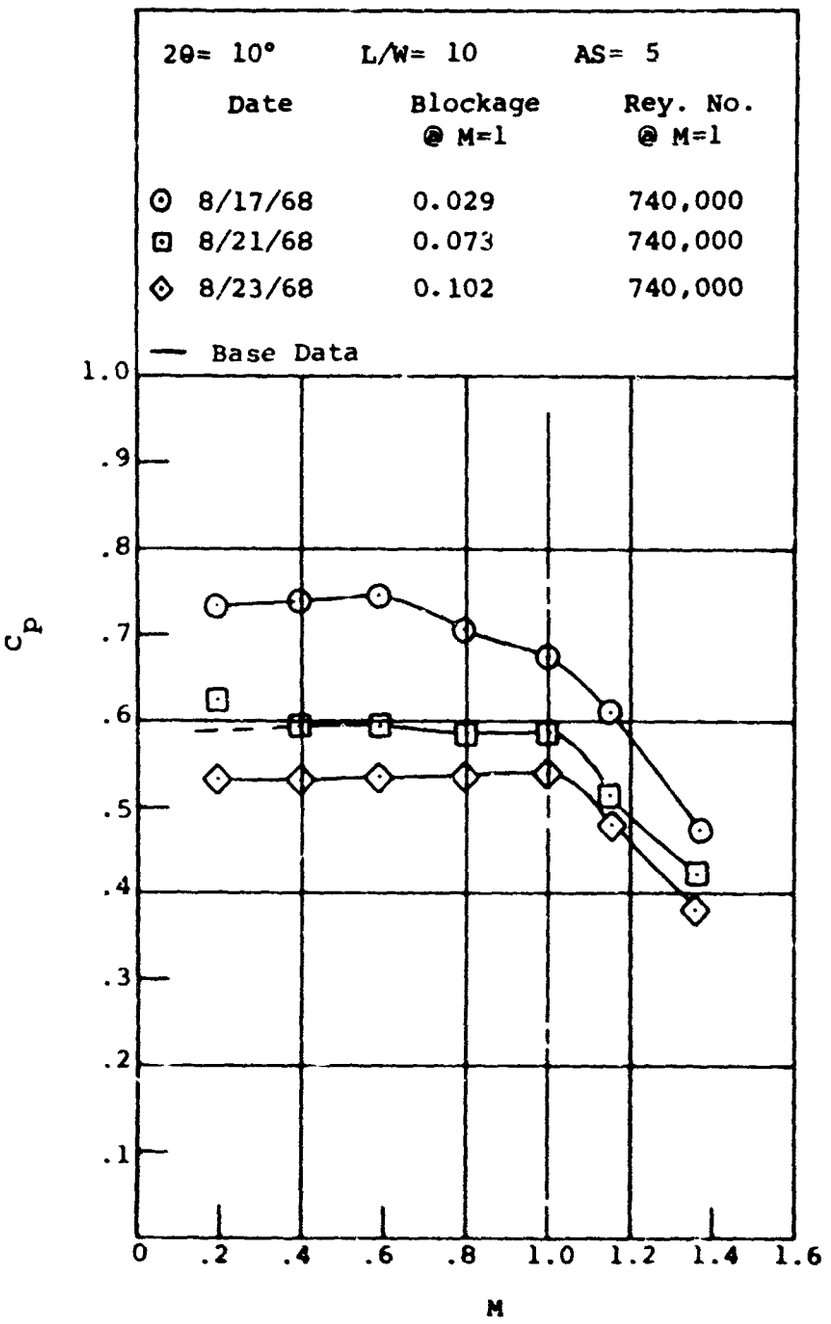

Figure 36. Pressure Recovery Versus Mach Number. Aspect Ratio = 5.0.

(3) Pressure recovery C_p vs. length-to-width ratio L/W_1. Throat blockage B is treated as a variable.

Selected examples of this form of cross-plotting for the three aspect ratios are presented in Figures 37 through 46. From these forms of presentation of the data, the final performance maps and other cross-plots of use to the designer have been made.

Only selected examples of the cross-plotted and "raw" data are shown in the main text.

Diffuser Performance Maps

Perhaps the most useful presentation of data is in terms of diffuser performance maps such as those given by Reneau et al (1964), shown in Figure 2.

For these performance maps, diffuser pressure recovery coefficient C_p is shown as a function of diffuser geometry (area ratio AR and diffuser length-to-width ratio L/W_1) for a given aspect ratio, inlet Mach number, throat blockage, and Reynolds number. When plotted in this form, pressure recovery C_p appears in the form of "contour hills", from which the performance of straight wall diffusers as a function of the geometric variables and inlet flow conditions can be most easily grasped. The base data are presented in this form for the three aspect ratios studied and for selected values of inlet Mach number and throat blockage. The range of variables on the performance maps is:

inlet Mach number M_t = 0.2, 0.4, 0.6, 0.8, 1.0

throat blockage B = 0.02, 0.04, 0.06, 0.08, 0.10, 0.12

The performance maps for aspect ratio AS = 0.25 are presented in Figures 47 through 76.

The performance maps for aspect ratio AS = 1.0 are presented in Figures 77 through 106.

The performance maps for aspect ratio AS = 5.0 are presented in Figures 107 through 136.

Aspect Ratio

The designer needs performance maps with a range of geometric and inlet parameters permitting a rational interpolation of diffuser performance between the available data. Values of blockage and inlet Mach number used in the present studies are sufficient to interpolate among these parameters. However, diffuser data are available only for aspect ratio = 0.25, 1.0, and 5.0 (for high inlet Mach number and blockage). Because pressure recovery is a strong function of aspect ratio, a greater amount of aspect ratio data would be desirable, particularly in the selection of the geometry for peak recovery. A significant variation in the shape and location of the pressure recovery "hills" occurs with a change in aspect ratio (and also with blockage and inlet Mach number). One of the most important factors related to diffuser design is the change in the magnitude and location of the geometry for peak recovery that occurs with a change in aspect ratio alone (holding blockage and Mach number fixed); i.e., a significant shifting occurs in the shape and location of the pressure recovery "hills". (A related factor is the change in pressure recovery for a fixed geometry, area ratio and length-to-width ratio constant, at a fixed Mach number and throat blockage as only diffuser aspect ratio is altered.)

The plots presented in Figures 137 through 141 show peak pressure recovery as a function of aspect ratio, with blockage as a variable for constant values of inlet Mach number.

It should be noted that for the three aspect ratio geometries studied, the range of geometric variables has been sufficient to find the peak recovery geometry only for the aspect ratio = 1.0 diffusers. For the aspect ratio = 0.25 and 5.0 diffusers, the highest L/W_1 values studied probably lie close to the peak recovery point on the performance maps. However, pressure recovery is still increasing above the highest L/W_1 values tested. For this reason, the cross-plots showing peak recovery may not actually show the highest recovery for the aspect ratio = 0.25 and 5.0 diffusers. In preparing these cross-plots, the highest values of pressure recovery actually measured (and their associated geometries in terms of L/W_1 and 2θ) have been used.

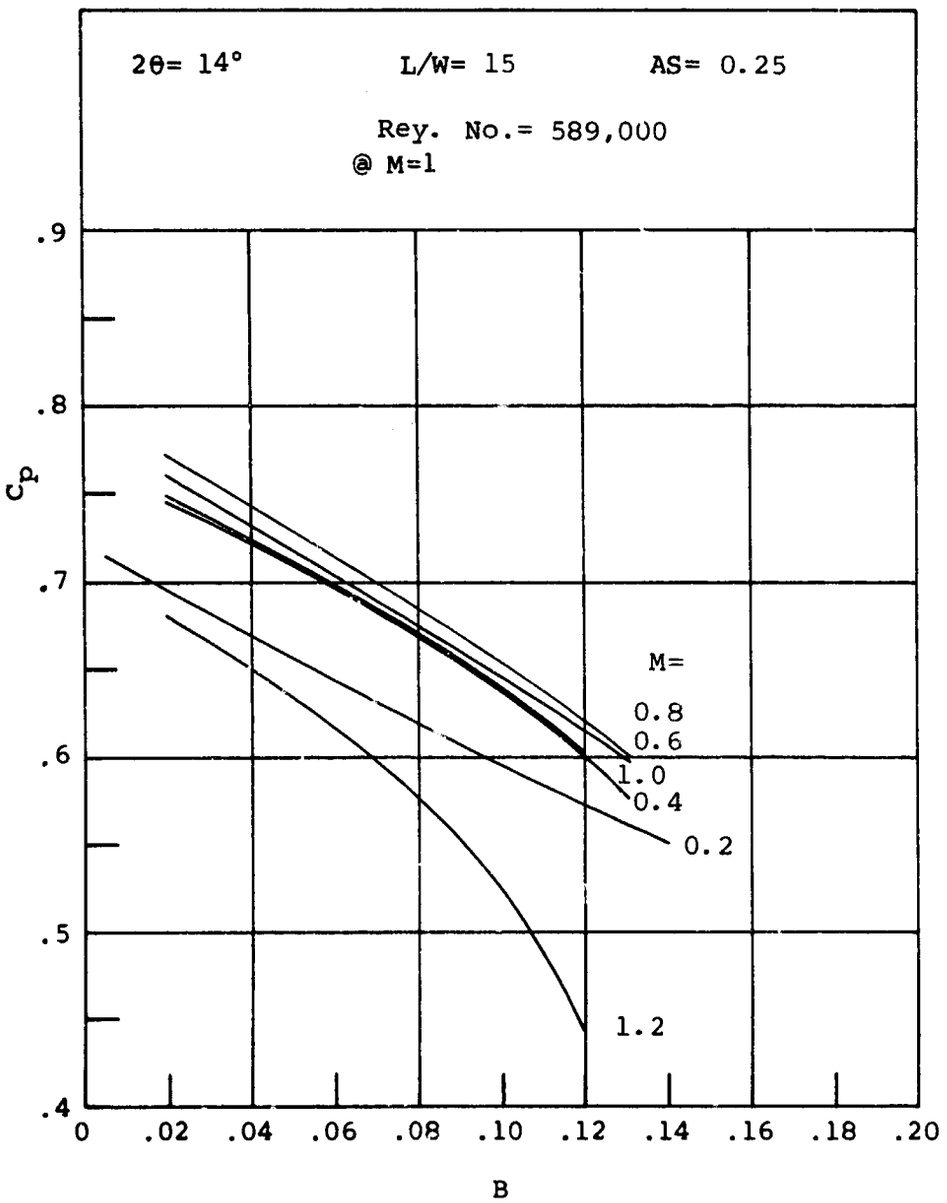

Figure 37. Pressure Recovery Versus Blockage. Aspect Ratio = 0.25.

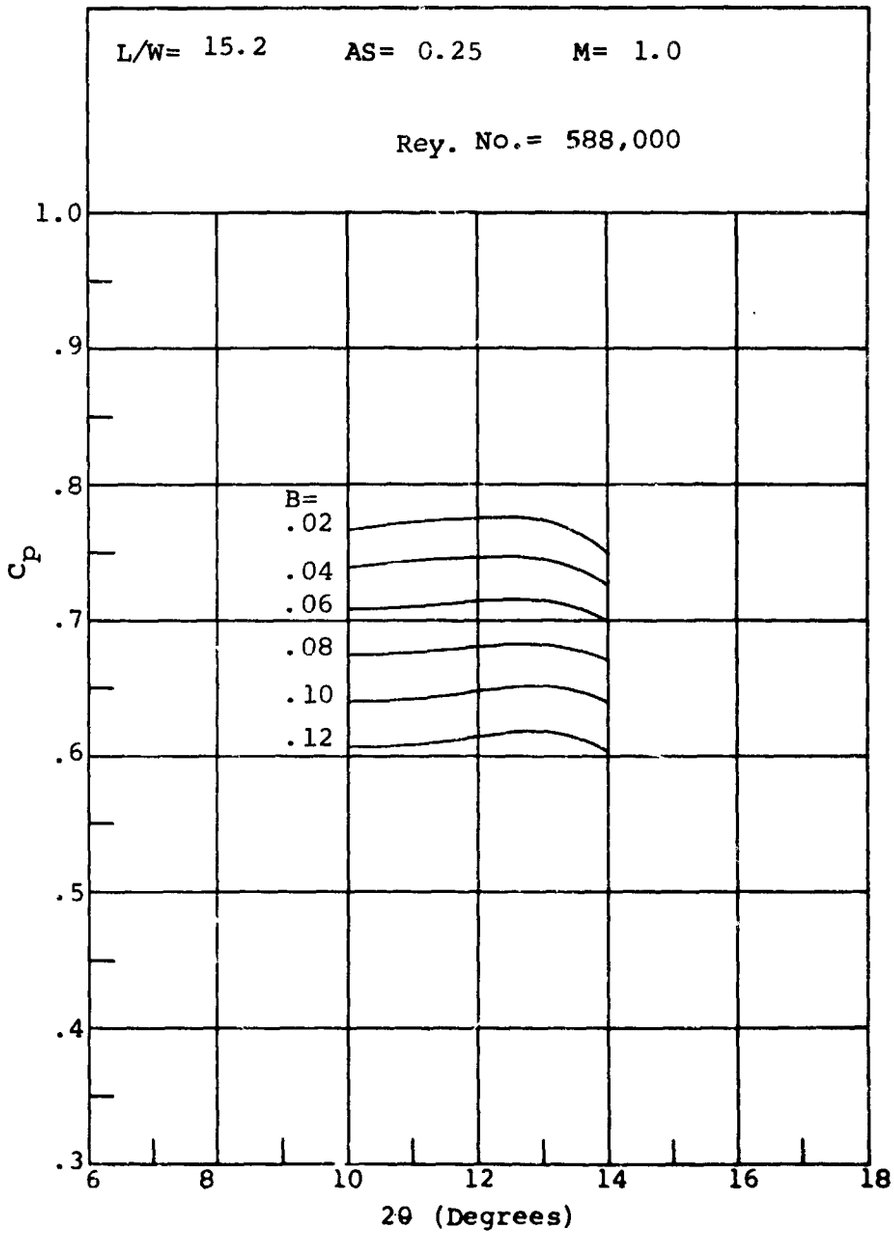

Figure 38. Pressure Recovery Versus Divergence Angle. Aspect Ratio = 0.25.

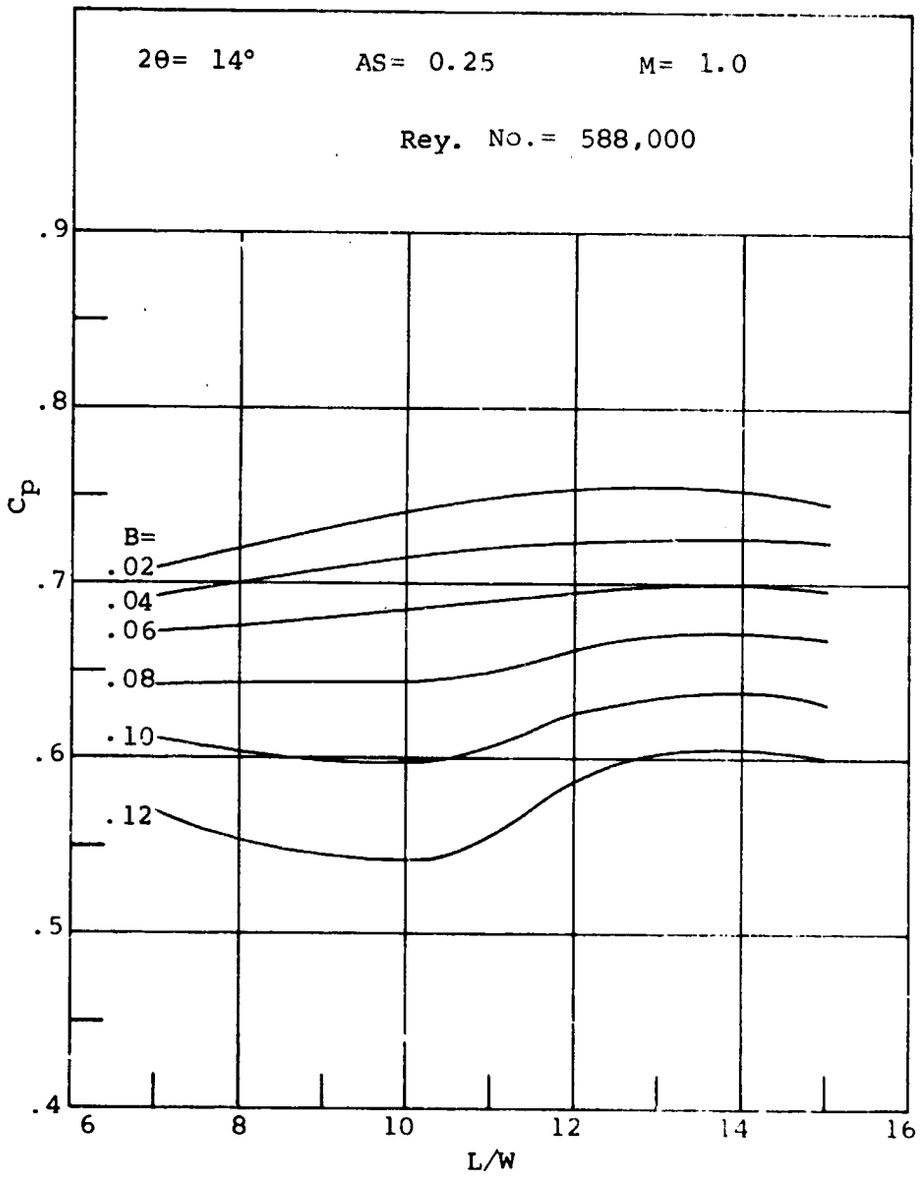

Figure 39. Pressure Recovery Versus Length-to-Throat Width Ratio. Aspect Ratio = 0.25.

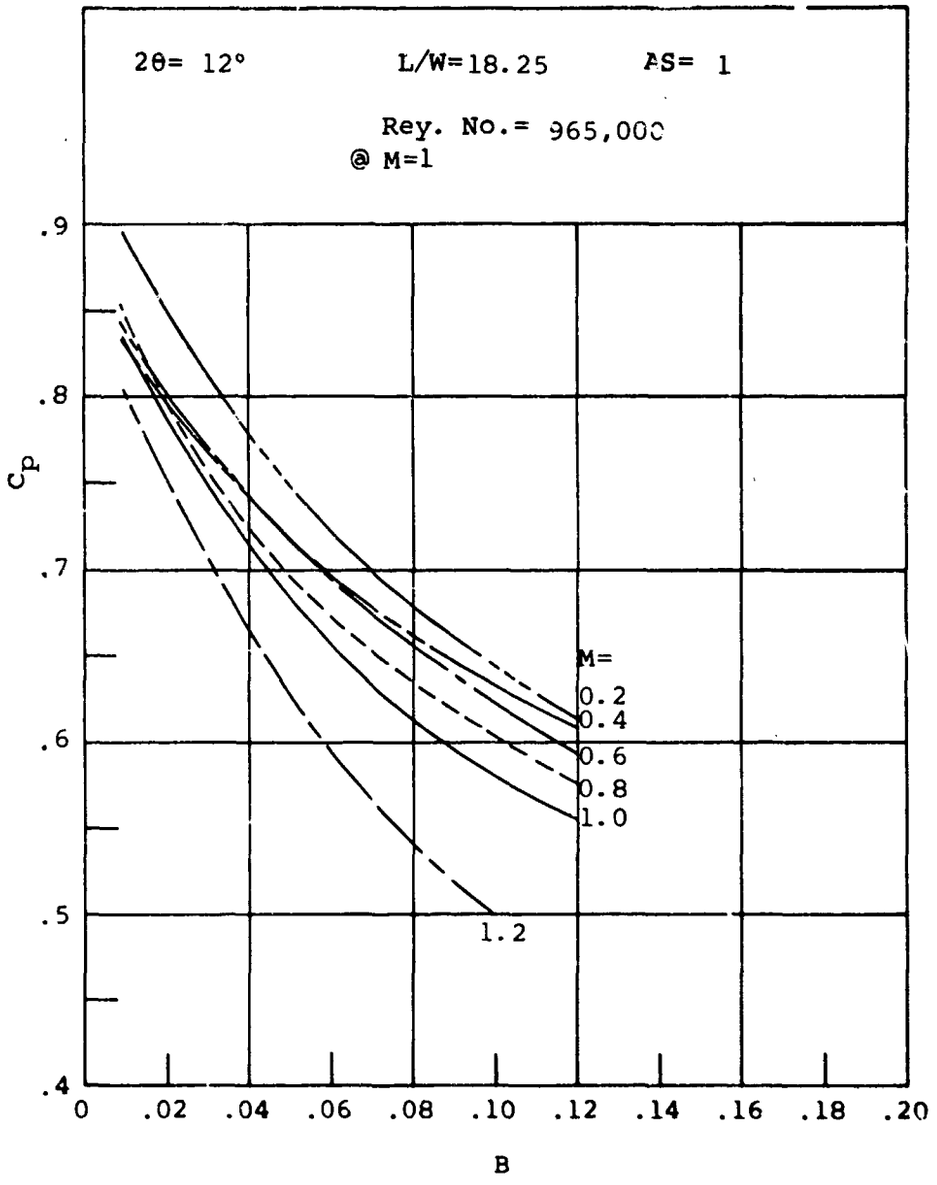

Figure 40. Pressure Recovery Versus Blockage. Aspect Ratio = 1.0.

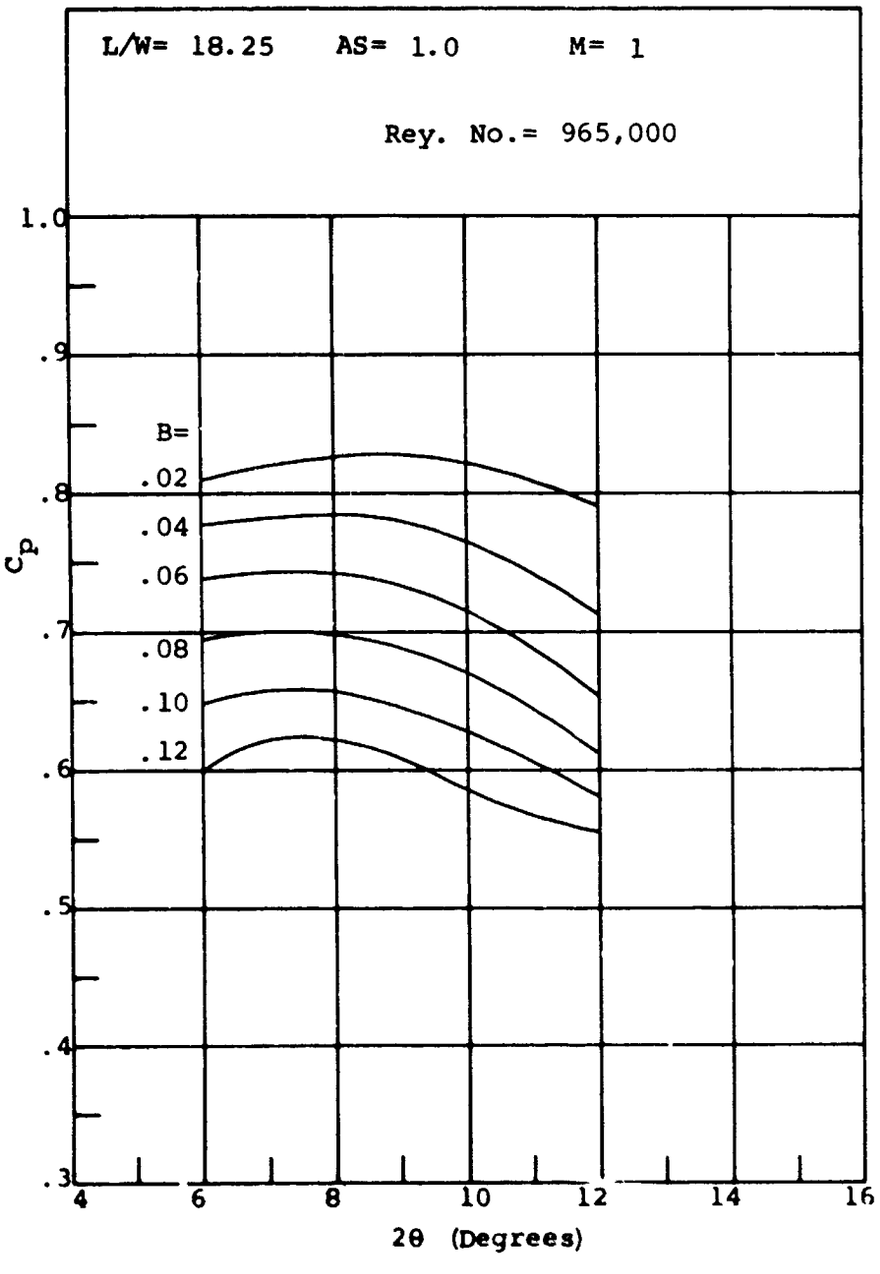

Figure 41. Pressure Recovery Versus Divergence Angle. Aspect Ratio = 1.0.

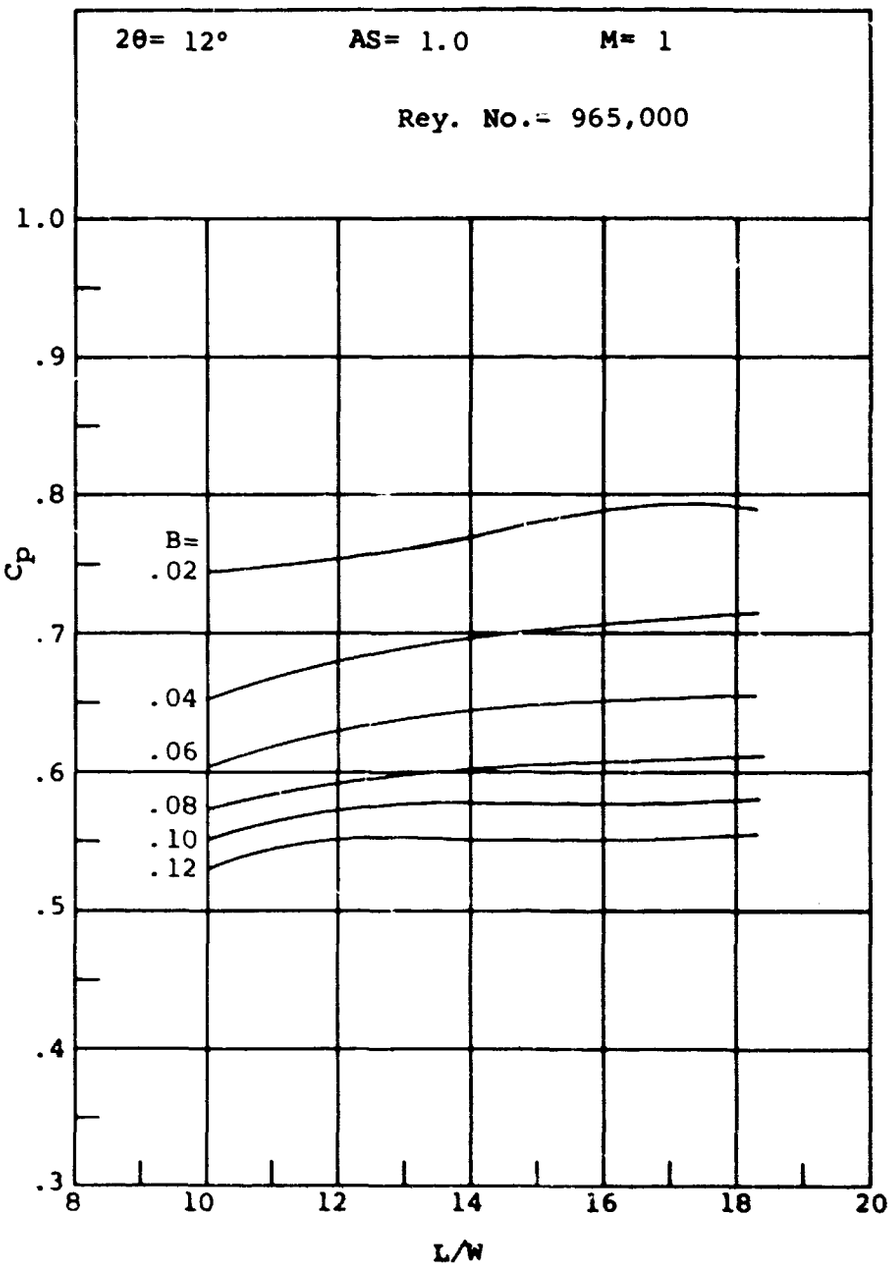

Figure 42. Pressure Recovery Versus Length-to-Throat Width Ratio. Aspect Ratio = 1.0.

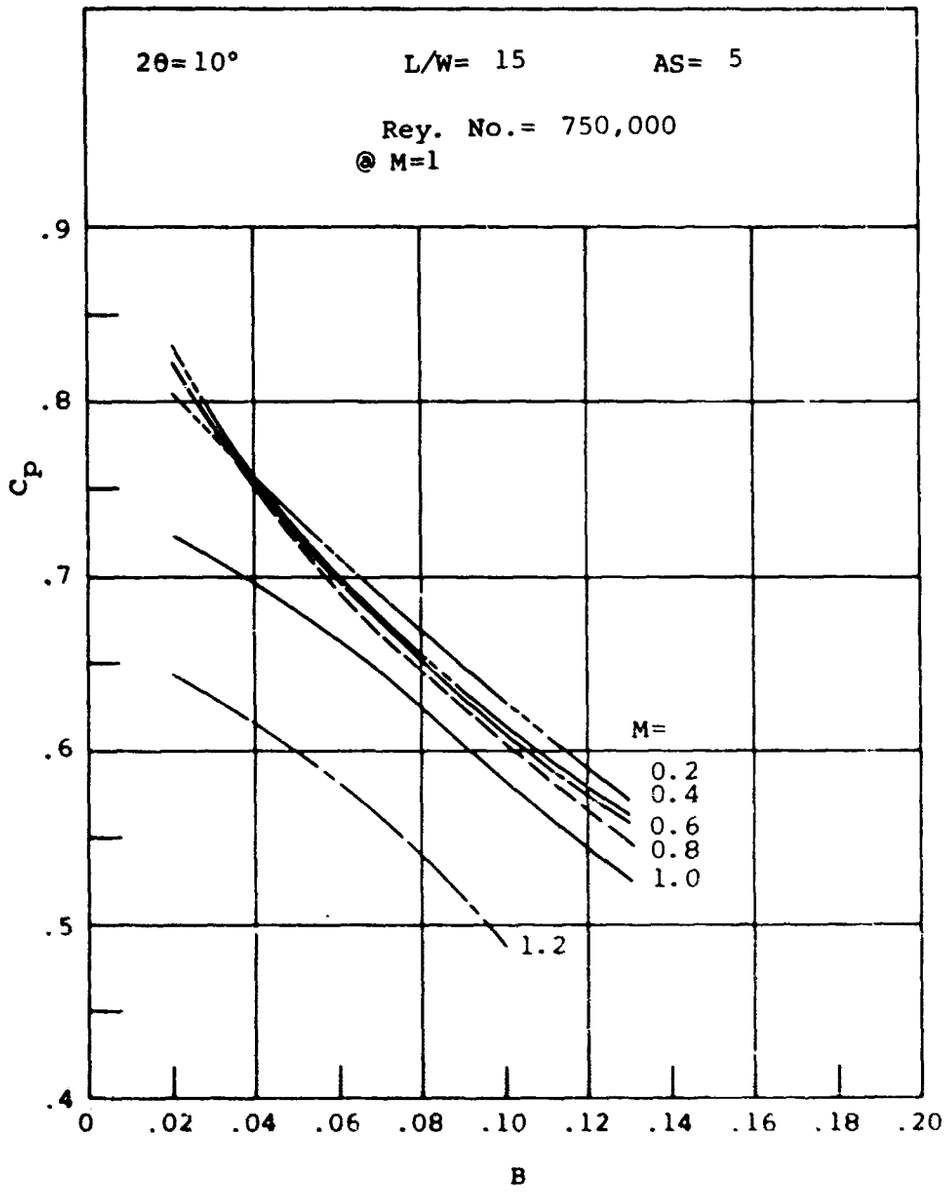

Figure 43. Pressure Recovery Versus Blockage. Aspect Ratio = 5.0.

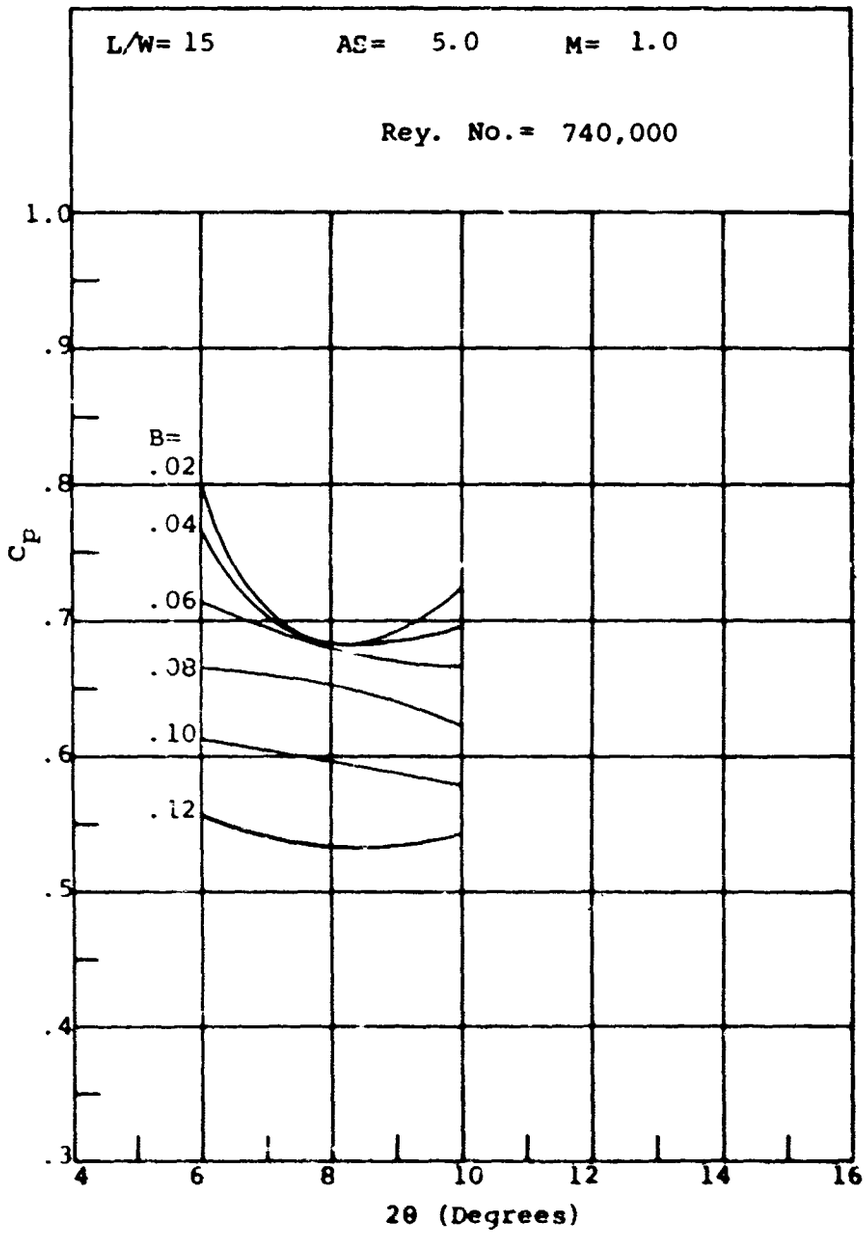

Figure 44. Pressure Recovery Versus Divergence Angle. Aspect Ratio = 5.0.

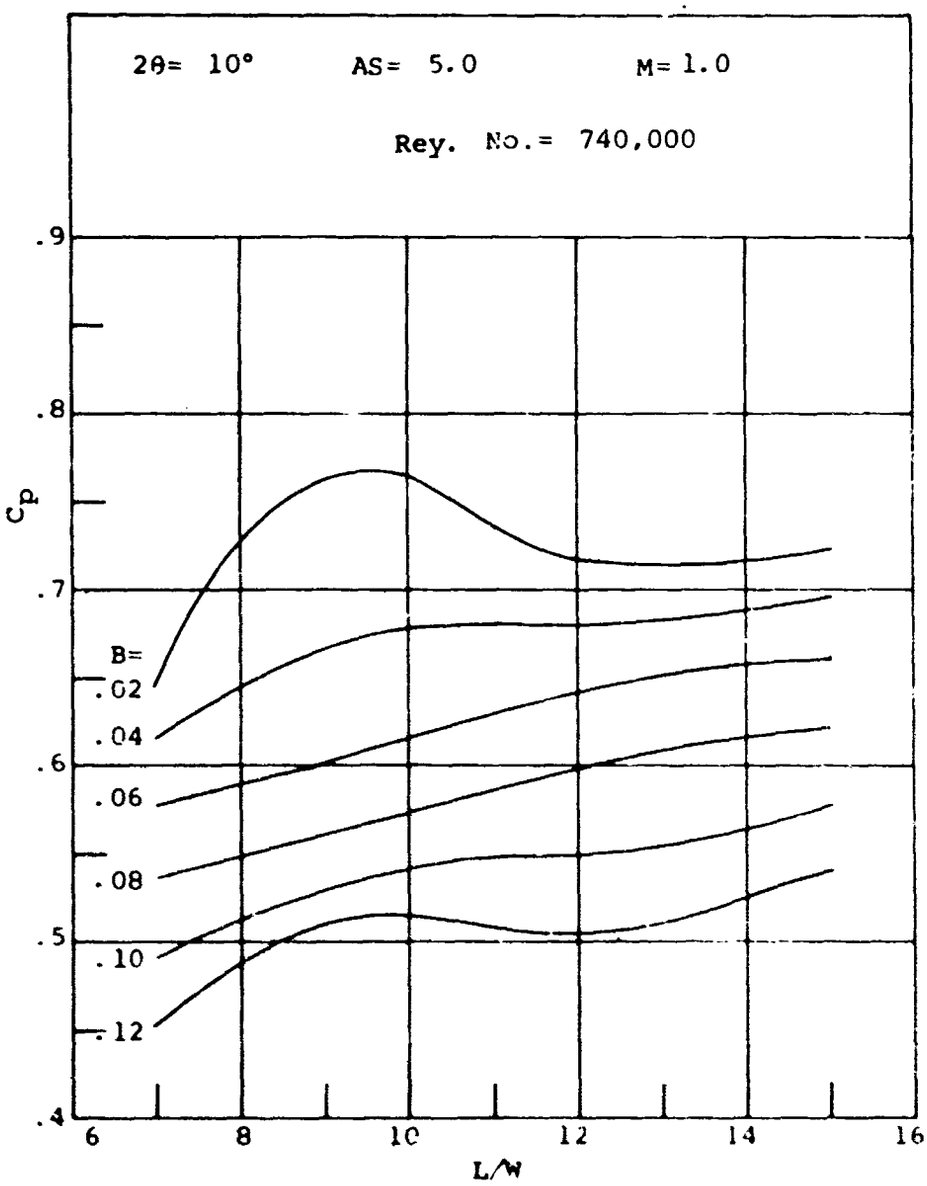

Figure 45. Pressure Recovery Versus Length-to-Throat Width Ratio. Aspect Ratio = 5.0.

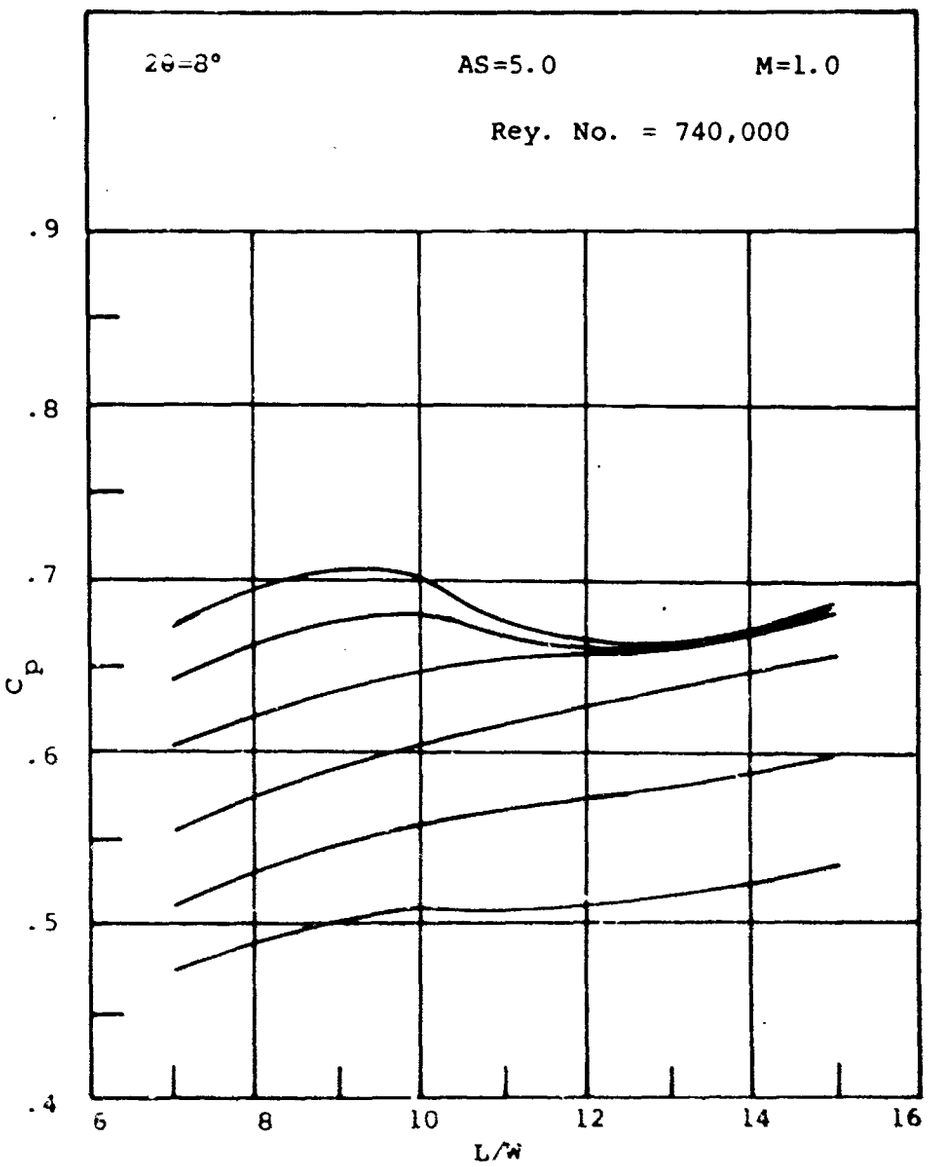

Figure 46. Pressure Recovery Versus Length-to-Throat Width Ratio. Aspect Ratio = 5.0.

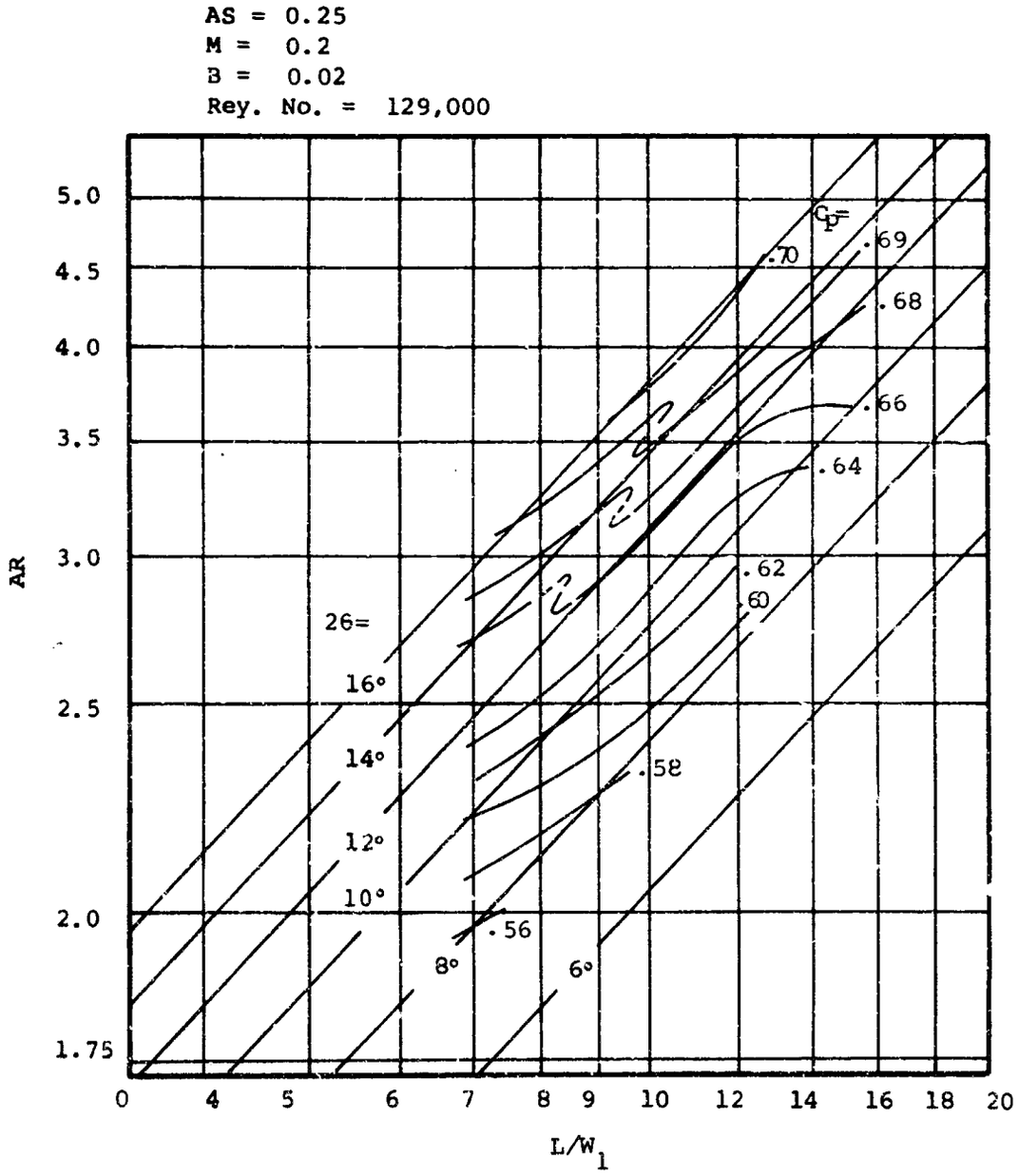

Figure 47. Performance Map - Aspect Ratio = 0.25.

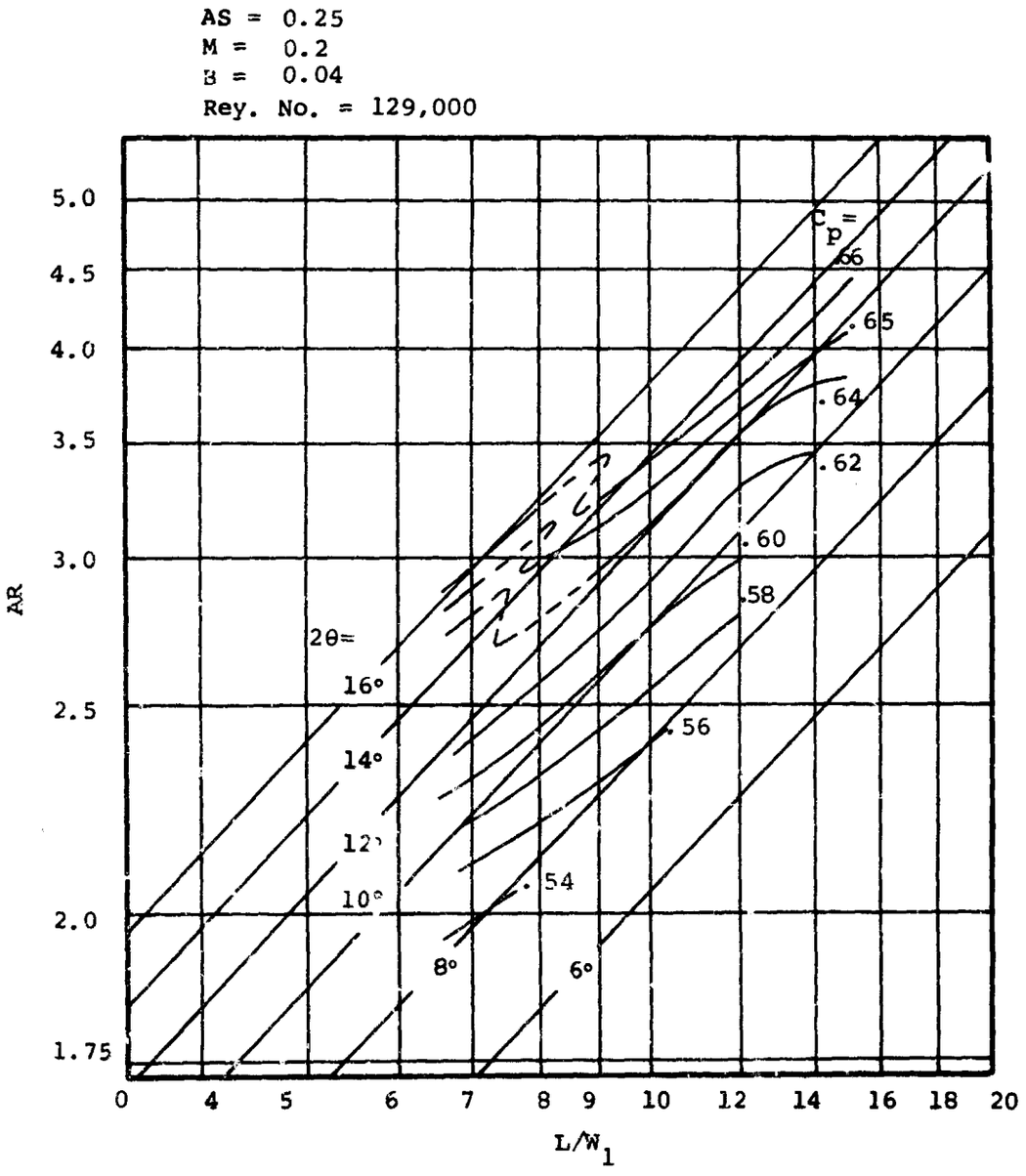

Figure 48. Performance Map - Aspect Ratio = 0.25.

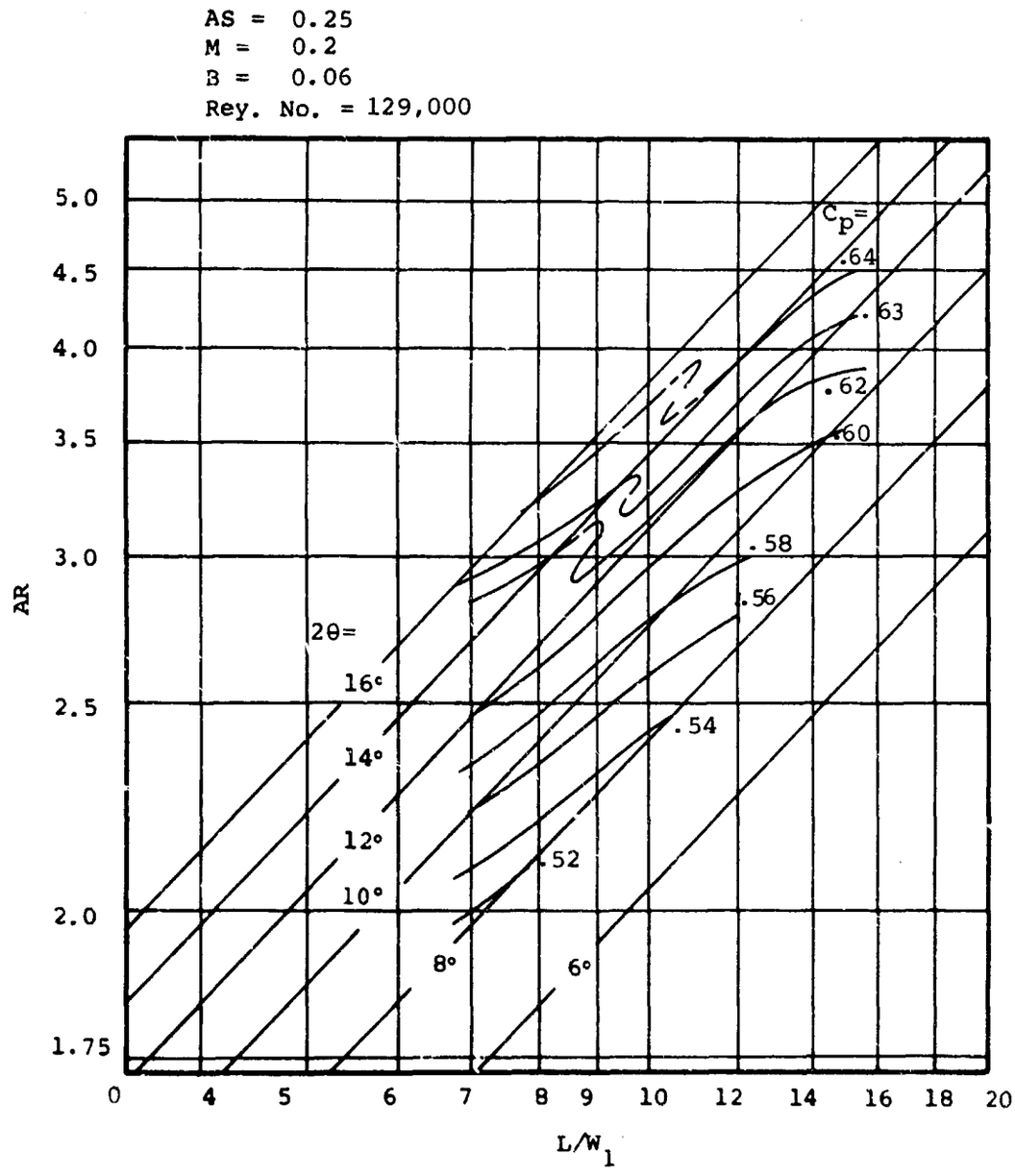

Figure 49. Performance Map - Aspect Ratio = 0.25.

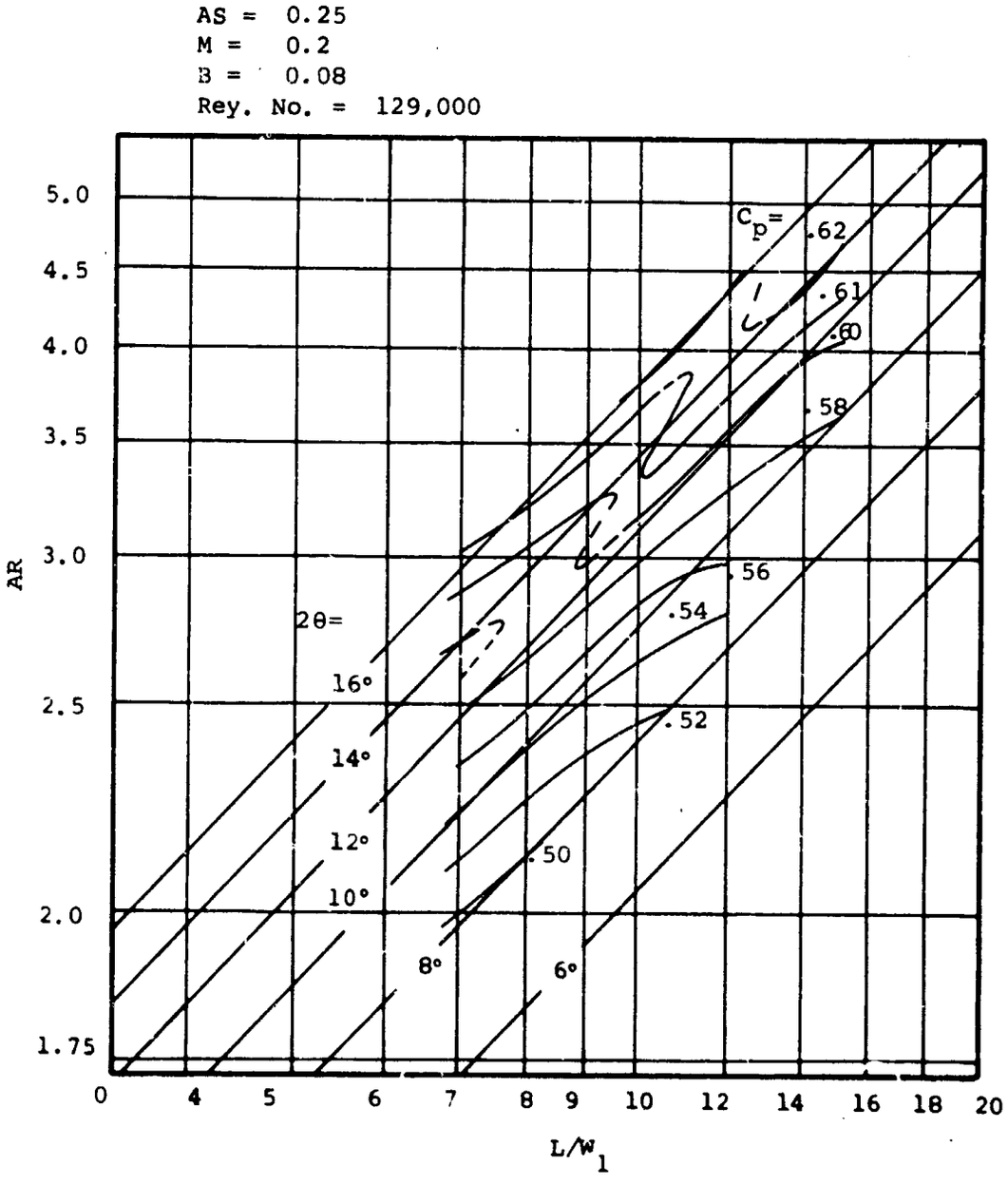

Figure 50. Performance Map - Aspect Ratio = 0.25.

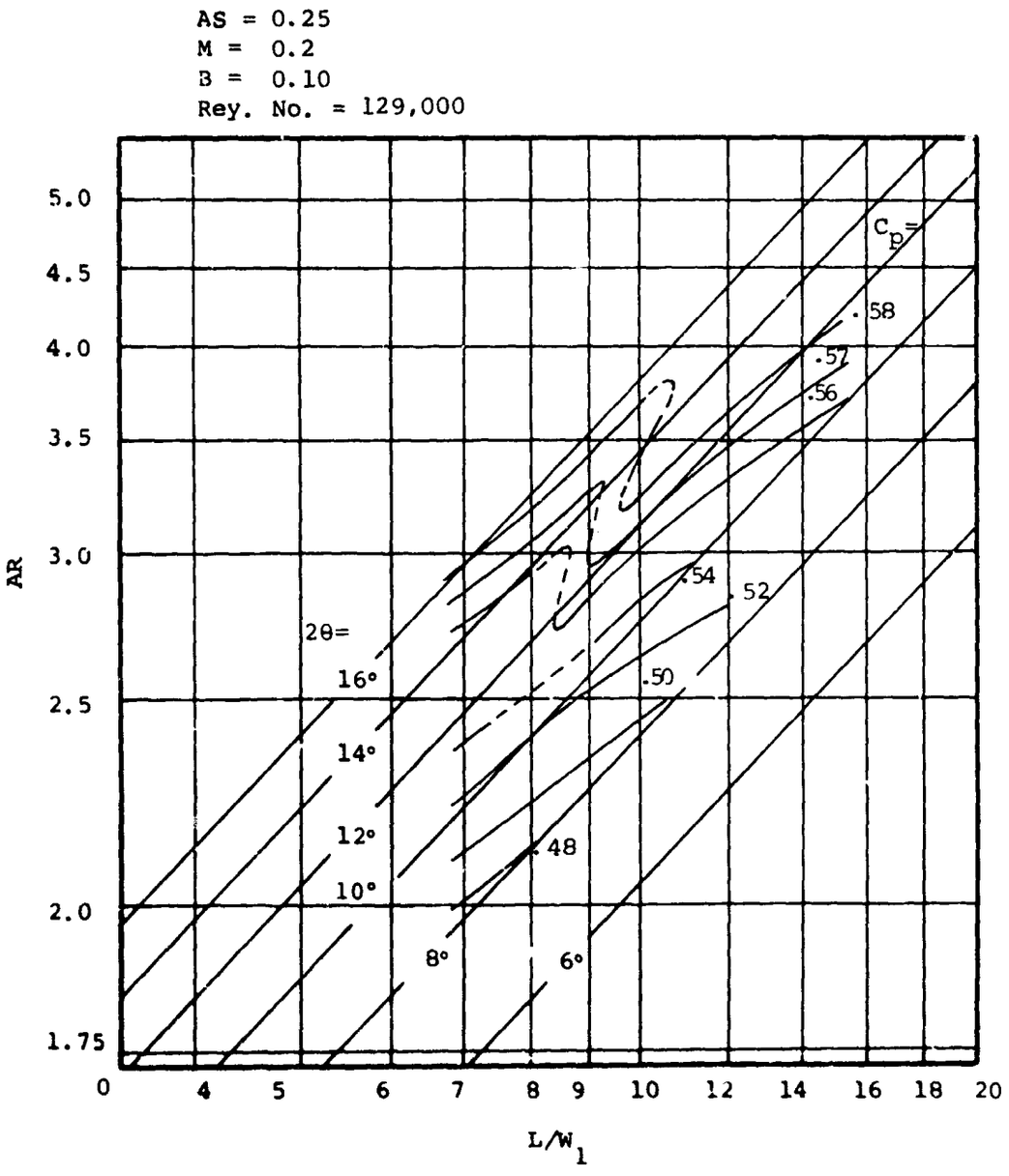

Figure 51. Performance Map - Aspect Ratio = 0.25.

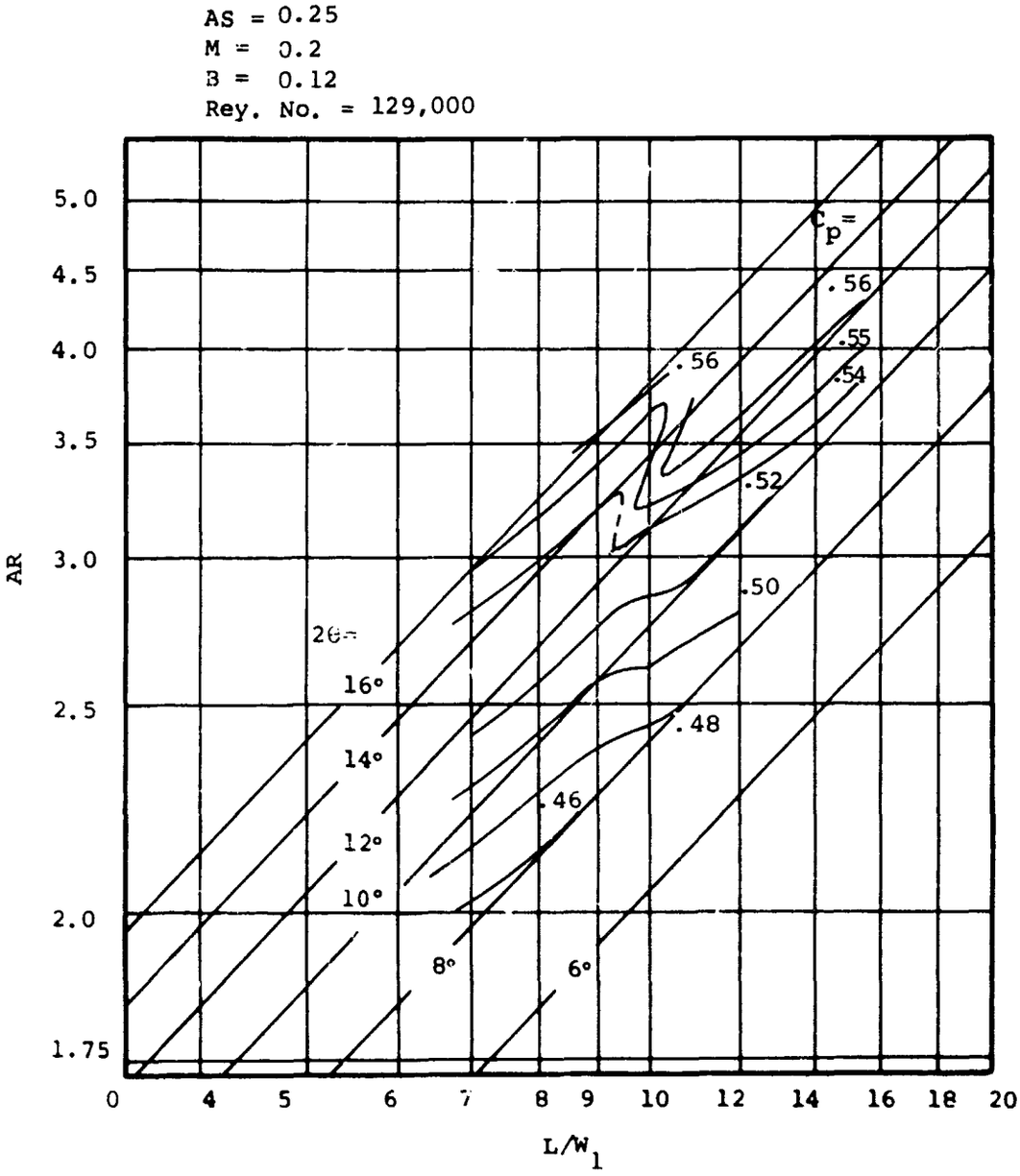

Figure 52. Performance Map - Aspect Ratio = 0.25.

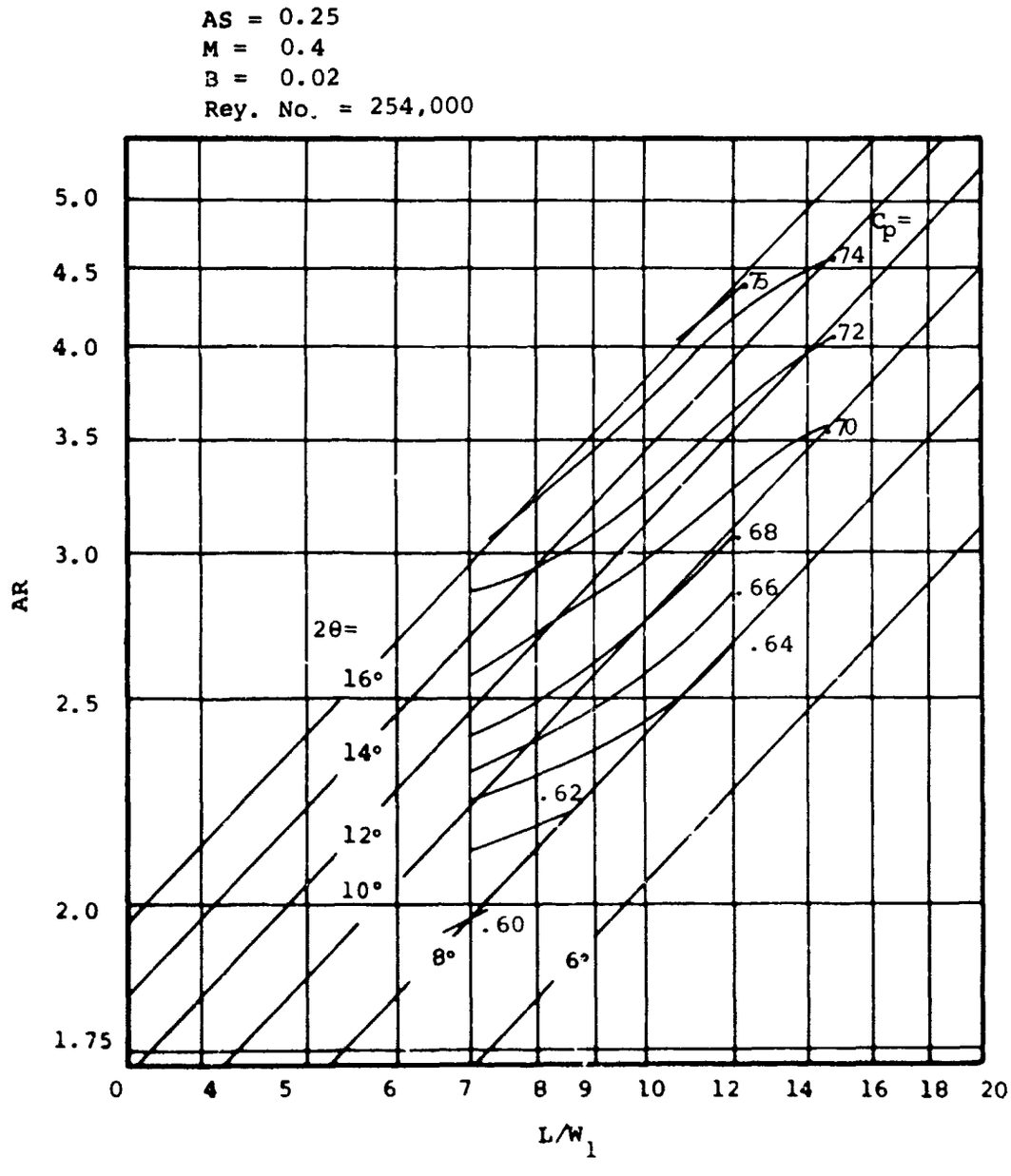

Figure 53. Performance Map - Aspect Ratio = 0.25.

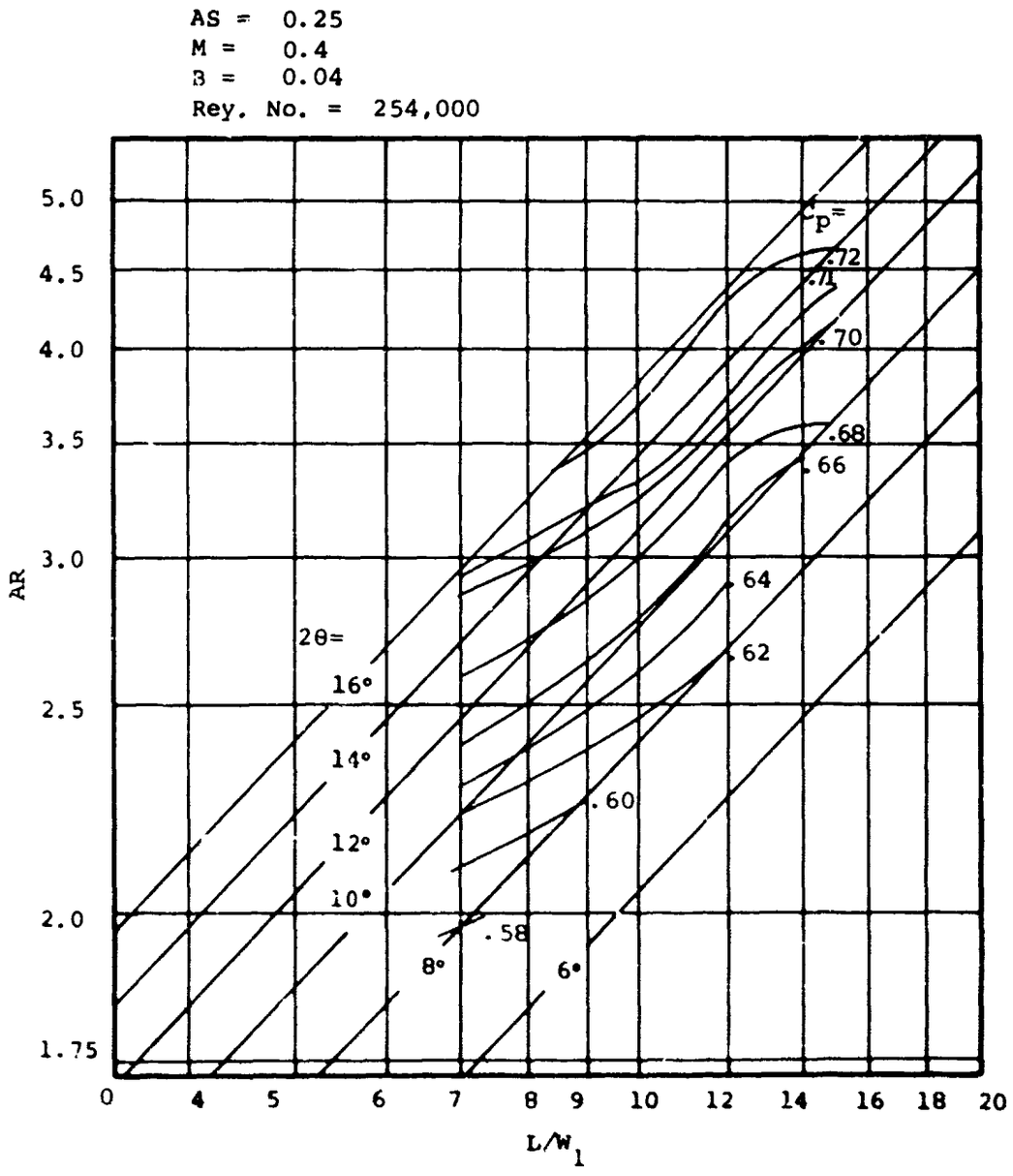

Figure 54. Performance Map - Aspect Ratio = 0.25.

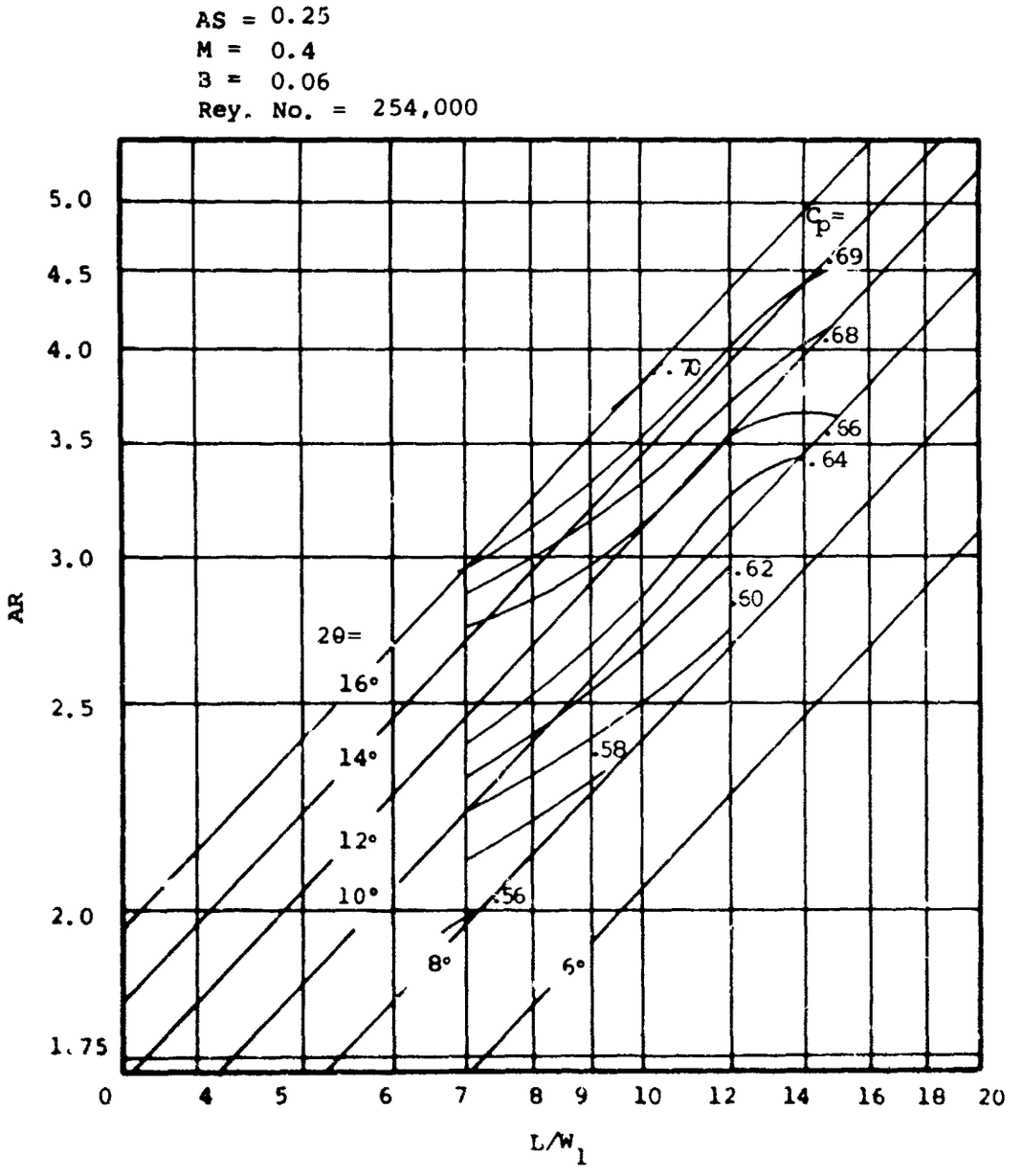

Figure 55. Performance Map - Aspect Ratio = 0.25.

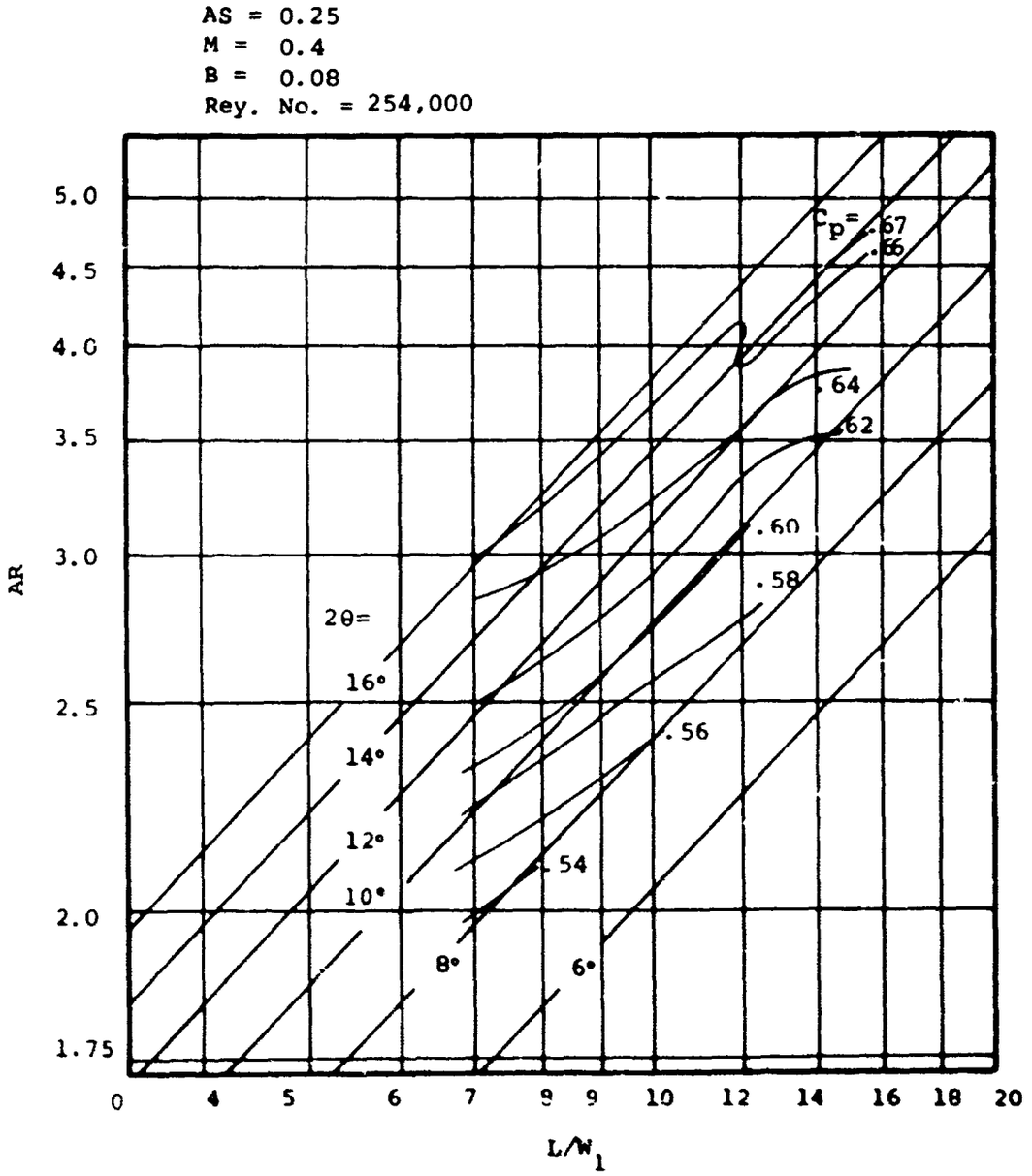

Figure 56. Performance Map - Aspect Ratio = 0.25.

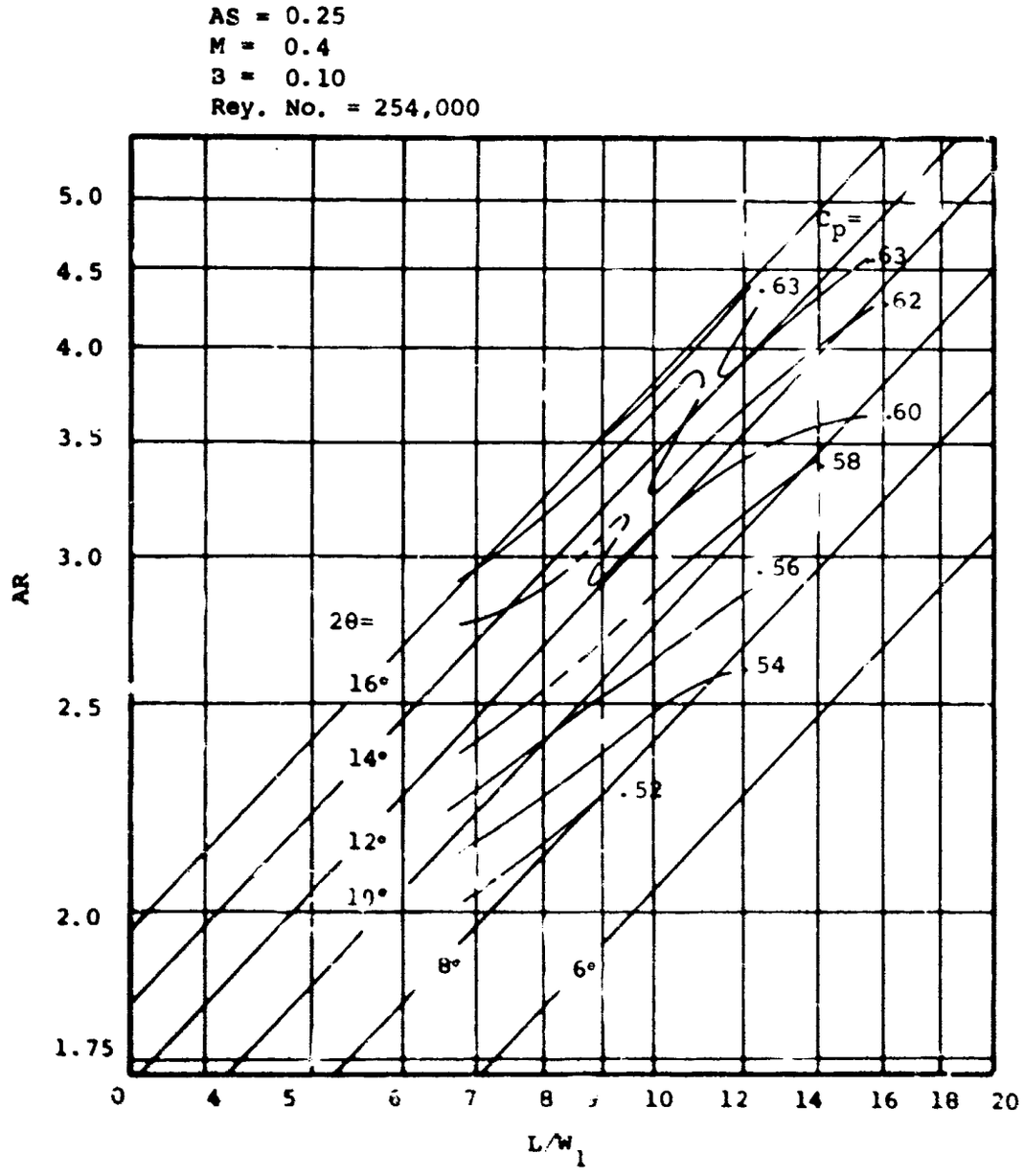

Figure 57. Performance Map - Aspect Ratio = 0.25.

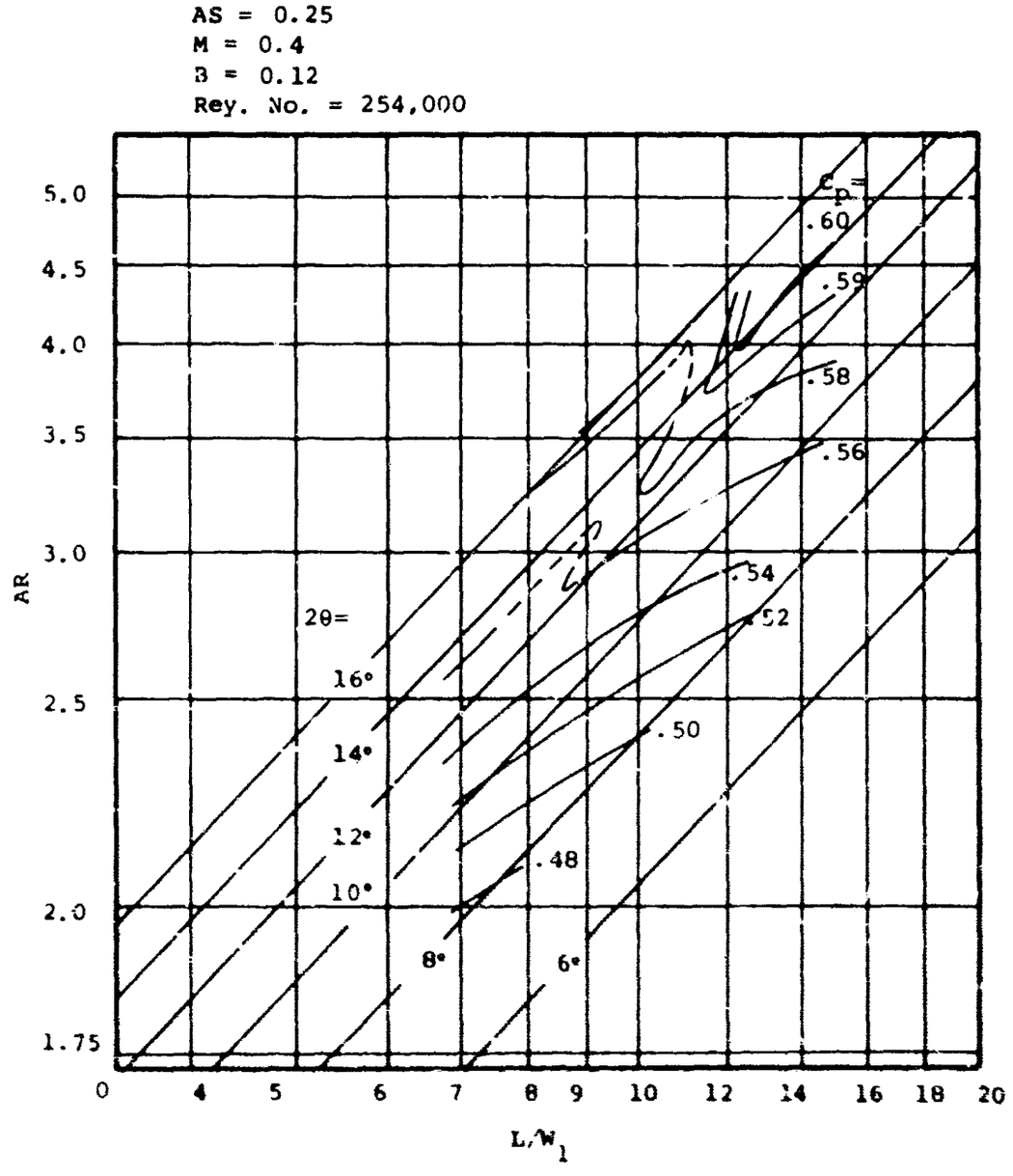

Figure 58. Performance Map - Aspect Ratio = 0.25.

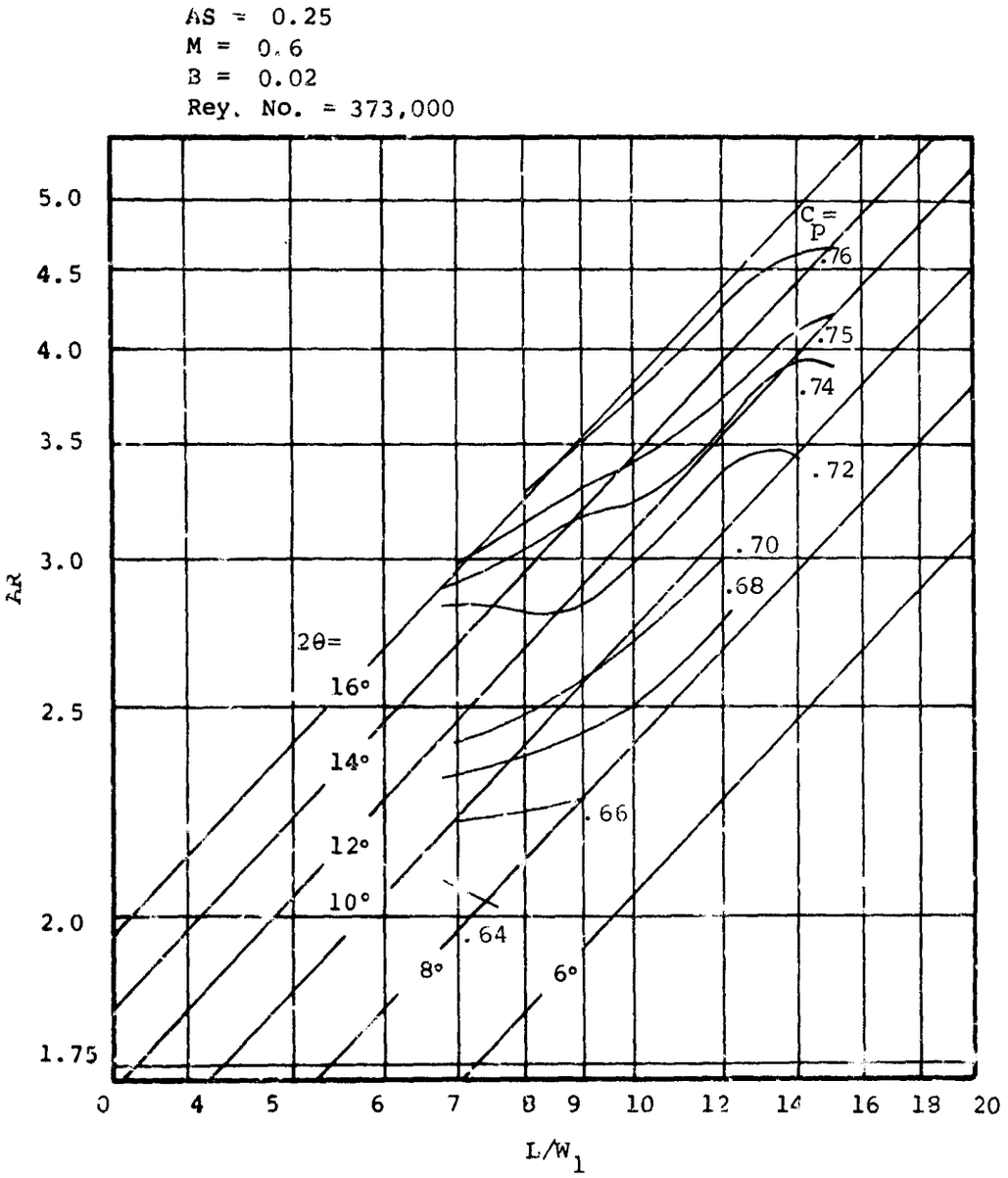

Figure 59. Performance Map - Aspect Ratio = 0.25.

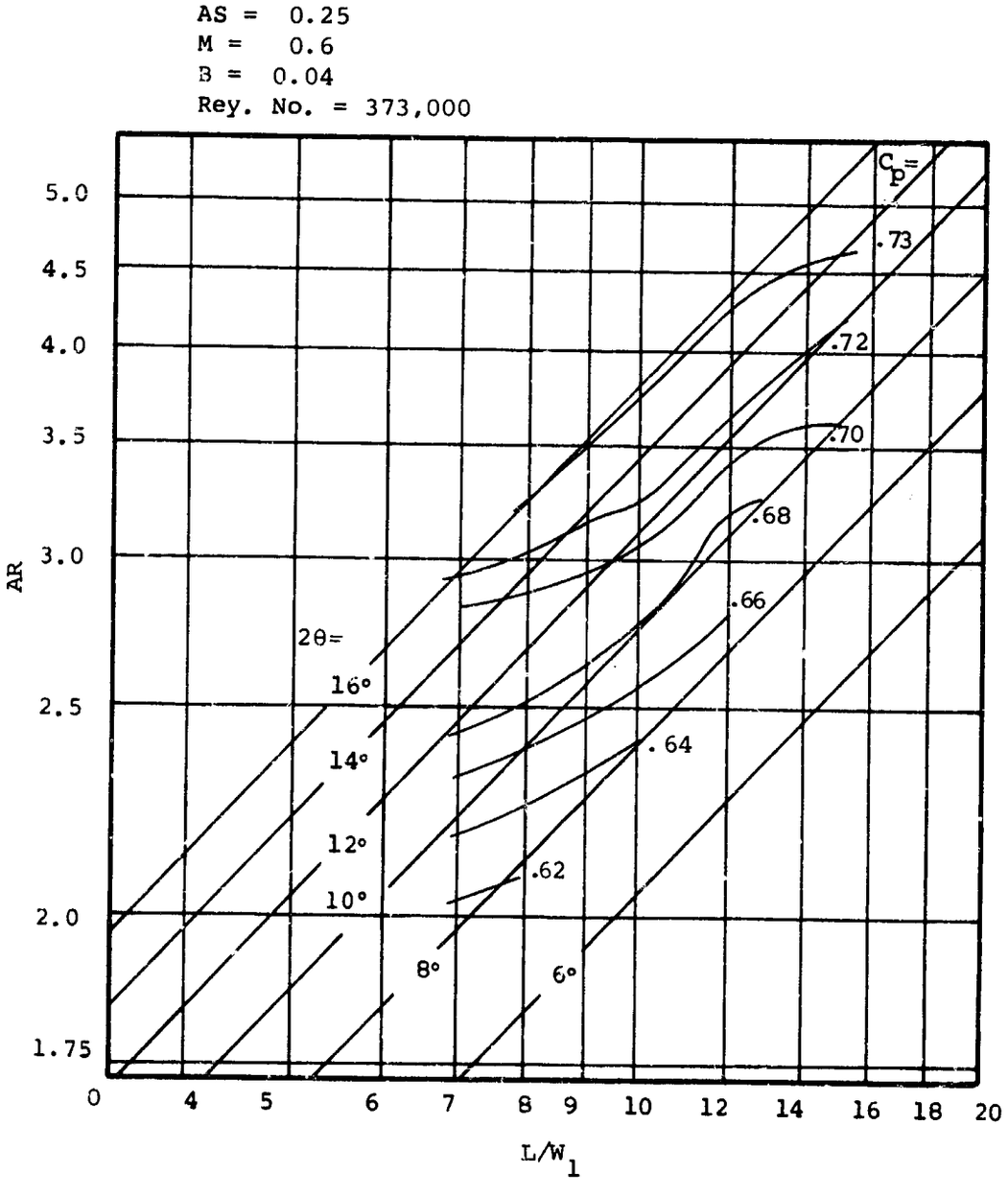

Figure 60. Performance Map - Aspect Ratio = 0.25.

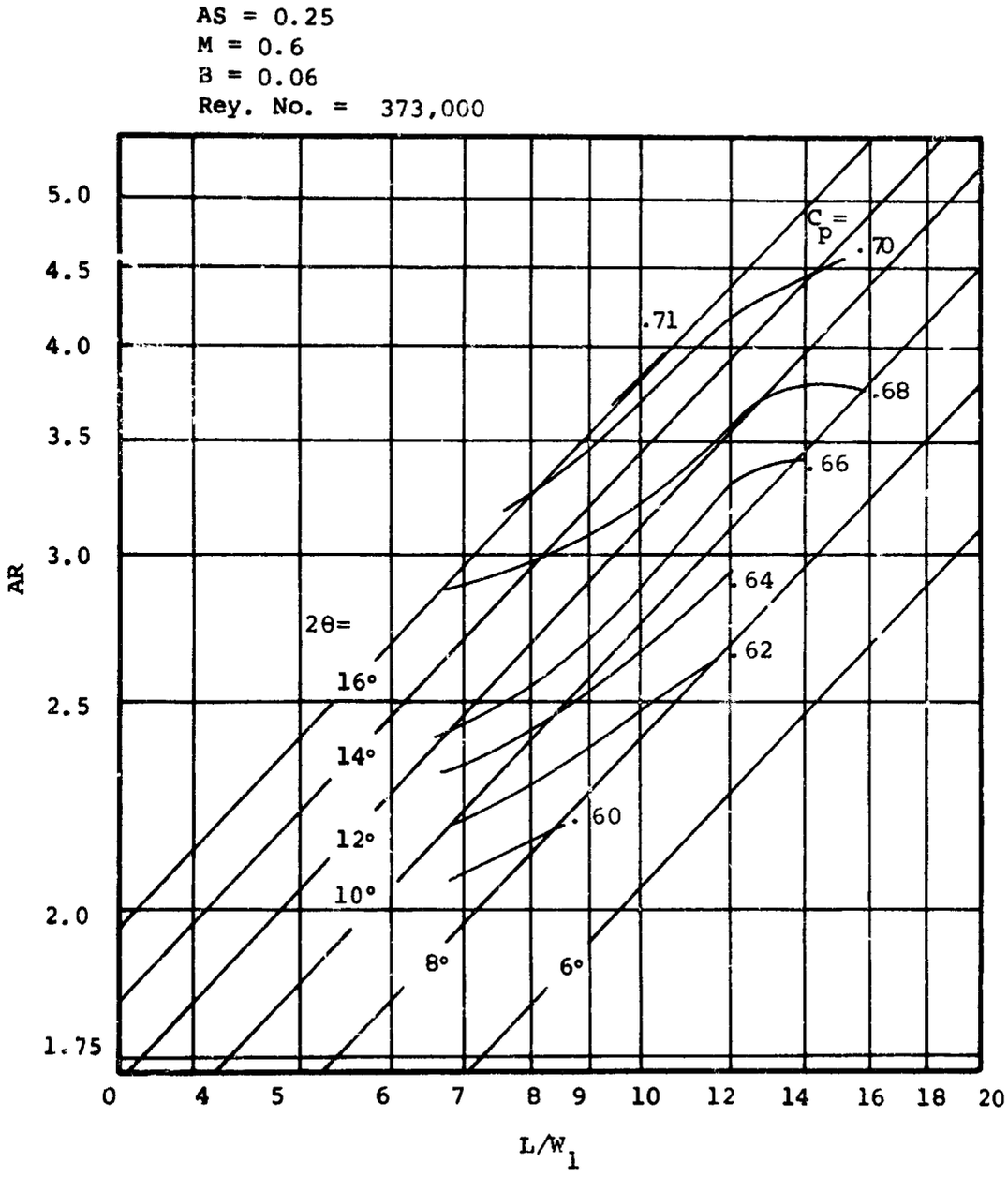

Figure 61. Performance Map - Aspect Ratio = 0.25.

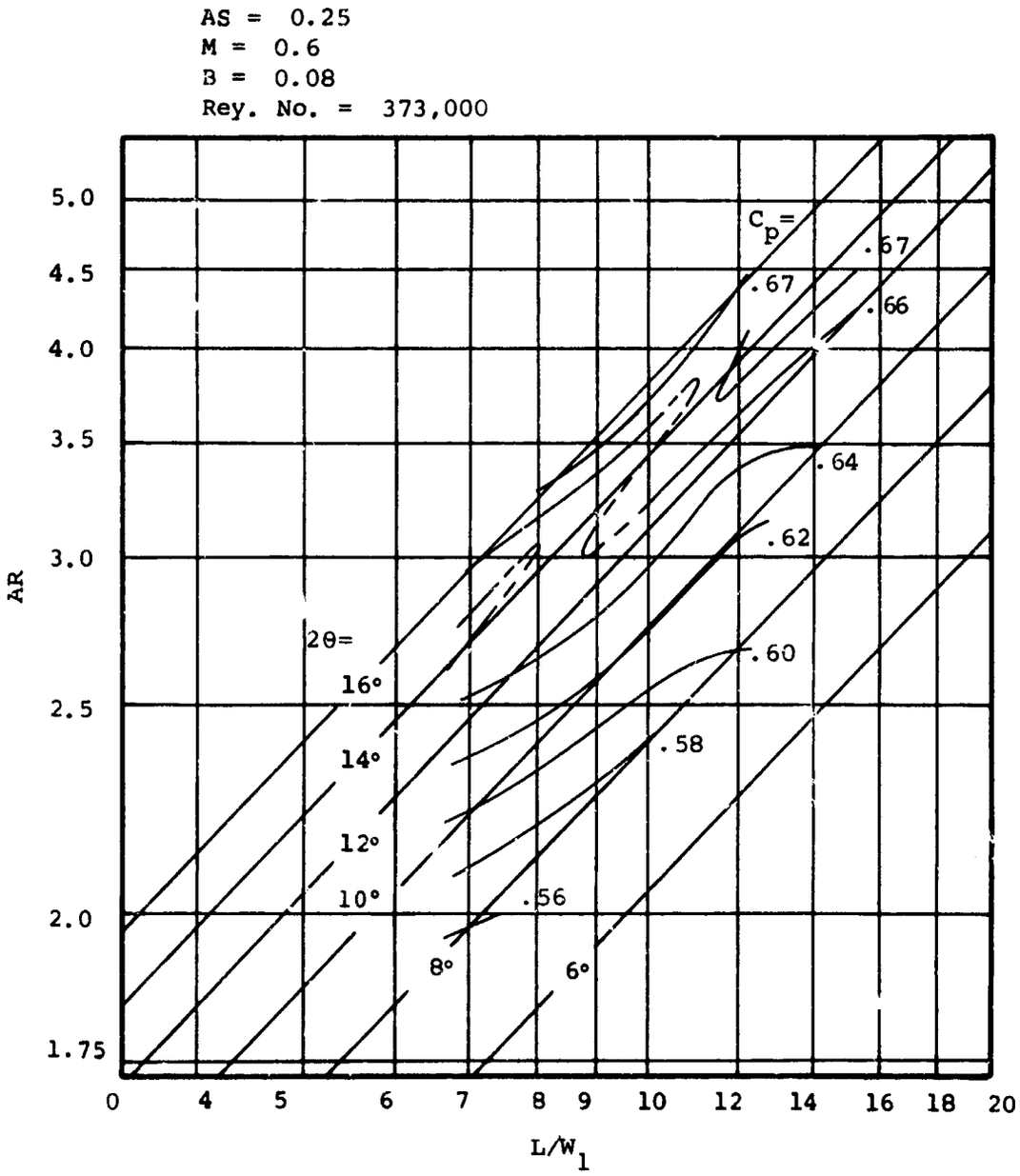

Figure 62. Performance Map - Aspect Ratio = 0.25.

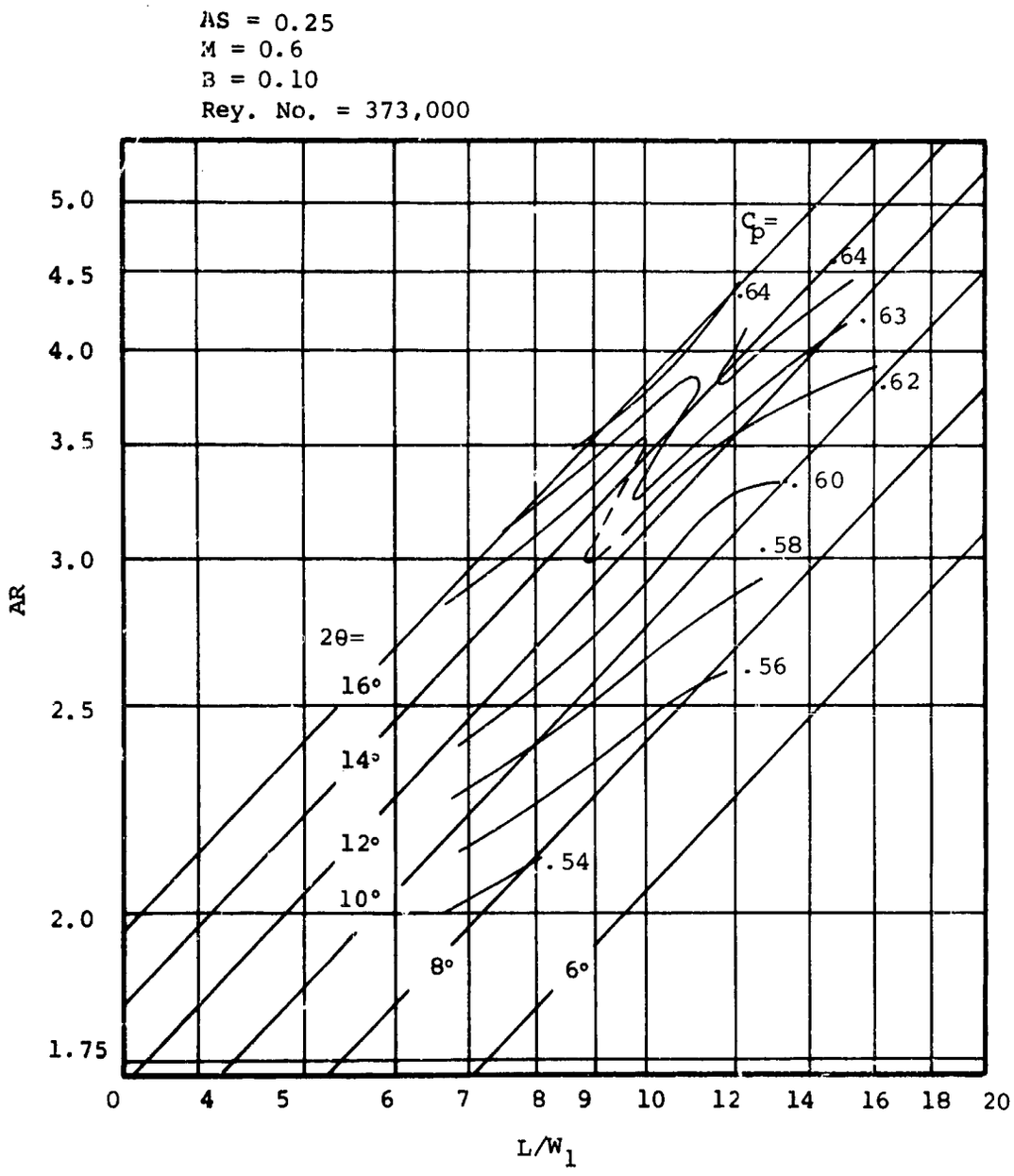

Figure 63. Performance Map - Aspect Ratio = 0.25.

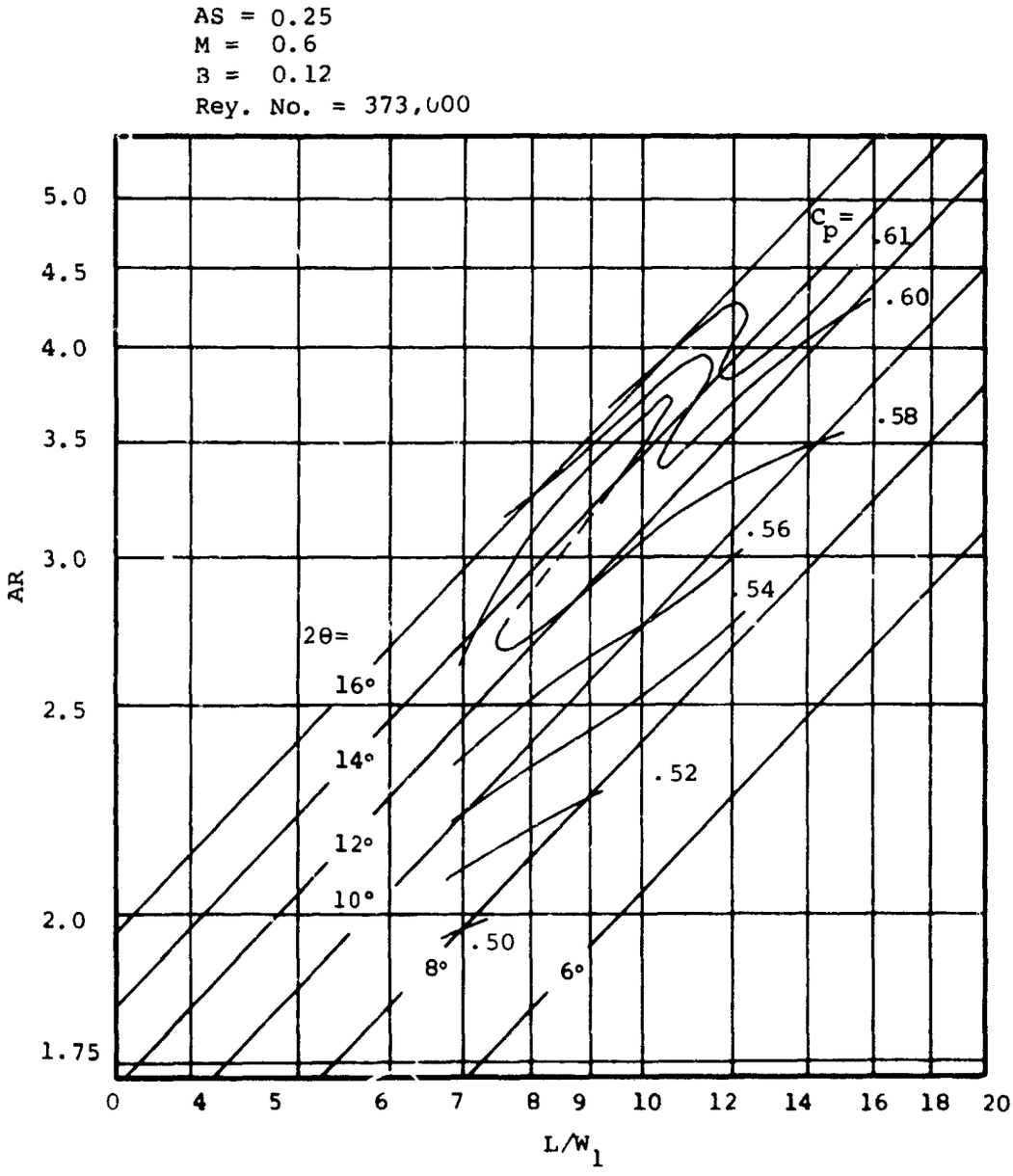

Figure 64. Performance Map - Aspect Ratio = 0.25.

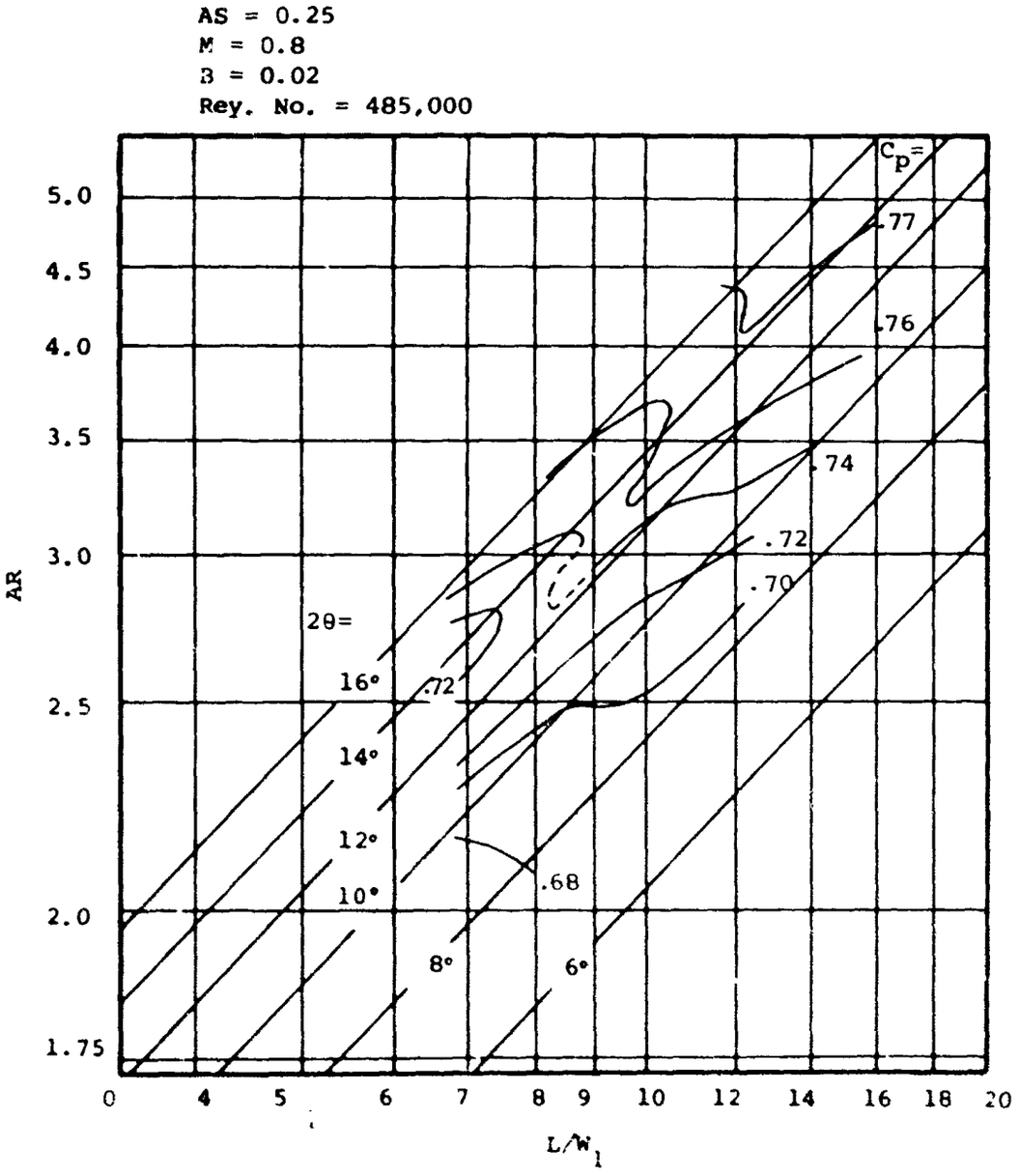

Figure 65. Performance Map - Aspect Ratio = 0.25.

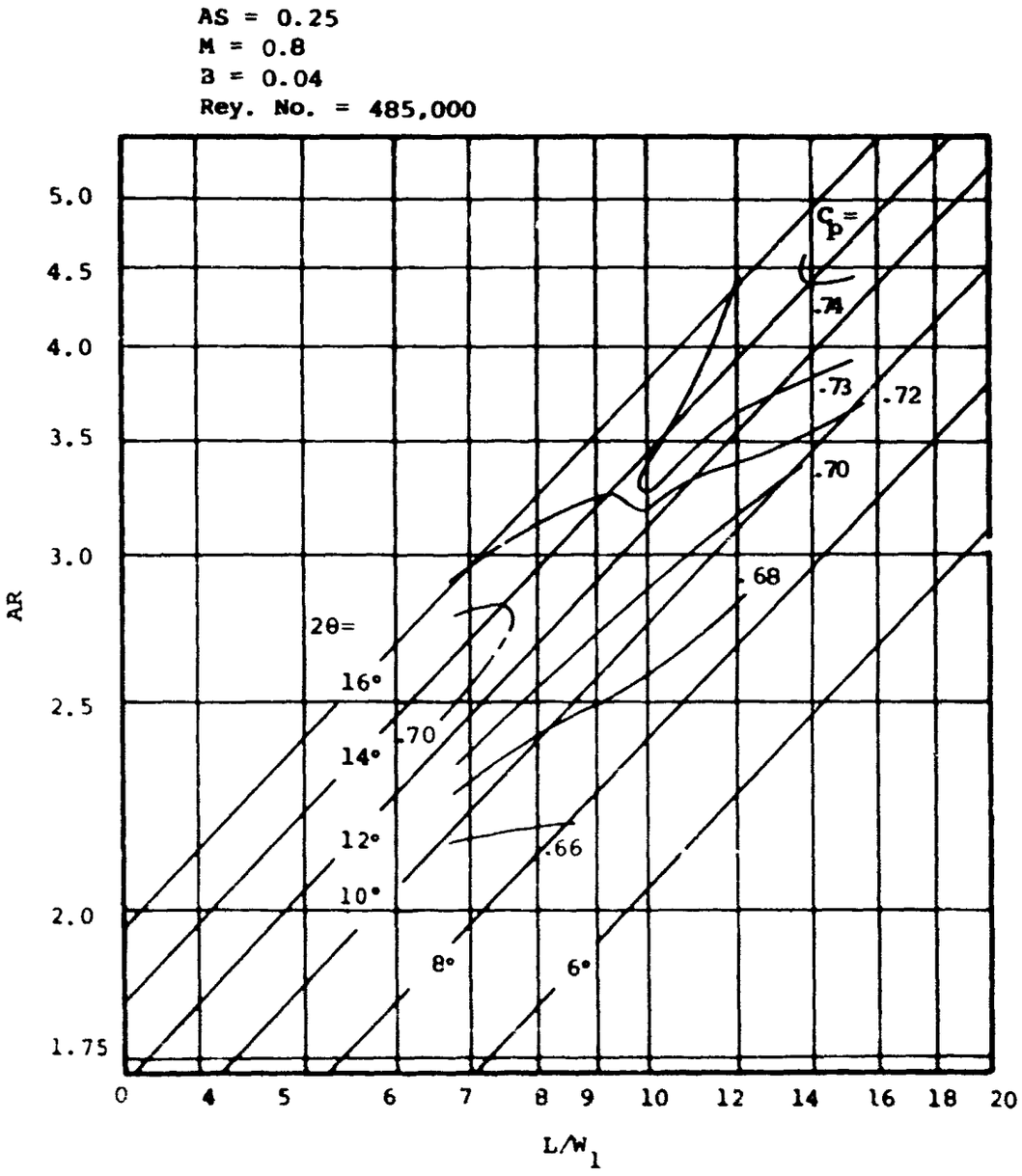

Figure 66. Performance Map - Aspect Ratio = 0.25.

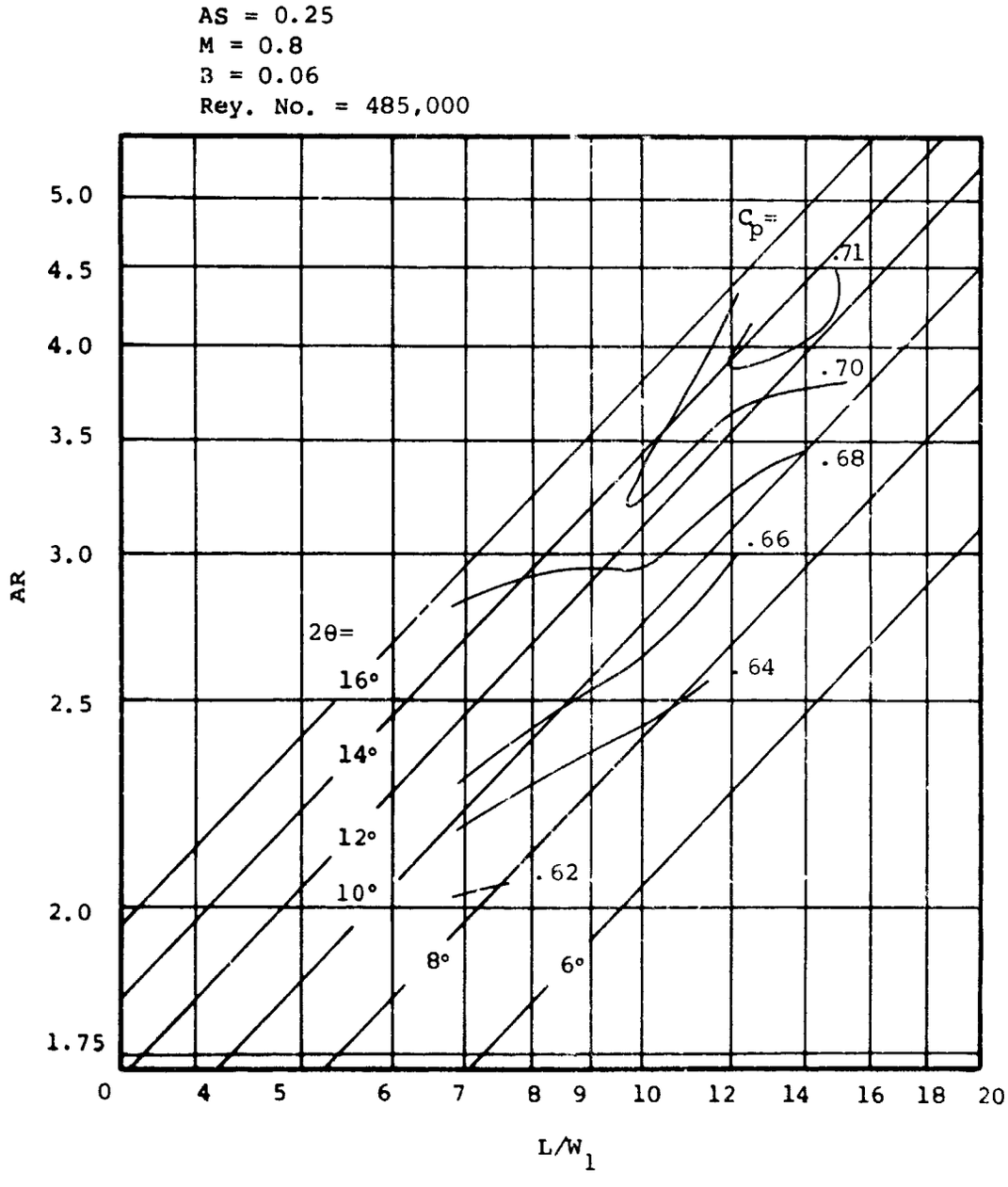

Figure 67. Performance Map - Aspect Ratio = 0.25.

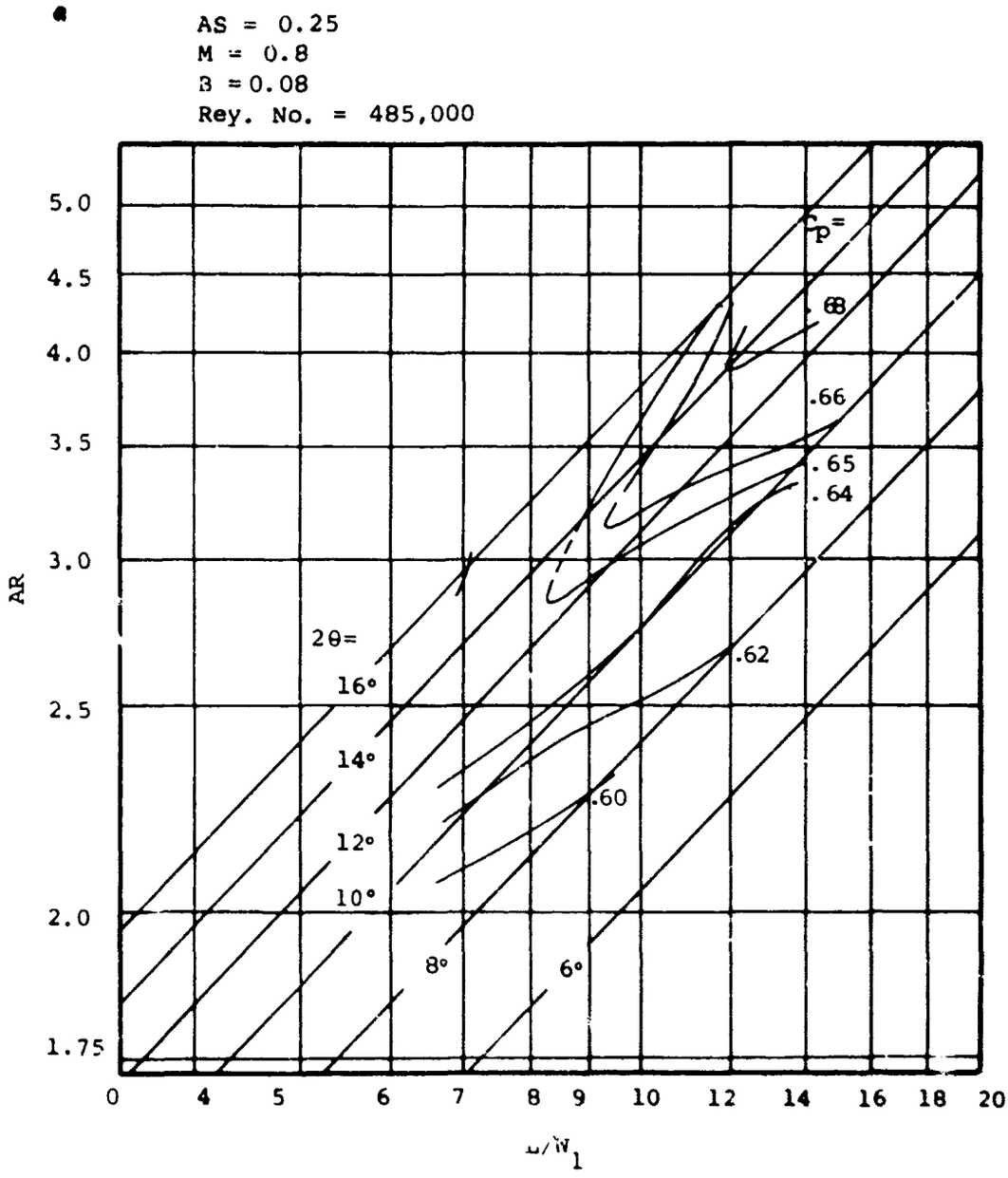

Figure 68. Performance Map - Aspect Ratio = 0.25.

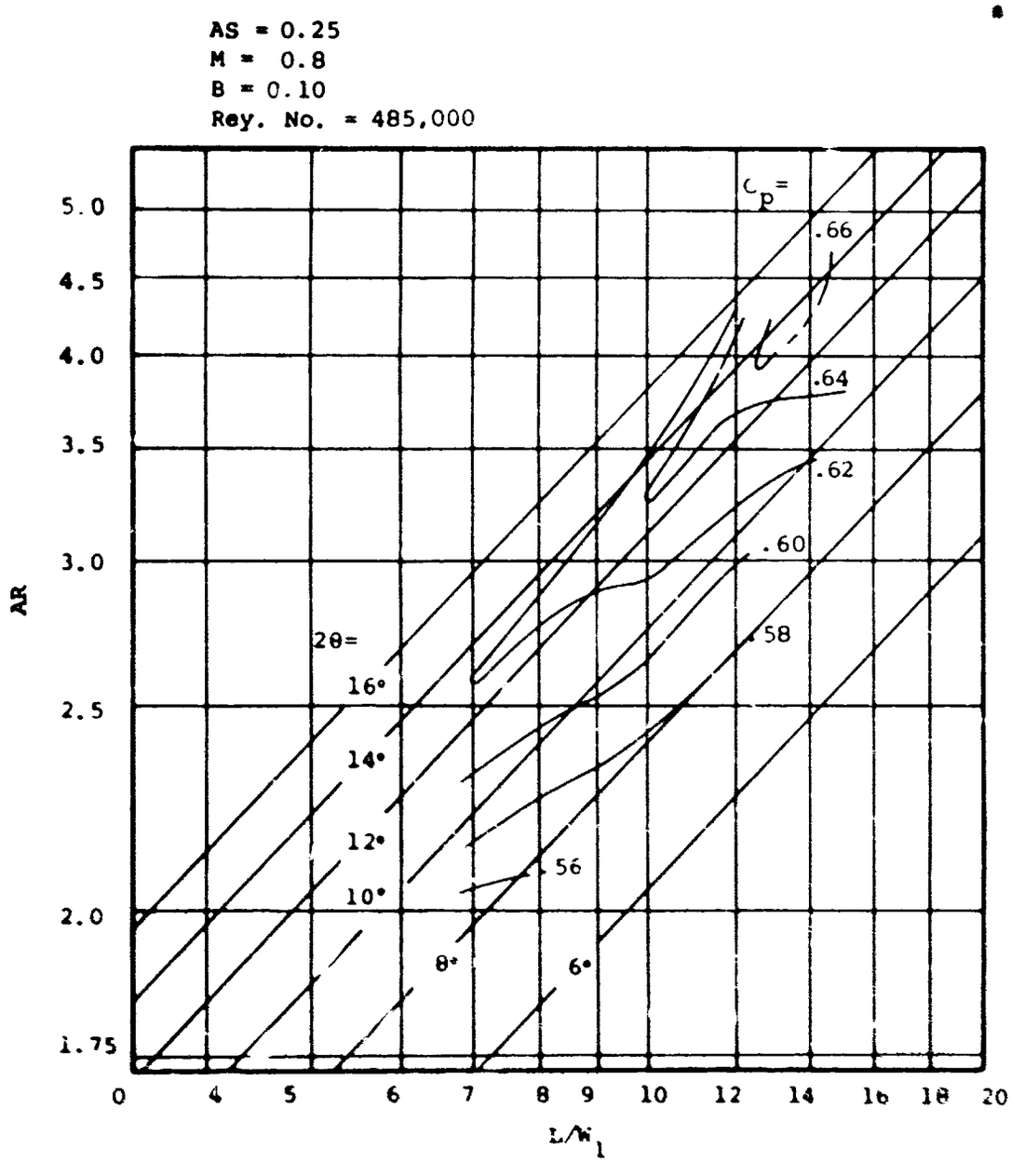

Figure 69. Performance Map - Aspect Ratio = 0.25.

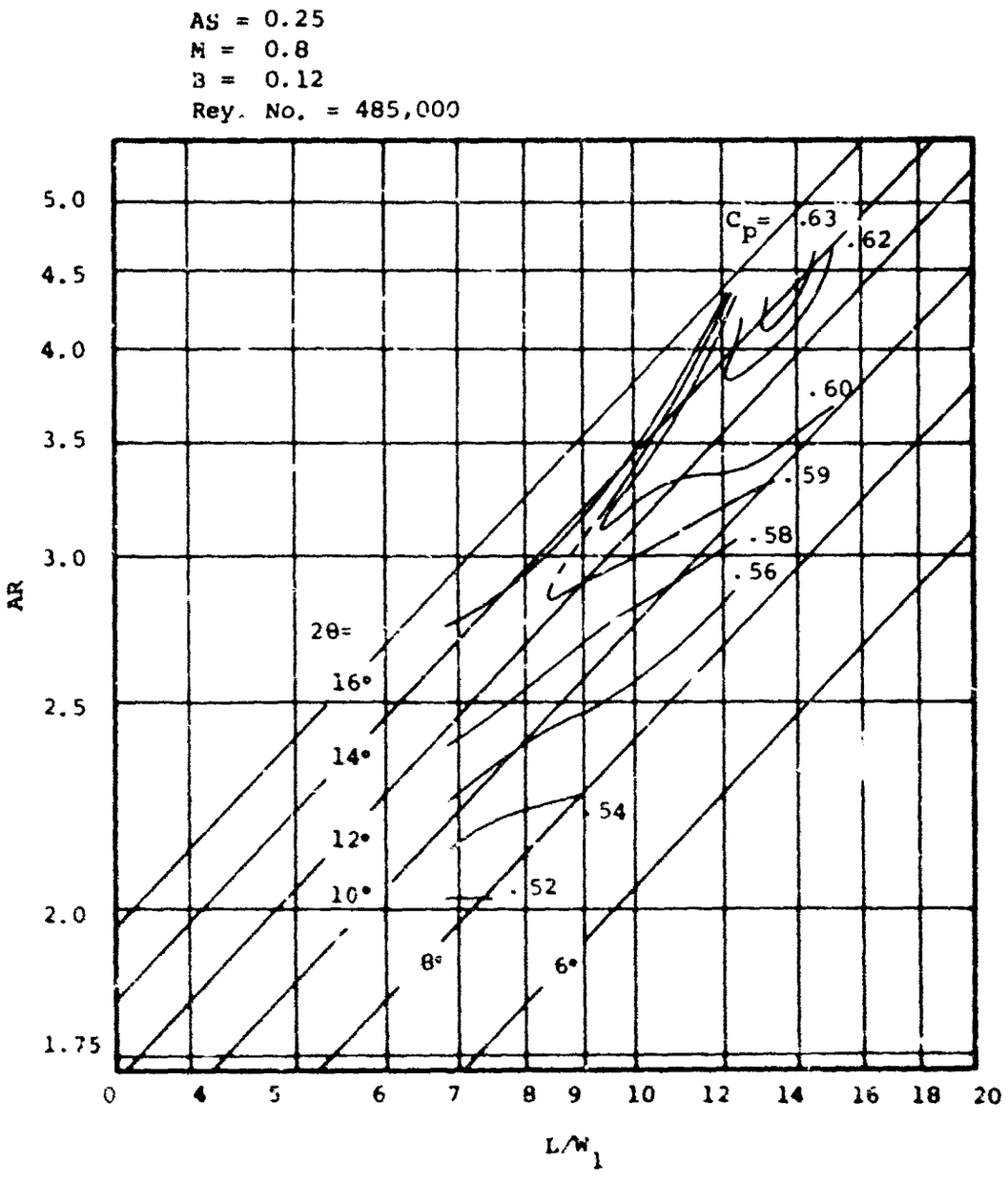

Figure 70. Performance Map - Aspect Ratio = 0.25.

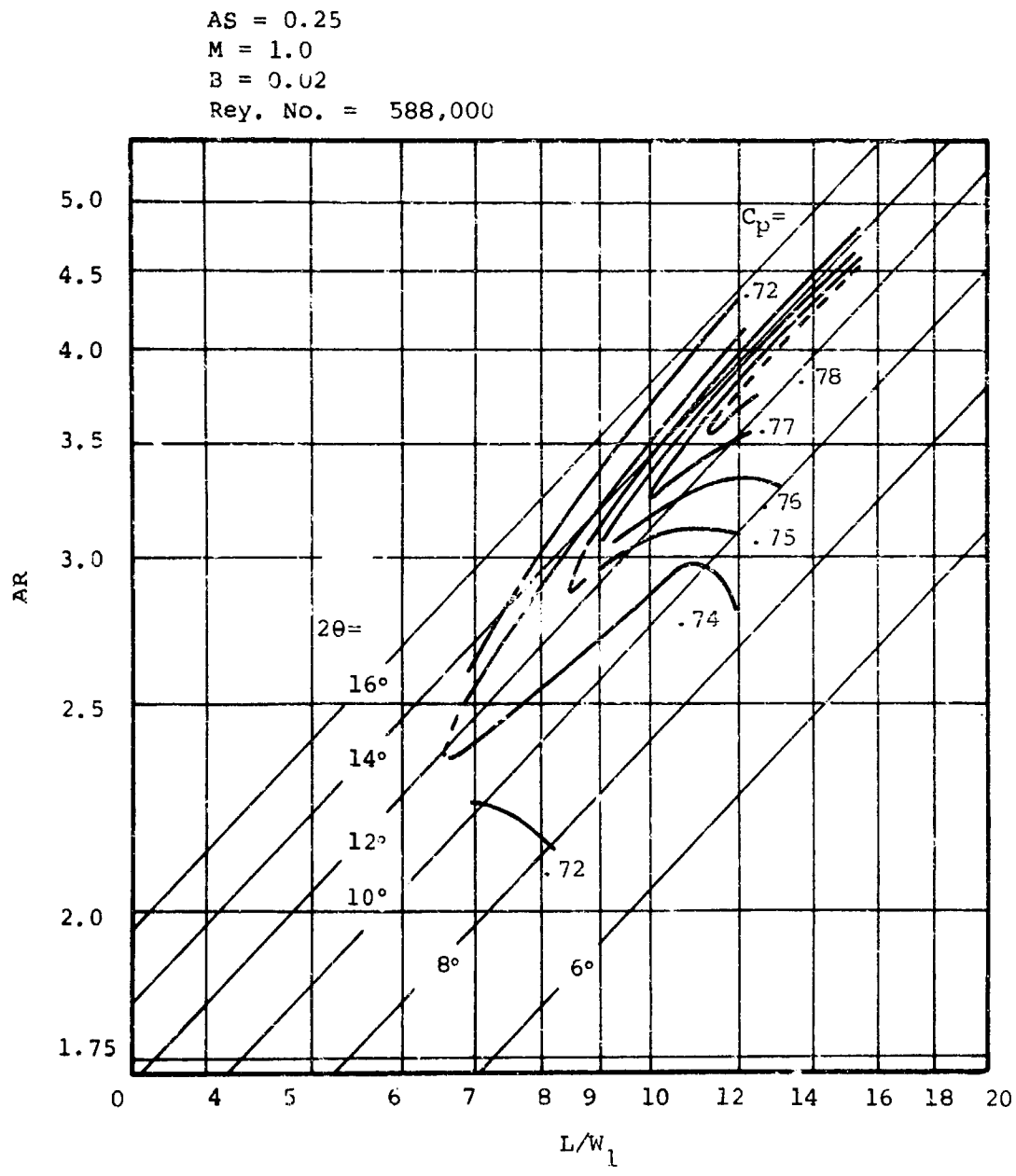

Figure 71. Performance Map - Aspect Ratio = 0.25.

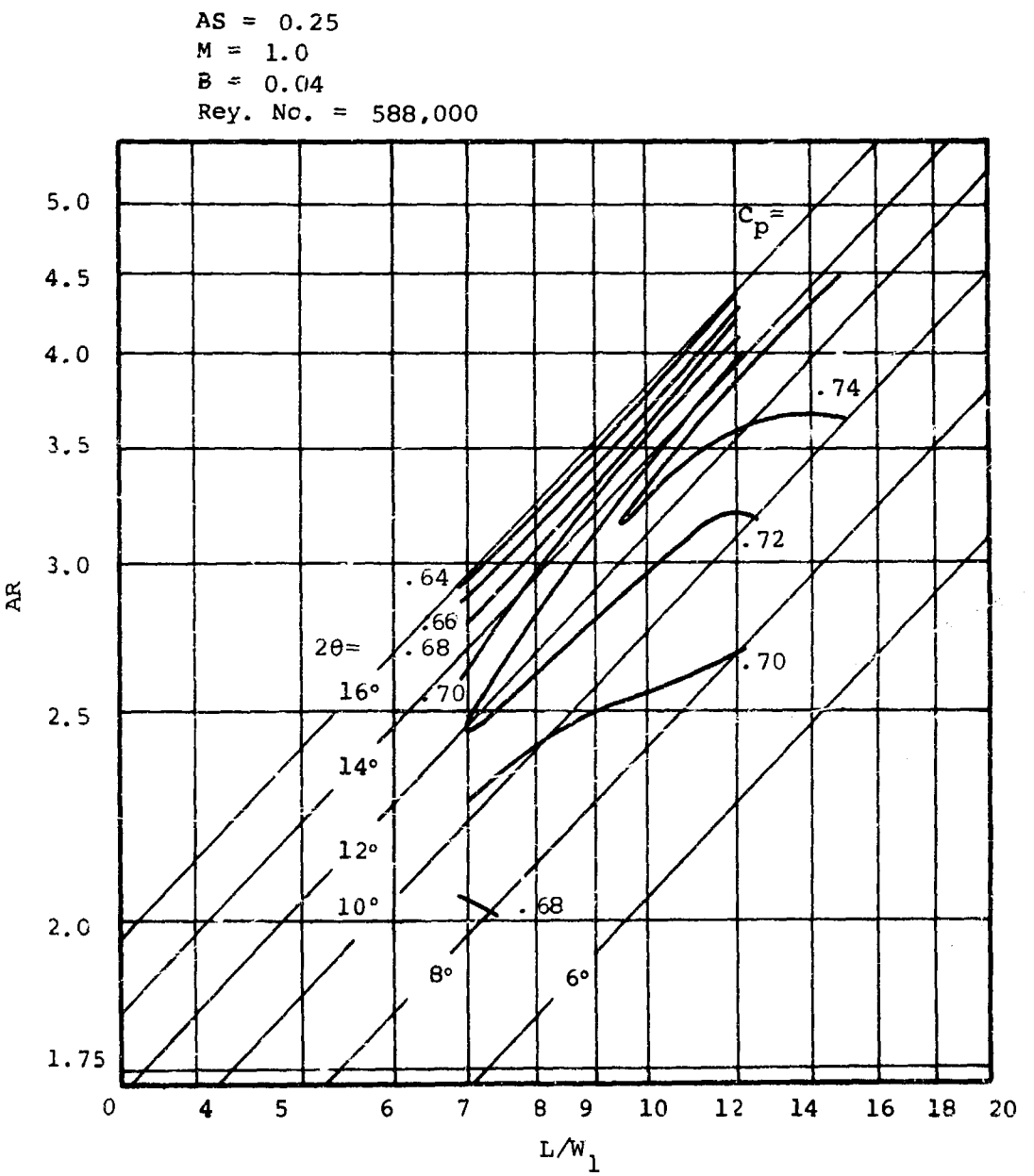

Figure 72. Performance Map - Aspect Ratio = 0.25.

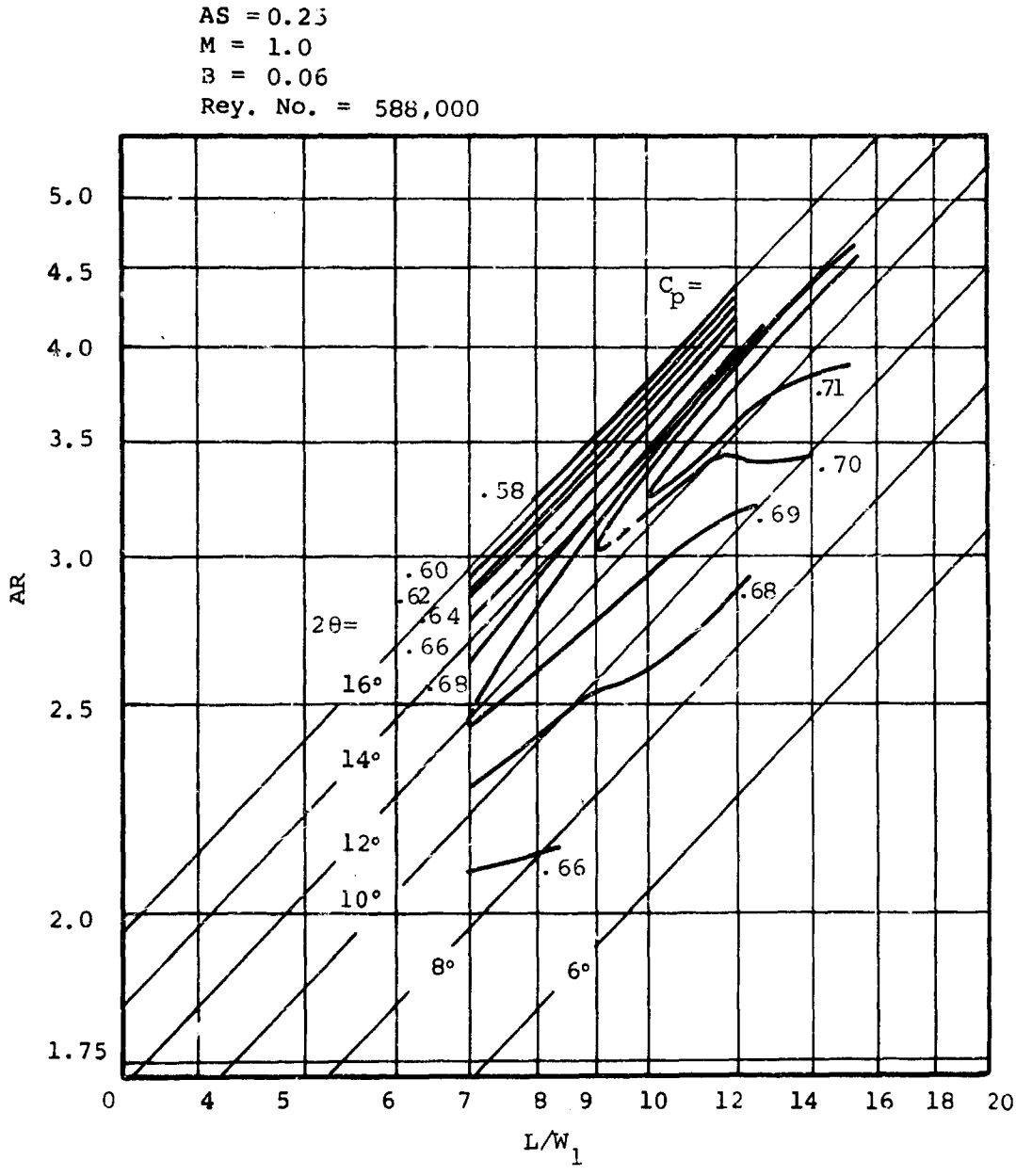

Figure 73. Performance Map - Aspect Ratio = 0.25.

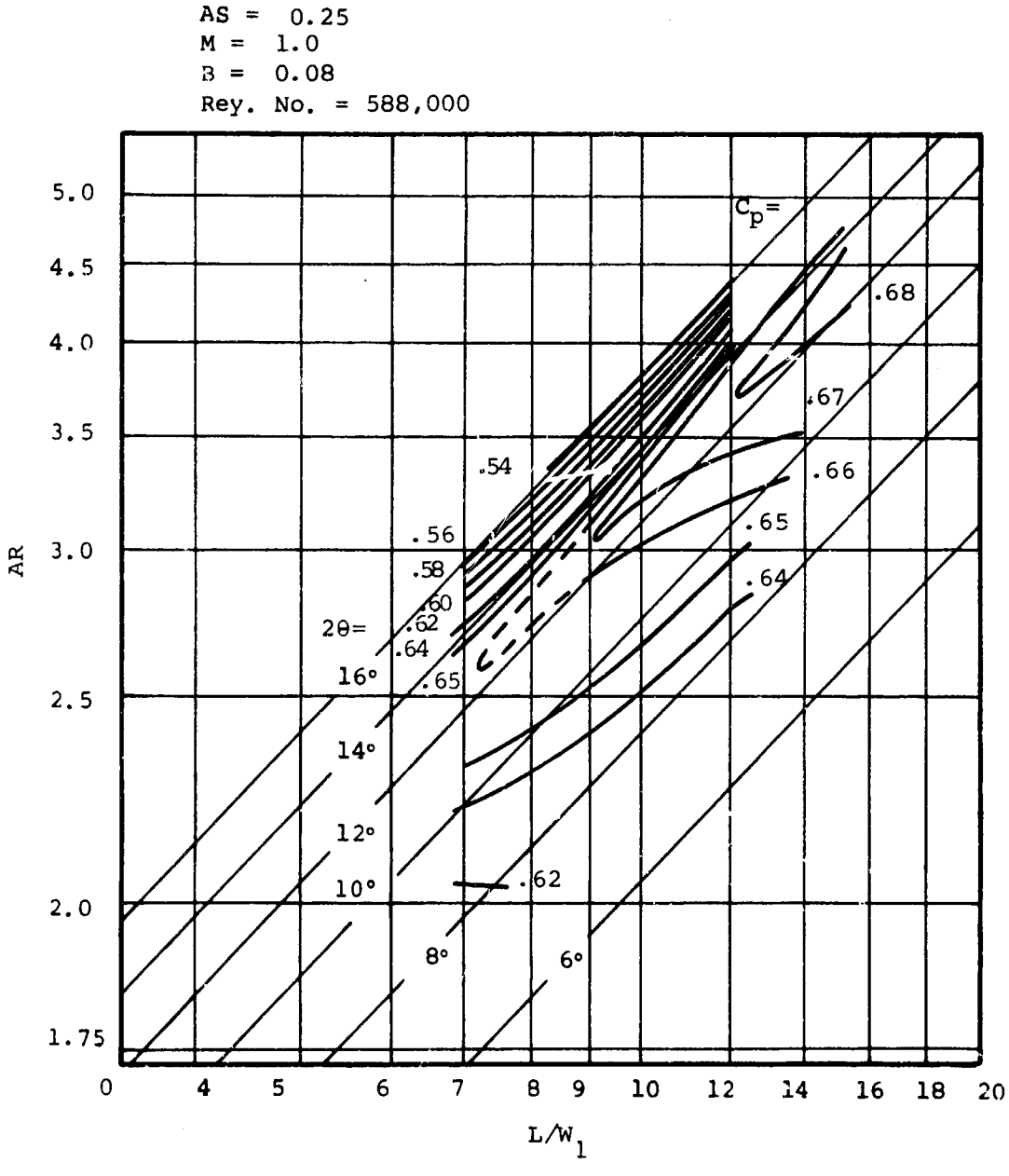

Figure 74. Performance Map - Aspect Ratio = 0.25.

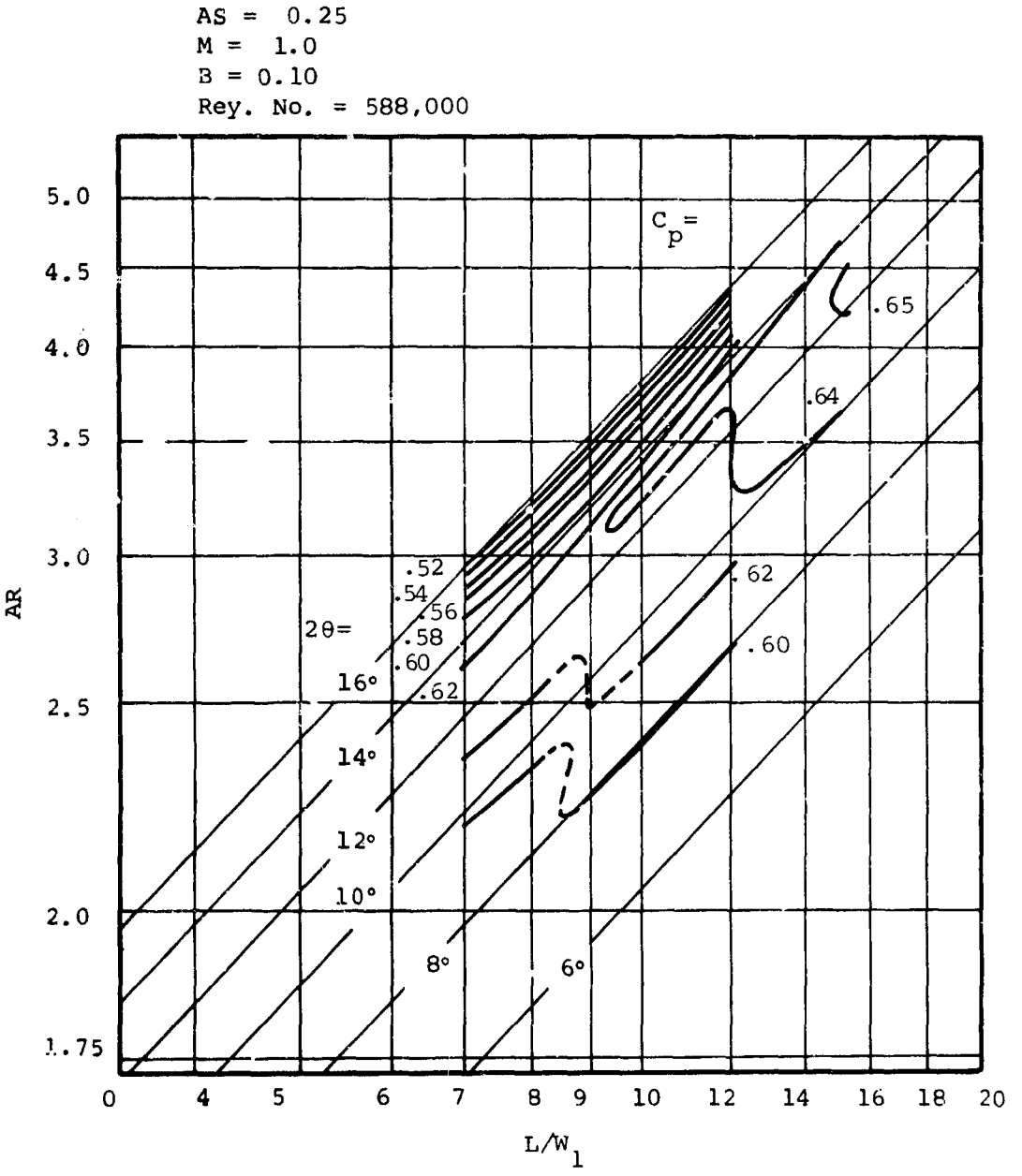

Figure 75. Performance Map - Aspect Ratio = 0.25.

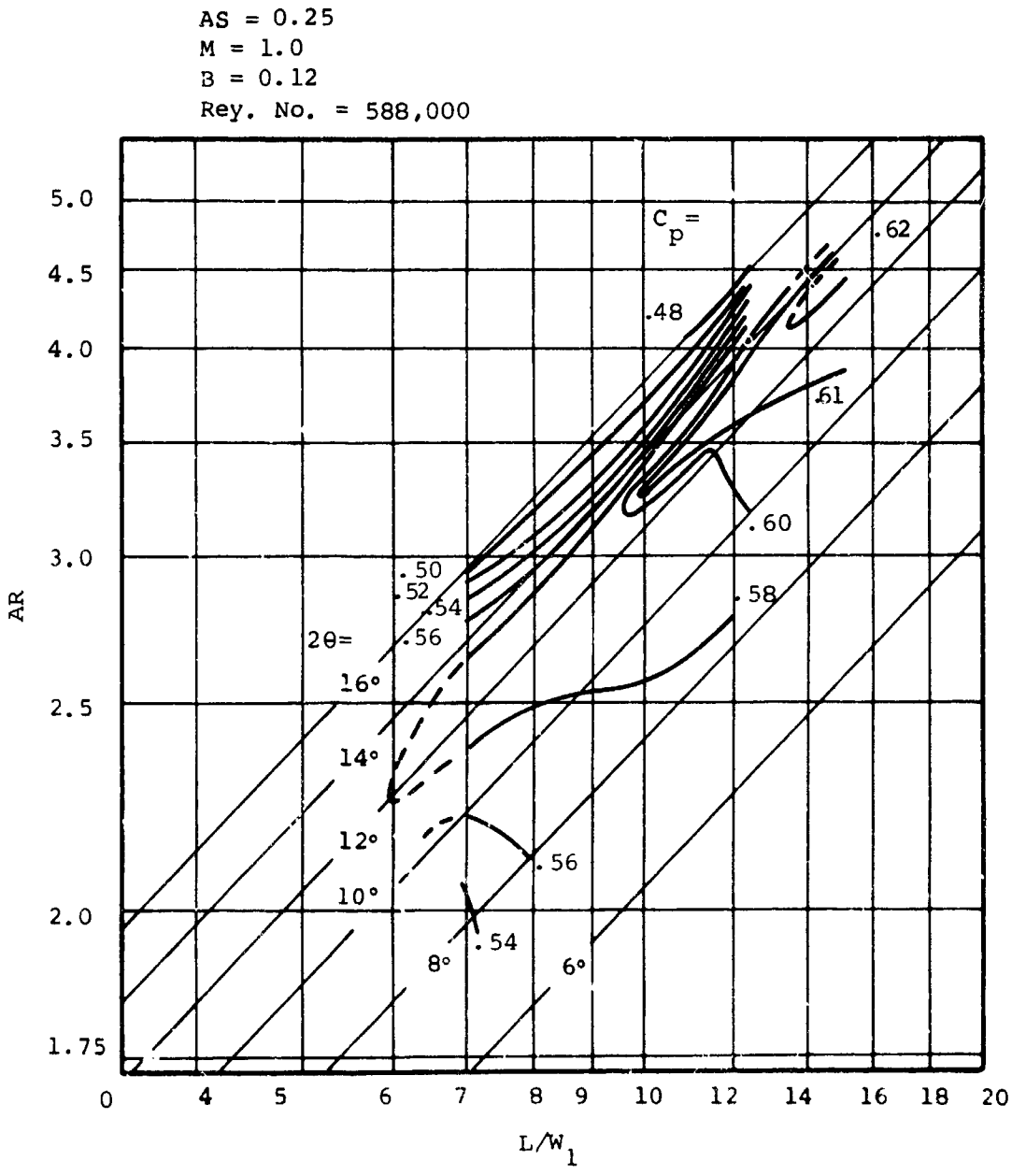

Figure 76. Performance Map - Aspect Ratio = 0.25.

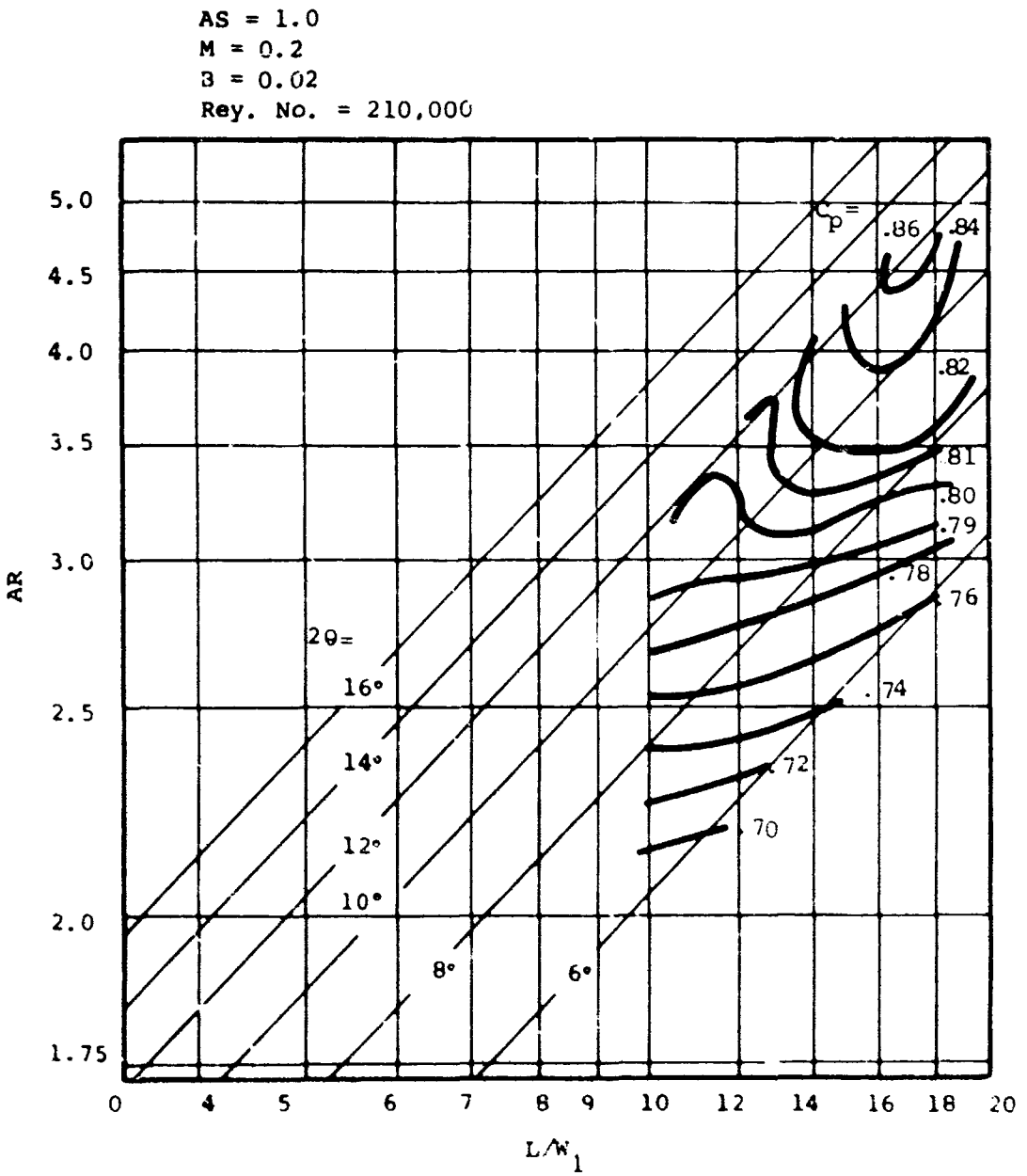

Figure 77. Performance Map - Aspect Ratio = 1.0.

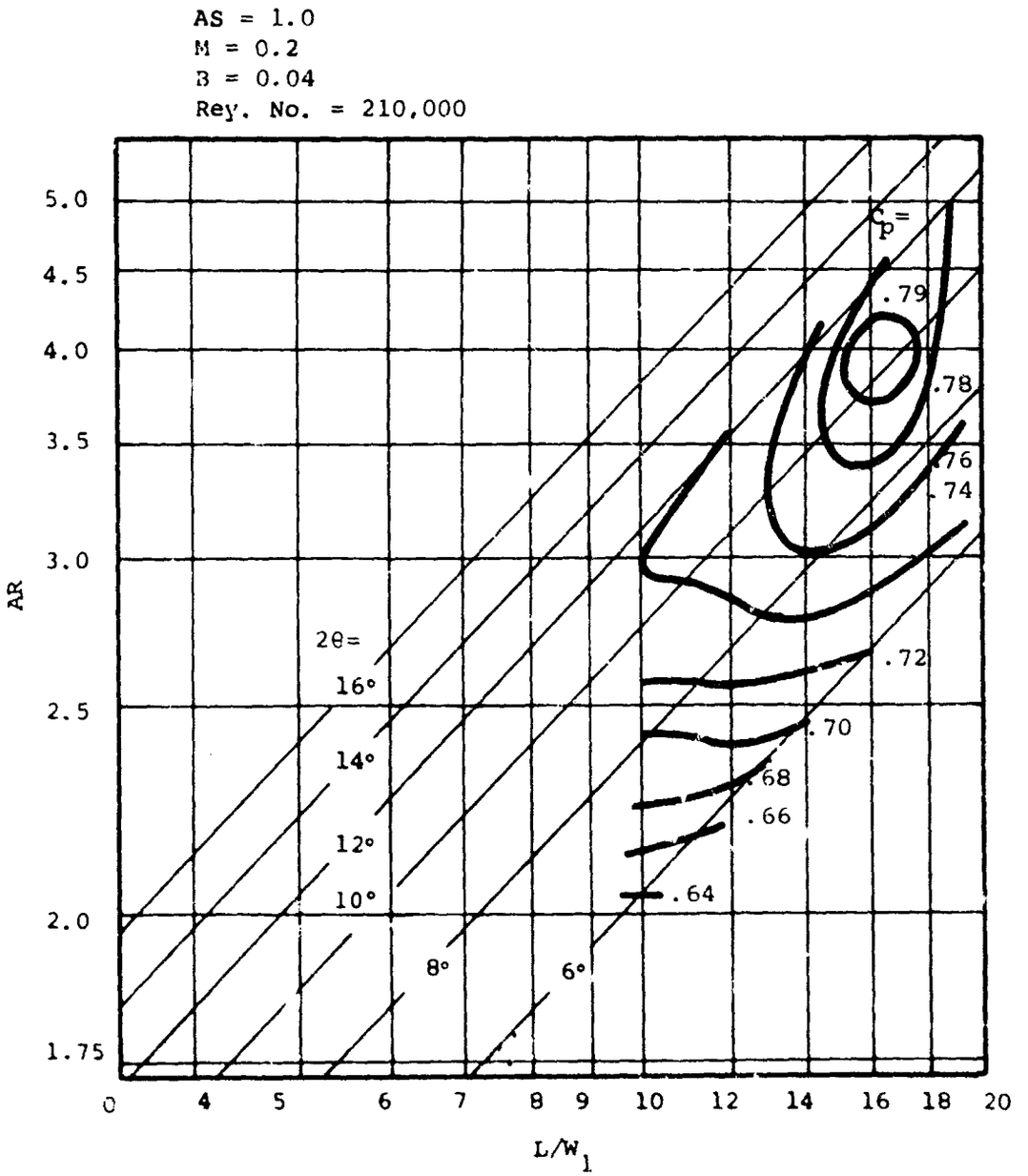

Figure 78. Performance Map - Aspect Ratio = 1.0.

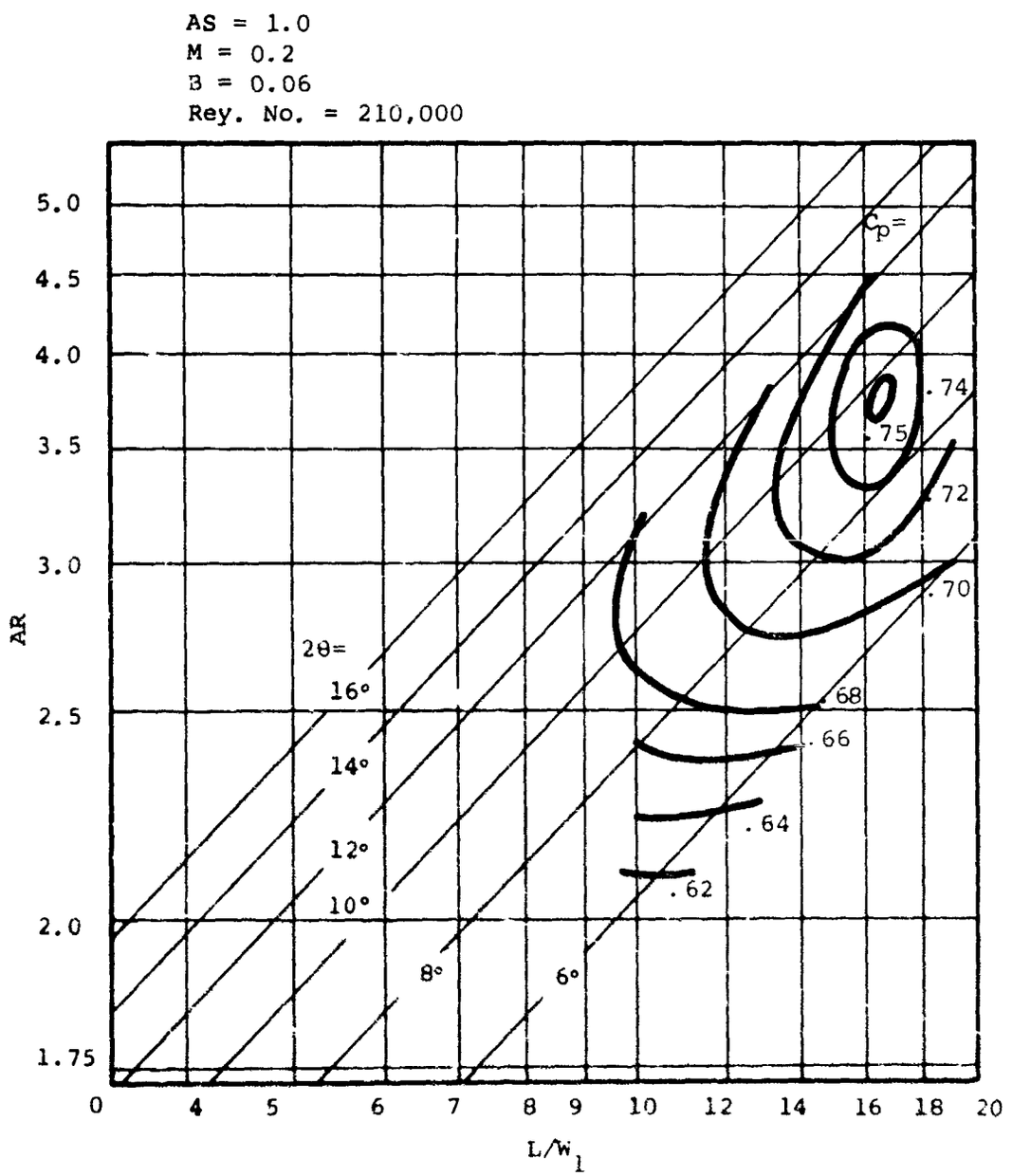

Figure 79. Performance Map - Aspect Ratio = 1.0.

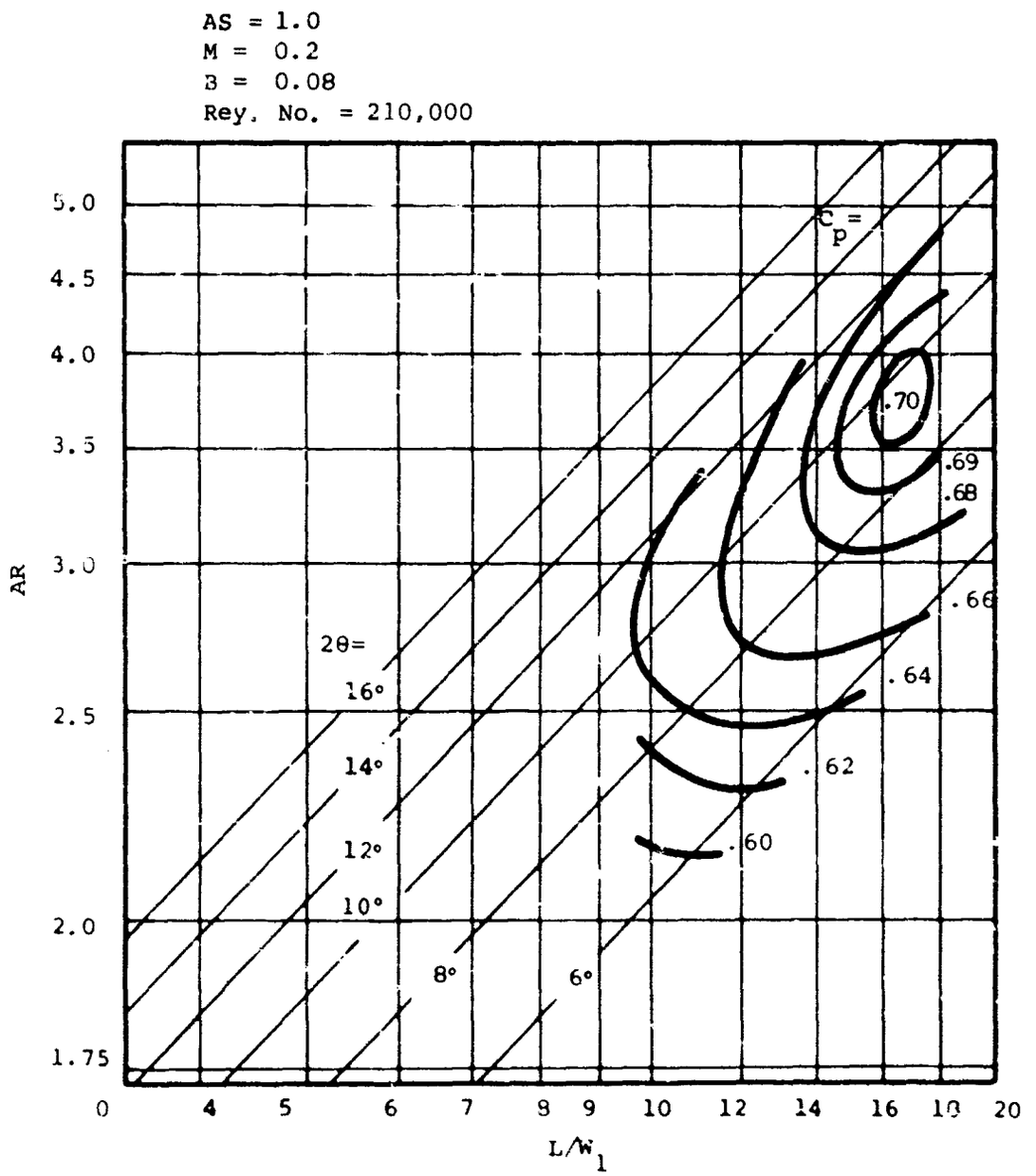

Figure 80. Performance Map - Aspect Ratio = 1.0.

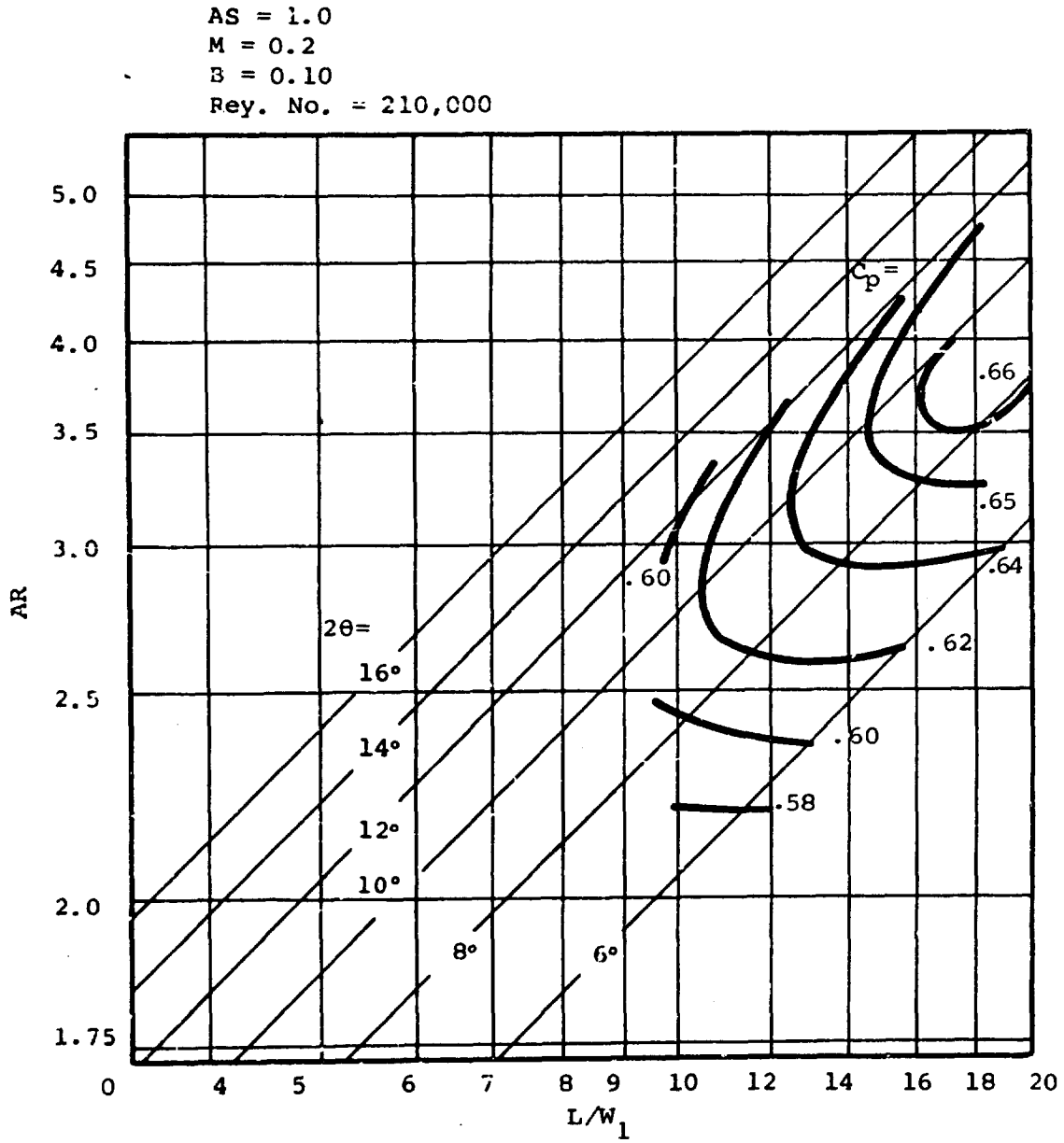

Figure 81. Performance Map - Aspect Ratio = 1.0.

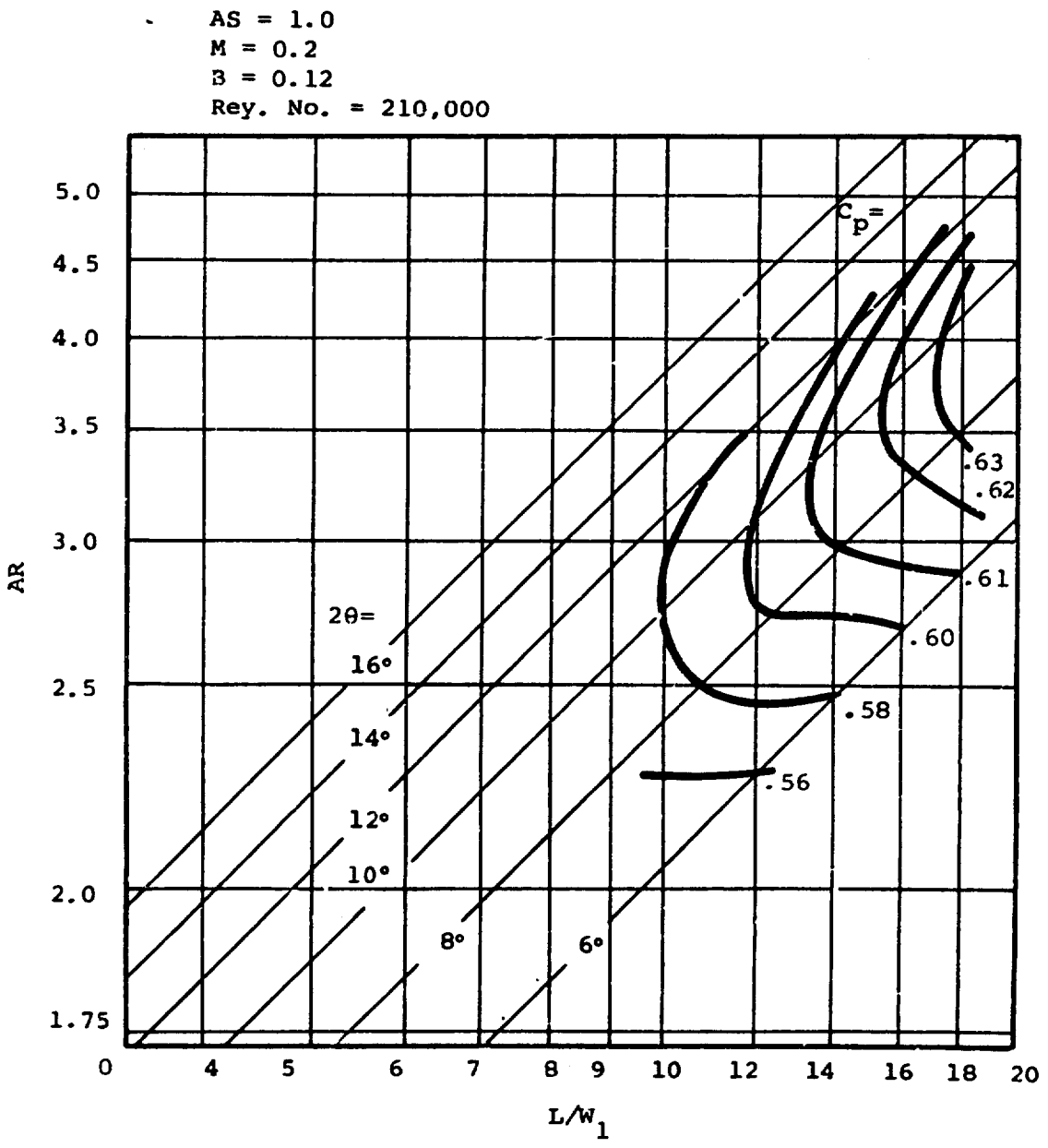

Figure 82. Performance Map - Aspect Ratio = 1.0.

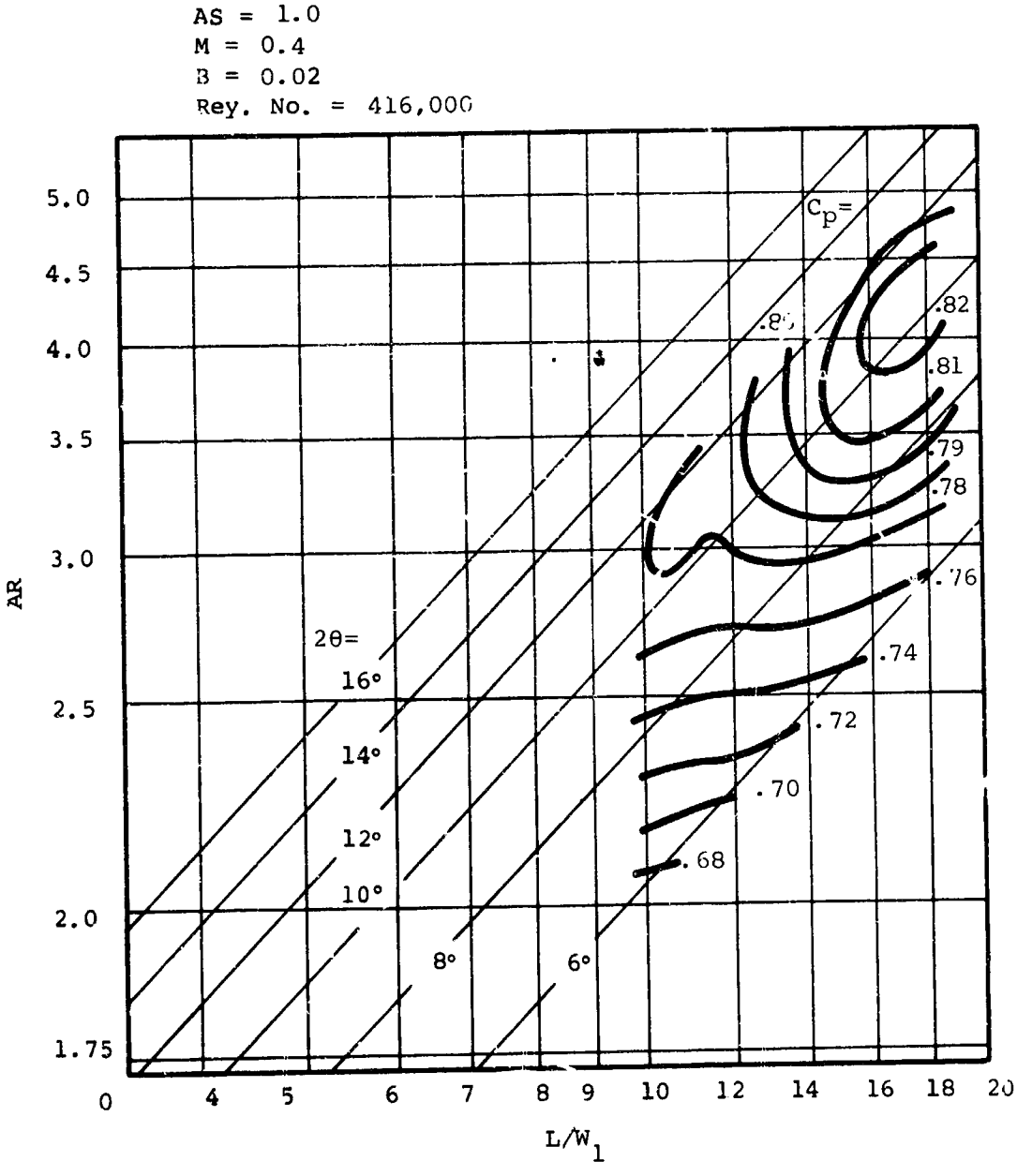

Figure 83. Performance Map - Aspect Ratio = 1.0.

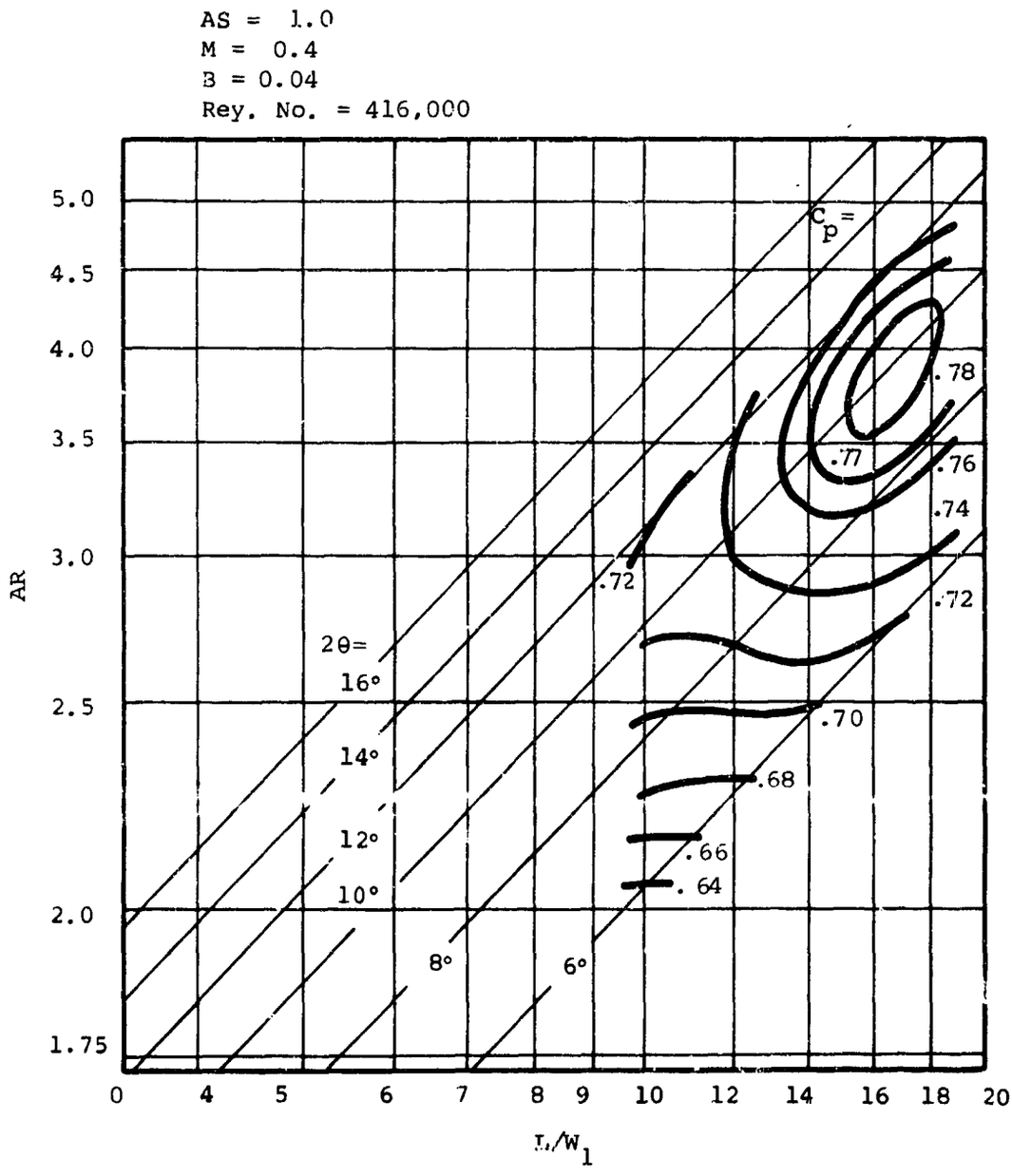

Figure 84. Performance Map - Aspect Ratio = 1.0.

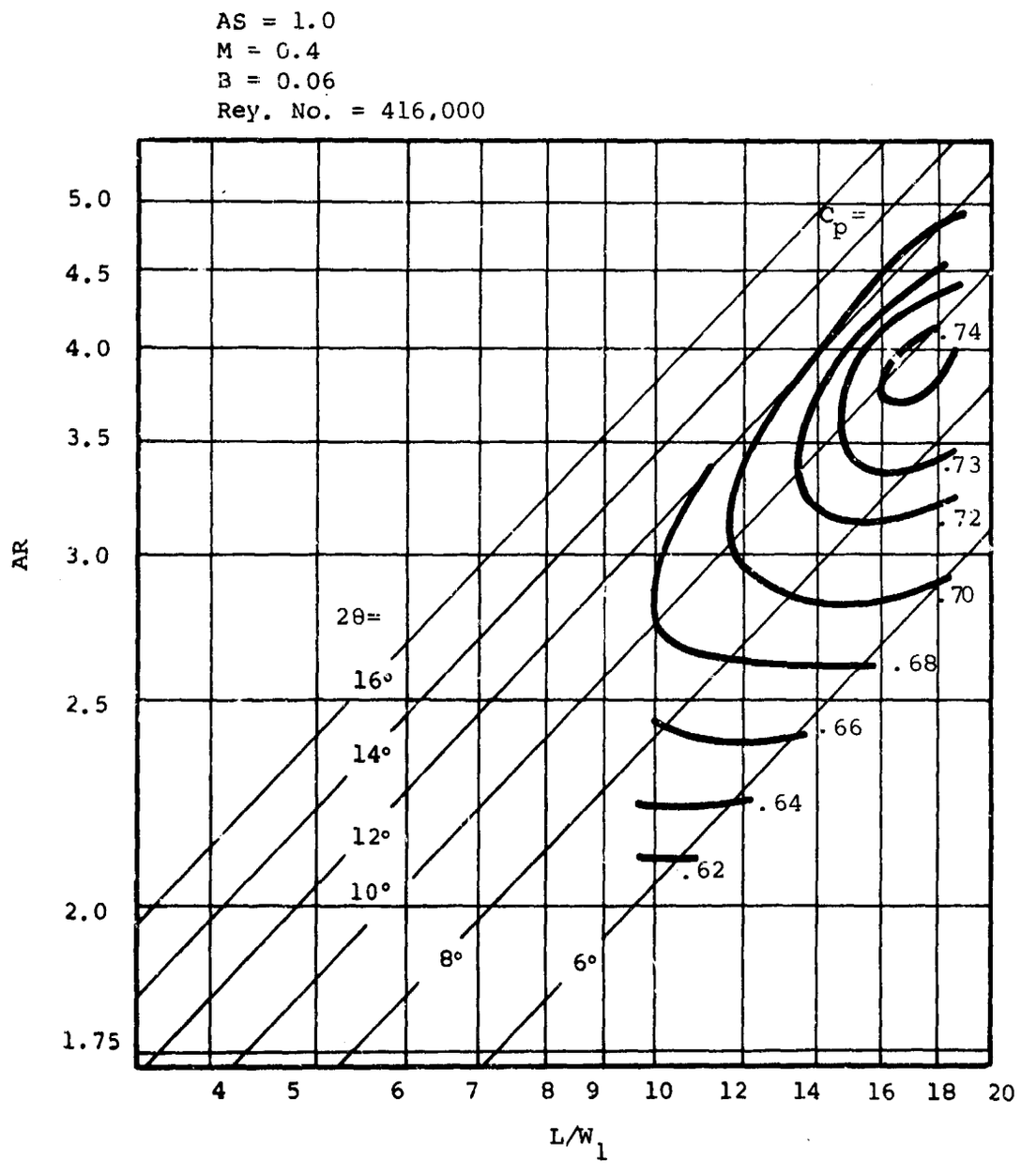

Figure 85. Performance Map - Aspect Ratio = 1.0.

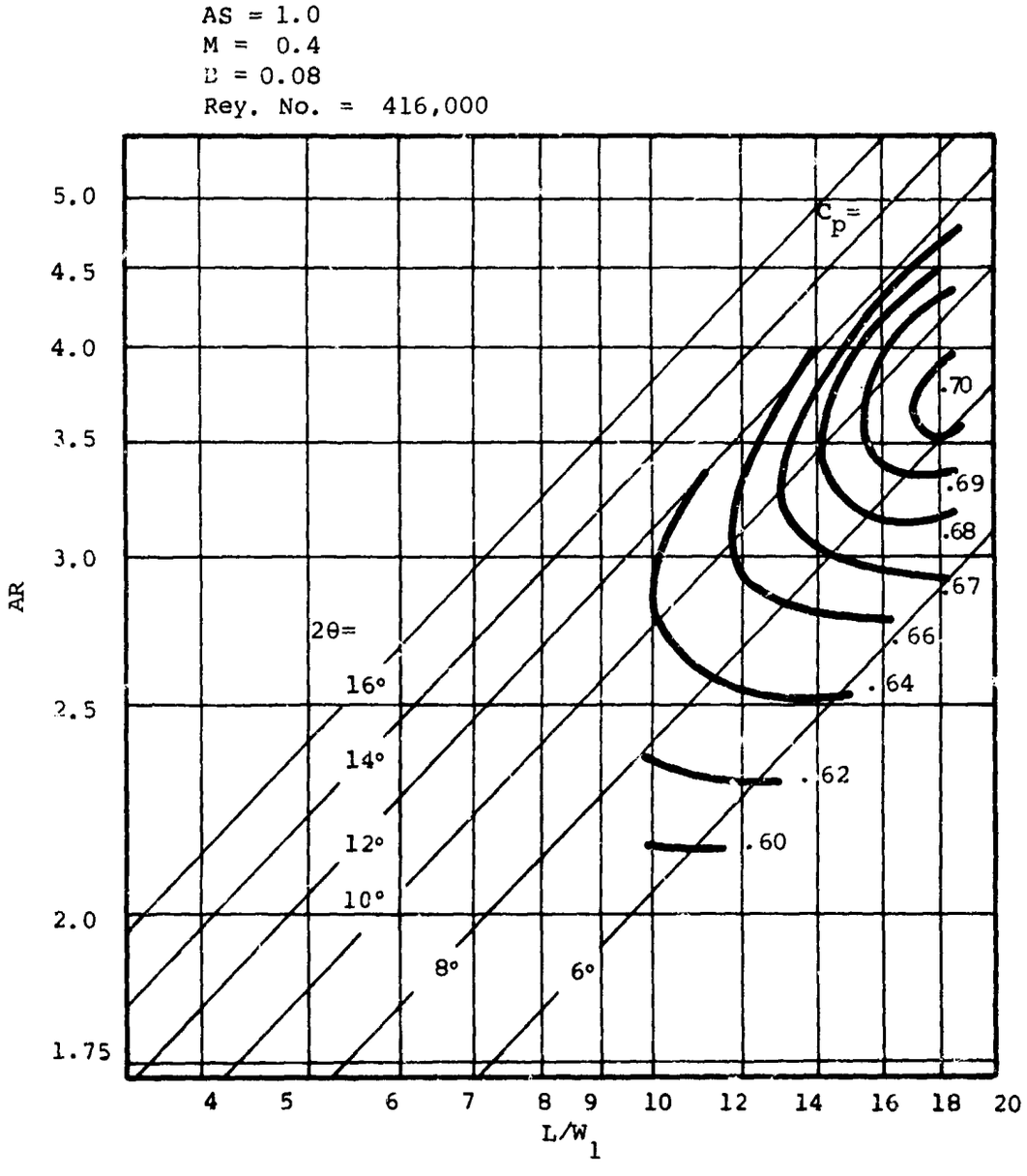

Figure 86. Performance Map - Aspect Ratio = 1.0.

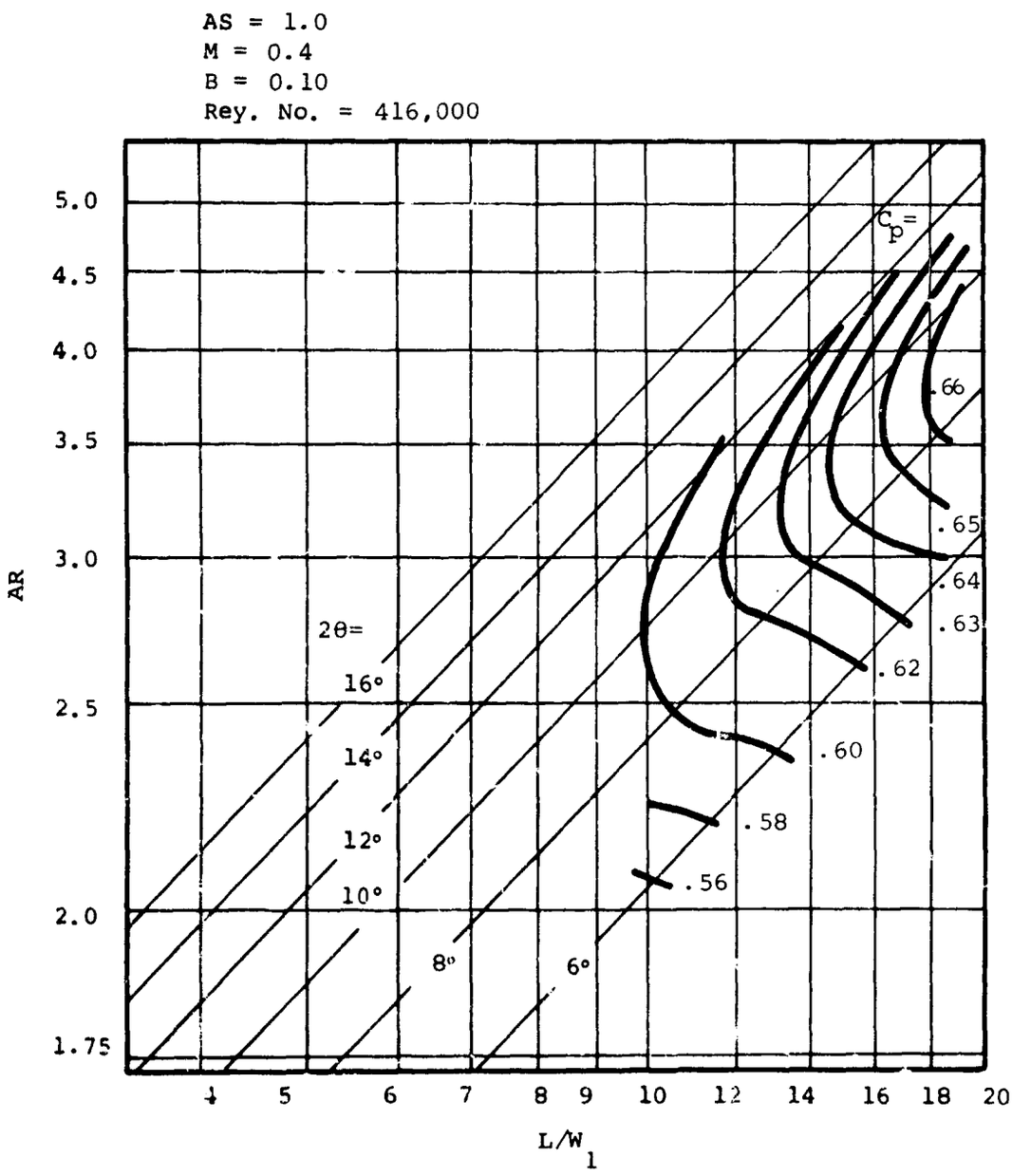

Figure 87. Performance Map - Aspect Ratio = 1.0.

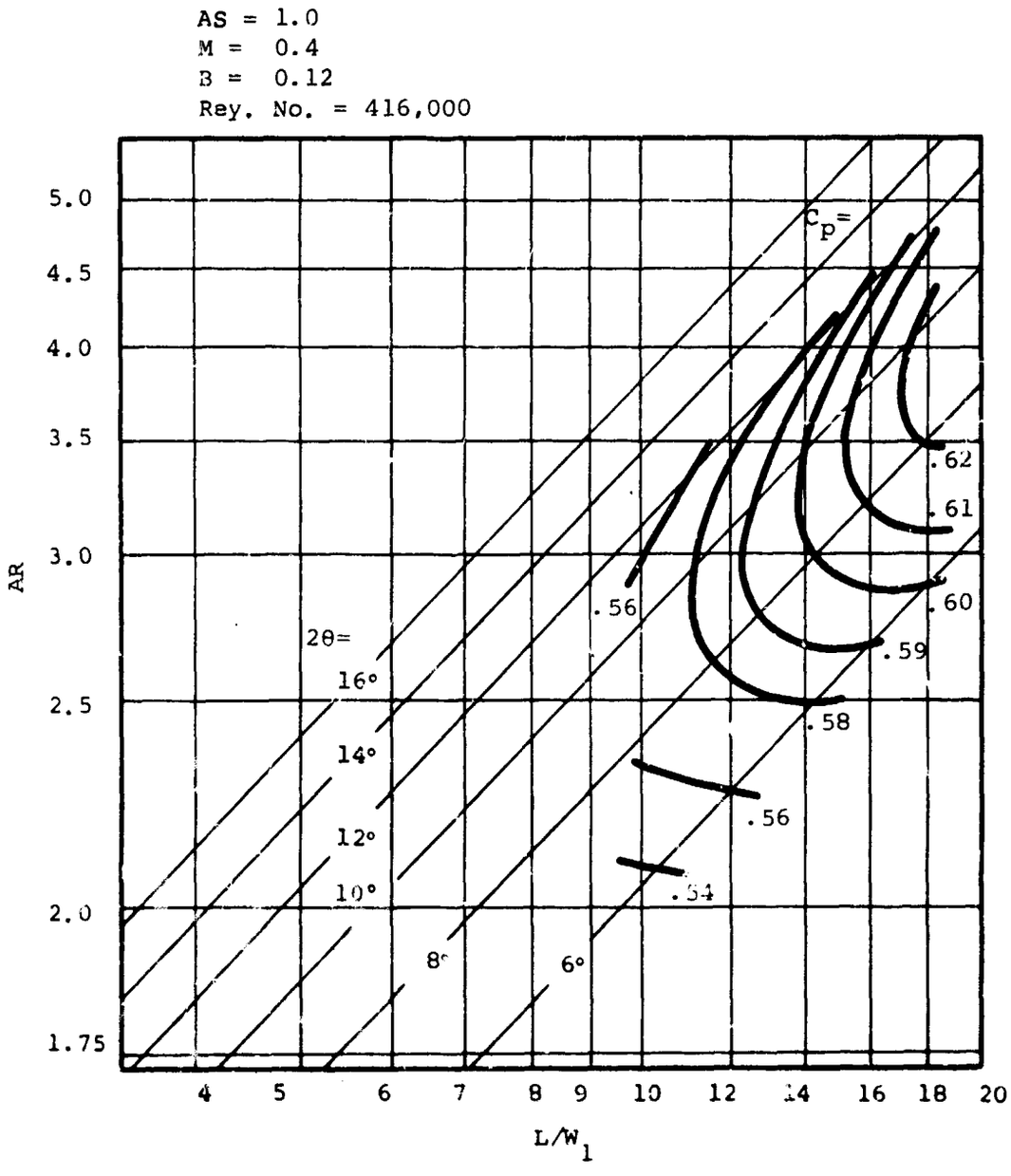

Figure 88. Performance Map - Aspect Ratio = 1.0.

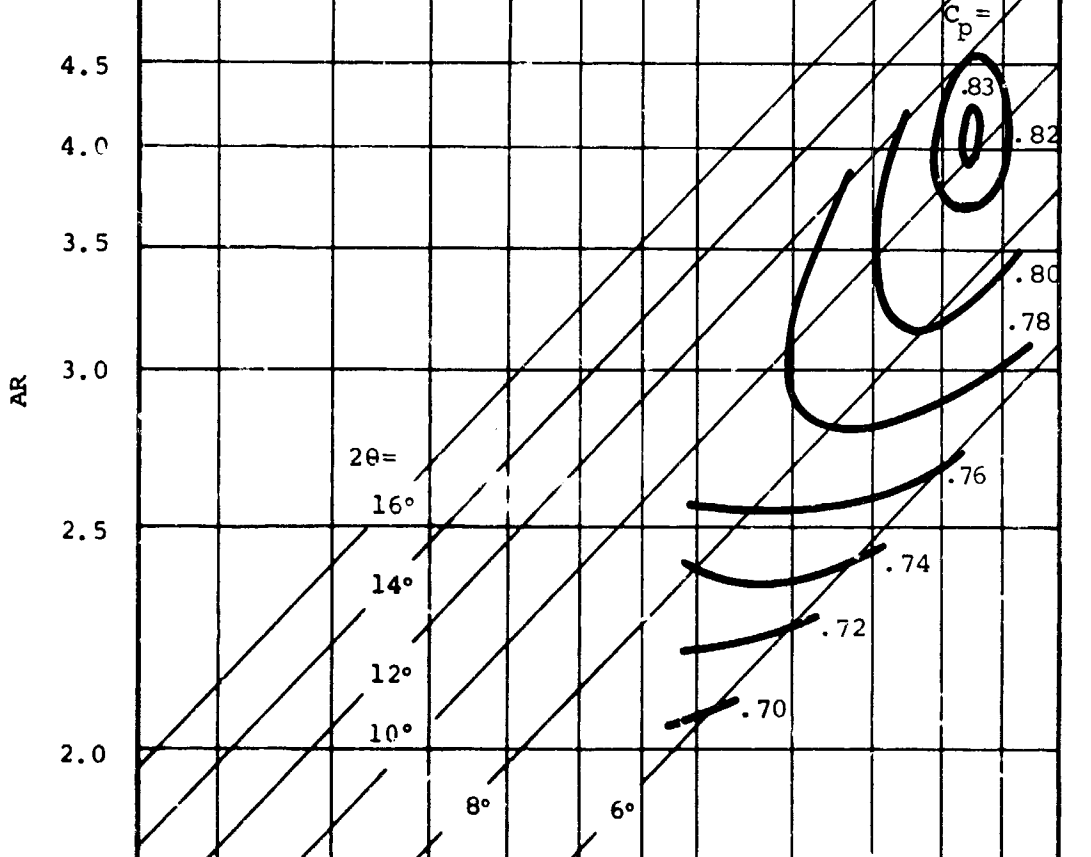

Figure 89. Performance Map - Aspect Ratio = 1.0.

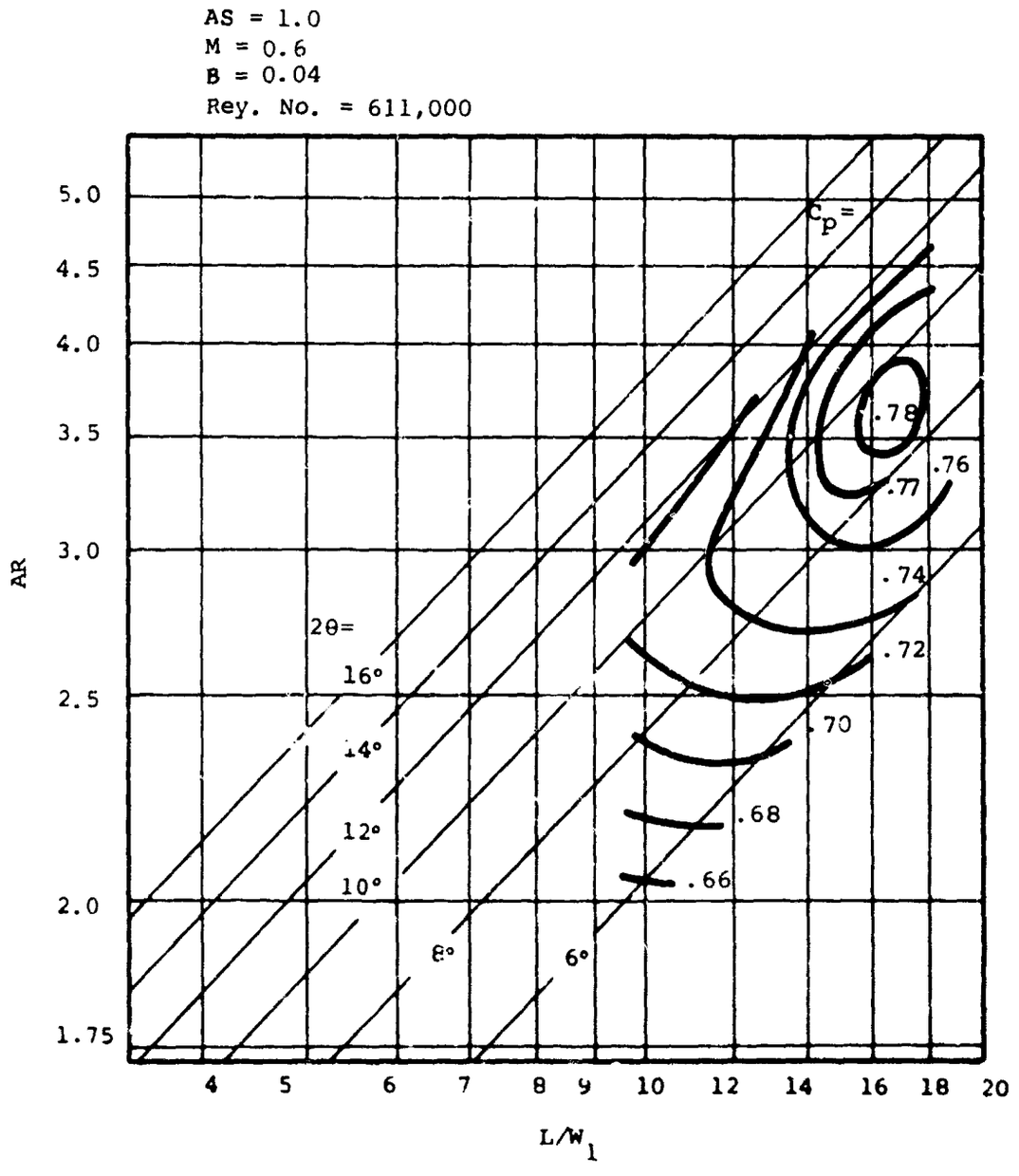

Figure 90. Performance Map - Aspect Ratio = 1.0.

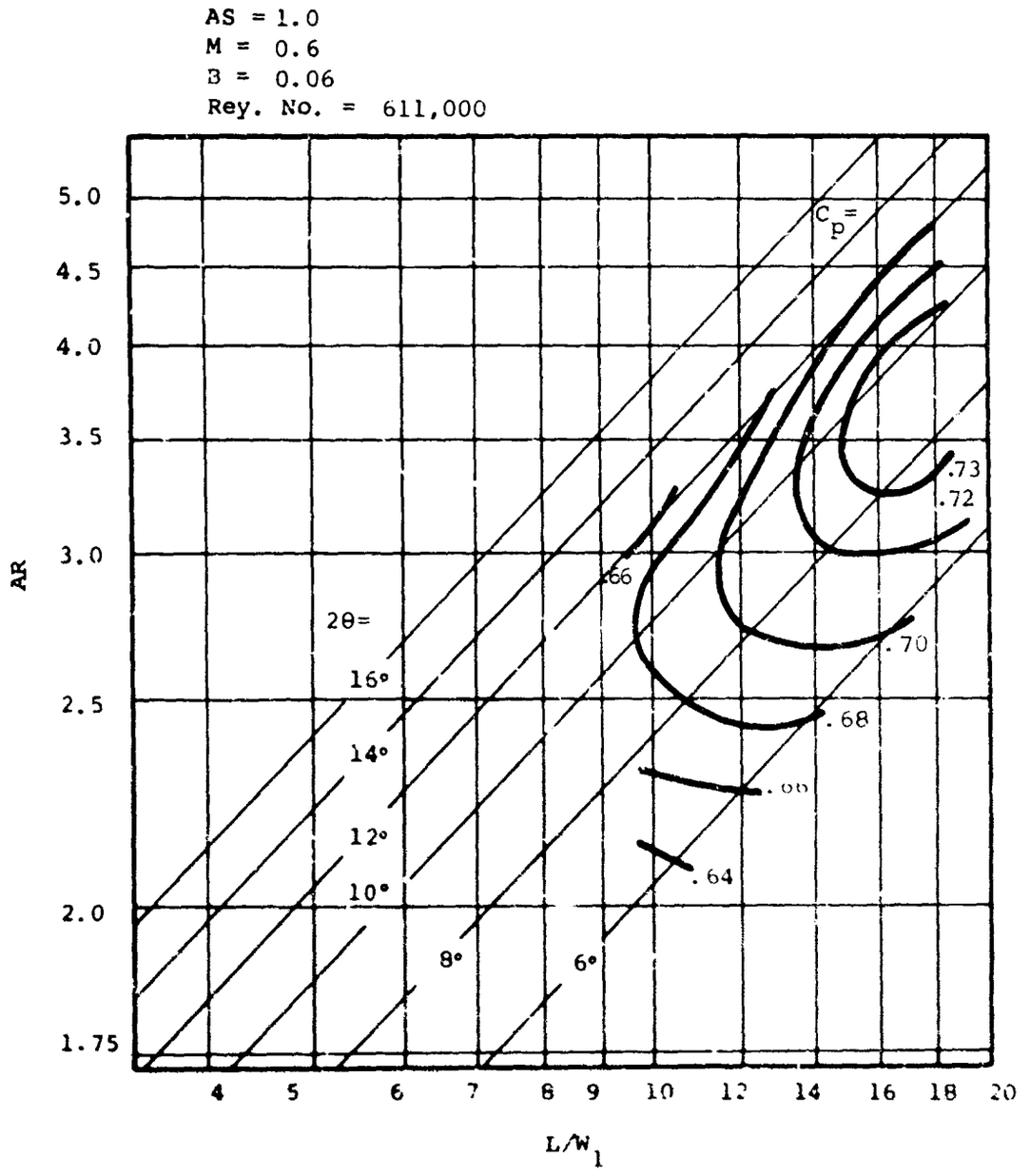

Figure 91. Performance Map - Aspect Ratio = 1.0.

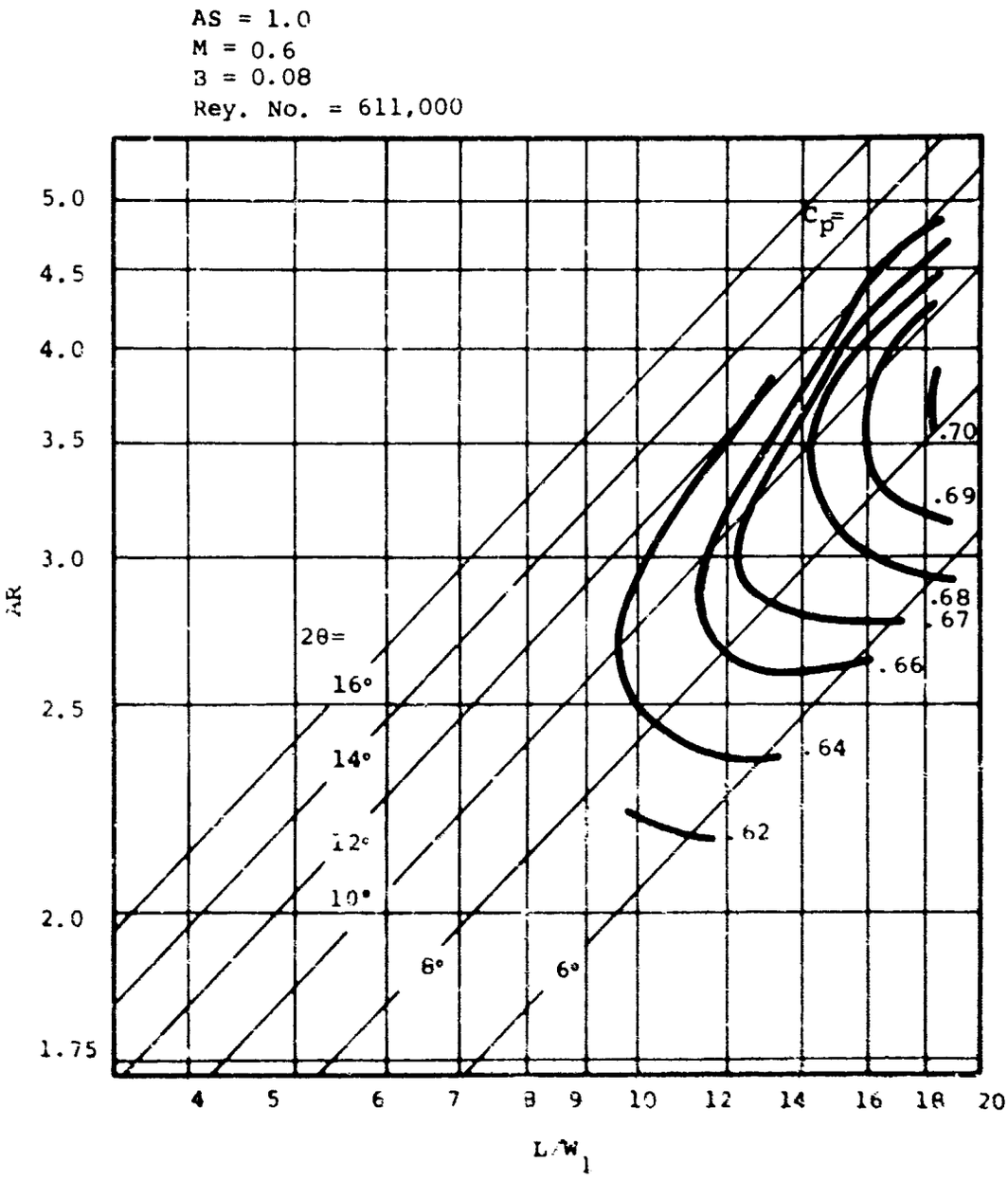

Figure 92. Performance Map - Aspect Ratio = 1.0.

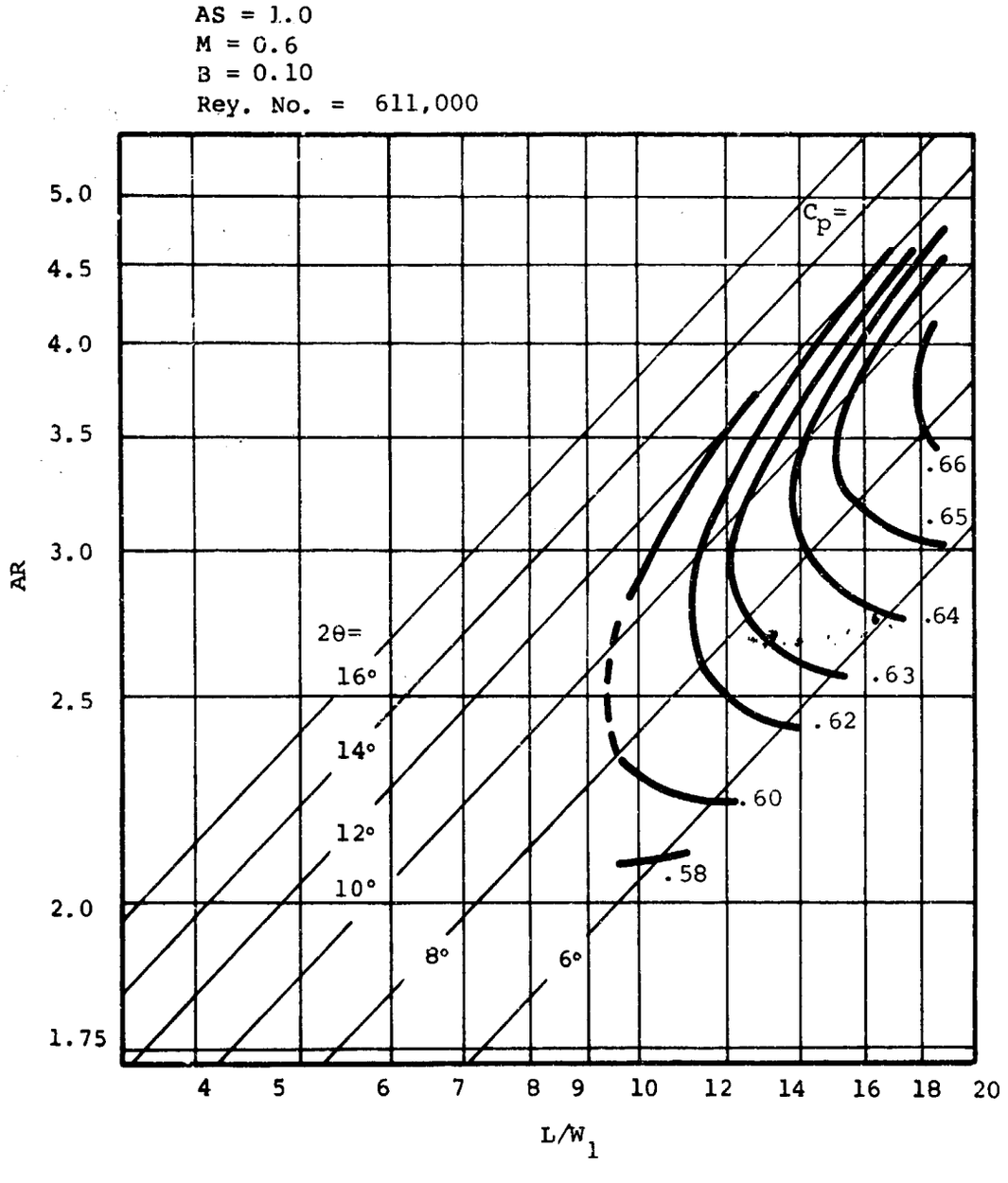

Figure 93. Performance Map - Aspect Ratio = 1.0.

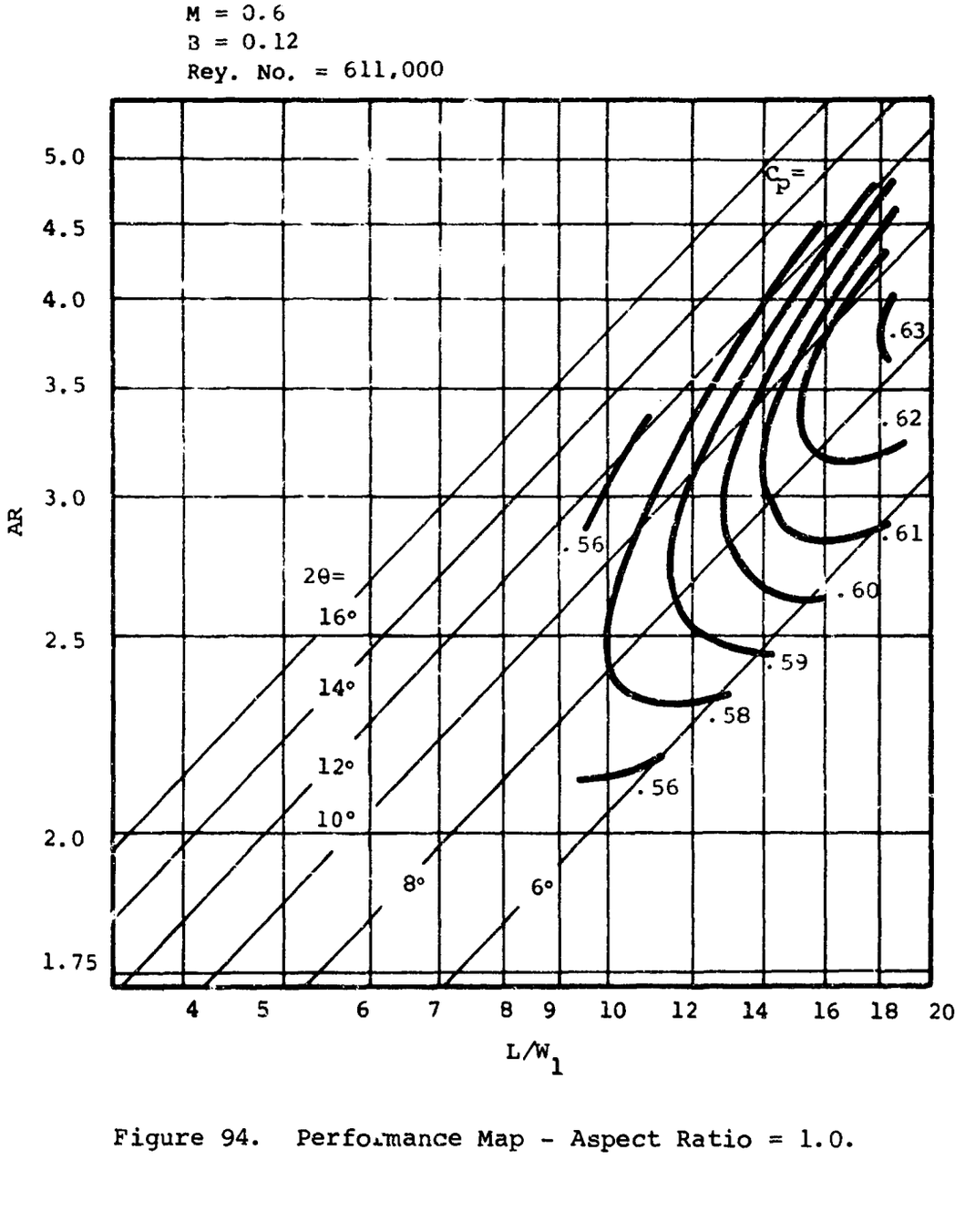

Figure 94. Performance Map - Aspect Ratio = 1.0.

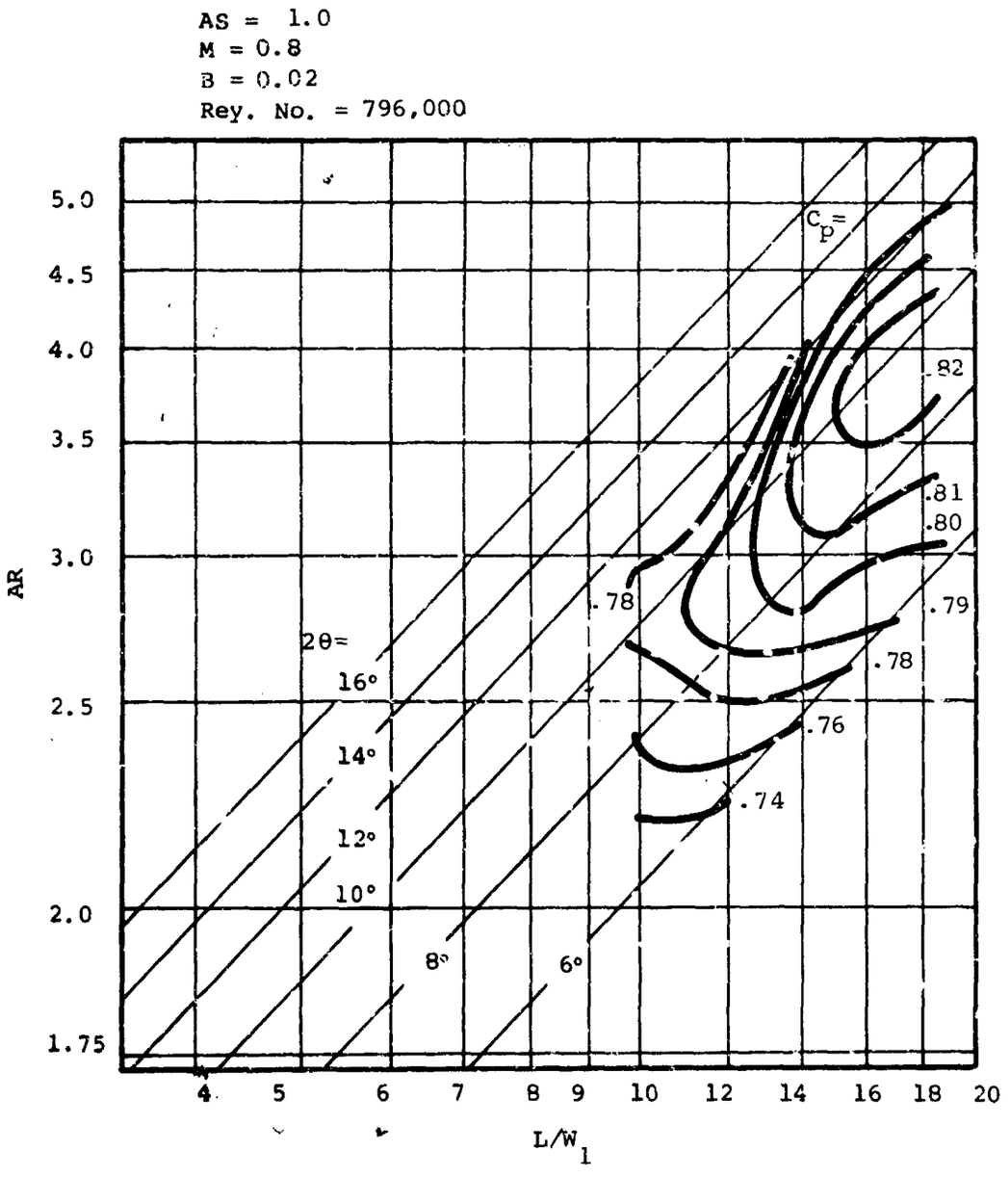

Figure 95. Performance Map - Aspect Ratio = 1.0.

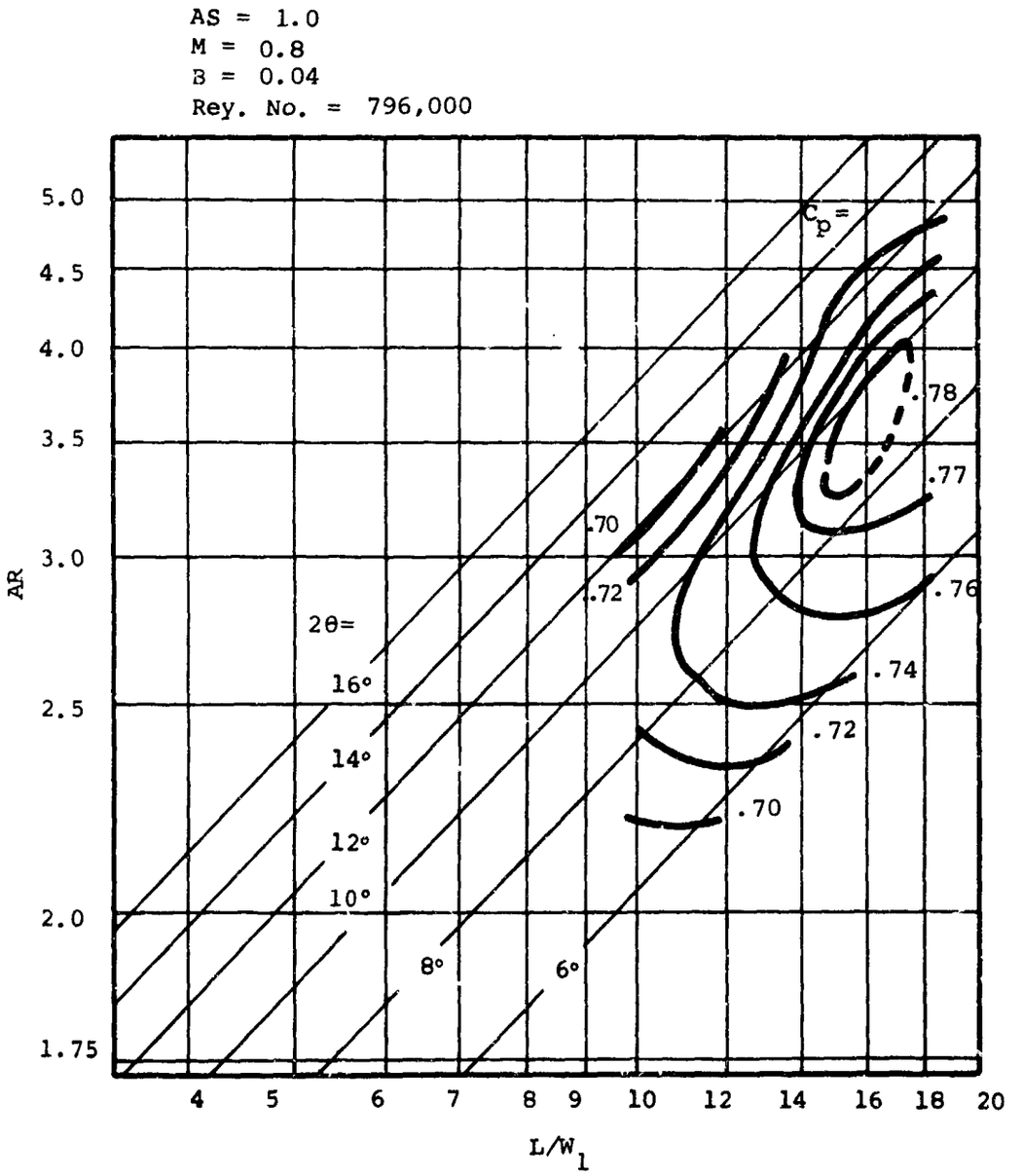

Figure 96. Performance Map - Aspect Ratio = 1.0.

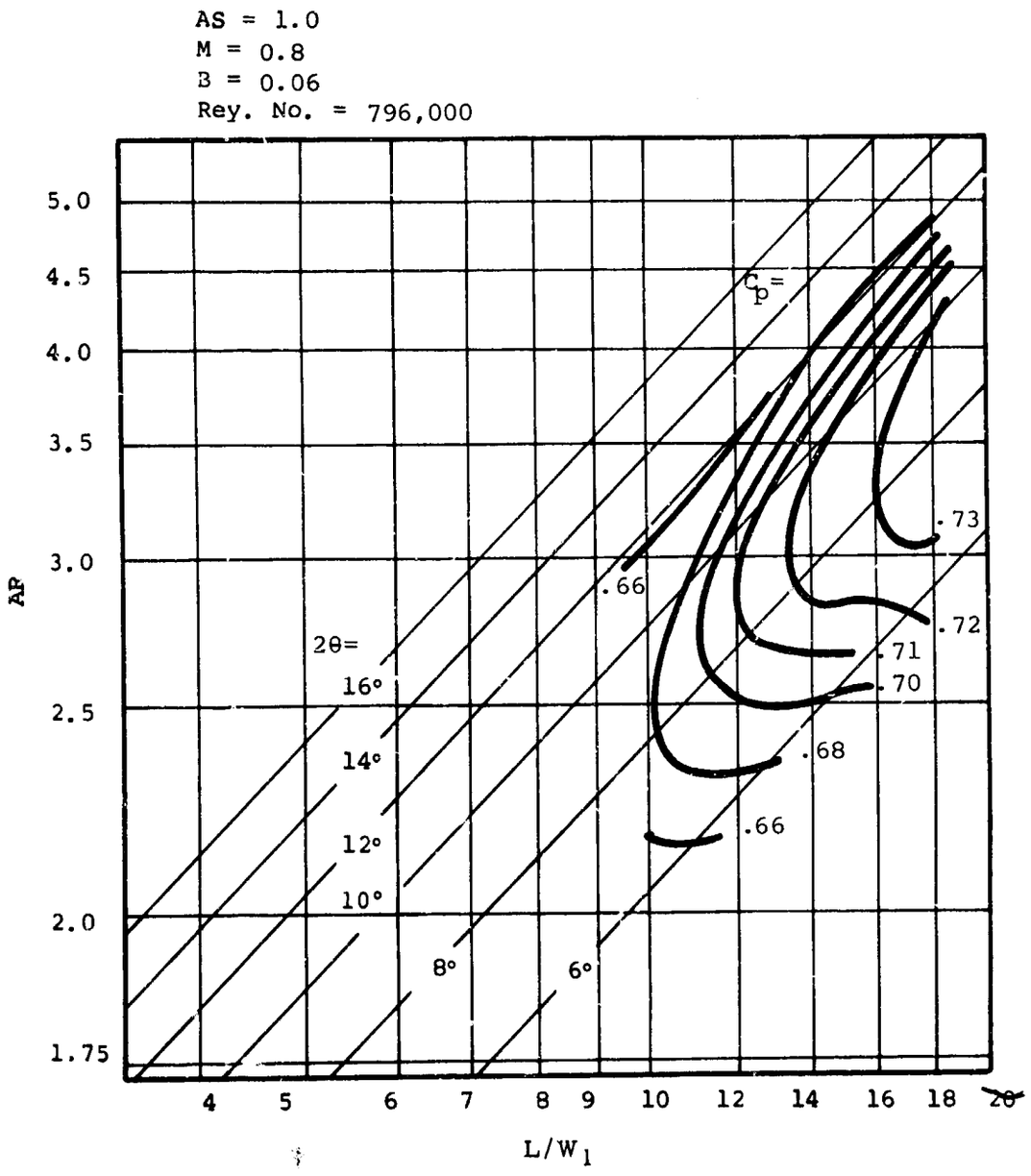

Figure 97. Performance Map - Aspect Ratio = 1.0.

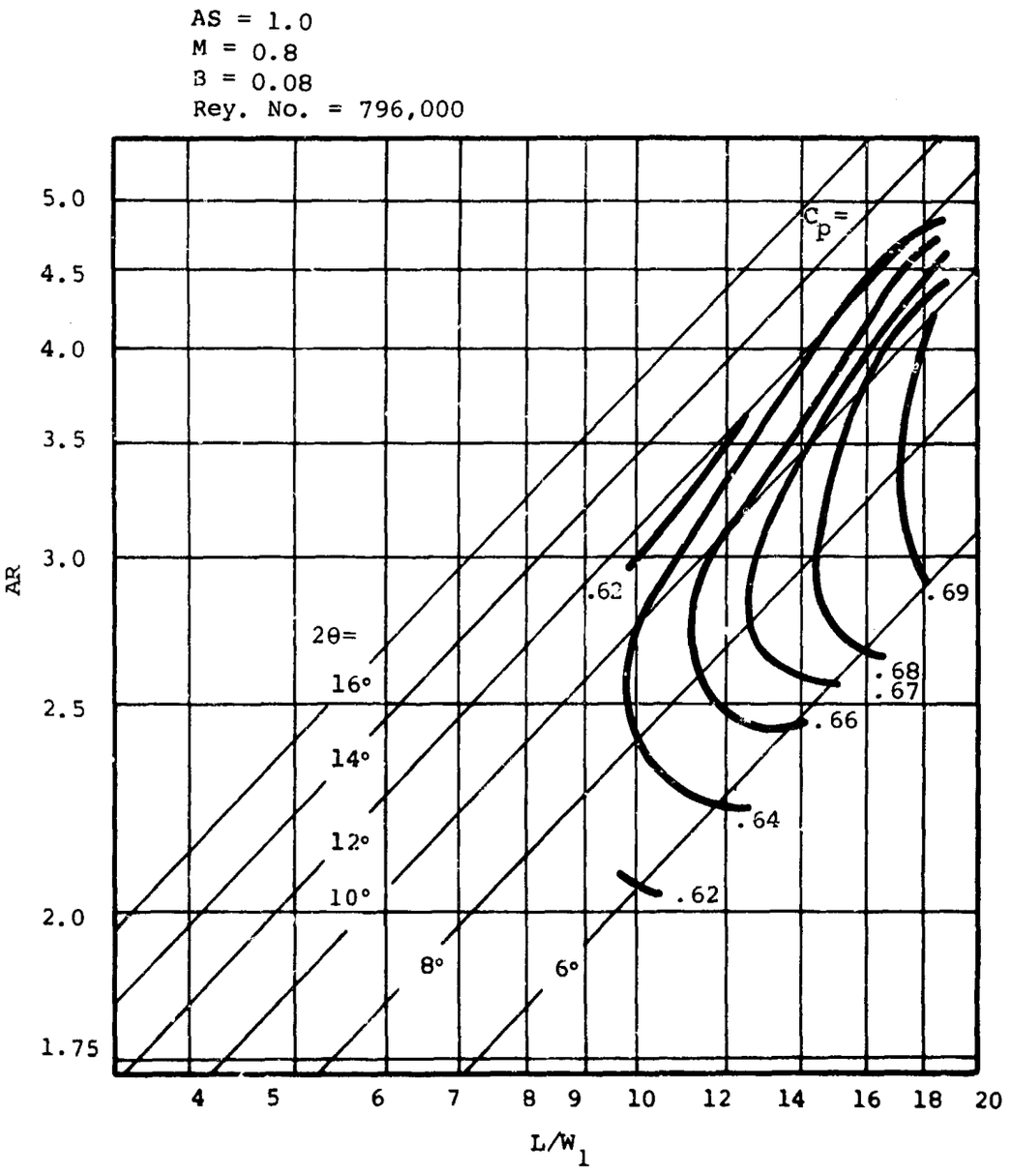

Figure 98. Performance Map - Aspect Ratio = 1.0.

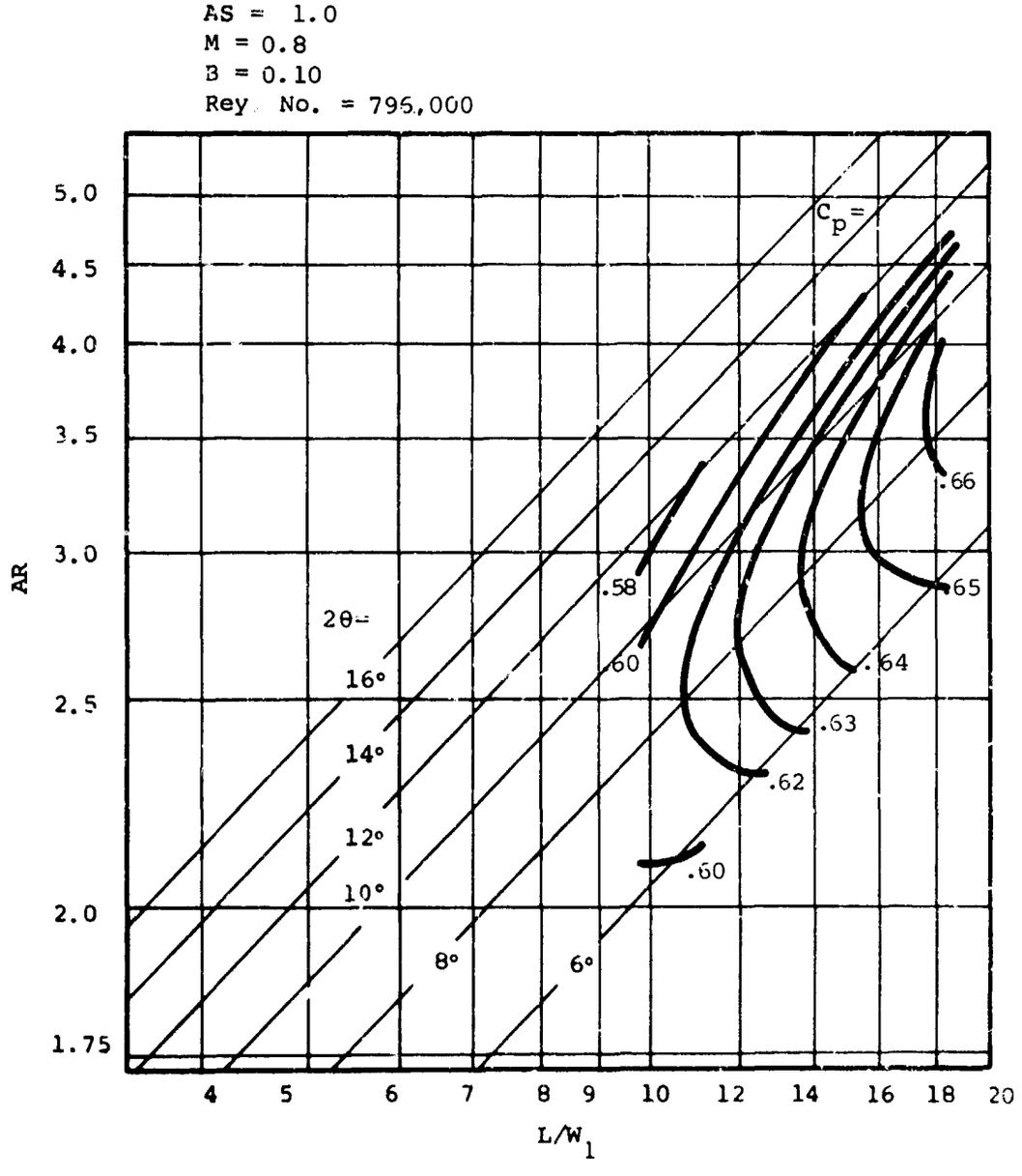

Figure 99. Performance Map - Aspect Ratio = 1.0.

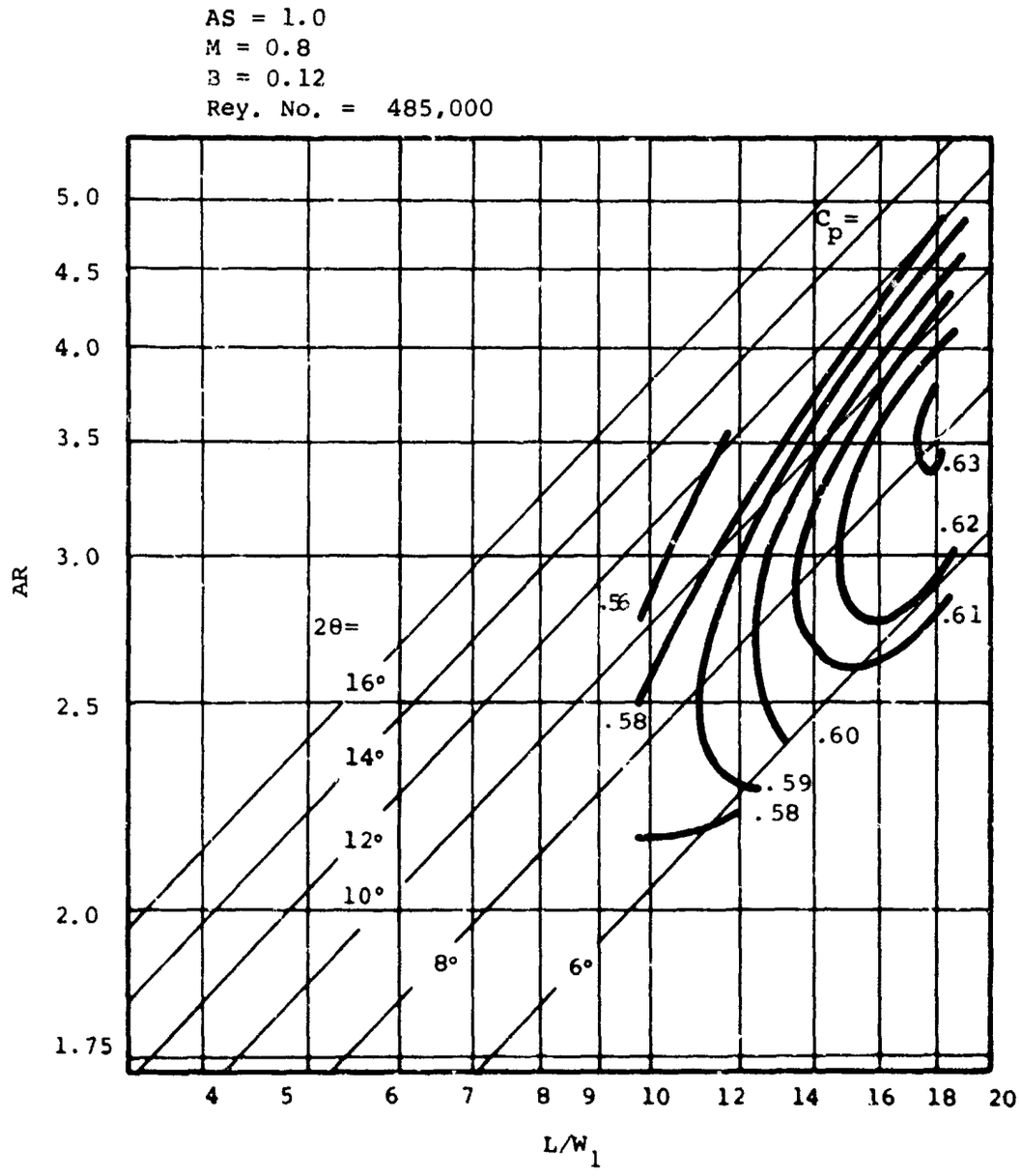

Figure 100. Performance Map - Aspect Ratio = 1.0.

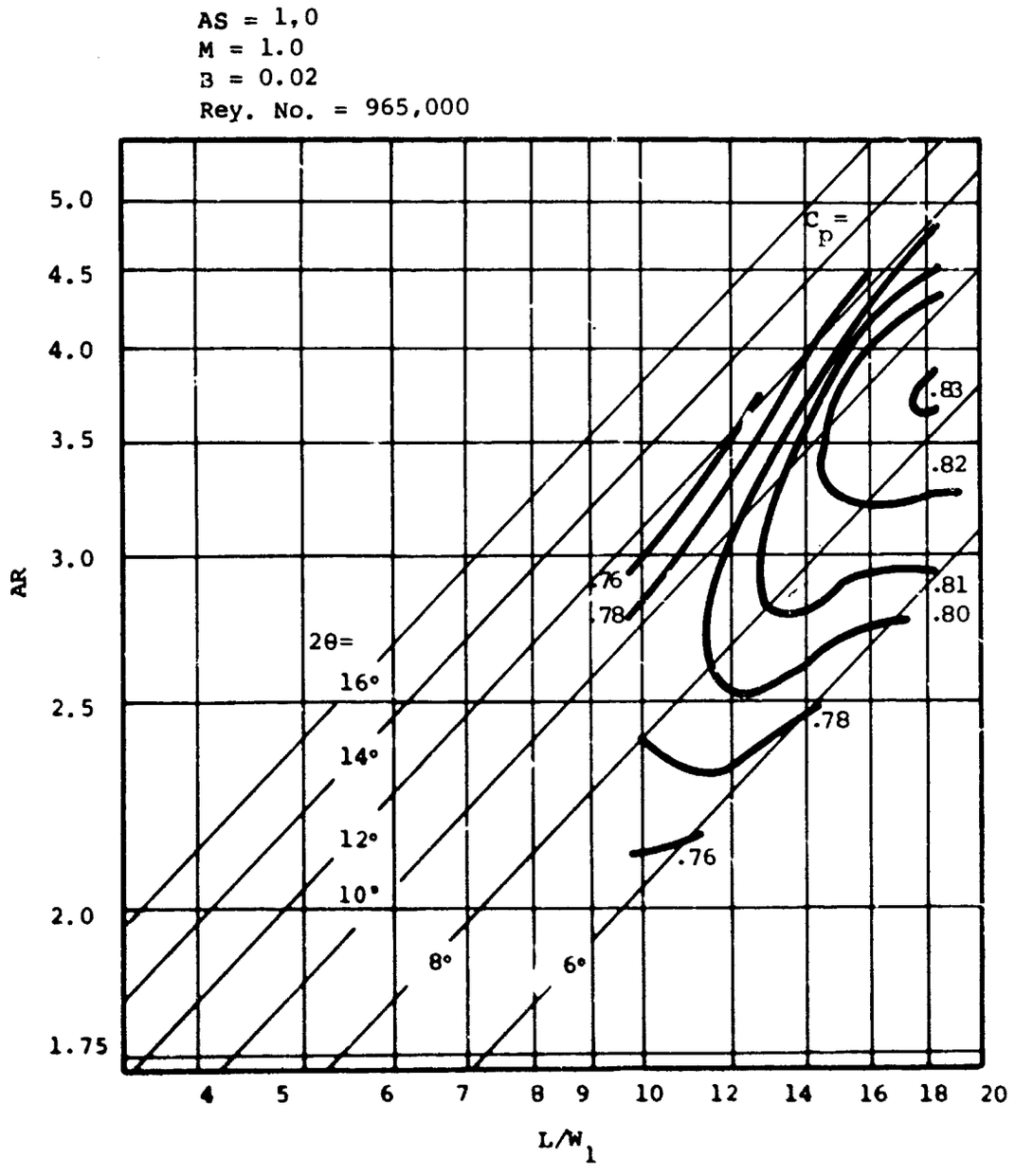

Figure 101. Performance Map - Aspect Ratio = 1.0.

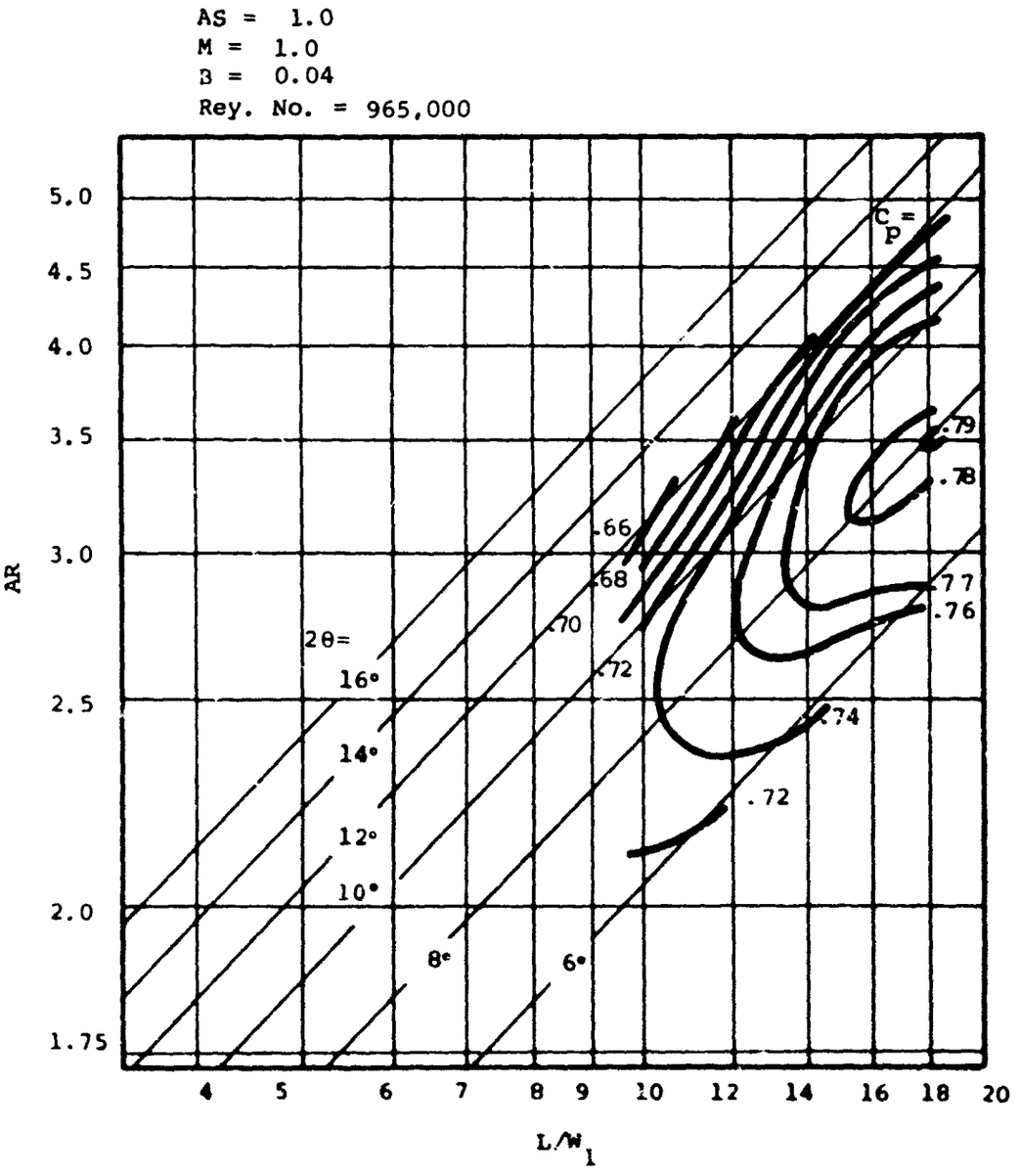

Figure 102. Performance Map - Aspect Ratio = 1.0.

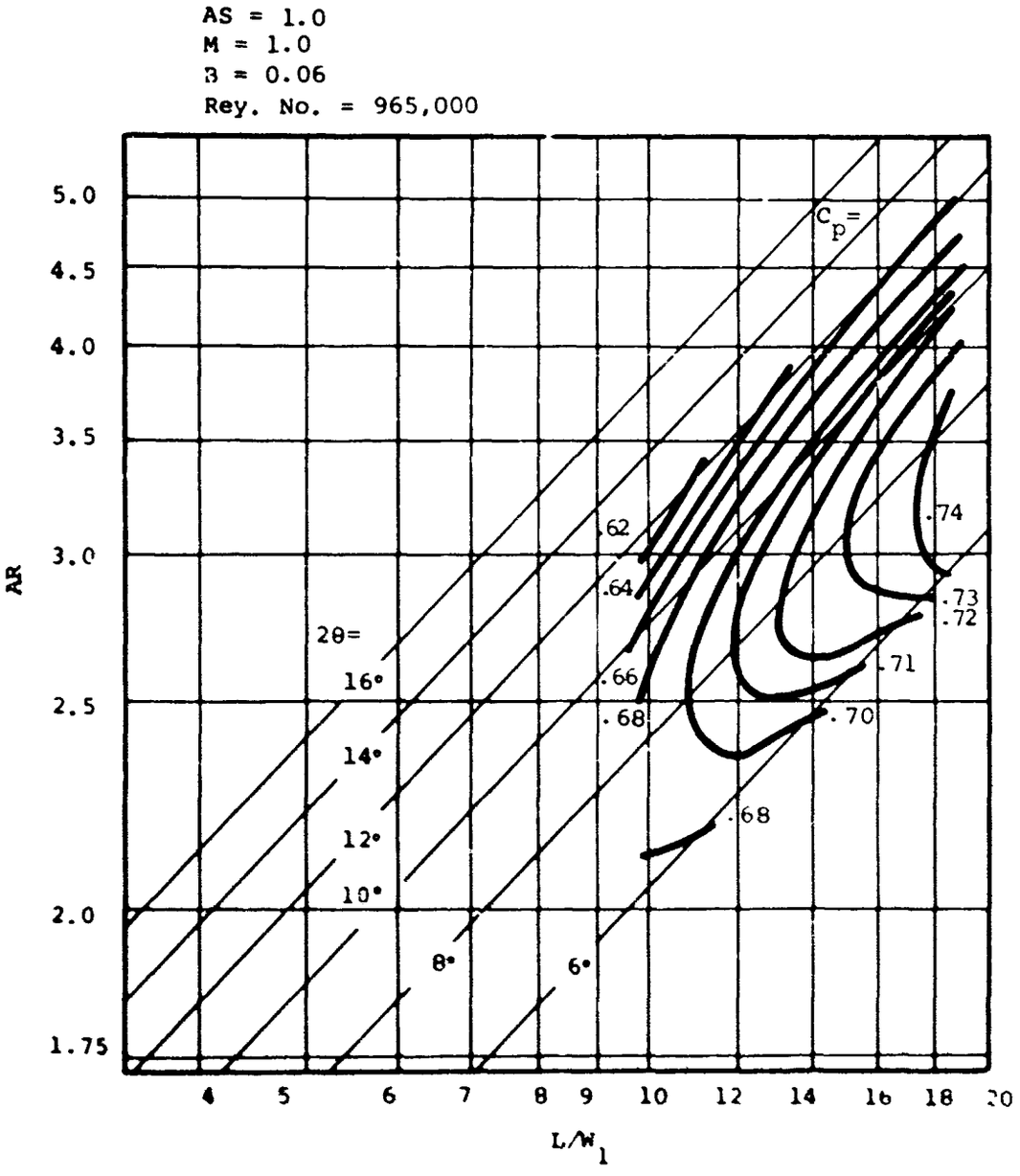

Figure 113. Performance Map - Aspect Ratio = 1.0.

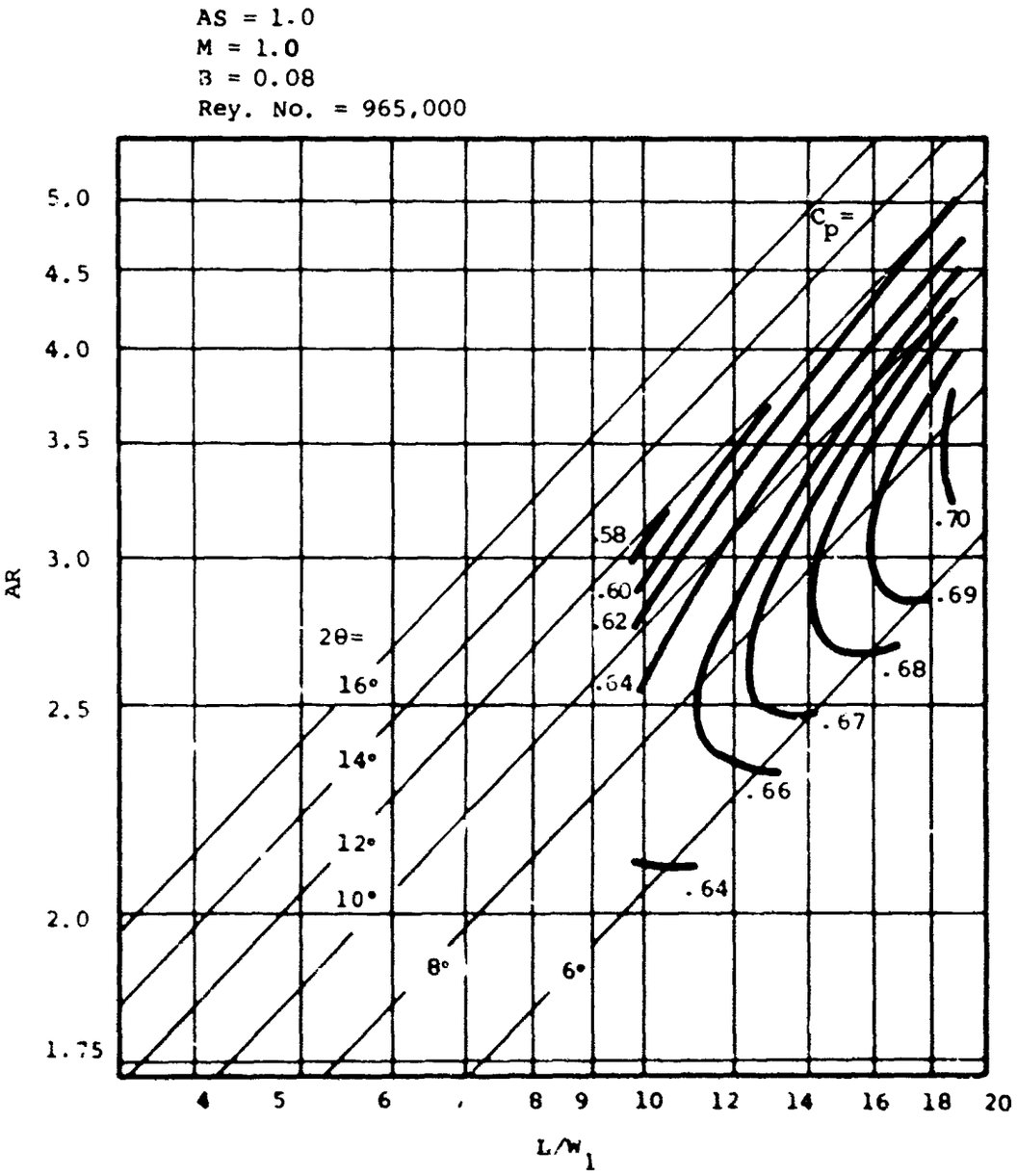

Figure 104. Performance Map - Aspect Ratio = 1.0.

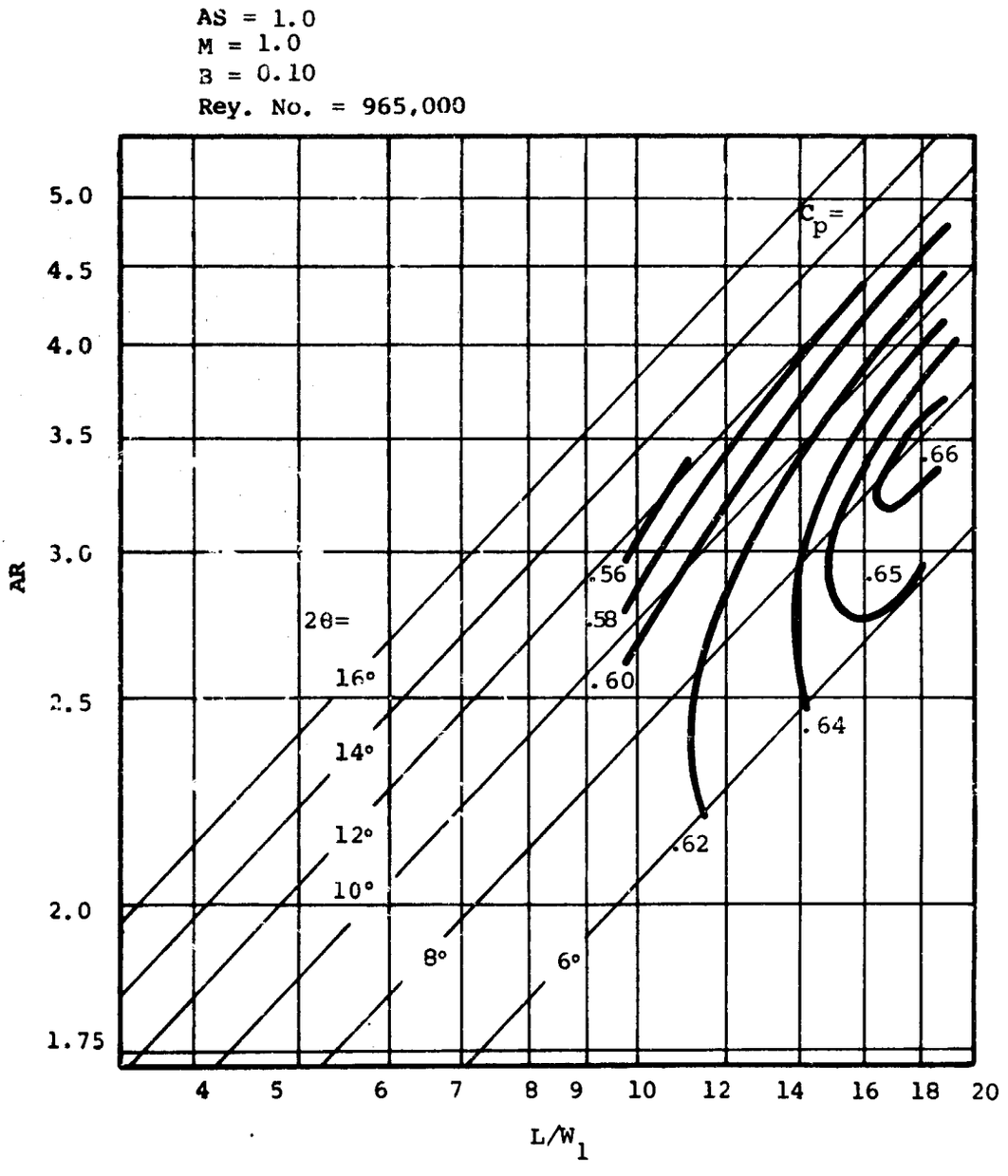

Figure 105. Performance Map - Aspect Ratio = 1.0.

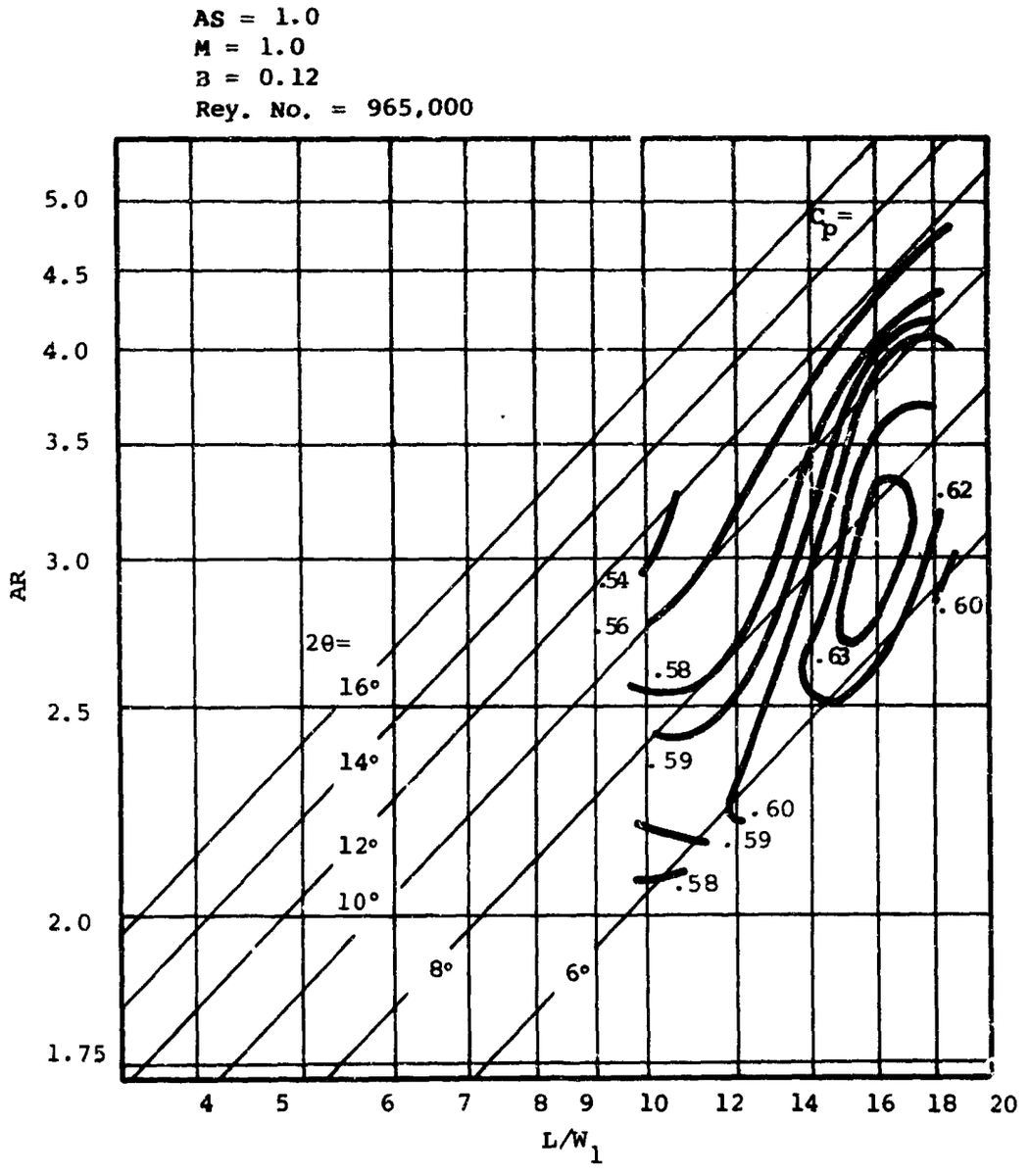

Figure 106. Performance Map - Aspect Ratio = 1.0.

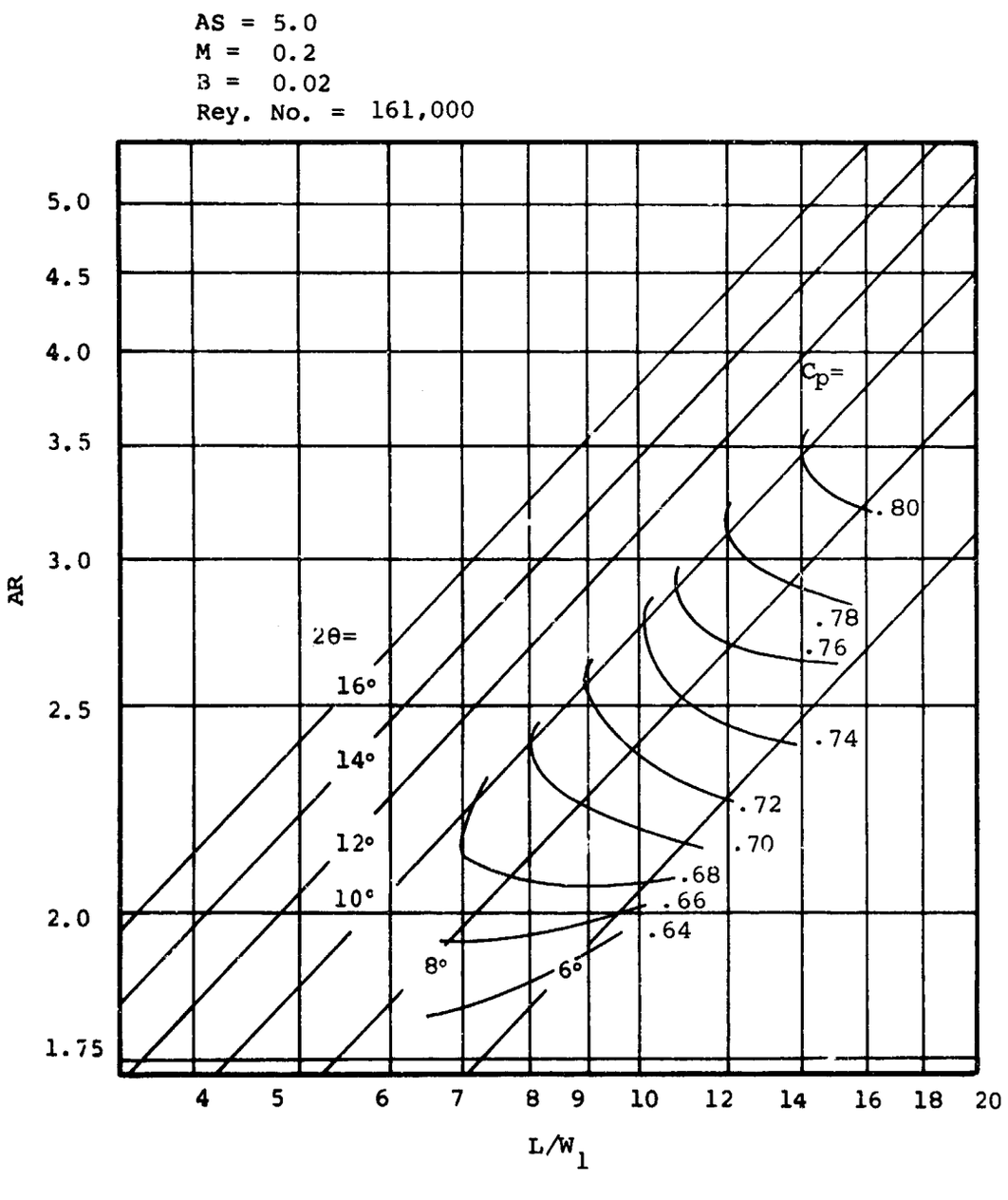

Figure 107. Performance Map - Aspect Ratio = 5.0.

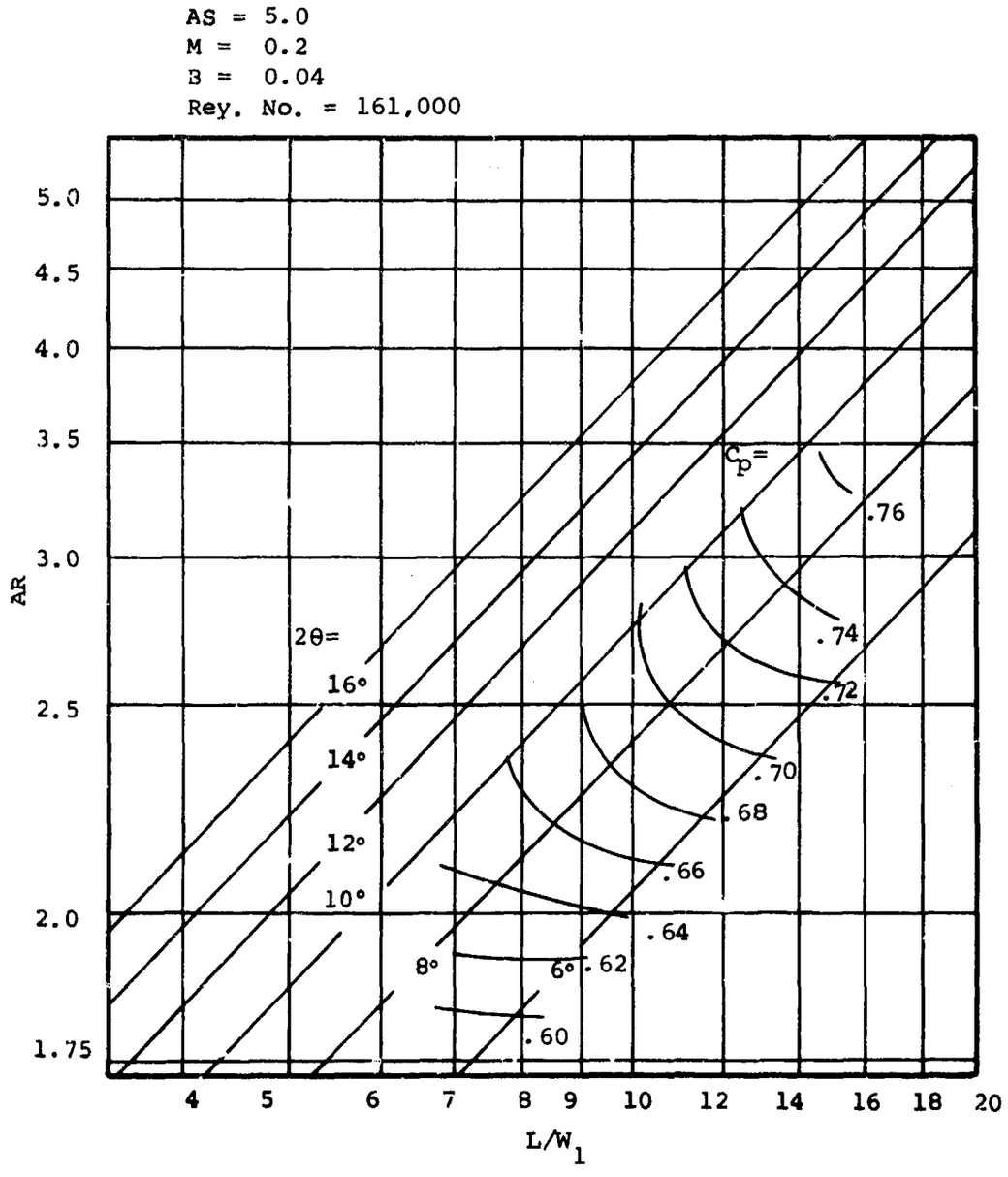

Figure 108. Performance Map - Aspect Ratio = 5.0.

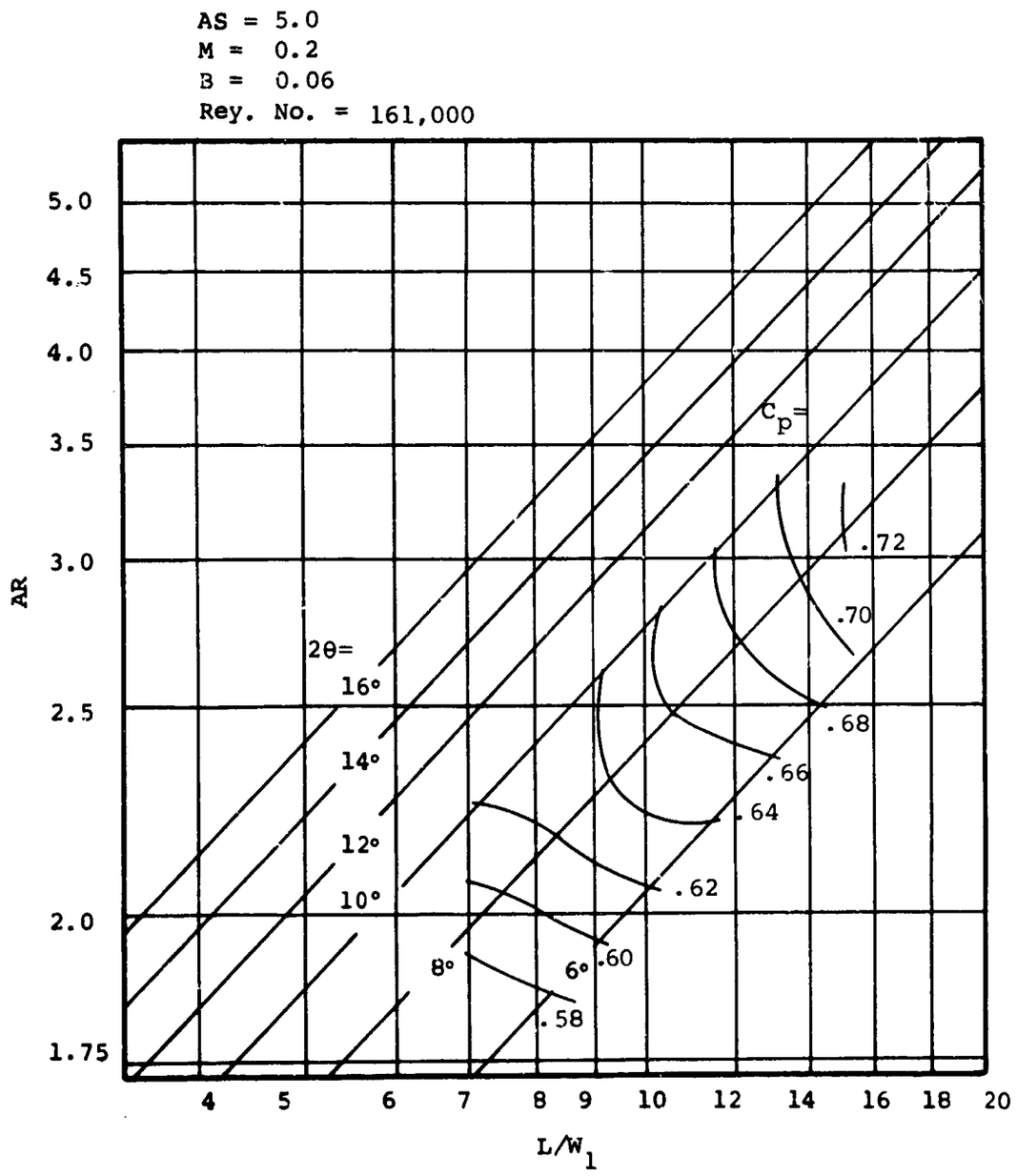

Figure 109. Performance Map - Aspect Ratio = 5.0.

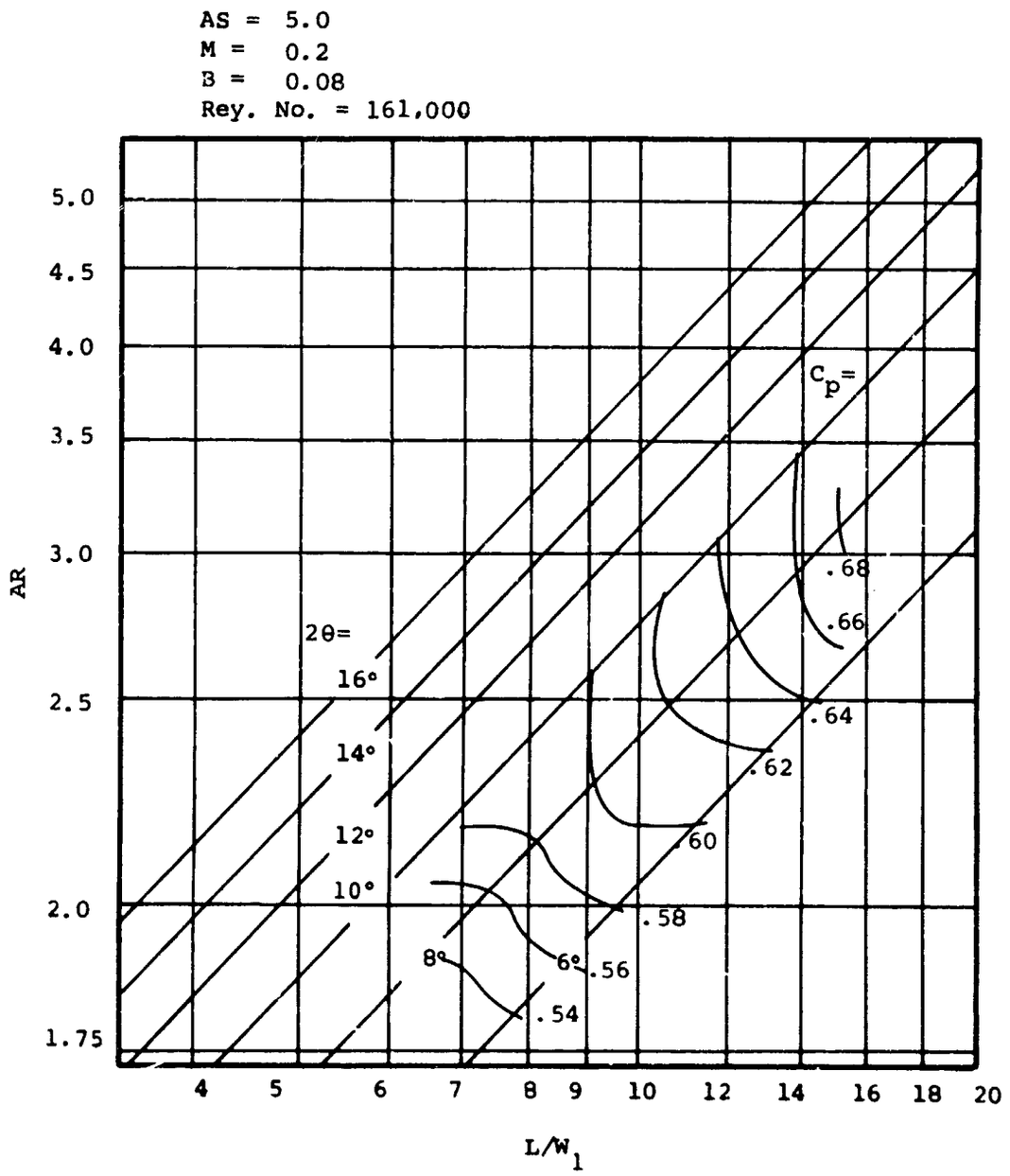

Figure 110. Performance Map - Aspect Ratio = 5.0.

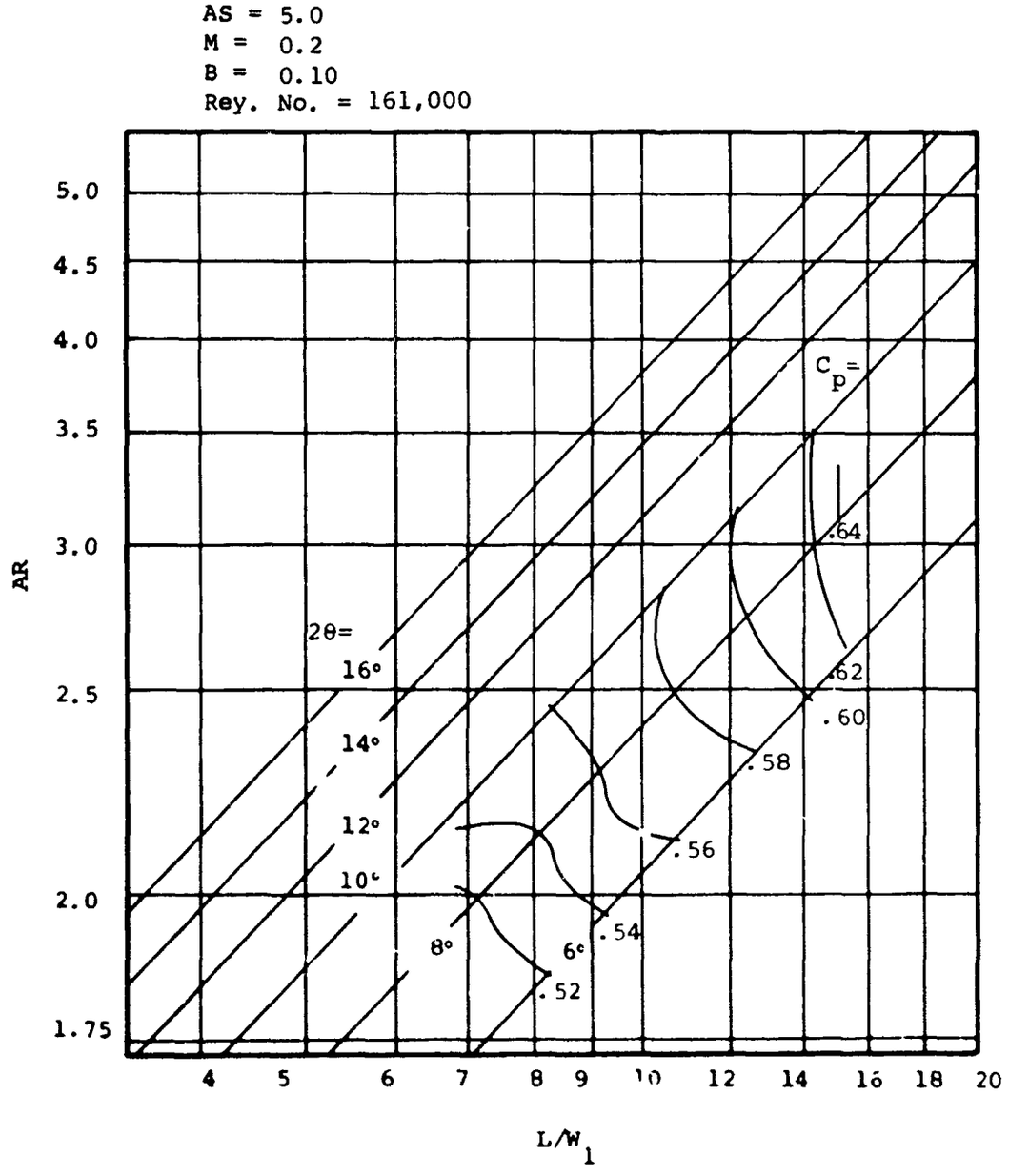

Figure 111. Performance Map - Aspect Ratio = 5.0.

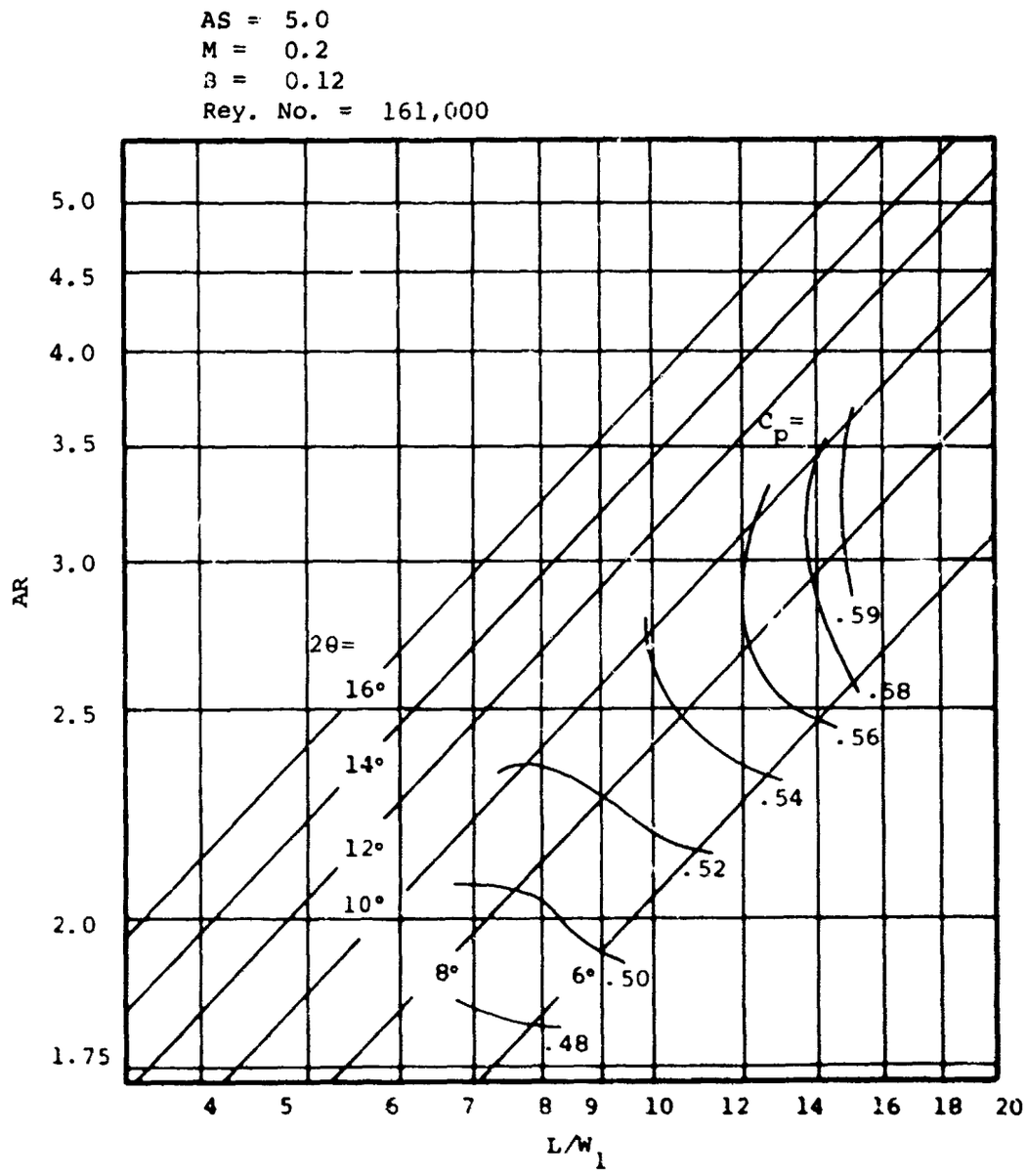

Figure 112. Performance Map - Aspect Ratio = 5.0.

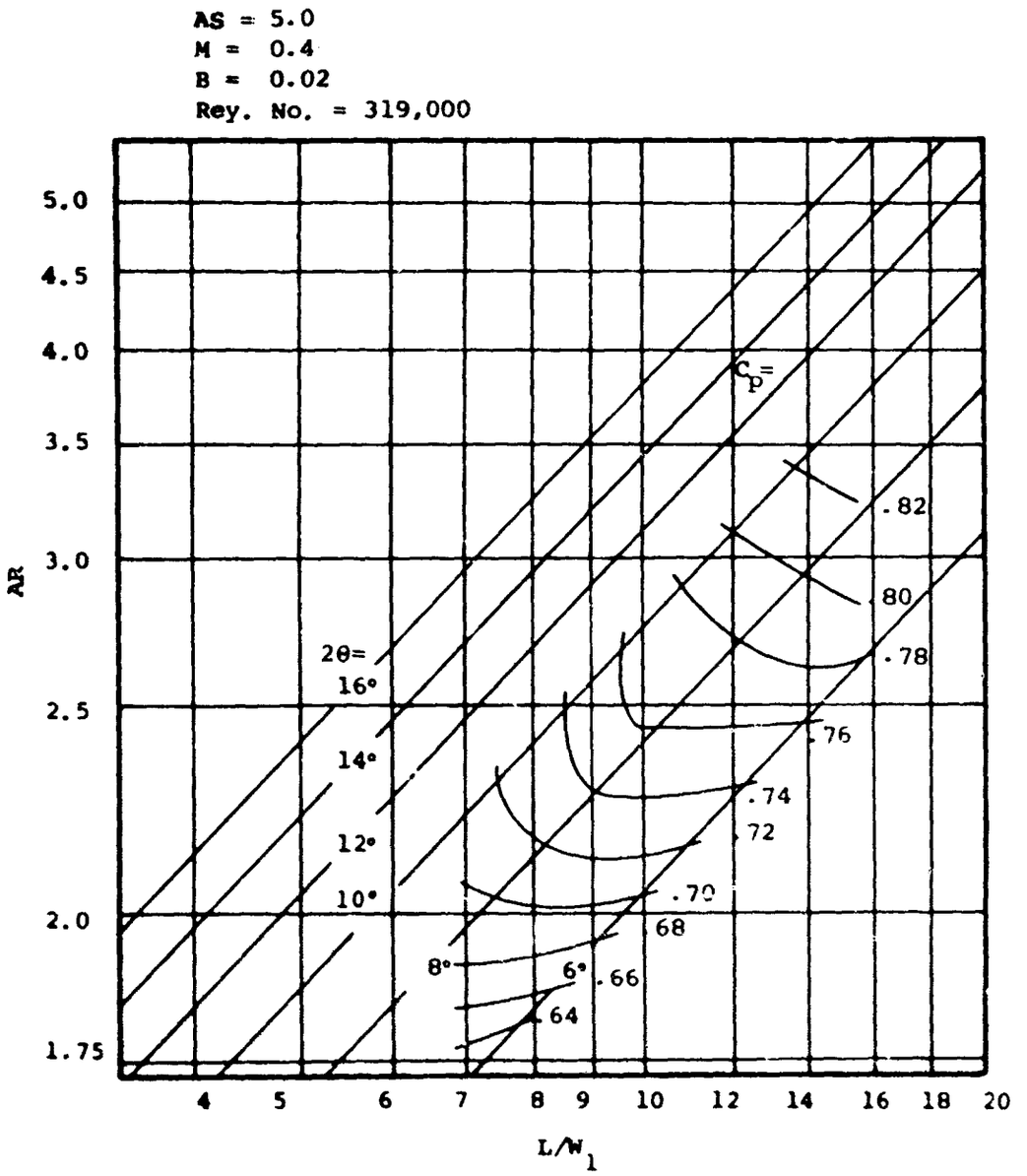

Figure 113. Performance Map - Aspect Ratio = 5.0.

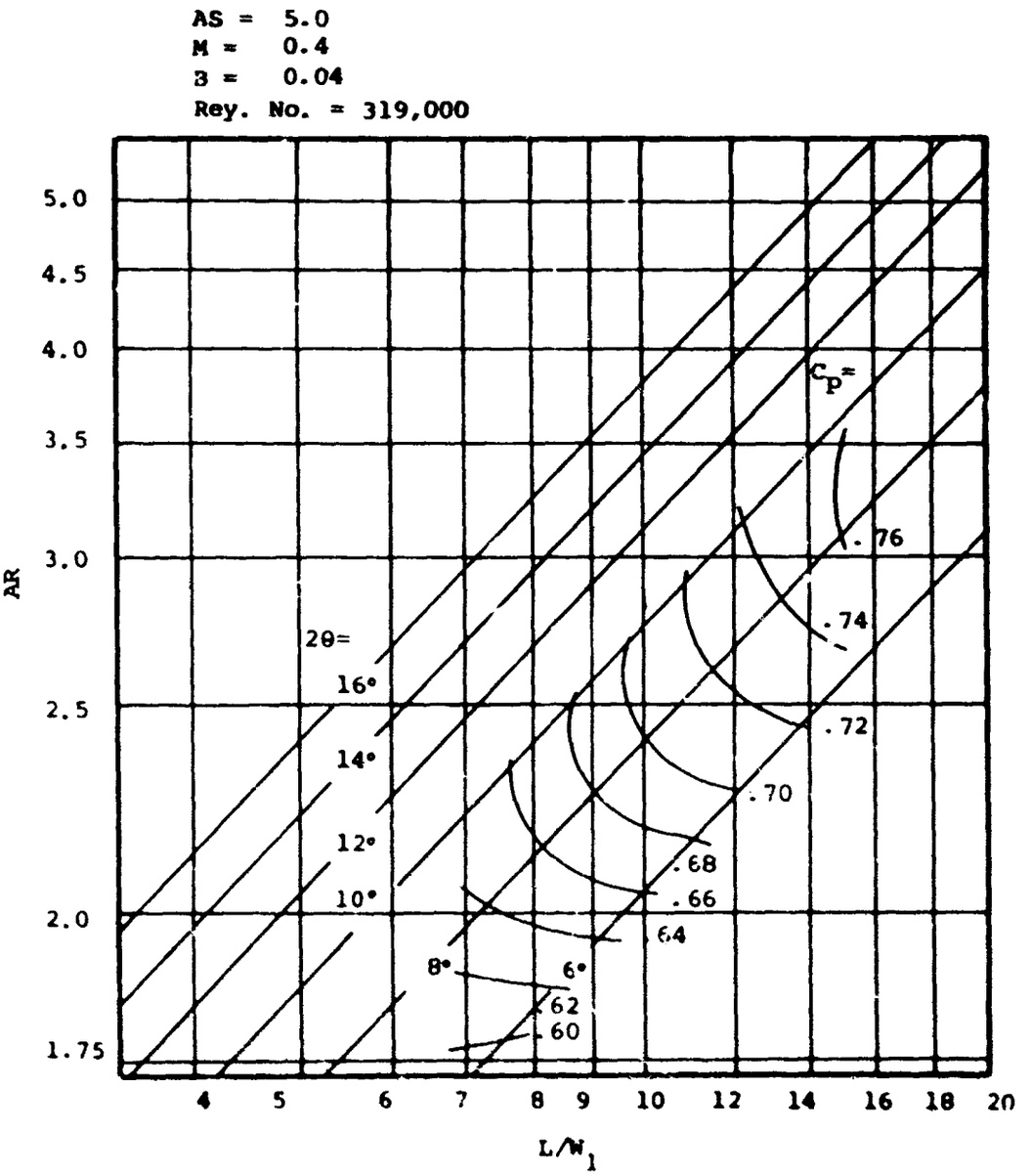

Figure 114. Performance Map - Aspect Ratio = 5.0.

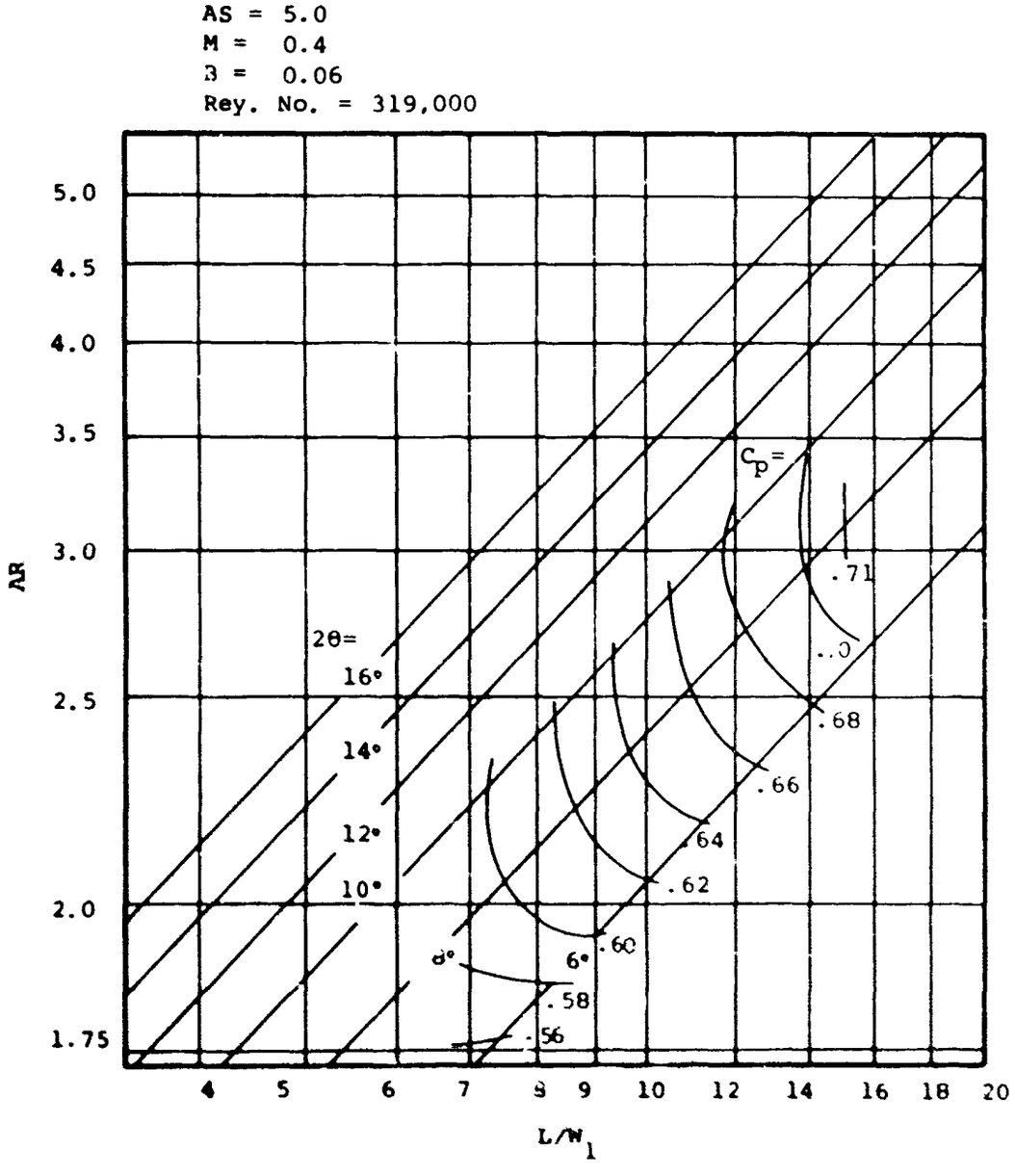

Figure 115. Performance Map - Aspect Ratio = 5.0.

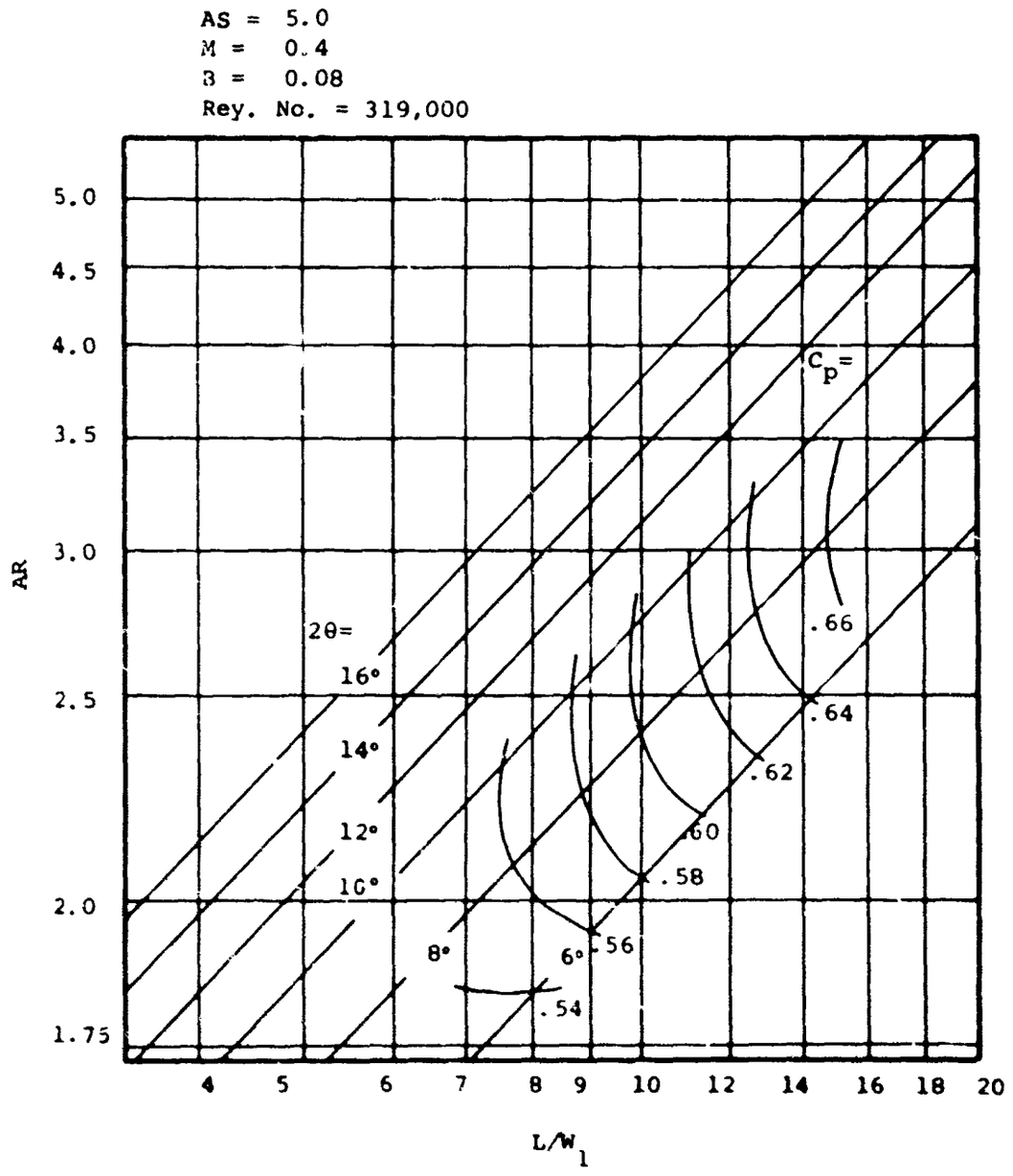

Figure 116. Performance Map - Aspect Ratio = 5.0.

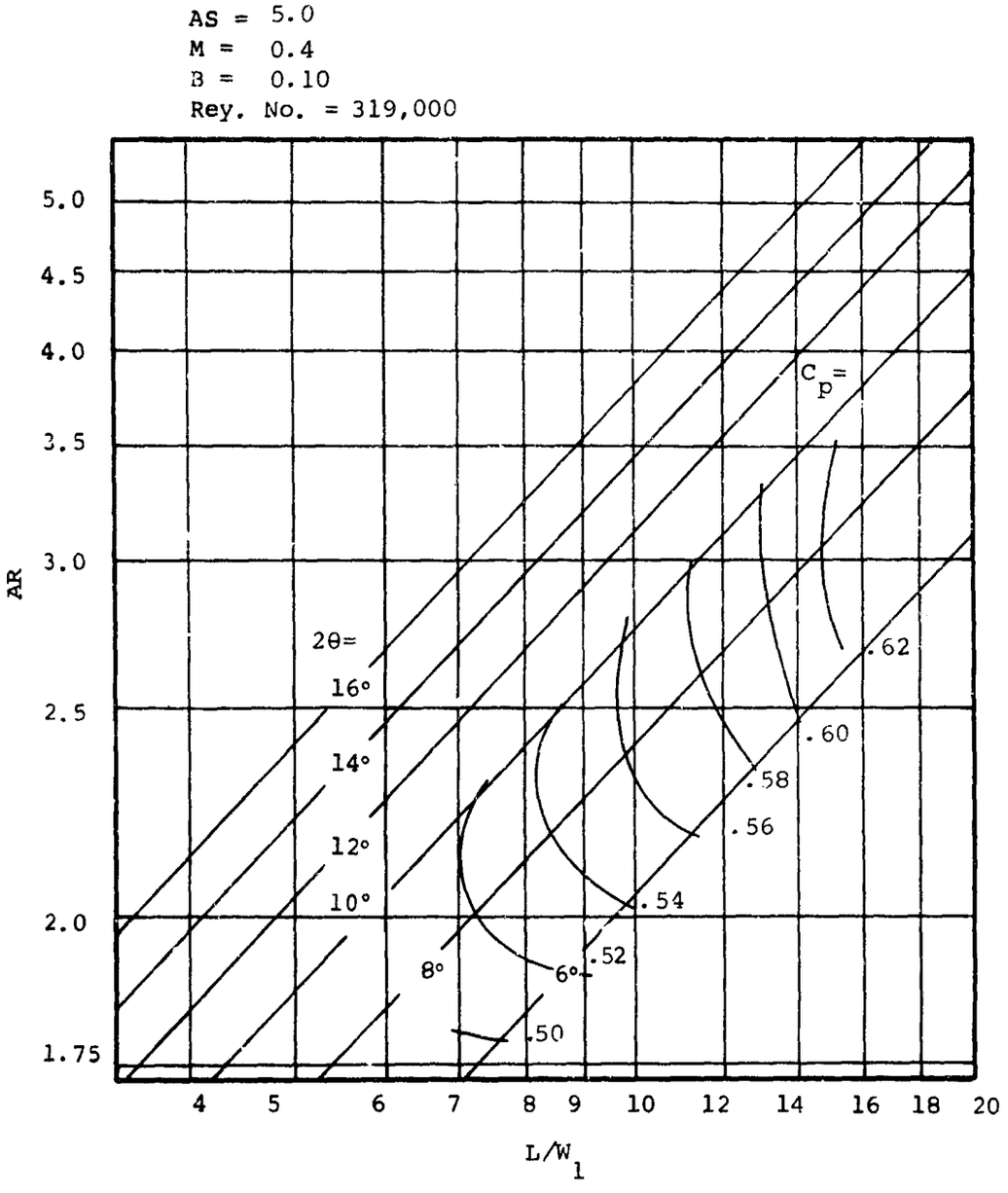

Figure 117. Performance Map - Aspect Ratio = 5.0.

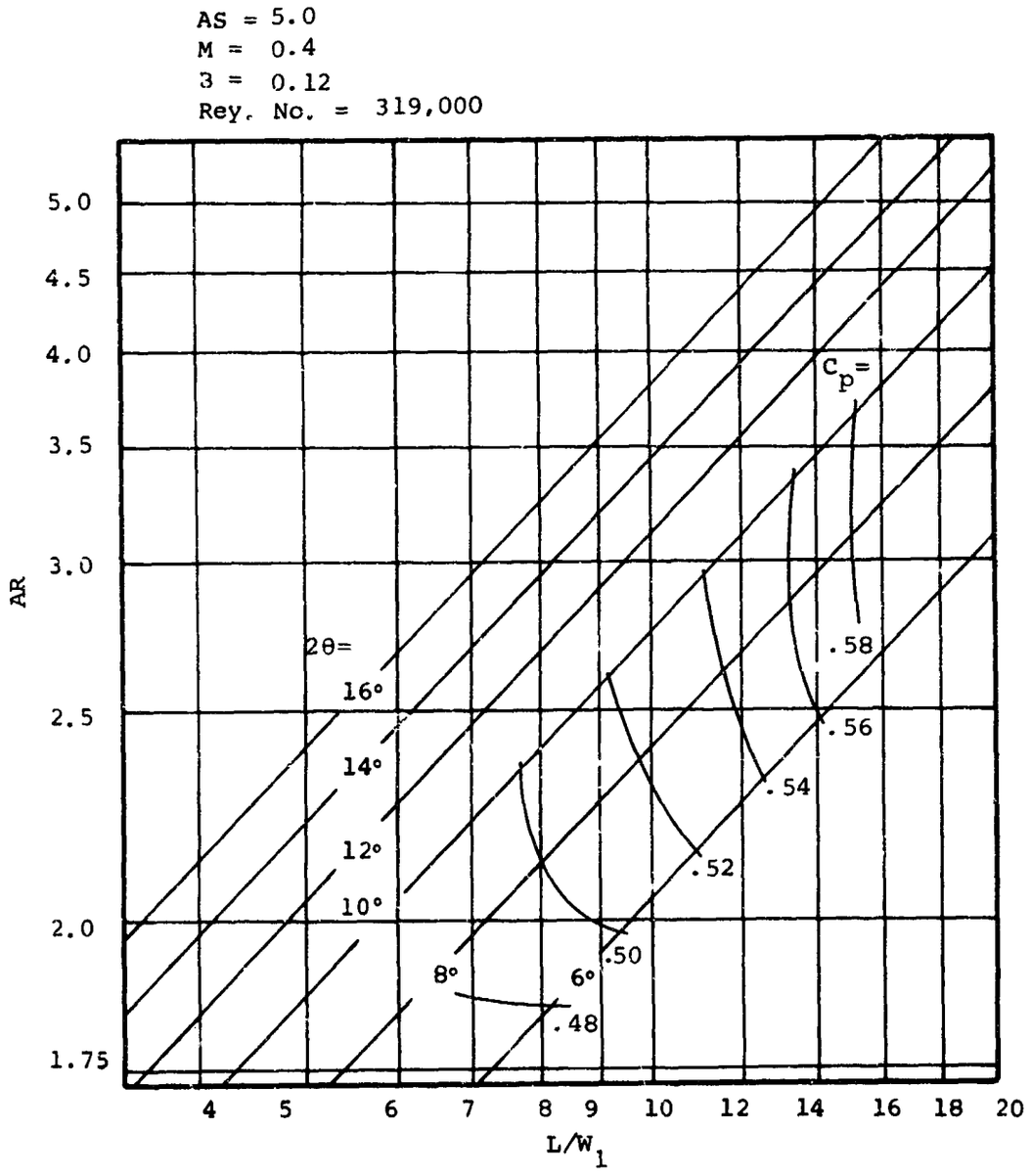

Figure 118. Performance Map - Aspect Ratio = 5.0.

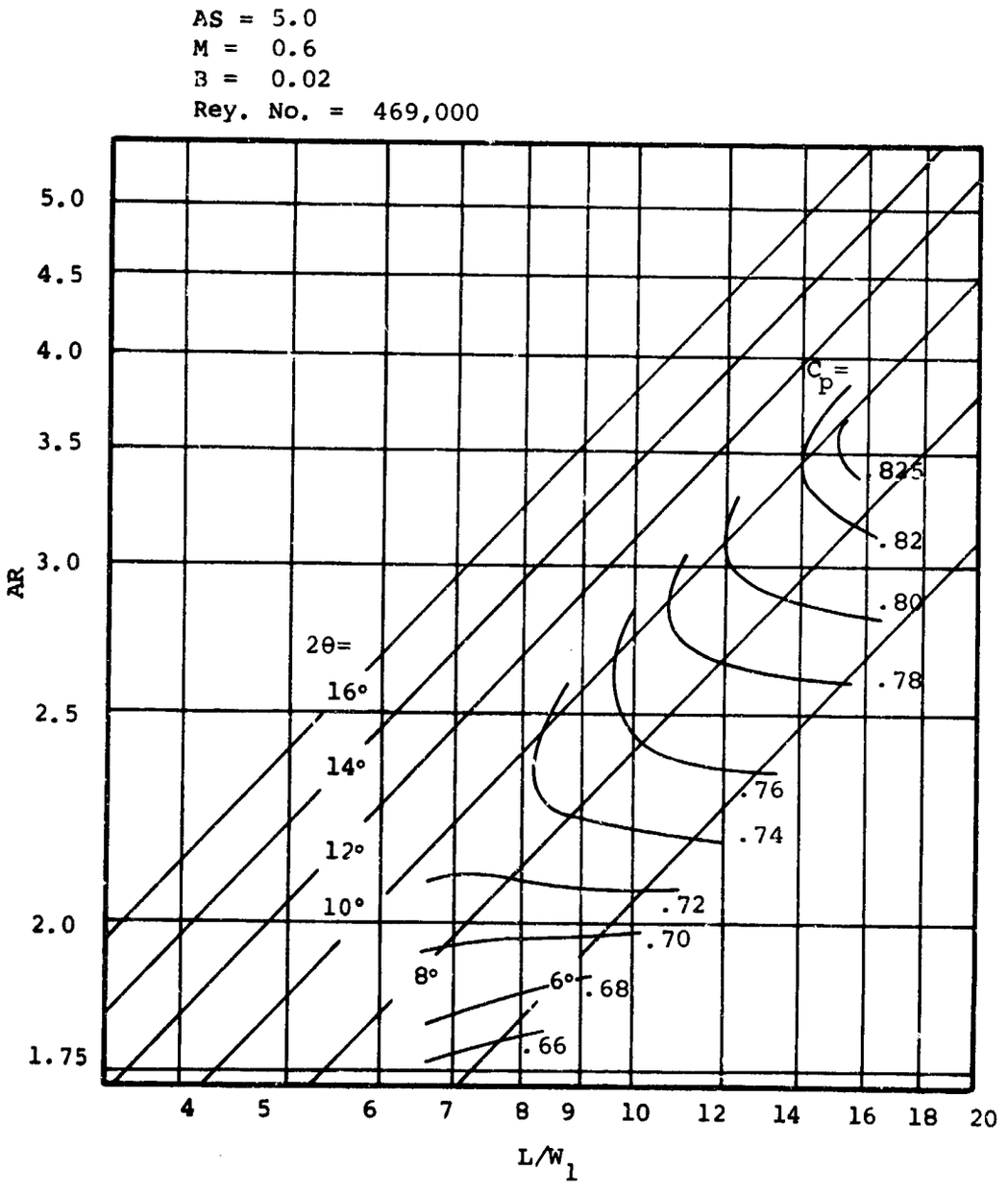

Figure 119. Performance Map - Aspect Ratio = 5.0.

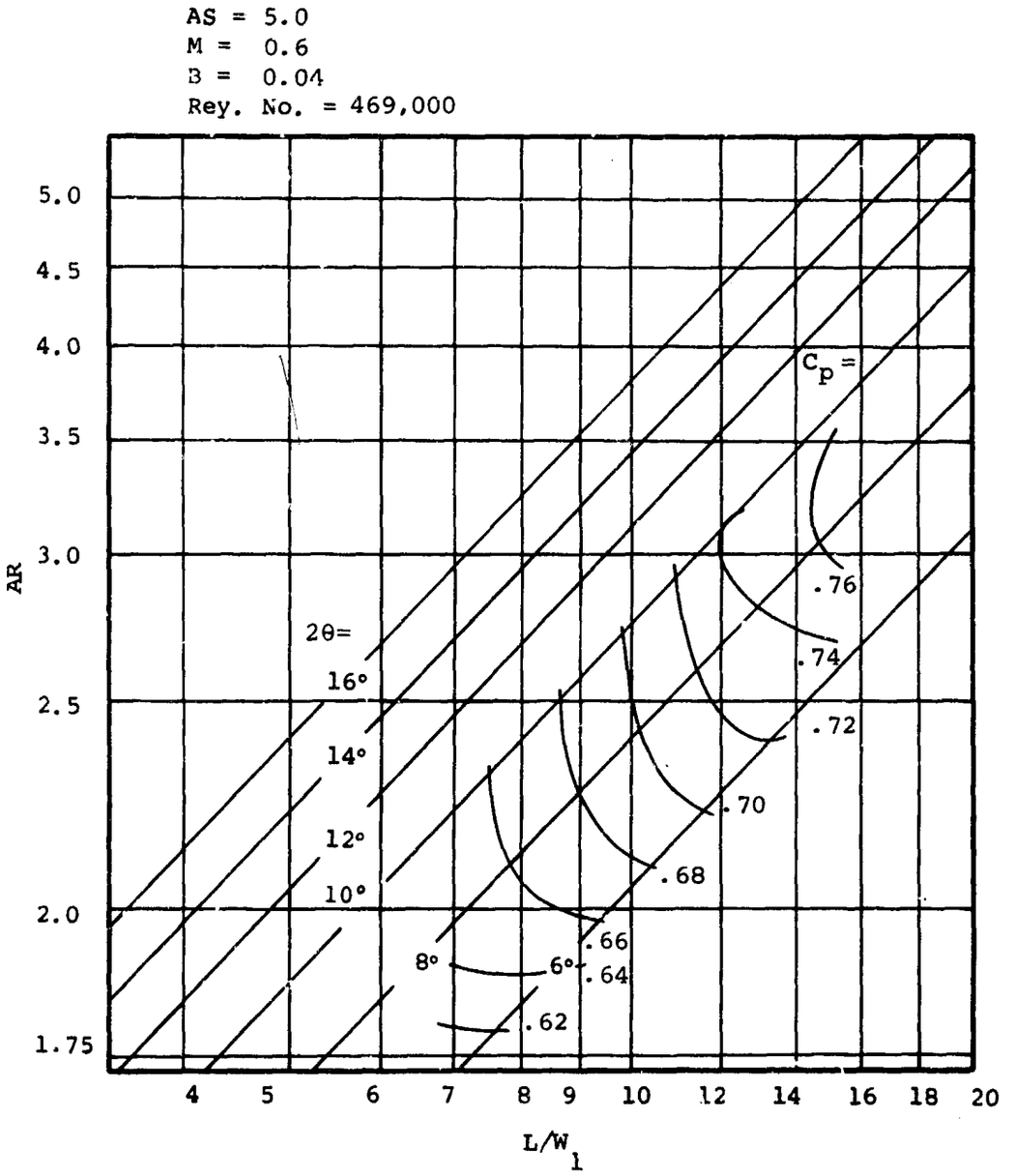

Figure 120. Performance Map - Aspect Ratio = 5.0.

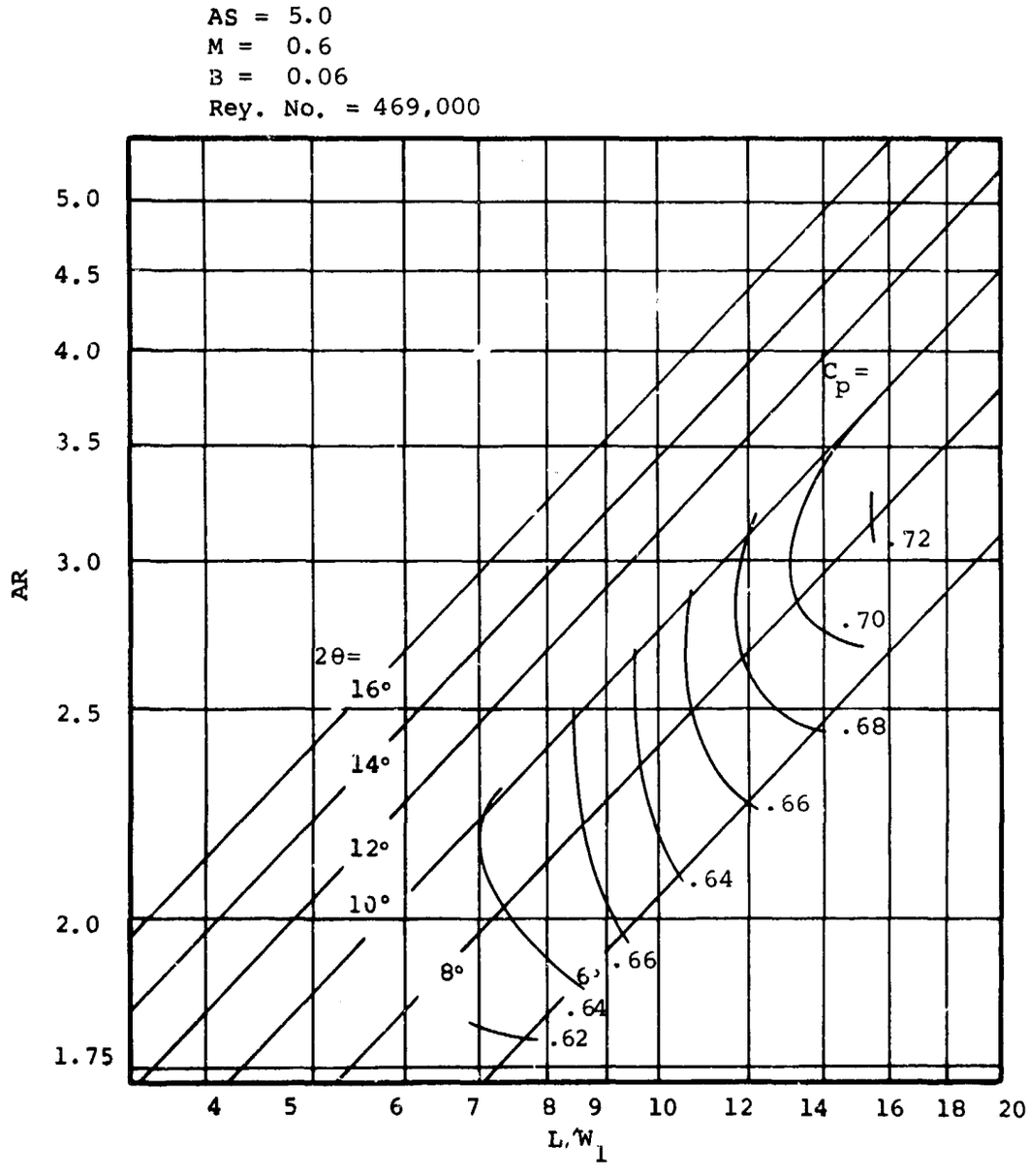

Figure 121. Performance Map - Aspect Ratio = 5.0.

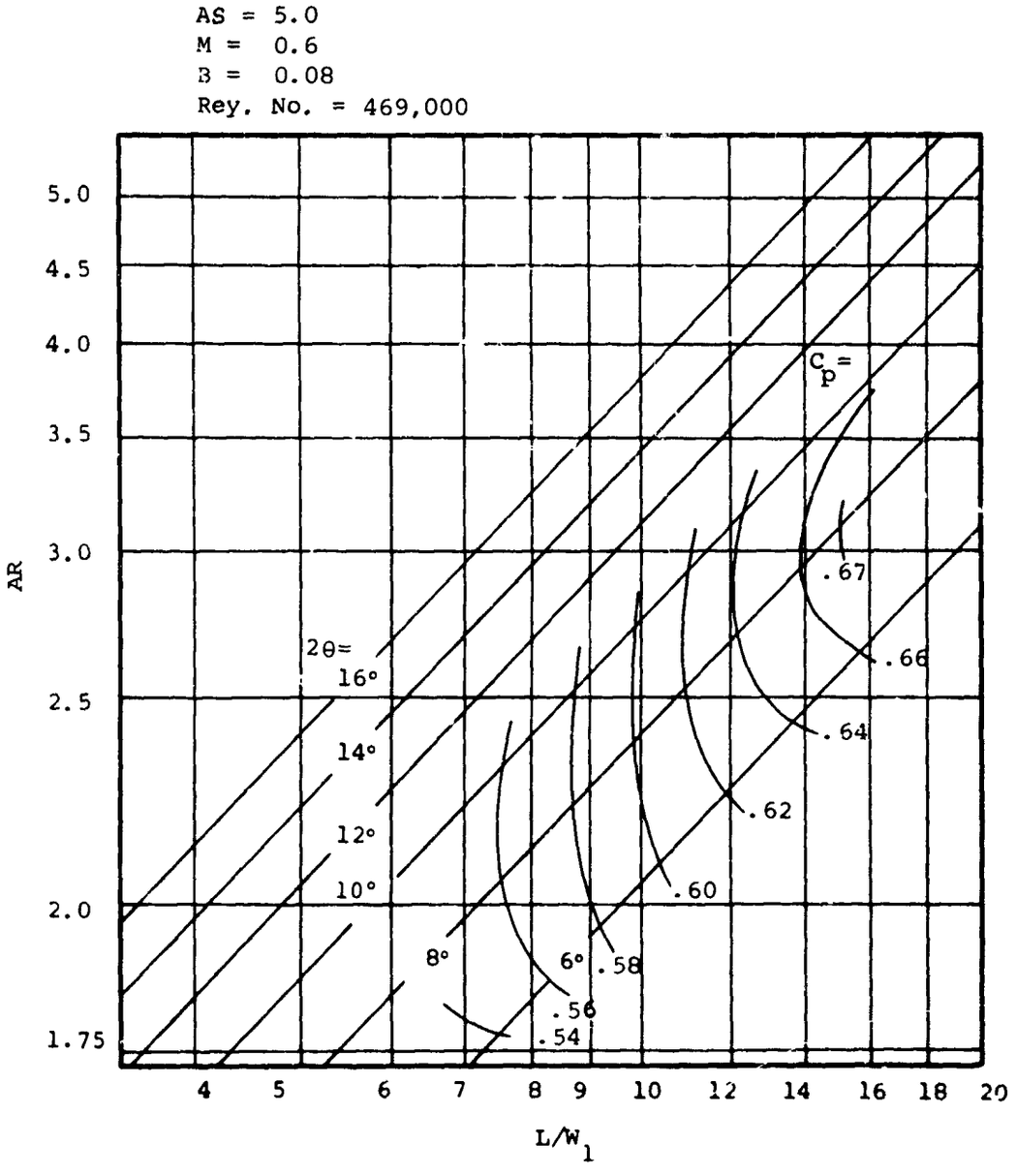

Figure 122. Performance Map - Aspect Ratio = 5.0.

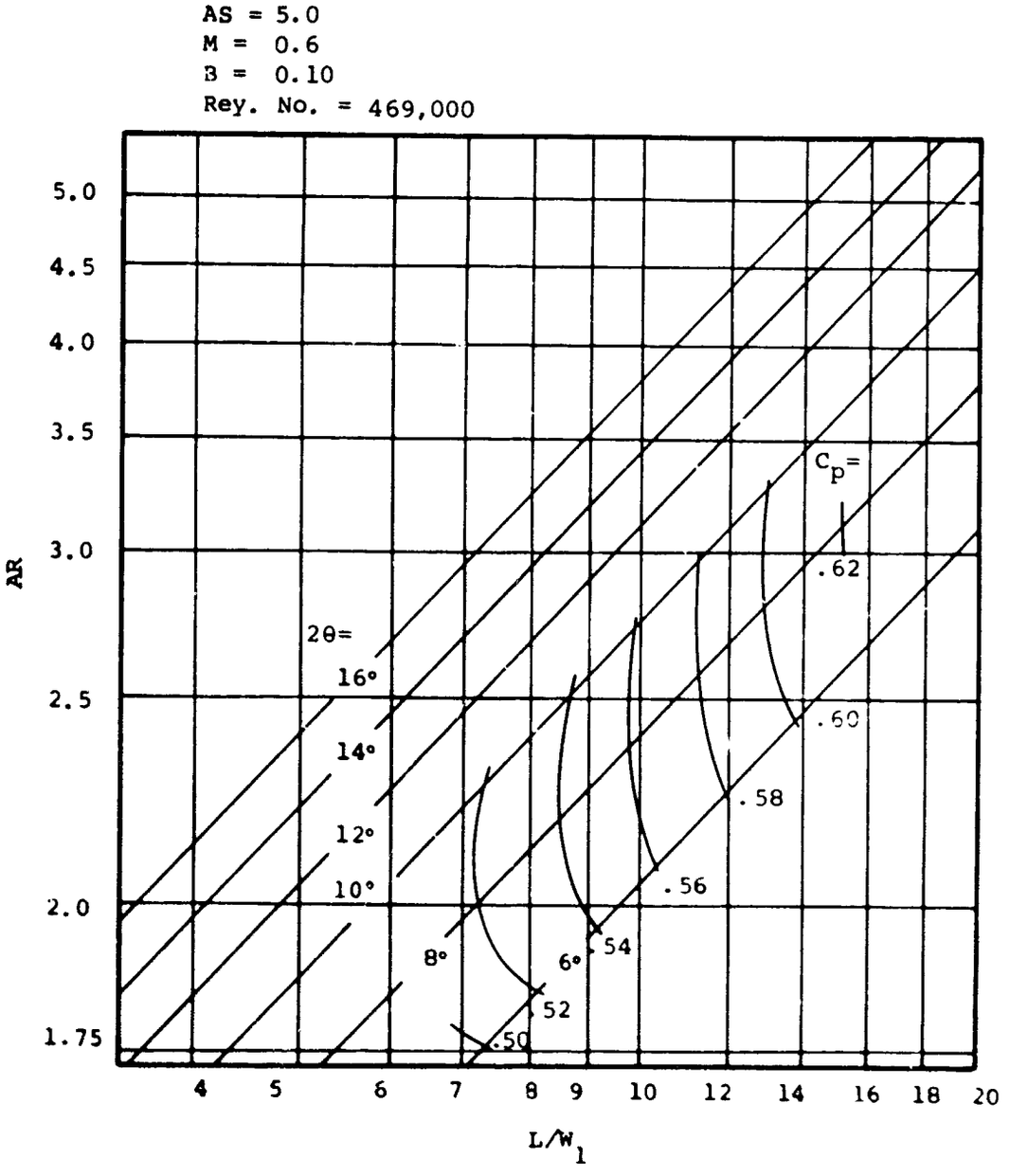

Figure 123. Performance Map - Aspect Ratio = 5.0.

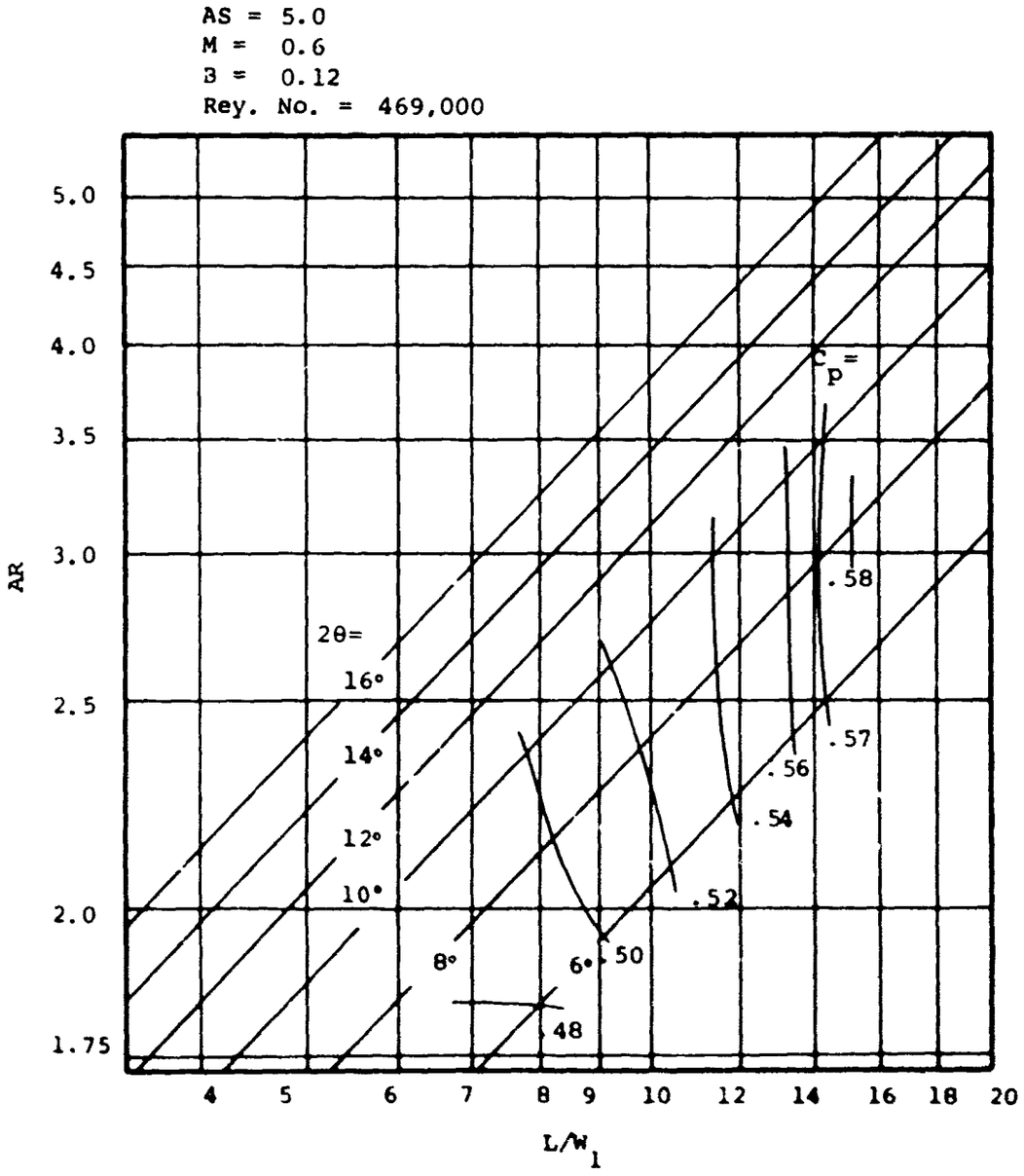

Figure 124. Performance Map - Aspect Ratio = 5.0.

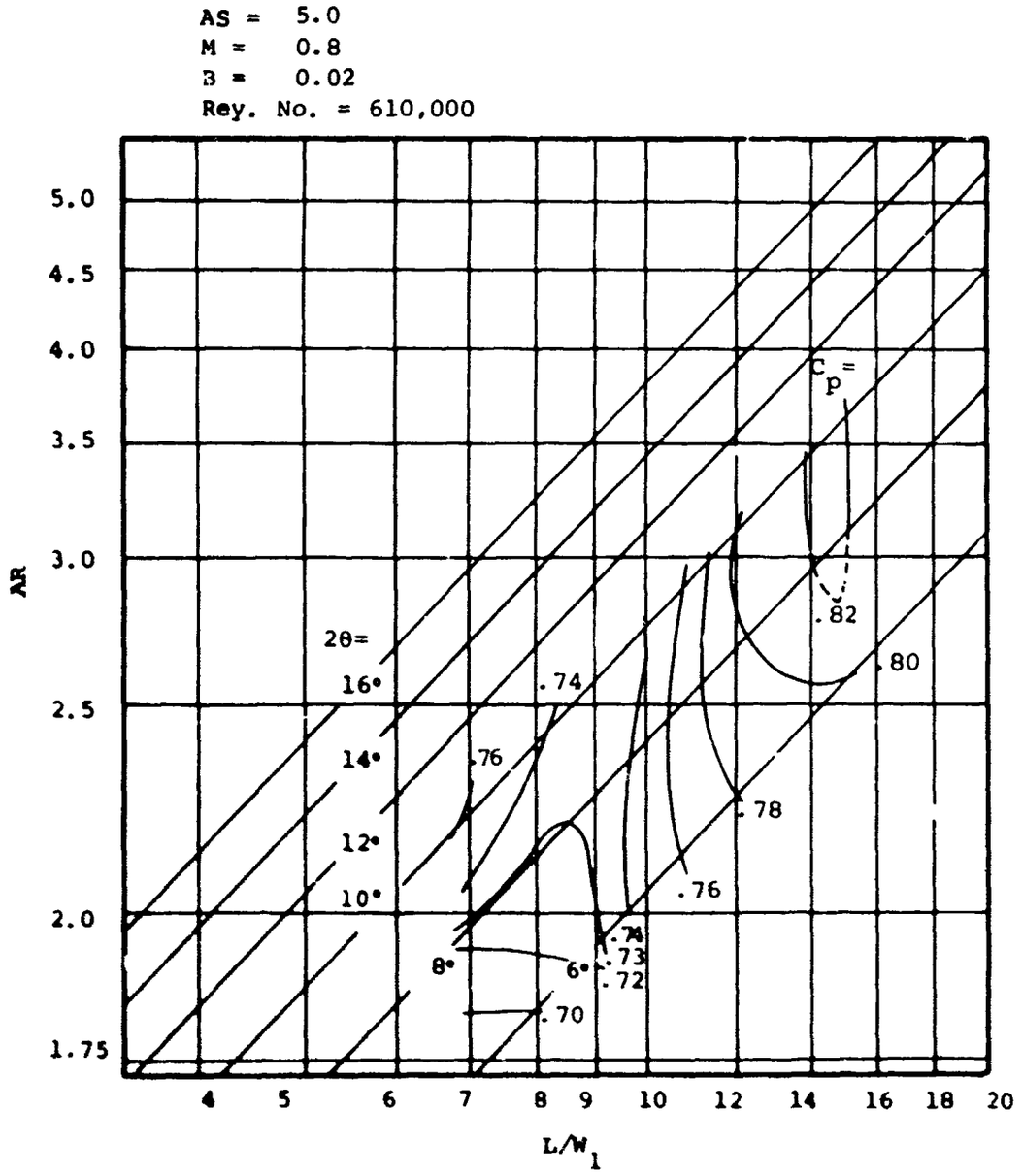

Figure 125. Performance Map - Aspect Ratio = 5.0.

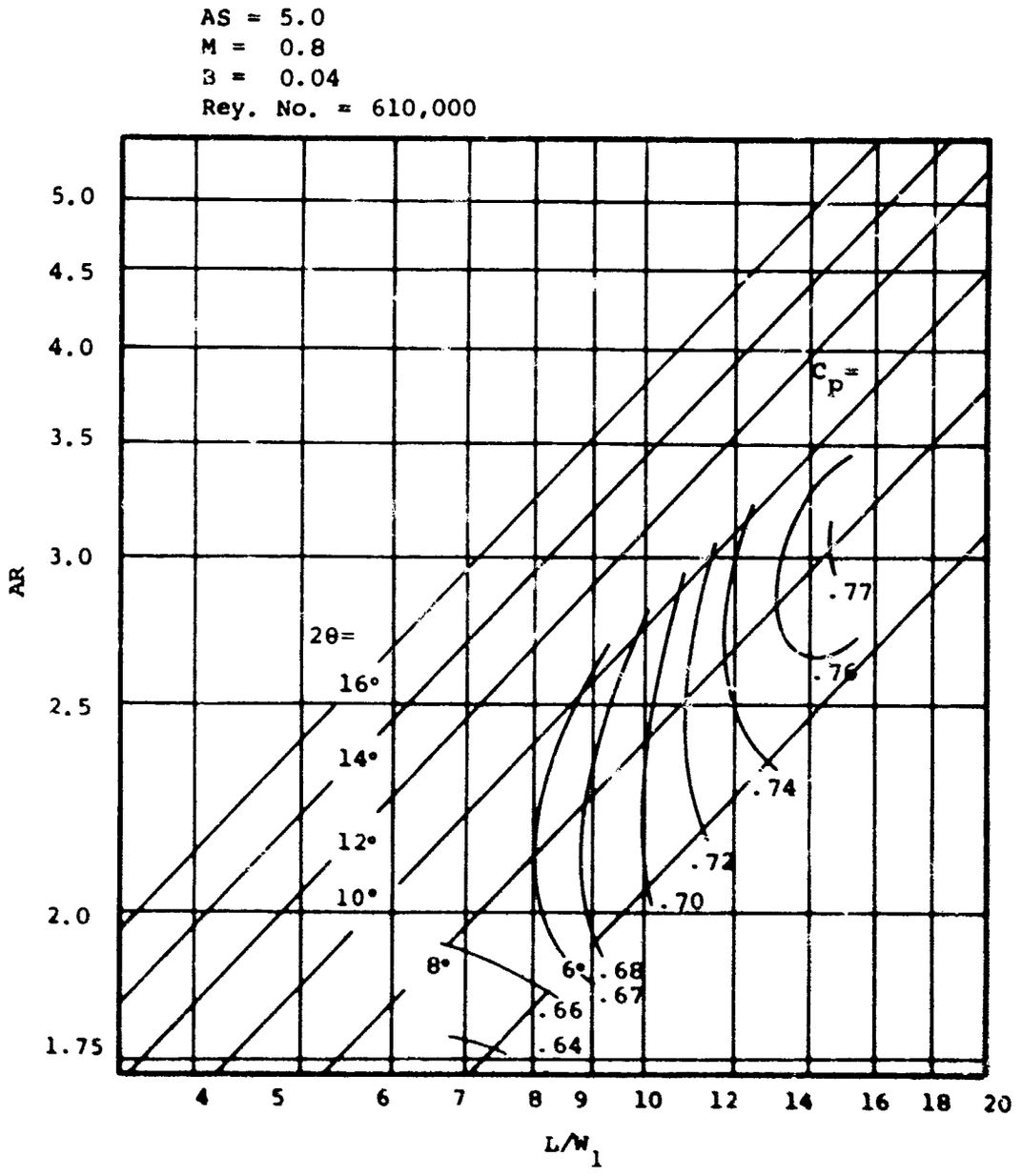

Figure 126. Performance Map - Aspect Ratio = 5.0.

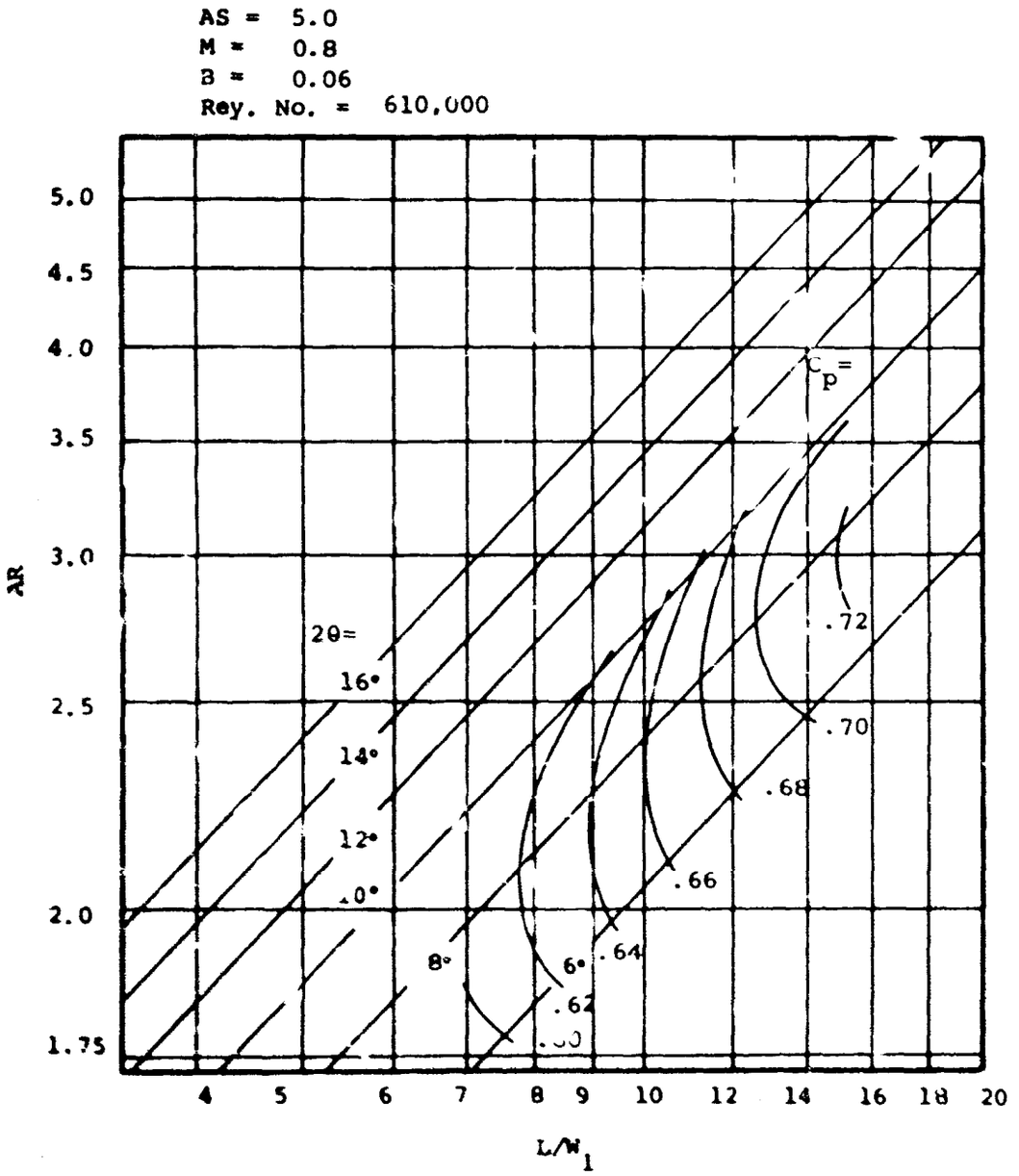

Figure 127. Performance Map - Aspect Ratio = 5.0.

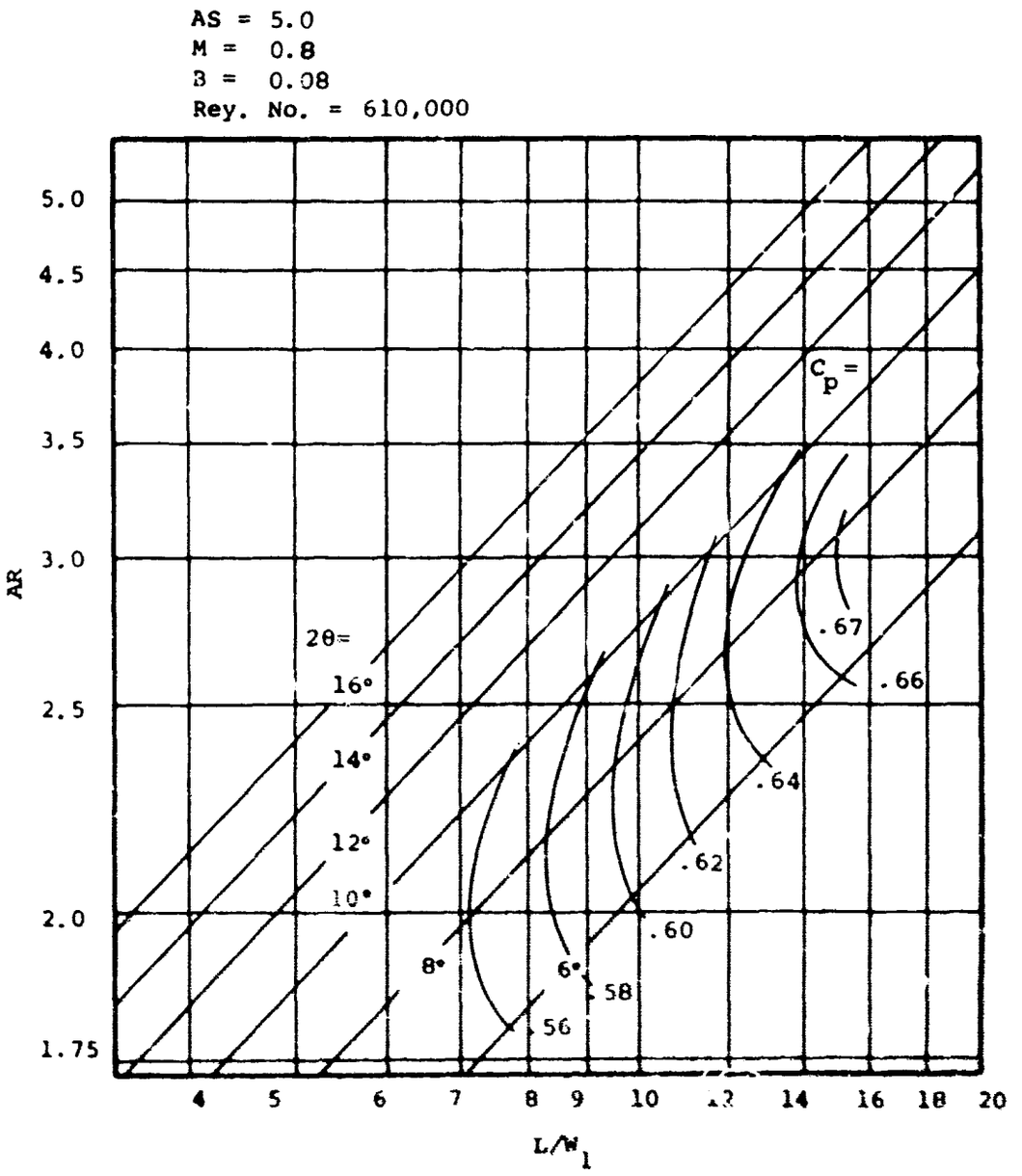

Figure 128. Performance Map - Aspect Ratio = 5.0.

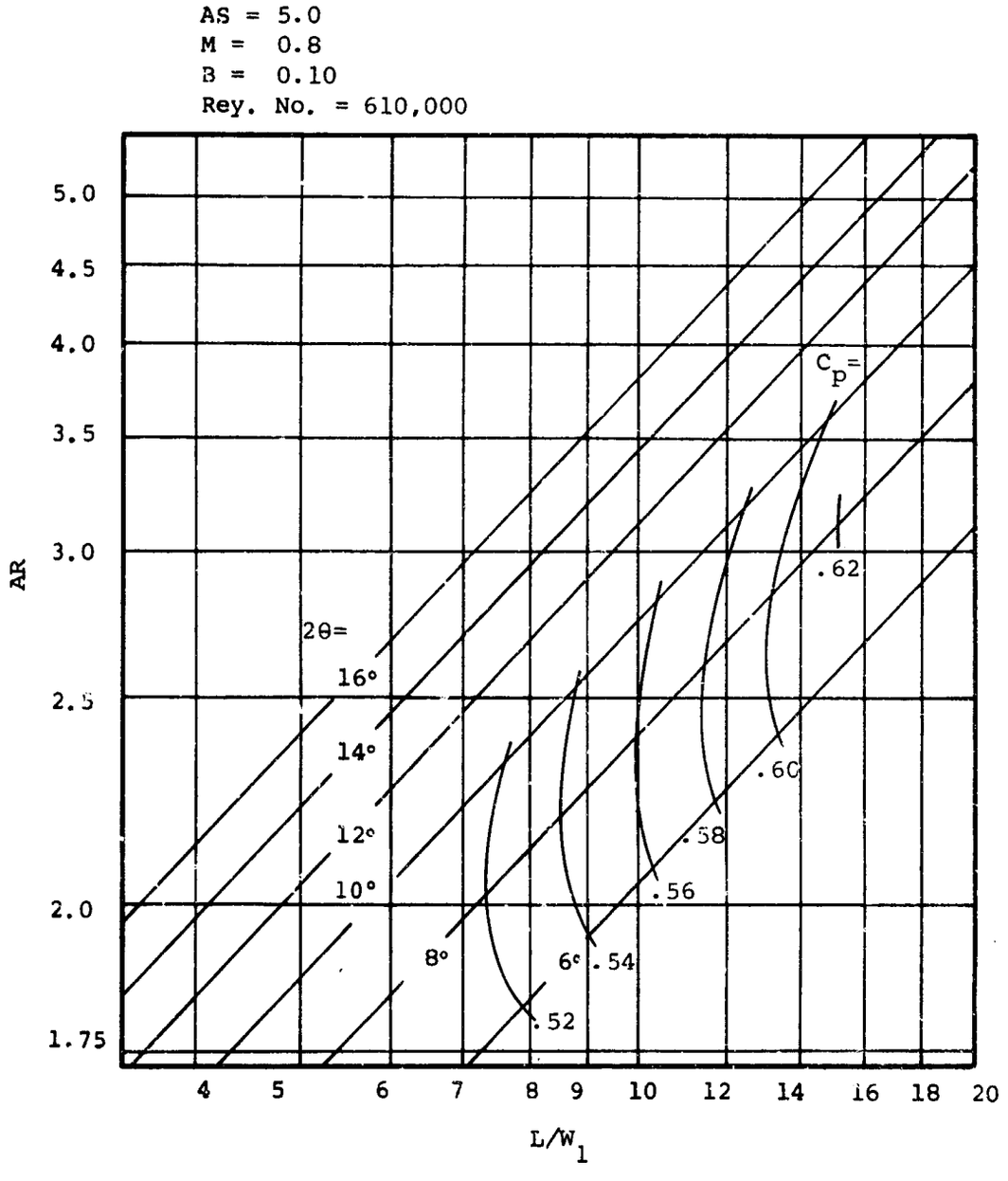

Figure 129. Performance Map - Aspect Ratio = 5.0.

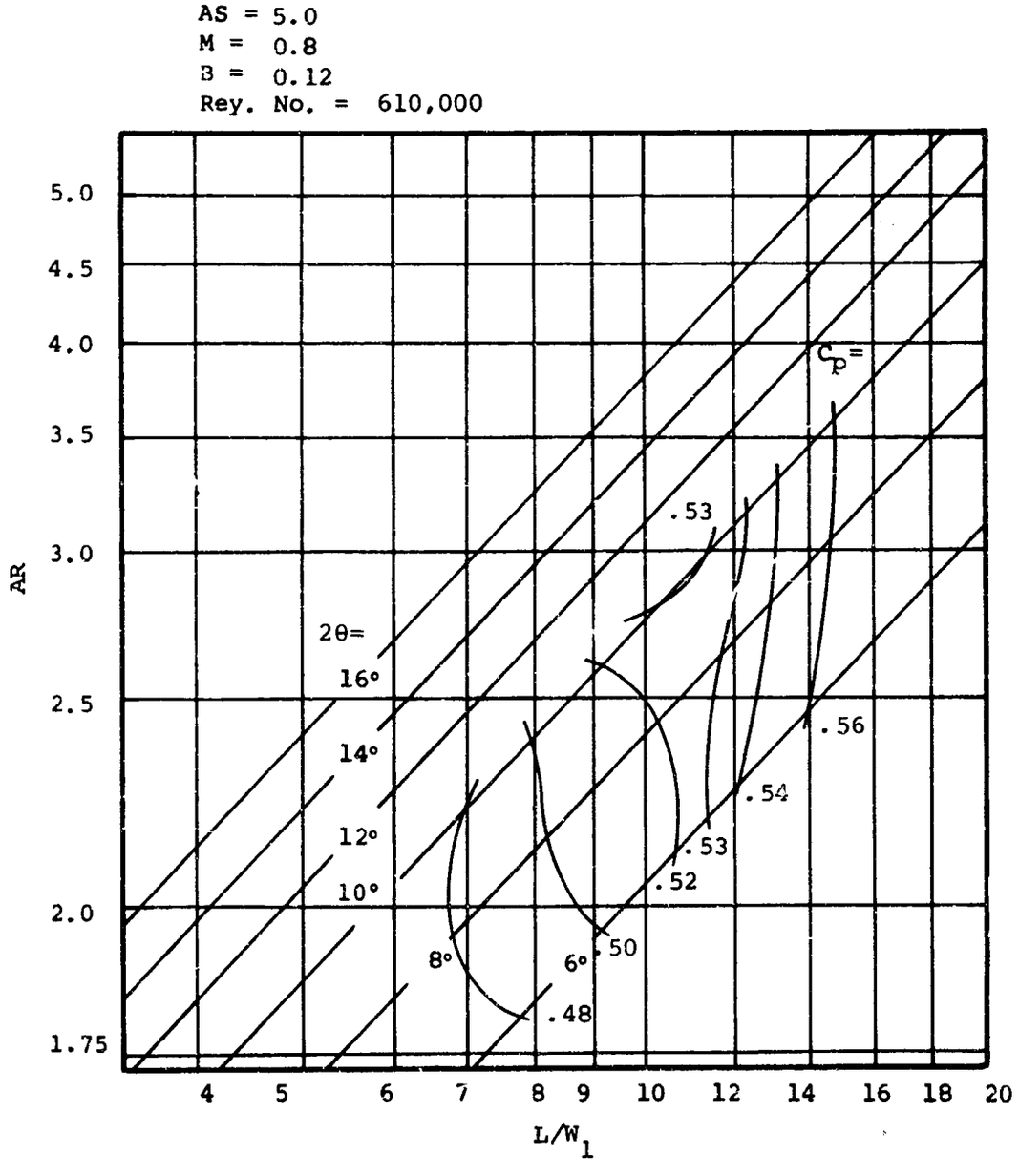

Figure 130. Performance Map - Aspect Ratio = 5.0.

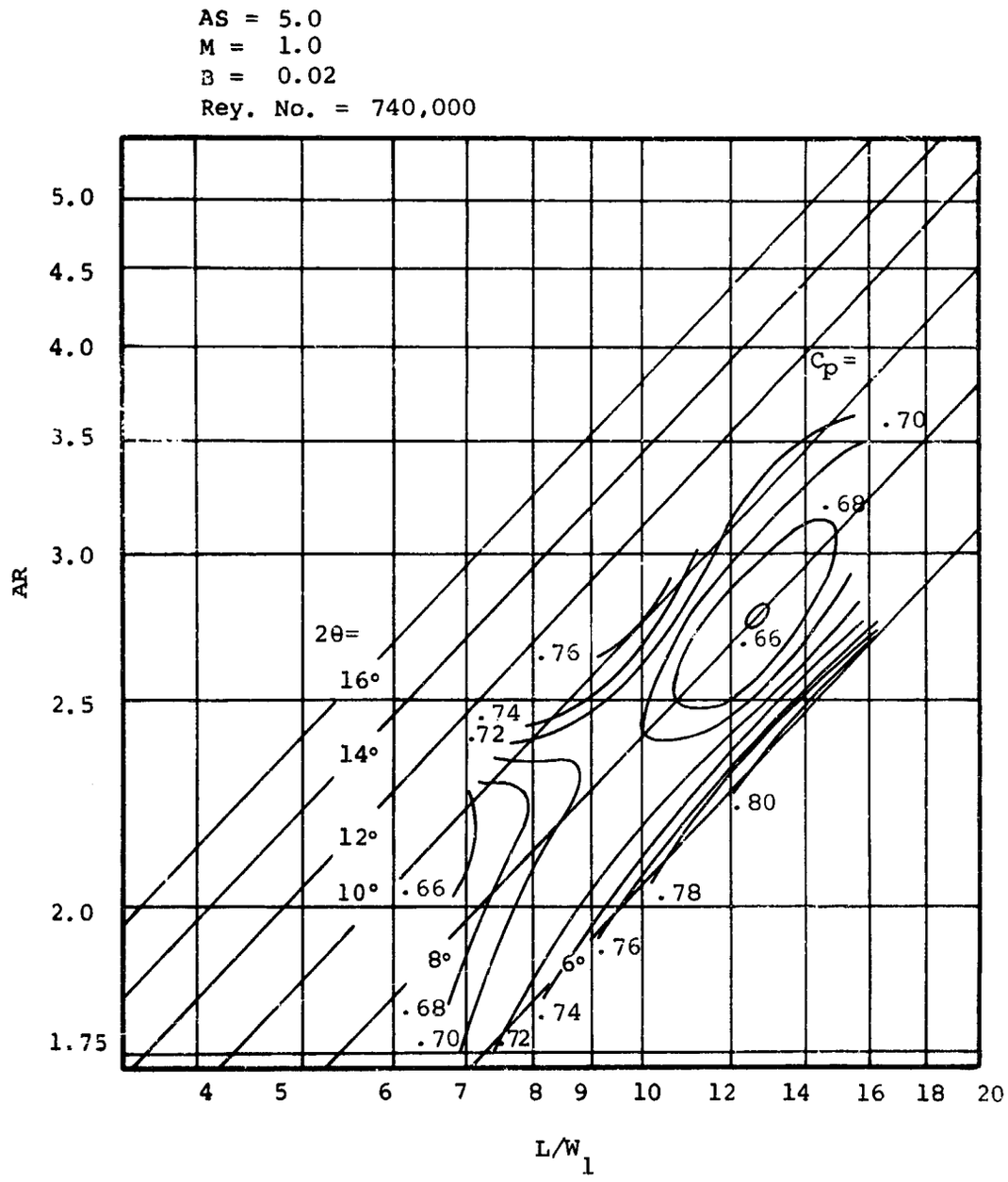

Figure 131. Performance Map - Aspect Ratio = 5.0.

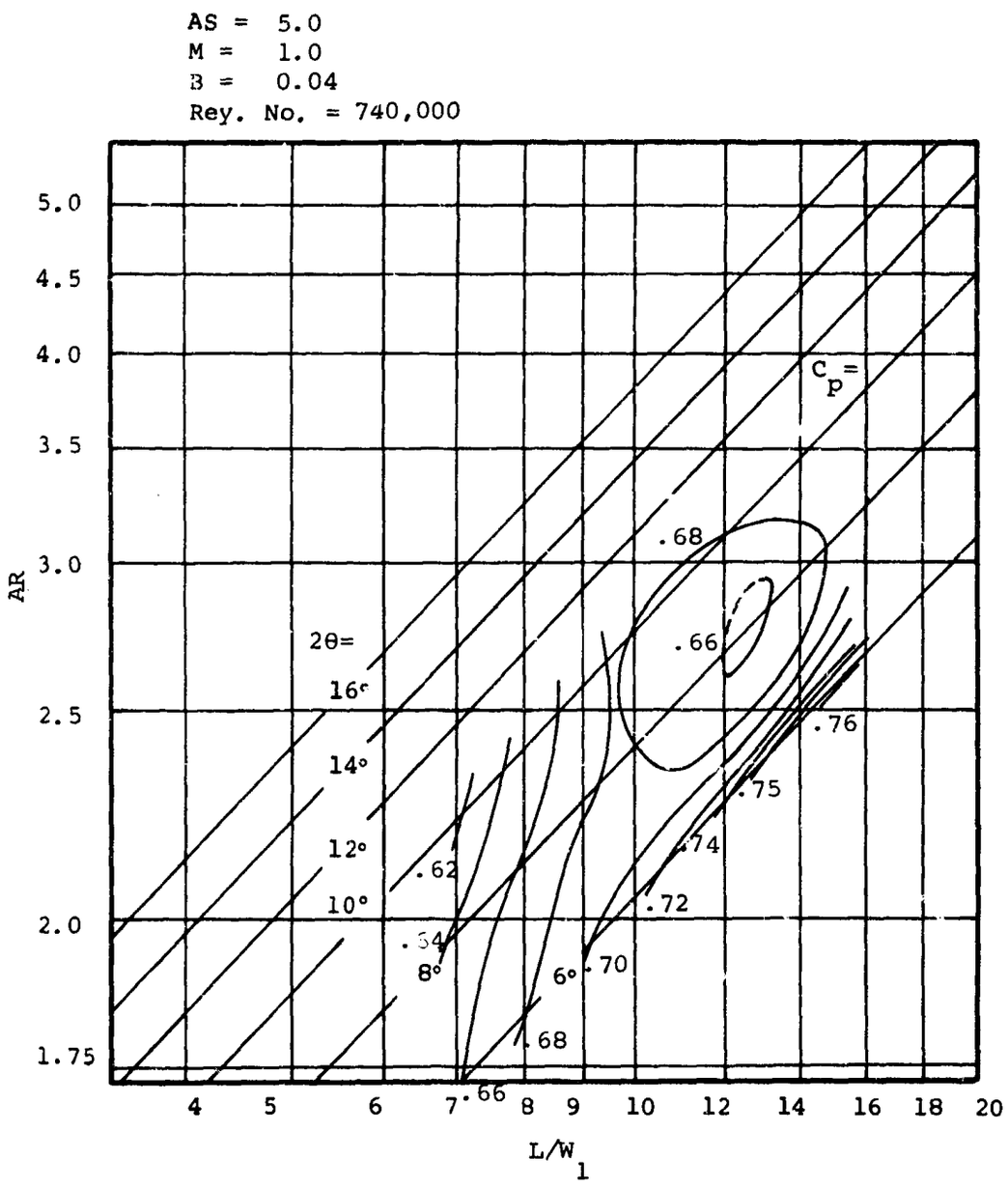

Figure 132. Performance Map - Aspect Ratio = 5.0.

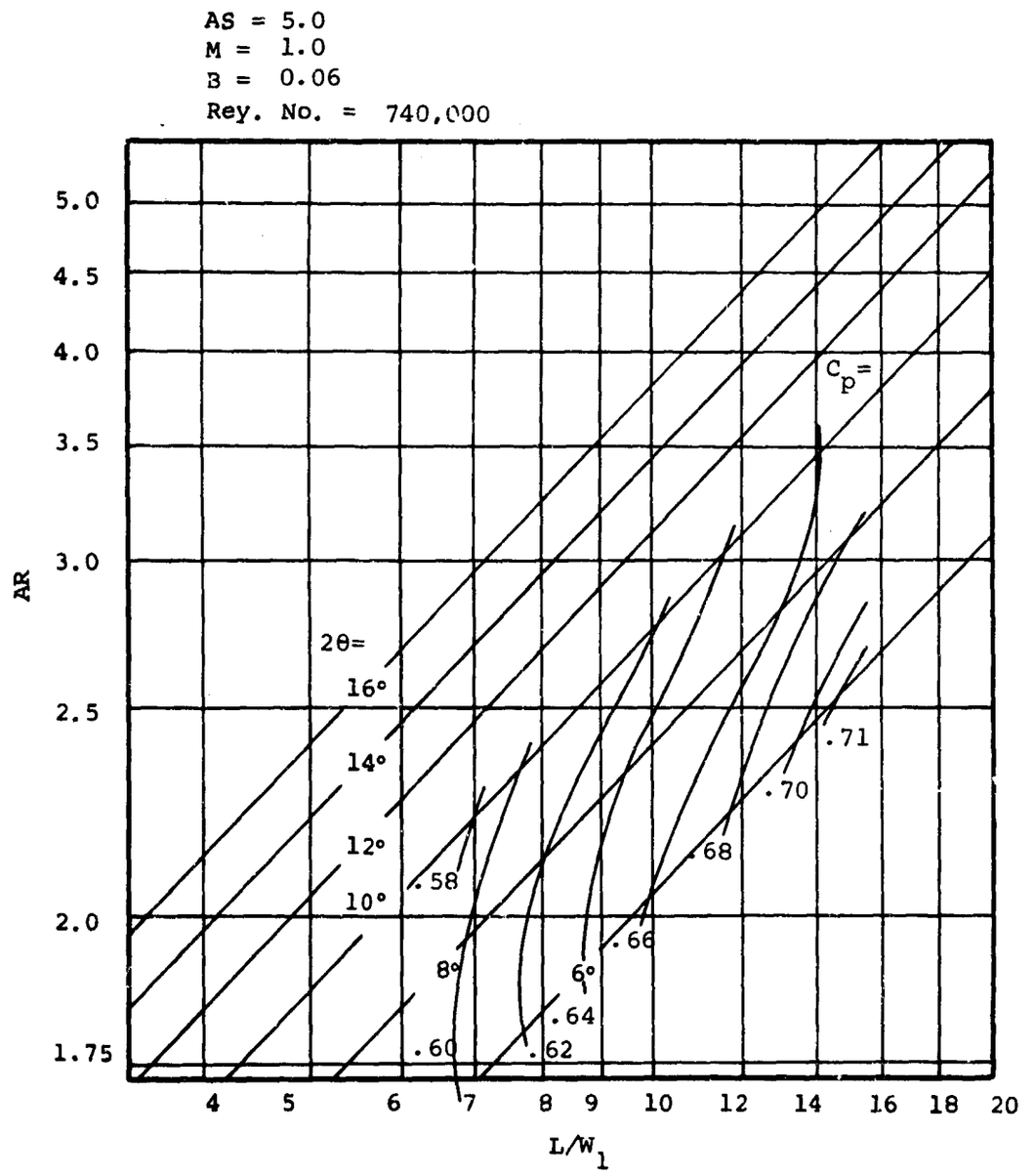

Figure 133. Performance Map - Aspect Ratio = 5.0.

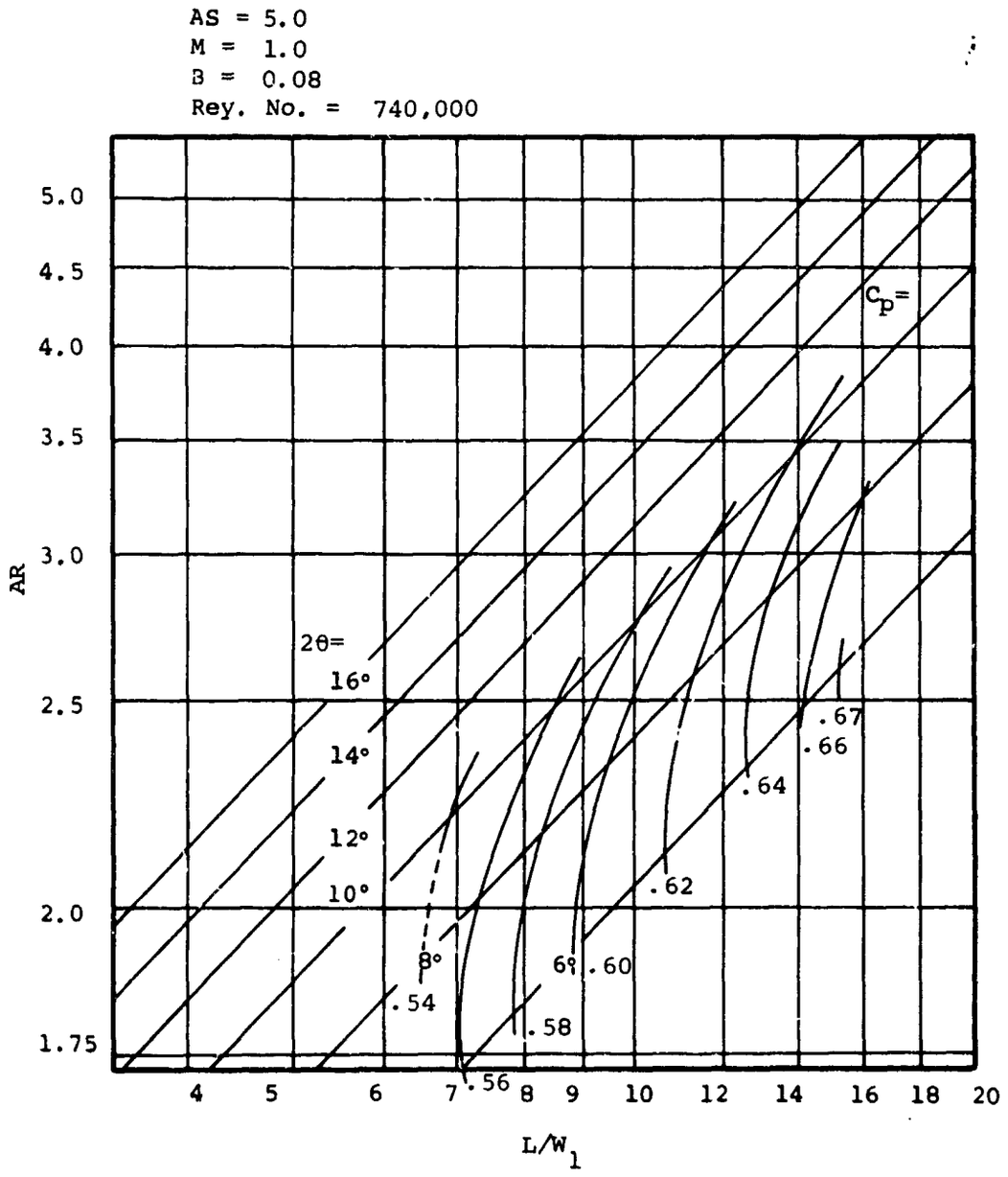

Figure 134. Performance Map - Aspect Ratio = 5.0.

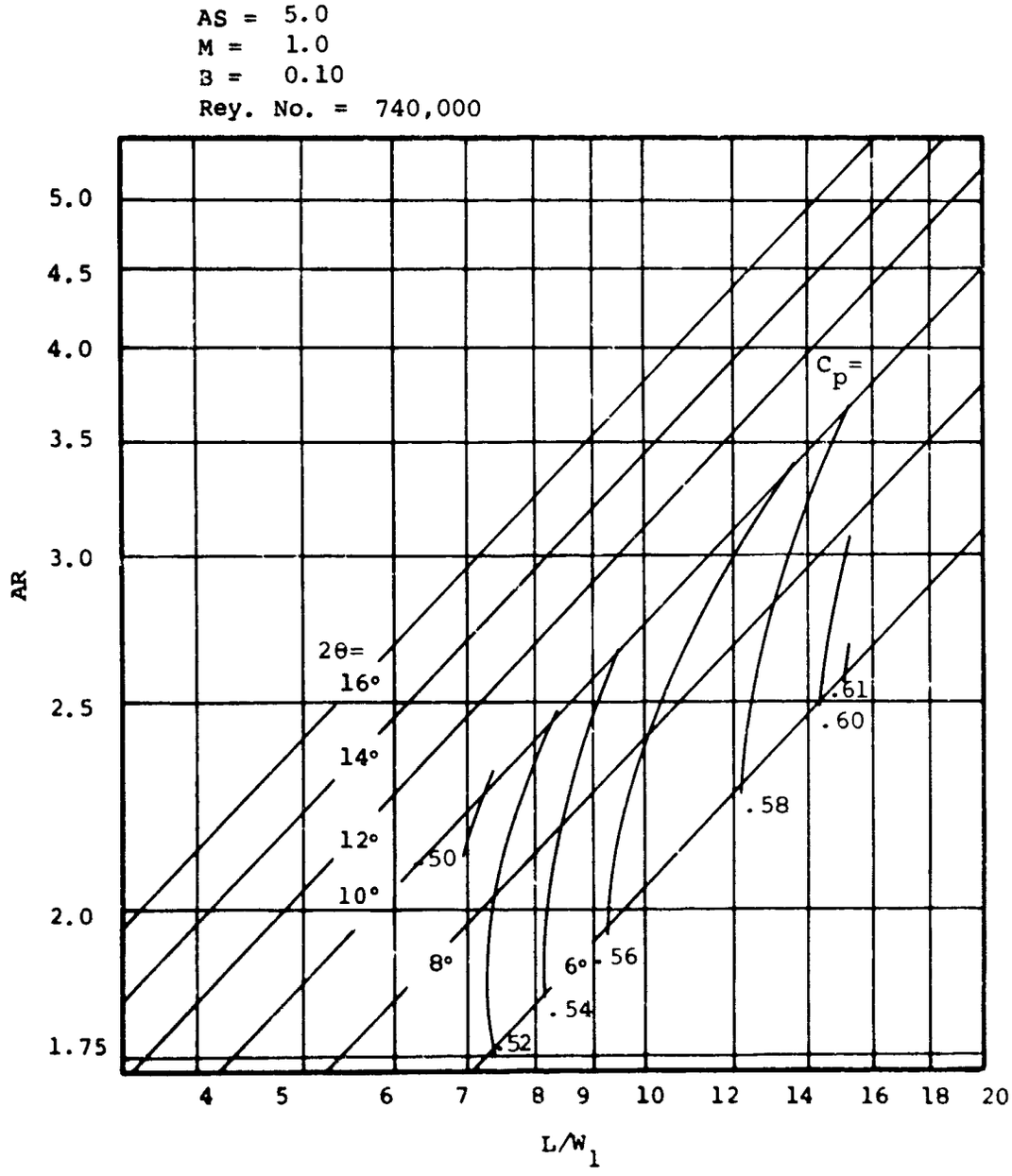

Figure 135. Performance Map - Aspect Ratio = 5.0.

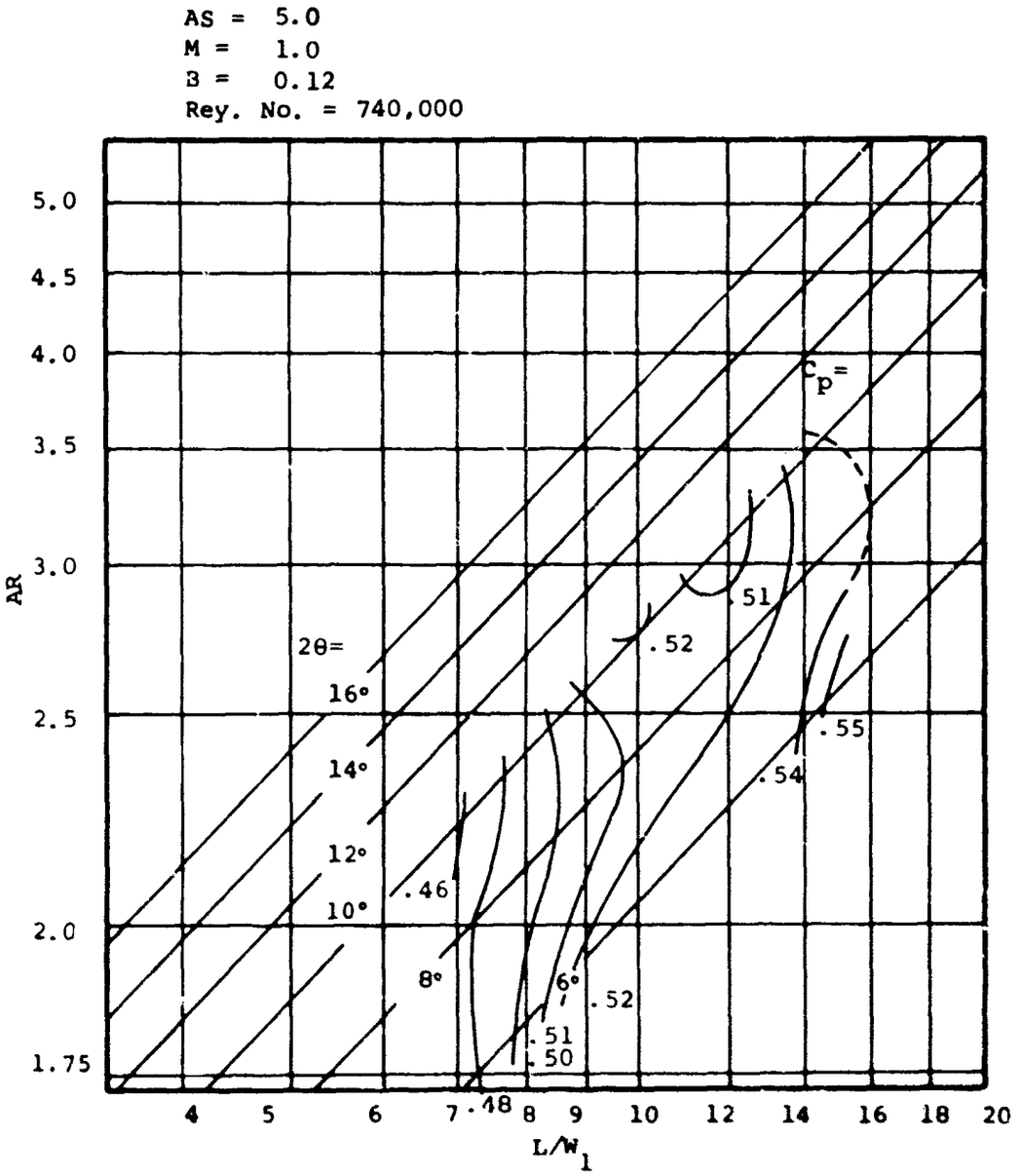

Figure 136. Performance Map - Aspect Ratio = 5.0.

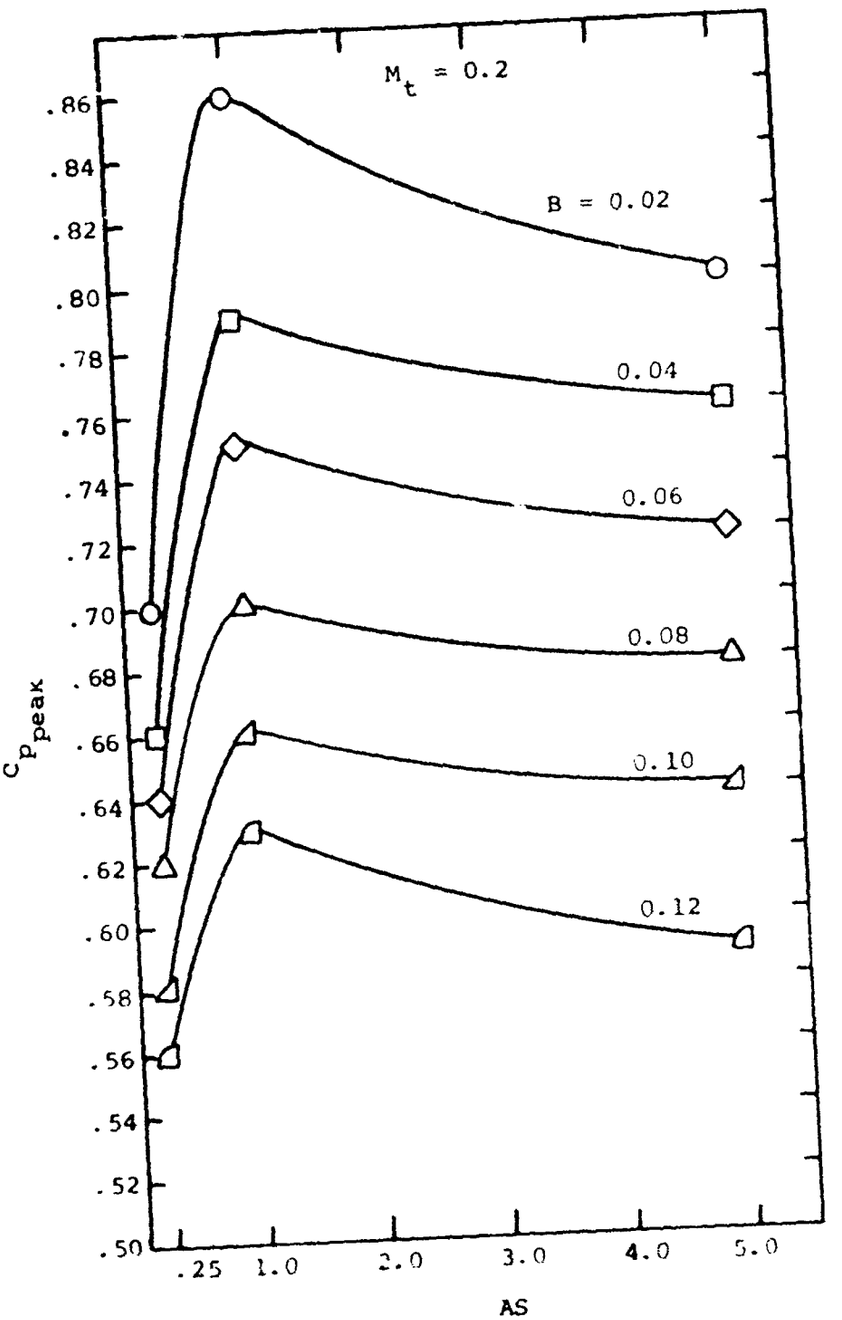

Figure 137. Peak Pressure Recovery Versus Aspect Ratio. Mach Number = 0.2.

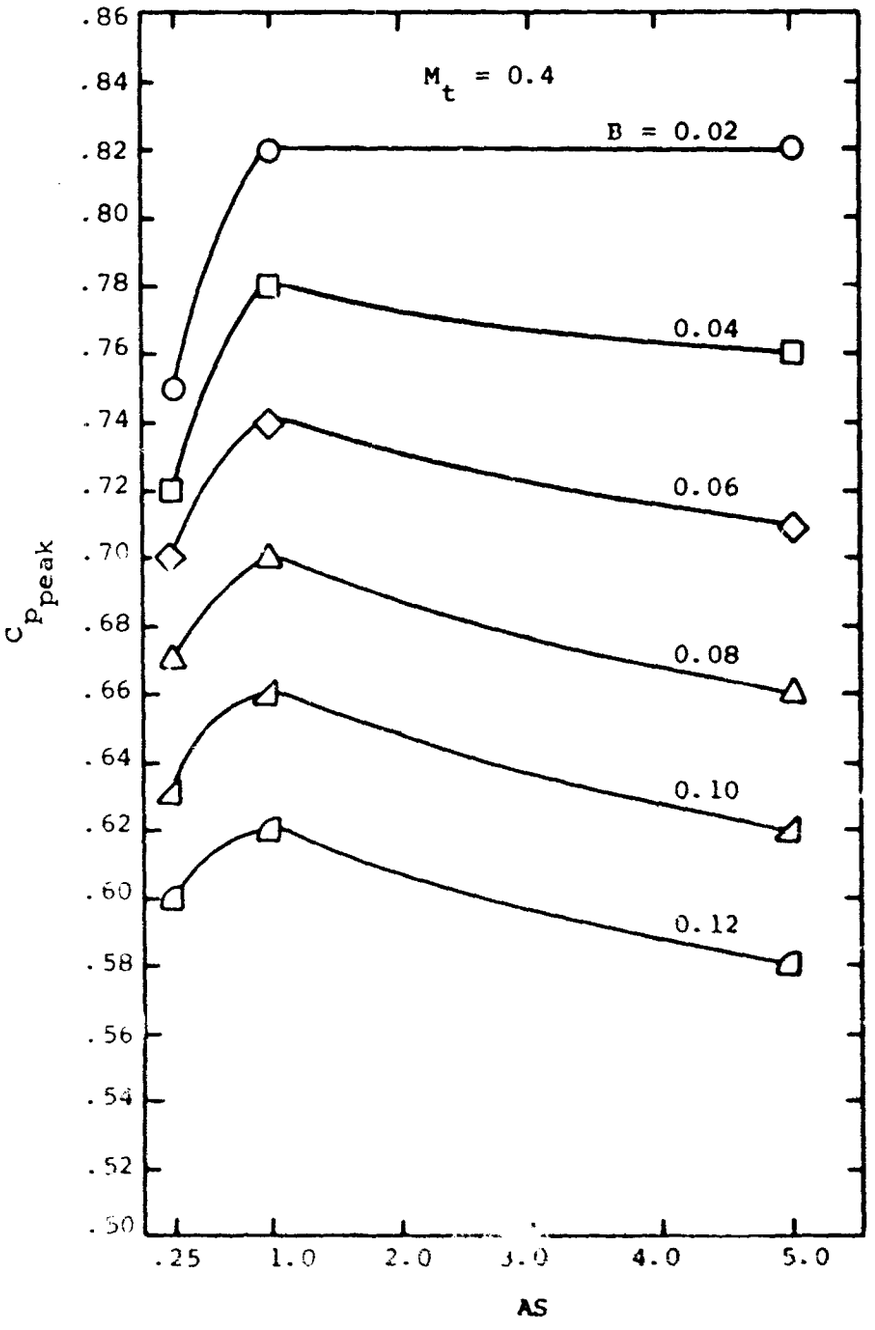

Figure 138. Peak Pressure Recovery Versus Aspect Ratio. Mach Number = 0.4.

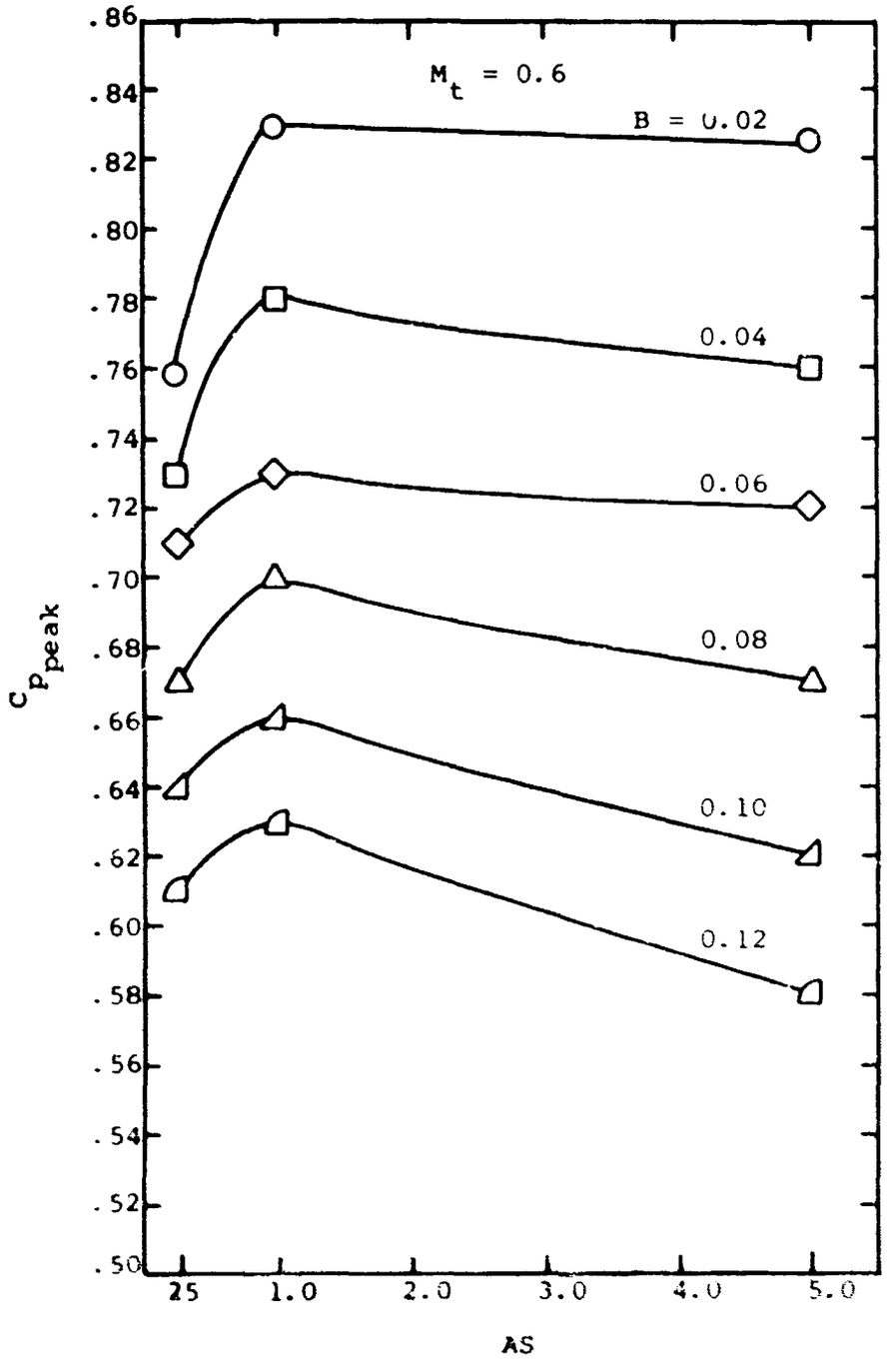

Figure 139. Peak Pressure Recovery Versus Aspect Ratio. Mach Number = 0.6.

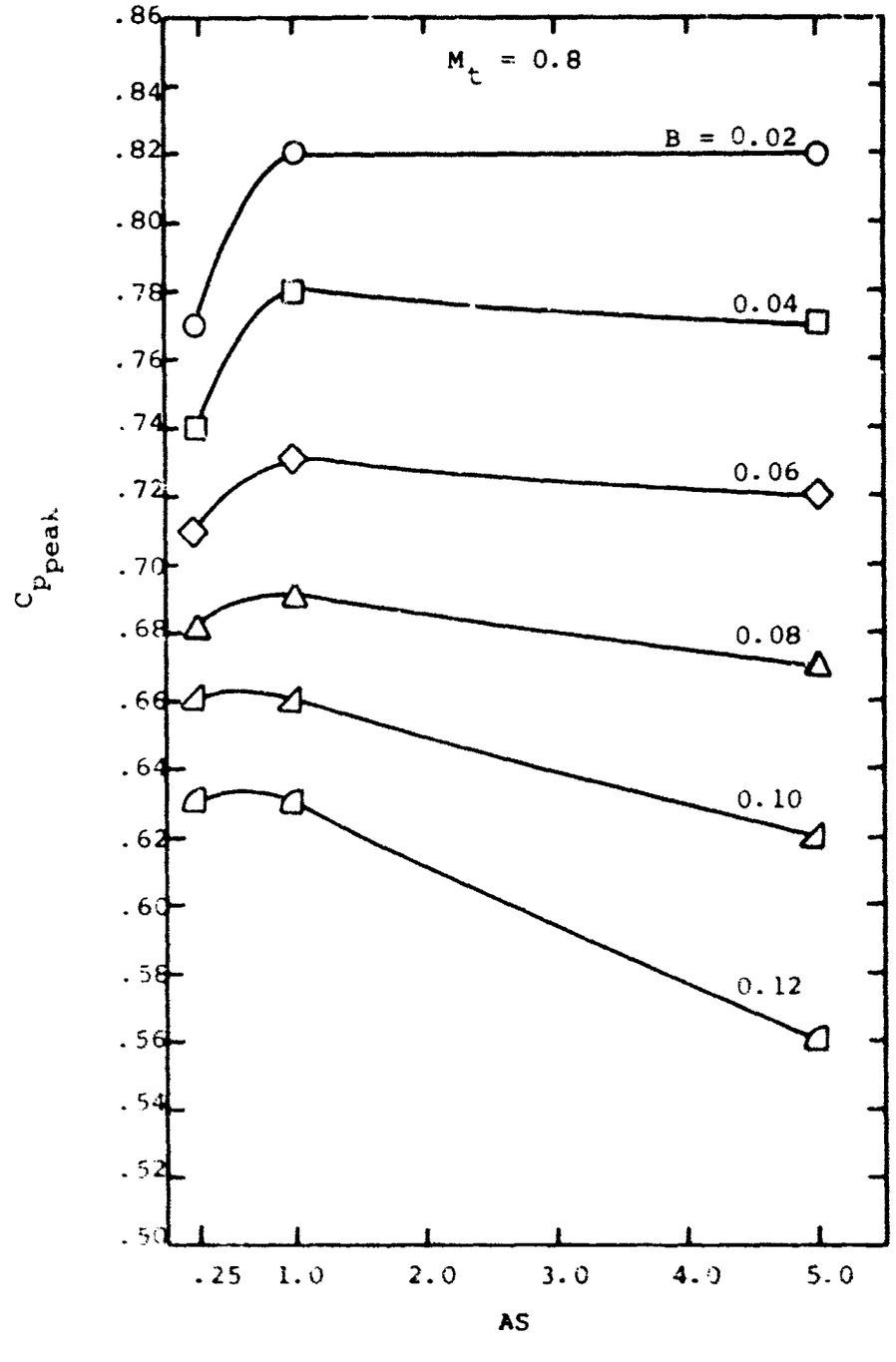

Figure 140. Peak Pressure Recovery Versus Aspect Ratio. Mach Number = 0.8.

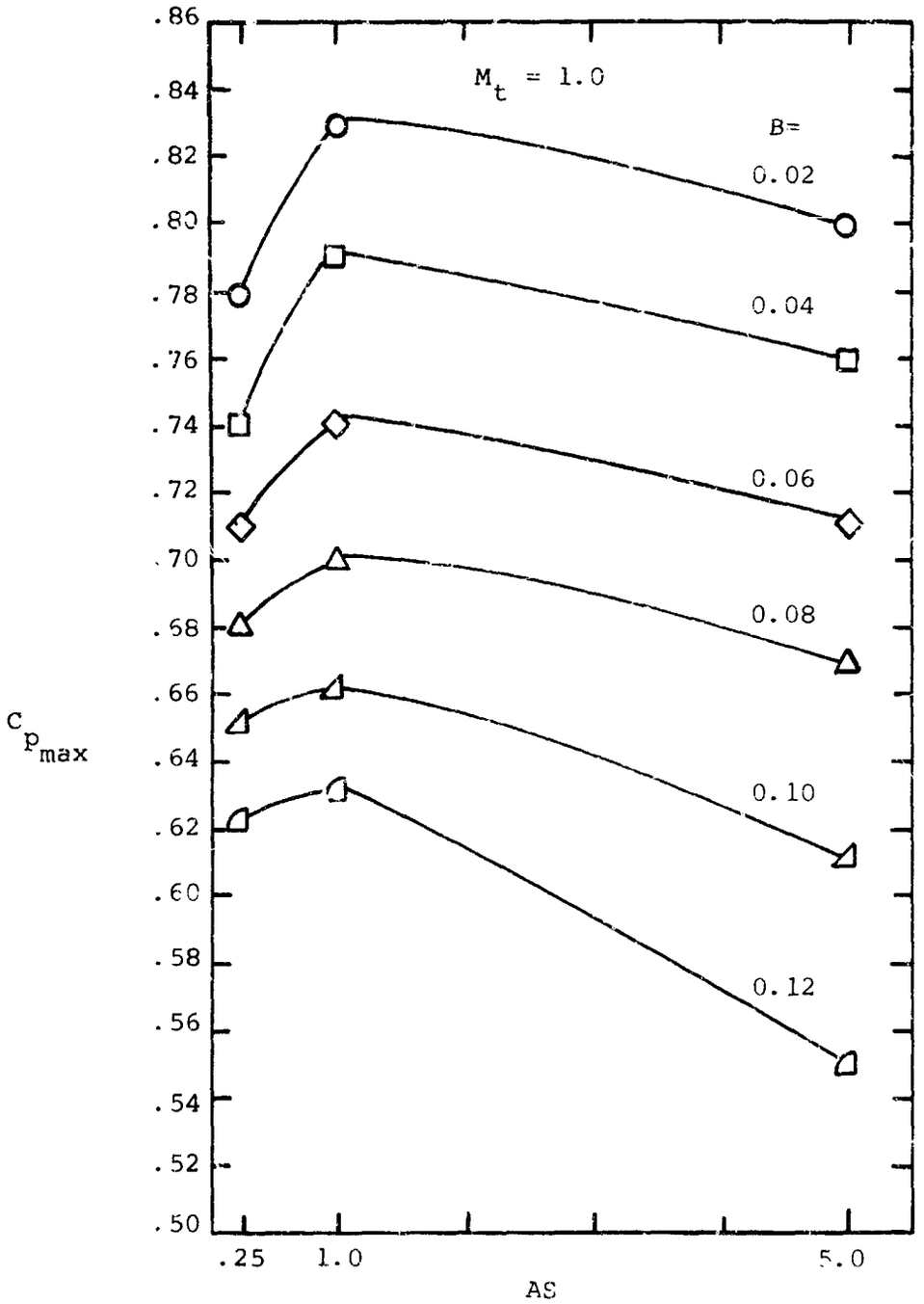

Figure 141. Peak Pressure Recovery Versus Aspect Ratio. Mach Number = 1.0.

Table VI lists the peak pressure recovery and corresponding geometry used in preparing these cross-plots. In plotting these curves for peak recovery, it has been assumed that very low aspect ratio diffusers have a significantly lower peak recovery than has been measured for aspect ratio = 0.25. Diffusers with aspect ratio greater than 5.0 are also assumed to have a slightly lower value of peak recovery*, so that the peak recovery curves still fall at aspect ratios above 5.0.

Figure 142 is a plot of the change in pressure recovery for a single fixed geometry and fixed inlet conditions (M_t = 1.0, B = 0.08, L/W_1 = 15, 2θ = 10°) as aspect ratio is changed.

In both types of plots (in the peak recovery plots and in Figure 142), we see that at small aspect ratio, pressure recovery changes rapidly. This is because recovery must fall rapidly as aspect ratio approaches zero. Because only three points are available to define the shape of the recovery vs. aspect ratio curves, the best aspect ratio is not clearly defined. For the curves of peak pressure recovery and for the curve of recovery for the constant geometry of Figure 142, the optimum geometry probably occurs at a small aspect ratio near 1.0.

Inlet Blockage

A critical aspect of diffuser behavior (other than the dependence on geometric parameters) is the dependence on throat boundary layer blockage. As has been shown for incompressible diffuser operation, a useful correlation parameter for inlet flow is the throat blockage B. Figures 37, 40, and 43 illustrate how greatly the blockage influences the pressure recovery for a given geometry. Of all the variables involved in the diffuser design problem, this is perhaps a predominant one in practice, since the designer can alter throat blockage appreciably by diffuser design changes. The pressure recovery behavior shown in Figures 37, 40, and 43 makes it clear that one is designing in the dark unless the relationship between diffuser recovery and blockage is understood.

*See the discussion on performance tests on aspect ratio = 8.0 diffusers.

TABLE VI. PEAK PRESSURE RECOVERY GEOMETRY

Aspect Ratio AS	Mach Number M_t	Throat Blockage B	Peak Pressure Recovery $C_{p_{peak}}$	Divergence Angle 2θ	Length-to-Width Ratio L/W_1
0.25	0.2	.02	.70	16	11
0.25	0.2	.04	.66	14	15
0.25	0.2	.06	.64	14	15
0.25	0.2	.08	.62	14	15
0.25	0.2	.10	.58	12	15
0.25	0.2	.12	.56	12	15
0.25	0.4	.02	.75	15	15
0.25	0.4	.04	.72	14	15
0.25	0.4	.06	.70	15	15
0.25	0.4	.08	.67	14	15
0.25	0.4	.10	.63	14	15
0.25	0.4	.12	.60	14	15
0.25	0.6	.02	.76	14	15
0.25	0.6	.04	.73	14	15
0.25	0.6	.06	.71	14	15
0.25	0.6	.08	.67	14	15
0.25	0.6	.10	.64	14	15
0.25	0.6	.12	.61	14	15
0.25	0.8	.02	.77	14	15
0.25	0.8	.04	.74	14	15
0.25	0.8	.06	.71	14	14
0.25	0.8	.08	.68	14	15
0.25	0.8	.10	.66	14	15
0.25	0.8	.12	.63	14	13.5
0.25	1.0	.02	.78	13	13
0.25	1.0	.04	.74	12	15
0.25	1.0	.06	.71	12	15
0.25	1.0	.08	.68	13	15
0.25	1.0	.10	.65	12.5	15
0.25	1.0	.12	.62	13.5	15
1.0	0.2	.02	.86	12	17
1.0	0.2	.04	.79	10.5	16
1.0	0.2	.06	.75	9.5	16.5
1.0	0.2	.08	.70	9.5	16.5

TABLE VI - Continued

Aspect Ratio AS	Mach Number M_t	Throat Blockage B	Peak Pressure Recovery $C_{p_{peak}}$	Divergence Angle 2θ	Length-to-Width Ratio L/W_1
1.0	0.2	.10	.66	9	18
1.0	0.2	.12	.63	9	18
1.0	0.4	.02	.82	10.5	17
1.0	0.4	.04	.78	10	17
1.0	0.4	.06	.74	9.5	17
1.0	0.4	.08	.70	8.5	18
1.0	0.4	.10	.66	9	18
1.0	0.4	.12	.62	9	18
1.0	0.6	.02	.83	10.5	17
1.0	0.6	.04	.78	9	16.5
1.0	0.6	.06	.73	9	16.5
1.0	0.6	.08	.70	8.5	18
1.0	0.6	.10	.66	8.5	18
1.0	0.6	.12	.63	8.5	18
1.0	0.8	.02	.82	10	17
1.0	0.8	.04	.78	9.5	16
1.0	0.8	.06	.73	8	18
1.0	0.8	.08	.69	8	18
1.0	0.8	.10	.66	8.5	18
1.0	0.8	.12	.63	8	18
1.0	1.0	.02	.83	8.5	18
1.0	1.0	.04	.79	8	18
1.0	1.0	.06	.74	7	18
1.0	1.0	.08	.70	7.5	18
1.0	1.0	.10	.66	7.5	17.5
1.0	1.0	.12	.63	7	16
5.0	0.2	.02	.80	9	15
5.0	0.2	.04	.76	9	15
5.0	0.2	.06	.72	8	15
5.0	0.2	.08	.68	8	15
5.0	0.2	.10	.64	8	15
5.0	0.2	.12	.59	8.5	15
5.0	0.4	.02	.82	9	15
5.0	0.4	.04	.76	9	15
5.0	0.4	.06	.71	8	15
5.0	0.4	.08	.66	8	15
5.0	0.4	.10	.62	8	15

TABLE VI - Continued

Aspect Ratio AS	Mach Number M_t	Throat Blockage B	Peak Pressure Recovery $C_{p_{peak}}$	Divergence Angle 2θ	Length-to-Width Ratio L/W_1
5.0	0.4	.12	.58	8.5	15
5.0	0.6	.02	.825	9.5	15
5.0	0.6	.04	.76	8.5	15
5.0	0.6	.06	.72	8	15
5.0	0.6	.08	.67	8	15
5.0	0.6	.10	.62	8	15
5.0	0.6	.12	.58	8	15
5.0	0.8	.02	.82	9	15
5.0	0.8	.04	.77	8	15
5.0	0.8	.06	.72	7.5	15
5.0	0.8	.08	.67	7.5	15
5.0	0.8	.10	.62	8	15
5.0	0.8	.12	.56	8	15
5.0	1.0	.02	.80	7	15
5.0	1.0	.04	.76	7	15
5.0	1.0	.06	.71	7	15
5.0	1.0	.08	.67	7	15
5.0	1.0	.10	.61	7	15
5.0	1.0	.12	.55	7	15

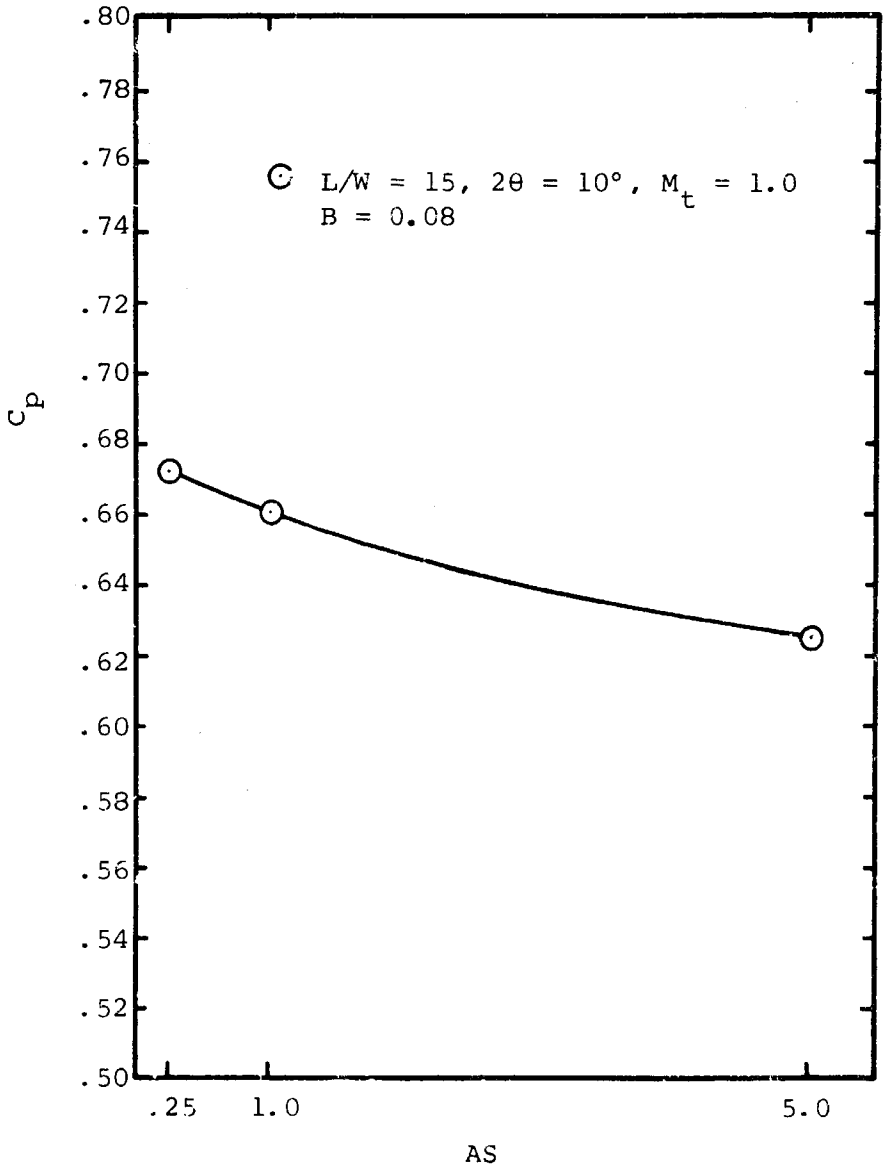

Figure 142. Peak Pressure Recovery for Fixed Geometry. Mach Number = 1.0. Throat Blockage = 0.08.

The optimum geometry as well as the peak achievable recovery is also strongly affected by blockage. Curves of peak recovery as a function of blockage for constant aspect ratio and Mach number are shown in Figures 143 through 147 and Table VI.

High Mach Number Operation

Figures 148 through 159 are examples of the recross-plotting of performance data, showing pressure recovery as a function of inlet Mach number at constant values of inlet blockage for a fixed geometry. Examples are shown for all three aspect ratios at both a high and low value of L/W_1 and a high and low value of divergence angle 2θ. It is obvious from the data that the concept of a "critical" subsonic Mach number above which diffuser pressure recovery drastically deteriorates is not entirely true. Diffusers actually do achieve good performance up to and beyond choke conditions at the throat.

The present studies do show, however, that at sufficiently large divergence angles, a reduction in pressure recovery does occur at a subsonic Mach number below choked conditions. However, if the divergence angle is not too large, the deterioration in performance is not appreciable. Moreover, at the lower divergence angles below and near that for peak recovery, the diffuser performance holds up well until choke, and even superchoked, operation is obtained.

This finding is entirely consistent with existing knowledge of shock wave boundary layer interaction [for example, as summarized by Pearcey (1961)]. The reason why many previous investigators have been misled about the concept of a "critical" subsonic Mach number should be understood.

In the past, the possibility of shocks near the throat corners of the diverging passage at high subsonic Mach numbers was cited as a reason for possible diffuser breakdown. Survey studies prior to the present investigations* revealed no shocks of any appreciable strength at these locations despite the fact that the diffusers had a sharp corner break in the wall at the throat.

*This result was obtained from survey studies where flow visualization through a transparent sidewall in the diffuser was possible. This work covered only relatively low diffuser divergence angles 2θ. The work is described in detail in Runstadler (1966).

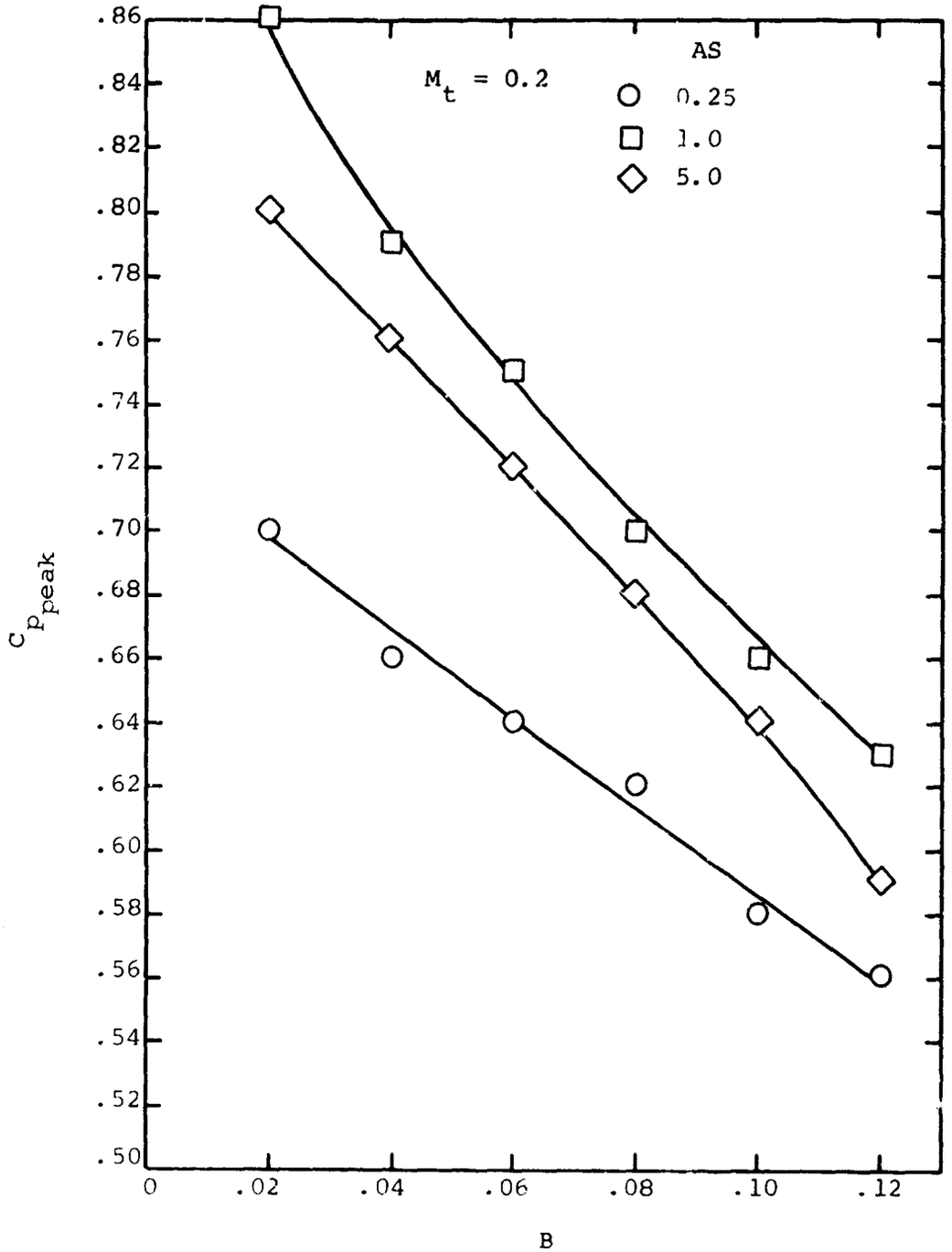

Figure 143. Peak Pressure Recovery Versus Blockage. Mach Number = 0.2.

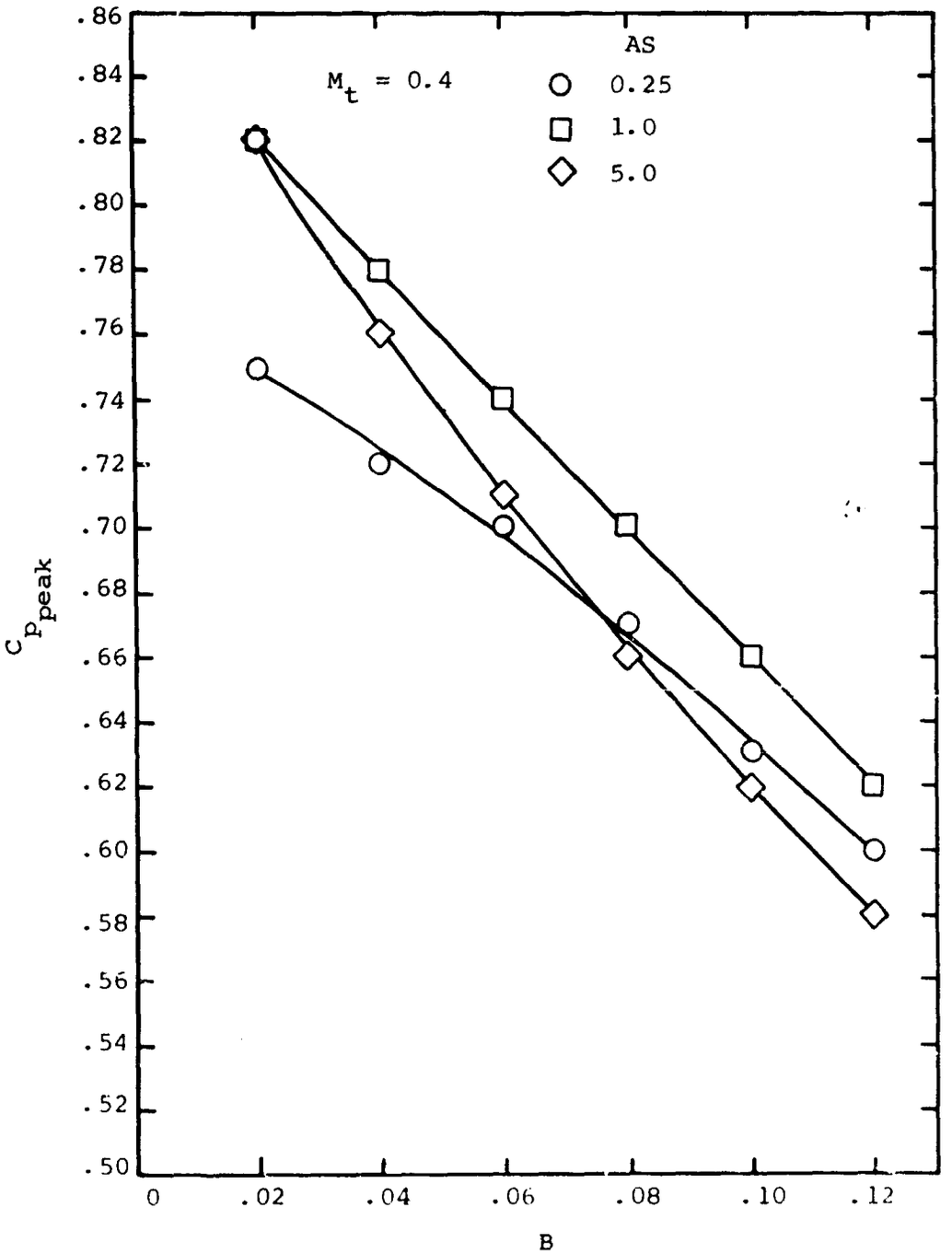

Figure 144. Peak Pressure Recovery Versus Blockage. Mach Number = 0.4.

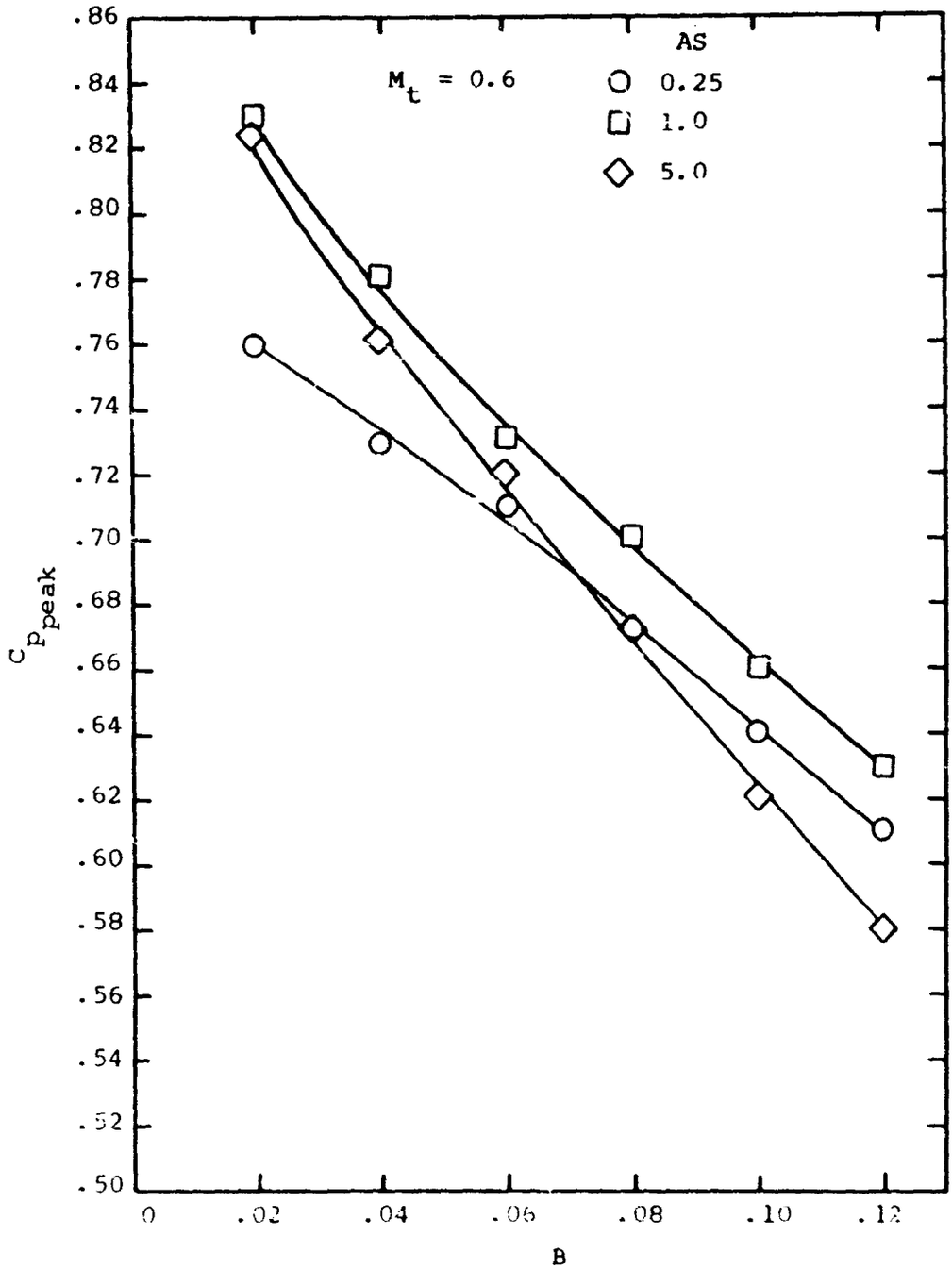

Figure 145. Peak Pressure Recovery Versus Blockage. Mach Number = 0.6.

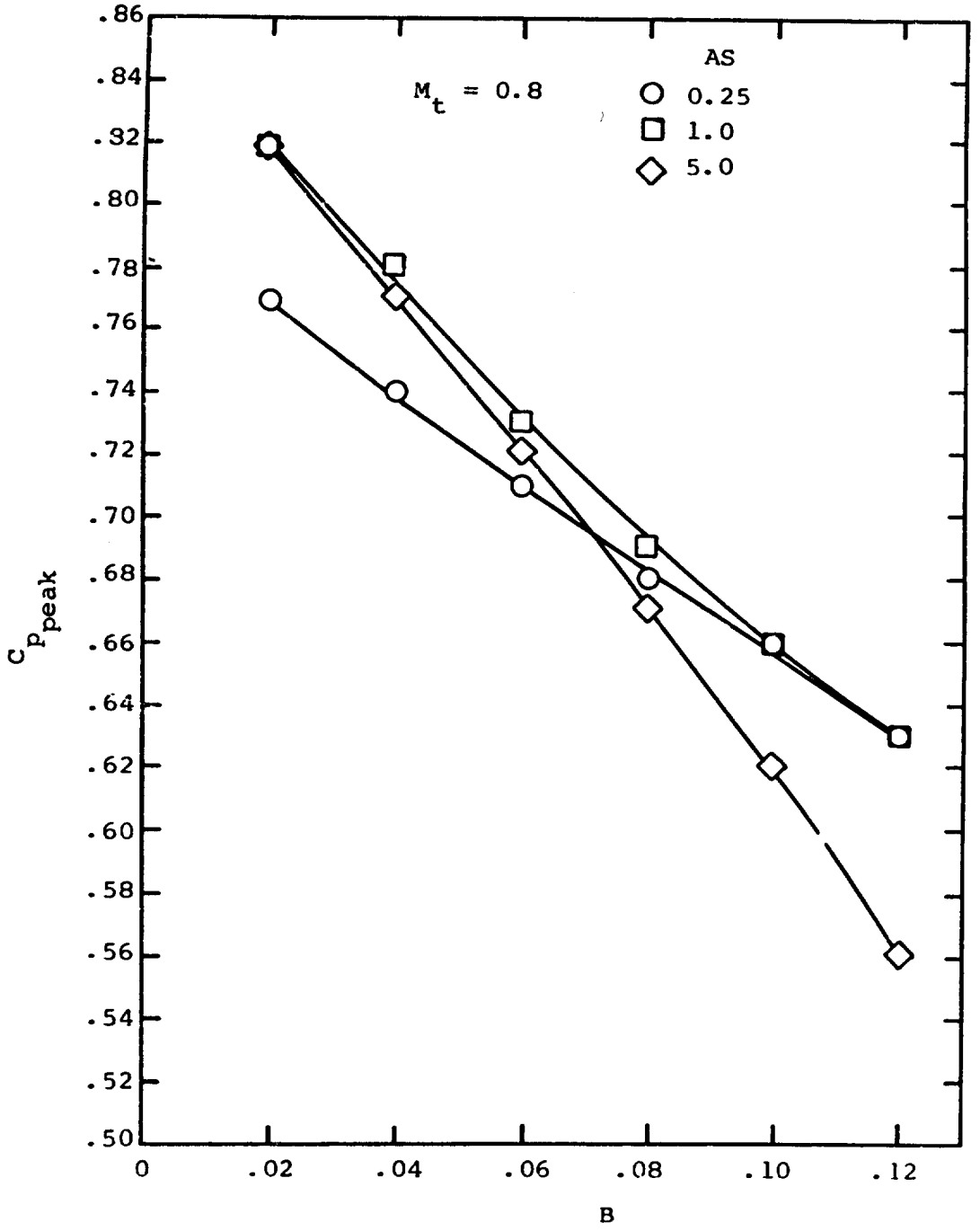

Figure 146. Peak Pressure Recovery Versus Blockage. Mach Number = 0.8.

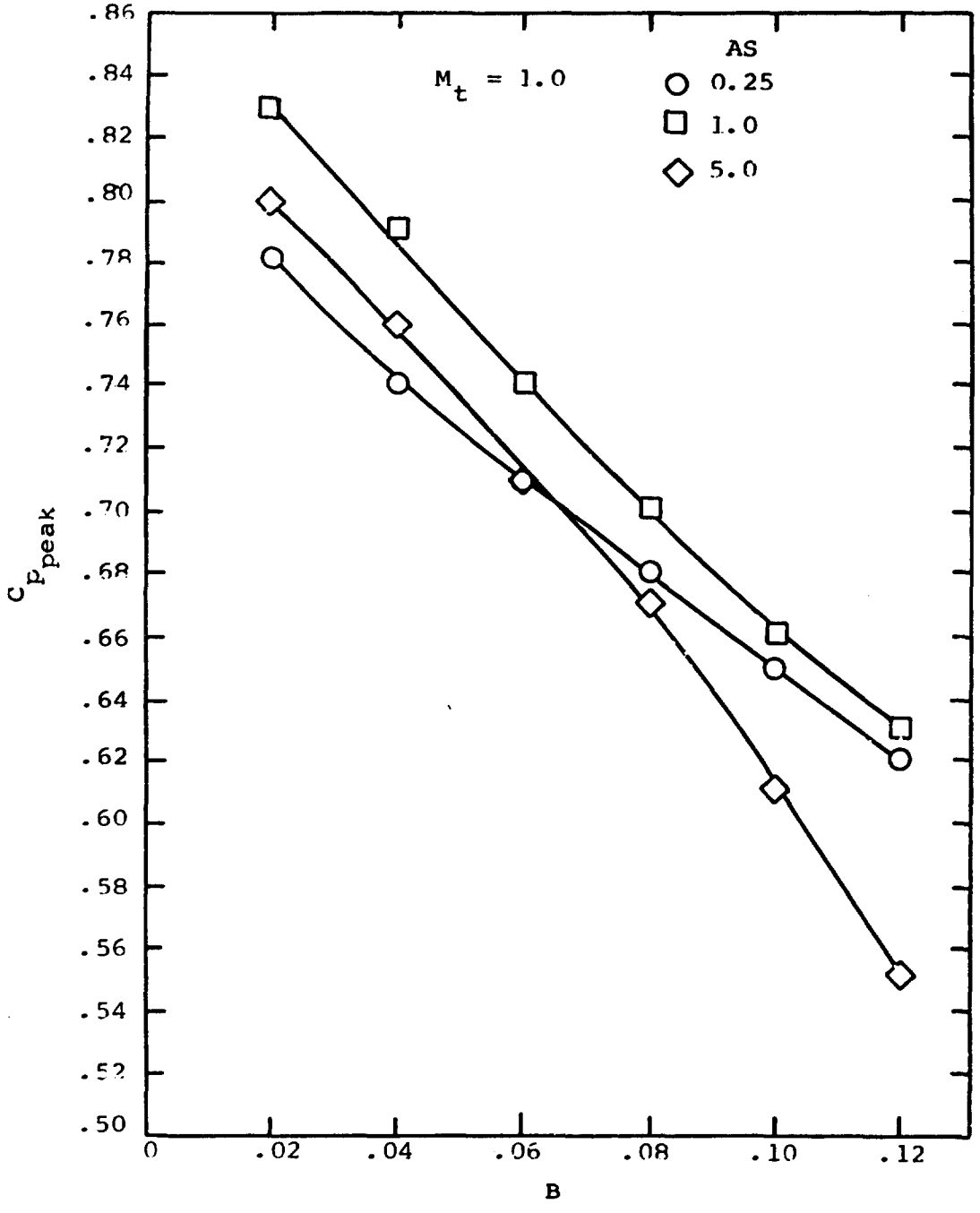

Figure 147. Peak Pressure Recovery Versus Blockage. Mach Number = 1.0.

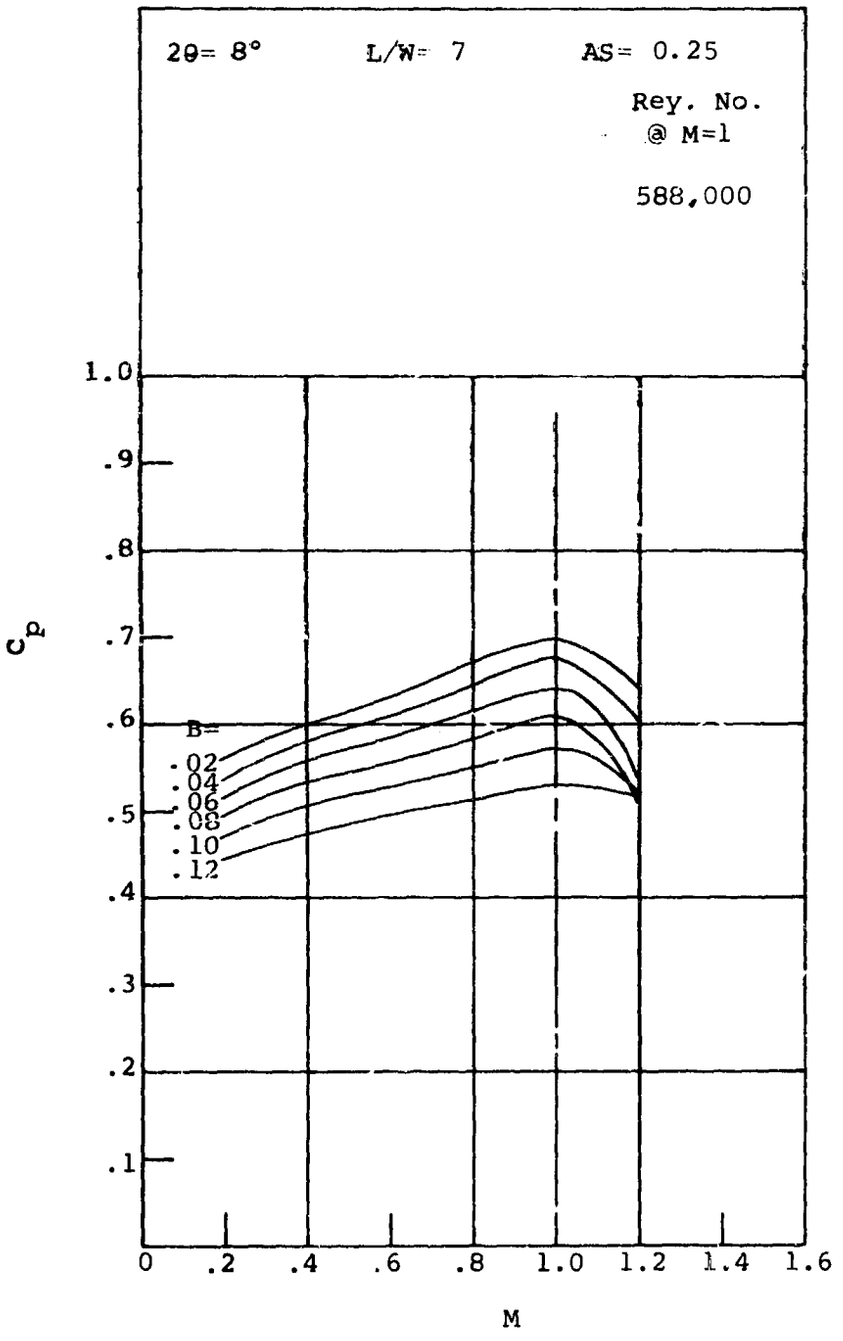

Figure 148. Pressure Recovery Versus Mach Number. Aspect Ratio = 0.25.

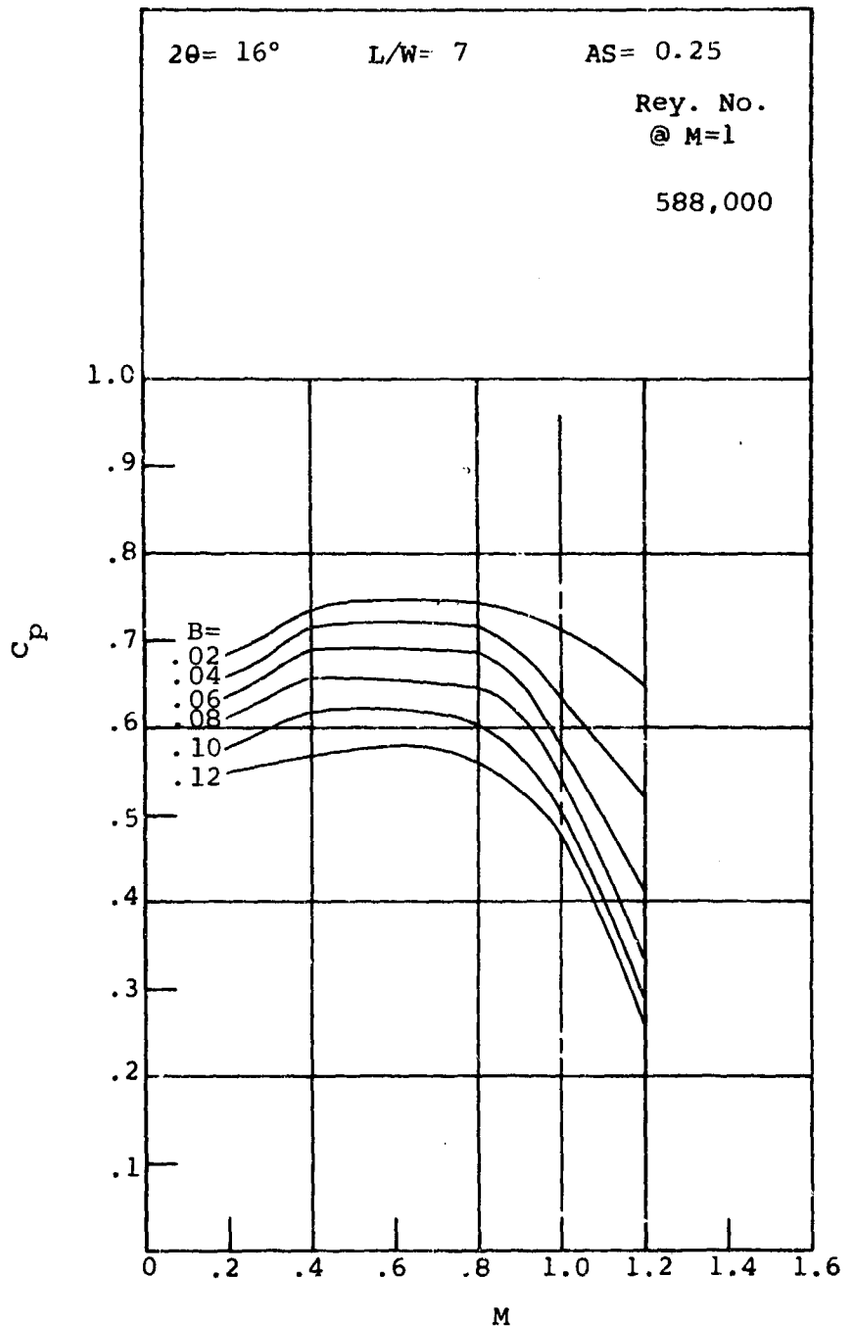

Figure 149. Pressure Recovery Versus Mach Number. Aspect Ratio = 0.25.

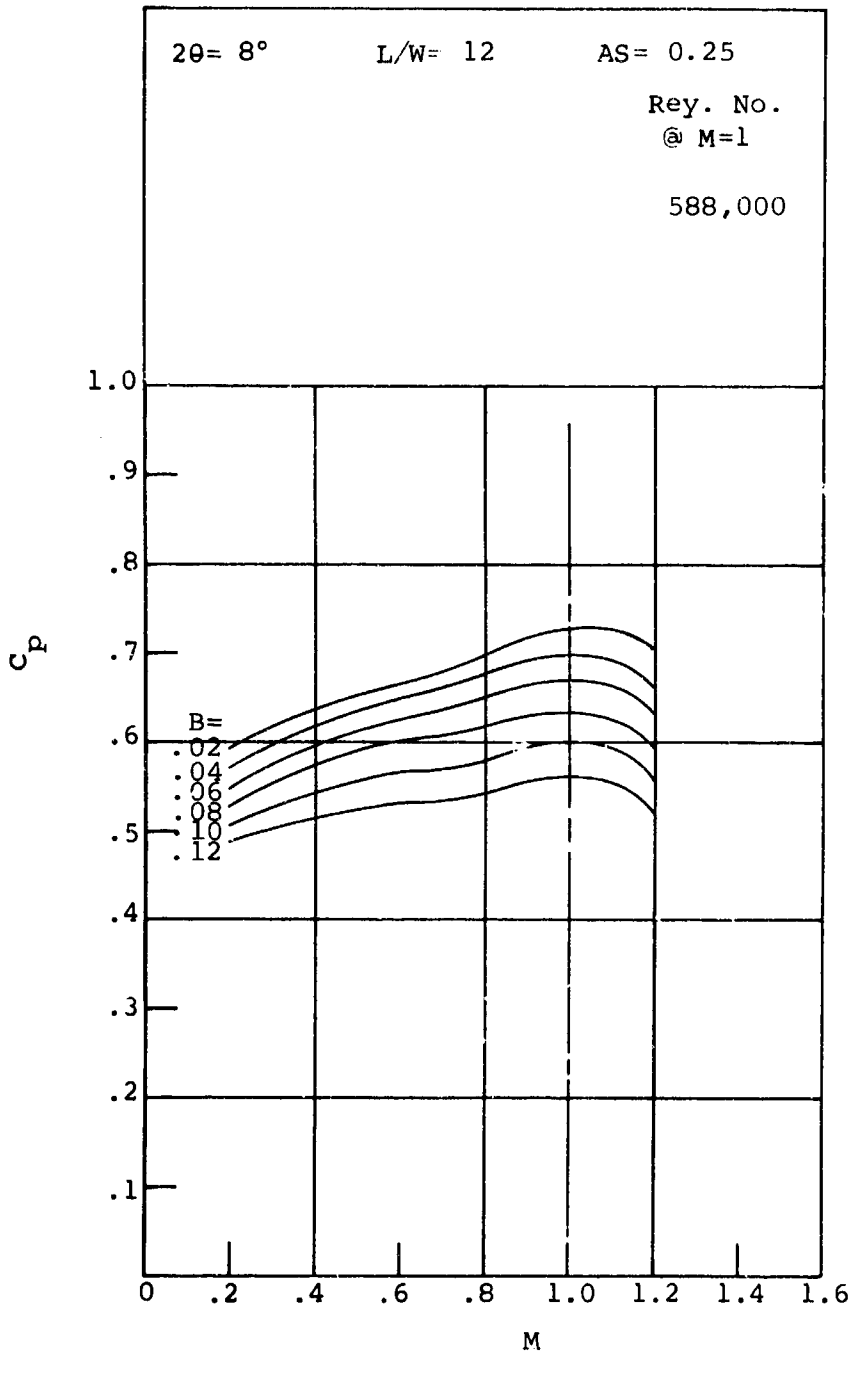

Figure 150. Pressure Recovery Versus Mach Number. Aspect Ratio = 0.25.

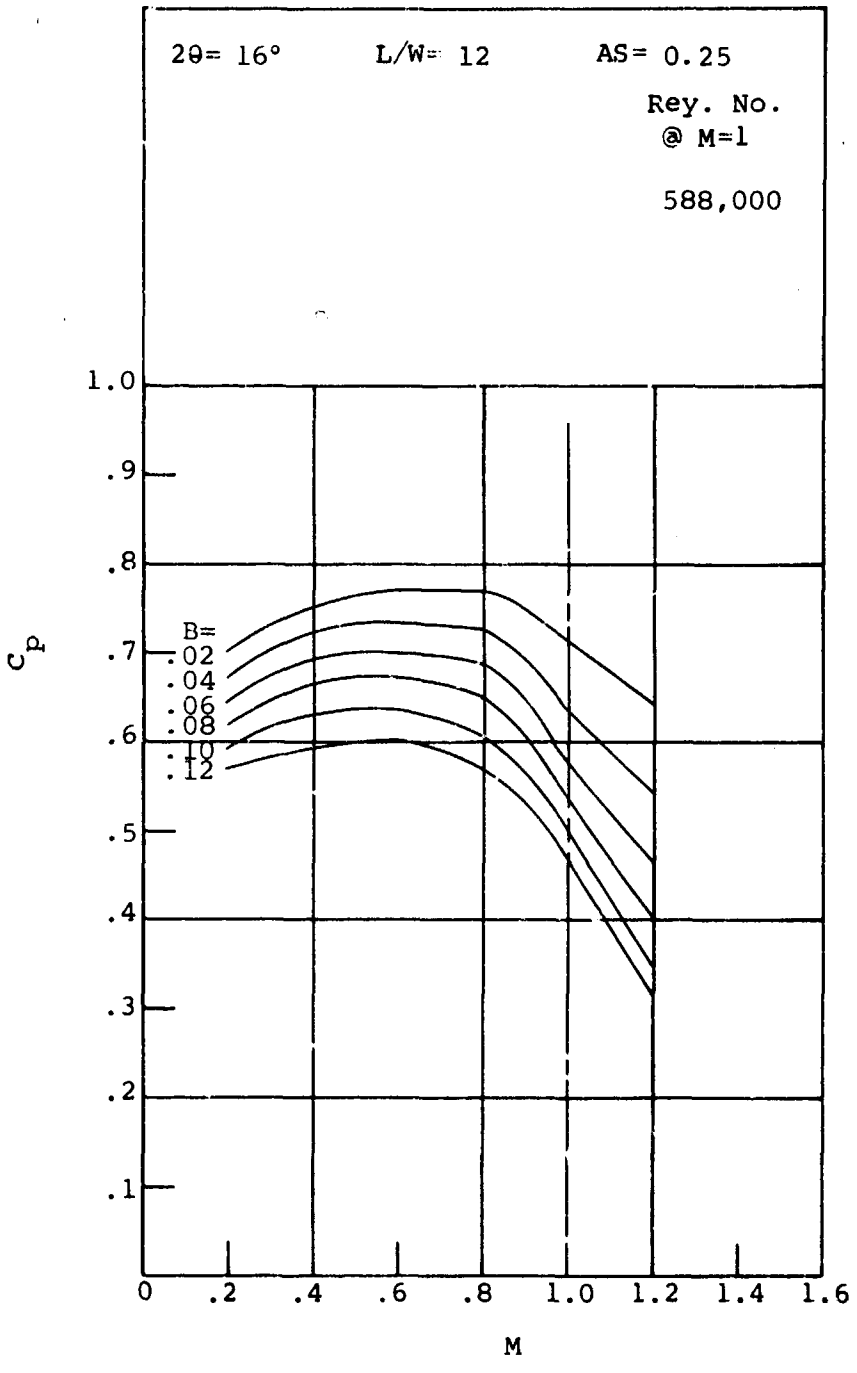

Figure 151. Pressure Recovery Versus Mach Number. Aspect Ratio = 0.25.

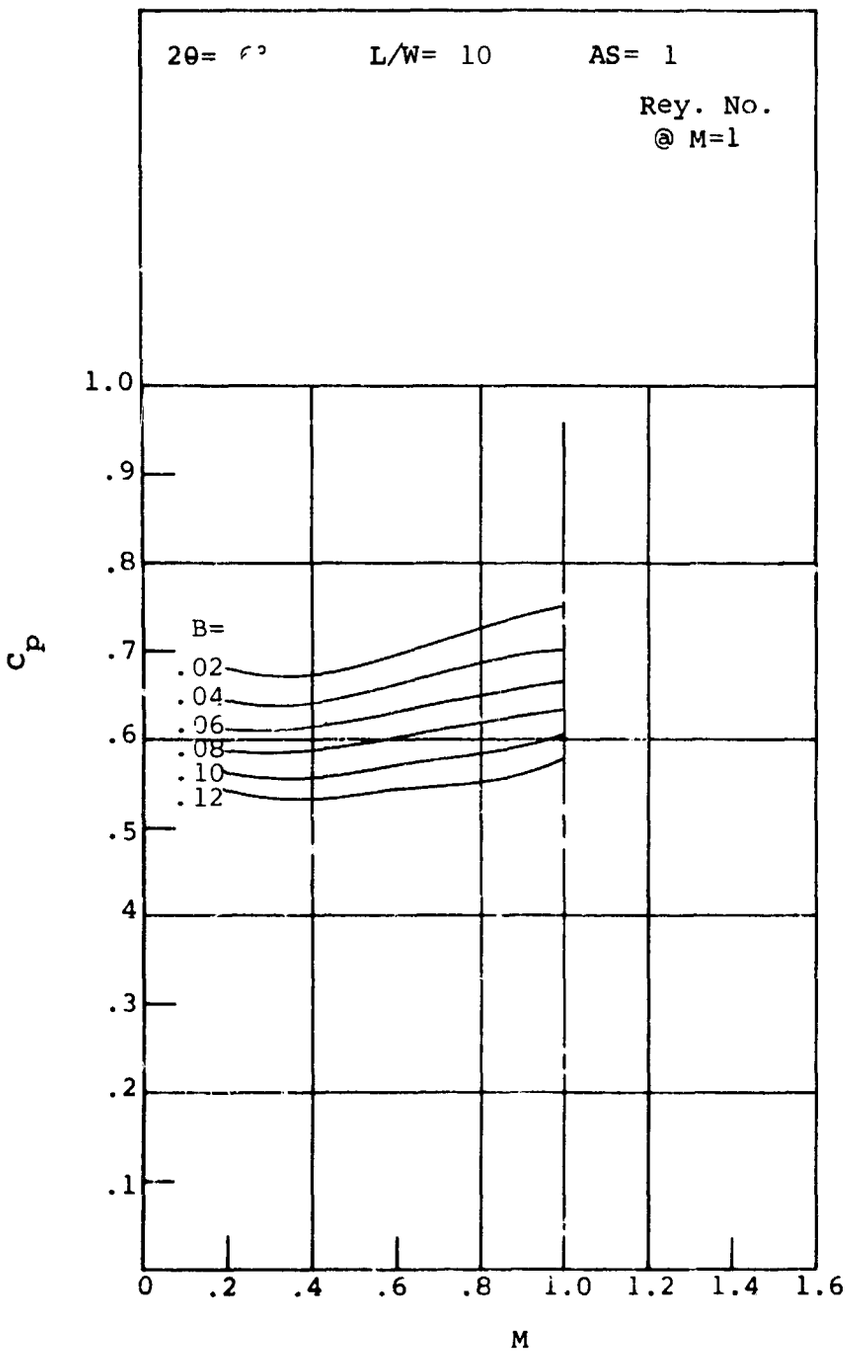

Figure 152. Pressure Recovery Versus Mach Number. Aspect Ratio = 1.0.

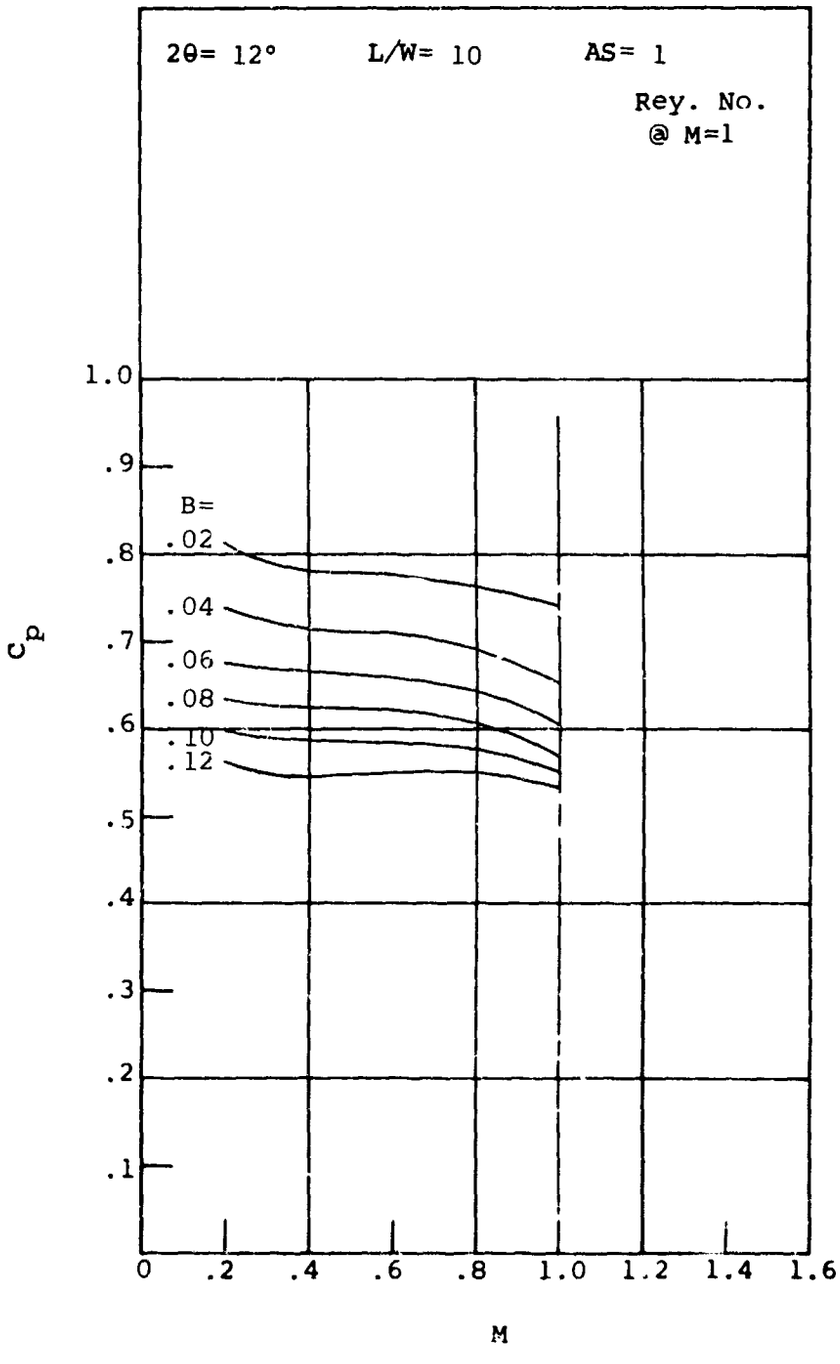

Figure 153. Pressure Recovery Versus Mach Number. Aspect Ratio = 1.0.

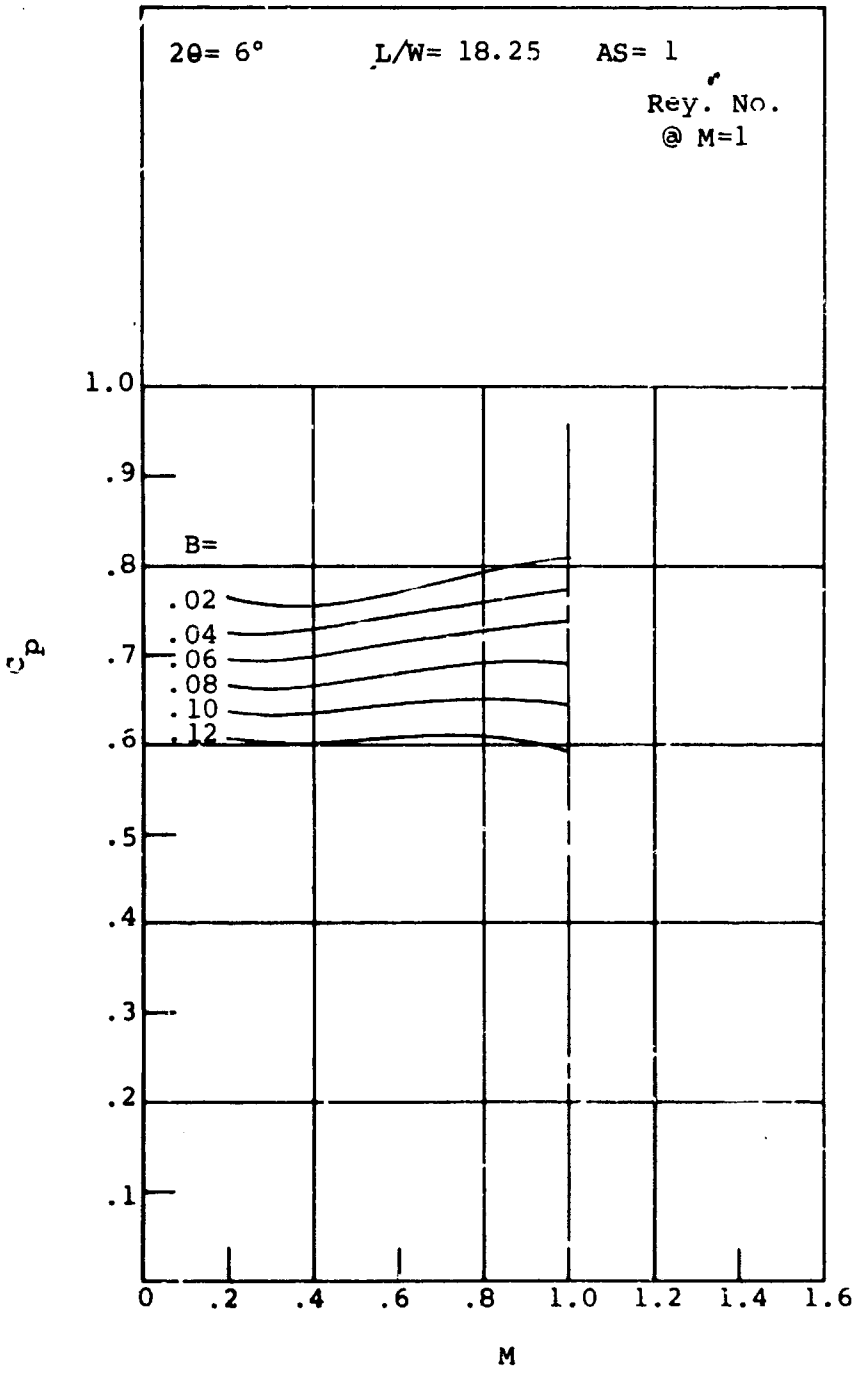

Figure 154. Pressure Recovery Versus Mach Number. Aspect Ratio = 1.0.

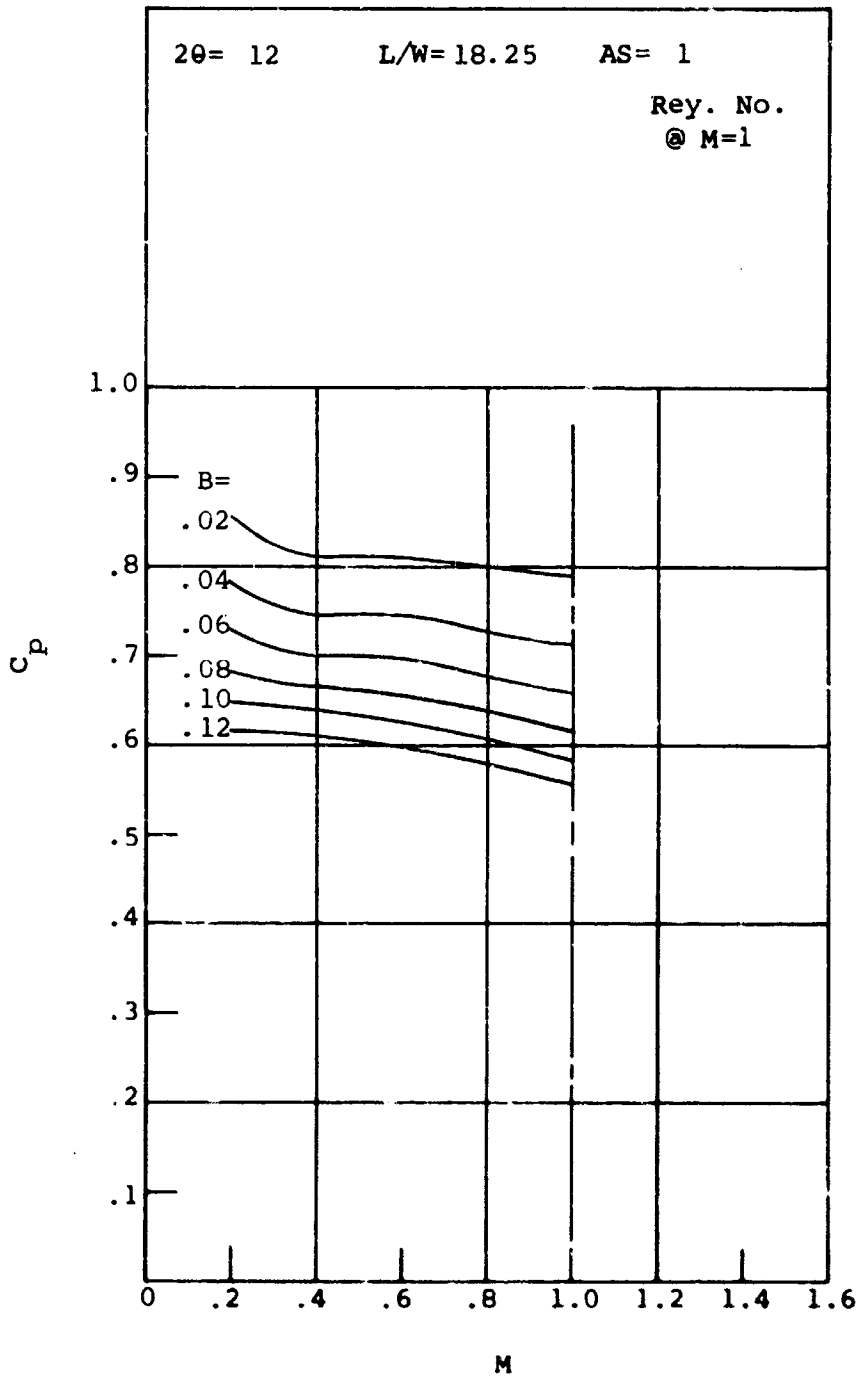

Figure 155. Pressure Recovery Versus Mach Number. Aspect Ratio = 1.0.

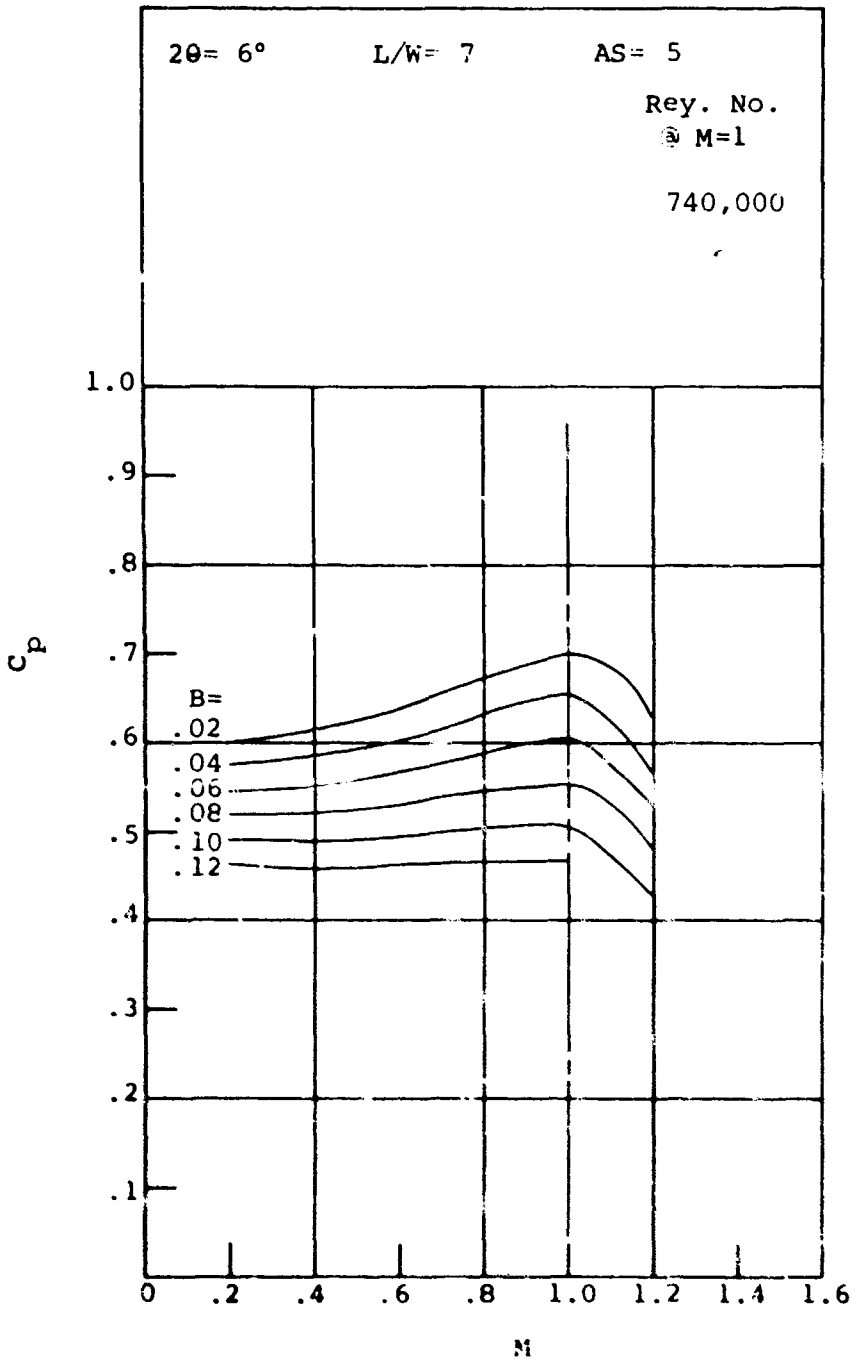

Figure 156. Pressure Recovery Versus Mach Number. Aspect Ratio = 5.0.

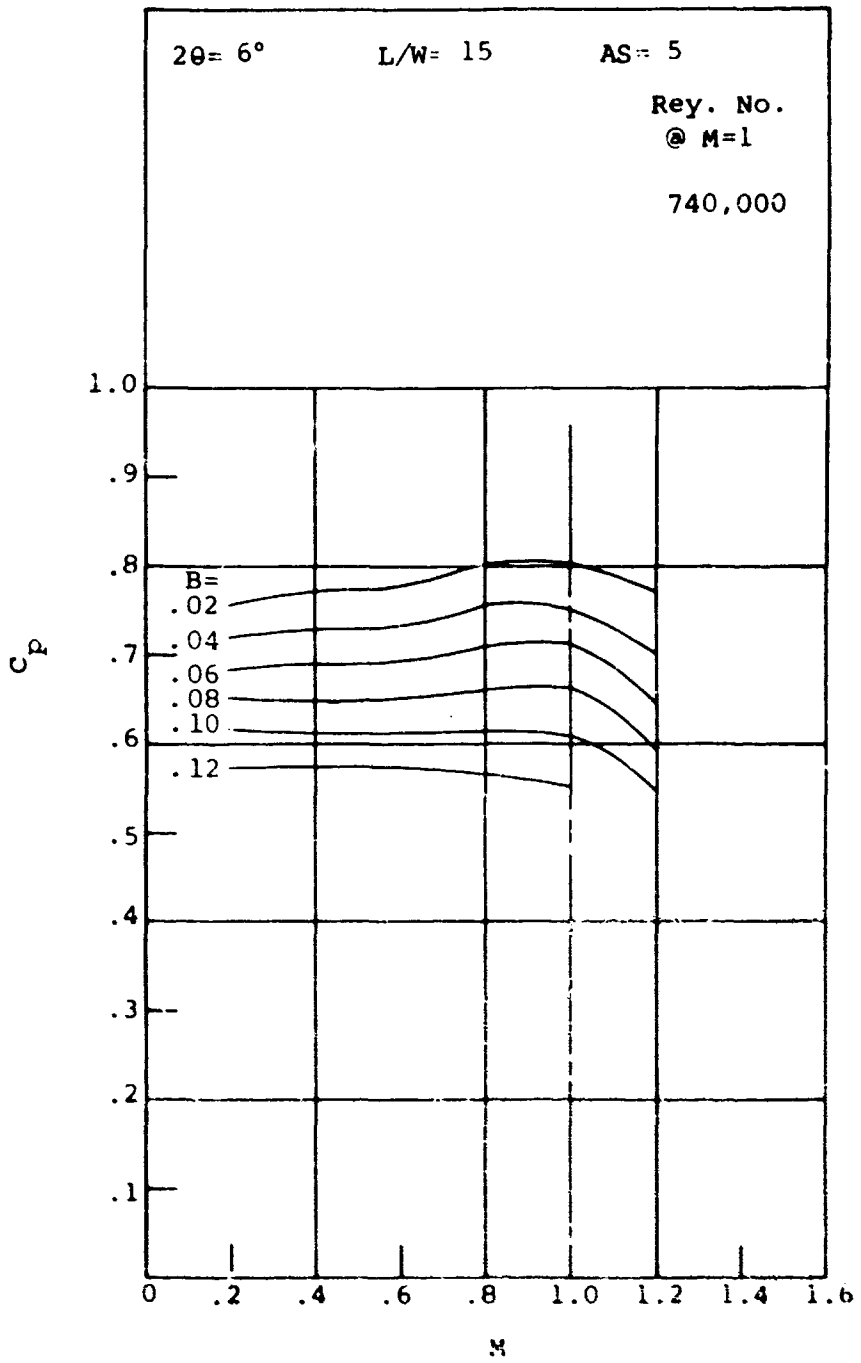

Figure 157. Pressure Recovery Versus Mach Number. Aspect Ratio = 5.0.

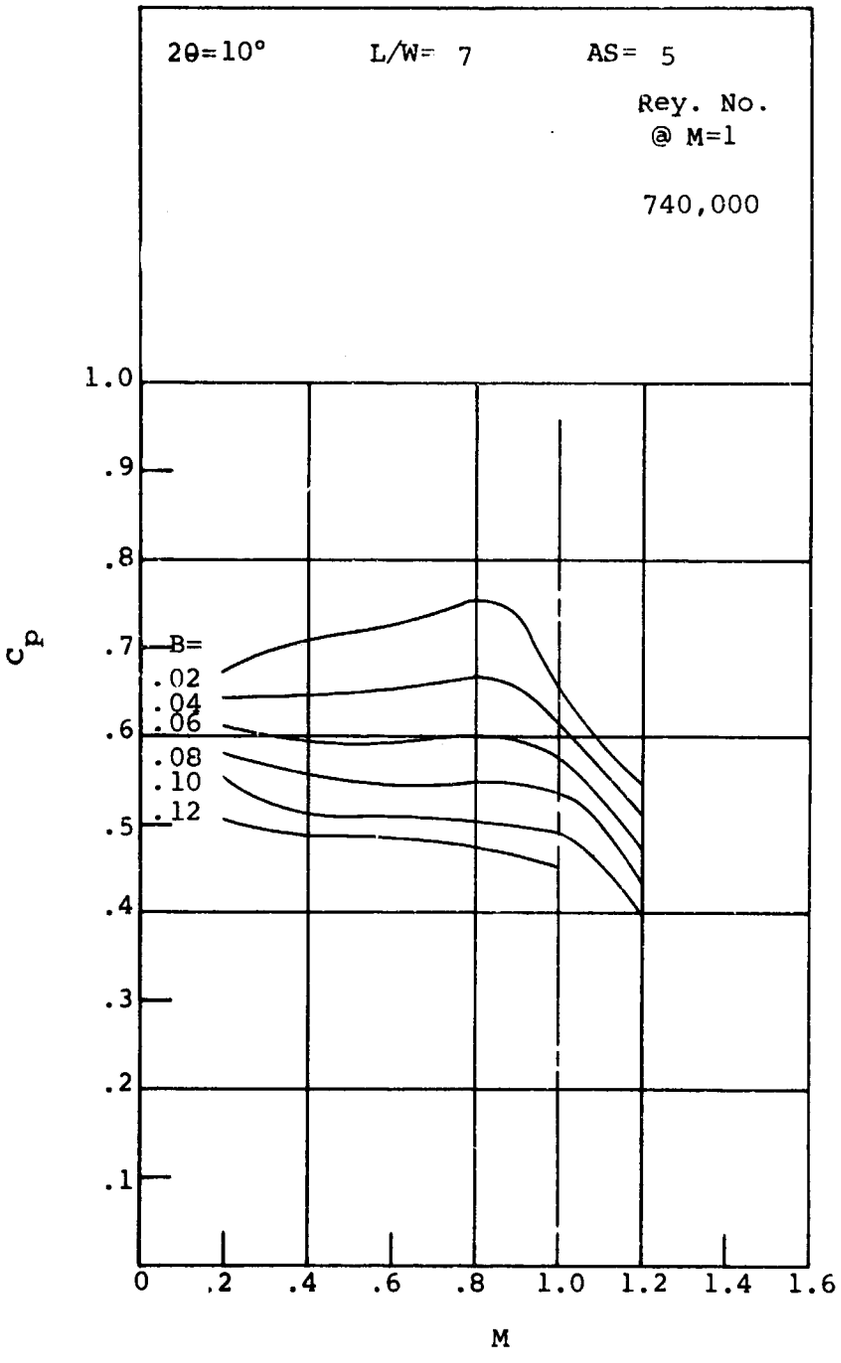

Figure 158. Pressure Recovery Versus Mach Number. Aspect Ratio = 5.0.

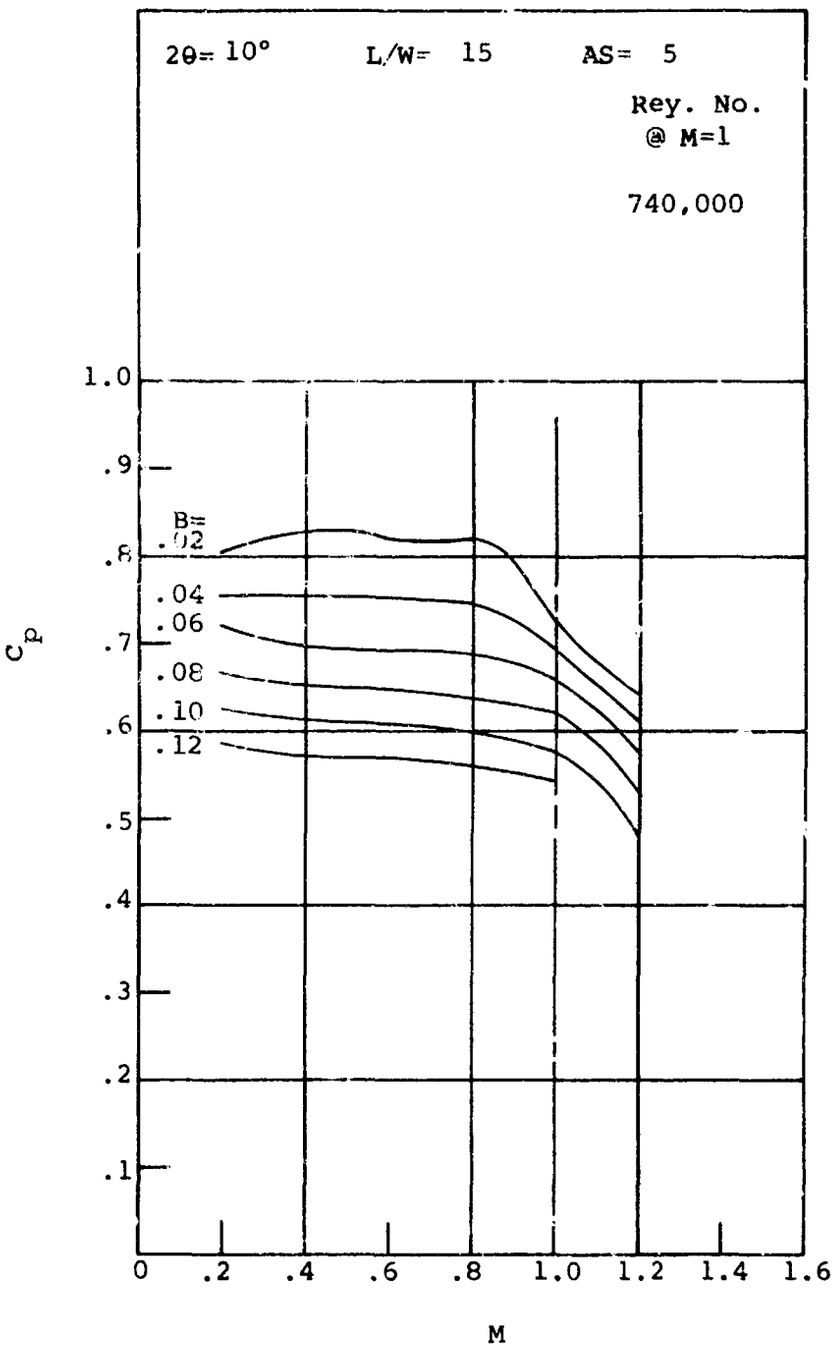

Figure 159. Pressure Recovery Versus Mach Number. Aspect Ratio = 5.0.

One reason that past diffuser researchers may have erroneously interpreted their data is that, as a diffuser approaches choking, the setting of experimental operating points becomes exceedingly sensitive. Operating points are usually established with a downstream throttling valve controlling back pressure. Between a centerline Mach number 0.8 and 1.0, however, only a 3.8% increase in flow occurs (based on one-dimensional flow arguments). In superchoked operation (a shock standing in the diffuser), almost no increase in flow occurs as the shock moves down the diffuser with a lowering in back pressure.

This small change in flow under superchoked conditions means that a throttling valve becomes extremely sensitive. In addition, the valve is usually choked so that the product of diffuser back pressure and the valve opening remains essentially constant. When the valve opening is increased 1%, the back pressure falls 1%; this is a change sufficient to move the shock a considerable distance in the diffuser. This extreme sensitivity, which in practice makes it very difficult to set a diffuser operating point, has probably been one of the principal causes of misinterpretation of actual diffuser operating states.

Another, and perhaps equally important, cause of misinterpretation is that usually a straight throat is incorporated at the inlet of the diffuser in order to put the inlet flow into a uniform pattern. But at high subsonic Mach numbers, boundary layer growth in a throat as short as one hydraulic diameter can cause substantial changes in static pressure. Figure 160 shows the pressure variation for a straight throat ahead of a diverging channel diffuser at $M_t = 1.0$. If wall static pressure taps are employed, a great many closely spaced taps must be installed in order to discover the minimum pressure in the throat. In contrast, by the use of a traverse static pressure probe along the centerline of the diffuser, the static pressure tap can be positioned in the diffuser without changing the diffuser geometry. By this means, the minimum pressure can be easily found. It has been possible to obtain excellent definition of the minimum pressure in the throat at each throat Mach number and the location of shocks when the diffuser flow is superchoked. In the present studies, any ambiguity and uncertainty in extrapolating readings from fixed pressure taps in a sidewall has been eliminated.

It should be noted that in the present studies the minimum pressure at the throat (for nonsuperchoked conditions) has been used to evaluate diffuser pressure recovery. In most

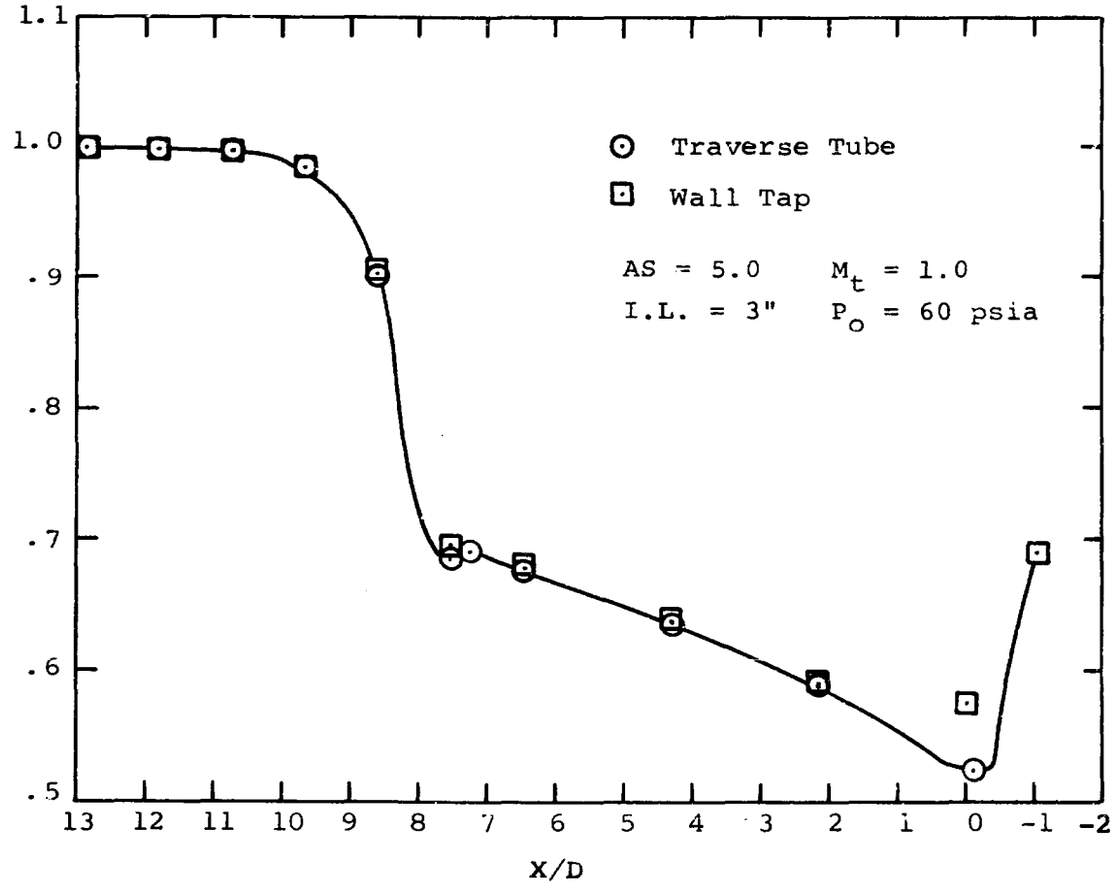

Figure 160. Static-to-Stagnation Pressure Ratio Versus Axial Distance. Inlet Length = 3". Mach Number = 1.0.

cases, this point of minimum pressure has not corresponded to the axial location of the geometric diffuser throat.

Table VII shows the relationship of the minimum pressure location to the geometric throat as a function of aspect ratio, Mach number, and inlet block length. On the basis of the present studies, there does not appear to be a significant correlation with either diffuser divergence angle 2θ or length-to-width ratio L/W_1. There is a continual movement of the minimum pressure point from a point upstream of the geometric throat at low Mach numbers ($M_t = 0.2$) to positions closer to the throat as Mach number is raised. At all Mach numbers, the difference between the location of minimum pressure and that of the geometric throat is small. At choked conditions, the minimum pressure point is essentially located at the diffuser geometric throat location.

The question has been raised* as to the usefulness in design of performance maps based on the minimum pressure; it is felt that the inlet flow configuration is an essential part of the overall diffuser geometry and that the designer will need information on pressure recovery for each combination of the diffuser/inlet geometry.

The basic premise of the present study is that the inlet/channel diffuser combination can be treated as a series of flow elements. The performance of the inlet/diffuser combination depends upon the flow characteristics of the inlet and diffuser separately, but the overall performance of the combination can be found by matching the characteristics of the inlet to those of the diffuser at the diffuser throat. If this approach is not valid, the designer will be required to test each inlet-diffuser combination separately. A general understanding of overall diffuser optimization will be an almost impossible task.

For subcritical (or subchoked), the point of minimum pressure has been used as the effective throat because it is in reality the point where the flow diffusion begins; as such, it is an essential part of the diffusion process. Consistent trends in recovery performance and a reduction in scatter of data have been possible by using only the minimum pressure rather than the static pressure at the geometric throat.

---

*See Fox (1969).

TABLE VII. THROAT MINIMUM PRESSURE LOCATION

Stagnation Pressure p_o (psia)	Aspect Ratio AS	Inlet Length I.L. (in.)	Mach Number M_t	Throat Location	Standard Deviation σ (in.)
60	0.25	0.5	0.2	-.184	.057
60	0.25	0.5	0.4	-.170	.050
60	0.25	0.5	0.6	-.150	.043
60	0.25	0.5	0.8	-.104	.038
60	0.25	0.5	1.0	-.029	.032
60	0.25	3.5	0.2	-.237	.055
60	0.25	3.5	0.4	-.206	.051
60	0.25	3.5	0.6	-.183	.045
60	0.25	3.5	0.8	-.142	.050
60	0.25	3.5	1.0	-.041	.038
60	0.25	6.5	0.2	-.272	.054
60	0.25	6.5	0.4	-.261	.058
60	0.25	6.5	0.6	-.216	.042
60	0.25	6.5	0.8	-.180	.118
60	0.25	6.5	1.0	-.099	.116
20	0.25	0.5	0.2	-.214	.073
20	0.25	0.5	0.4	-.189	.066
20	0.25	0.5	0.6	-.160	.071
20	0.25	0.5	0.8	-.123	.051
20	0.25	0.5	1.0	+.004	.027
20	0.25	3.5	0.2	-.251	.038
20	0.25	3.5	0.4	-.200	.050
20	0.25	3.5	0.6	-.171	.050
20	0.25	3.5	0.8	-.141	.030
20	0.25	3.5	1.0	-.055	.009
20	0.25	6.5	0.2	-.245	.043
20	0.25	6.5	0.4	-.226	.042
20	0.25	6.5	0.6	-.180	.023
20	0.25	6.5	0.8	-.127	.024
20	0.25	6.5	1.0	-.069	.018
60	1.0	0.5	0.2	-.307	.059
60	1.0	0.5	0.4	-.261	.043
60	1.0	0.5	0.6	-.186	.037

TABLE VII - Continued

Stagnation Pressure P_o (psia)	Aspect Ratio AS	Inlet Length I.L. (in.)	Mach Number M_t	Throat Location	Standard Deviation σ (in.)
60	1.0	0.5	0.8	-.124	.024
60	1.0	0.5	1.0	+.019	.023
60	1.0	6.5	0.2	-.326	.098
60	1.0	6.5	0.4	-.289	.110
60	1.0	6.5	0.6	-.239	.106
60	1.0	6.5	0.8	-.155	.050
60	1.0	6.5	1.0	-.043	.038
60	1.0	9.5	0.2	-.322	.094
60	1.0	9.5	0.4	-.271	.067
60	1.0	9.5	0.6	-.222	.057
60	1.0	9.5	0.8	-.165	.044
60	1.0	9.5	1.0	-.052	.031

The actual situation facing the designer is schematically sketched in Figure 161. The curves drawn show the actual pressure distribution through an inlet diffuser combination and the inlet distribution that would be calculated in a design situation. Point A is the minimum pressure point in the actual distribution that has been used to evaluate recovery performance. Point B is the actual geometric throat static pressure which is higher than Point A, since A is the minimum pressure point. Point C is the static pressure at the geometric throat (end of the inlet geometry) that a designer might estimate based on calculation of the flow in the inlet, neglecting the presence of the diffuser.

Of course, the real flow situation is represented by the actual static pressure distribution curve passing through A and B, and the designer should develop proper flow models to represent this inlet/diffuser flow situation. However, this probably does not represent a reasonable task until much more detailed information is available on the flow behavior at the throat.

Assuming that the inlet flow is calculated as if the diffuser were not present (Point C is calculated), a greater error will be incurred in design calculations by using the actual geometric throat pressure B than by using the minimum pressure Point A. This is because the difference between C and B is greater than the difference between C and A.

From the present studies, however, it appears to make little difference to the accuracy of overall pressure recovery whether the recovery performance is based on the pressure B or the pressure A.

Inlet traverse tube static pressure measurements are shown in Figures 160 and 162 through 166 for the aspect ratio = 5.0 diffusers for throat Mach numbers of 0.2, 0.6, and 1.0. These figures illustrate the minimum pressure point and static pressure distributions near the diffuser throat region. Because of the small pressure gradients at low Mach number, the minimum pressure point value of static pressure does not make an appreciable difference in the calculation of pressure recovery compared with that calculated using the static pressure at the geometric throat. On the other hand, the relatively large pressure gradients that occur at high Mach numbers do not affect the calculated difference in recovery, because the steep gradients are offset by the nearness of the minimum pressure

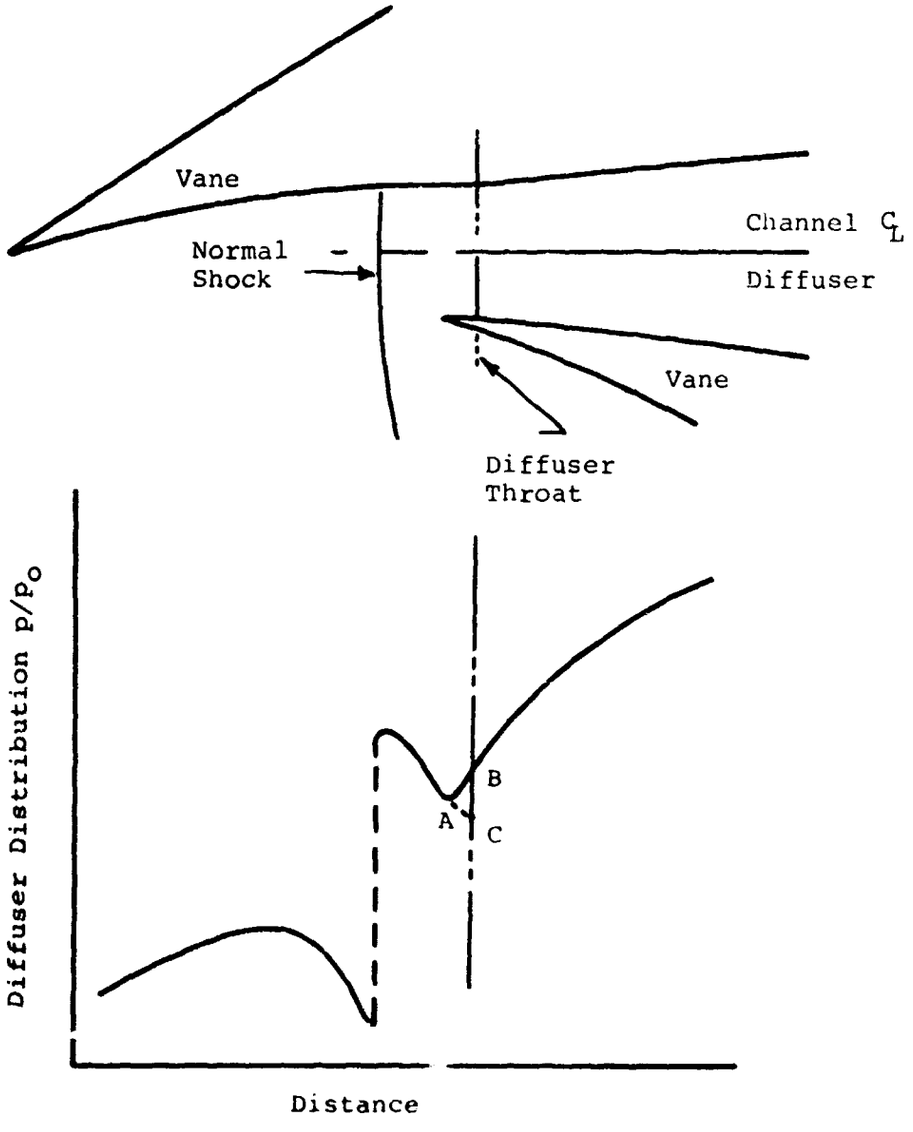

Figure 161. Vane-Island Channel Diffuser Inlet Pressure Distribution.

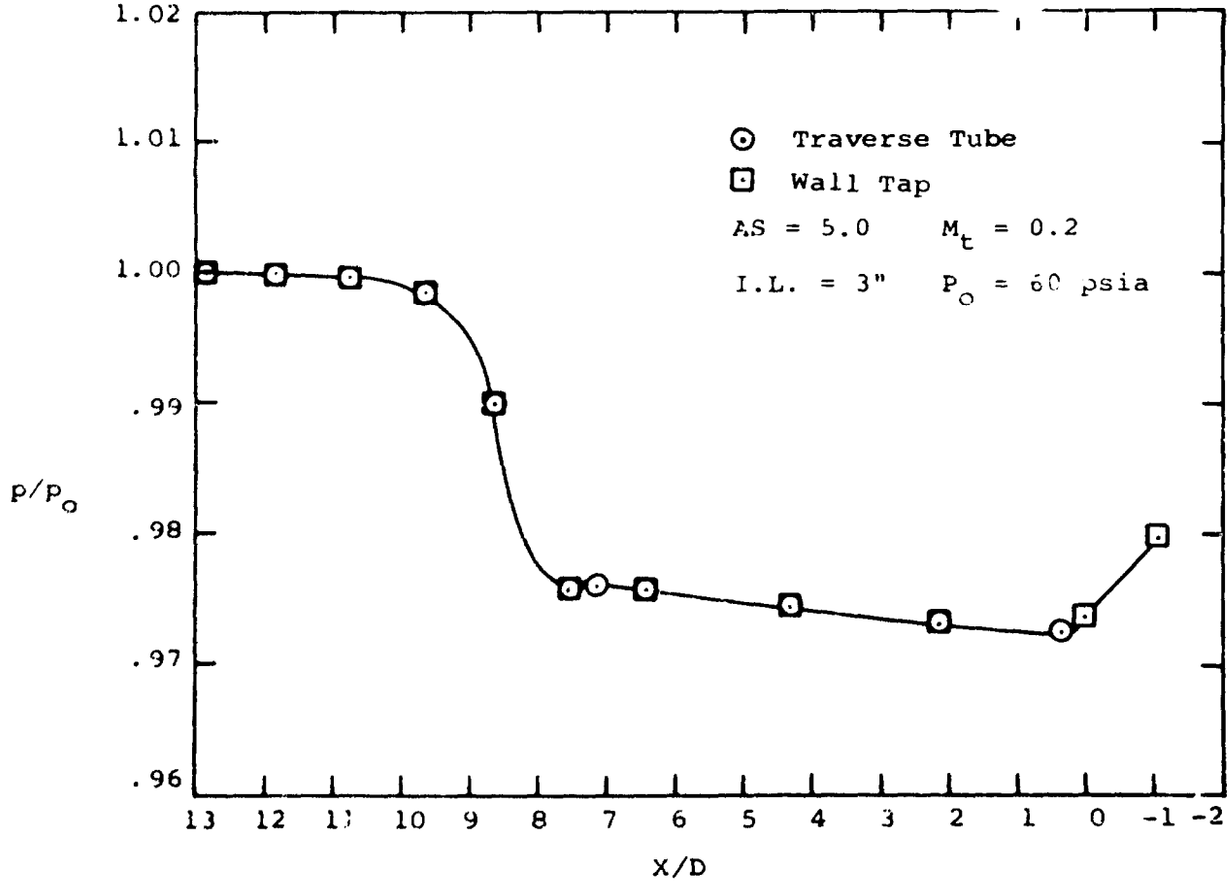

Figure 162. Static-to-Stagnation Pressure Ratio Versus Axial Distance. Inlet Length = 3". Mach Number = 0.2.

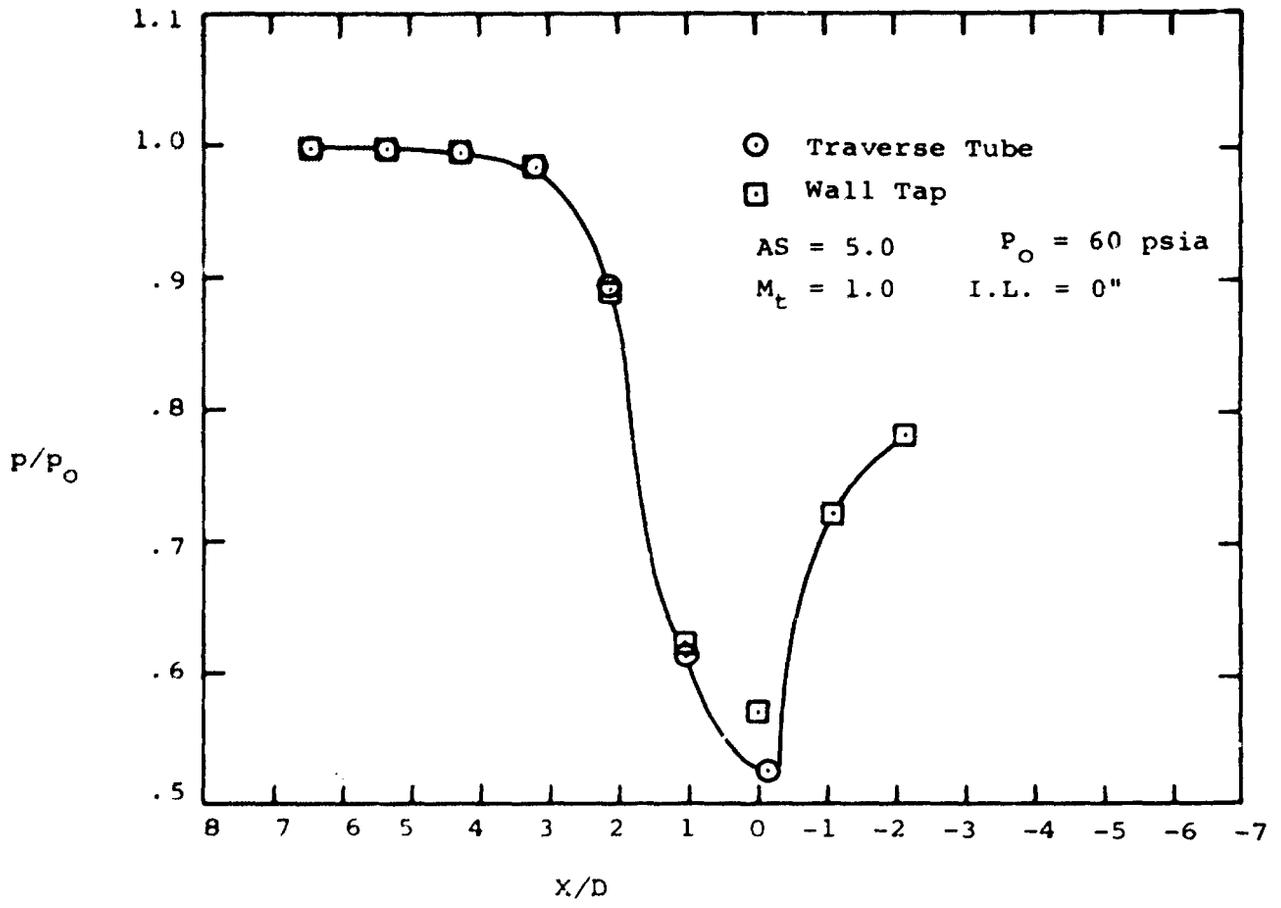

Figure 163. Static-to-Stagnation Pressure Ratio Versus Axial Distance. Inlet Length = 0". Mach Number = 1.0.

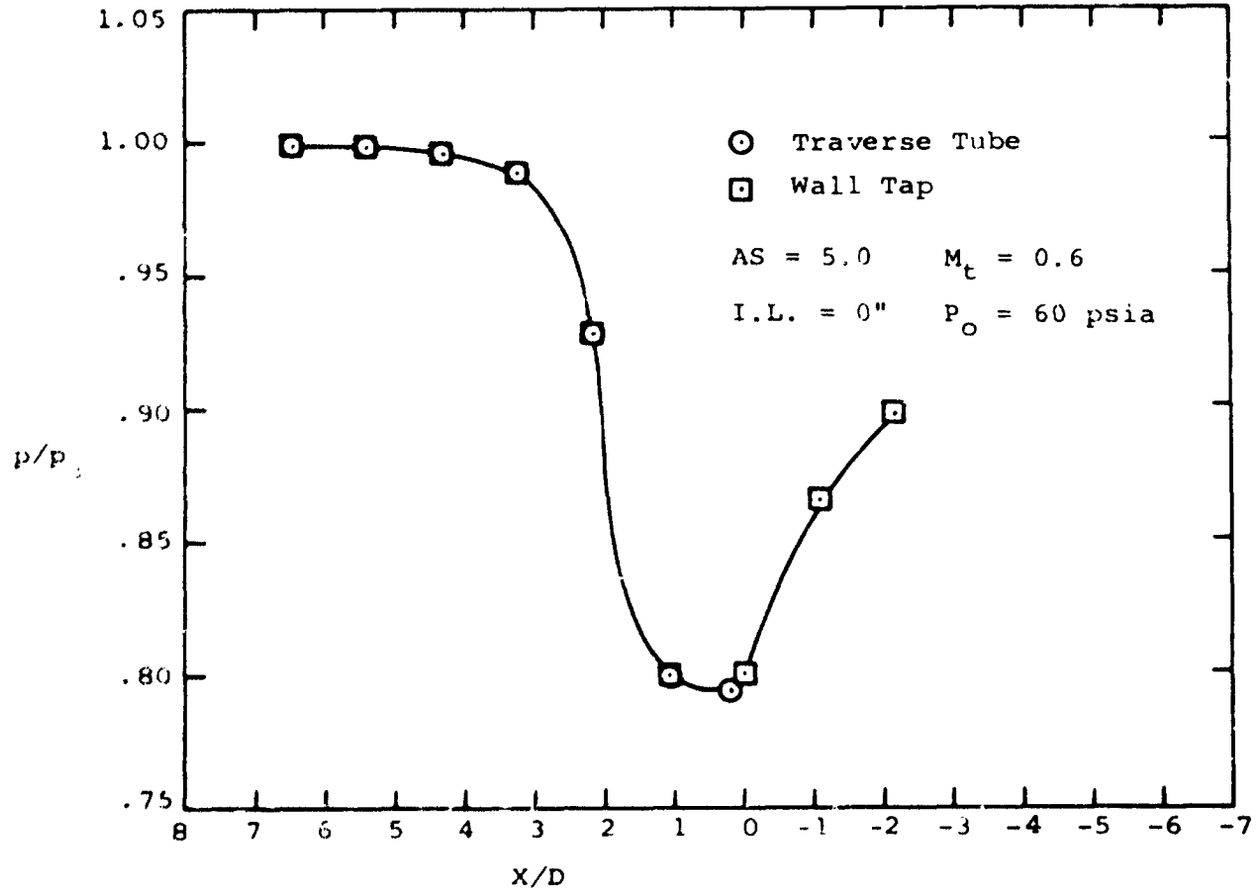

Figure 164. Static-to-Stagnation Pressure Ratio Versus Axial Distance. Inlet Length = 0". Mach Number = 0.6.

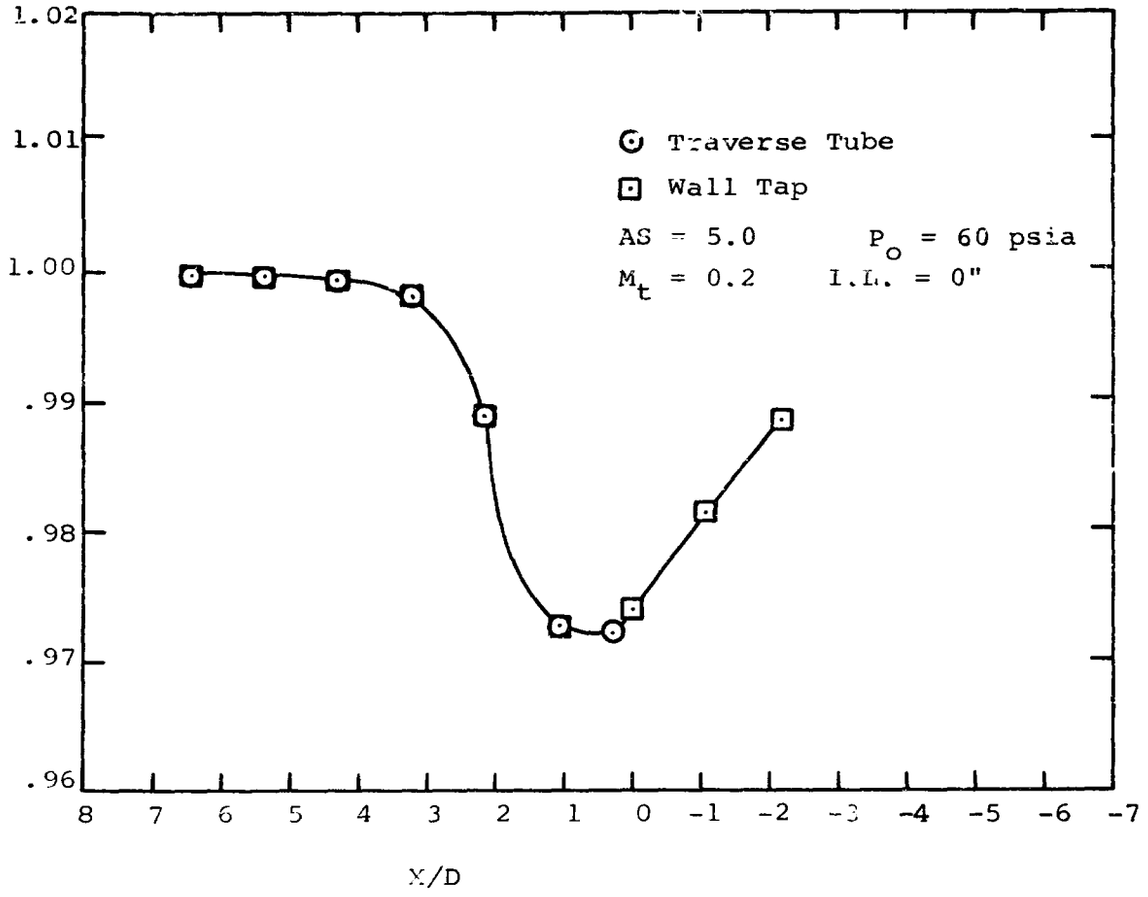

Figure 165. Static-to-Stagnation Pressure Ratio Versus Axial Distance. Inlet Length = 0". Mach Number = 0.2.

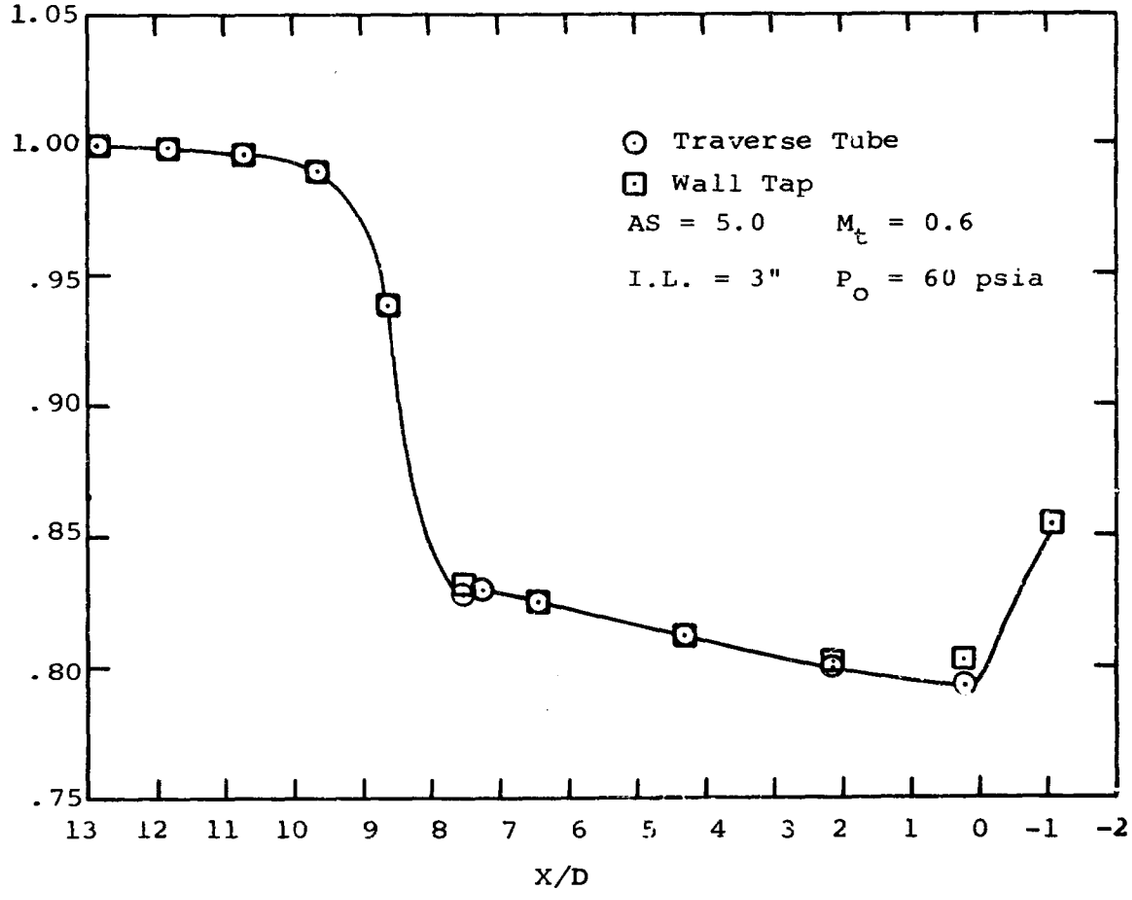

Figure 166. Static-to-Stagnation Pressure Ratio Versus Axial Distance. Inlet Length = 3". Mach Number = 0.6.

point to the geometric throat. Thus, there is very little difference in the value of C_p calculated at the geometric throat and at the minimum pressure point over the entire Mach number range.

Another cause for confusion in the diffuser literature is the occasional location of taps on curved sidewalls or on the walls of axisymmetric diffusers. The two-dimensional nature of a flow in the vicinity of a curved wall makes the use of such tap indication most difficult when attempting to determine the average throat conditions. Streamline curvature effects around curved walls can lead to an erroneous, high indication of the true core flow throat Mach number at high subsonic conditions.

A final possible source of misinterpretation is that when the diffuser goes into superchoked operation, the distribution of pressures in the throat does not change. We suspect that many investigators have only observed throat and exit static pressure taps and therefore were unaware of the fact that their diffusers were operating in the superchoked region with a shock standing in the diverging channel. A lack of numerous taps near the throat can lead one to ignore the presence of the superchoked flow regime near choked conditions.

Mach number is thus not a very powerful variable until the Mach number ahead of the shock in the diverging portion of the diffuser under superchoked flow exceeds about 1.15. At this point, performance degenerates rapidly because increases in the shock strength are sufficient to separate the diffuser boundary layer.

Despite the fact that Mach numbers in the subsonic range do not have an overwhelming influence on diffuser performance, the variation with Mach number is important to the achievement of the very highest performance. In many turbomachine applications, such small gains are important to the overall performance of the fluid machines or devices, and the behavior of diffuser recovery with inlet throat Mach number cannot be ignored.

Diffuser Effectiveness

A measure of the insufficient and inefficient diffusion in the diffuser channel is provided by comparing the actual

measured pressure recovery coefficient C_p with the ideal pressure recovery coefficient C_{p_i} and is the effectiveness ε:

$$\varepsilon = C_p/C_{p_i}$$

Figures 167 through 178 give representative plots of the effectiveness of fixed geometry diffusers as a function of inlet Mach number with inlet blockage as a variable. Samples are shown from each aspect ratio for fixed L/W with increasing divergence angle 2θ.

A comparison of the effectiveness plots with the diffuser performance maps shows a direct correlation between the trends in effectiveness and the configuration and location of the pressure recovery "contour" hills.

For fixed length-to-width ratio L/W_1 when the divergence angle 2θ is small, the geometry lies on the unstalled and gentle sloping side of the pressure recovery "hill". As divergence angle is increased, the geometry approaches the optimum ridge on which lie the lines C_p^* and C_p^{**}, after which the pressure recovery falls very rapidly on the steep slope of the pressure recovery "hill" as divergence angle is further increased.

For the 0.25 aspect ratio geometries, the optimum lines C_p^* and C_p^{**} are at large divergence angles (approximately 12° and above). Most of the geometries studied thus lie on the gently sloping side of the pressure recovery "hill" where recovery is increasing with divergence angle. On the basis of low Mach number visualization studies, the low angles on this side of the "hill" correspondto unstalled diffuser flow. As the divergence angle is increased at constant length-to-throat width ratio, the diffuser enters into a transitory stall regime, and the ridge of optimum recovery (C_p^* or C_p^{**}) occurs at slightly higher divergence angles. At yet still higher divergence angles, the diffuser enters fully stalled separating conditions in which the recovery rapidly declines.

Fox (1969) has described a similar behavior for conical diffusers at high inlet Mach numbers and low inlet blockage.

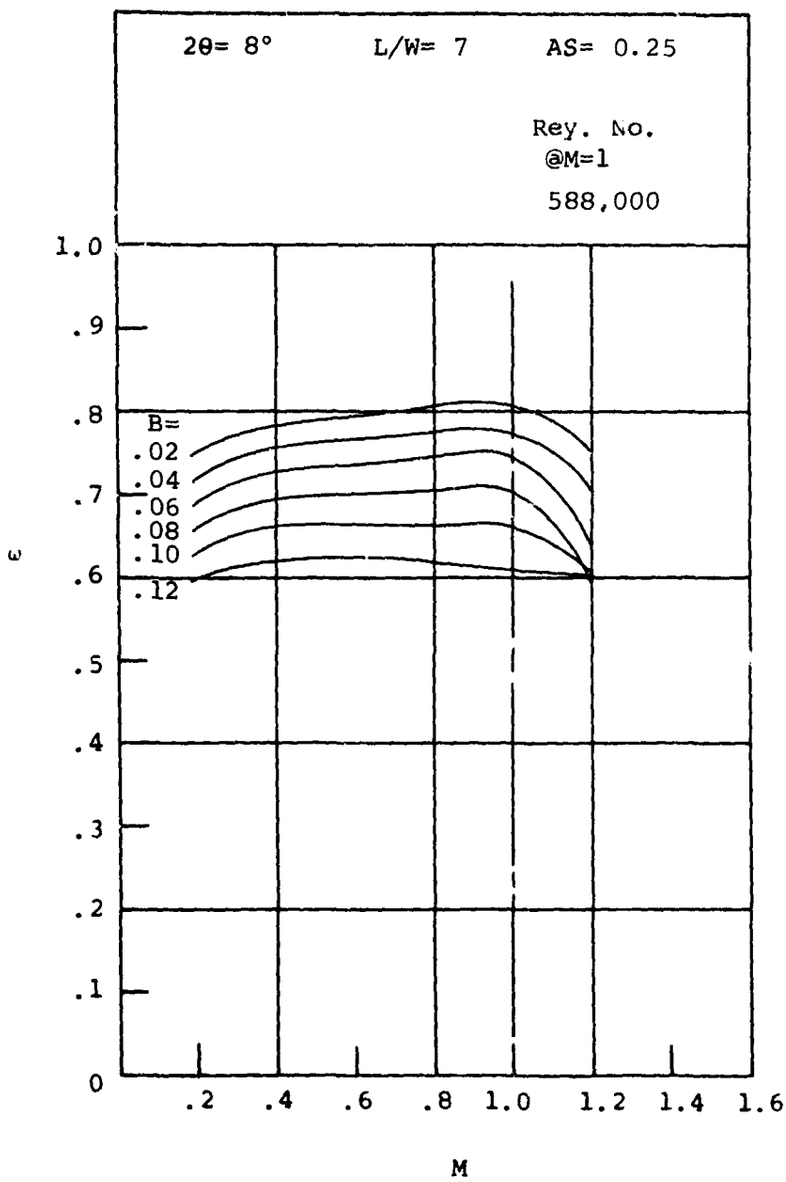

Figure 167. Effectiveness Versus Mach Number. Aspect Ratio = 0.25.

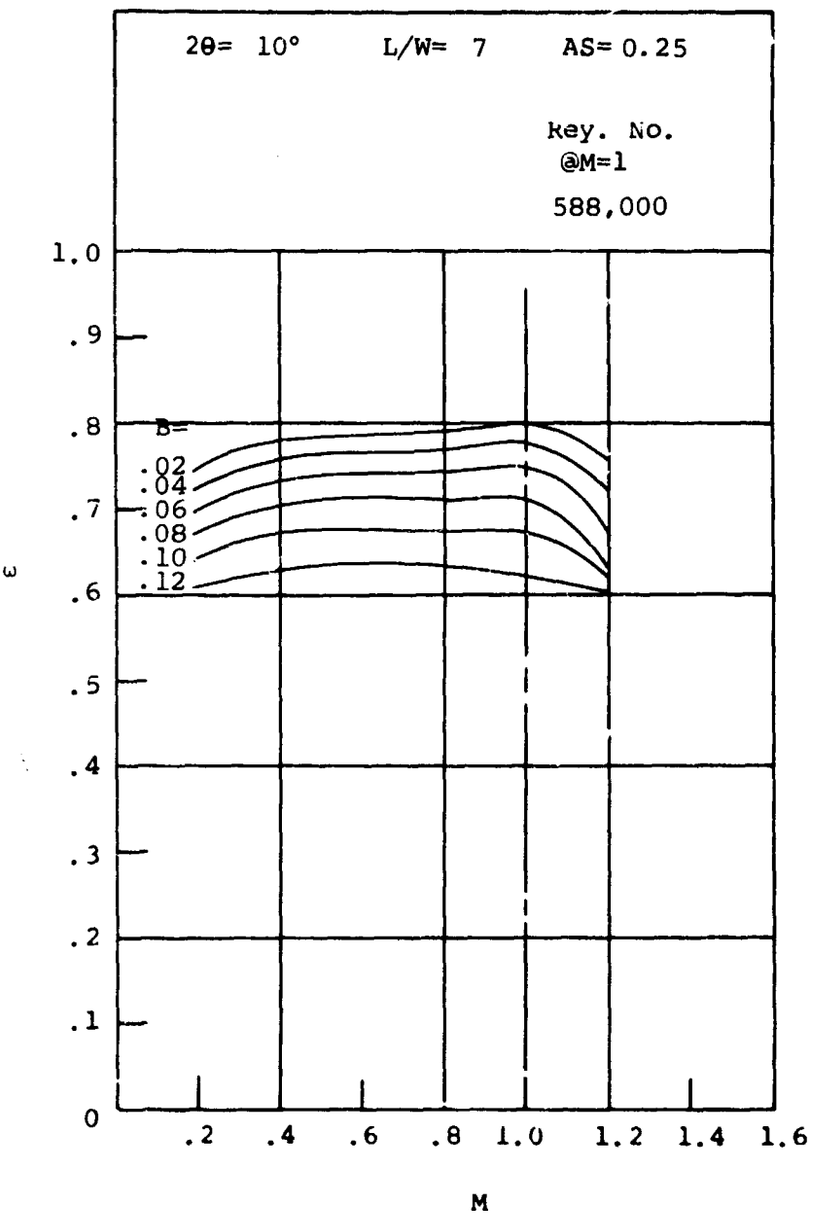

Figure 168. Effectiveness Versus Mach Number. Aspect Ratio = 0.25.

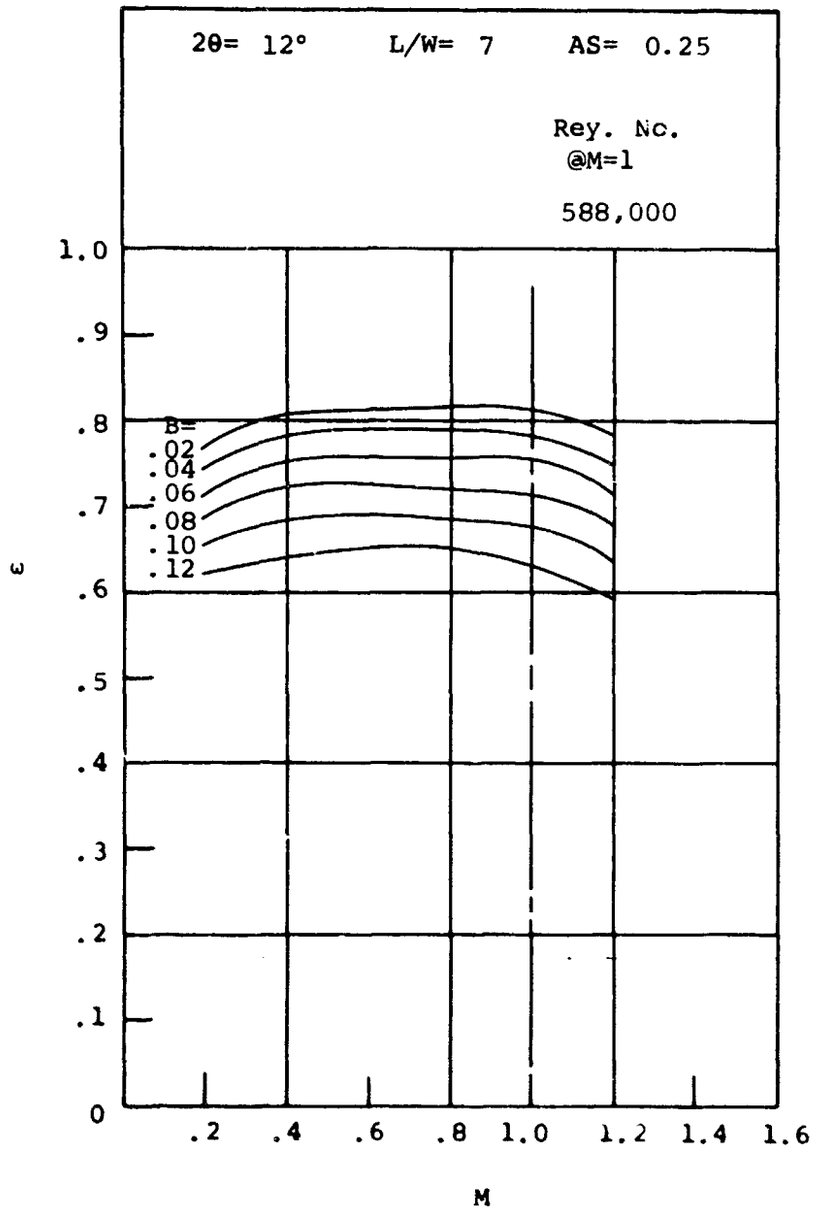

Figure 169. Effectiveness Versus Mach Number. Aspect Ratio = 0.25.

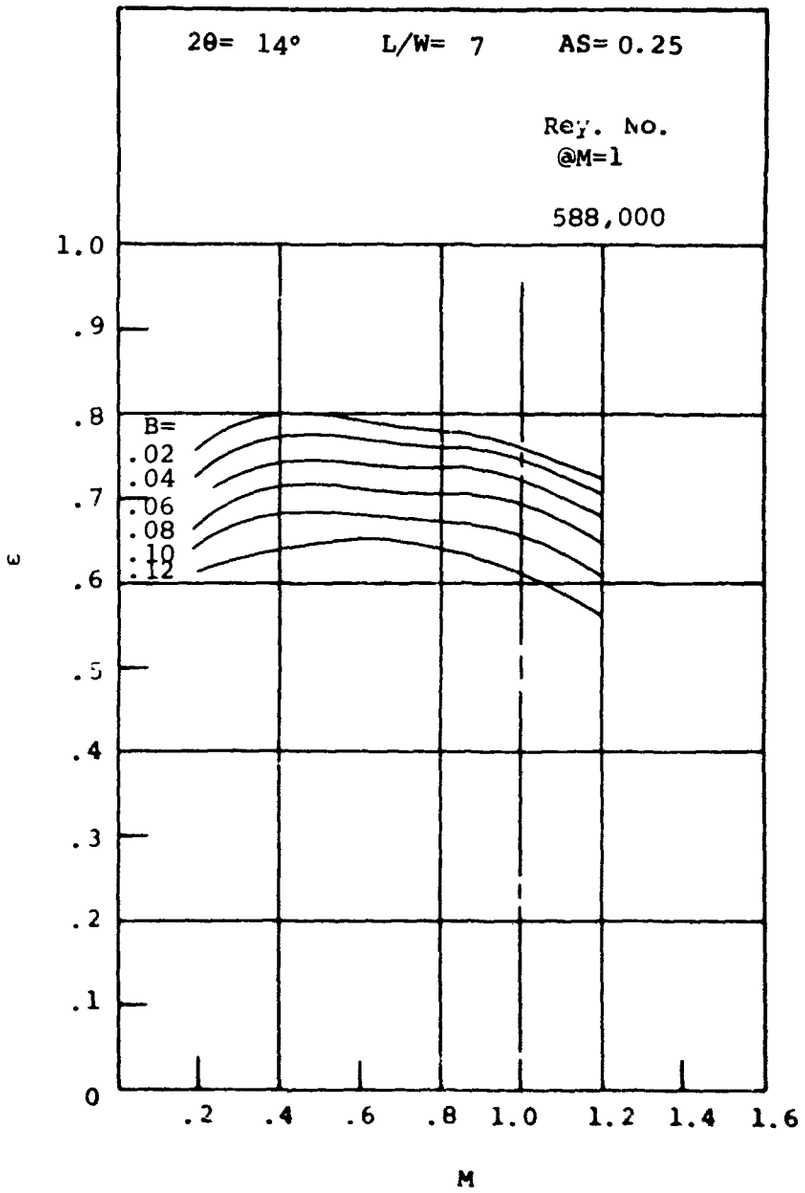

Figure 170. Effectiveness Versus Mach Number. Aspect Ratio = 0.25.

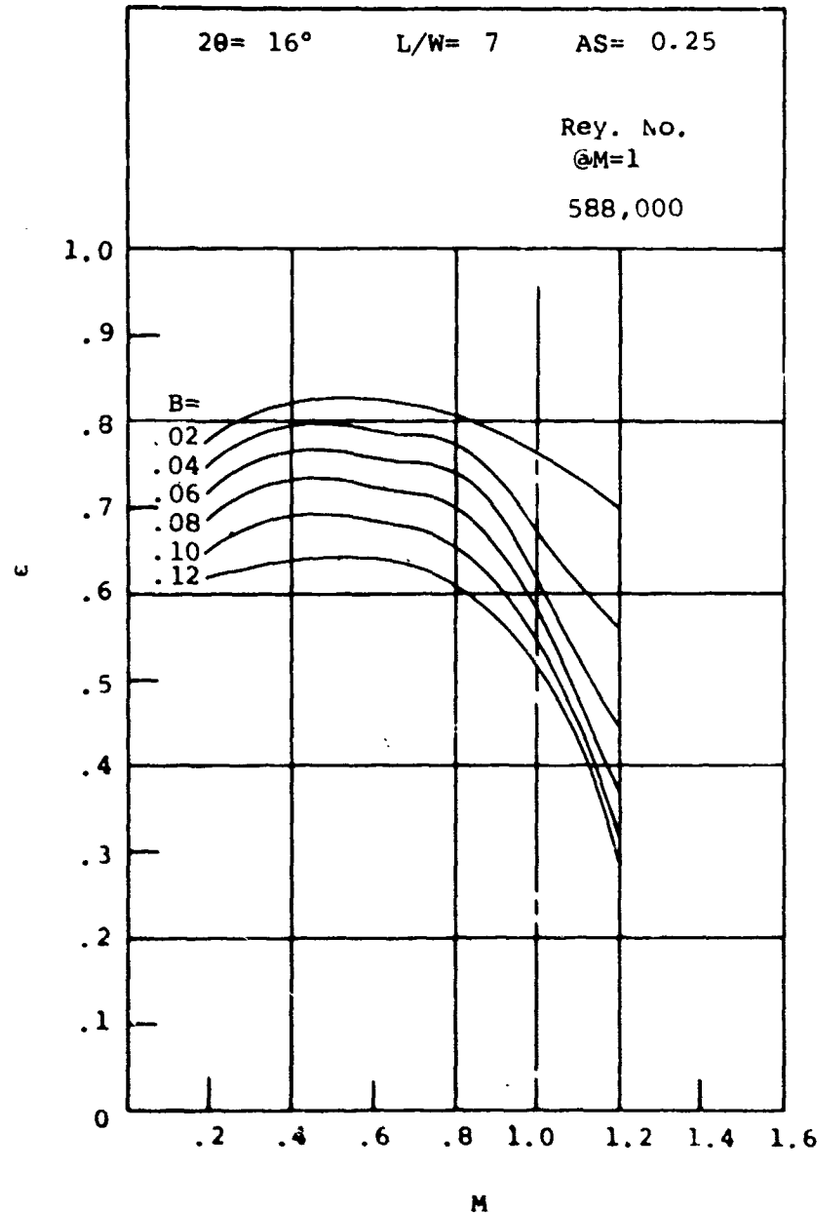

Figure 171. Effectiveness Versus Mach Number. Aspect Ratio = 0.25.

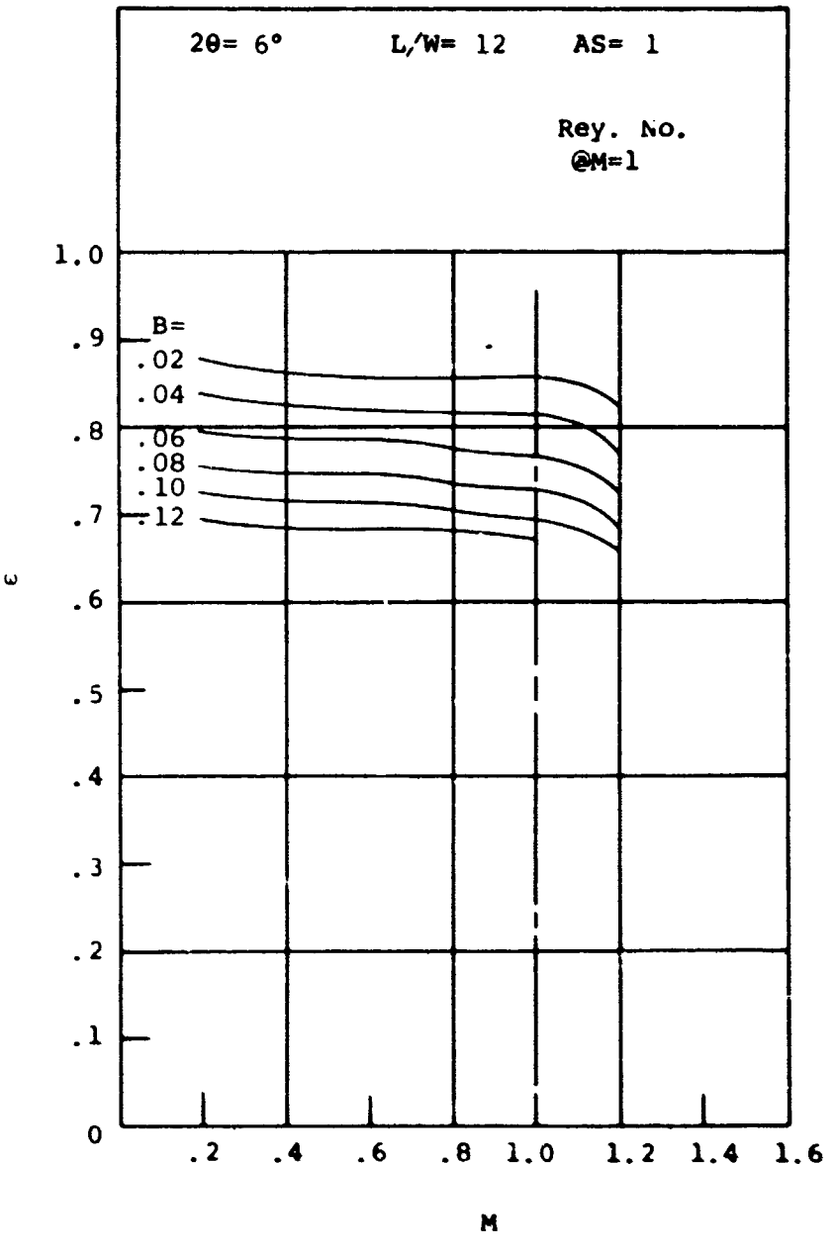

Figure 172. Effectiveness Versus Mach Number. Aspect Ratio = 1.0.

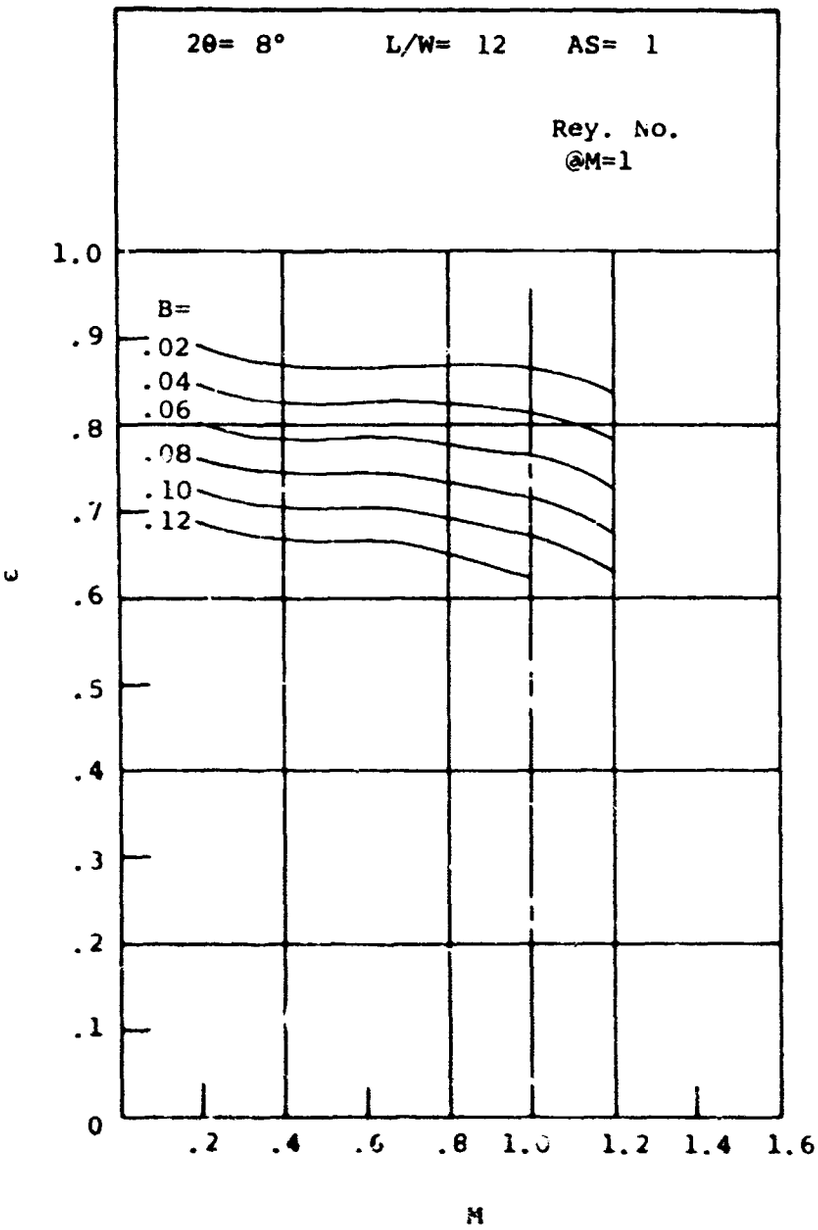

Figure 173. Effectiveness Versus Mach Number. Aspect Ratio = 1.0.

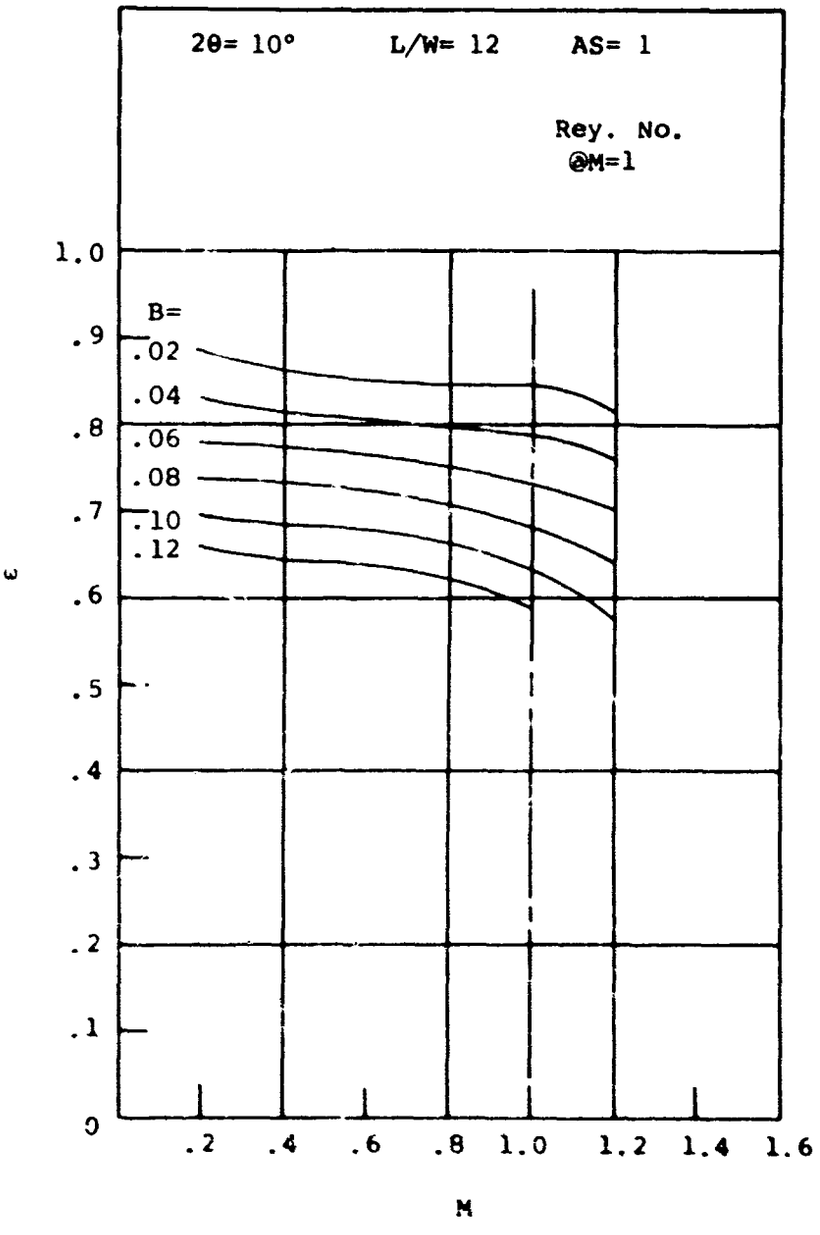

Figure 174. Effectiveness Versus Mach Number. Aspect Ratio = 1.0.

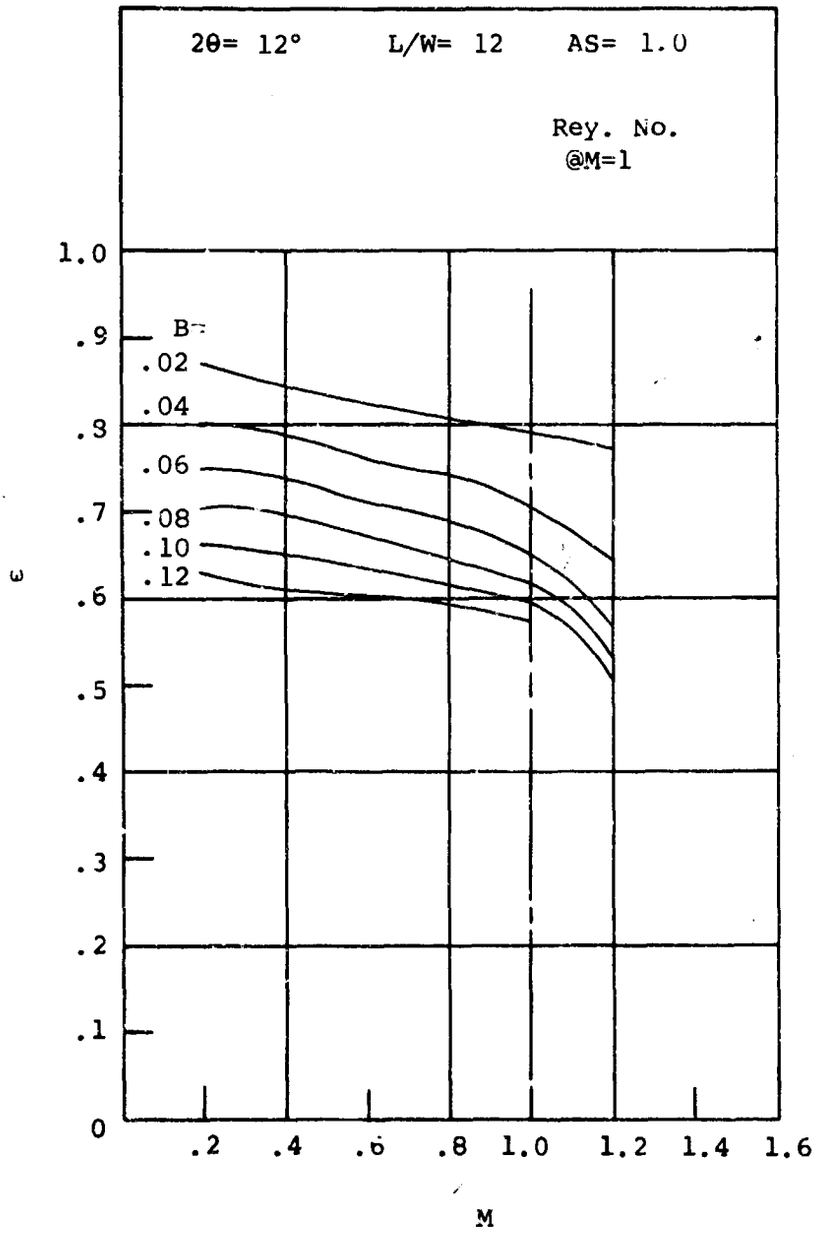

Figure 175. Effectiveness Versus Mach Number. Aspect Ratio = 1.0.

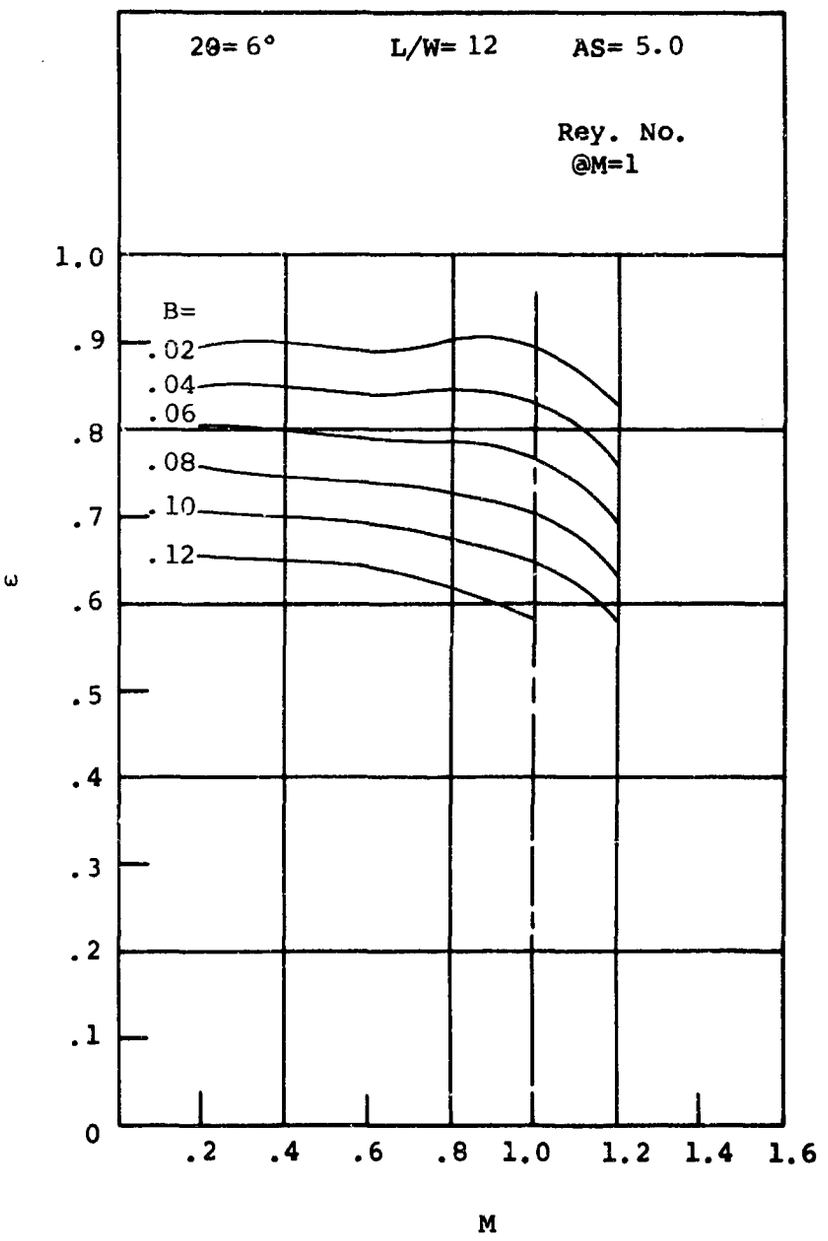

Figure 176. Effectiveness Versus Mach Number. Aspect Ratio = 5.0.

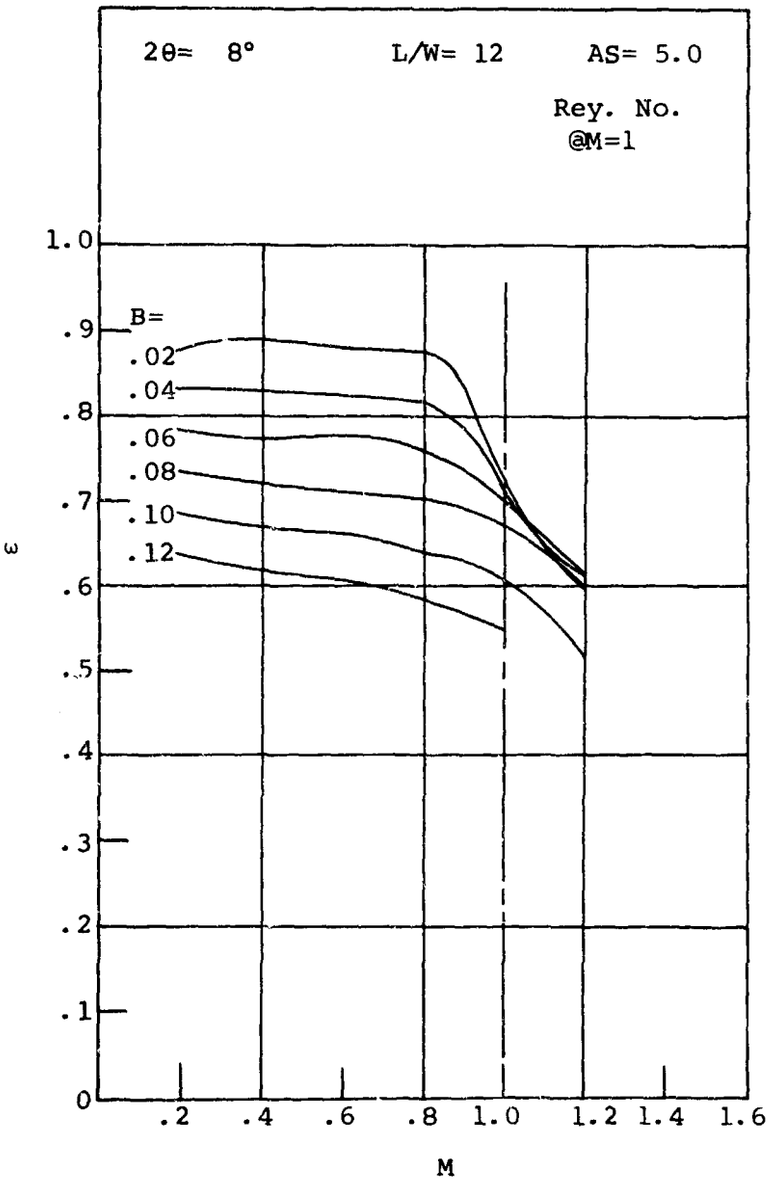

Figure 177. Effectiveness Versus Mach Number. Aspect Ratio = 5.0.

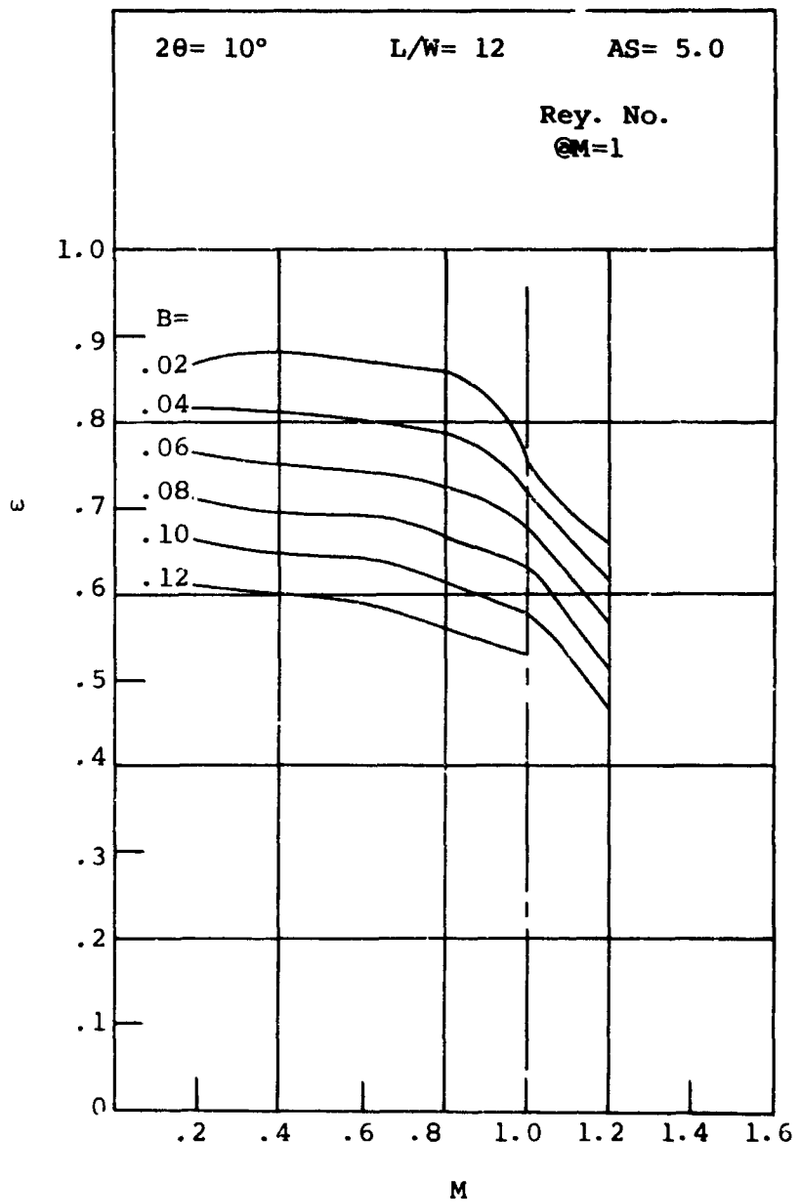

Figure 178. Effectiveness Versus Mach Number. Aspect Ratio = 5.0.

In Fox's study, the diffuser performance would be classified into three categories which could be broadly correlated with the location of the diffuser geometry relative to the line of first appreciable stall found for incompressible flow in conical diffusers.

1) For diffusers below the line of first appreciable stall, there is a moderate increase in C_p with increasing M_t.

2) For geometries in the neighborhood of the line, C_p remains constant with increasing M_t.

3) Above the line of first appreciable stall, there is a moderate decrease in C_p with increasing M_t.

Since ideal pressure recovery increases with increasing inlet Mach number, as can be seen from Figure 4, the effectiveness based upon the above three categories will show the following characteristics. For diffuser geometries at area ratios below the line of the first appreciable stall (corresponding to low diffuser angles for the aspect ratio 0.25 data), the moderate increase in C_p approximately corresponds with the moderate increase in C_{p_i}, producing constant values of effectiveness ε.

When the diffuser begins to stall at higher divergence angles, the near-constant pressure recovery when nondimensionalized with C_{p_i} will produce a falling effectiveness ε with increasing Mach number. At still higher divergence angles and area ratios, the moderate decrease in C_p will produce a still more rapidly falling variation of effectiveness with inlet Mach number.

For the aspect ratio 0.25 data, these characteristics are observed to be relative to the location of the optimum ridge defining the lines C_p^* and C_p^{**} in the region of diffuser divergence angle $2\theta = 12°$ to $14°$.

As aspect ratio increases, the pressure recovery "hill" shifts to produce C_p^* and C_p^{**} optimum lines at lower divergence angles. In terms of the effectiveness plots presented, the low divergence angles shown are now closer to the optimum lines; the effectiveness plots show a decreasing effectiveness at lower divergence angles as a consequence. This is true for both the aspect ratio 1.0 and 5.0 geometries.

The increase in effectiveness indicated for the 6° and 8° diffusers at 0.25 aspect ratio is not as easily understood. It is suspected that if performance were measured at lower divergence angles for the 1.0 and 5.0 aspect ratio diffusers, similar effectiveness versus Mach number plots would be obtained (the diffuser geometries now lying lower upon the pressure recovery "hill").

Diffuser Static Pressure Distribution

For most of the base data, static pressure distributions through the diffuser were measured using wall pressure taps located in the bottom plate of the diffuser test section. Comparative measurements between wall tap static pressure readings and static pressure readings measured by the traverse pressure tube are presented in Figures 179 and 180 for throat Mach number M_t = 1.0, 2θ = 8°, and aspect ratios AS = 0.25 and 1.0 respectively. The measurements agree well.

Static pressure distributions have not been plotted for the complete range of base data. This information is available on the original data record sheets for each test.

Correlation of Data

It has been suggested* that the performance data may correlate better if other parameters are used to define the diffuser geometry and inlet conditions.

Instead of using the present performance maps, whose coordinates are "length-to-initial-width ratio L/W_1" and "area ratio AR", the performance map coordinates should be "stretched" to reflect the change in aspect ratio AS and throat Mach number.

It has been suggested that the diffuser length should be non-dimensionalized on the inlet hydraulic radius D/2 rather than the width W_1 of the flow passage at the inlet. For large aspect ratios, the equivalent hydraulic diameter is approximately equal to twice the throat width. For other diffuser geometries,

*See Sapiro (1968), (1969).

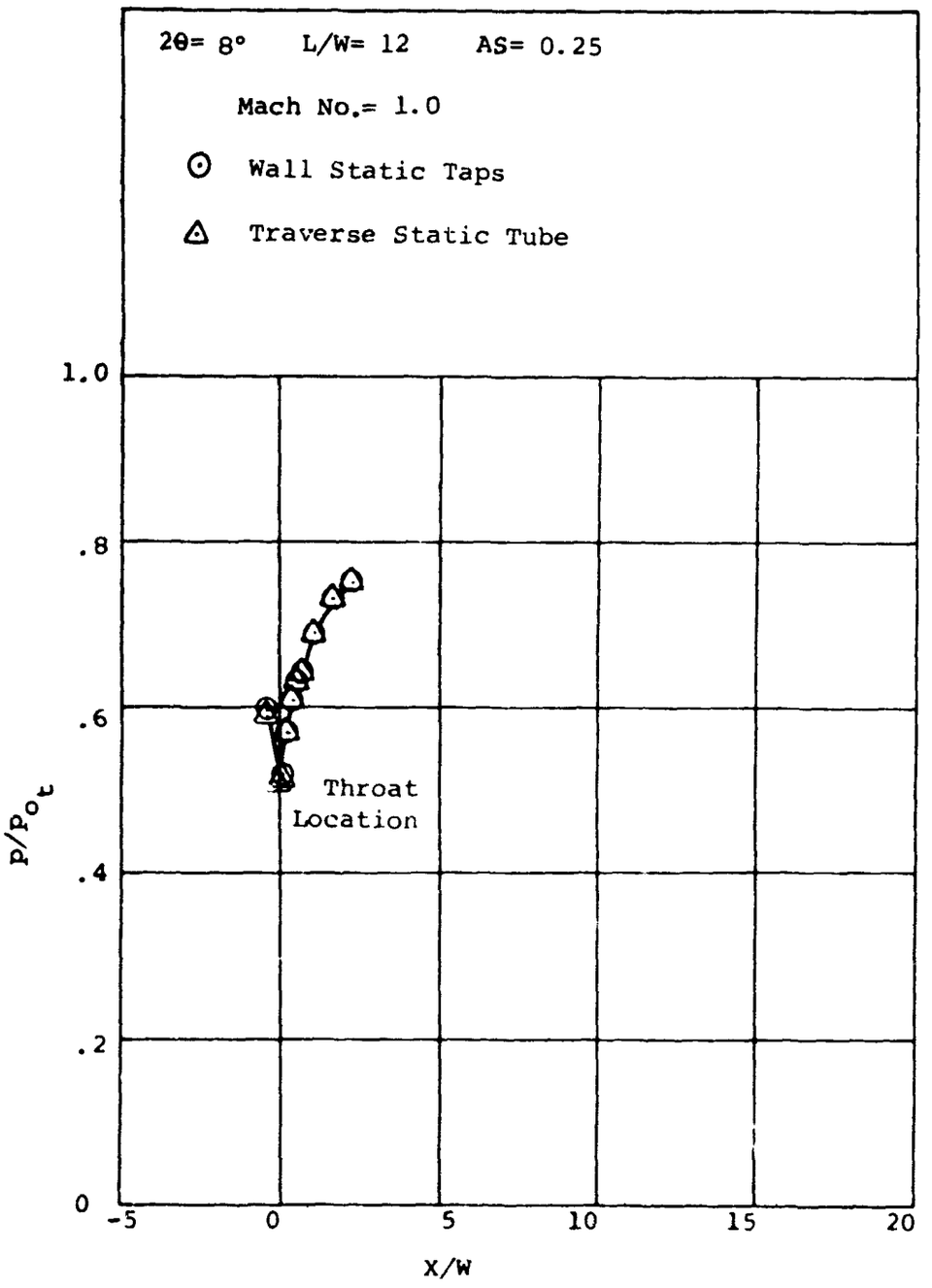

Figure 179. Diffuser Static Pressure Distribution. Aspect Ratio = 0.25. Mach Number = 1.0.

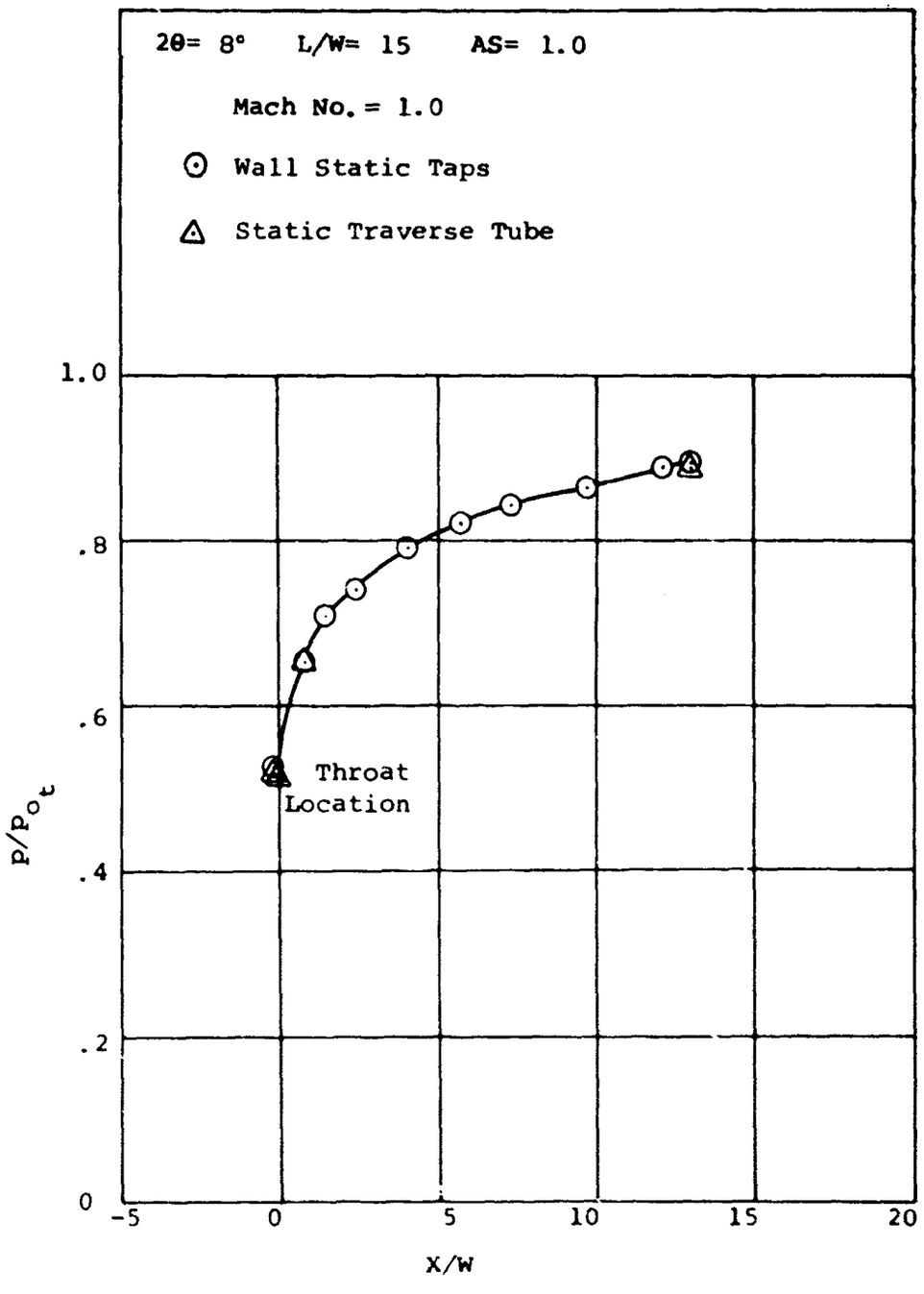

Figure 180. Diffuser Static Pressure Distribution. Aspect Ratio = 1.0. Mach Number = 1.0.

e.g., conical diffusers and annular diffusers, the correlation length parameters that have been found useful to correlate data are L/R (the length-to-initial radius ratio) and L/ΔR (the length-to-initial height ratio) respectively. It has been pointed out that the different definitions of nondimensional length that have been applied to straight wall diffusers in the literature correspond uniquely to "twice the length-to-initial hydraulic diameter ratio". For the single plane, symmetric divergence diffuser, this ratio is

$$\frac{2L}{D} = \frac{L}{W_1}\left(1 + \frac{1}{AS}\right) \tag{36}$$

For low Mach number flow where the inlet conditions are described completely by the inlet blockage B and the Reynolds number R_D, the pressure recovery coefficient is a function of the geometric and inlet variables

$$C_p = C_p\,(B,\ R_D,\ L,\ W_1,\ 2\theta,\ b) \tag{37}$$

From dimensional analysis arguments, it is possible to define the pressure recovery by a set of five nondimensional pi's; e.g.,

$$C_p = C_p\,(B,\ R_D,\ AS,\ L/W_1,\ 2\theta)$$

The above arguments have suggested that the pressure recovery performance can perhaps be reduced to four nondimensional pi's by appropriately combining the two geometric parameters L/W_1 and $AS = b/W_1$:

$$C_p = C_p\left[B,\ R_D,\ 2\theta,\ L/W_1\left(1 + \frac{1}{AS}\right)\right] \tag{38}$$

A comparison of the present data at low Mach numbers with that of Reneau for incompressible flow is presented in Table VIII. Comparison values of pressure recovery for aspect ratios 0.25, 1.0, and 5.0 are presented using the "stretched" coordinate L/D for both the present data and that of Reneau. Sample values of L/D for a range of divergence angle 2θ are shown. Examination of the table indicates that the difference in pressure recovery ΔC_p $(= C_{p_{\text{present data}}} - C_{p_{\text{Reneau}}})$ varies widely over the performance map and varies with aspect ratio.

TABLE VIII. COMPARISON OF BASE DATA AND DATA OF RENEAU, ET AL, ON 2 L/D AND $AR_{EQUIVALENT}$ COORDINATES

Mach No. M_t	Throat Blockage B	Aspect Ratio AS	Length-to-Throat Width Ratio L/W_1	Length-to-Hydraulic Diameter Ratio 2 L/D	Divergence Angle 2θ	Pressure Recovery - Present Data C_{p_A}	Pressure Recovery - Reneau Data C_{p_B}	Pressure Recovery Difference $C_{p_A} - C_{p_B}$
0.2	.05	0.25	7.0	35.0	8°	.525	.575	-.050
0.2	.05	0.25	7.0	35.0	10°	.570	.575	-.005
0.2	.05	0.25	7.0	35.0	12°	.610	.575	.035
0.2	.05	0.25	7.0	35.0	14°	.615	.575	.040
0.2	.05	0.25	7.0	35.0	16°	.645	.575	.070
0.2	.05	0.25	10.0	50.0	8°	.545	.575	-.030
0.2	.05	0.25	10.0	50.0	10°	.585	.575	.010
0.2	.05	0.25	10.0	50.0	12°	.630	.575	.055
0.2	.05	0.25	10.0	50.0	13°	.645	.575	.070
0.2	.05	0.25	10.0	50.0	14°	.650	.575	.075
0.2	.05	0.25	10.0	50.0	16°	.660	.575	.085
0.2	.03	0.25	7.0	35.0	8°	.545	.700	-.155
0.2	.03	0.25	7.0	35.0	10°	.585	.680	-.095
0.2	.03	0.25	7.0	35.0	12°	.630	.660	-.030
0.2	.03	0.25	7.0	35.0	14°	.640	.620	.020
0.2	.03	0.25	7.0	35.0	16°	.670	.600	.070
0.2	.05	1.0	10.0	20.0	6°	.675	.575	.100
0.2	.05	1.0	10.0	20.0	8°	.685	.575	.110

TABLE VIII - Continued

Mach No. M_t	Throat Blockage B	Aspect Ratio AS	Length-to Throat Width Ratio L/W_1	Length-to-Hydraulic Diameter Ratio 2 L/D	Divergence Angle 2θ	Pressure Recovery-Present Data C_{p_A}	Pressure Recovery-Reneau Data C_{p_B}	Pressure Recovery Difference $C_{p_A} - C_{p_B}$
0.2	.05	1.0	10.0	20.0	10°	.725	.575	.150
0.2	.05	1.0	10.0	20.0	12°	.705	.575	.130
0.2	.05	1.0	18.25	36.5	6°	.710	.575	.135
0.2	.05	1.0	18.25	36.5	8°	.750	.575	.175
0.2	.05	1.0	18.25	36.5	10°	.750	.575	.175
0.2	.05	1.0	18.25	36.5	12°	.750	.575	.175
0.2	.03	1.0	10.0	20.0	6°	.710	.710	0
0.2	.03	1.0	10.0	20.0	8°	.725	.710	.015
0.2	.03	1.0	10.0	20.0	10°	.760	.680	.080
0.2	.03	1.0	10.0	20.0	12°	.765	.660	.105
0.2	.03	1.0	18.25	36.5	6°	.740	.720	.020
0.2	.03	1.0	18.25	36.5	8°	.780	.700	.080
0.2	.03	1.0	18.25	36.5	10°	.790	.670	.120
0.2	.03	1.0	18.25	36.5	12°	810	.660	.150
0.2	.05	5.0	7.0	8.4	6°	.560	.575	-.015
0.2	.05	5.0	7.0	8.4	8°	.600	.650	-.050
0.2	.05	5.0	7.0	8.4	10°	.630	.650	-.020
0.2	.05	5.0	10.0	12.0	6°	.680	.650	.030
0.2	.05	5.0	10.0	12.0	8°	.670	.600	.070
0.2	.05	5.0	10.0	12.0	10°	.630	.575	.055

TABLE VIII - Continued

Mach No. M_t	Throat Blockage B	Aspect Ratio AS	Length-to-Throat Width Ratio L/W_1	Length-to-Hydraulic Diameter Ratio 2 L/D	Divergence Angle 2θ	Pressure Recovery-Present Data C_{P_A}	Pressure Recovery-Reneau Data C_{P_B}	Pressure Recovery Difference $C_{P_A} - C_{P_B}$
0.2	.05	5.0	12.0	14.4	6°	.660	.620	.040
0.2	.05	5.0	12.0	14.4	8°	.690	.575	.115
0.2	.05	5.0	12.0	14.4	10°	.710	.575	.135
0.2	.05	5.0	15.0	18.0	6°	.705	.575	.130
0.2	.05	5.0	15.0	18.0	8°	.735	.575	.160
0.2	.05	5.0	15.0	18.0	10°	.735	.575	.160
0.2	.03	5.0	7.0	8.4	6°	.585	.630	-.045
0.2	.03	5.0	7.0	8.4	8°	.640	.670	-.030
0.2	.03	5.0	7.0	8.4	10°	.660	.670	-.010
0.2	.03	5.0	10.0	12.0	6°	.740	.670	.070
0.2	.03	5.0	10.0	12.0	8°	.710	.710	0
0.2	.03	5.0	10.0	12.0	10°	.670	.680	.010
0.2	.03	5.0	12.0	14.4	6°	.705	.710	-.005
0.2	.03	5.0	12.0	14.4	8°	.735	.710	.025
0.2	.03	5.0	12.0	14.4	10°	.760	.680	.080
0.2	.03	5.0	15.0	18.0	6°	.730	.720	.010
0.2	.03	5.0	15.0	18.0	8°	.775	.710	.065
0.2	.03	5.0	15.0	18.0	10°	.775	.680	.095

Table IX presents the peak pressure recovery data (at the peak pressure recovery geometry) for aspect ratio 1.0 and M_t = 1.0 compared with the Reneau data. The data are compared for blockage values of .02, .03, and .05 corresponding to the performance maps presented by Reneau.

These data incorporate, in addition to the "stretched" non-dimensional length coordinate, an equivalent or "stretched" area ratio. This area ratio is based upon the assumption that the incompressible flow relation between area ratio and ideal pressure recovery

$$AR = [1/(1-C_{p_i})_{\text{incompressible}}]^{1/2} \tag{39}$$

holds throughout the entire subsonic Mach number range. The expression for equivalent area ratio is thus

$$AR = [1/(1-C_{p_i})]^{1/2} \tag{40}$$

This equivalent area ratio, in effect, takes into account the increase in ideal pressure recovery which occurs as a function of Mach number at constant area ratio (presented in Figure 4).

Again the difference in recovery ΔC_p varies greatly. Only the aspect ratio 1.0 data are compared, because only these data have geometries that include or are very close to the geometry for peak recovery.

Table X is a comparison of some independent data by Johnston and Powars (1967) at low aspect ratio. Again the data are compared on the basis of an "equivalent length" and the true geometric area ratio since their data are for incompressible flow. The Johnston and Powars data have been compared for aspect ratio 1.0 and 4 where their measured blockage is close to that of the performance maps provided by Reneau, et al. Here again the difference in pressure recovery ΔC_p varies appreciably over the range of parameters studied.

It does not appear that for either incompressible or compressible flow conditions that a simple stretching of coordinates, using the hydraulic diameter and inlet Mach number,

TABLE IX. COMPARISON OF PEAK PRESSURE RECOVERY OF BASE DATA AND DATA OF RENEAU, ET AL, ON 2 L/D AND $AR_{EQUIVALENT}$ COORDINATES

Mach Number M_t	Throat Blockage B	Aspect Ratio AS	Length-to-Throat-Width Ratio L/W_1	Length-to-Hydraulic Diameter Ratio 2 L/D	Area Ratio AR	Equivalent Area Ratio $AR_{equivalent}$	Pressure Recovery-Present Data C_{p_A}	Pressure Recovery-Reneau Data C_{p_B}	Pressure Recovery Difference $C_{p_A} - C_{p_B}$
1.0	.02	1.0	18	36	3.7	5.06	.83	.80+	.030-
1.0	.03	1.0	18	36	3.5	4.94	.80	.72-	.080+
1.0	.05	1.0	18	36	3.5	4.94	.76	.575	.185

TABLE X. COMPARISON OF PRESSURE RECOVERY DATA OF JOHNSTON AND POWARS AND DATA OF RENEAU, ET AL, ON 2 L/D AND $AR_{EQUIVALENT}$ COORDINATES

Mach Number M_t	Throat Blockage B	Aspect Ratio AS	Length-to-Throat-Width Ratio L/W_1	Length-to-Hydraulic Diameter Ratio 2 L/D	Area Ratio AR	Pressure Recovery Johnston & Powers C_{P_A}	Pressure Recovery Reneau, et al C_{P_B}	Pressure Recovery Difference $C_{P_A} - C_{P_B}$
<0.2	.027	1.0	6	12	1.5	0.44	0.46	-0.020
<0.2	.027	1.0	6	12	2.1	0.615	0.67	-0.055
<0.2	.027	1.0	6	12	3.0	0.525	0.69	-0.165
<0.2	.017	4.0	6	7.5	1.5	0.455	0.50	-0.045
<0.2	.017	4.0	6	7.5	2.1	0.620	0.67	-0.050
<0.2	.017	4.0	6	7.5	3.0	0.490	0.66	-0.170

is sufficient to provide much improved correlation of the data. This is indeed unfortunate, since such a correlation would be extremely valuable in interpolating and/or extrapolating the existing data to cover other geometries and flow conditions. Because of the complex nature of the fluid dynamics, if such a correlation exists, it will probably be difficult to find and will depend upon an improved knowledge of the fluid dynamics of the separation phenomena within the diffuser.

Comparison With Other Channel Diffuser Data

There are little data available that can be used for a direct comparison of the pressure recovery performance of the symmetric, single plane divergence channel diffusers studied under the present program. The only data for which blockage information is available are that contained in the performance maps of Reneau, et al (1964), and the low aspect ratio data of Johnston and Powars (1967). Johnston and Powars obtained pressure recovery as a function of aspect ratio for a selected set of diffuser geometries.

High Aspect Ratio Data

Reneau, et al (1964) have a complete set of performance maps for incompressible flow as a function of throat blockage B. The data are all for high aspect ratio diffusers. On the basis of the information they had available, they suggest that the performance maps they present should be valid for aspect ratio diffusers of 8 and greater.

The Reneau data are for constant values of $2\delta_1^*/W_1 = 0.007$, 0.015, 0.03, and 0.05. Assuming that the blockage is due to boundary layer flow uniformly distributed around the throat periphery, we find that the throat blockage is related to $2\delta_1^*/W_1$ by

$$B = \frac{2\delta_1^*}{W_1}\left(1 + \frac{1}{AS}\right) \qquad (41)$$

Figures 181, 182, and 183 give a comparison of the recovery data taken for aspect ratio 5 (which should closely agree with the Reneau data) and the performance data for the same geometries taken from the performance maps of Reneau. The data are compared on the basis of equivalent throat blockage, geometry, and inlet conditions.

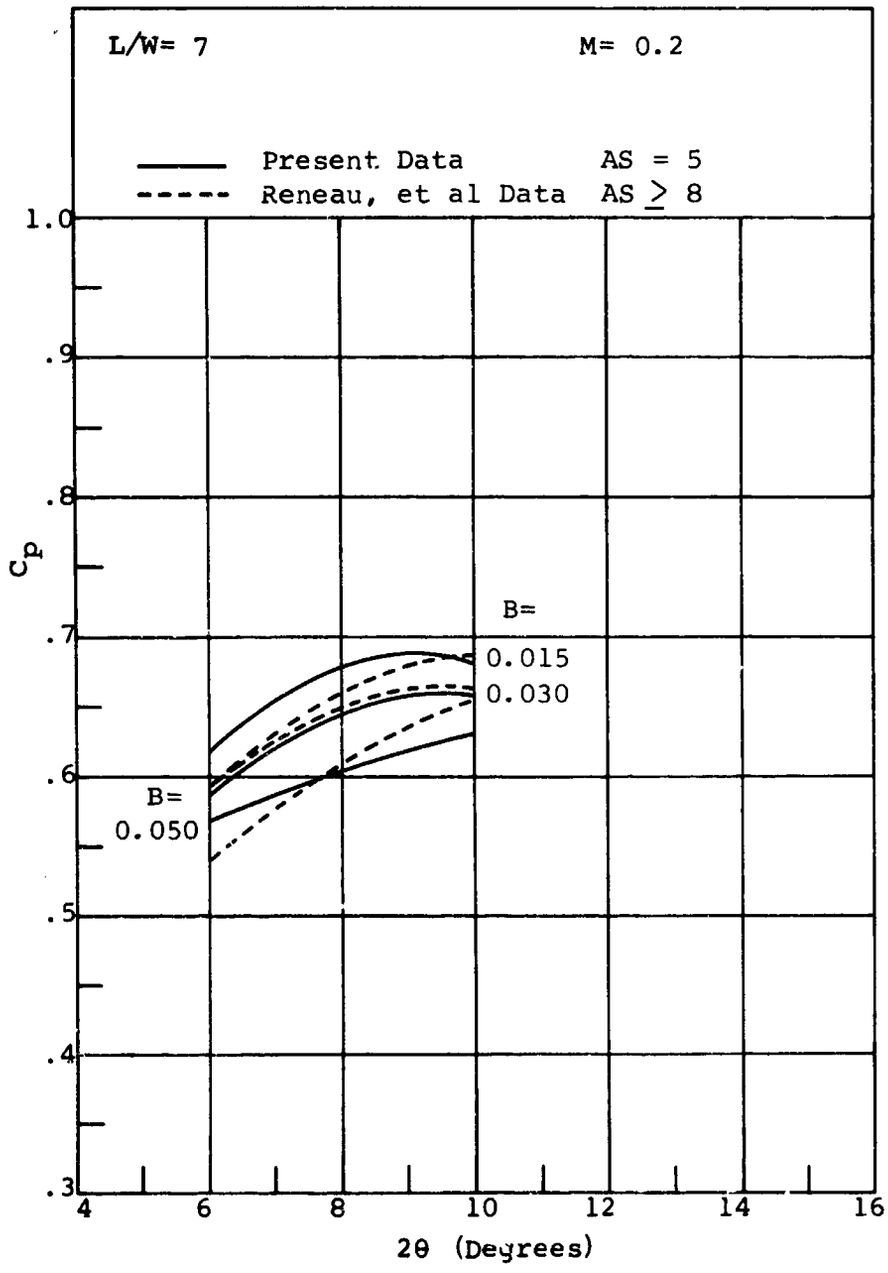

Figure 181. Pressure Recovery Versus Divergence Angle. Comparison of Base Data and Data of Reneau, et al (1967).

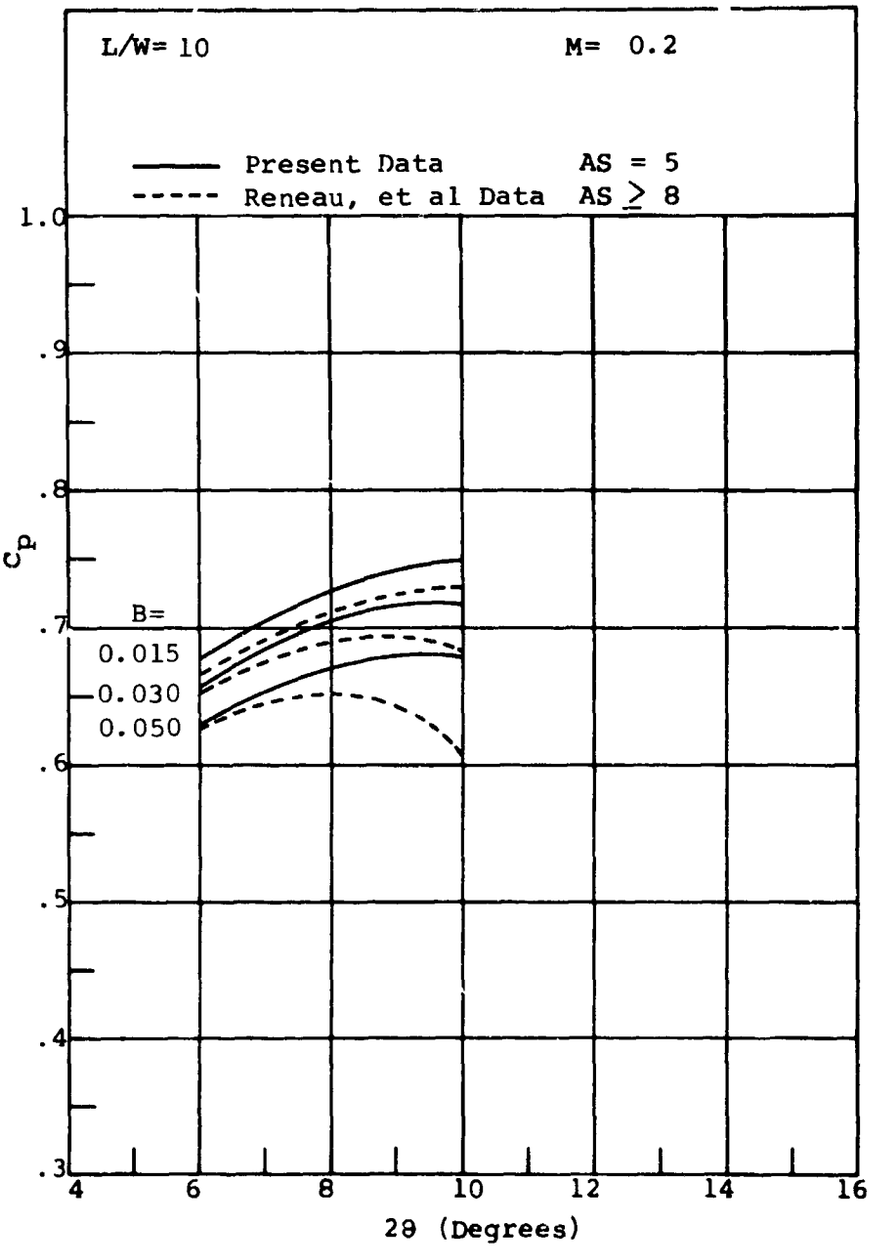

Figure 182. Pressure Recovery Versus Divergence Angle. Comparison of Base Data and Data of Reneau, et al (1967).

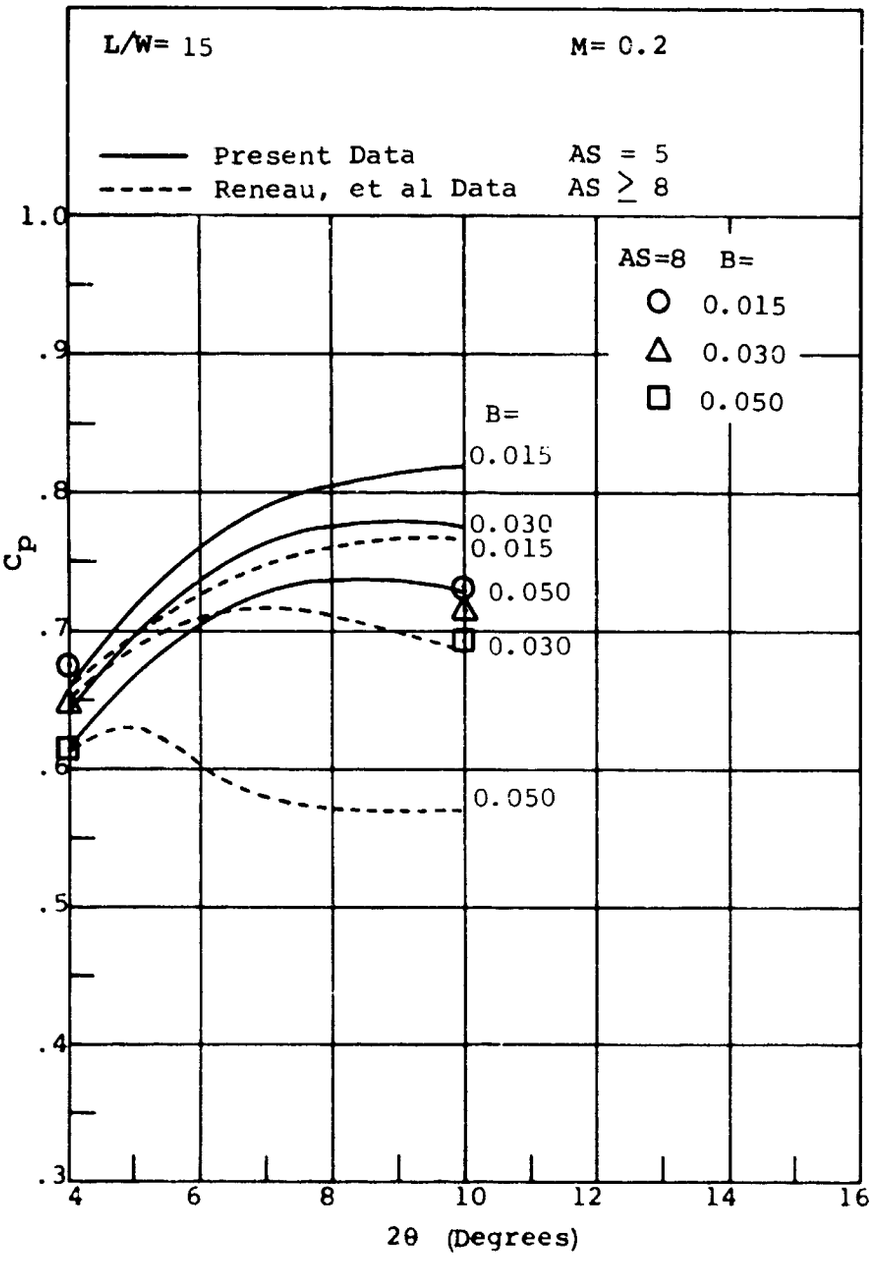

Figure 183. Pressure Recovery Versus Divergence Angle. Comparison of Base Data and Data of Reneau, et al (1967).

At L/W_1 = 7, differences do exist between the two sets of data. However, the agreement is within the uncertainty reported in the data of Reneau and the uncertainty for the present data.

For the L/W_1 = 10 and 15 data, however, a rather large and significant difference appears between the two sets of data (2θ = 8° and 10° for L/W_1 = 10 at the larger values of blockage and 2θ = 6°, 8°, and 10° for L/W_1 = 15). In fact, at the highest blockage considered (B = .0506 for the L/W_1 = 15 data), there is a difference of 15.5 points in C_p at 2θ = 10°, and whereas the Reneau data indicate an optimum in C_p at $2\theta \tilde{=} 5°$, the present data indicate a considerably higher optimum recovery at $2\theta \tilde{=} 9°$ at L/W_1 = 15.

Because of this large difference in recovery behavior between aspect ratio 5 and 8, a small number of geometries were tested under the present program at aspect ratio 8 to see if a large fall in recovery occurred between aspect ratio 5 and 8 as indicated.

The geometries tested were 2θ = 4° and 10° at L/W_1 = 15 over the range of inlet blockages provided by the set of three inlet blocks used on the base data studies.

The results are indicated in Figure 183 by symbols. While there is a decrease in recovery between the aspect ratio 5 and 8 data, the decrease is small compared to the difference between the present data and the data given by Reneau. At 2θ = 10°, which still appears to be near the optimum recovery at constant L/W_1, the difference between the aspect ratio 8 data and that of Reneau is still 11.5 points in recovery.

The uncertainty in the aspect ratio 8 data is approximately that for the aspect ratio 5. While Mach number 0.2 data do have a larger uncertainty than that at other Mach numbers, the uncertainty is far less than the difference that exists between the aspect ratio 8 data and that of Reneau.

The disagreement with the data of Reneau is disconcerting. We feel that the aspect ratio 8 data reported are good, and we have no reason to suspect any gross inaccuracy that can account for the discrepancy shown in Figure 183.

The data reported by Reneau are a compilation of pressure recovery performance taken on diffusers of various aspect ratios. The smallest aspect ratio reported is 8. An intercomparison of the data by Reneau lead to the belief that performance maps presented in their data were valid, at least for diffuser aspect ratios of 8 and above. If the present data taken at aspect ratio 8 are correct, and we believe it is, then it is probable that there will continue to be a significant difference in pressure recovery as aspect ratio is varied above aspect ratio = 8.

The only other explanation that may account for the discrepancy between the two sets of data is that the present data was taken under test conditions known to have rather large static pressure oscillations at the throat of the diffuser. While experiments were performed to examine the effect of a reduction in the level of static pressure fluctuations, the minimum level of pressure fluctuations attained may still have been significant in affecting overall performance.

The possibility of throat static pressure fluctuations producing a marked improvement in pressure recovery could be a significant factor in diffuser applications. For example, the centrifugal compressor diffuser is known to operate under conditions of unsteady flow and rather large pressure fluctuations at the throat as a result of the flow off the impeller (although these occur at a high frequency compared to the frequencies observed in the present studies). Further measurements repeating some of the present study data without throat static pressure fluctuations will be necessary to resolve this question.

Low Aspect Ratio Data

The data obtained by Johnston and Powars (1967) were taken at $L/W_1 = 6.0$ and, unfortunately, do not lie within the range of geometries covered by the present aspect ratio data. However, the aspect ratio 0.25 data do include $L/W_1 = 7$ recovery information, which is felt to be close enough to the data of Johnston and Powars to permit a quite reasonable extrapolation. The data for aspect ratio = 1.0 have a lowest L/W_1 value = 10, and the extrapolation to $L/W_1 = 6$ is therefore more uncertain. The range of extrapolation of data for

aspect ratio 5 is too great to make a readable comparison with the data of Johnston and Powars.

The data extrapolation to $L/W_1 = 6$ is indicated in Figure 184, labeled "present data", and is compared with the Johnston and Powars data. The Johnston and Powars data were obtained with variable inlet blockage as a function of aspect ratio. The present data shown in Figure 184 are for the same inlet blockage B as obtained by Johnston and Powars.

The data comparison for aspect ratio 0.25 and 1.0 is quite good. Data have not been extrapolated and compared for the aspect ratio = 1.0 and 3.0 data because of the uncertainty in extrapolating this far from the base data performance maps.

4.5 THROAT INLET REYNOLDS NUMBER TESTS

For selected geometries at aspect ratios 0.25 and 1.0, tests for the full range of Mach number and blockage were made at 20 psia upstream stagnation pressure and at 60 psia. The purpose was to determine if there is a strong influence of inlet flow Reynolds number upon diffuser pressure recovery performance. It is to be noted that the Reynolds number is based on the centerline core flow velocity, the inlet throat hydraulic diameter, and the fluid kinematic viscosity.

Insufficient data were obtained at 20 psia to obtain cross-plots of the low Reynolds number information in the form of performance maps. Instead, the data have been presented on the original cross plot forms. One of the most useful cross plots for this purpose is the comparison of pressure recovery C_p against throat Mach number for constant geometry with inlet blockage B as a variable. Figures 185 through 212 present this information. For each geometry and upstream stagnation pressure, the throat Reynolds number is a function of throat Mach number M_t, as presented in Table XI. Under these conditions, as the inlet Mach number is reduced, the Reynolds number is decreased.

For this reason, the data should be compared between the 20 psia tests and the 60 psia tests at a constant value of inlet Mach number.

TABLE XI. TEST REYNOLDS NUMBERS

Stagnation Pressure p_o (psia)	Aspect Ratio AS	Mach Number M_t	Reynolds Number R_D
60	0.25	0.2	129,000
60	0.25	0.4	254,000
60	0.25	0.6	373,000
60	0.25	0.8	485,000
60	0.25	1.0	588,000
60	1.0	0.2	210,000
60	1.0	0.4	416,000
60	1.0	0.6	611,000
60	1.0	0.8	796,000
60	1.0	1.0	965,000
60	5.0	0.2	161,000
60	5.0	0.4	319,000
60	5.0	0.6	469,000
60	5.0	0.8	610,000
60	5.0	1.0	740,000
20	0.25	0.2	43,000
20	0.25	0.4	84,666
20	0.25	0.6	124,333
20	0.25	0.8	161,666
20	0.25	1.0	196,000
20	1.0	0.2	70,000
20	1.0	0.4	138,666
20	1.0	0.6	203,666
20	1.0	0.8	265,333
20	1.0	1.0	321,666
20	5.0	0.2	53,666
20	5.0	0.4	106,333
20	5.0	0.6	156,333
20	5.0	0.8	203,333
20	5.0	1.0	246,666

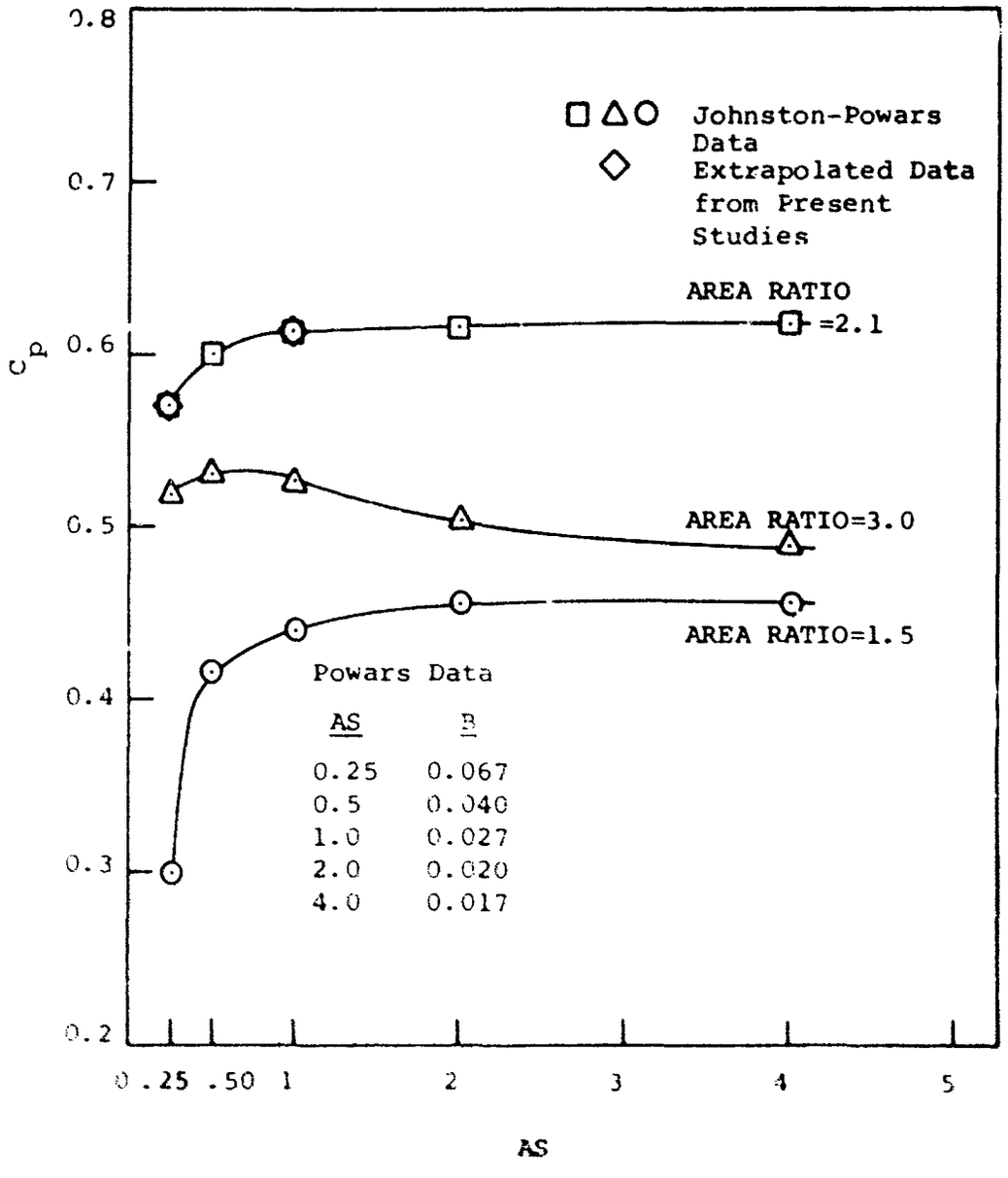

Figure 184. Pressure Recovery Versus Aspect Ratio. Comparison of Base Data and Data of Johnston and Powars (1967).

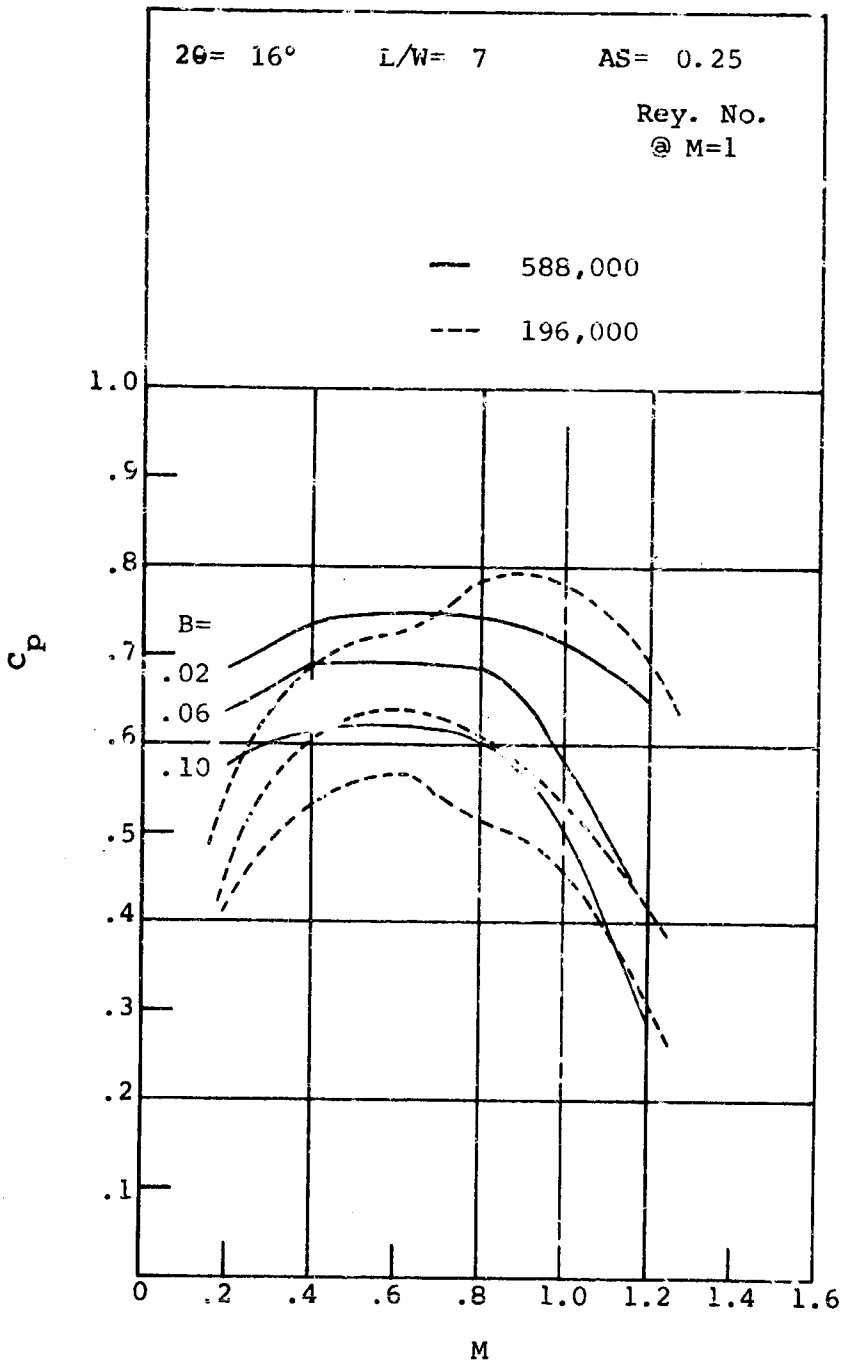

Figure 185. Pressure Recovery Versus Mach Number. Aspect Ratio = 0.25.

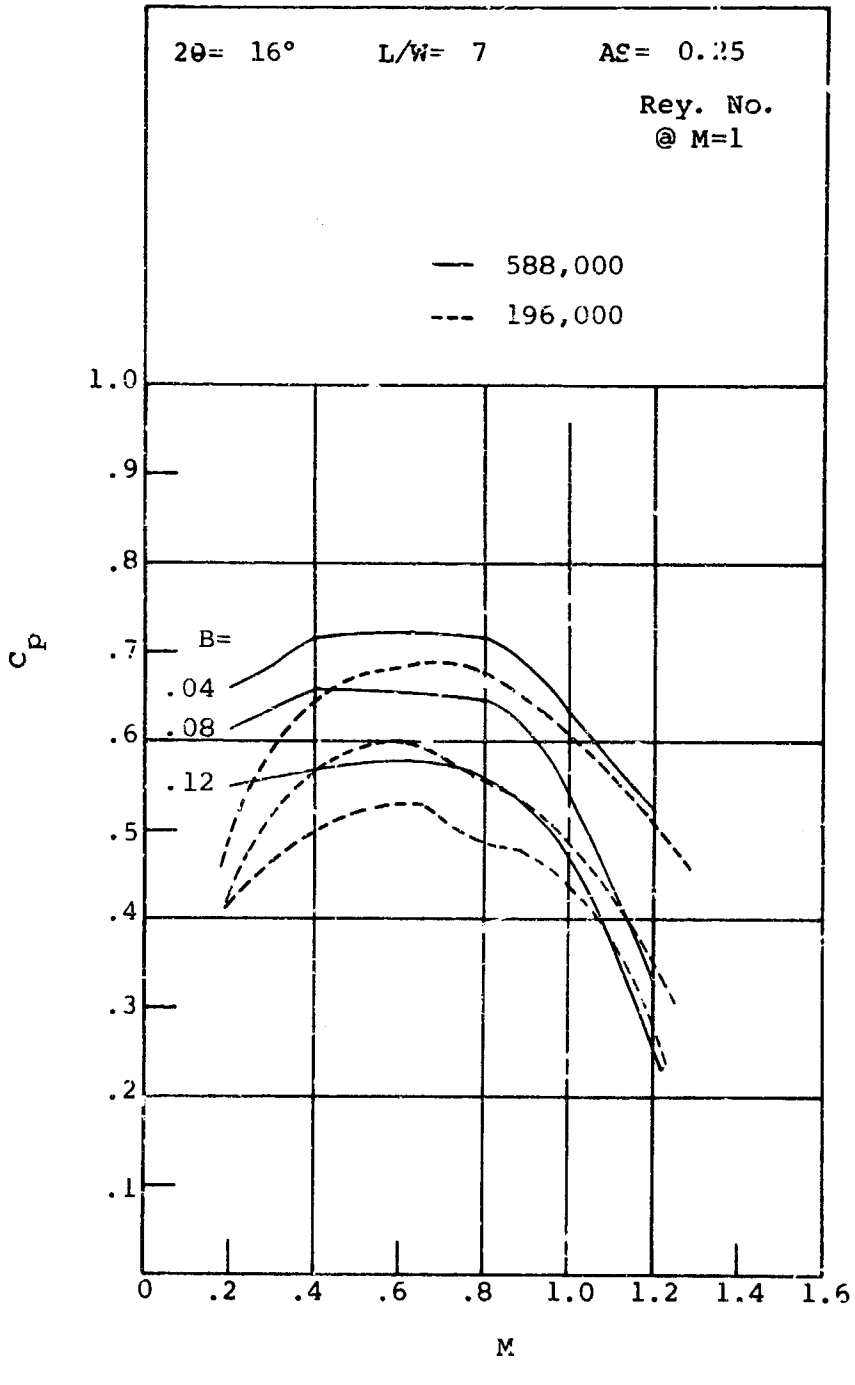

Figure 186. Pressure Recovery Versus Mach Number. Aspect Ratio = 0.25.

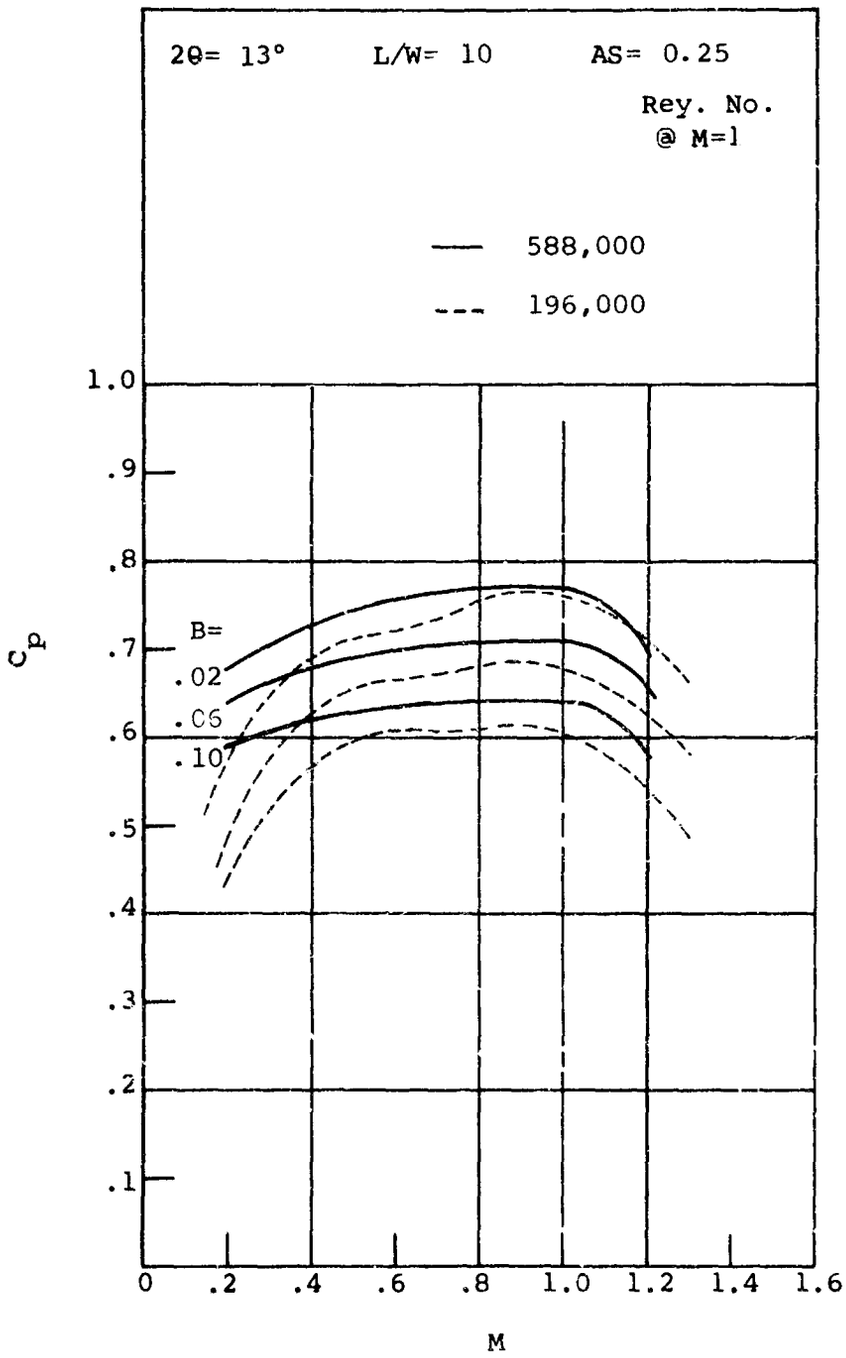

Figure 187. Pressure Recovery Versus Mach Number. Aspect Ratio = 0.25.

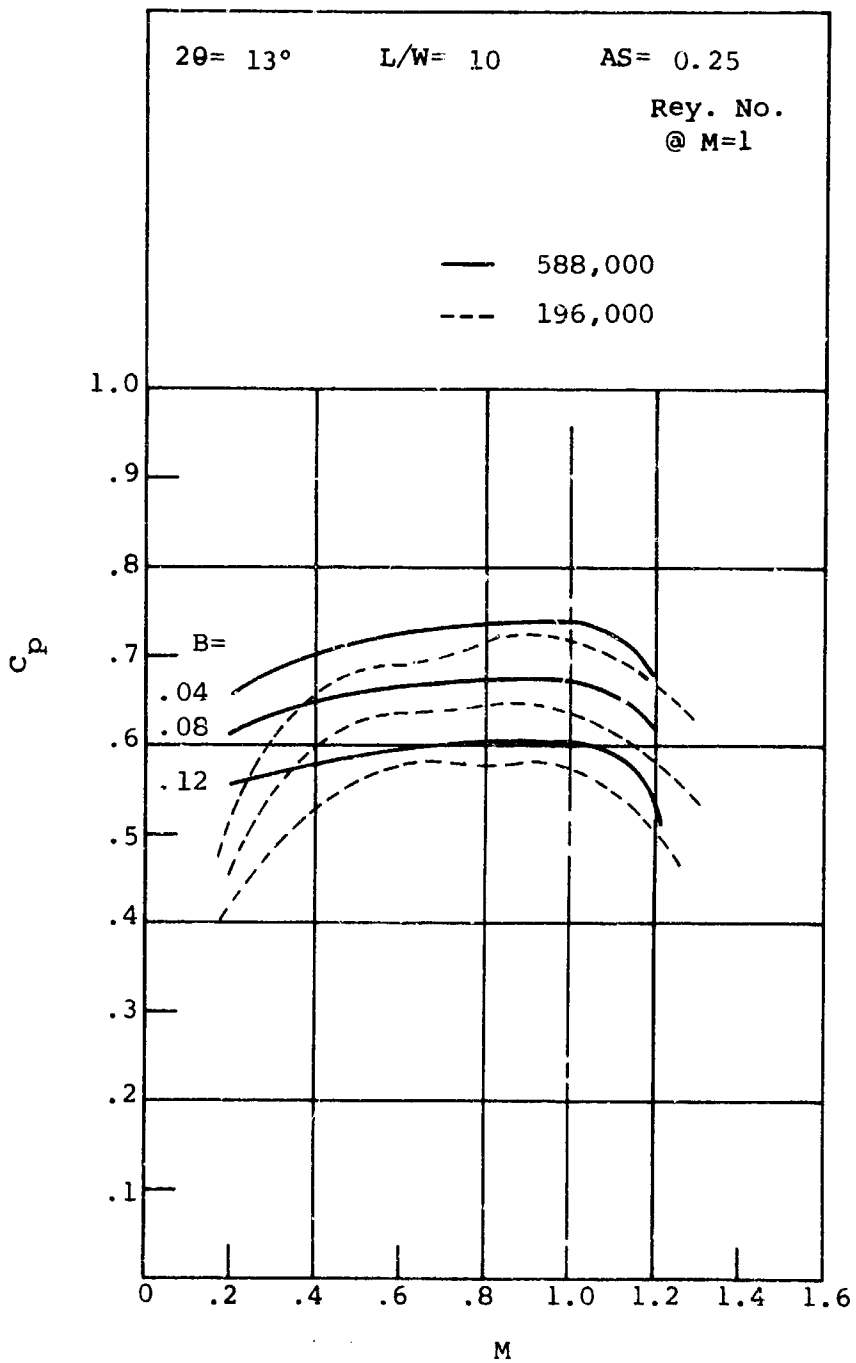

Figure 188. Pressure Recovery Versus Mach Number. Aspect Ratio = 0.25.

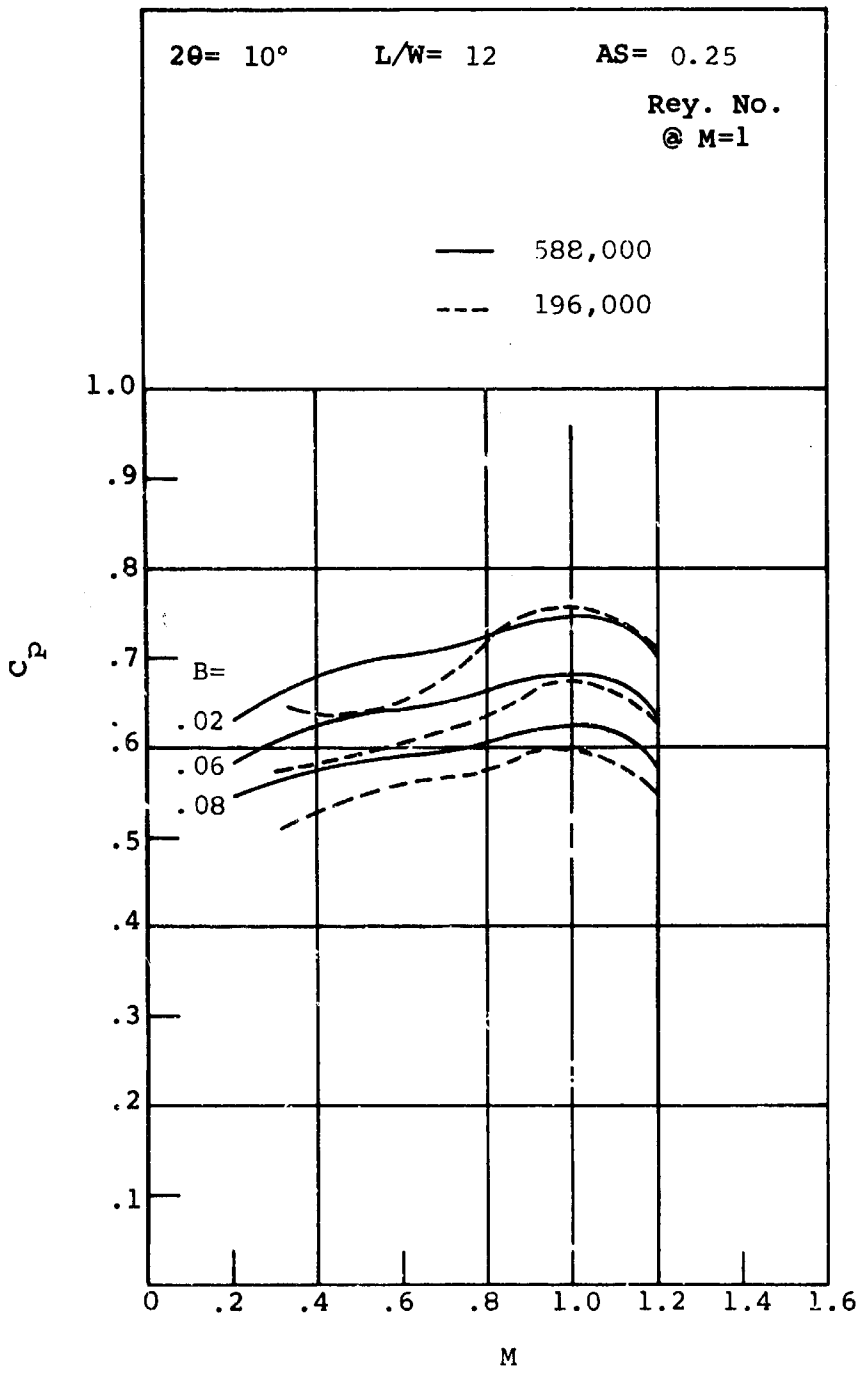

Figure 189. Pressure Recovery Versus Mach Number. Aspect Ratio = 0.25.

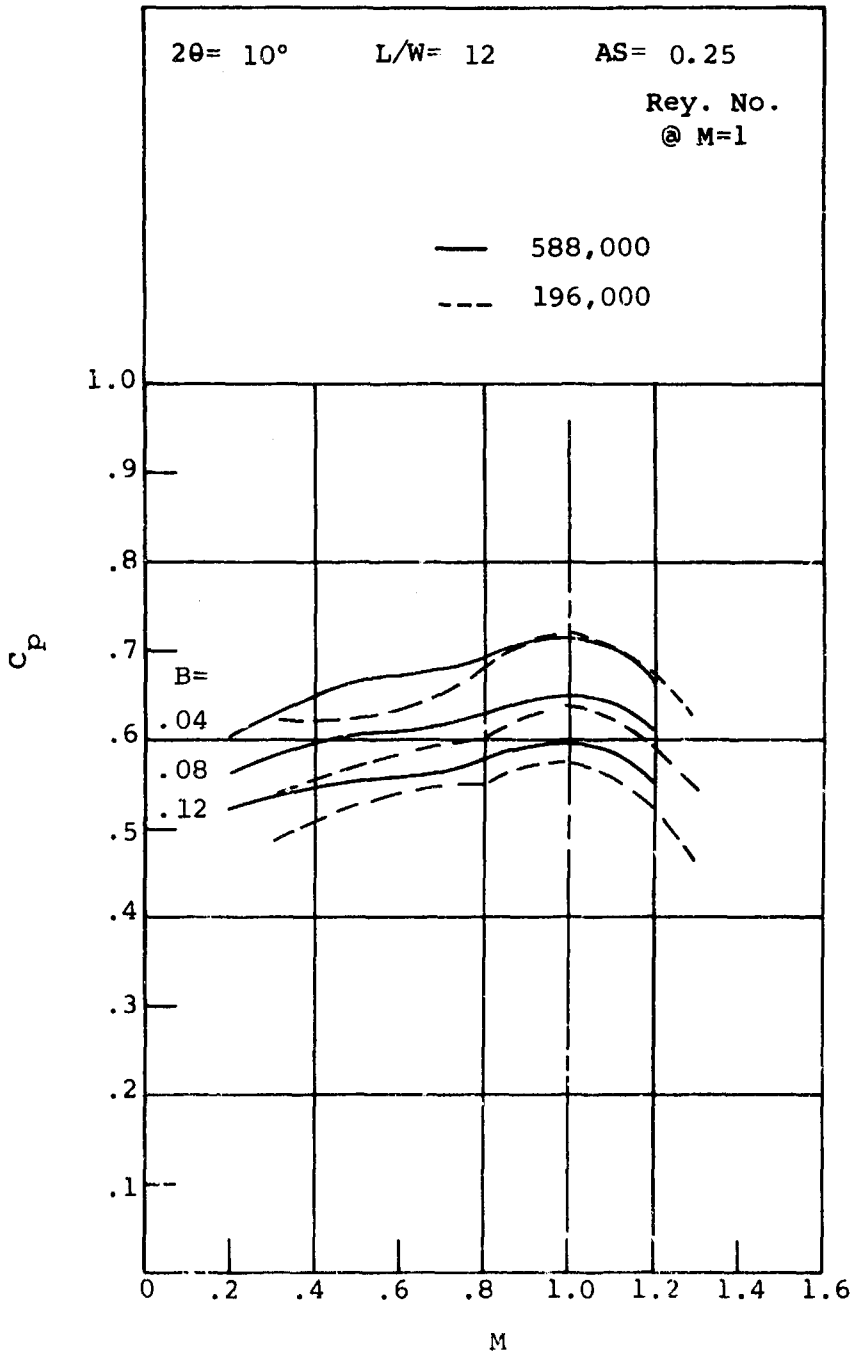

Figure 190. Pressure Recovery Versus Mach Number. Aspect Ratio = 0.25.

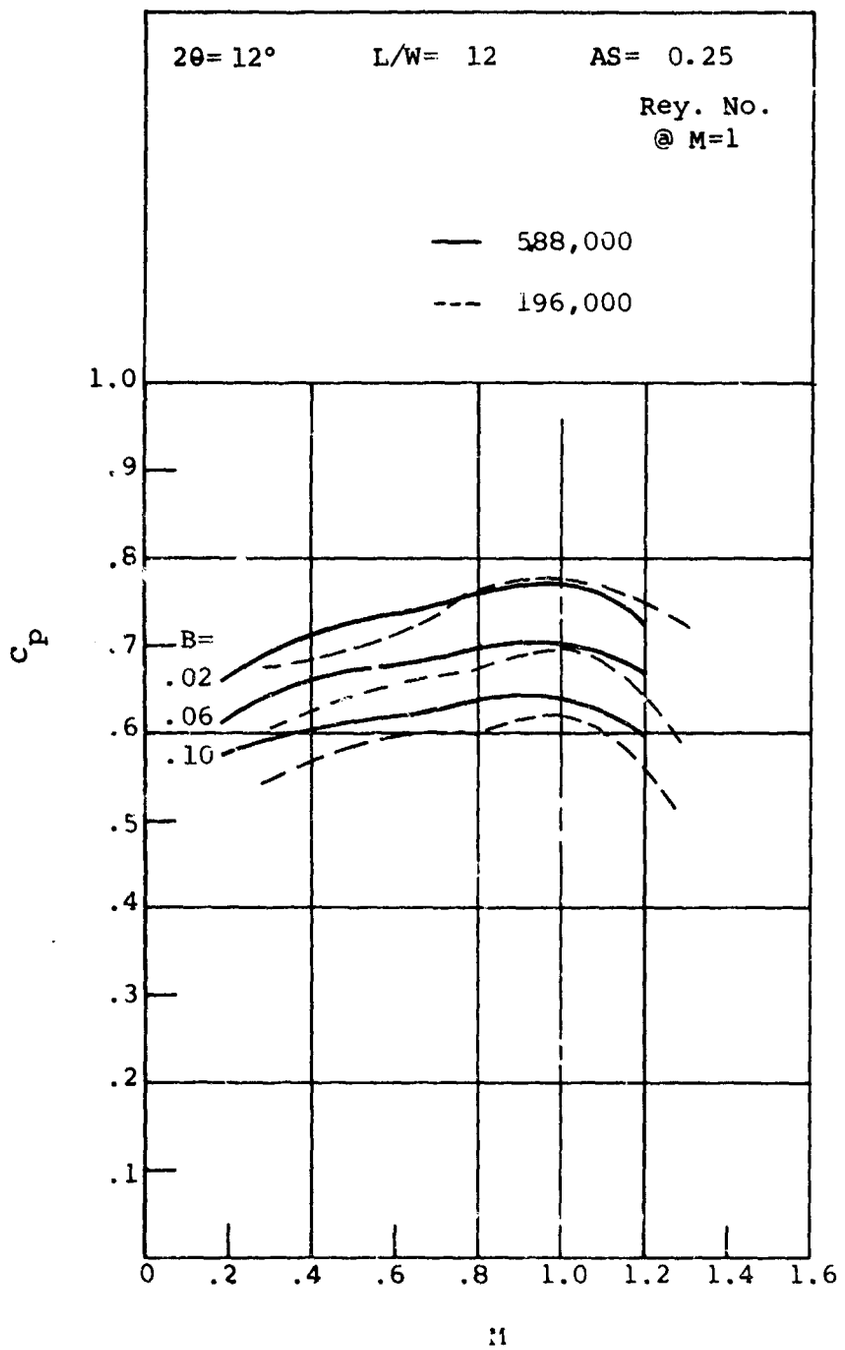

Figure 191. Pressure Recovery Versus Mach Number, Aspect Ratio = 0.25.

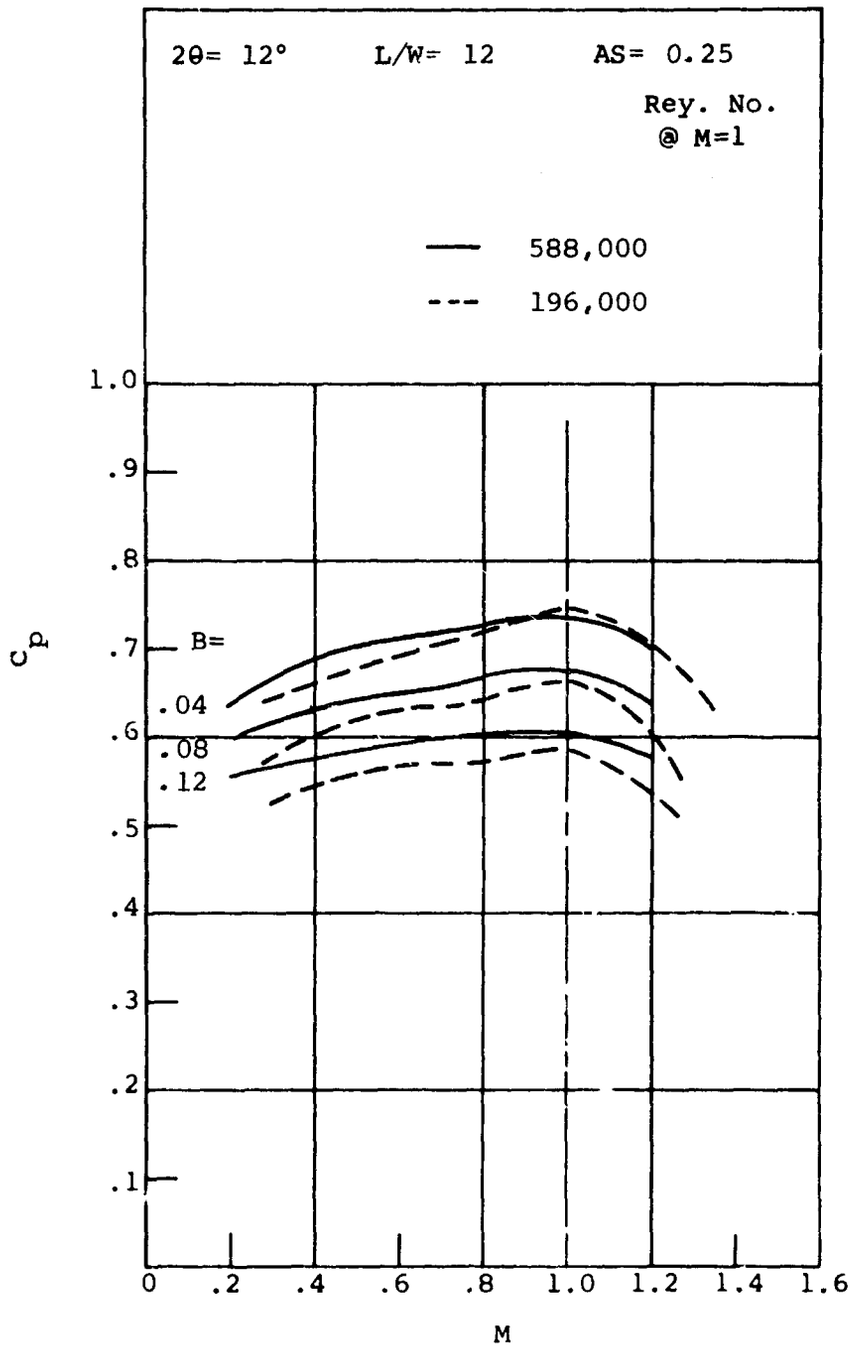

Figure 192. Pressure Recovery Versus Mach Number. Aspect Ratio = 0.25.

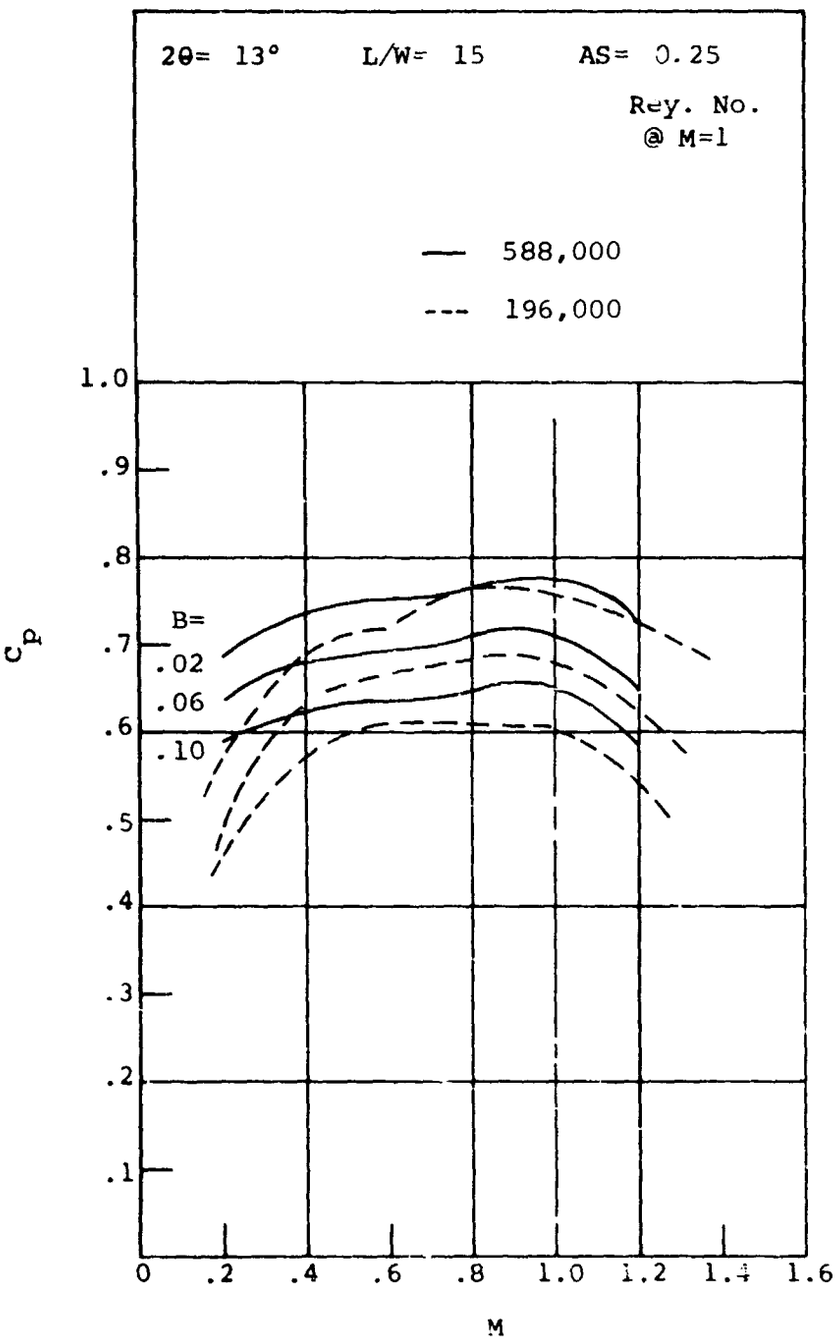

Figure 193. Pressure Recovery Versus Mach Number. Aspect Ratio = 0.25.

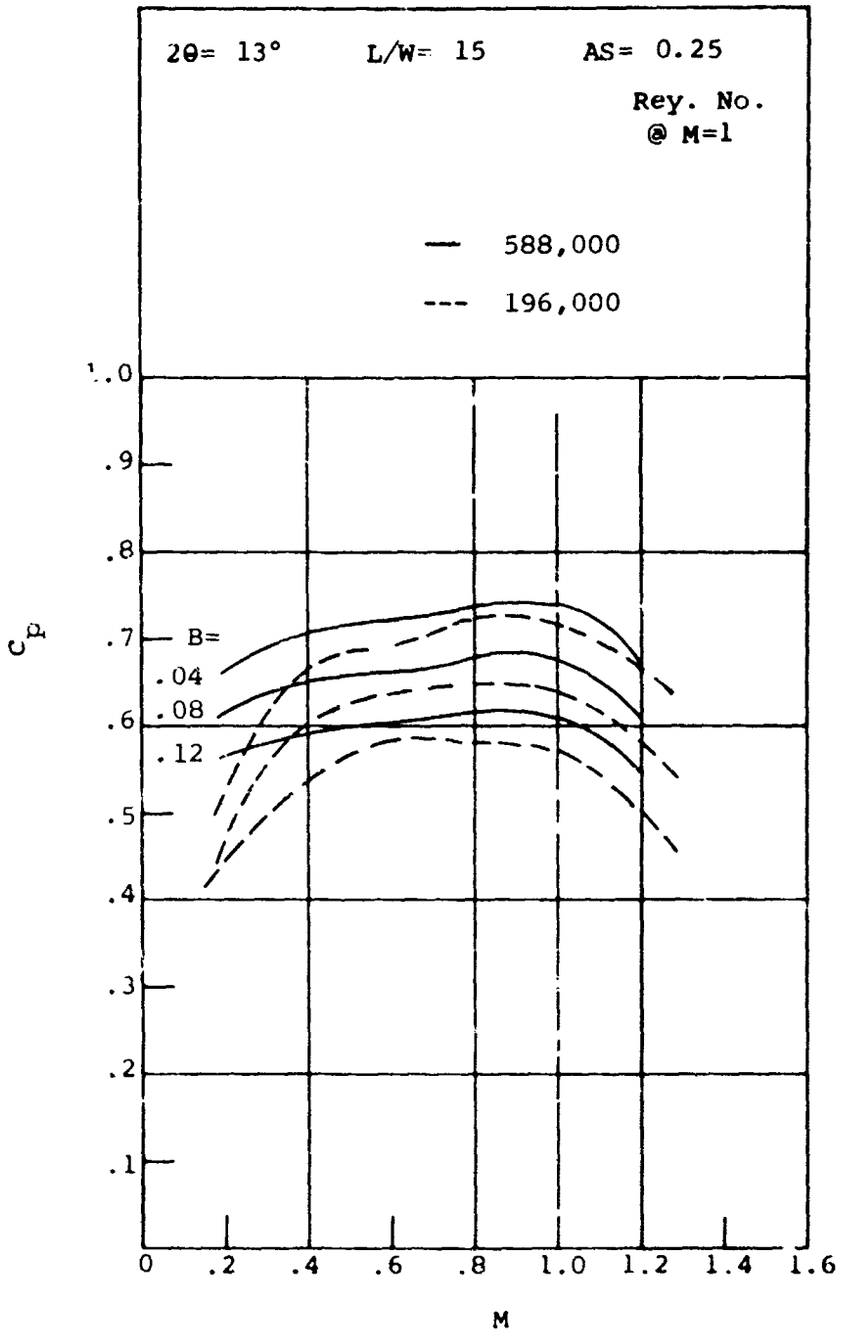

Figure 194. Pressure Recovery Versus Mach Number. Aspect Ratio = 0.25.

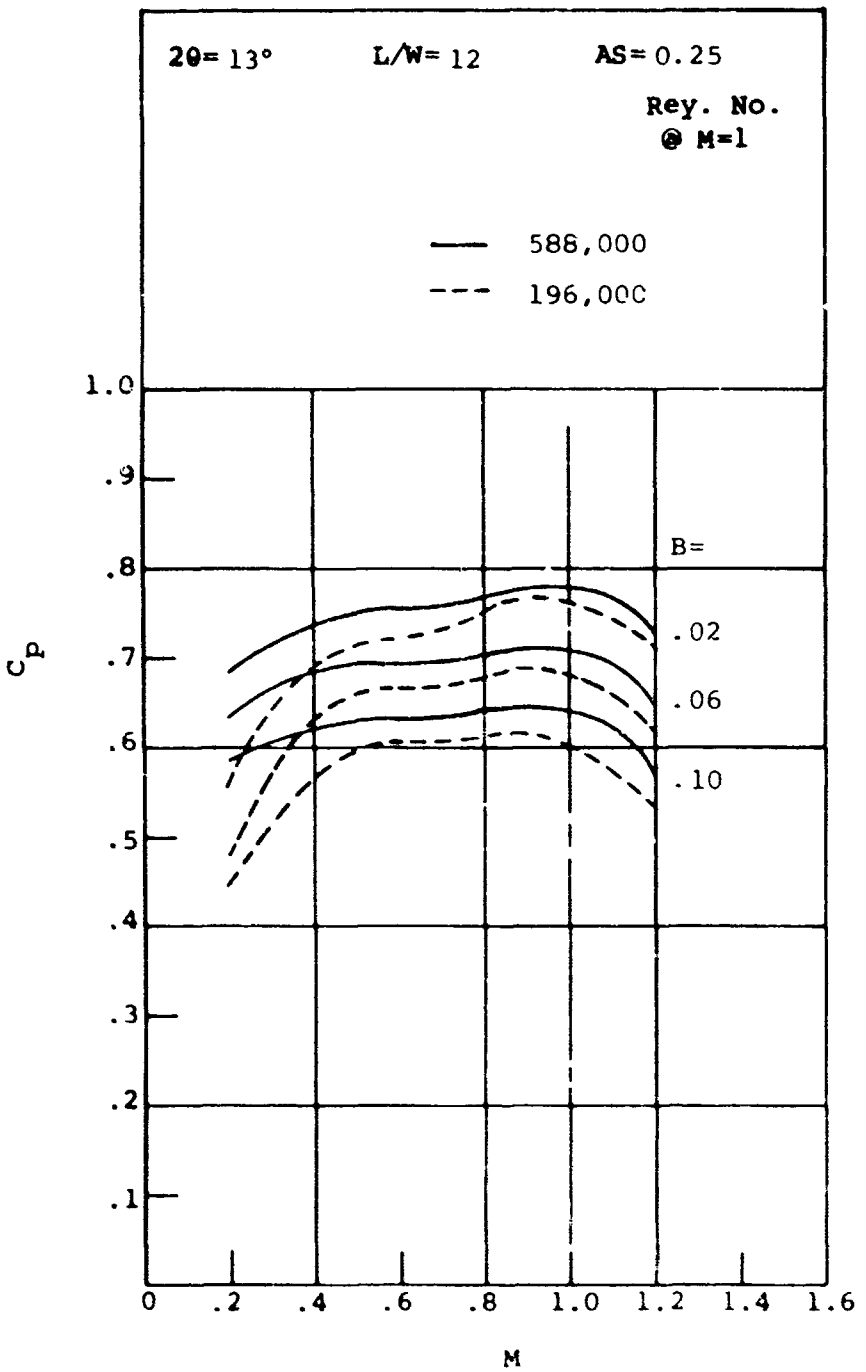

Figure 195. Pressure Recovery Versus Mach Number. Aspect Ratio = 0.25.

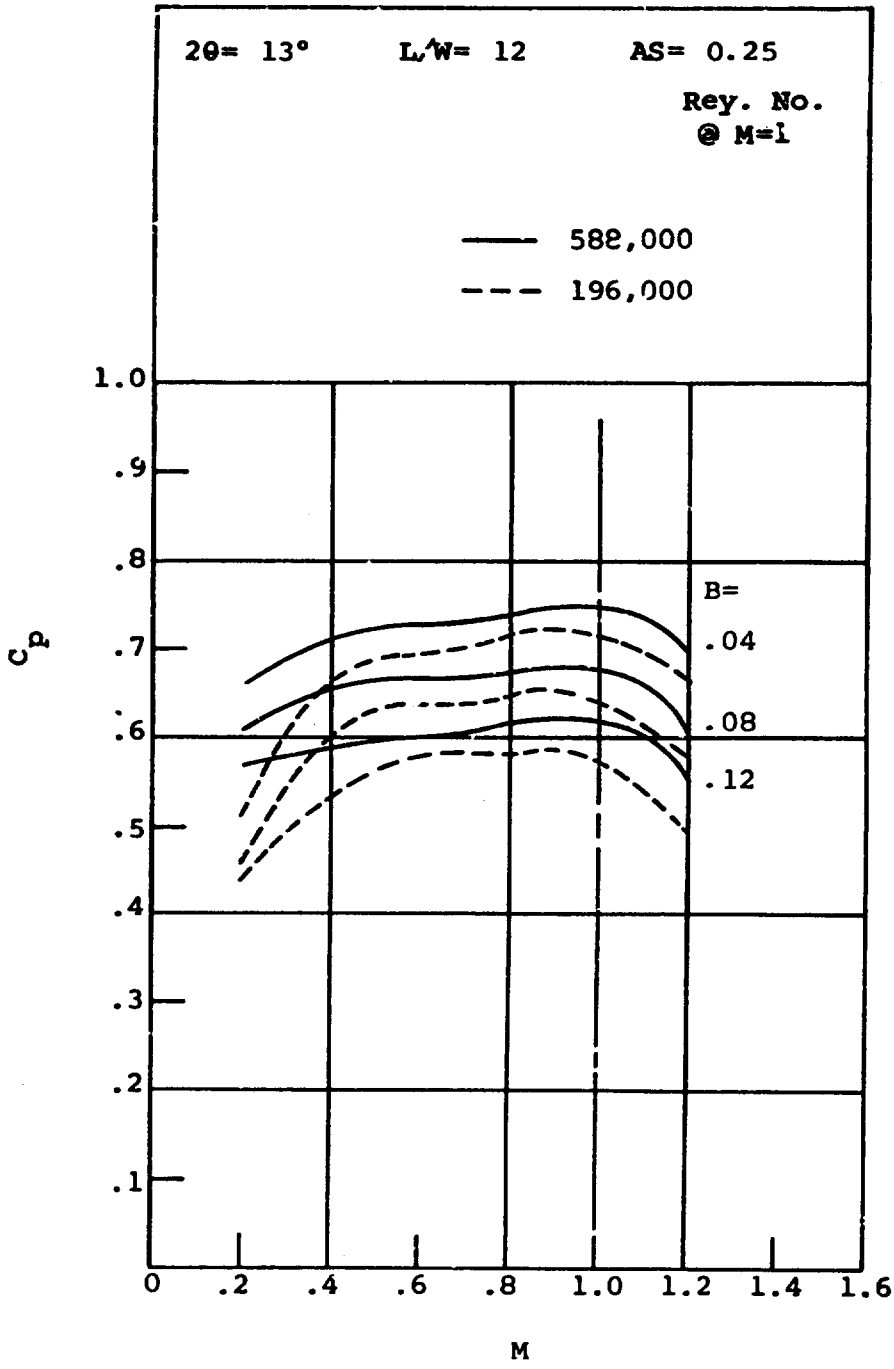

Figure 196. Pressure Recovery Versus Mach Number. Aspect Ratio = 0.25.

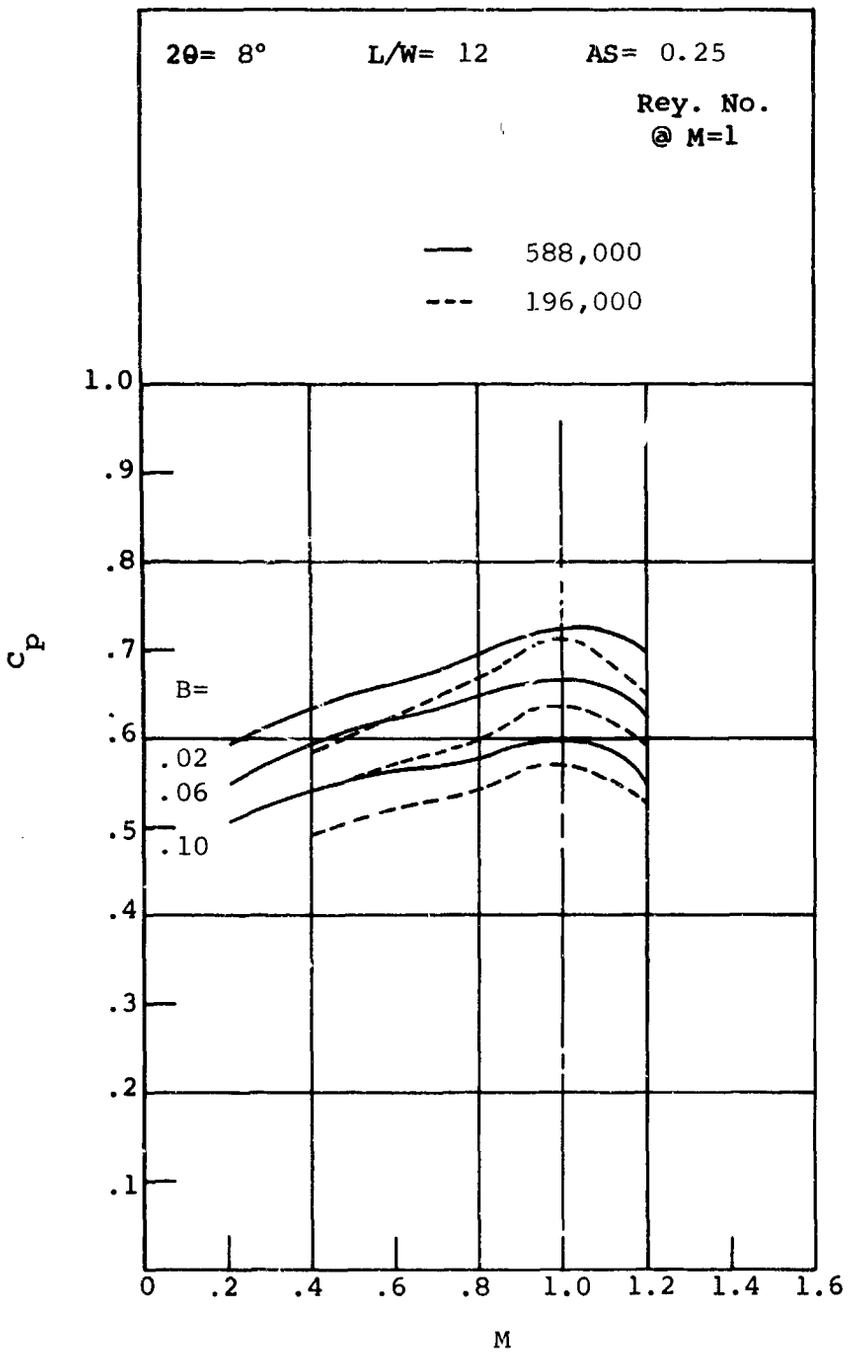

Figure 197. Pressure Recovery Versus Mach Number. Aspect Ratio = 0.25.

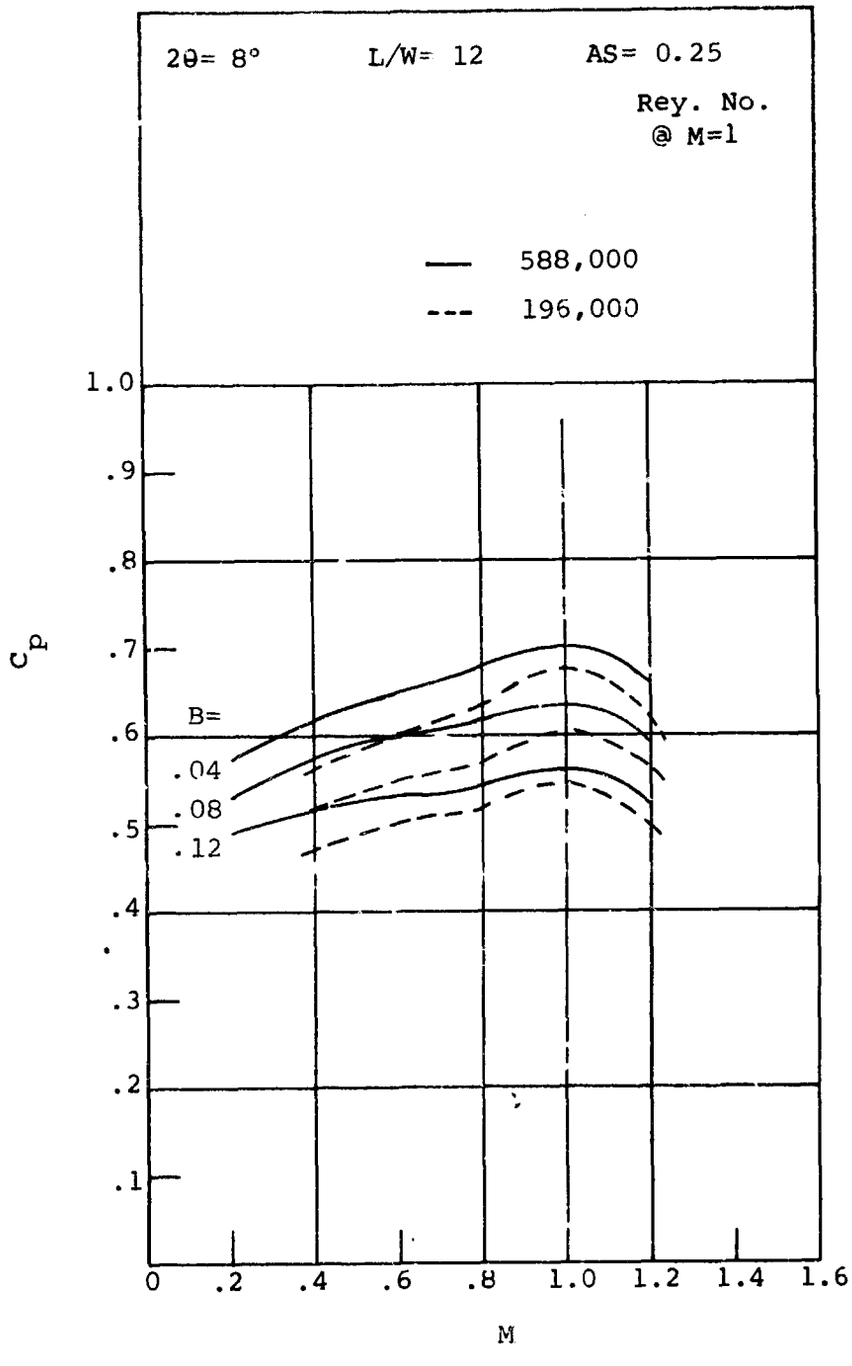

Figure 198. Pressure Recovery Versus Mach Number. Aspect Ratio = 0.25.

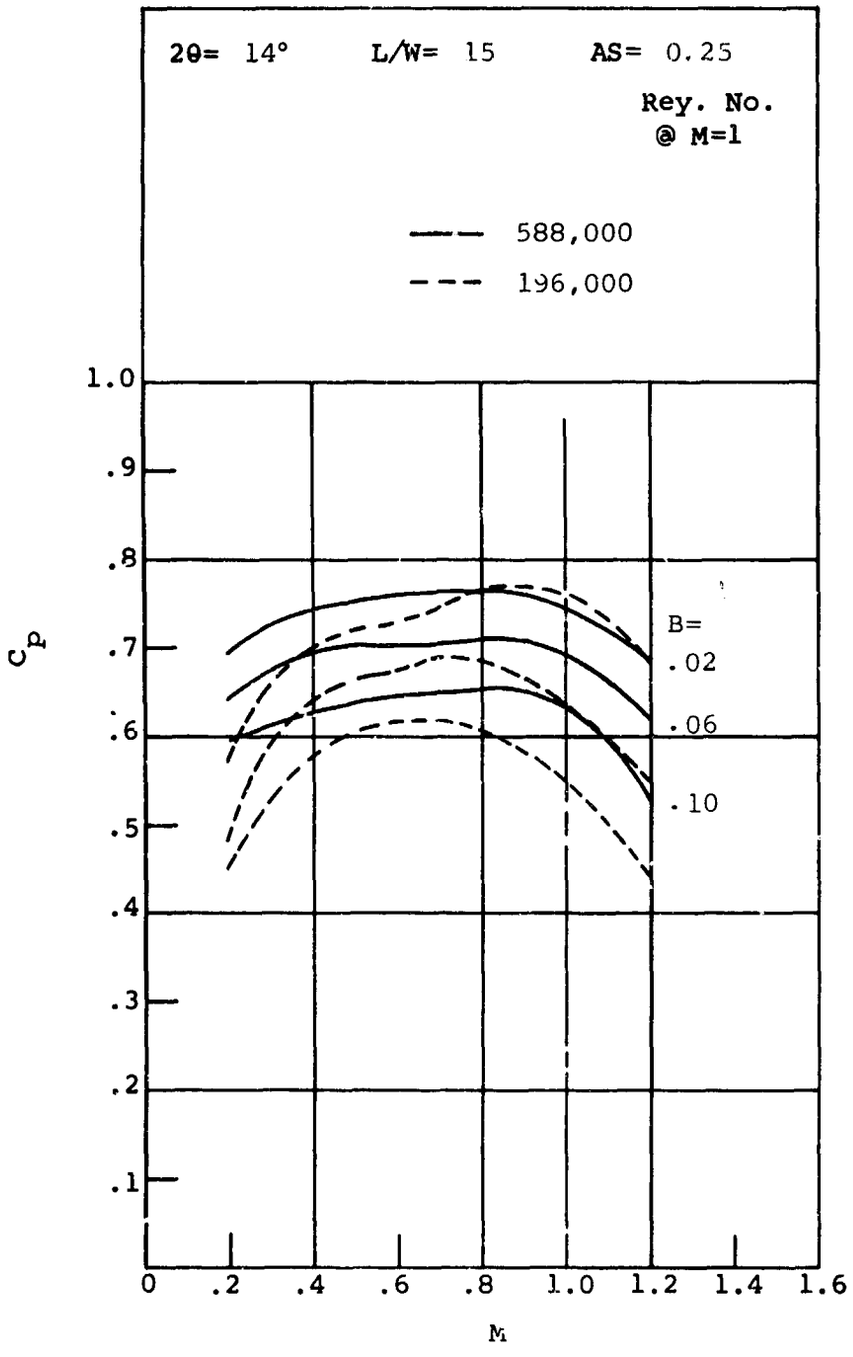

Figure 199. Pressure Recovery Versus Mach Number. Aspect Ratio = 0.25.

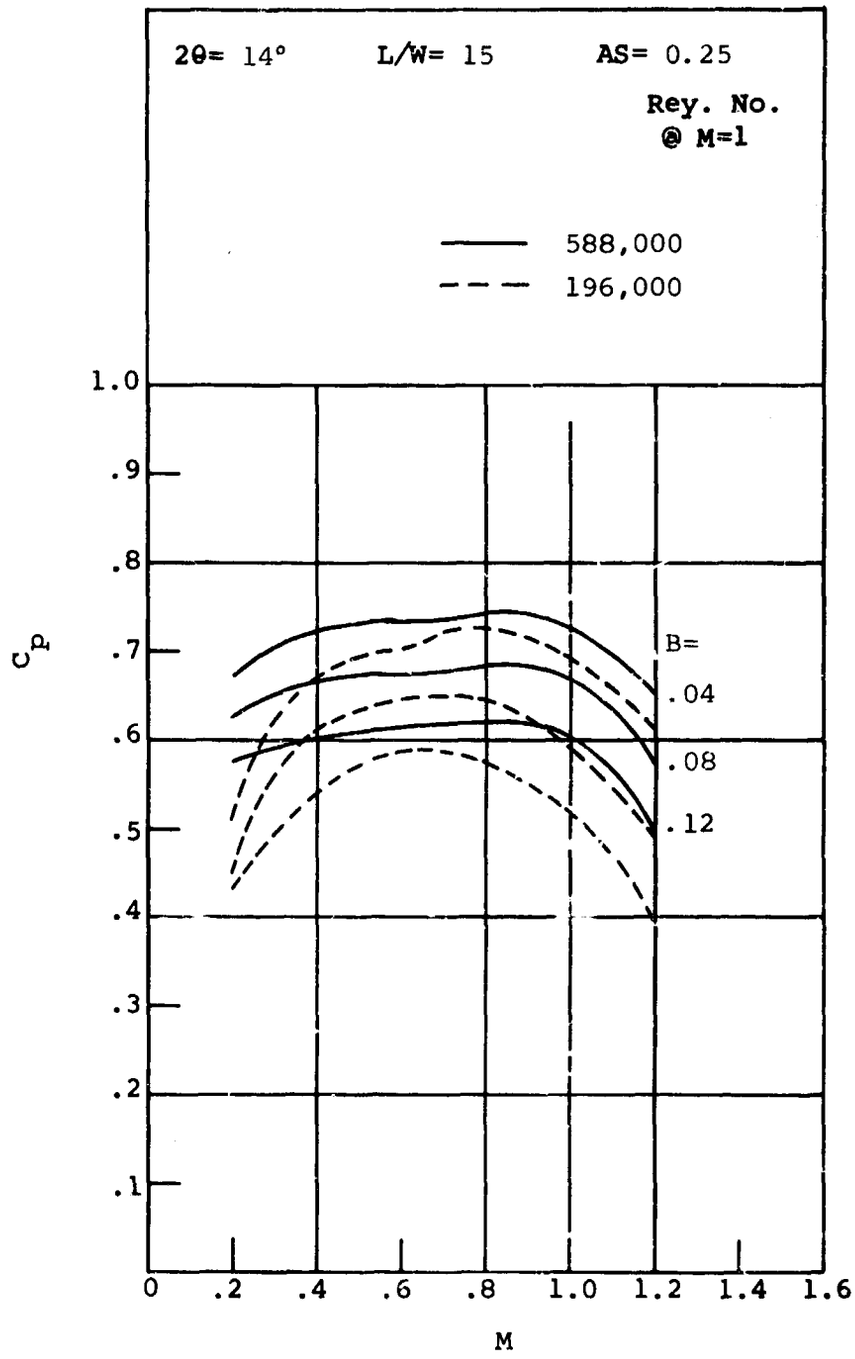

Figure 200. Pressure Recovery Versus Mach Number. Aspect Ratio = 0.25.

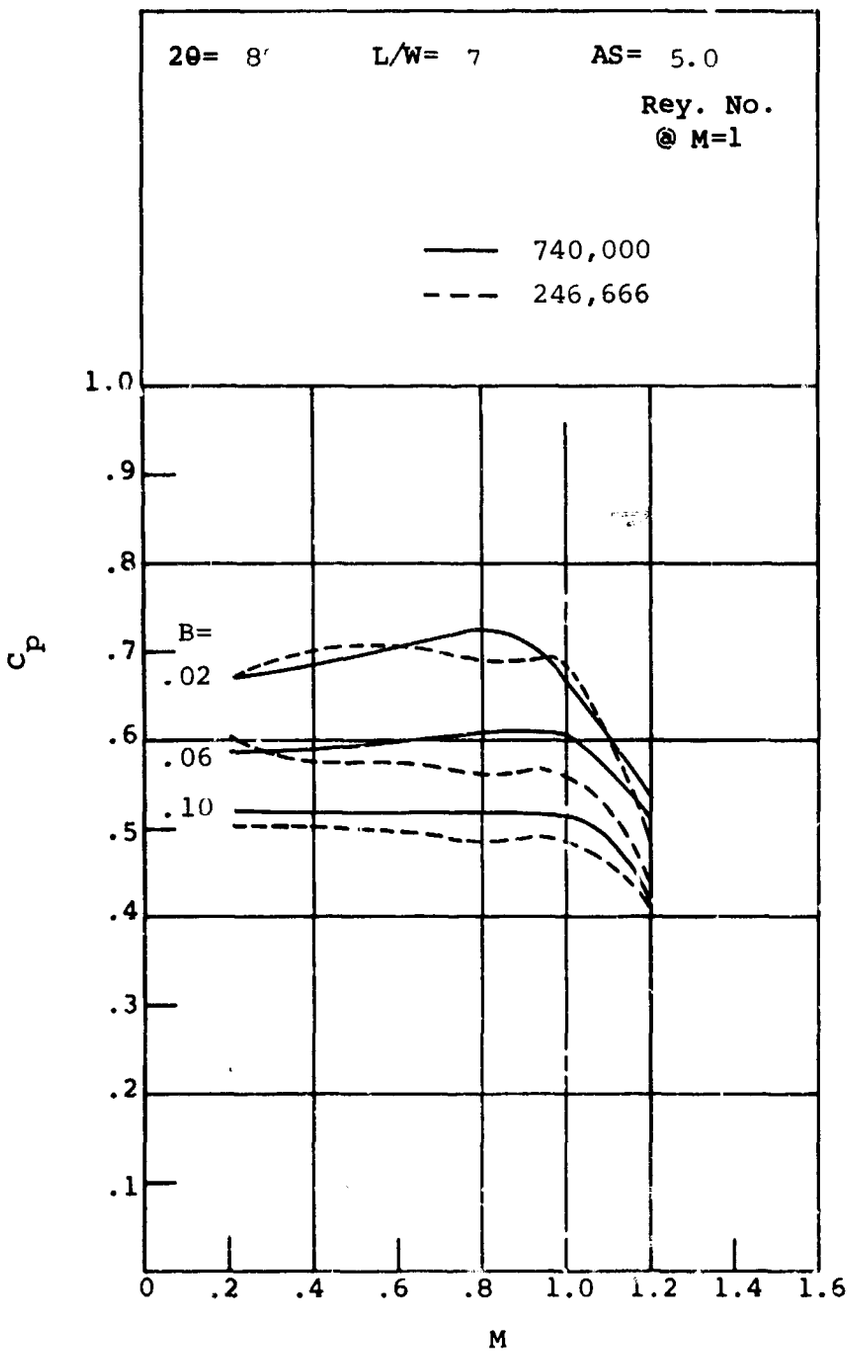

Figure 201. Pressure Recovery Versus Mach Number. Aspect Ratio = 5.0.

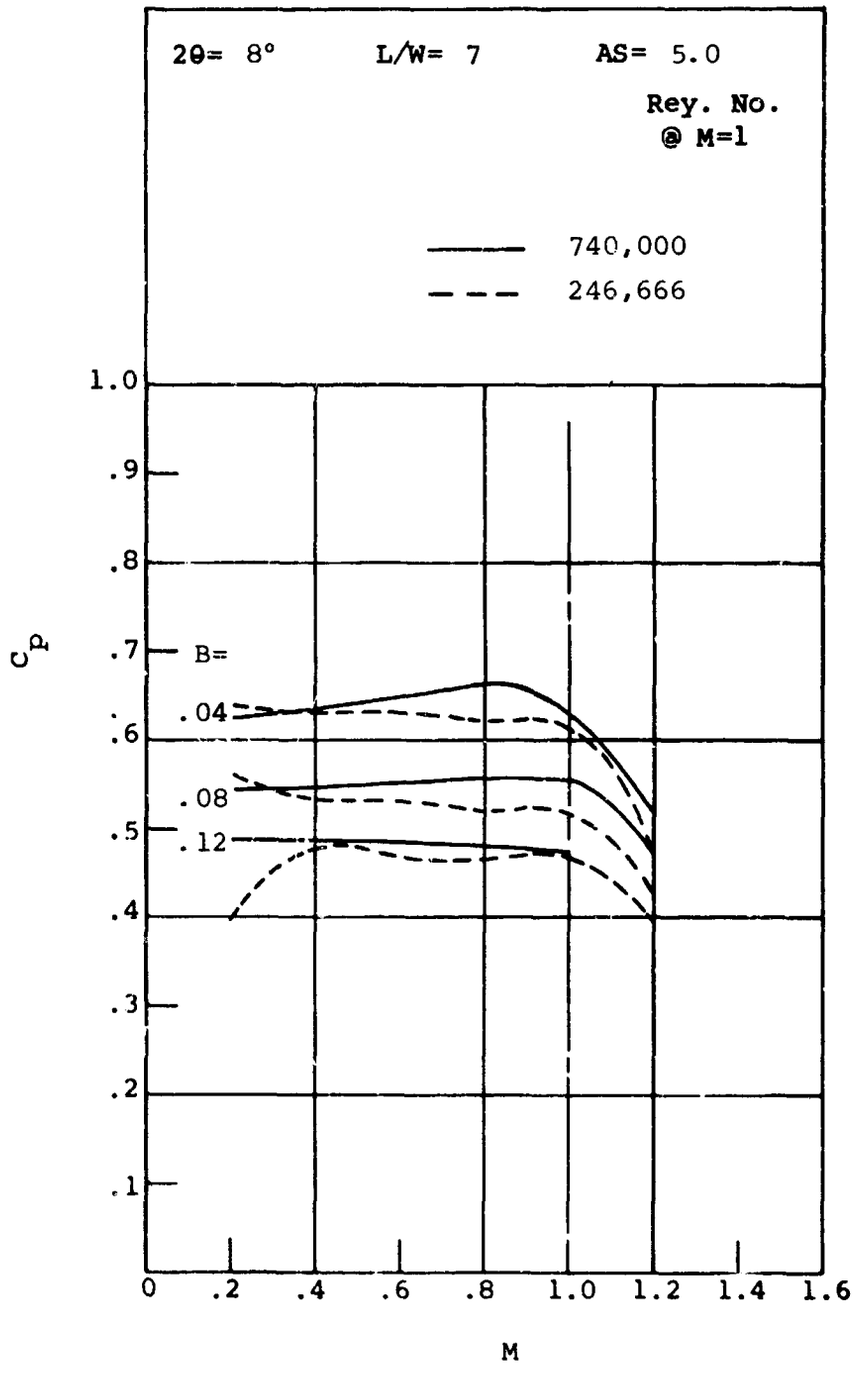

Figure 202. Pressure Recovery Versus Mach Number. Aspect Ratio = 5.0.

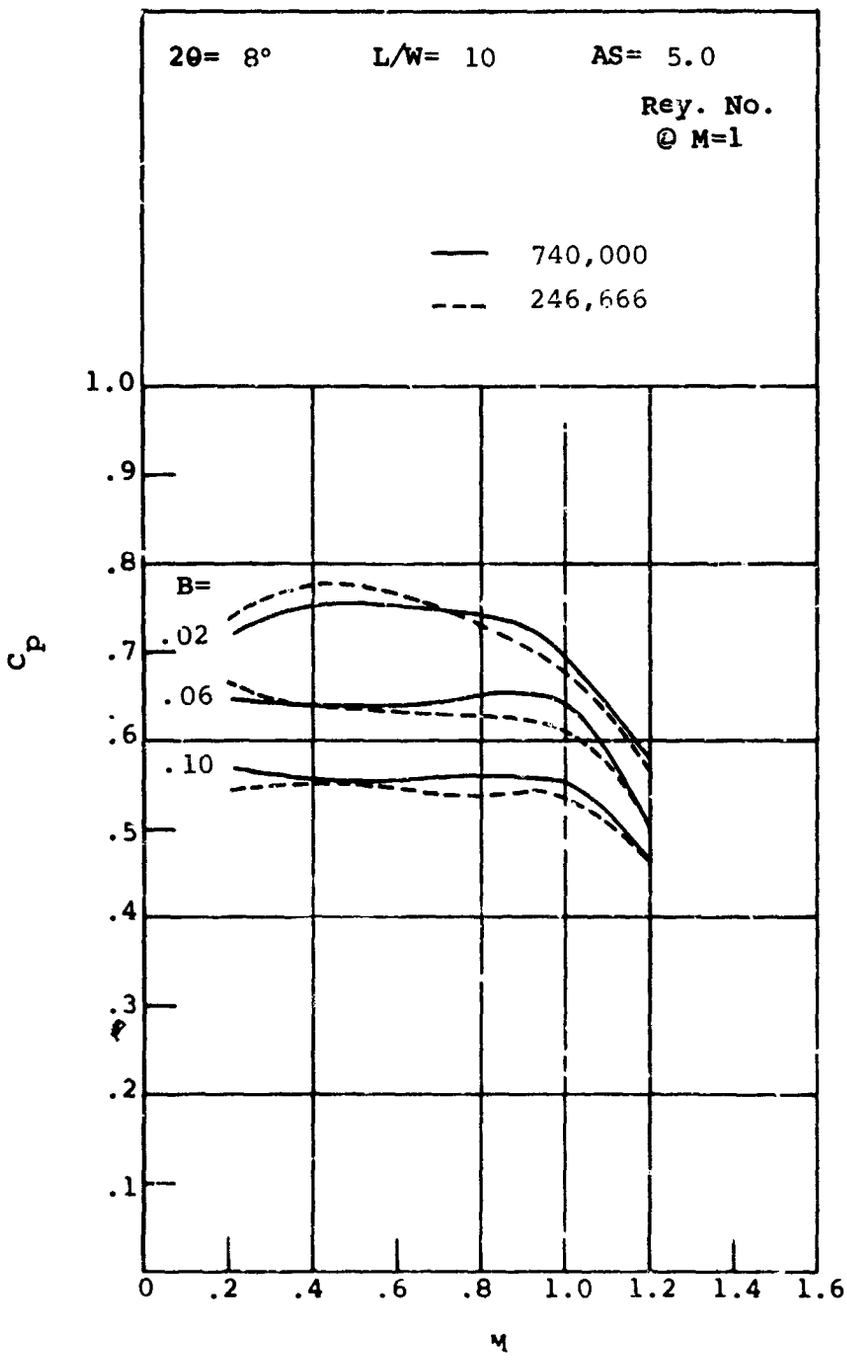

Figure 203. Pressure Recovery Versus Mach Number. Aspect Ratio = 5.0.

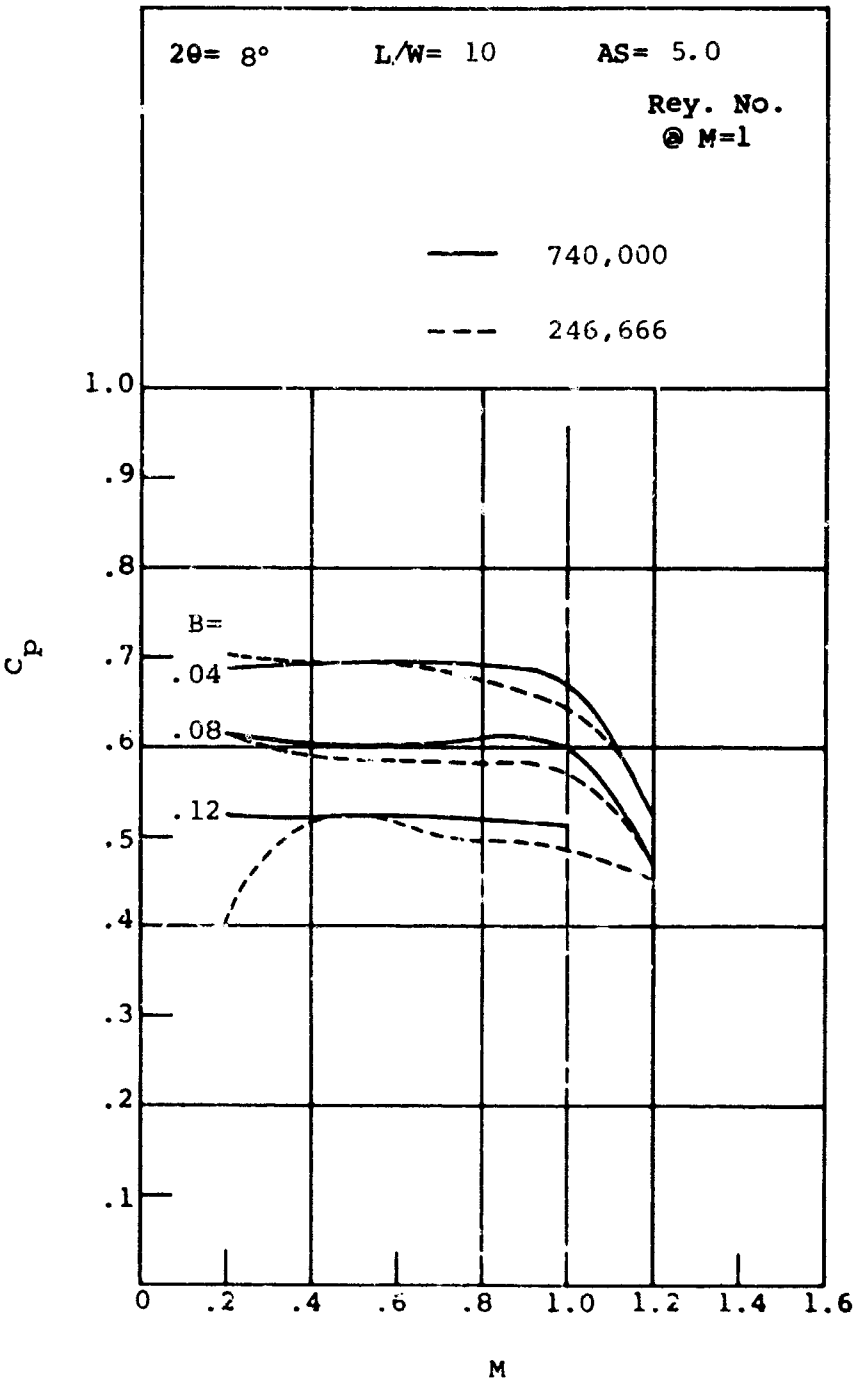

Figure 204. Pressure Recovery Versus Mach Number. Aspect Ratio = 5.0.

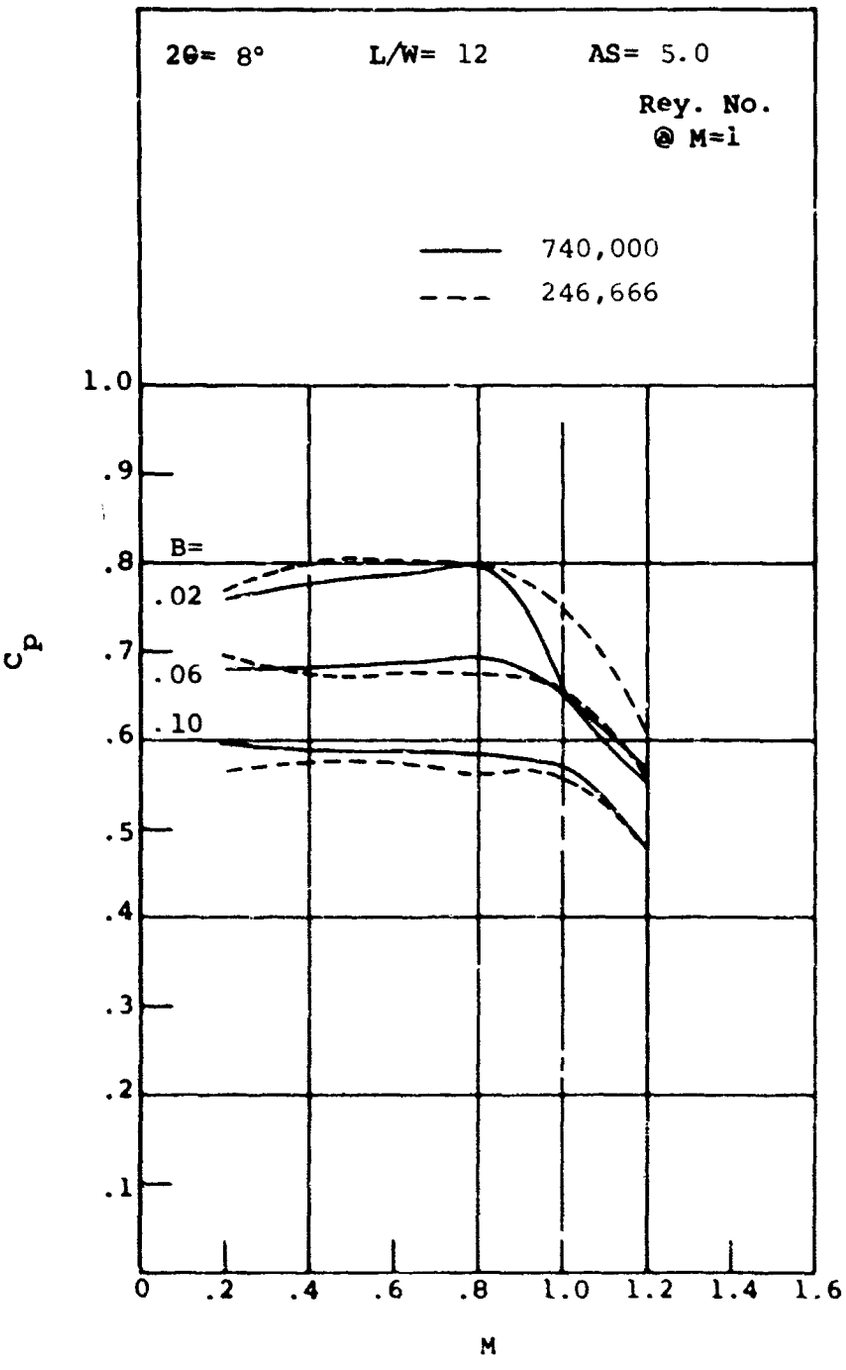

Figure 205. Pressure Recovery Versus Mach Number. Aspect Ratio = 5.0.

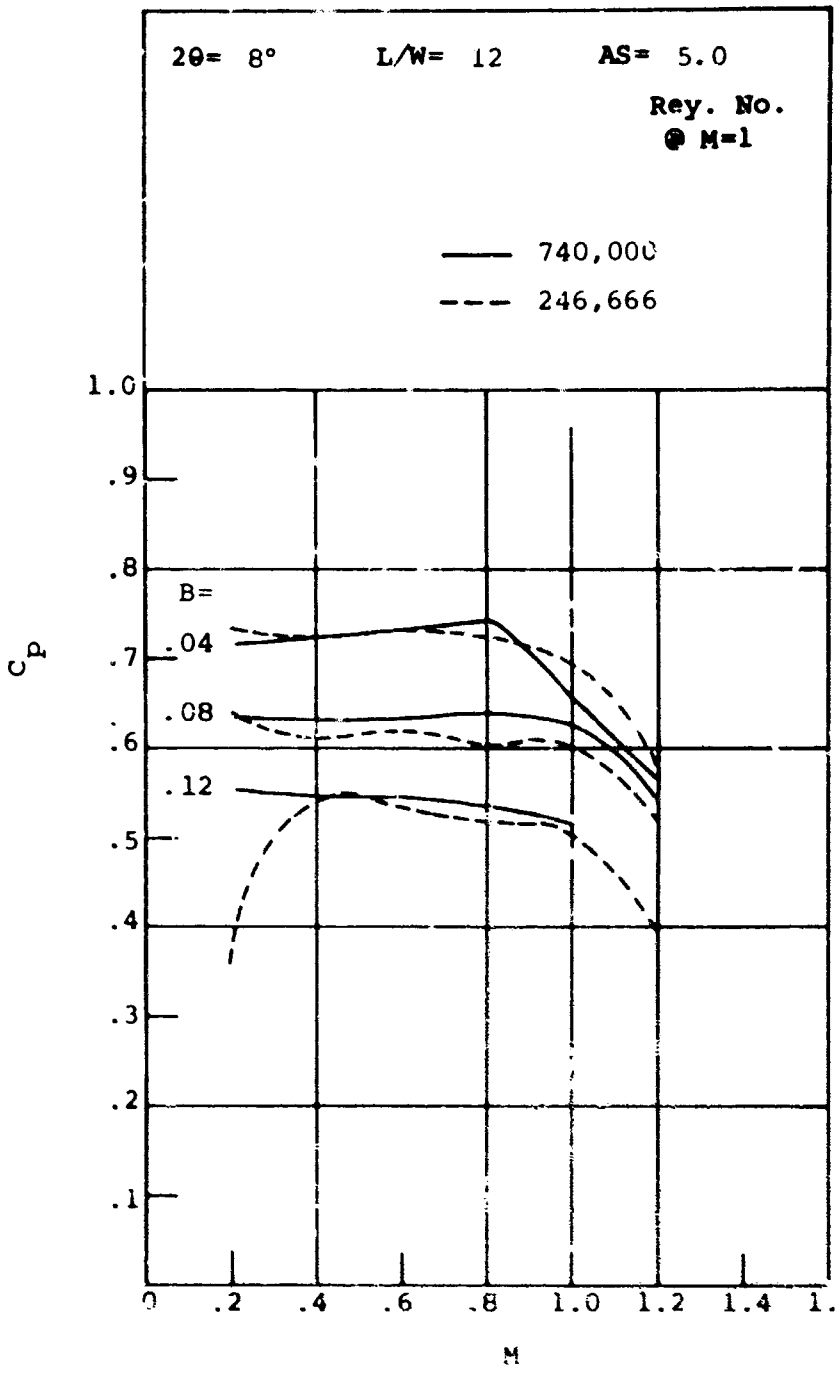

Figure 206. Pressure Recovery Versus Mach Number. Aspect Ratio = 5.0.

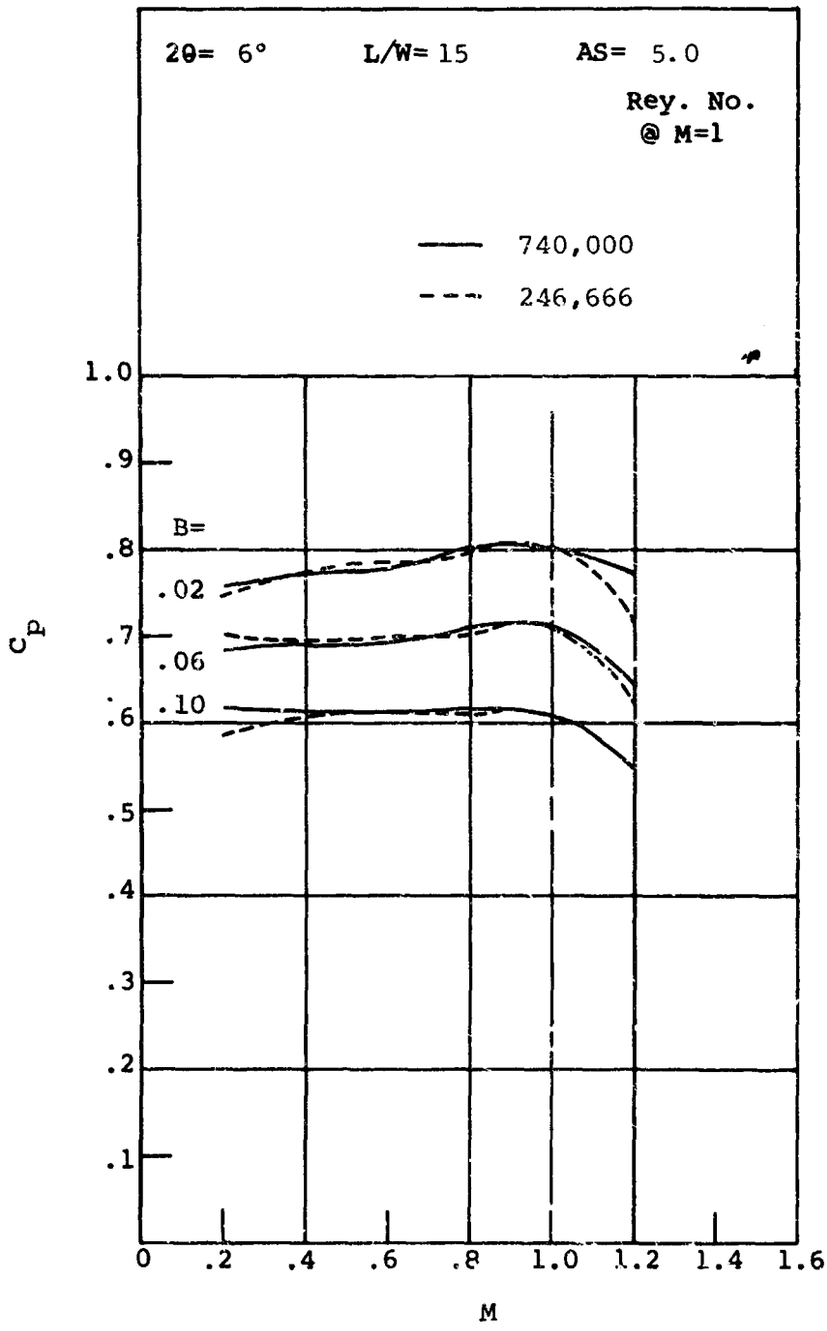

Figure 207. Pressure Recovery Versus Mach Number. Aspect Ratio = 5.0.

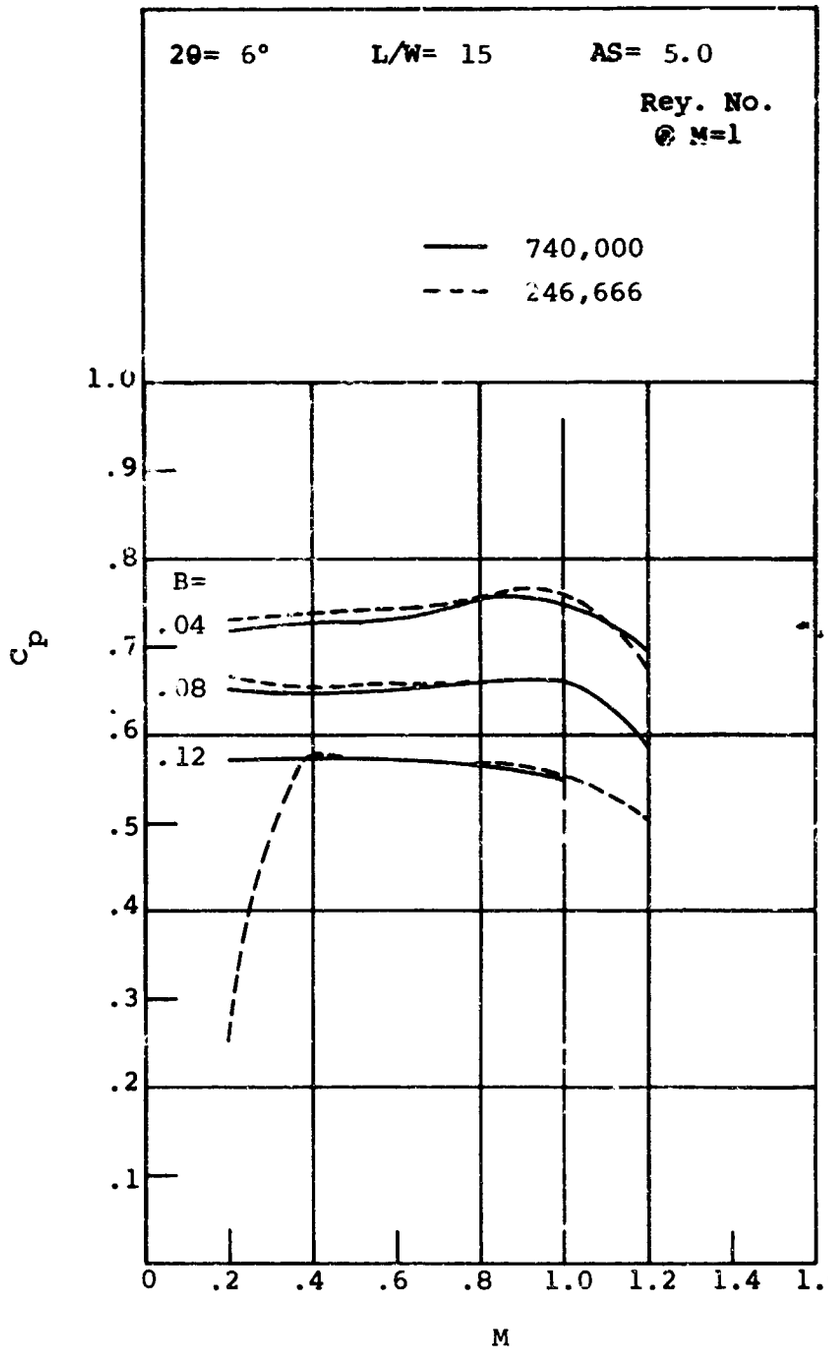

Figure 208. Pressure Recovery Versus Mach Number. Aspect Ratio = 5.0.

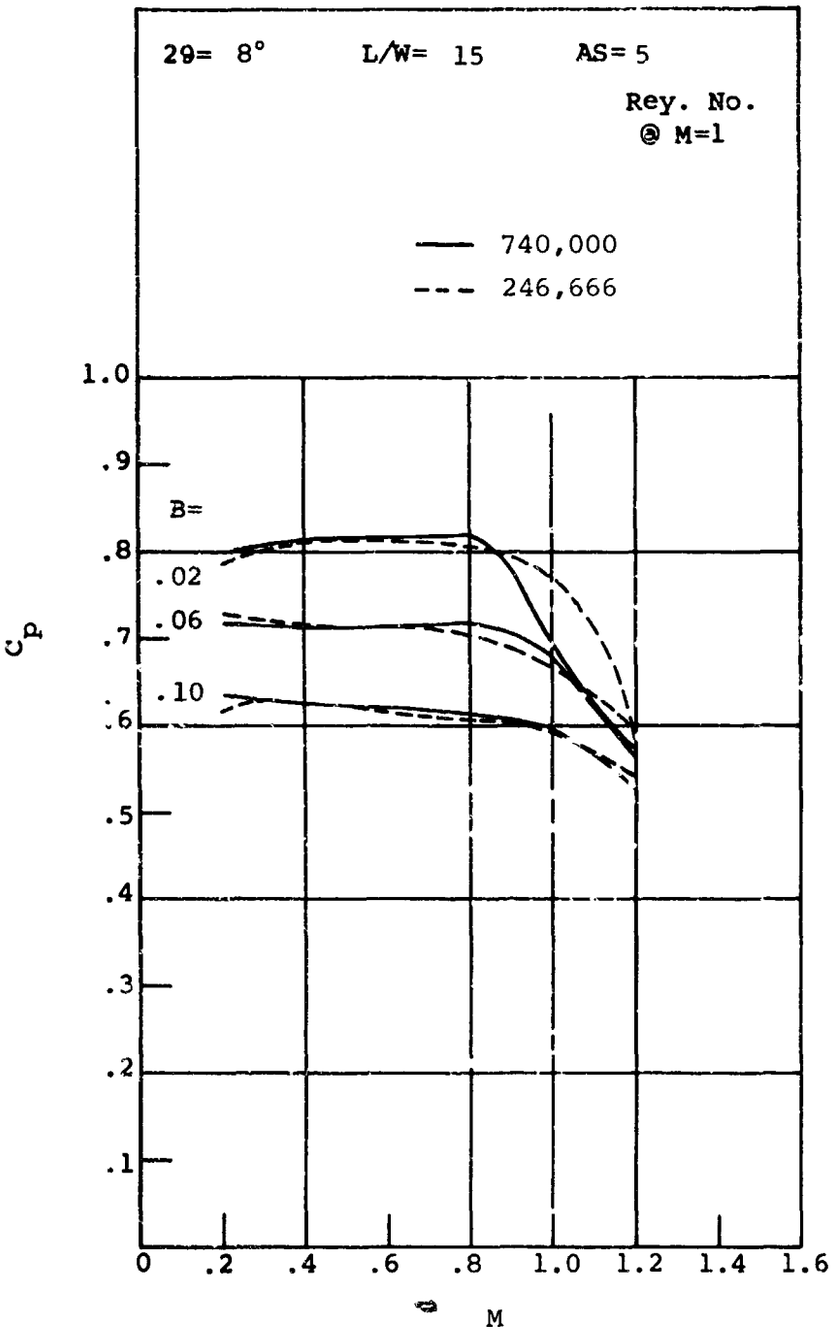

Figure 209. Pressure Recovery Versus Mach Number. Aspect Ratio = 5.0.

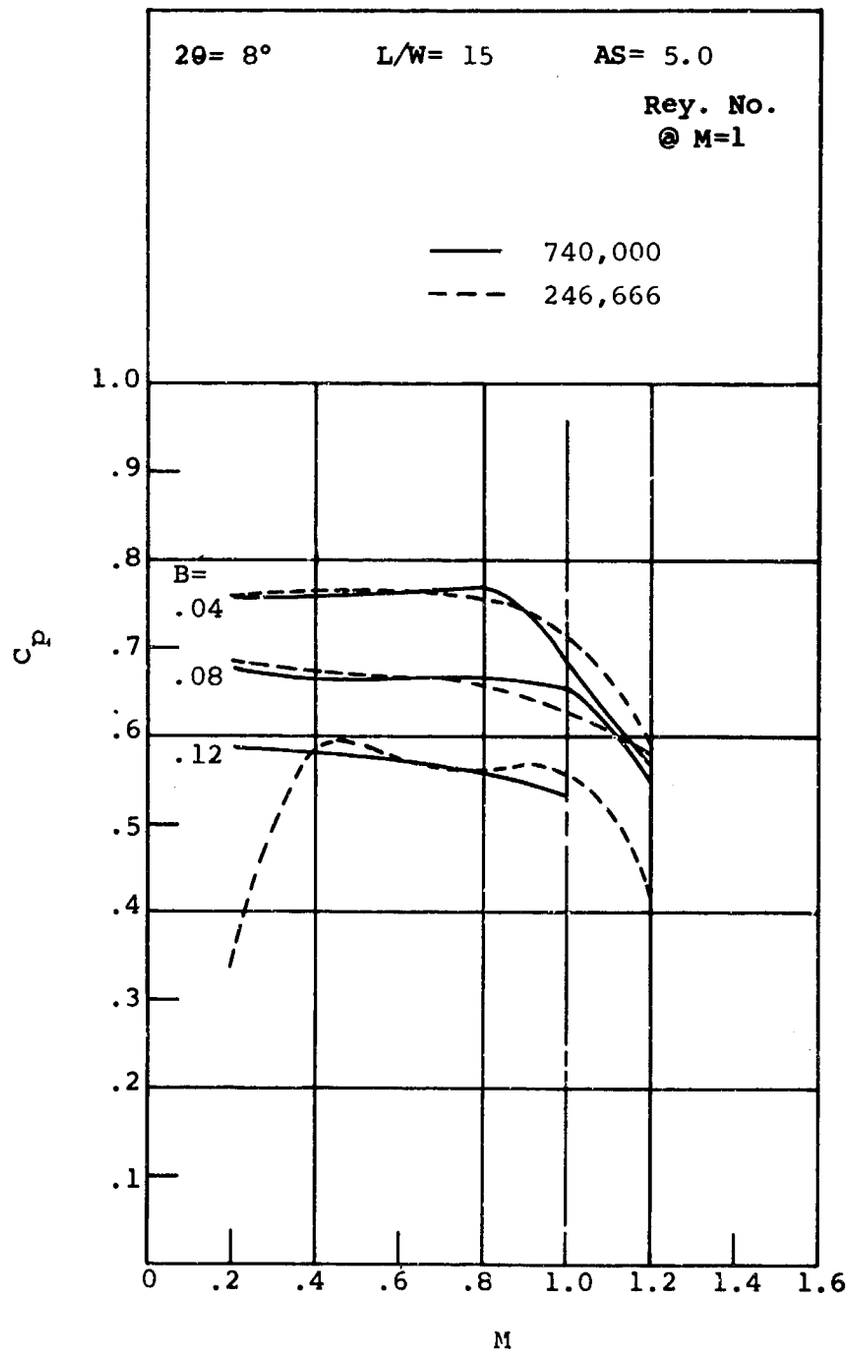

Figure 210. Pressure Recovery Versus Mach Number. Aspect Ratio = 5.0.

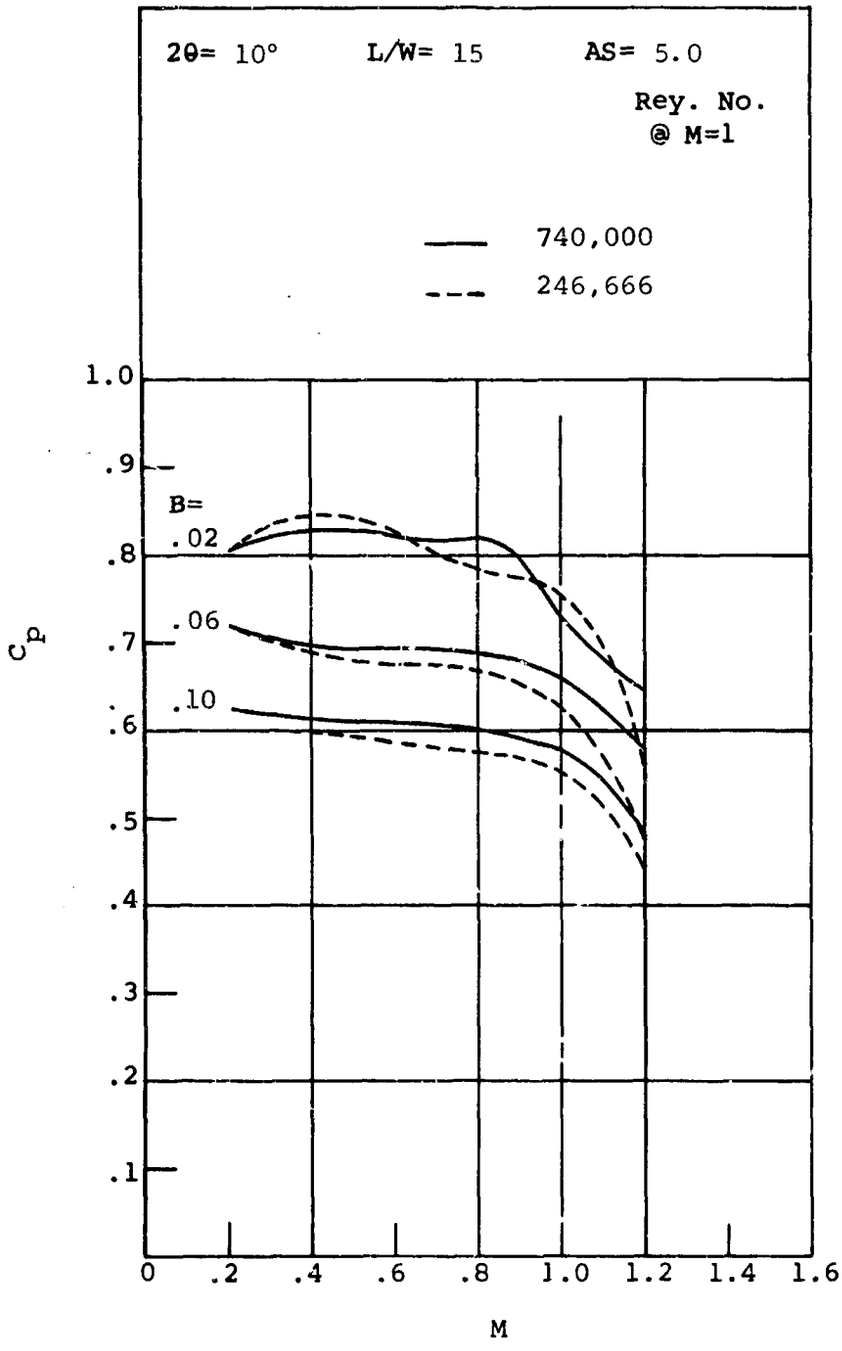

Figure 211. Pressure Recovery Versus Mach Number. Aspect Ratio = 5.0.

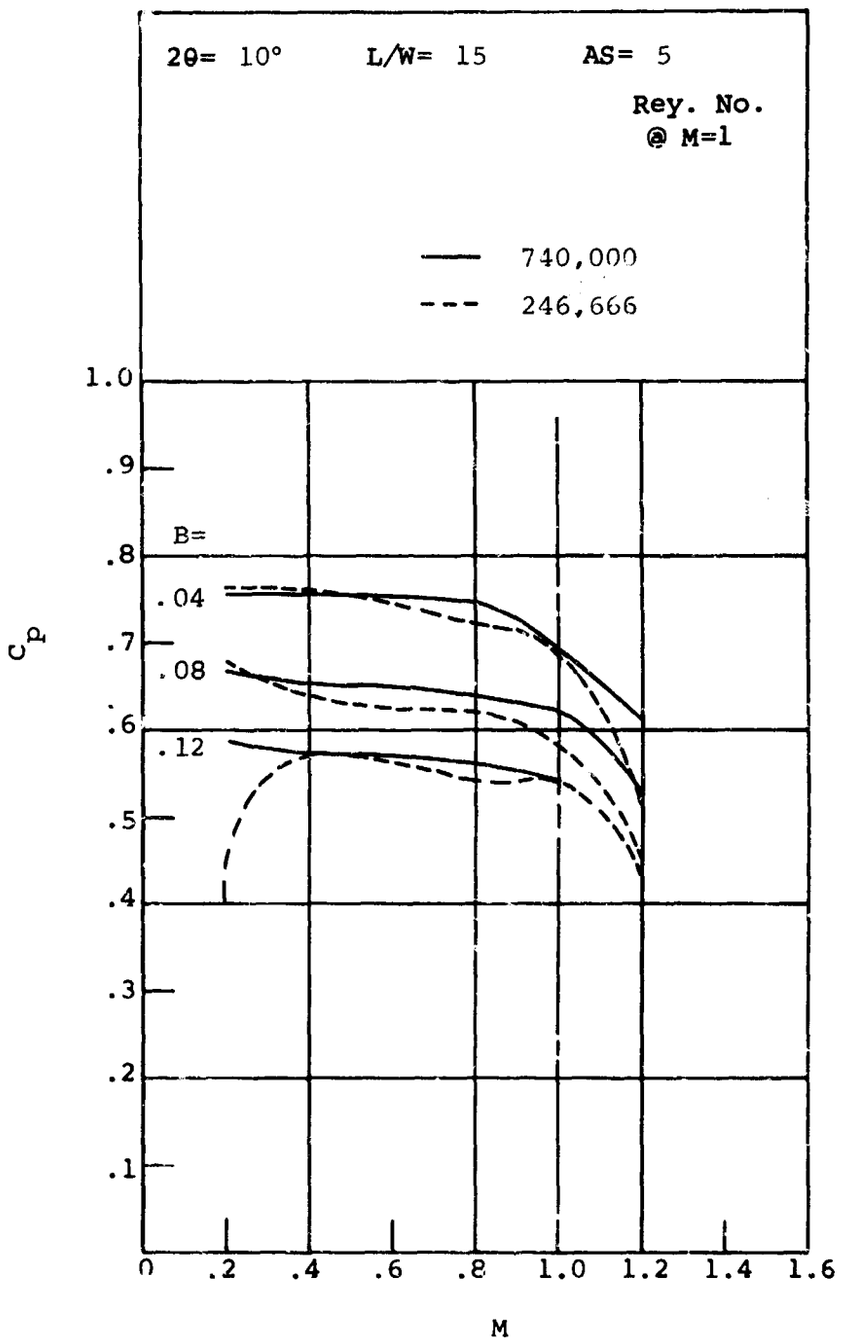

Figure 212. Pressure Recovery Versus Mach Number. Aspect Ratio = 5.0.

It is easier to discuss the data in terms of the difference in C_p between the 60 psia and 20 psia data. This difference varies appreciably with aspect ratio and divergence angle.

For low angles (low compared to angles corresponding to the ridge of optimum recovery, C_p* and C_p**) for the 0.25 aspect ratio data, the 20 psia data varies from 2 to 5 points below the 60 psia data. (Although the 0.2 Mach number data has been shown, it is felt that this data may have a considerable fixed error in blockage greater than that shown in Table V for M_t = 0.4; the very low flow rates at this Mach number and stagnation pressure are at the very low end of the range of the flowmeter.) The trends in C_p vary in much the same manner for both the 20 and 60 psia data.

At high angles, however, where the divergence angle falls on the steep side of the ridge of optimum recovery (2θ = 16°), there is a much greater variation in the C_p difference with Mach number and blockage; some of the data at B = .02 has the 20 psia recovery data higher than the 60 psia data, while at B = 0.12, the 20 psia data is as much as 8 points lower than the data for the high stagnation pressure.

The same comments can be made for the 5.0 aspect ratio data except that the differences in C_p are smaller than was found for aspect ratio 0.25. For the lowest angles shown, much of the data is, in fact, almost coincident between the two stagnation pressures.

It is difficult to generalize the Reynolds number behavior because of the differences found as aspect ratio, divergence angle, and length-to-throat-width ratio are varied. However, for diffuser geometries at angles corresponding to or below the ridge of recovery optima (which includes peak recovery), the low Reynolds number recovery is below the recovery measured for the higher Reynolds number. Since the leverage of overall diffuser recovery on compressor efficiency is about 1:3 for high pressure ratio stages, the general effect of Reynolds number could be to produce a 1-to-2 point (or greater) difference in stage efficiency. In general, the recovery differences produced by Reynolds number effects become less as the throat Mach number approach unity.

Unless some other effect on the inlet flow that has not been accounted for has been produced by changing the inlet stagnation pressure (we have no reason to suspect that any such effect has occurred), the designer should strive to achieve high throat Reynolds number in order to optimize diffuser recovery. The present data is limited as to the range of Reynolds numbers covered but should serve as a guide in estimating the effect to be expected as Reynolds number is varied

4.6 BOUNDARY LAYER SHAPE FACTOR TESTS

A number of tests were run early in the experimental program to study the effect of the nearness of the inlet boundary layers to separation on pressure recovery performance. The tests were made on selected diffuser geometries at aspect ratio 0.25.

Turbulent boundary layer calculation techniques often attempt to predict the onset of boundary layer separation in terms of a boundary layer shape factor. The shape factor may be one of several integral parameters of the boundary layer flow. The present tests are referred to as "boundary layer shape factor studies", although direct measurement of boundary layer velocity profiles or shape factors have not been made. Instead, different shapes of inlet geometry have been used to provide a variation in boundary layer growth conditions and hence boundary layer shape factor.

All of the base data inlet geometries are typical of accelerating pressure gradients ($dp/dx < 0$). Boundary layers under such conditions can be classified as being far from separation.

The boundary layers used for the shape factor studies were developed on the inlet geometry shown in Figure 213. These inlet blocks have been called "H-factor blocks". This inlet geometry provides a channel shape in which the inlet flow accelerates through a converging nozzle and then decelerates ahead of the diffuser throat. The objective is to simulate pressure gradient effects on the boundary layer flow that will approximate those found in centrifugal compressor diffusers immediately ahead of the diffuser throat. The converging-diverging nozzle provides an adverse pressure gradient boundary layer shape factor ahead of the diffuser.

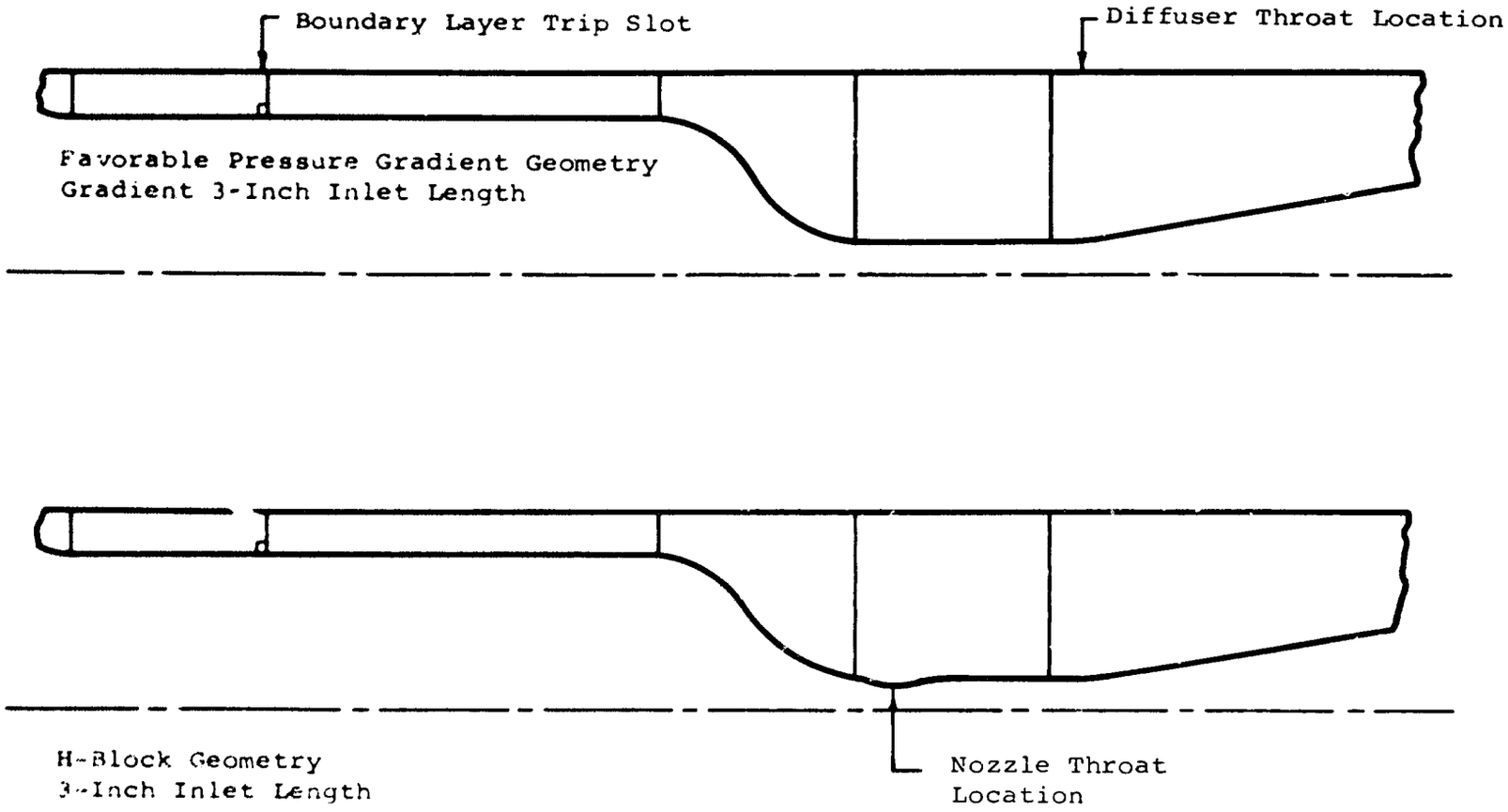

Figure 213. Adverse Pressure Gradient Inlet Geometry.

At Mach numbers at the entrance to the diffuser less than about 0.8, the flow accelerates through the sine block and the nozzle contraction of the H-block. The flow then decelerates to the throat of the diffuser as the flow passes through the diverging portion of the H-block downstream of the primary throat. However, the magnitude of the adverse pressure gradient is not large, and the boundary layer characteristics are probably not extremely different in terms of nearness to separation from the boundary layer characteristics generated in the favorable pressure gradient inlets used in the base studies. The H-factor blocks were designed with the primary purpose of studying the high Mach number recovery behavior. In order to establish the proper Mach number behavior in the diverging portion of the upstream nozzle at high throat Mach numbers, the area ratio expansion of the nozzle must be kept small. At low Mach number, the boundary layer growth and the small area expansion combine to produce a mild adverse pressure gradient in the nozzle expansion, followed by an acceleration in the straight inlet immediately ahead of the throat because of boundary layer growth.

At Mach numbers at the entrance to the diffuser greater than about 0.8, the flow is first accelerated to sonic conditions at the nozzle throat and then accelerated further to supersonic conditions in the diverging portion of the nozzle. By adjusting the back pressure downstream of the diffuser, a shock can be established in the diverging portion of the converging-diverging nozzle. The core flow decelerates across this shock to a subsonic Mach number and then accelerates again to the throat Mach number in the diffuser because of boundary layer growth over the straight length of parallel section of inlet channel. The abruptness and steepness of the pressure rise imposed by the shock on the boundary layer can be seen from Figure 214.

The H-factor block geometry was designed to produce a shock Mach number (immediately ahead of the shock) of approximately 1.2 to 1.3. The exact Mach number developed in the inlet depends on the amount of boundary layer growth and hence the core flow area expansion in the diverging portion of the nozzle. Upstream Mach numbers of about 1.2 to 1.3 represent the maximum shock Mach number which should be allowed in centrifugal compressor diffuser design to avoid severe shock boundary layer interaction and separation.

The static pressure distribution (measured with the traverse static pressure tube) in the H-factor block geometry inlet is shown in Figure 214 . The downstream pressure conditions were set to establish choked flow at the diffuser throat. The pressure distribution indicates a shock strength near the downstream end of the H-factor block of about 1.3. The flow accelerates over the 1.75" length of parallel channel ahead of the diffuser throat from a subsonic Mach number immediately downstream of the shock, M_y = .78, to sonic flow at the diffuser throat.

In calculating the diffuser performance for the H-factor block geometry, the throat stagnation pressure has been calculated using the upstream stagnation pressure corrected for the stagnation pressure loss across the shock using one-dimensional normal shock tables.

Figures 215 through 219 show a comparison of the pressure recovery performance of diffuser geometries studied in the H-factor tests with the recovery of the same diffusers from the base data studies with favorable inlet pressure gradients.

Figures 215 and 216 show inlet blockage as a function of Mach number for the 0-inch and 3-inch H-factor block inlet geometries for L/W = 12 and 2θ = 8°, 10°, and 12°. The 0-inch geometry (Figure 213) has a larger scatter in blockage among the three tests than does the 3-inch geometry. In both cases, recovery performance has been compared with the base data using the arithematic mean value of the blockage data for each inlet length; these values are indicated by the dashed lines in Figures 215 and 216.

The pressure recovery data are compared with the base data (the base data have been plotted for the same values of blockage as shown by the mean curves for the H-factor data) in Figures 217, 218, and 219 for 2θ = 8°, 10°, and 12°.

For all three angles, the 0 inch inlet data are the same as or very slightly below (at high Mach numbers) the base data recovery values. Thus, at inlet blockage of approximately 0.09 (and below), the data indicate that a strong shock-boundary layer interaction upstream of the throat has virtually no effect on diffuser recovery.

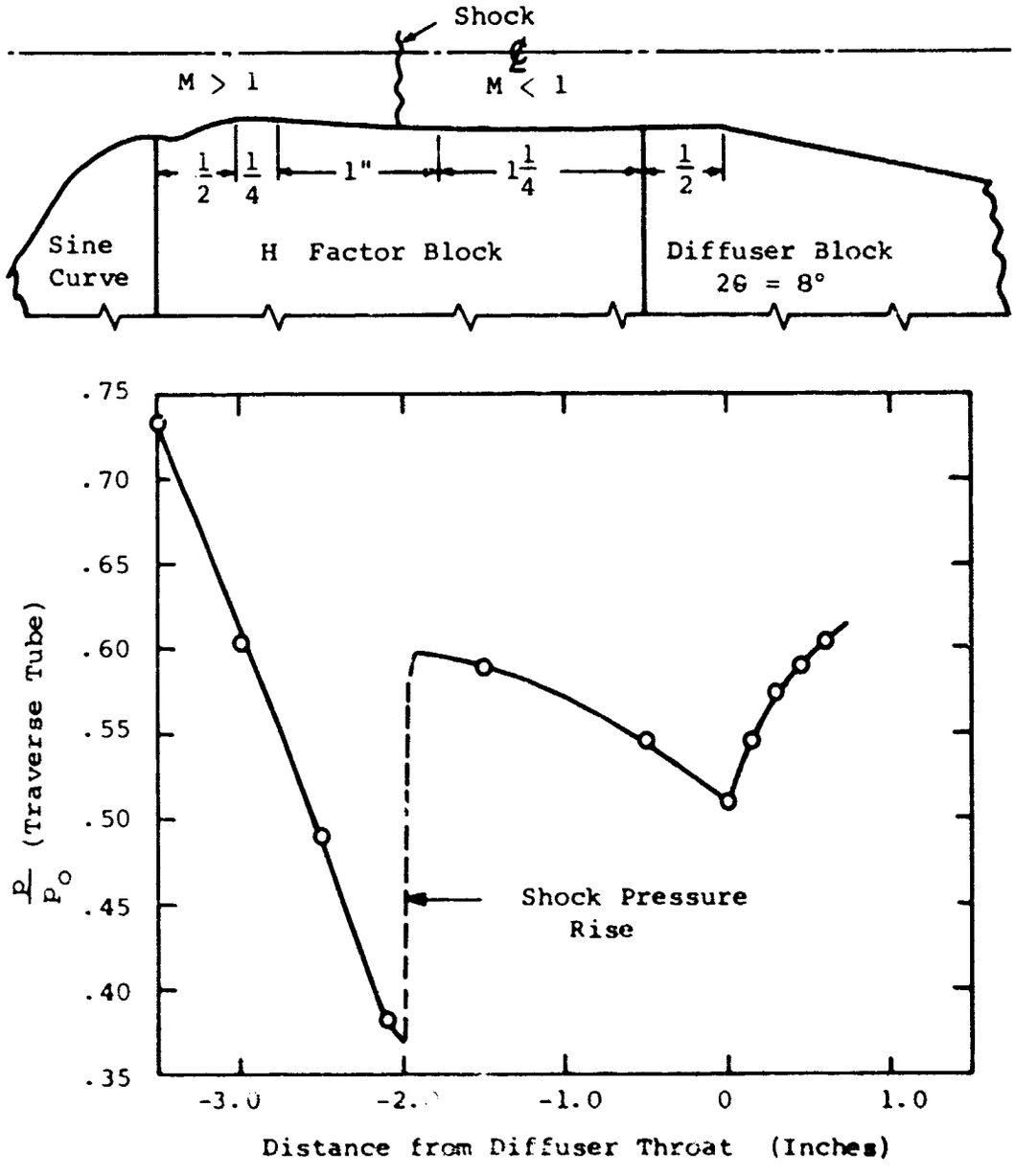

Figure 214. Static-to-Stagnation Pressure Ratio Distribution in Adverse Pressure Gradient Inlet Geometry.

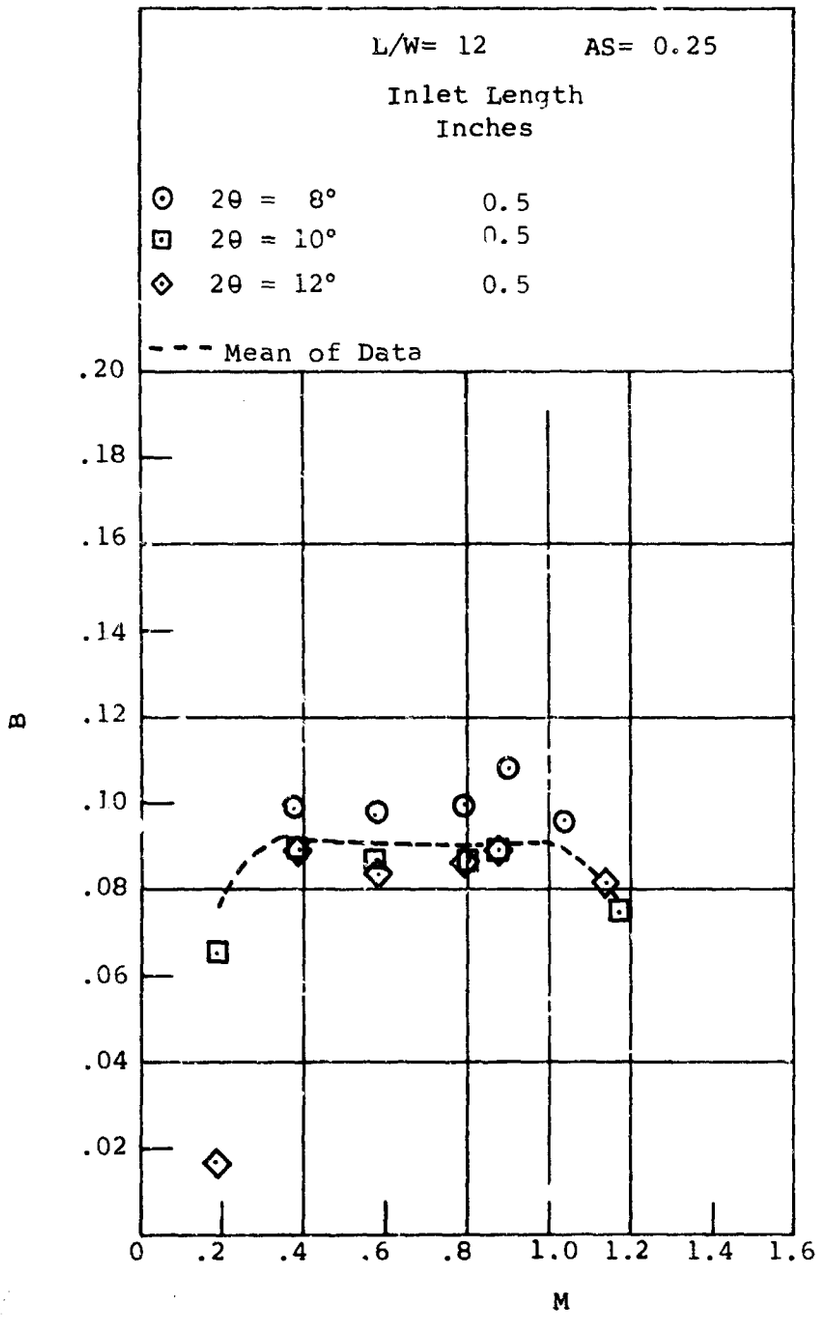

Figure 215. Blockage Versus Mach Number. Shape Factor Studies.

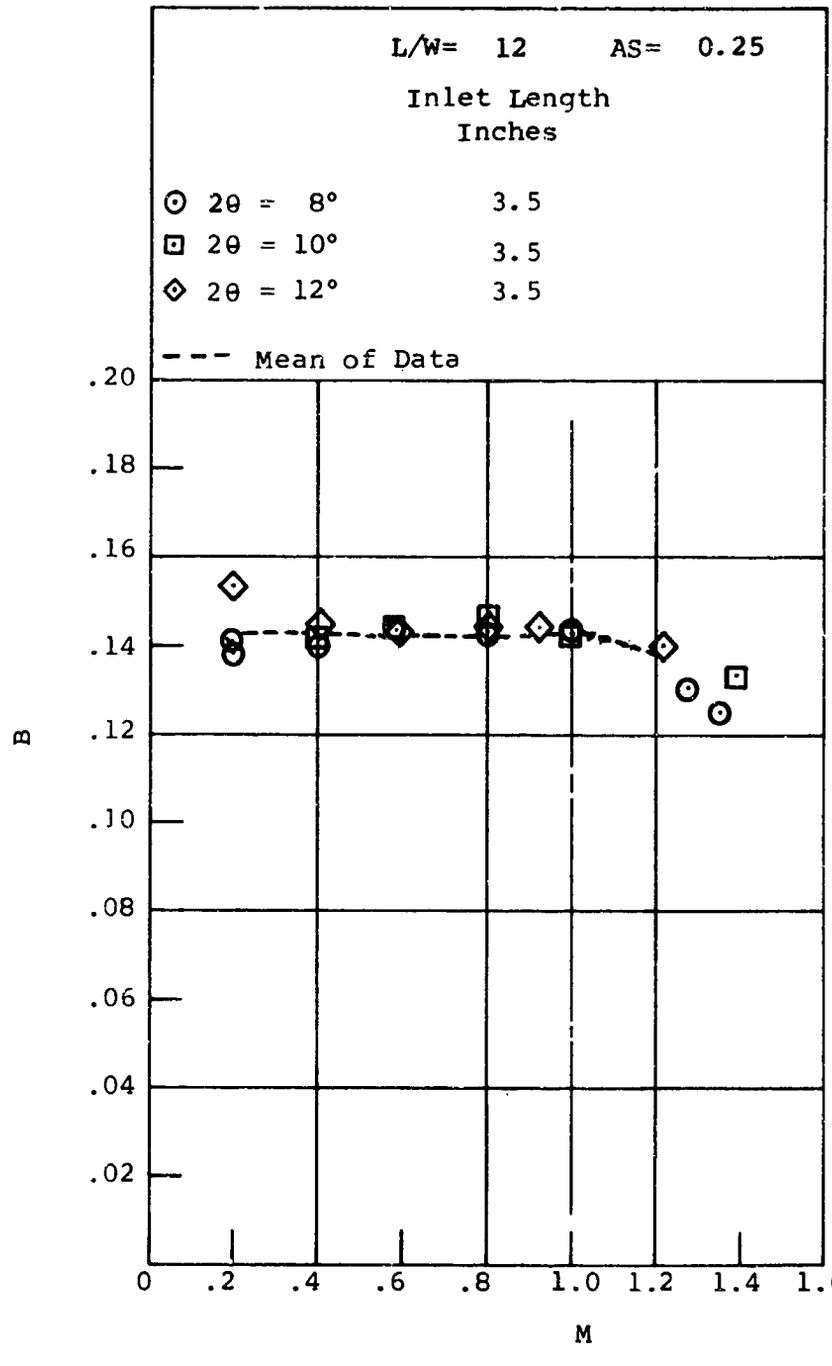

Figure 216. Blockage Versus Mach Number. Shape Factor Studies.

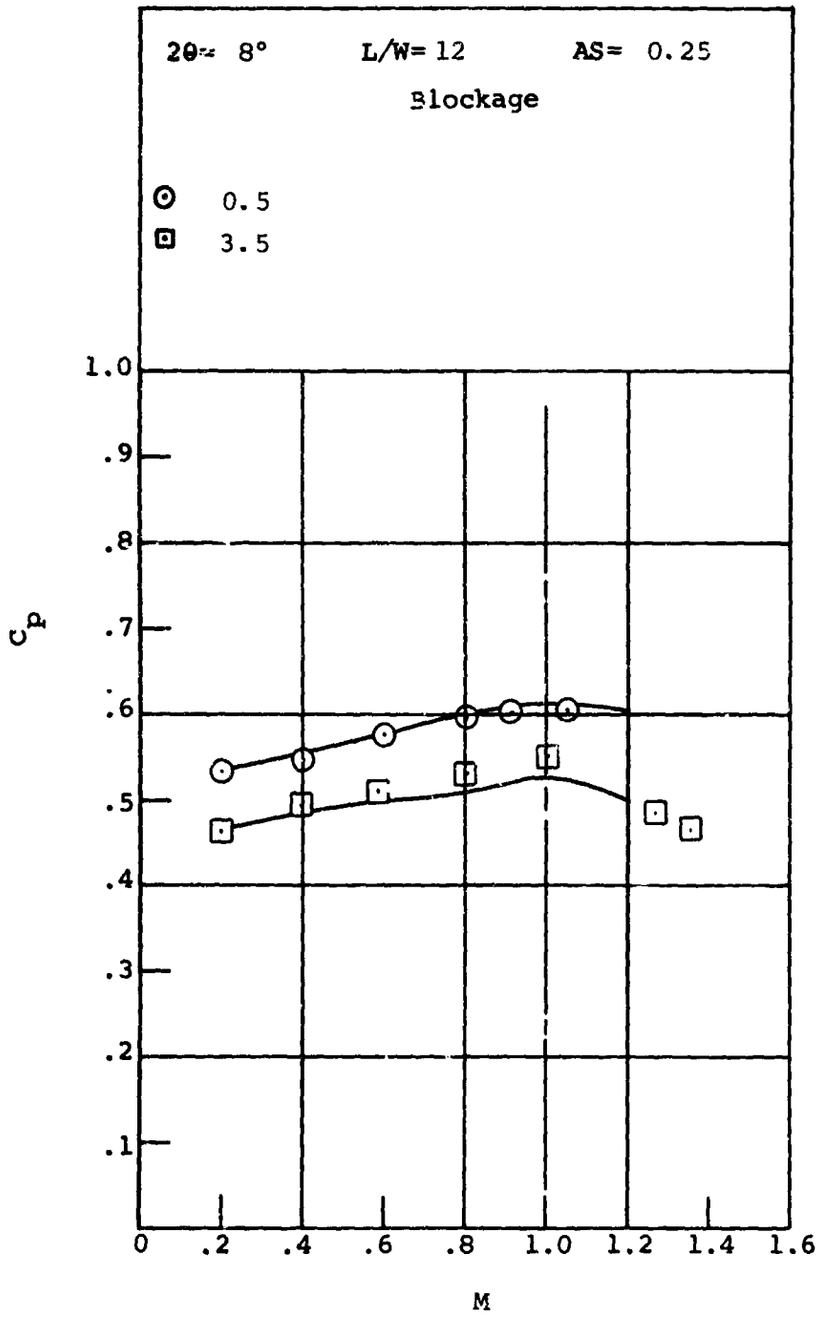

Figure 217. Pressure Recovery Versus Mach Number. Shape Factor Studies.

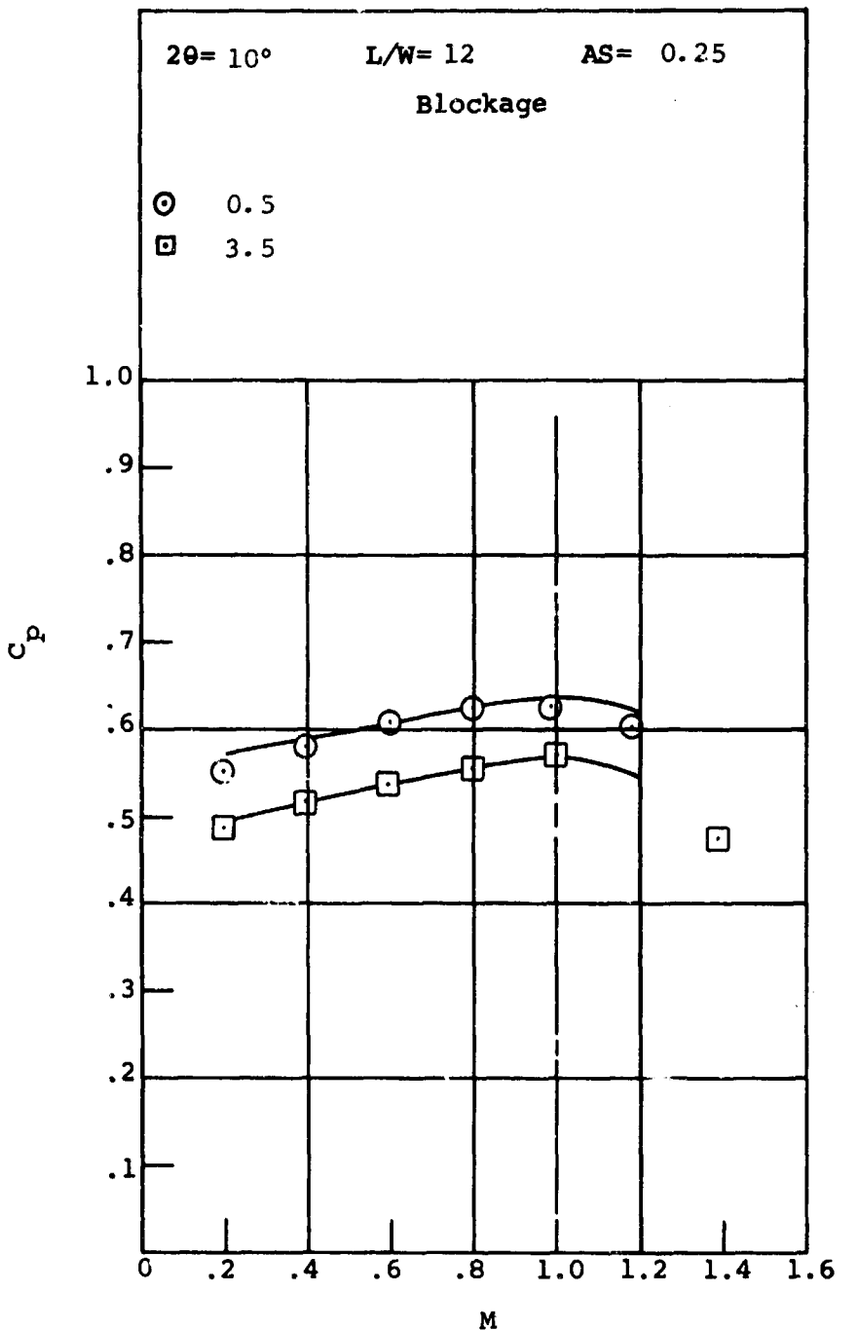

Figure 218. Pressure Recovery Versus Mach Number. Shape Factor Studies.

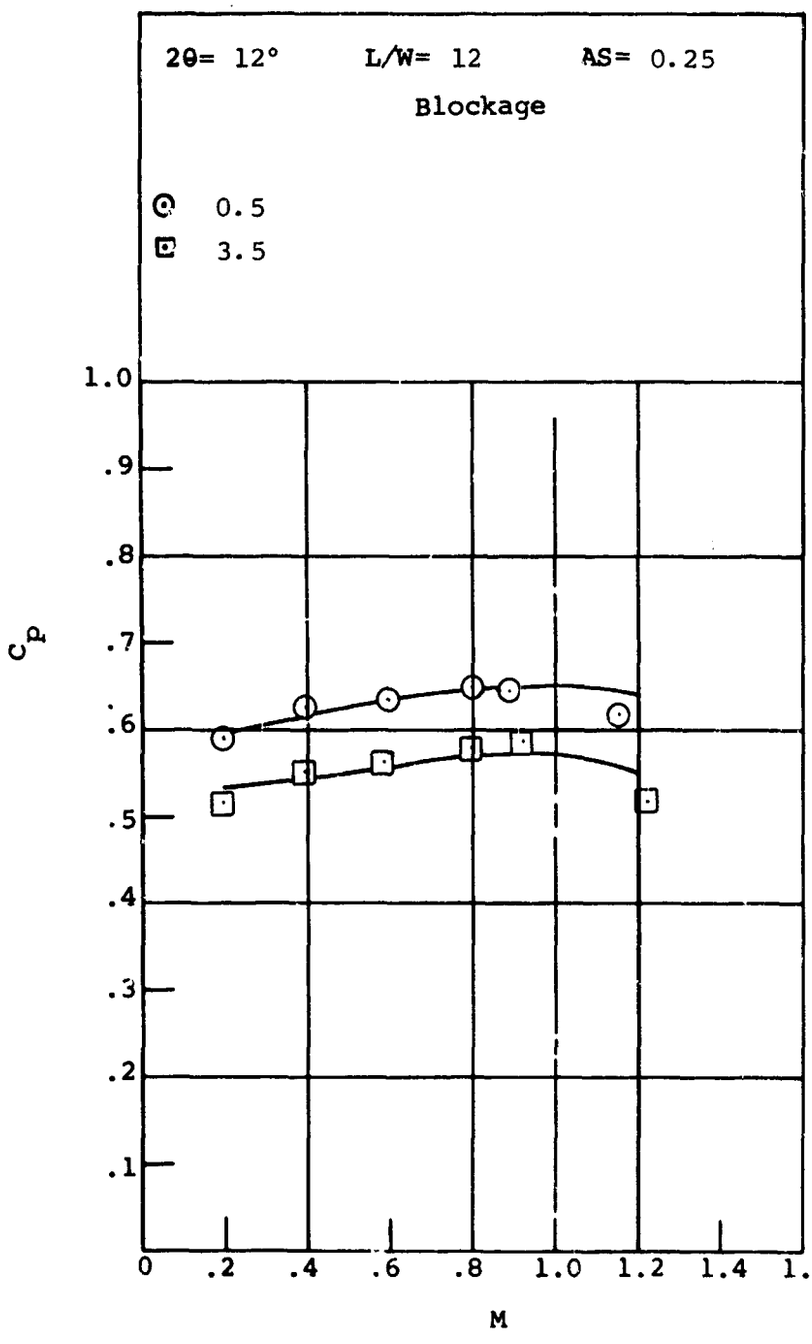

Figure 219. Pressure Recovery Versus Mach Number. Shape Factor Studies.

The 3-inch inlet data indicate a slight increase (1.5 to 2.0 points improvement) in recovery at the higher Mach numbers for $2\theta = 8°$ and 12° only. However, this increase is very slight (this would amount to only 2/3 of a point improvement in overall compressor efficiency for a pressure ratio 10 to 12 compressor) and is not consistent among all three divergence angles tested. If account is taken of the uncertainty in recovery for both the base data and the H-factor data, the difference in pressure recovery is quite small for these tests.

The geometry of the H-factor blocks (Figure 213) may in part explain the high recovery of the H-factor data. The traverse static tube readings showed that the shock ahead of the diffuser at high Mach numbers was located at or near the exit of the diverging portion of the upstream nozzle (Figure 214). Thus, even the highest value of Mach number of 1.3 attained in the inlet occurred about 1-3/4" upstream of the diffuser geometric throat. Even if boundary layer separation occurs because of the high Mach number shock/boundary layer interaction, the boundary layer will reattach and adjust to the accelerating flow conditions in the parallel inlet immediately ahead of the diffuser throat. This reacceleration of the flow immediately ahead of the throat has largely offset the adverse effects on the inlet boundary layer (i.e., pushing the boundary layer more toward separation) developed by the adverse pressure gradients created by the H-factor inlet block geometry. Also, the additional turbulence created immediately outside the boundary layer, if the boundary layer separates after a shock, will help to maintain good diffuser recovery by helping to energize the boundary layer and forestall diffuser separation.

A more conclusive test of the importance of boundary layer shape factor would be obtained if tests as described here were carried out with the exit of the upstream nozzle located very close to the diffuser throat. This would not allow much of a reacceleration of the boundary layer ahead of the throat; it would more truly measure diffuser performance with inlet boundary layers with characteristics closer to separation.

4.7 ASYMMETRIC INLET BLOCKAGE DISTRIBUTION

The boundary layer flow on the sidewalls of the vaneless and semivaneless space of a centrifugal diffuser is subjected to

a radial pressure gradient. The boundary layer has a tendency, because of the inwardly directed radial pressure gradient, to "slide off" the sidewalls and the vane suction surface in the semivaneless space and to move back toward the impeller. This secondary flow "bleeding" of the boundary layers on the sidewalls and vane suction surface results in buildup of boundary layer fluid on the vane pressure surface at the throat of the channel diffuser.* A schematic of the secondary flow behavior in a vane-island diffuser geometry and the resulting distribution of boundary layer thickness δ (and hence blockage) at the diffuser throat is shown in Figure 220.

To simulate this entrance flow behavior in the test channel diffusers, suction was applied to one of the sidewalls of the inlet flow channel. Tests were conducted for aspect ratio = 0.25 and 1.0. Diffuser geometries were studied near peak pressure recovery on the base data diffuser performance maps. In each case, suction was applied to one of the sidewalls that form the diverging walls of the diffuser. Inlet lengths of 1, 6, and 9" (corresponding inlet lengths in the basic studies were 0, 6, and 9") were used to cover the inlet blockage range from approximately .02 to 0.12.

The suction studies include the following geometries:

1) aspect ratio = 0.25
   $L/W_1 = 15$
   $2\theta = 10°, 12°, 14°,$ and $16°$

2) aspect ratio = 1.0
   $L/W_1 = 15$
   $2\theta = 6°, 8°, 10°,$ and $12°$

The three inlet lengths tested for each geometry were chosen to simulate the range of inlet blockage values as were obtained for the base studies without suction. The purpose was to provide the same range of inlet conditions, i.e., inlet blockage and Reynolds number, in order to compare data with and without asymmetric blockage distribution. Because the diffuser blocks are built with a 1/2" run of straight section ahead of the sharp corner of the block, suction on the inlet passage wall actually

*That such flow does indeed occur is supported by measurements of total pressure in a channel diffuser geometry by Welliver and Acurio (1967).

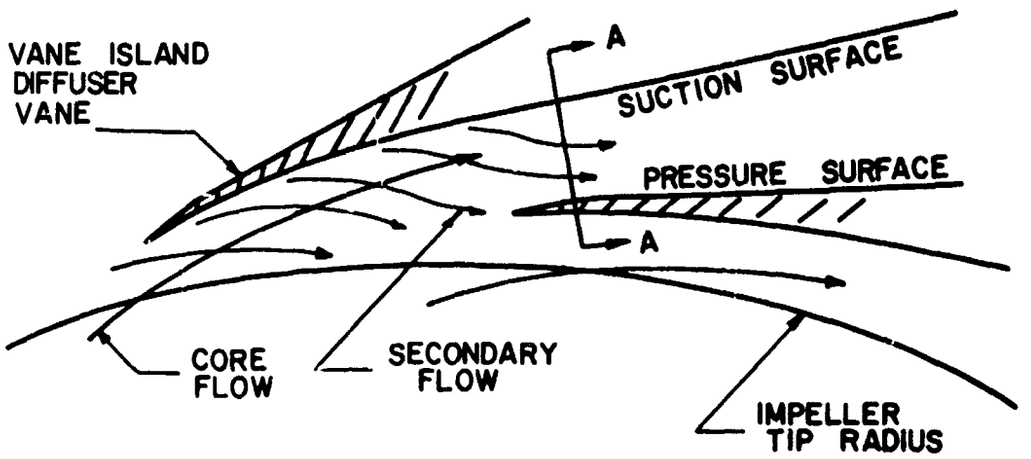

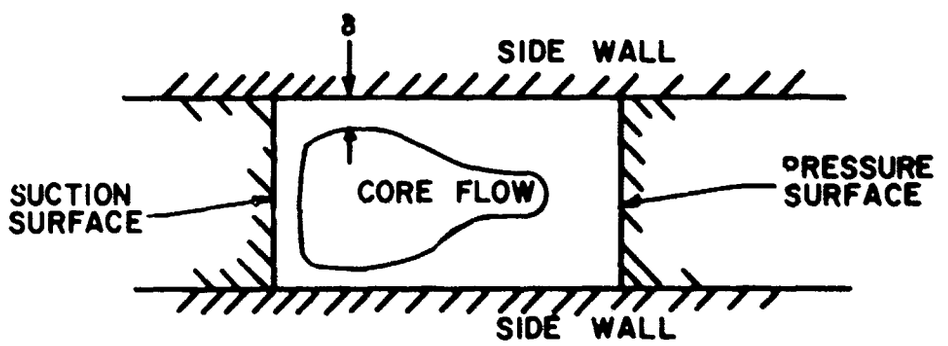

SECTION A-A

Figure 220. Secondary Flow Pattern in Vane-Island Diffuser.

ceases 1/2" upstream of the geometric throat. Because a suction block had to be provided for the smallest inlet length, the shortest inlet length possible was a 1" inlet length (length of the suction block) instead of the 0" inlet length of the base studies.

The inlet blocks (fitting between the sine blocks and the diffuser blocks at the inlet) were a combination of the plain, straight inlet blocks used in the base studies modified to include a 1" suction block on one wall.

The 1" length of suction block has a 3/4" length of porous surface mounted flush with the rest of the inlet channel wall. A suction well is provided behind the porous material and suction is applied to the boundary layer passing over the suction block. The suction flow leaves the test section through a hole in the top plate. A sketch of the suction geometry is shown in Figure 221. The hole between the suction block and the top plate was sealed using O-rings.

The suction surface is made from porous bronze. The bronze is approximately 1/8" thick and has a rather large porosity.* The porous material was epoxied into the suction block on 1/16" wall ledges surrounding the suction well. Although no tests were attempted to determine suction distribution over the suction surface, it is assumed that the porous material thickness and the large suction well provide a quite uniform suction flow rate. Great care was taken in mounting the porous surface to provide a flush and smooth junction between the solid material of the suction block and the porous surface.

The photograph of Figure 222 gives an indication of the porosity and finish of the suction surface.

Suction was applied to the blocks from a point downstream of the flow control valving. This enabled the wind tunnel to be operated as a closed loop unit.

It is common to discuss suction flow rates in terms of the ratio of the normal component of suction velocity at the wall v_o to the stream velocity U_∞ (the stream velocity being the

---

*The material used has the trade name of Poral and was purchased from the Carbone Corporation, Boonton, New Jersey. The porosity is not specified. The material is Poral grade 25.

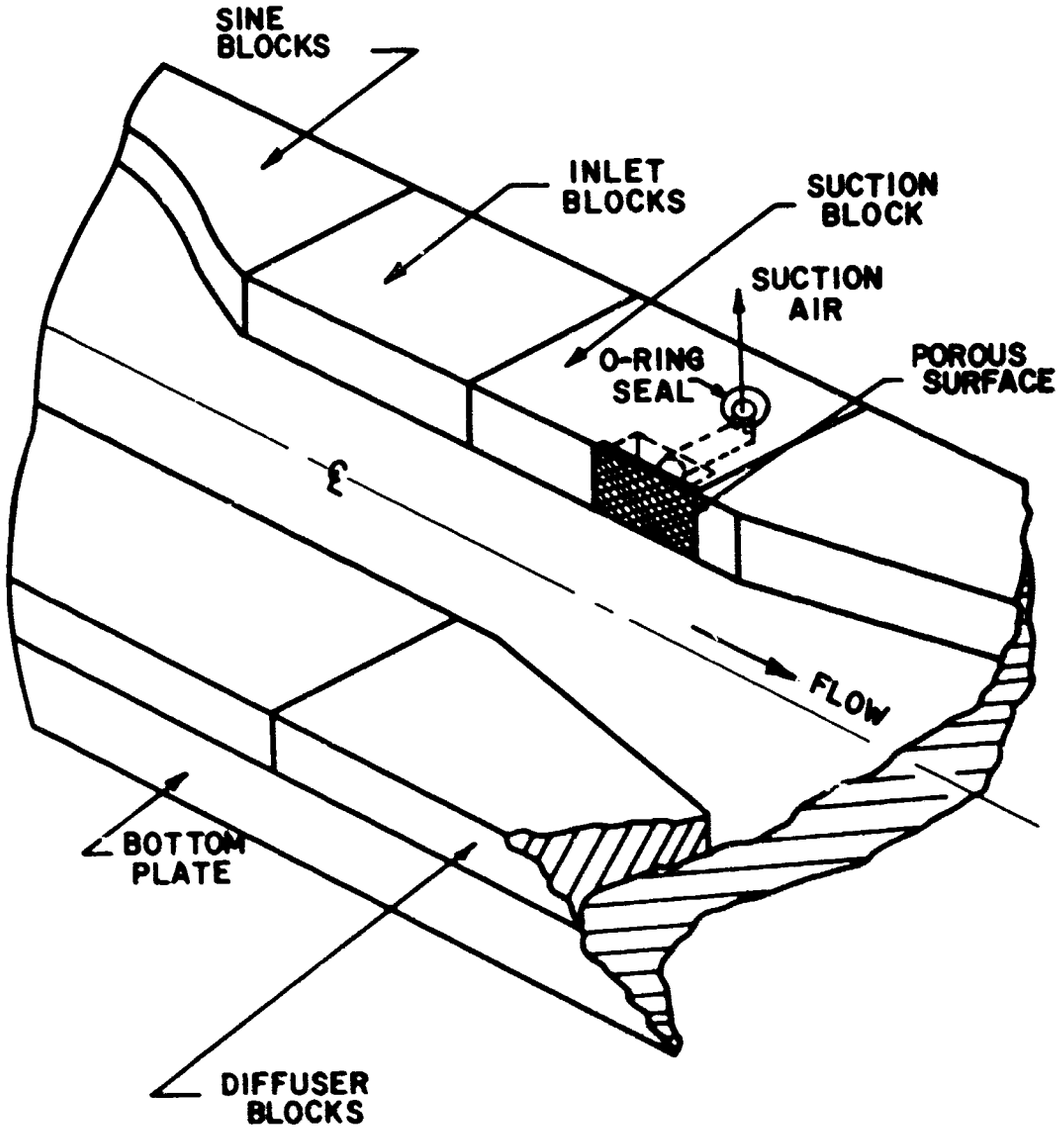

Figure 221. Inlet Channel Suction Geometry.

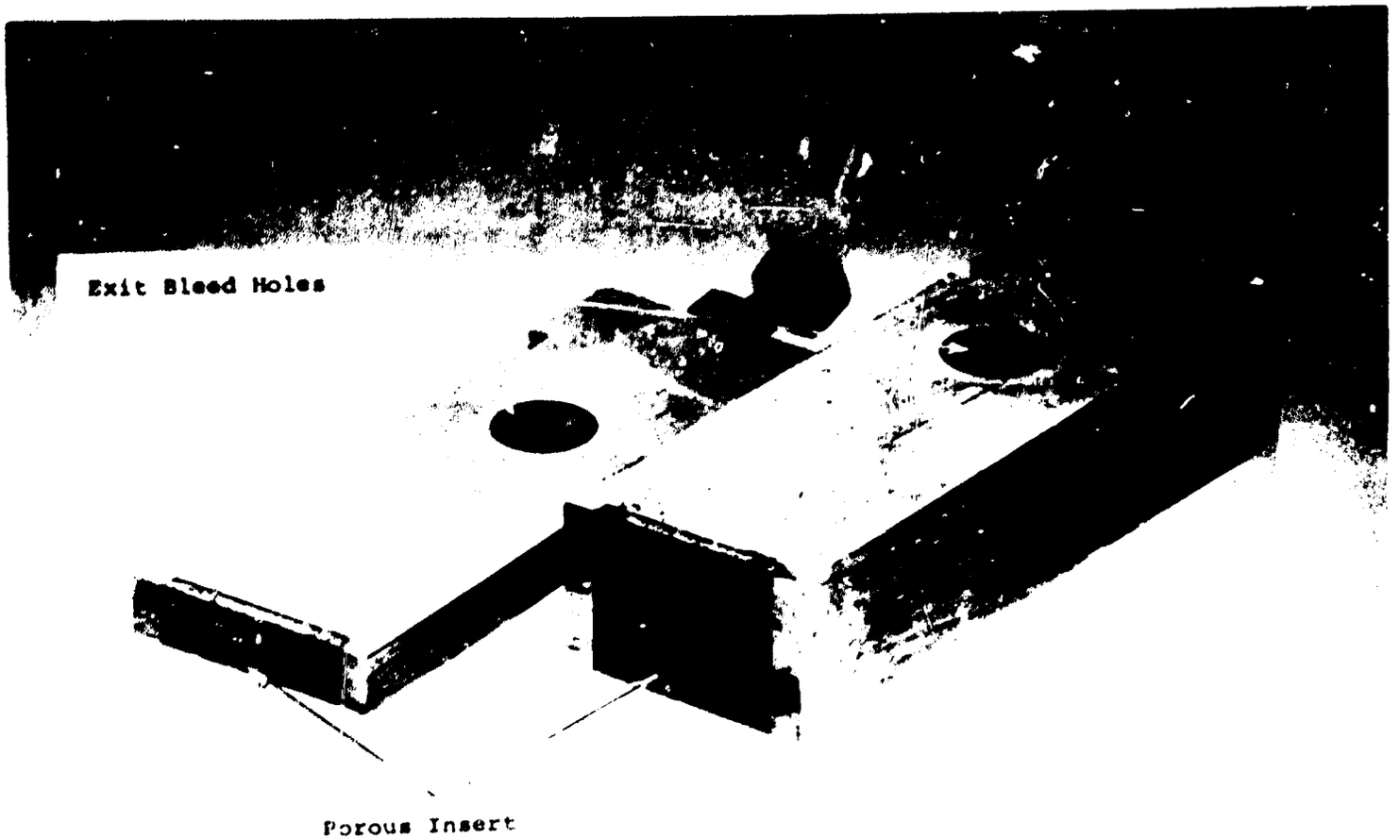

Figure 222. Suction Blocks.

potential flow velocity outside of the boundary layer). Velocity ratios can be quite small and still produce significant effects upon boundary layer characteristics, e.g., $0.0001 < v_o/U_\infty < 0.01$.

Suction data are also sometimes expressed in terms of the rate of fluid removed Q_s and in terms of a volume coefficient C_Q defined as

$$C_Q = \frac{Q}{AU_\infty} \tag{42}$$

where $A = bL$ (denotes the suction area)
b = suction area width
L = suction area length

since

$$Q = b \int_o^{\ell} v_o(x)\, dx \tag{43}$$

$$C_Q = \frac{1}{\ell U_\infty} \int_o^{\ell} v_o(x)\, dx \tag{44}$$

Thus for uniform suction (v_o = constant),

$$C_Q = \frac{v_o \ell}{\ell U_\infty} = \frac{v_o}{U_\infty} \tag{45}$$

Initial experiments were conducted over the range of suction rates $0 \leq C_Q \leq 0.017$. The upper limit on the suction rate corresponds to the removal of about 2% of the total flow through the diffuser. This flow rate corresponds (approximately) to the product of suction wall width, displacement thickness of the boundary layer, and core velocity; e.g.,

$$Q_{s_{max}} = b\delta^* U_\infty \tag{46}$$

This largest suction flow rate has been called the 100% suction rate. Initial tests were conducted for a range of suction rates of 0, 25, 50, 75, and 100% suction. What has here been called 100% suction corresponds to a rather large bleed rate on the boundary layer in terms of boundary layer control technology.

The initial tests covered a range of suction flow rates and showed that a 25% suction rate consistently gave the best pressure recovery performance whenever an increase in performance as a result of boundary layer bleed was observed. Only the 25% suction rate (and the 0% bleed rate for the purpose of providing a base for comparison) was used for about half of the tests.

The 100% suction rate removes an appreciable volume of the low-velocity fluid in the boundary layer near the wall. This low-velocity fluid near the wall must be replaced by higher velocity fluid outside this region as the boundary layer leaves the suction surface. Thus, a decrease in displacement thickness δ^* on the suction wall is achieved relative to the displacement thickness present on the three remaining walls of the inlet channel. If at the end of the suction surface we estimate a new boundary layer displacement thickness based on the profile approaching the suction surface minus the portion of the profile which has been sucked away, the ratio of displacement thickness leaving the suction surface to that approaching it (and hence approximately the ratio of the displacement thickness on the suction wall surface to the displacement thickness on the other channel walls) is approximately 0.54 for 100% suction. Measurements were not made of the velocity profiles in the boundary layer leaving the suction surface; hence a direct measurement of the distribution of blockage around the throat periphery was not obtained. However, the alteration in displacement thickness on the suction wall should produce blockage conditions similar to those observed in actual centrifugal compressor diffusers.

In discussing the suction data, the following terms will be used. The original data taken prior to these studies without suction will be denoted as the "base" data. Data taken to replicate the original "base" data during these studies are called the "solid wall" data. Any data taken with the suction blocks in place are denoted as the "porous wall" data and are described by the amount of suction used, e.g., by 0, 25, 50%, etc.

The 25% suction data for all the geometries studied have very close to the same throat blockage B for the same throat Mach number M_t as the original base data. Apparently the reason for this is that although the blockage should be reduced by the effect of suction on the one wall, the change in the pressure gradient distribution through the suction block region reduces the amount of acceleration present in the inlet channel and causes the boundary layers on the remaining three walls to grow more rapidly. The reduction in blockage by suction is nearly balanced by the increase in blockage due to the less favorable pressure gradient in the suction block region on the remaining boundary layers.

Comparison of Bleed Data and Base Data

A comparison of the measured blockage as a function of Mach number for the three inlet lengths (1, 6, and 9") for the aspect ratio = 1.0 geometry is shown in Figures 223 through 228. Blockage data for aspect ratio = 0.25 and 1, 3, and 6" inlet lengths are shown in Figures 229 through 234. In these plots, the solid lines represent the average of the base data and the bars around the solid lines represent the estimate of the uncertainty in measurement of base data blockage at each Mach number. The dashed lines are the mean of the porous wall data at 0% bleed rate. For the 1" inlet length, there are no base data available since the base data were taken with a 0" inlet length.

Blockage measurements for the porous wall data were very repeatable. However, the porous wall data lie largely above the uncertainty limits of the base data, although the mean value has the same trend with Mach number. Thus, the blockage values for the porous wall data, with or without suction, are higher than the values obtained for the base data.

There are two effects which can account for this increased blockage for the porous wall data taken under otherwise similar conditions (i.e. zero bleed) as the base data. First, instead of a smooth inlet wall upstream of the diffuser, a porous, "rough" wall of 3/4" length in the flow direction has been used. This surface provides a hydraulically "rough" surface on which an increase in the growth of the boundary layer greater than that which occurs over a smooth wall can occur.

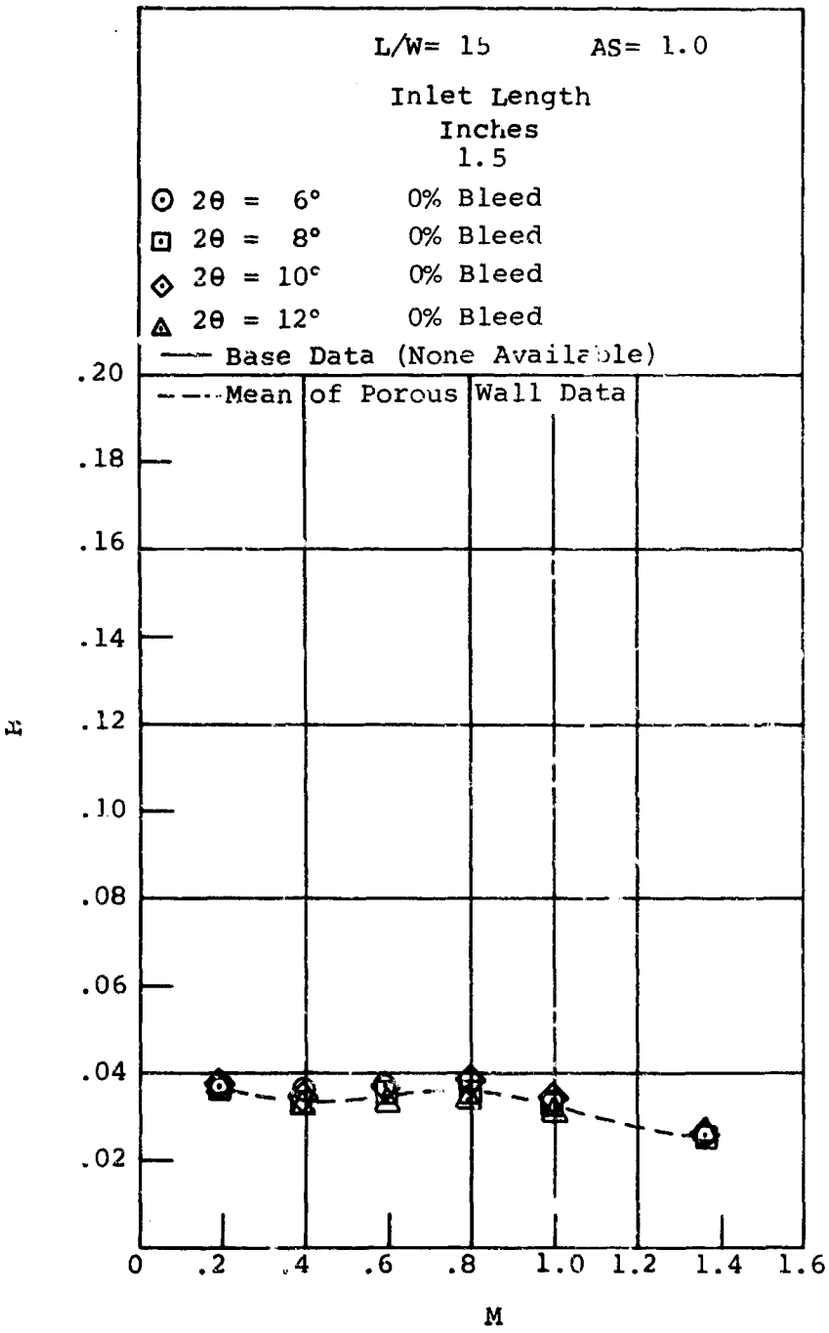

Figure 223. Blockage Versus Mach Number. Aspect Ratio = 1.0. Asymmetric Blockage Distribution Studies.

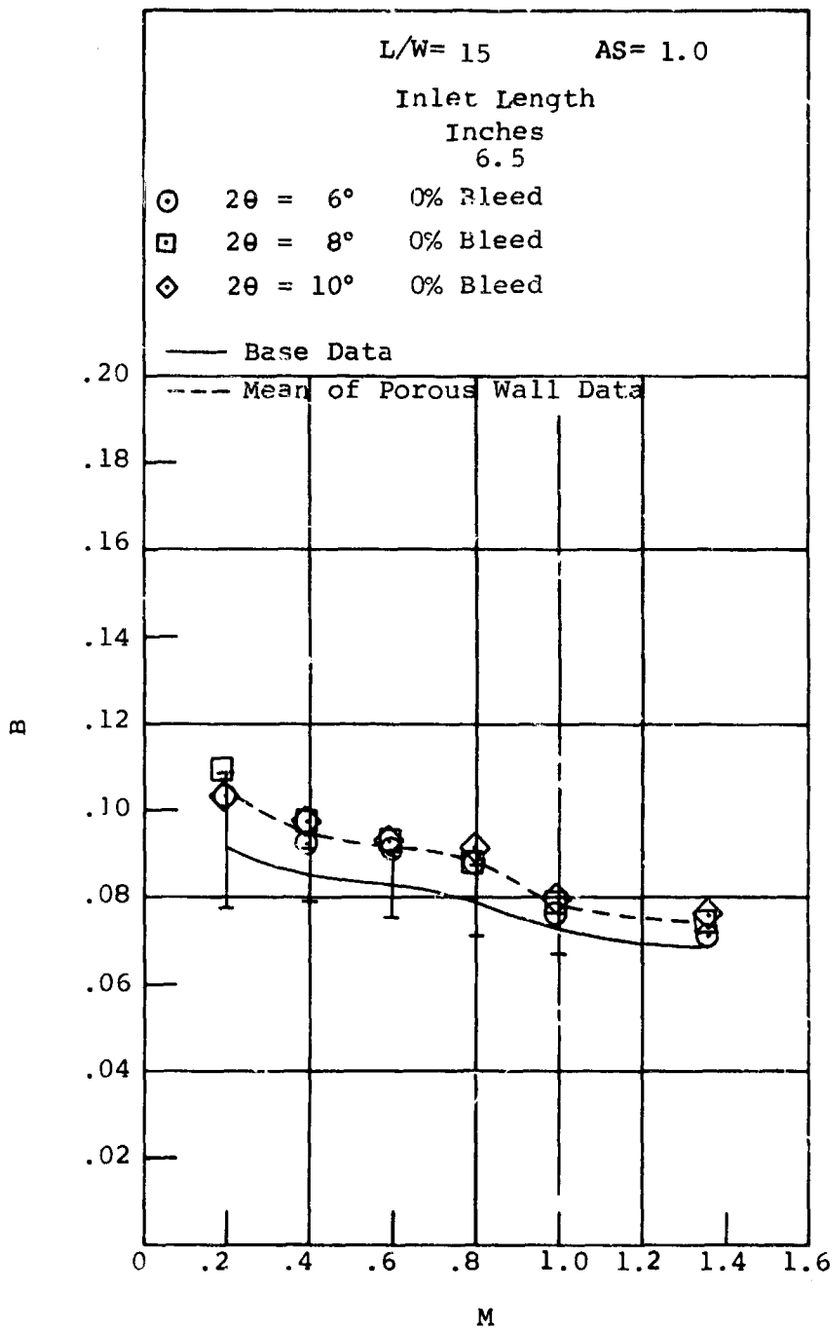

Figure 224. Blockage Versus Mach Number. Aspect Ratio = 1.0. Asymmetric Blockage Distribution Studies.

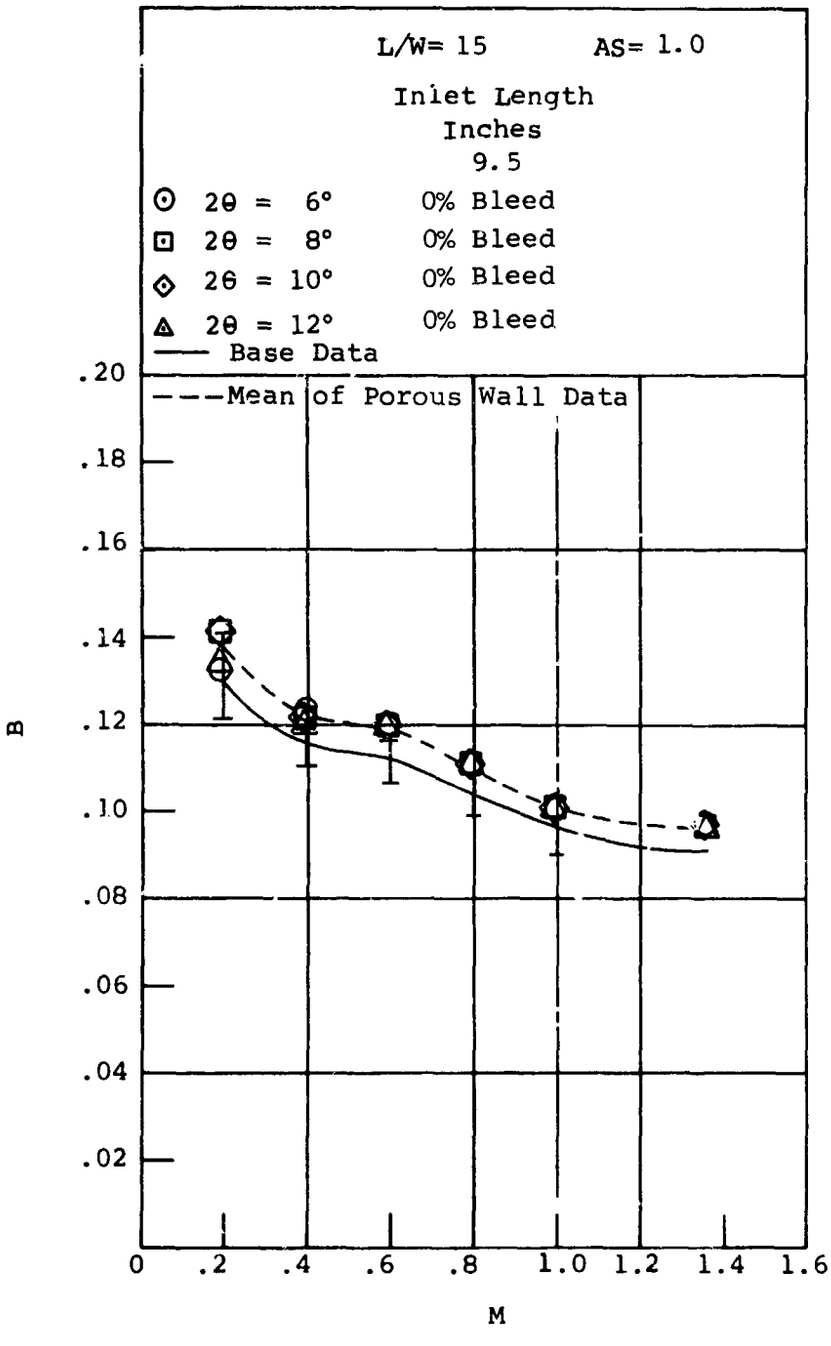

Figure 225. Blockage Versus Mach Number. Aspect Ratio = 1.0. Asymmetric Blockage Distribution Studies.

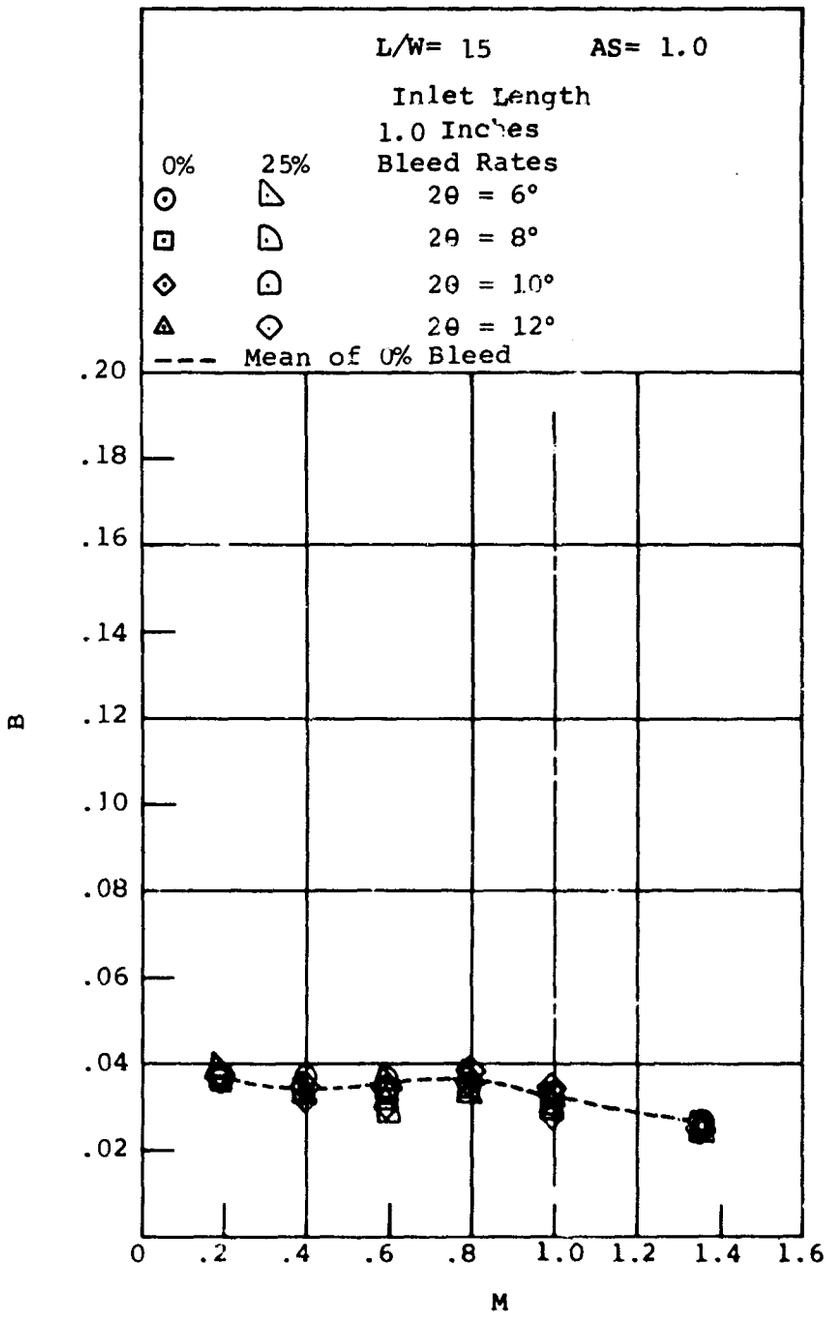

Figure 226. Blockage Versus Mach Number. Aspect Ratio = 1.0. Asymmetric Blockage Distribution Studies.

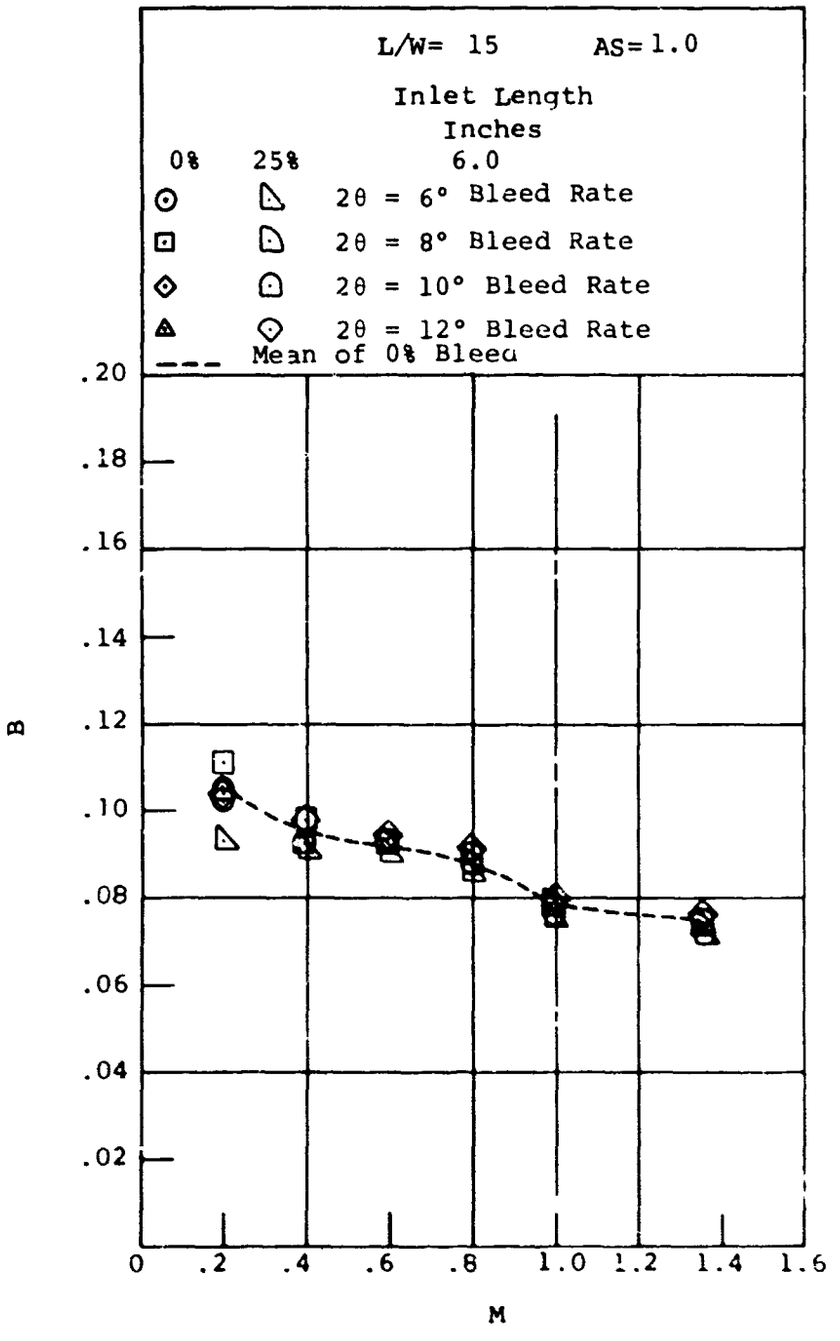

Figure 227. Blockage Versus Mach Number. Aspect Ratio = 1.0. Asymmetric Blockage Distribution Studies.

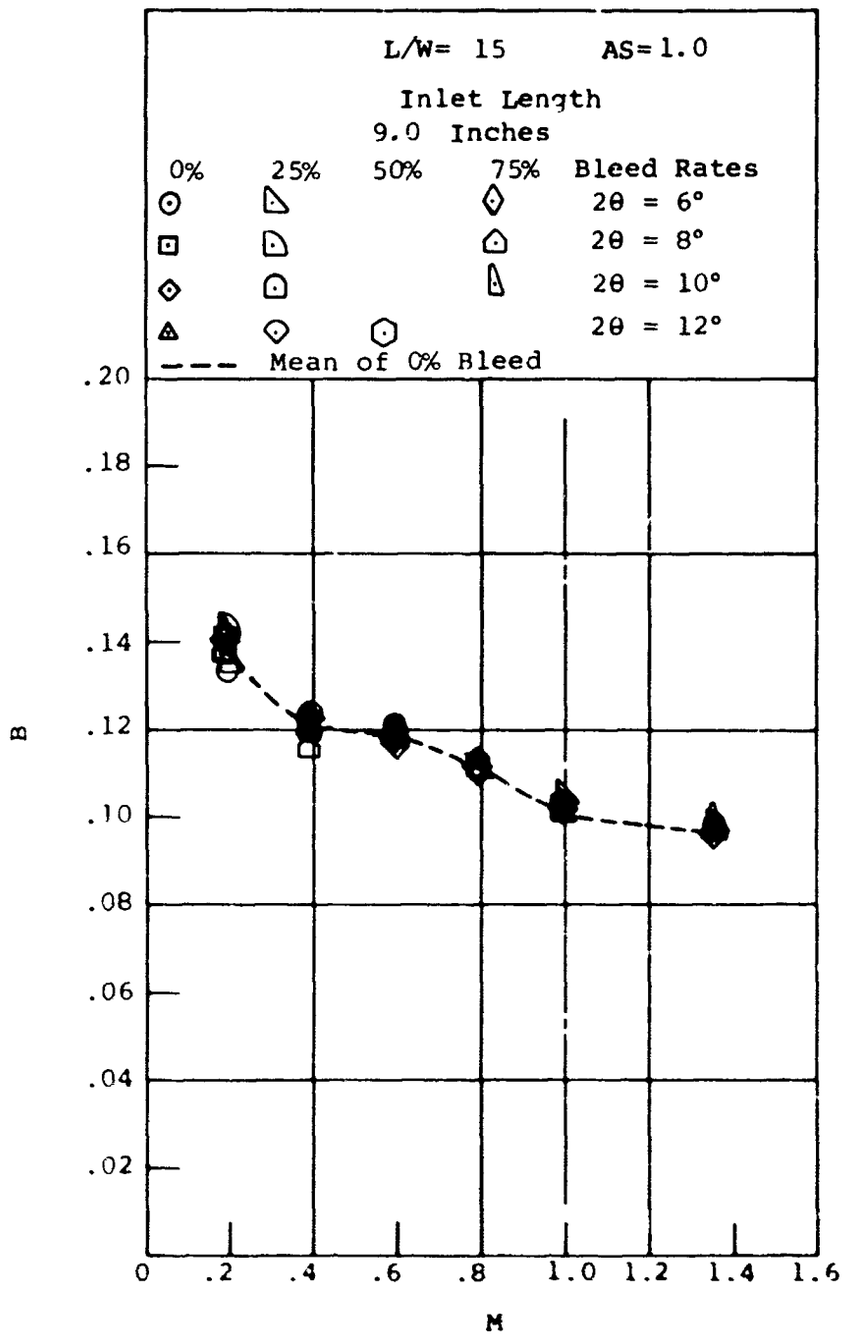

Figure 228. Blockage Versus Mach Number. Aspect Ratio = 1.0. Asymmetric Blockage Distribution Studies.

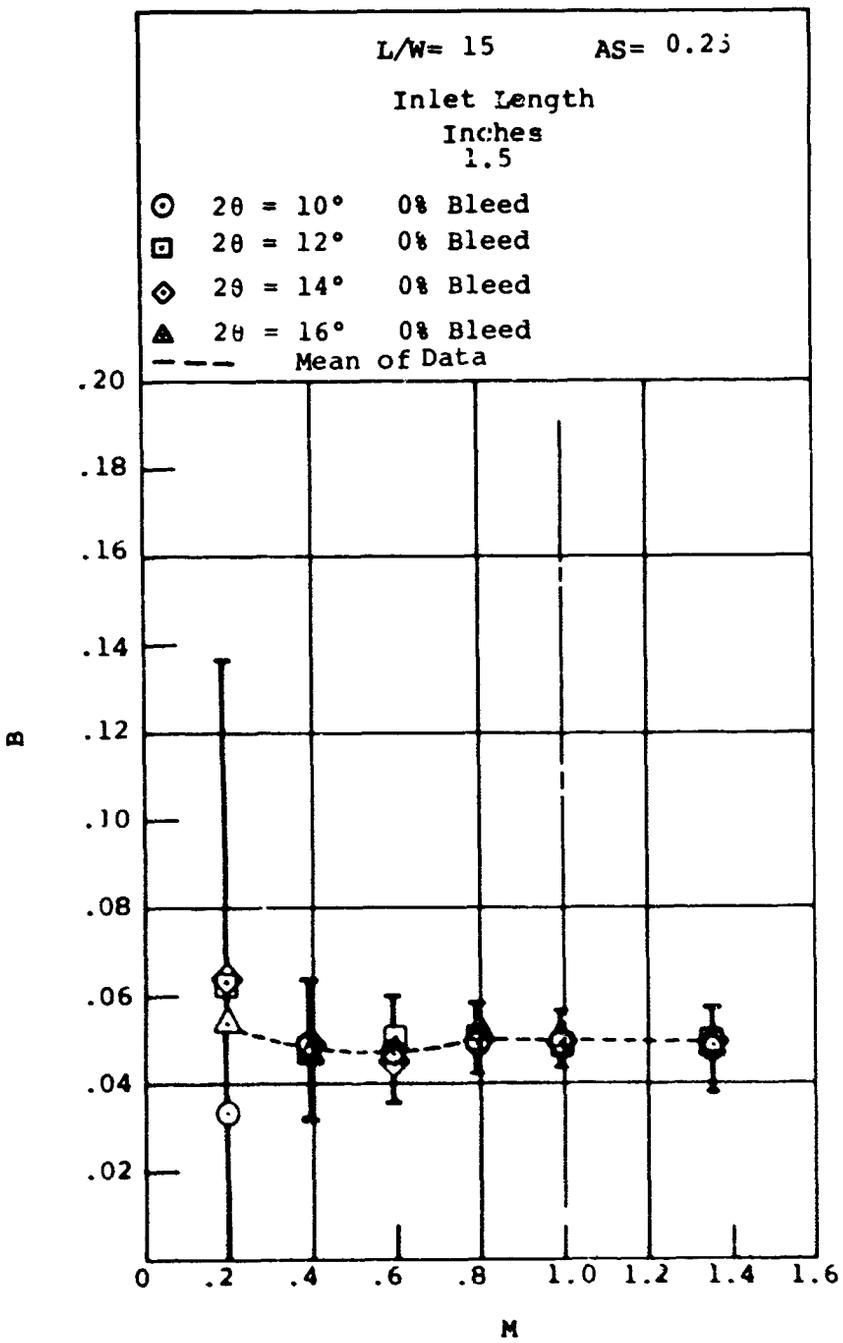

Figure 229. Blockage Versus Mach Number. Aspect Ratio = 0.25. Asymmetric Blockage Distribution Studies.

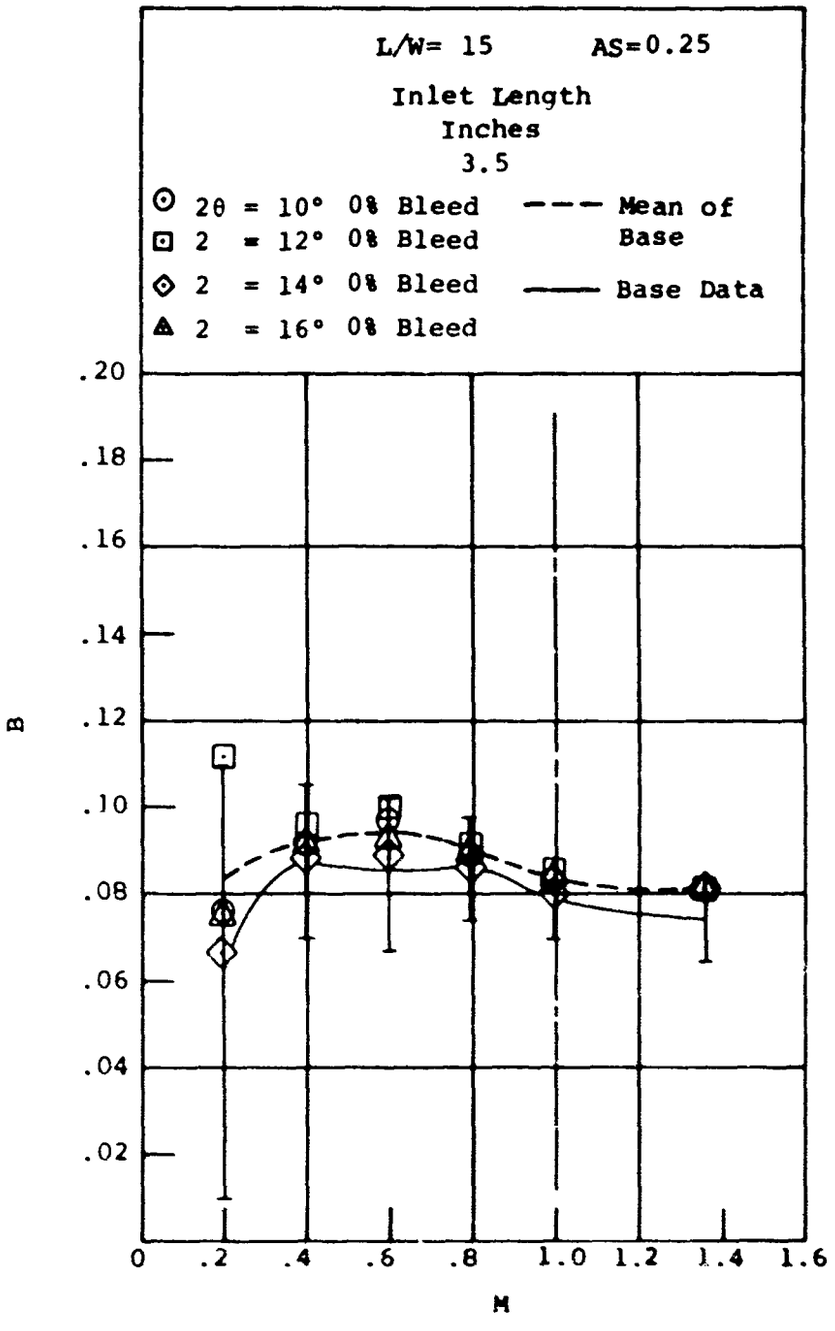

Figure 230. Blockage Versus Mach Number. Aspect Ratio = 0.25. Asymmetric Blockage Distribution Studies.

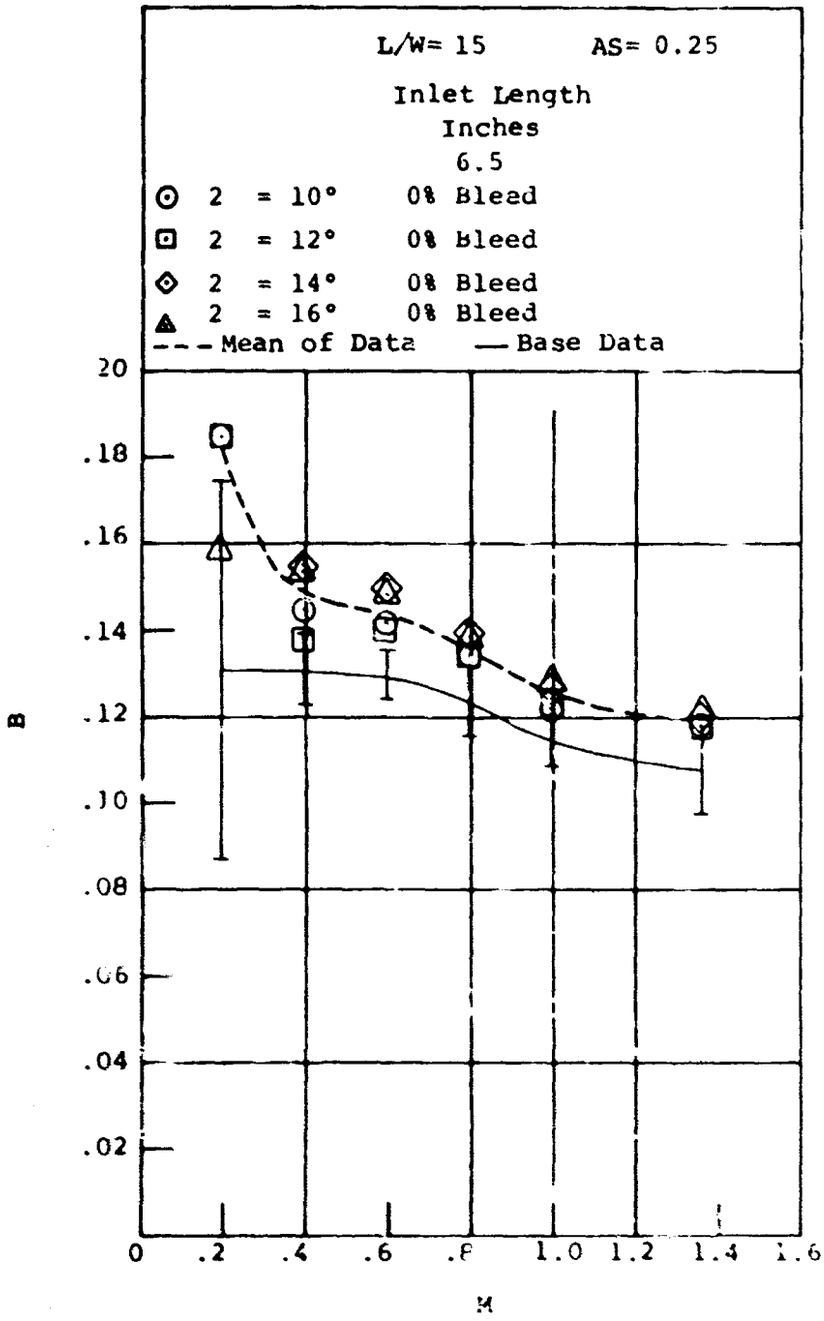

Figure 231. Blockage Versus Mach Number. Aspect Ratio = 0.25. Asymmetric Blockage Distribution Studies.

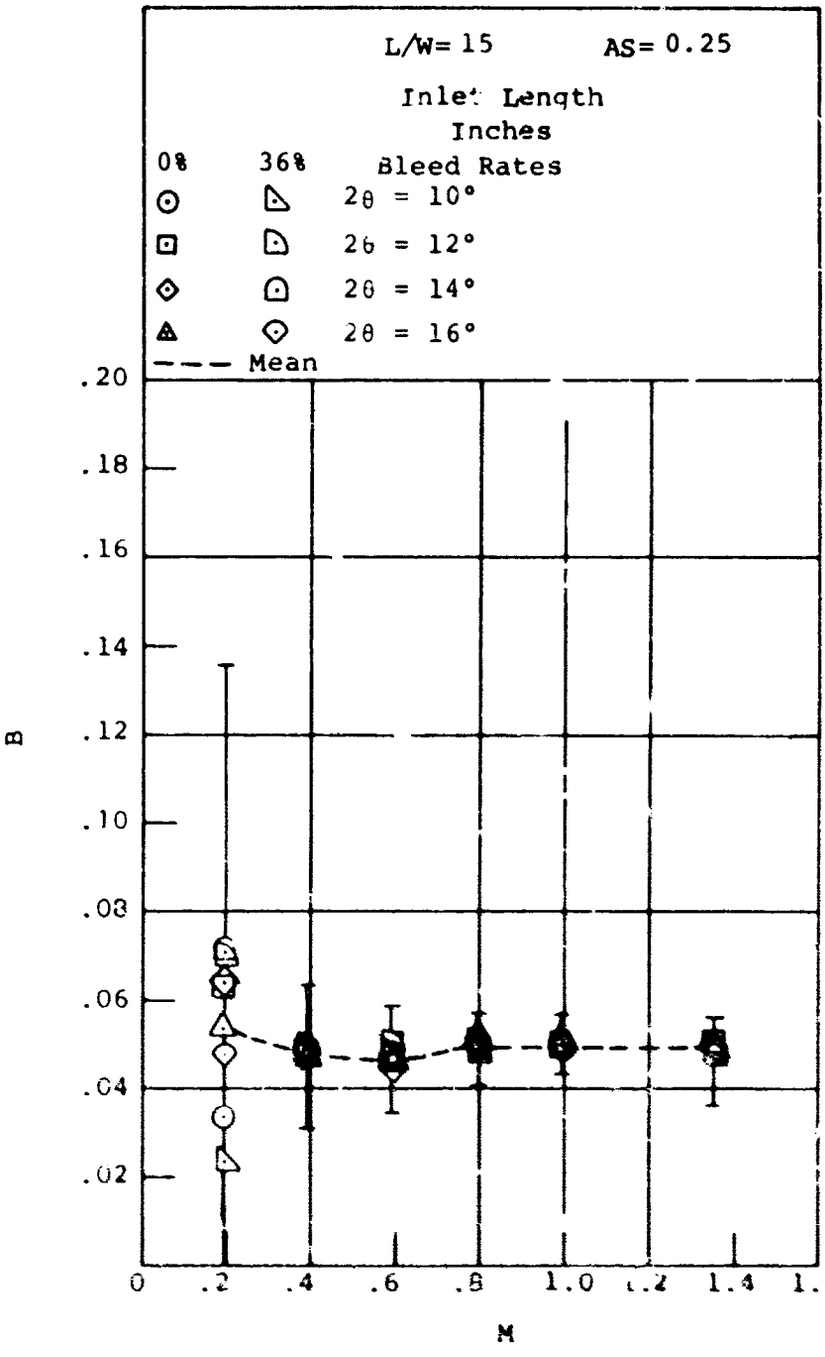

Figure 232. Blockage Versus Mach Number. Aspect Ratio = 0.25. Asymmetric Blockage Distribution Studies.

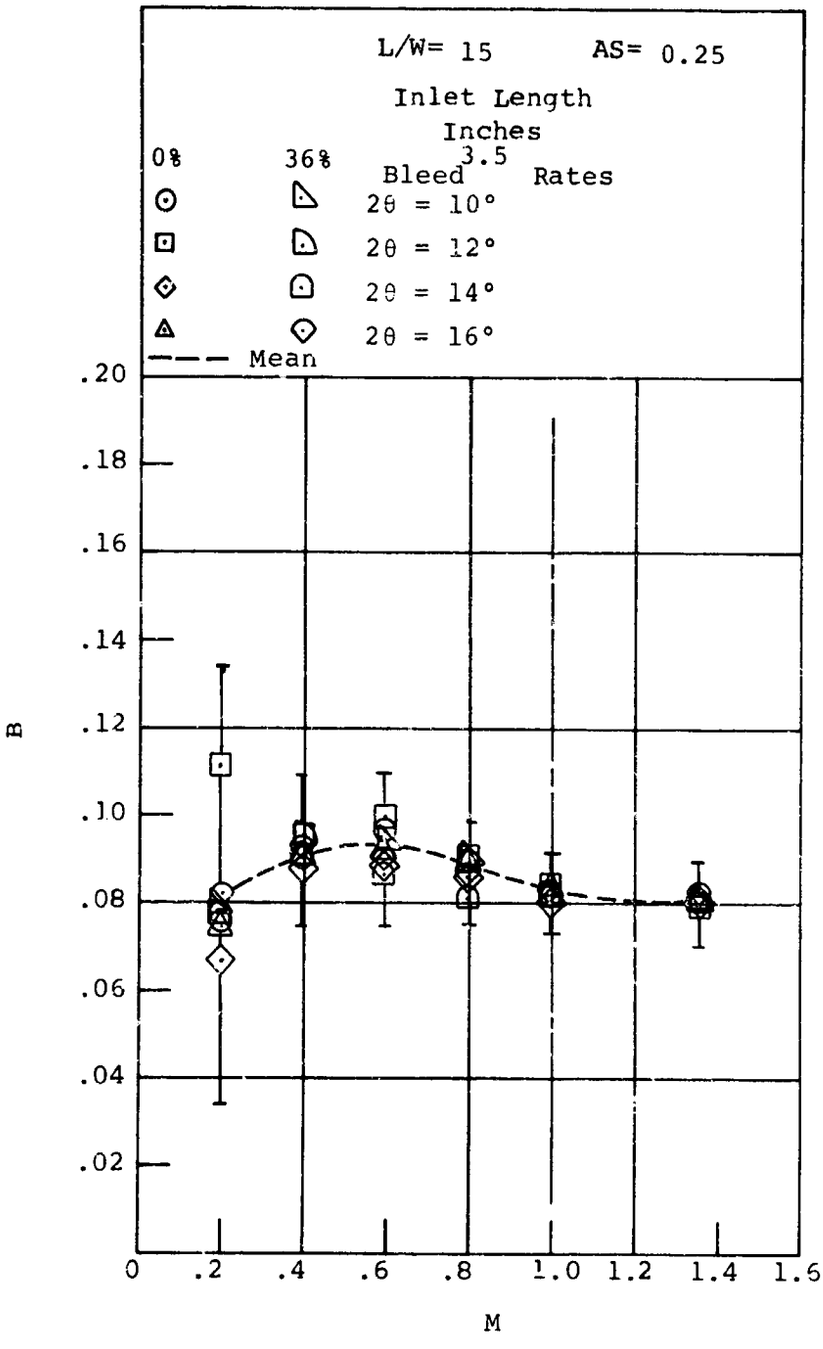

Figure 233. Blockage Versus Mach Number. Aspect Ratio = 0.25. Asymmetric Blockage Distribution Studies.

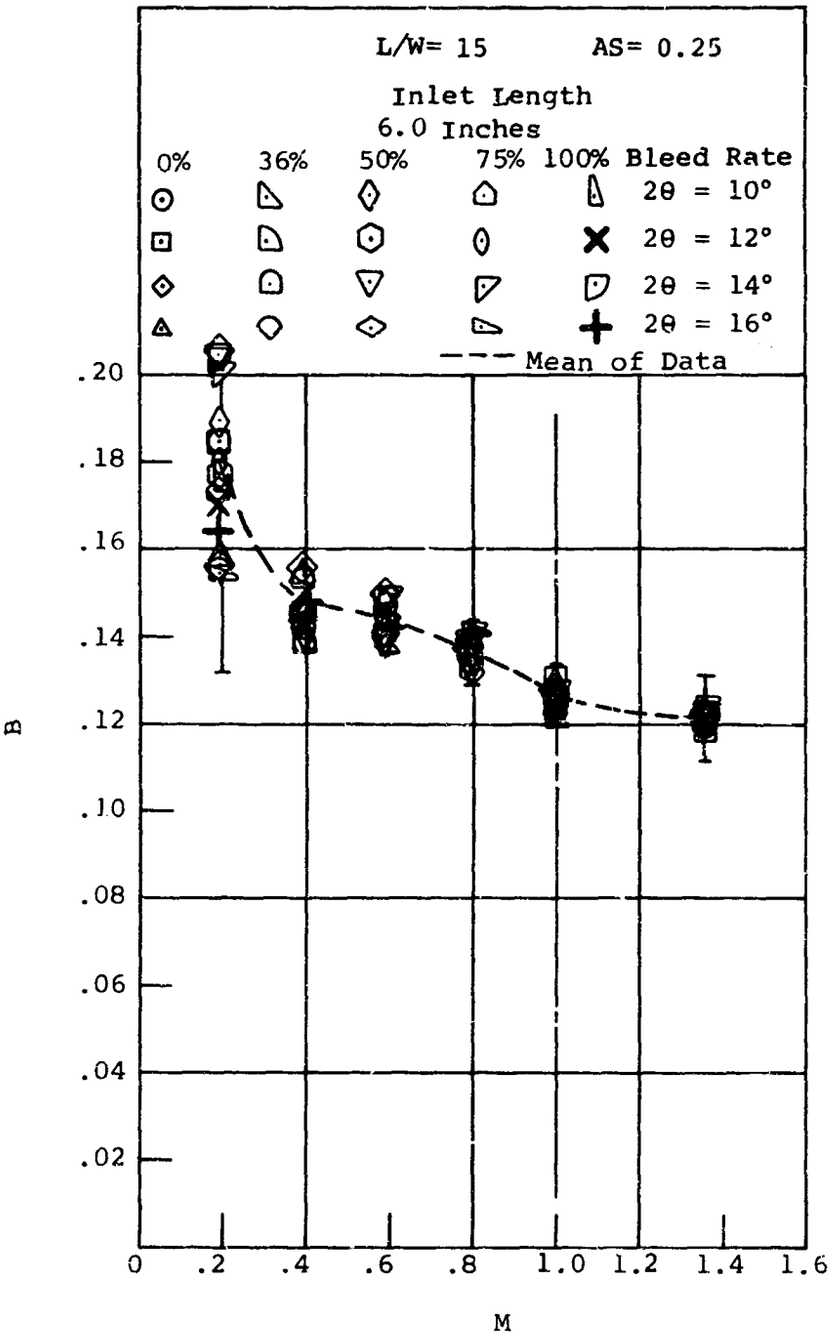

Figure 234. Blockage Versus Mach Number. Aspect Ratio = 0.25. Asymmetric Blockage Distribution Studies.

Secondly, and perhaps more importantly, the base data studies have shown that there are rather large pressure fluctuations at the throat of the diffuser under most test conditions. However, in the base studies these fluctuations, when altered substantially in magnitude, produced no influence on either the measured blockage or pressure recovery performance. In the case of the porous wall experiments, the corresponding pressure fluctuations can cause movement of air in and out through the porous wall section even under zero bleed conditions. This could have the effect of producing an increased relative "roughness" of the inlet porous wall surface. Thus, the increased roughness of the porous surface from both of these effects should produce an increase in boundary layer growth, and hence throat blockage, as observed.

A comparison of the pressure recovery performance of the porous wall data (using the mean values of the blockage data at 0% bleed) with the base data (at the same blockage) is shown in Figures 235 through 238 for 2θ = 6°, 8°, 10°, and 12° and aspect ratio = 1.0. Figures 239 through 247 show the same type of data for AS = 0.25 and 2θ = 14°, 12°, and 10°. In most cases, the measured pressure recovery with the porous wall at 0% bleed is slightly higher than the corresponding base data. A general trend between the 0% bleed rate data and the base data is observed as divergence angle is changed. At the smallest angles studied, the difference between recovery is small or nonexistent. At the larger angles, however, the 0% bleed recovery falls below the base data at high Mach numbers. The reason for this is not entirely understood.

One might expect that the porous wall data at 0% bleed, when compared under the same blockage conditions, should agree with the base data. However, the effects of a porous wall section on the boundary layer as described above may alter the boundary layer characteristics sufficiently to change the recovery as observed. Indeed, slight changes in boundary layer characteristics (e.g., changes in inlet Reynolds number as discussed in 4.5) have been observed to alter the diffuser recovery from that found in the base data studies. It does not seem unreasonable that such effects may be occurring with the porous wall 0% bleed data because of increased hydraulic "roughness" effects. Such effects would be expected to produce an increased turbulence intensity level within the boundary layer

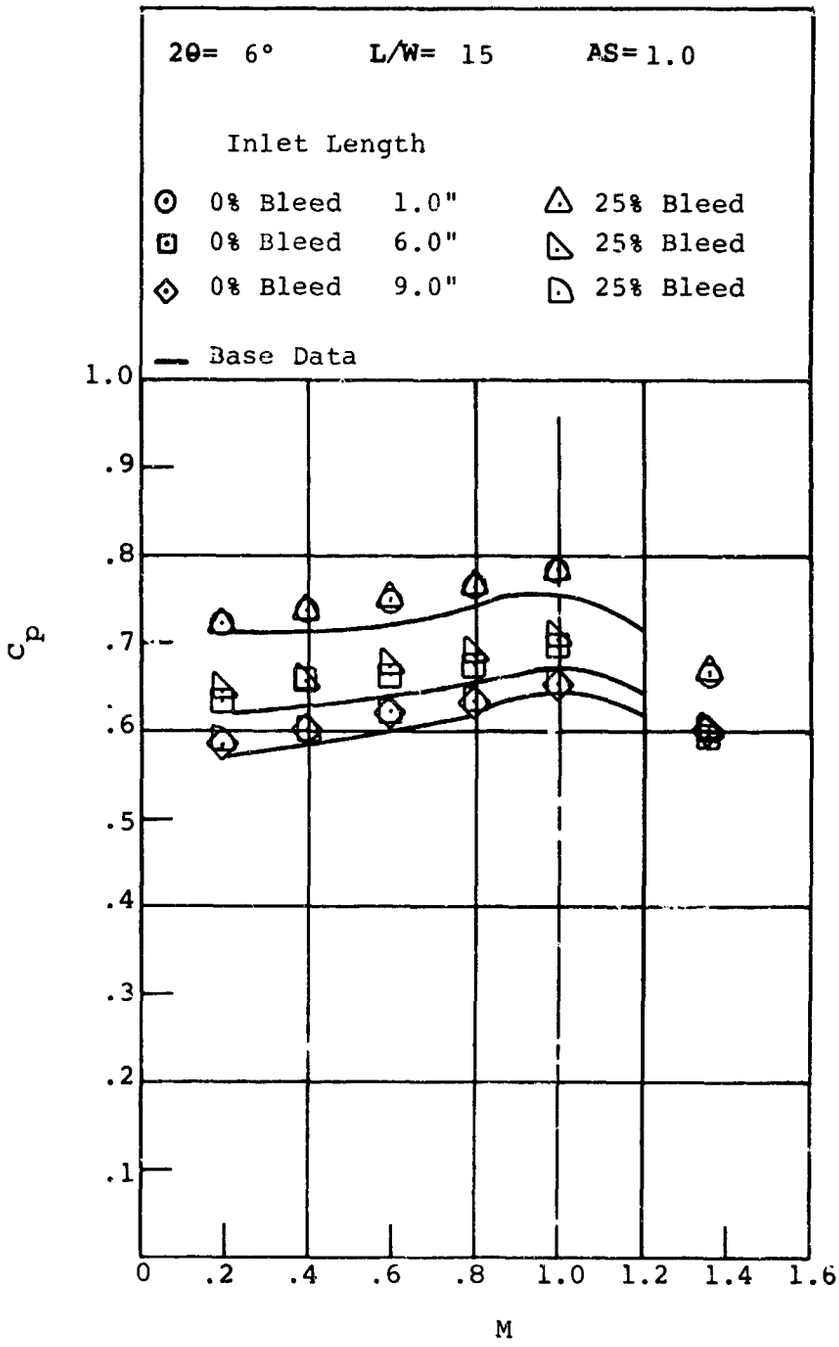

Figure 235. Pressure Recovery Versus Mach Number. Aspect Ratio = 1.0. Asymmetric Blockage Distribution Studies.

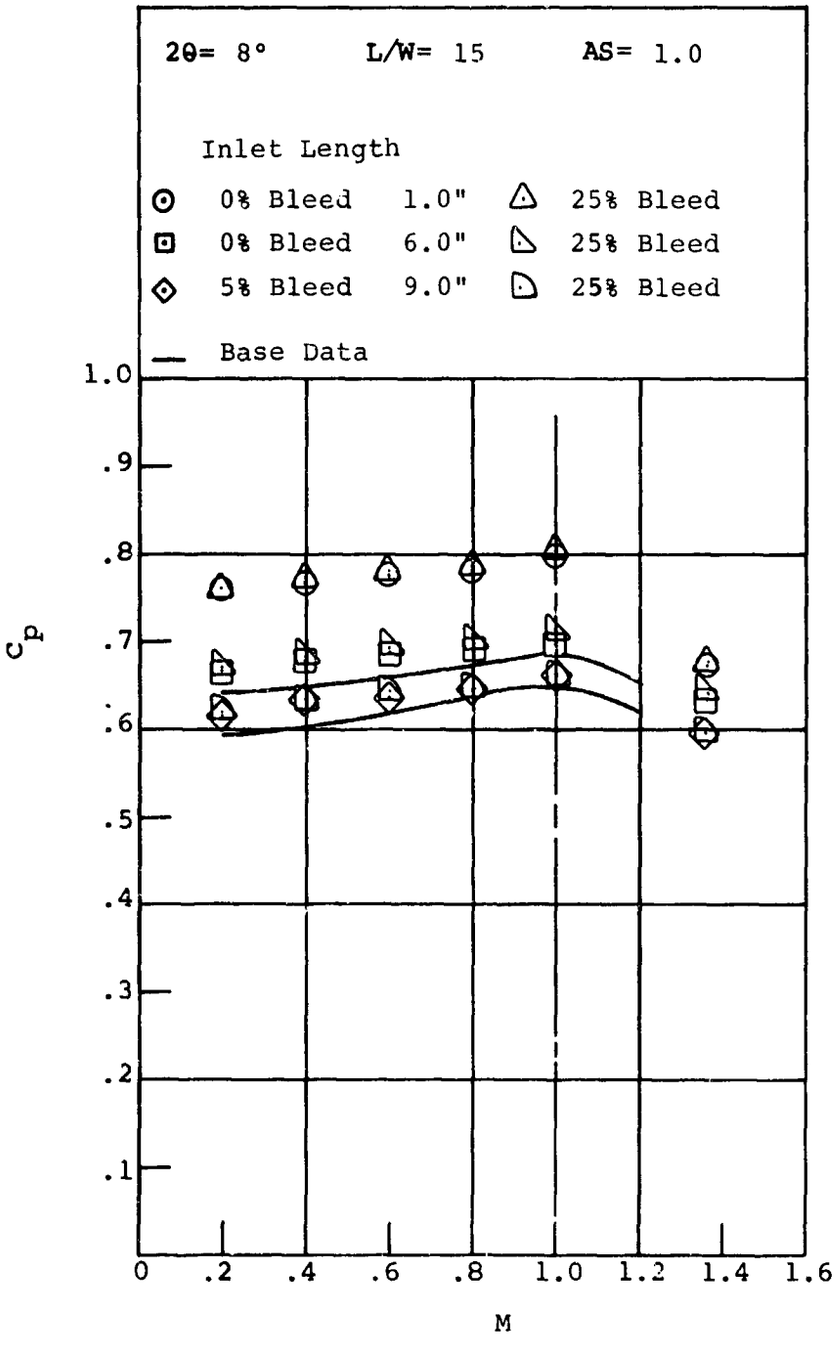

Figure 236. Pressure Recovery Versus Mach Number. Aspect Ratio = 1.0. Asymmetric Blockage Distribution Studies.

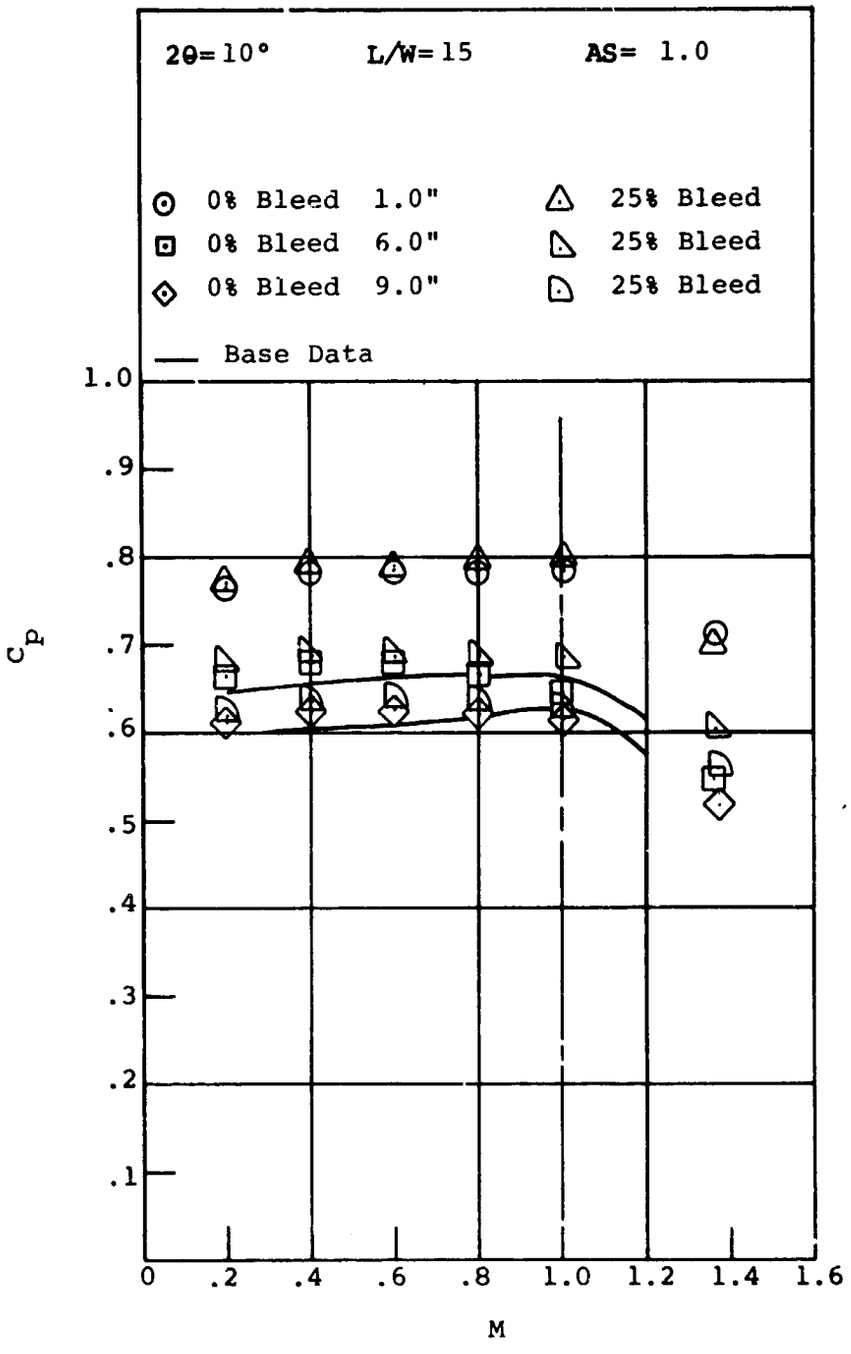

Figure 237. Pressure Recovery Versus Mach Number. Aspect Ratio = 1.0. Asymmetric Blockage Distribution Studies.

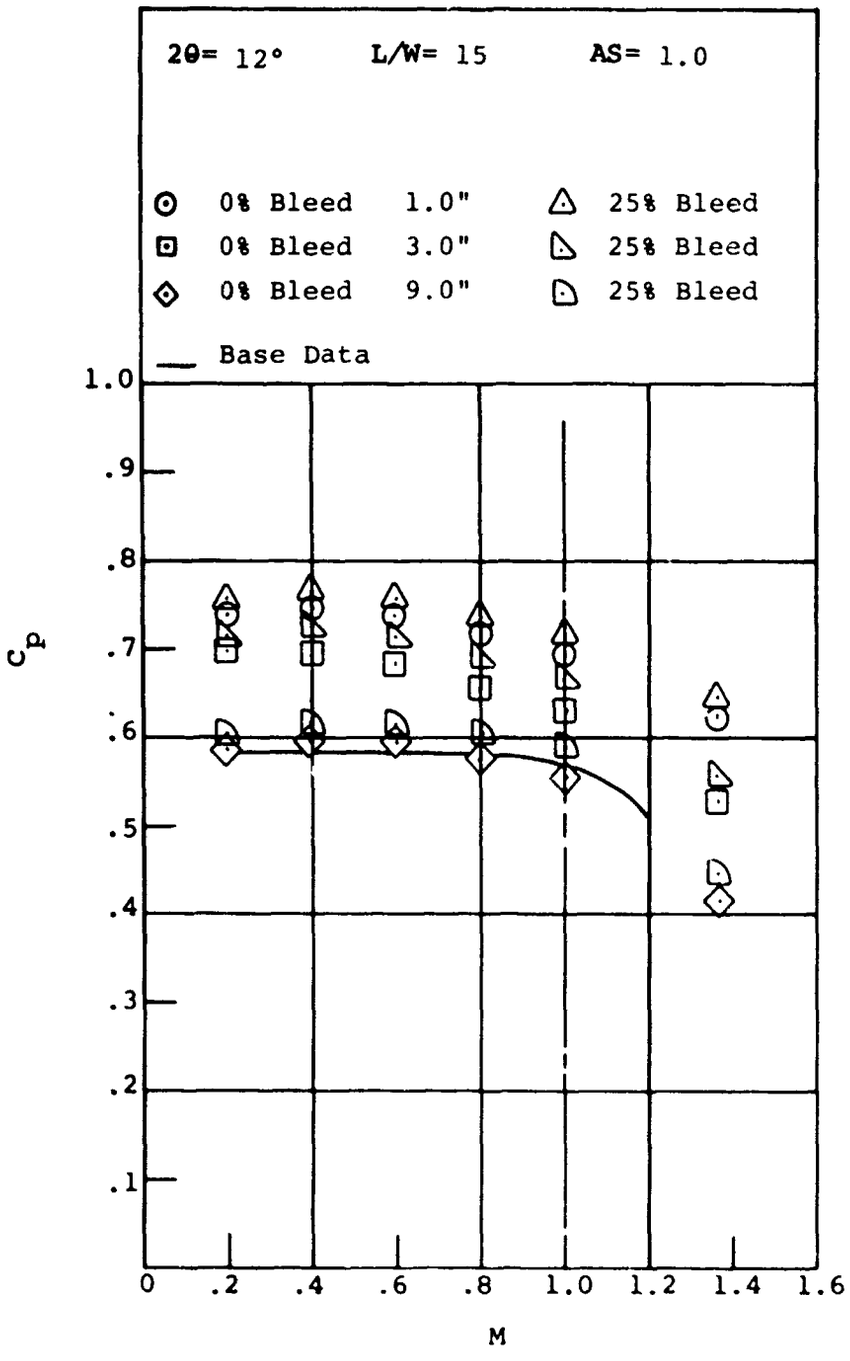

Figure 238. Pressure Recovery Versus Mach Number. Aspect Ratio = 1.0. Asymmetric Blockage Distribution Studies.

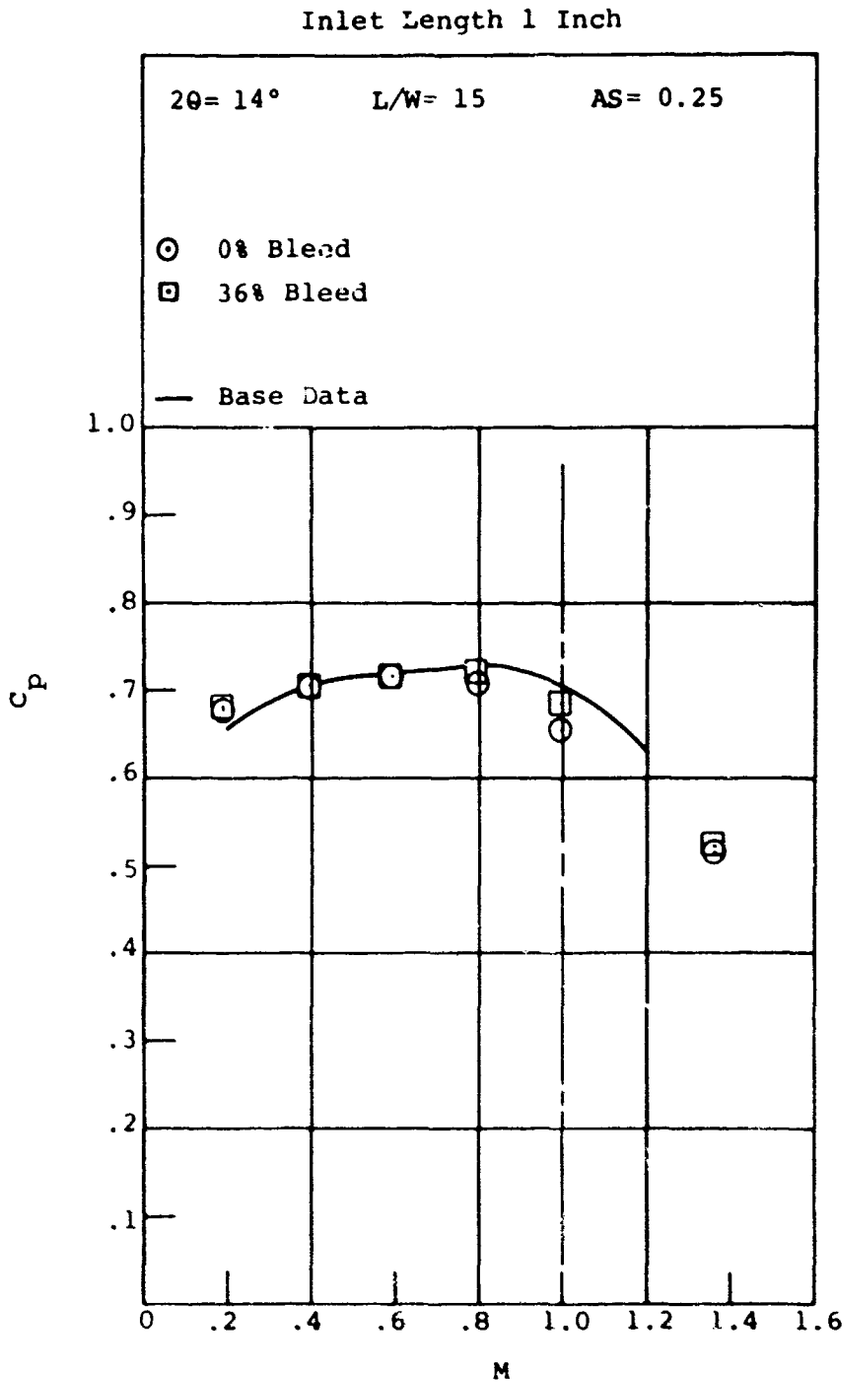

Figure 239. Pressure Recovery Versus Mach Number. Aspect Ratio = 0.25. Asymmetric Blockage Distribution Studies.

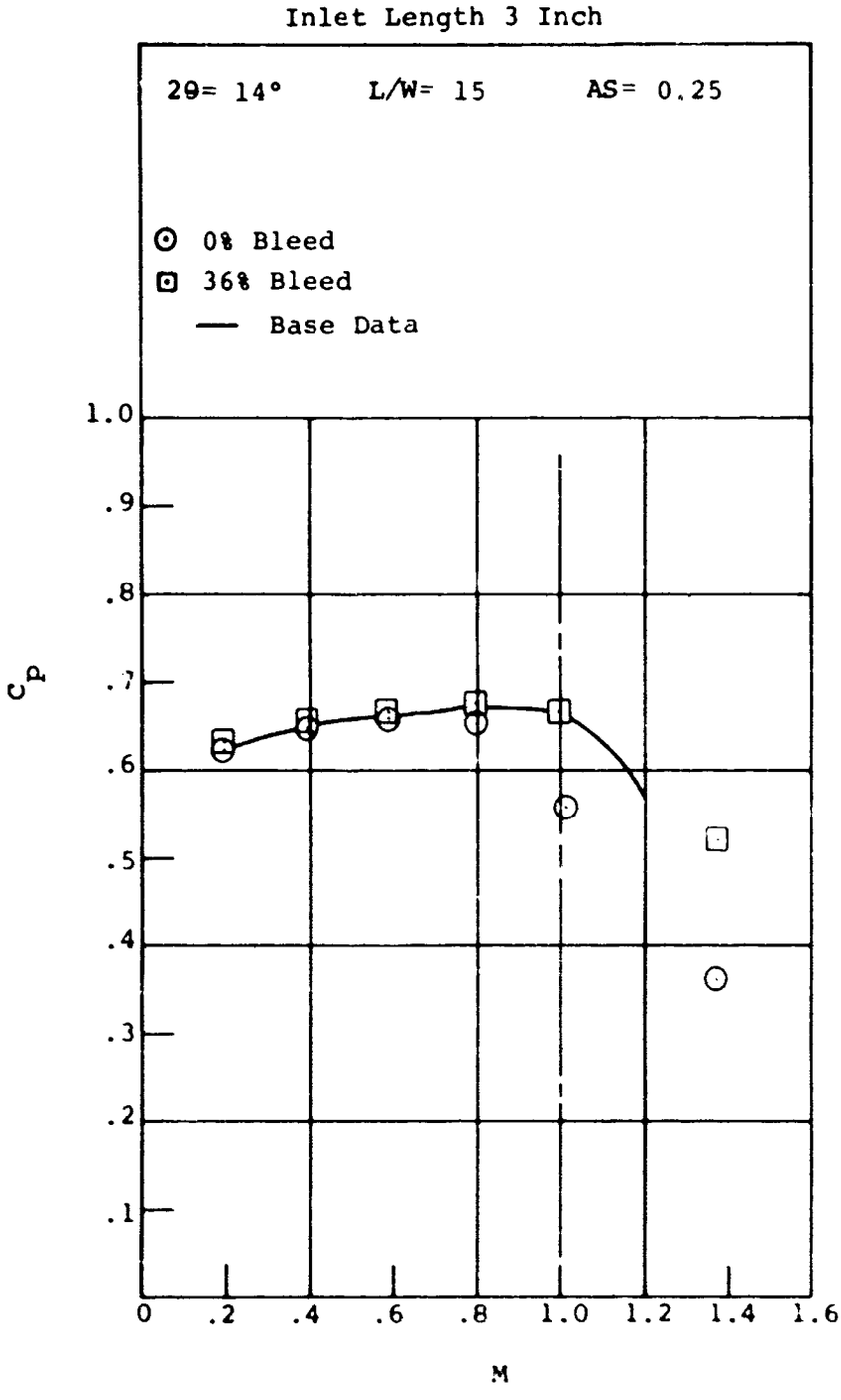

Figure 240. Pressure Recovery Versus Mach Number. Aspect Ratio = 0.25. Asymmetric Blockage Distribution Studies.

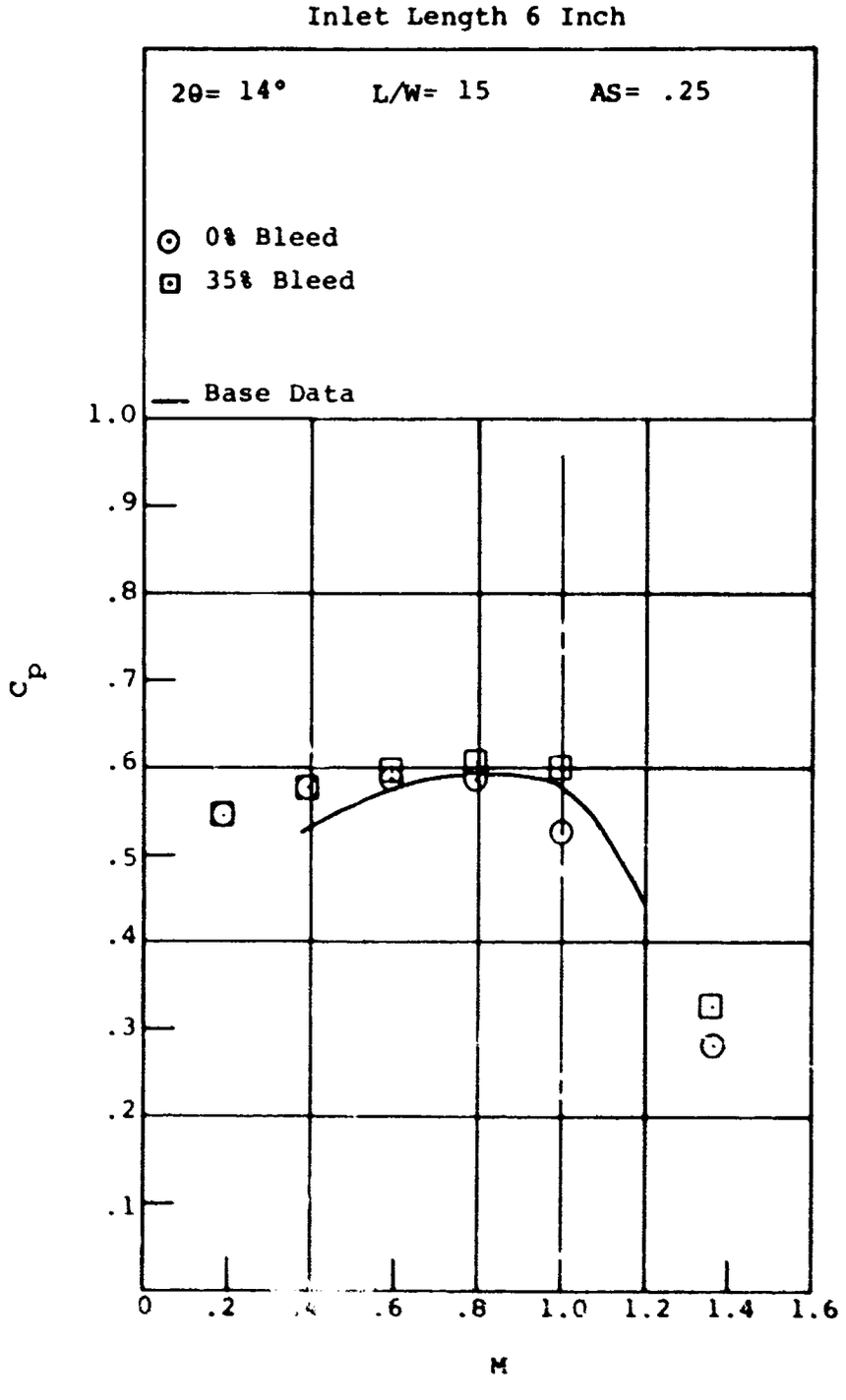

Figure 241. Pressure Recovery Versus Mach Number. Aspect Ratio = 0.25. Asymmetric Blockage Distribution Studies.

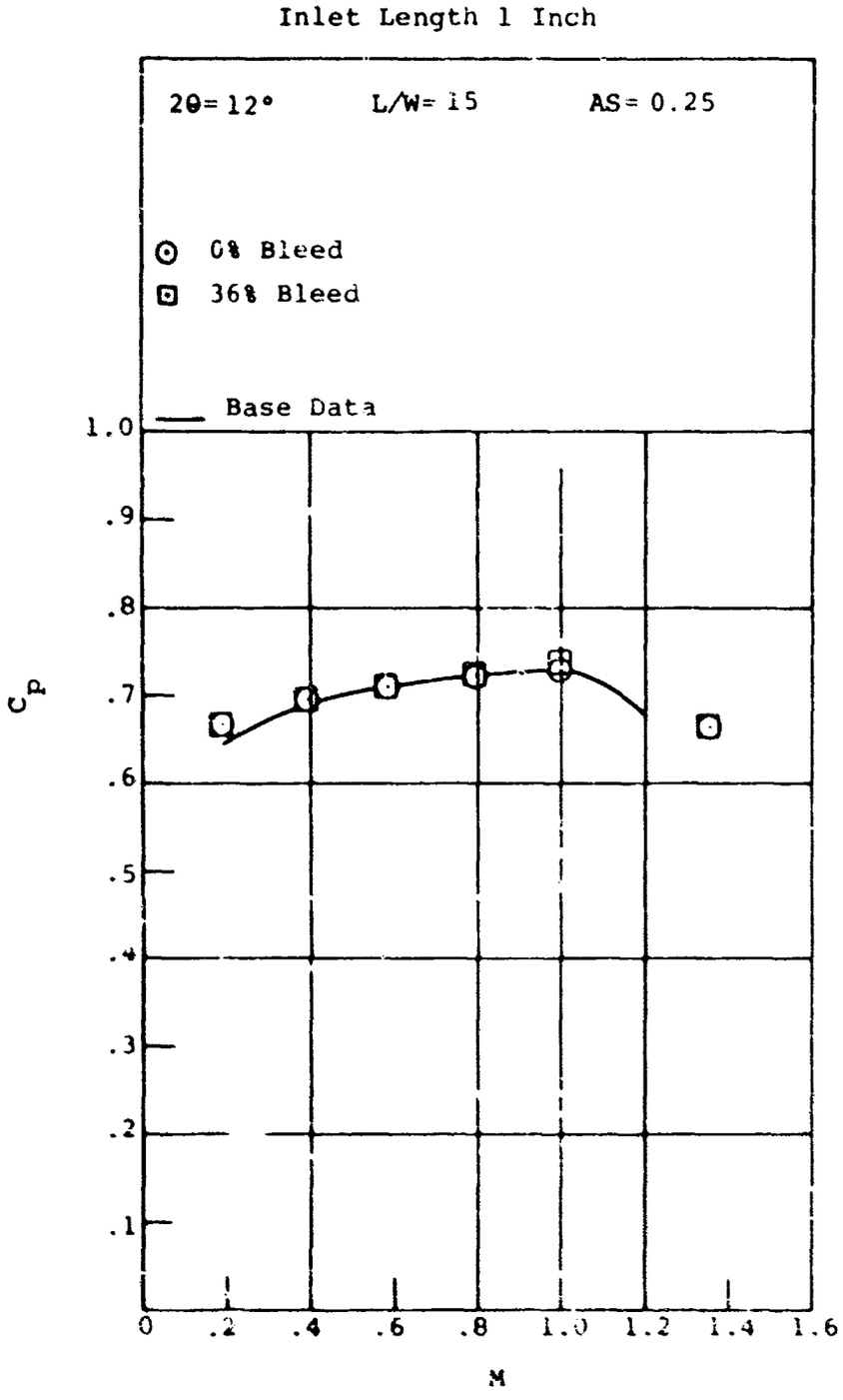

Figure 242. Pressure Recovery Versus Mach Number. Aspect Ratio = 0.25. Asymmetric Blockage Distribution Studies.

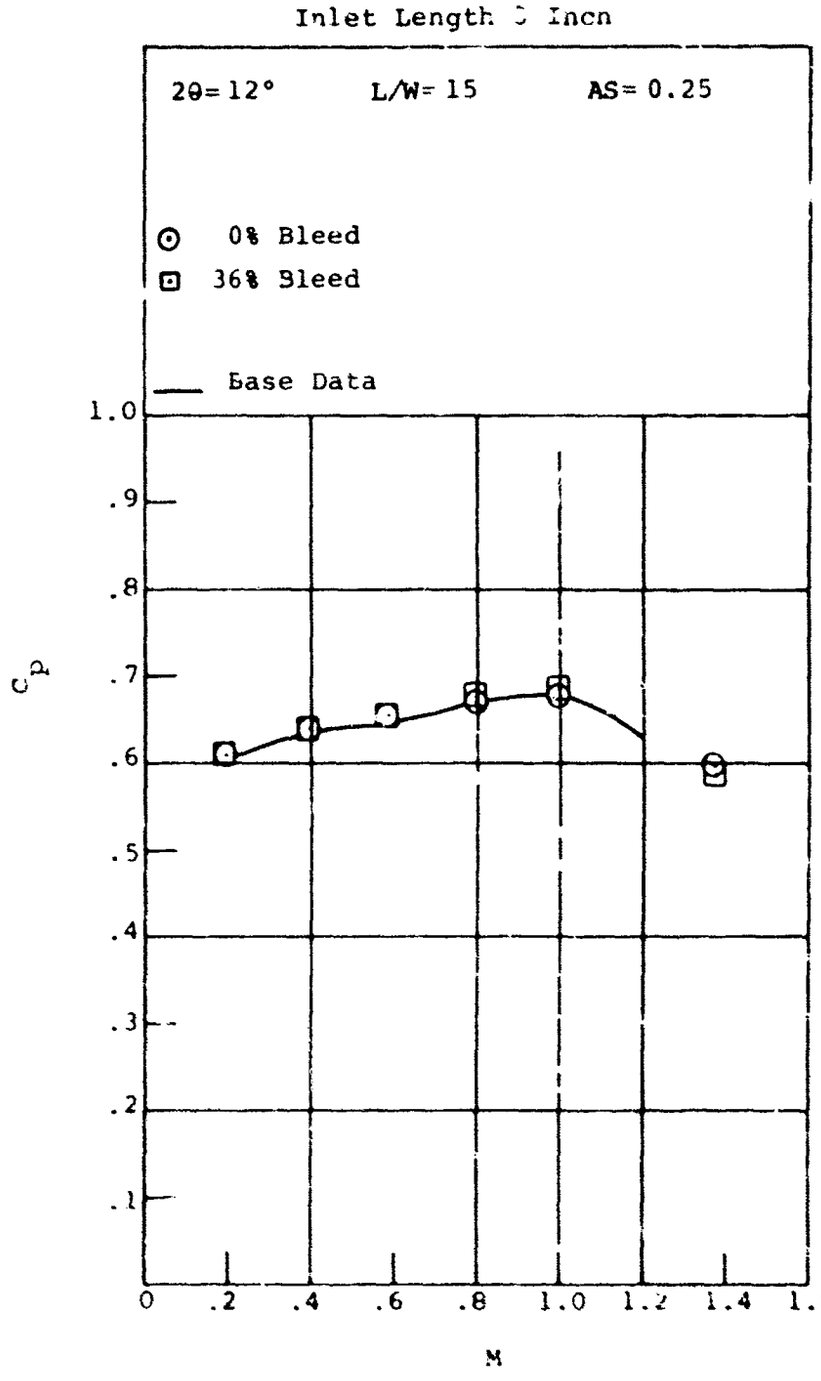

Figure 243. Pressure Recovery Versus Mach Number. Aspect Ratio = 0.25. Asymmetric Blockage Distribution Studies.

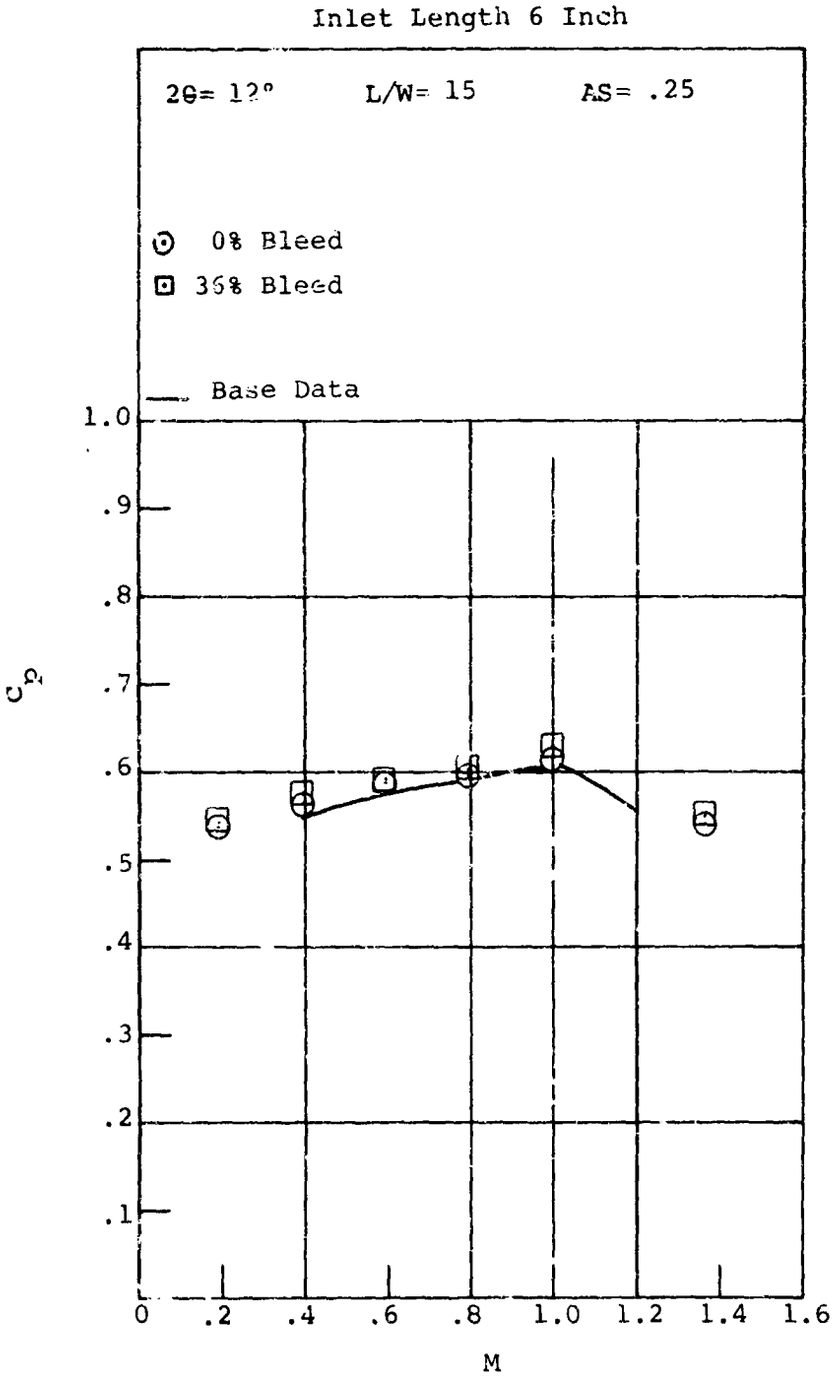

Figure 244. Pressure Recovery Versus Mach Number. Aspect Ratio = 0.25. Asymmetric Blockage Distribution Studies.

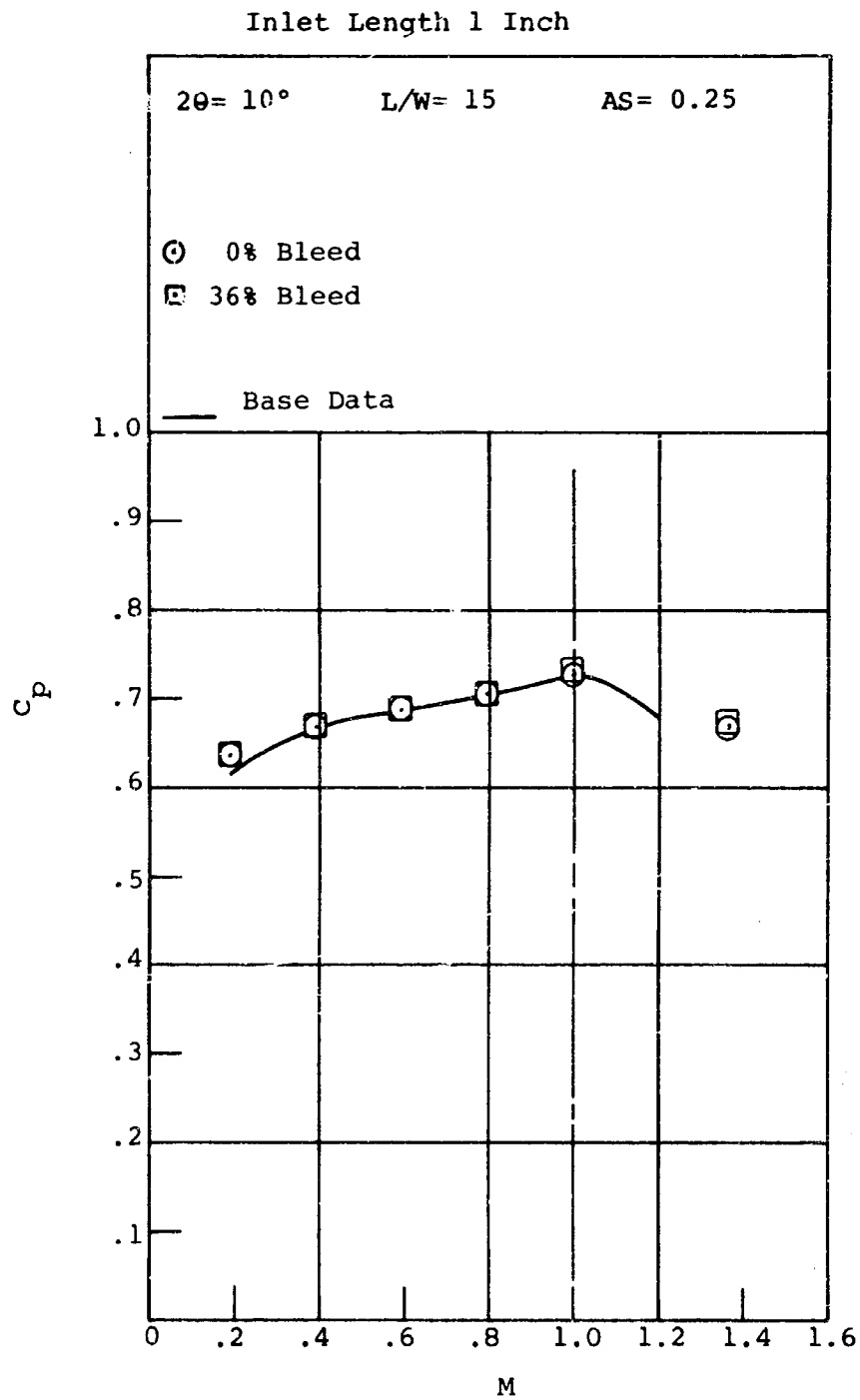

Figure 245. Pressure Recovery Versus Mach Number. Aspect Ratio = 0.25. Asymmetric Blockage Distribution Studies.

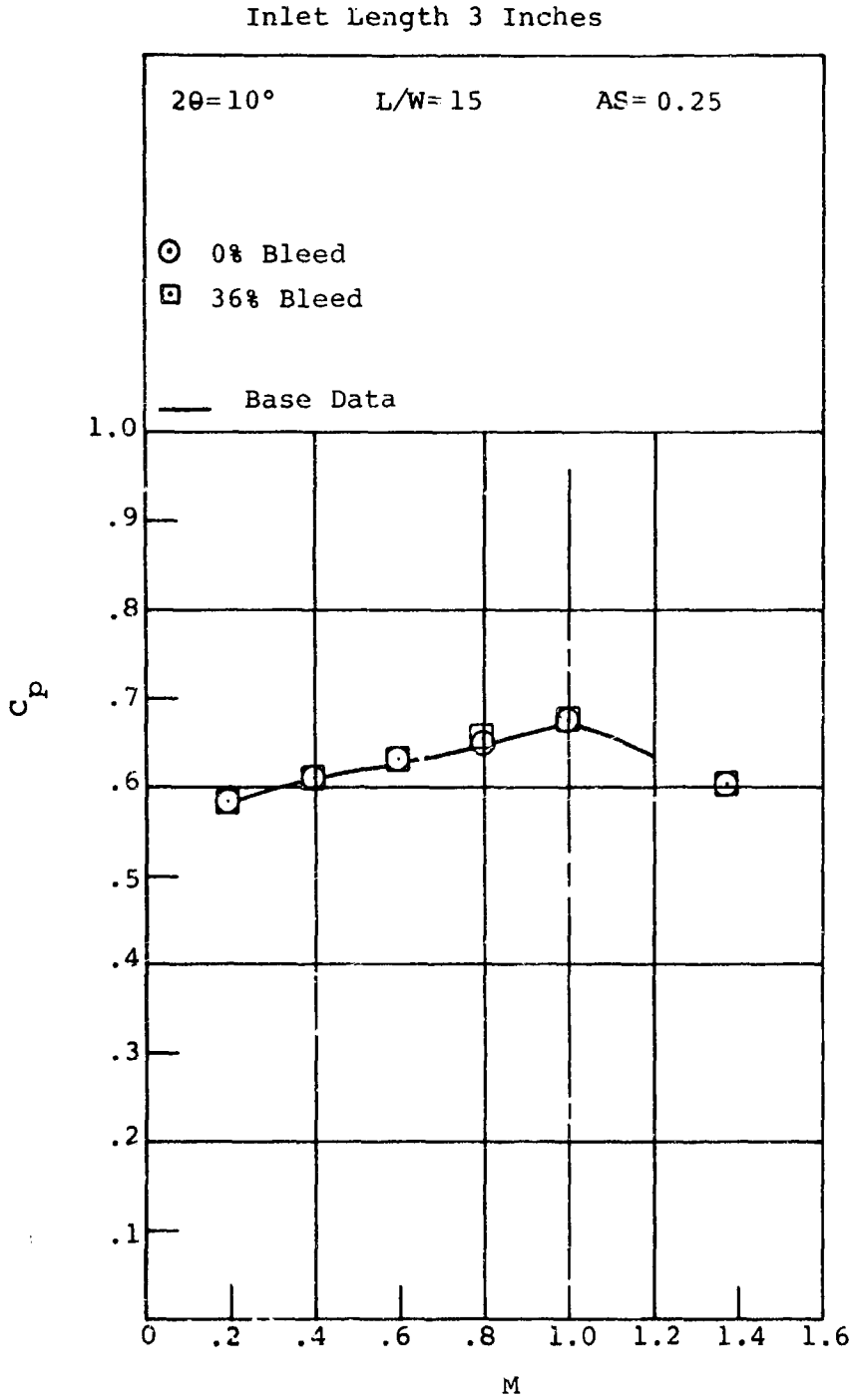

Figure 246. Pressure Recovery Versus Mach Number. Aspect Ratio = 0.25. Asymmetric Blockage Distribution Studies.

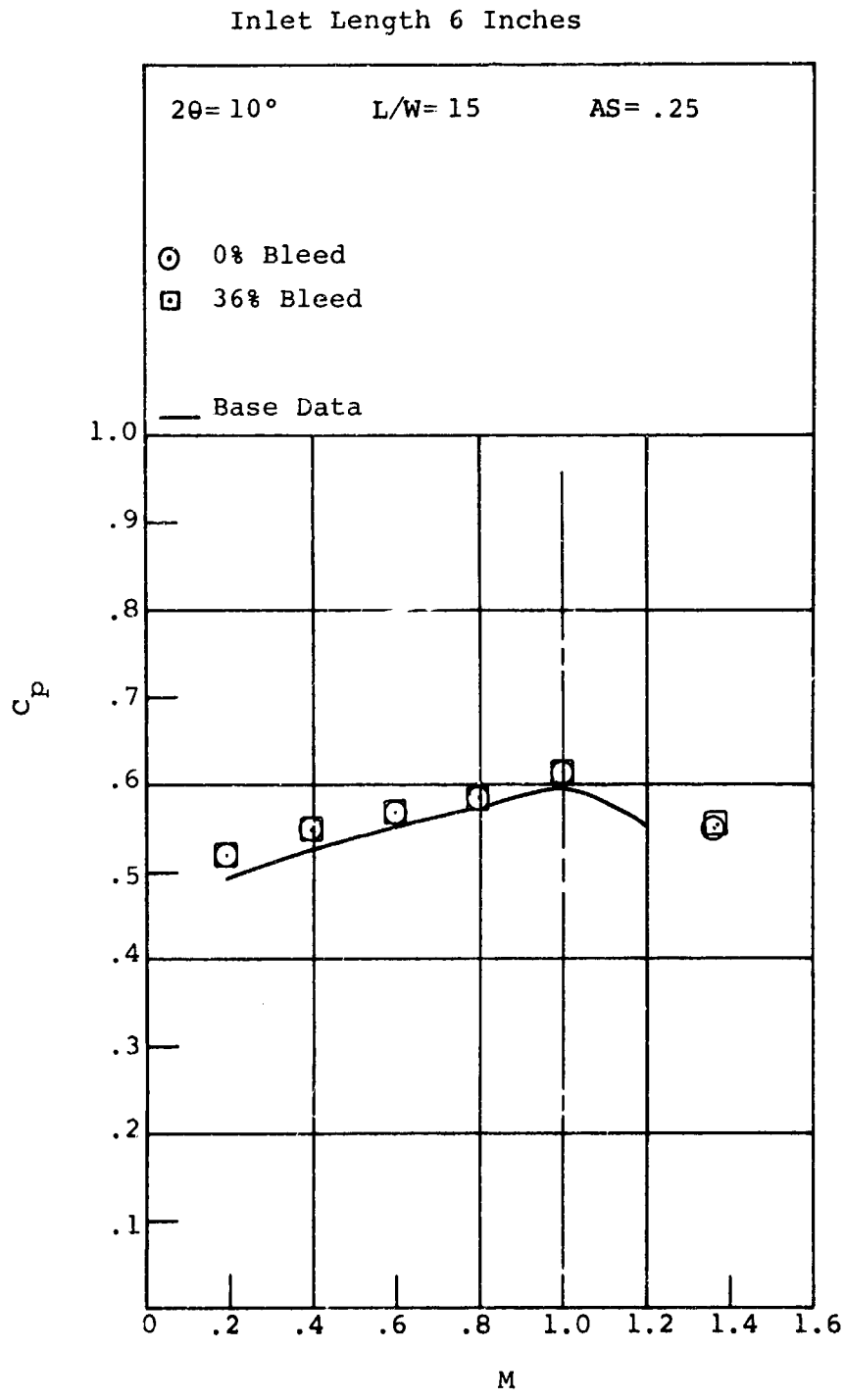

Figure 247. Pressure Recovery Versus Mach Number. Aspect Ratio = 0.25. Asymmetric Blockage Distribution Studies.

and hence improve the boundary layer's ability to negotiate the adverse pressure gradient within the diffuser. This should increase the pressure recovery performance of the diffuser geometry as is observed in most cases.

Comparison of Solid Wall and Base Data

During the suction studies, a few geometries were tested with a solid wall inlet (exactly the same test section geometry as used in the original base data tests) as a check upon the experimental repeatability in obtaining pressure recovery data. Figure 248 shows the comparison between the measured throat blockage for the solid wall and base data as a function of Mach number for $2\theta = 6°$ and 12°, and aspect ratio = 1.0. Here again, the base data are represented by the solid lines. The variation of blockage with Mach number and inlet length reproduces the original base data satisfactorily.

A comparison of the pressure recovery performance for the solid wall data and base data is shown in Figures 249, 250, and 251 for $2\theta = 6°$, 8°, and 12°, and aspect ratio = 1.0. Although some of the data (for example, $2\theta = 6°$, inlet length = 0", and $2\theta = 12°$, inlet length = 6") reproduce the base data very well, the other data show a slightly higher pressure recovery performance (1.5 to 2 points in some cases) than the original data. The present solid wall tests were only repeated on separate days, but the test section was disassembled and reassembled between tests. In all cases the pressure recovery performance of the solid wall data was reproducible to about 0.2 points (0.002 in C_p).

Repeat tests were also conducted with the original diffuser blocks at $L/W = 10$ and $2\theta = 6°$ for the aspect ratio = 1.0 geometry. The results are shown in Figures 252 and 253. Here the data repeat well the base data except for the highest inlet length at $M_t = 0.2$ and $M_t = 1.365$. Because of the shock in the diffuser at $M_t = 1.365$, some scatter between tests is expected at this condition of superchoked flow.

The same type of comparison was also made between solid wall data and base data for aspect ratio = 0.25. For all tests, the aspect ratio = 0.25 data agree well with the base data.

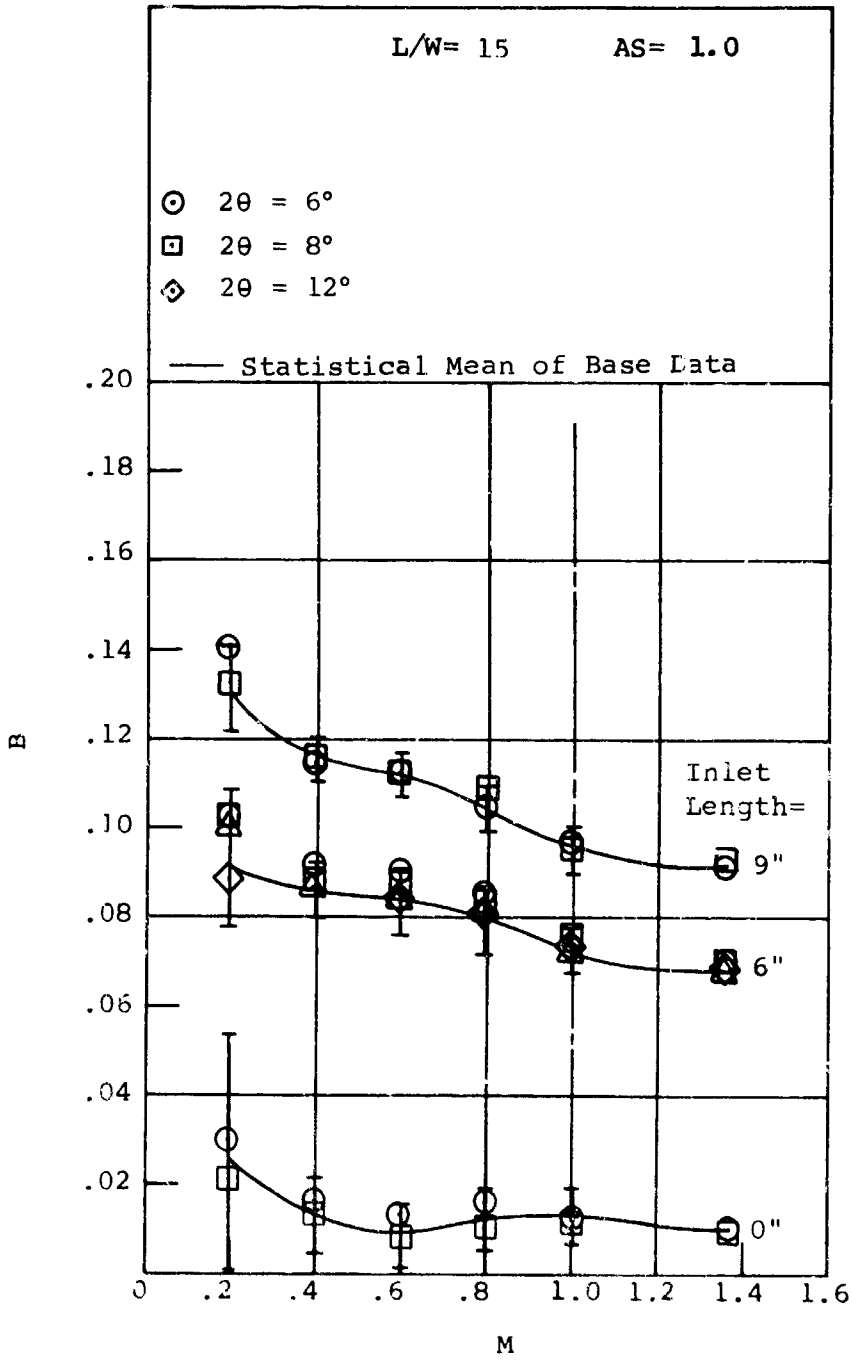

Figure 248. Blockage Versus Mach Number. Aspect Ratio = 1.0. "Solid Wall" Data.

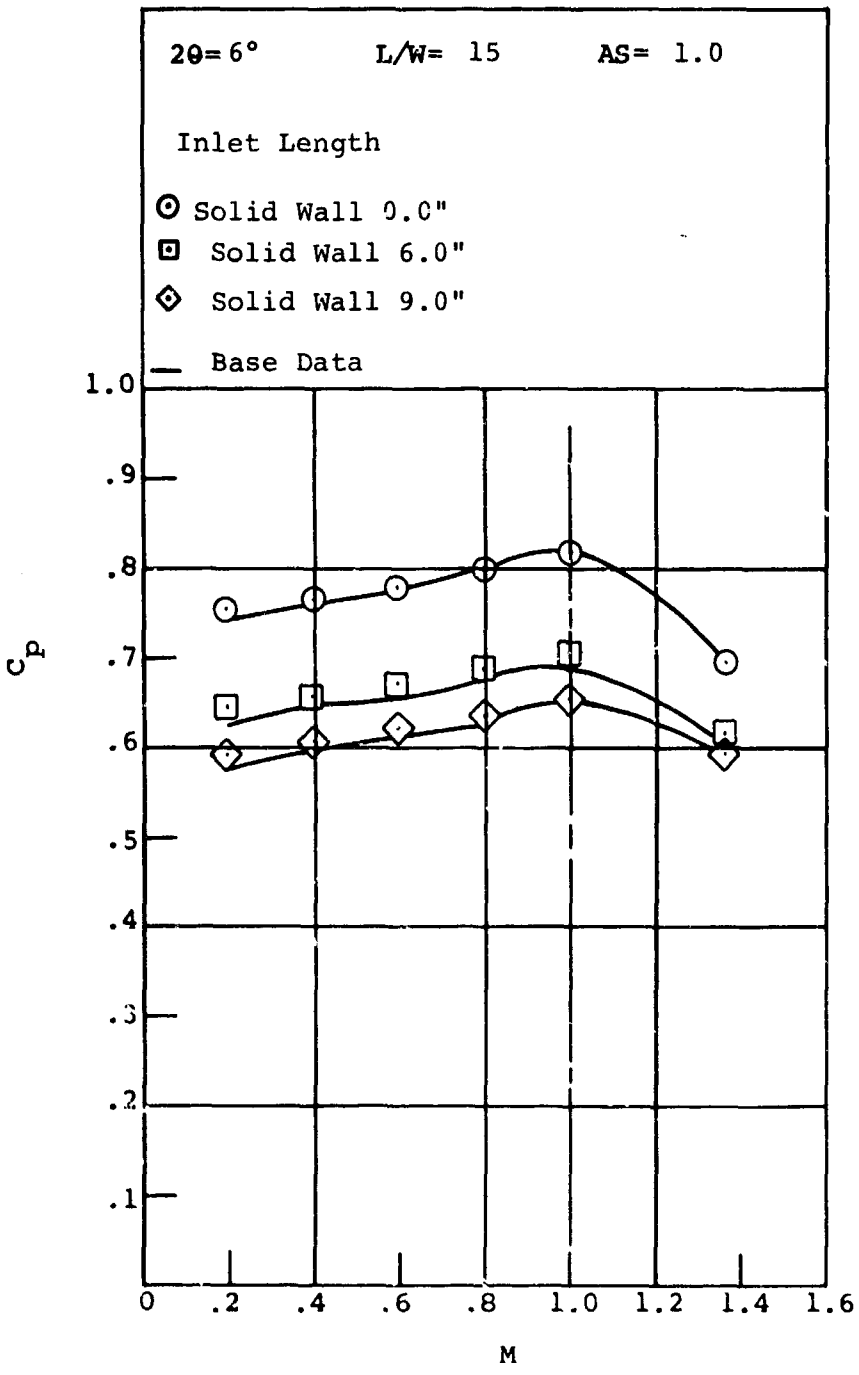

Figure 249. Pressure Recovery Versus Mach Number. Aspect Ratio = 1.0. "Solid Wall" Data.

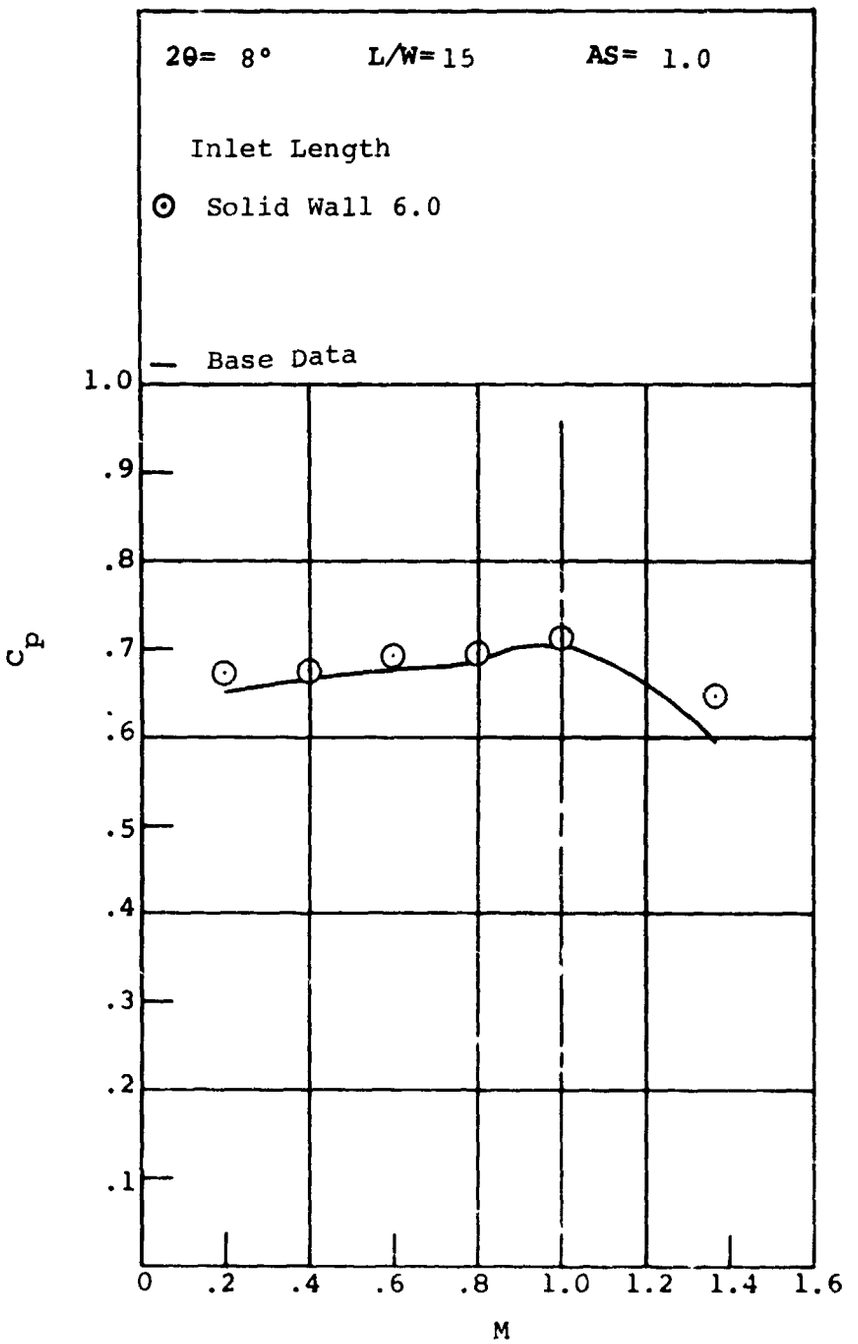

Figure 250. Pressure Recovery Versus Mach Number. Aspect Ratio = 1.0. "Solid Wall" Data.

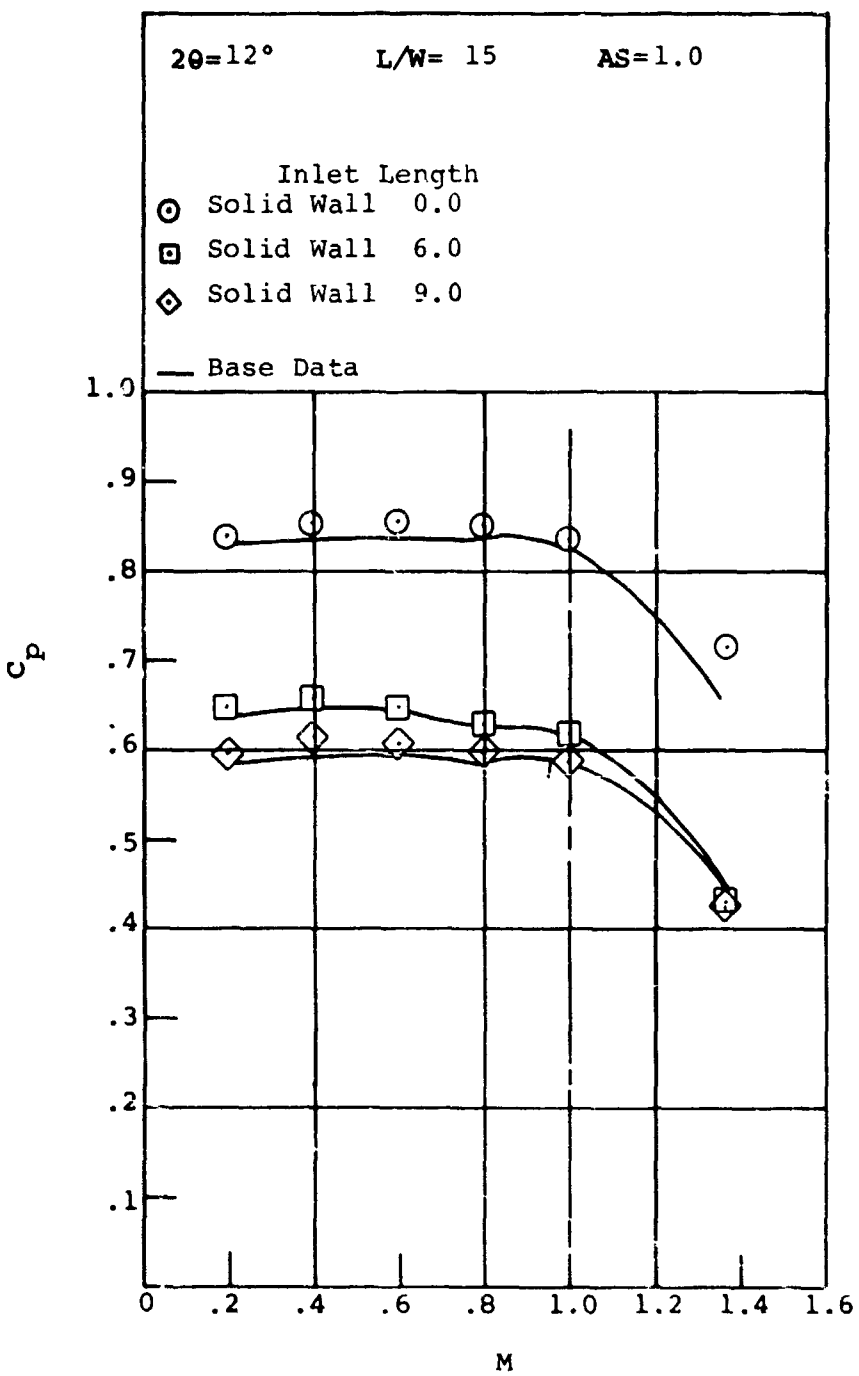

Figure 251. Pressure Recovery Versus Mach Number. Aspect Ratio = 1.0. "Solid Wall" Data.

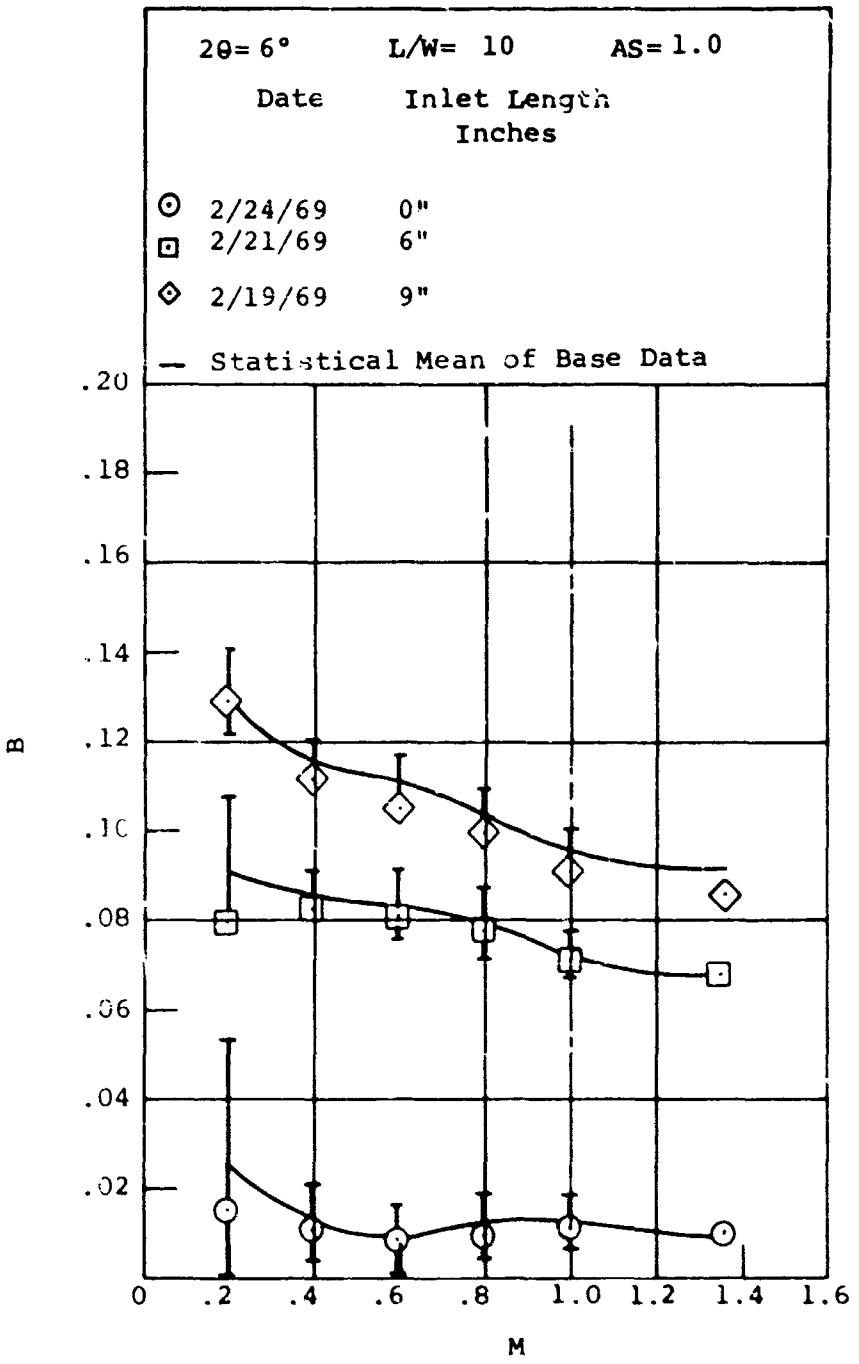

Figure 252. Blockage Versus Mach Number. Aspect Ratio = 1.0. "Solid Wall" Data.

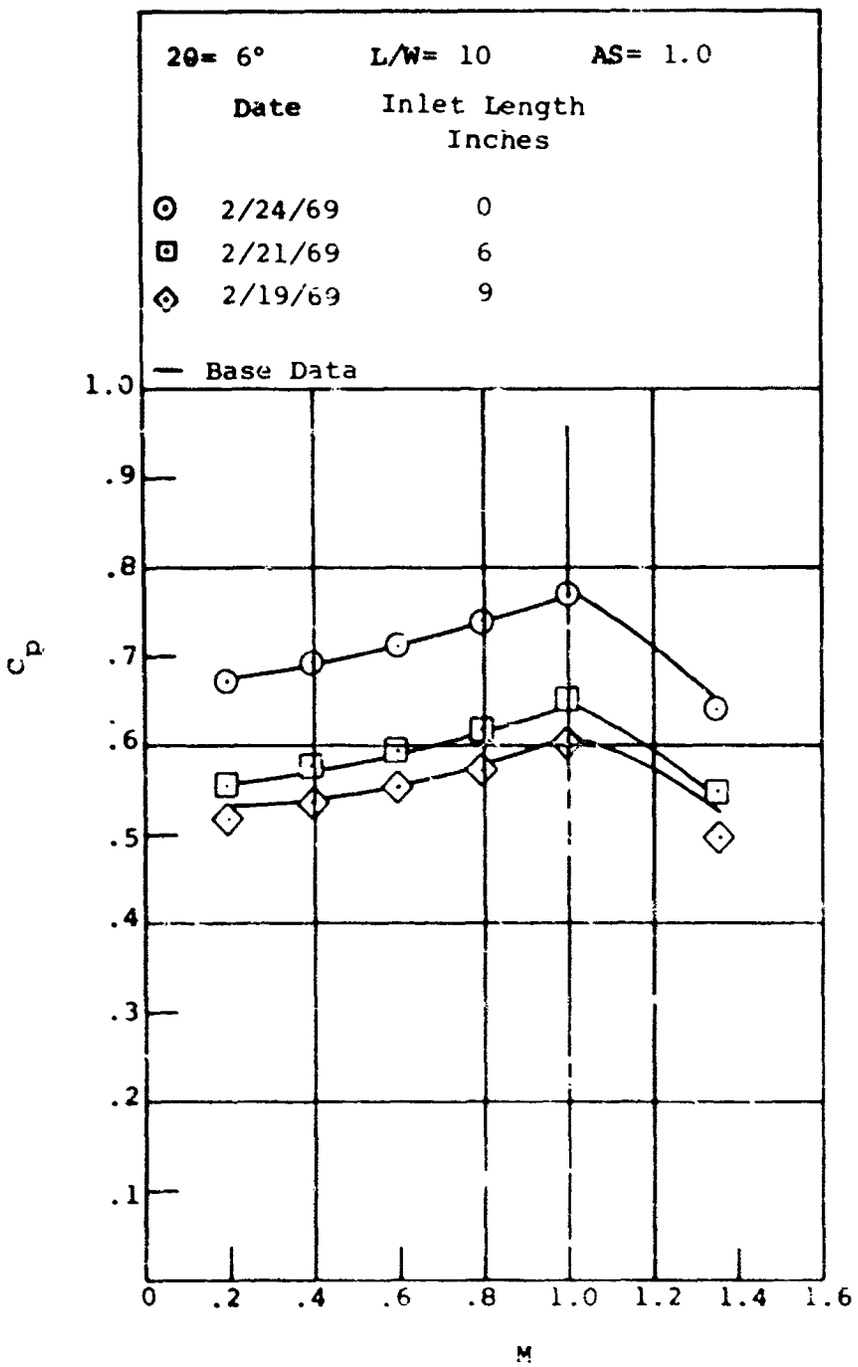

Figure 253. Pressure Recovery Versus Mach Number. Aspect Ratio = 1.0. "Solid Wall" Data.

Figures 254, 255, and 256 show the comparison of the two sets of data for $2\theta = 10°$ and $14°$ for $L/W_1 = 15$.

As far as can be determined, all conditions have been reproduced exactly between the solid wall tests and the original base studies. The only difference in the diffuser geometry between the two sets of studies has been a modification of the diffuser test section top plate. The suction experiments necessitated the drilling of a number of holes in the top plate to provide for suction bleed. It is possible that this may have weakened the top plate slightly. However, solid wall tests were run (1) with additional strengthening of the top plate (using large C-clamps and strongbacks to additionally clamp the sandwich construction together) and (2) with the O-rings removed between the top plate and inlet blocks. These tests produced no changes in pressure recovery performance greater than the 0.2 points in C_p.

All calibration tests with the pressure measuring system have shown that the system was operating according to calibration over all of the tests in these studies (including the base studies). The reason for the small differences in pressure recovery for the aspect ratio = 1.0 data, as shown in Figures 249 through 251, is not really understood. Although there is an uncertainty in the evaluation of C_p, the uncertainty is less than the indicated difference between the base data and the solid wall data. Since the solid wall data repeat extremely well, it is assumed that there may be a small fixed error in measuring pressure recovery C_p for some aspect ratio 1.0 geometries of the base data; although for the geometries which have been intercompared, it appears that any such error in the base data would be on the conservative side. That is, the base data show a slightly lower value of C_p than the solid wall data.

It is emphasized that the differences observed (Figures 249 to 251) are small and that all other checks made on the repeatability of test data for a given geometry show an astonishing repeatability of pressure recovery coefficient (i.e., less than 0.2 points in C_p).

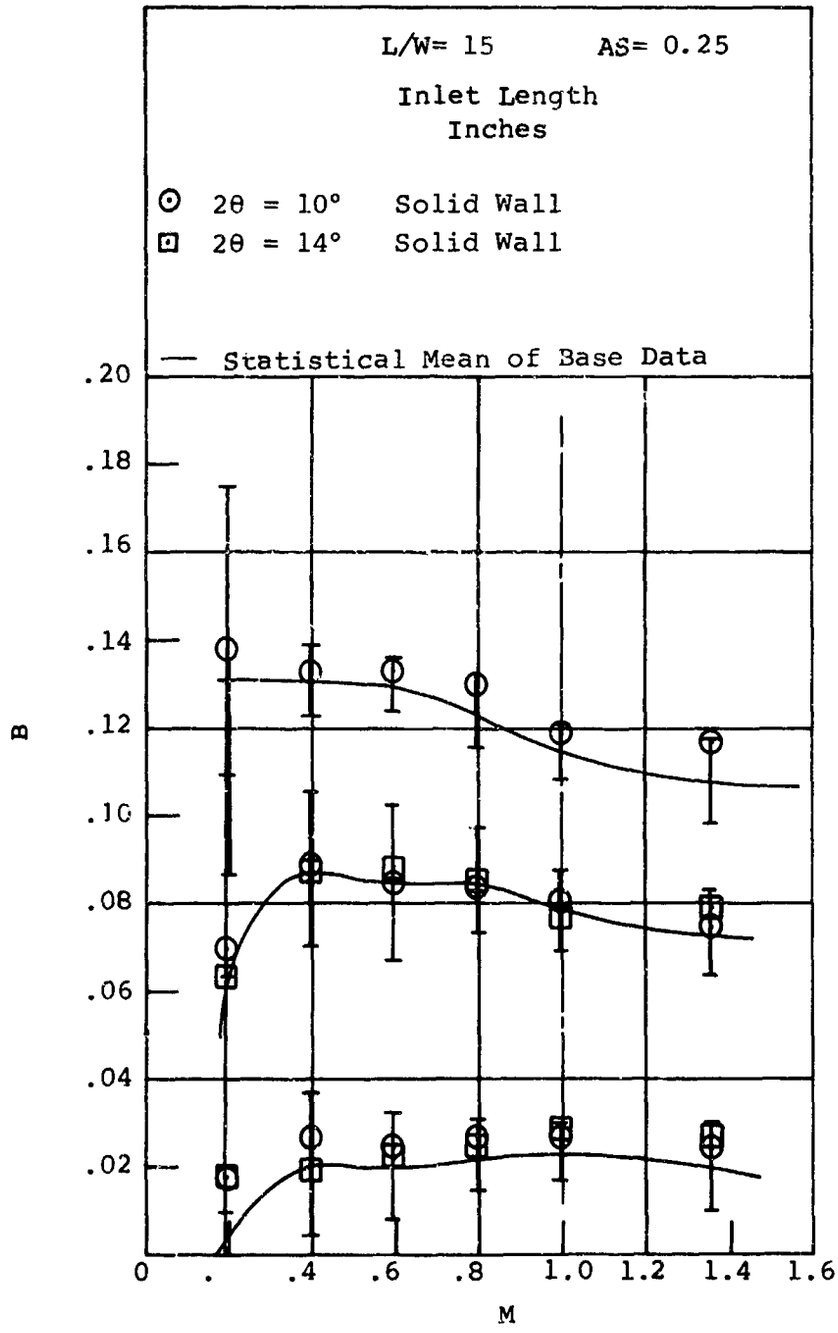

Figure 254. Blockage Versus Mach Number. Aspect Ratio = 0.25. "Solid Wall" Data.

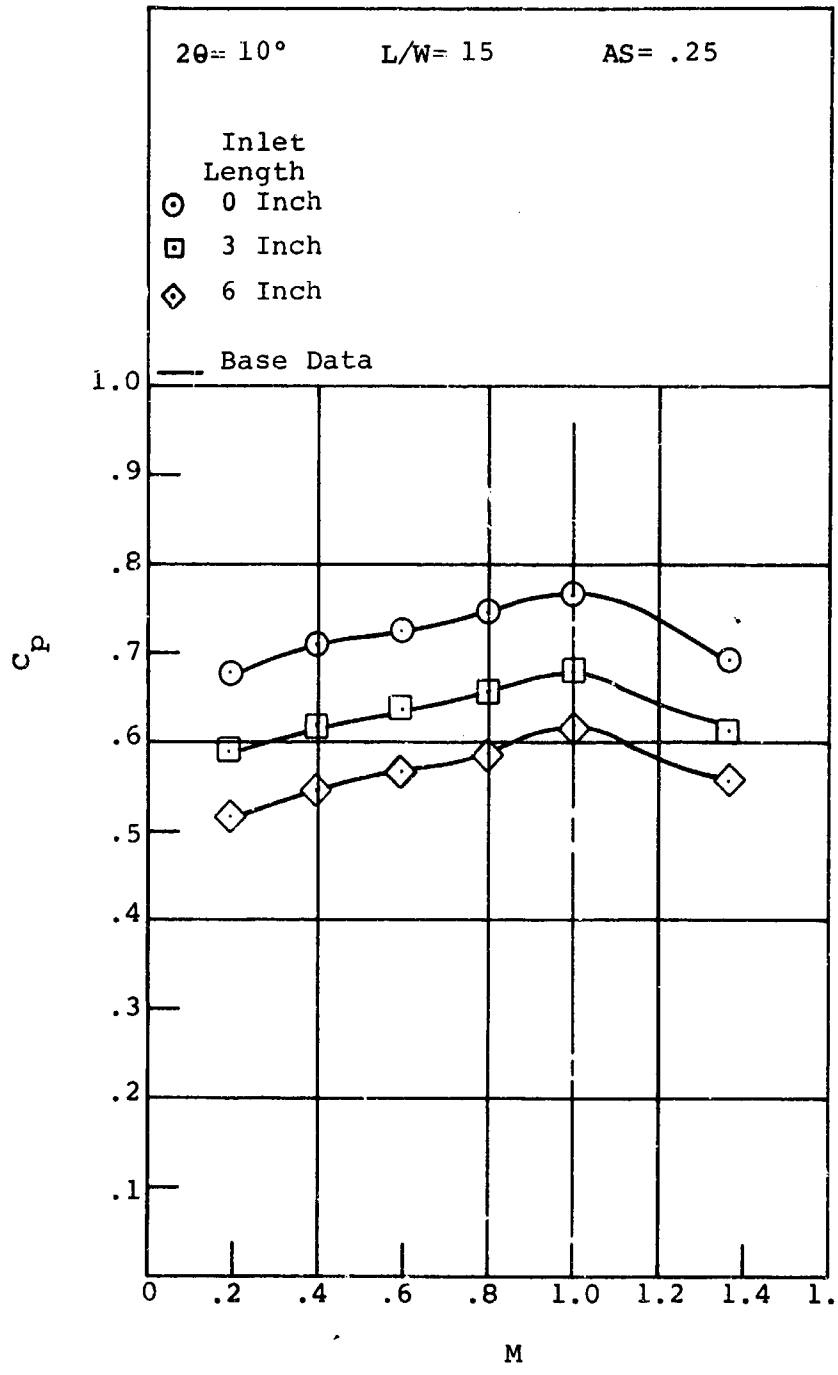

Figure 255. Pressure Recovery Versus Mach Number. Aspect Ratio = 0.25. "Solid Wall" Data.

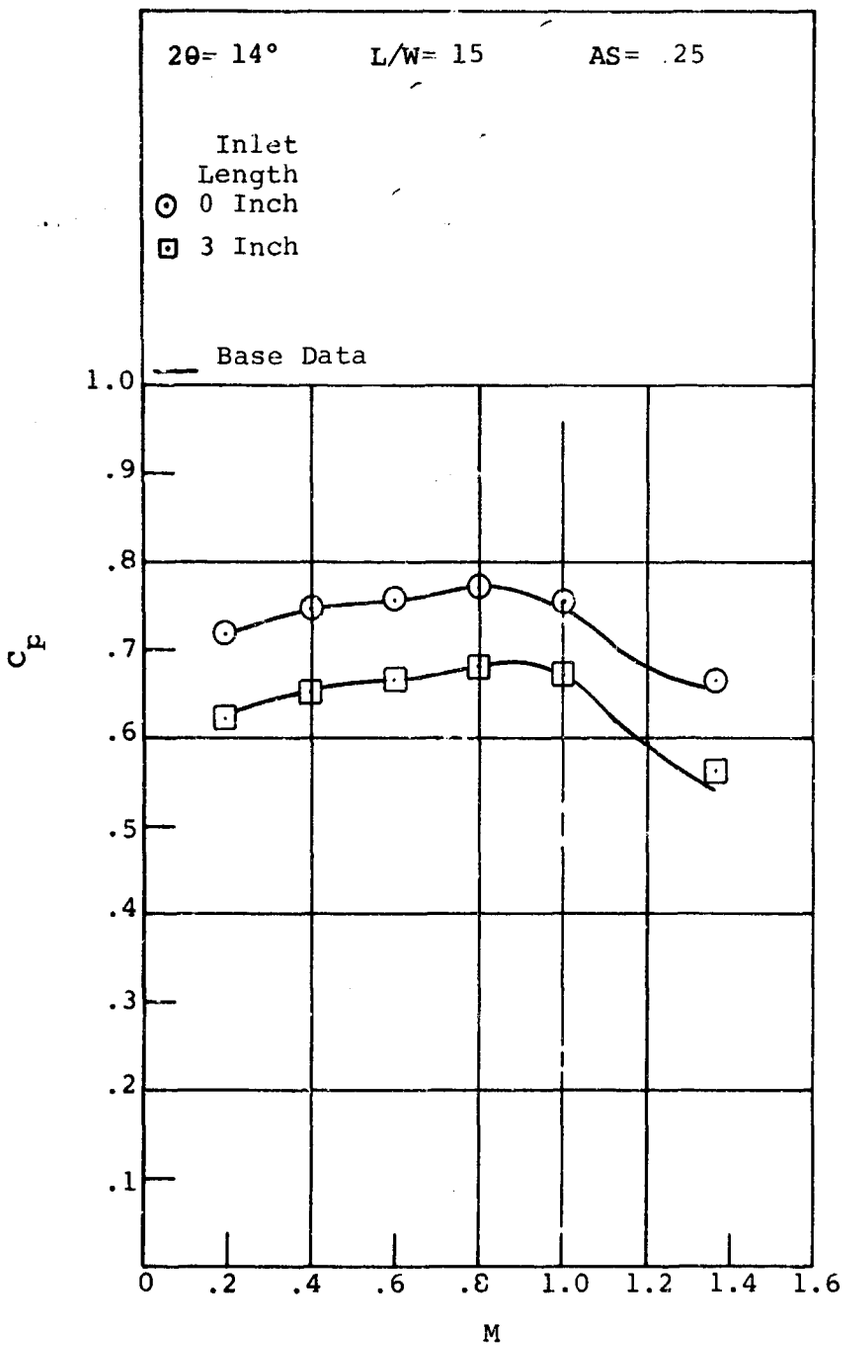

Figure 256. Pressure Recovery Versus Mach Number. Aspect Ratio = 0.25. "Solid Wall" Data.

Pressure Recovery Performance as a Function of Suction Rate

In terms of these performance maps, the test geometries can be described by increasing the diffuser angle 2θ along a line of constant L/W_1. The tests with variable suction rates show that below the angle corresponding to the ridge of optimum recovery little or no increase in diffuser performance at constant inlet blockage is obtained by applying suction to obtain an asymmetric distribution in inlet blockage. At low angles, 2θ = 6° and 8° for aspect ratio = 1.0 and 2θ = 10° and 12° for aspect ratio = 0.25 (these geometries being below the optimum diffuser angle for maximum recovery at constant L/W_1 = 15), there was virtually no indicated change in diffuser pressure recovery over the range of boundary layer bleed used. This is shown in Figures 257 through 260 for aspect ratio = 1.0 and in Figures 261 through 264 for aspect ratio = 0.25.

At large diffuser angles, i.e., above the optimum ridge, 2θ = 12° for aspect ratio = 1.0 (Figure 260) and 2θ = 16° for aspect ratio = 0.25 (Figures 264 and 265 through 267), an increase in pressure recovery performance of at least 1.5 to 2 points is obtained across the Mach number range at approximately the 25% bleed rate. However, for higher and lower bleed rates the amount of performance gain is reduced.

In Figures 257 through 267, the 0% bleed data are used as the comparison "base" data for the effect of nonuniform distribution of throat blockage produced by suction because of the effect of increased relative roughness of the porous suction surface as has been discussed.

All of the suction tests, from greater than 0% bleed to 100% bleed, should be effective in producing some nonuniform distribution in throat blockage. The 100% suction rate should be most effective in the amount of asymmetry created. However, from the test results, it would appear that a nonuniform distribution of blockage is not the major parameter affecting the diffuser recovery; diffuser recovery is increased most effectively by applying approximately a 25% suction rate. This is a result that occurs in all of the tests in which variable suction rates were applied. These results lead to the speculation that it is some other characteristics of the inlet boundary layer flow and not the distribution of blockage which is governing the change in performance observed in the suction tests. On the basis of physical arguments about the type of boundary

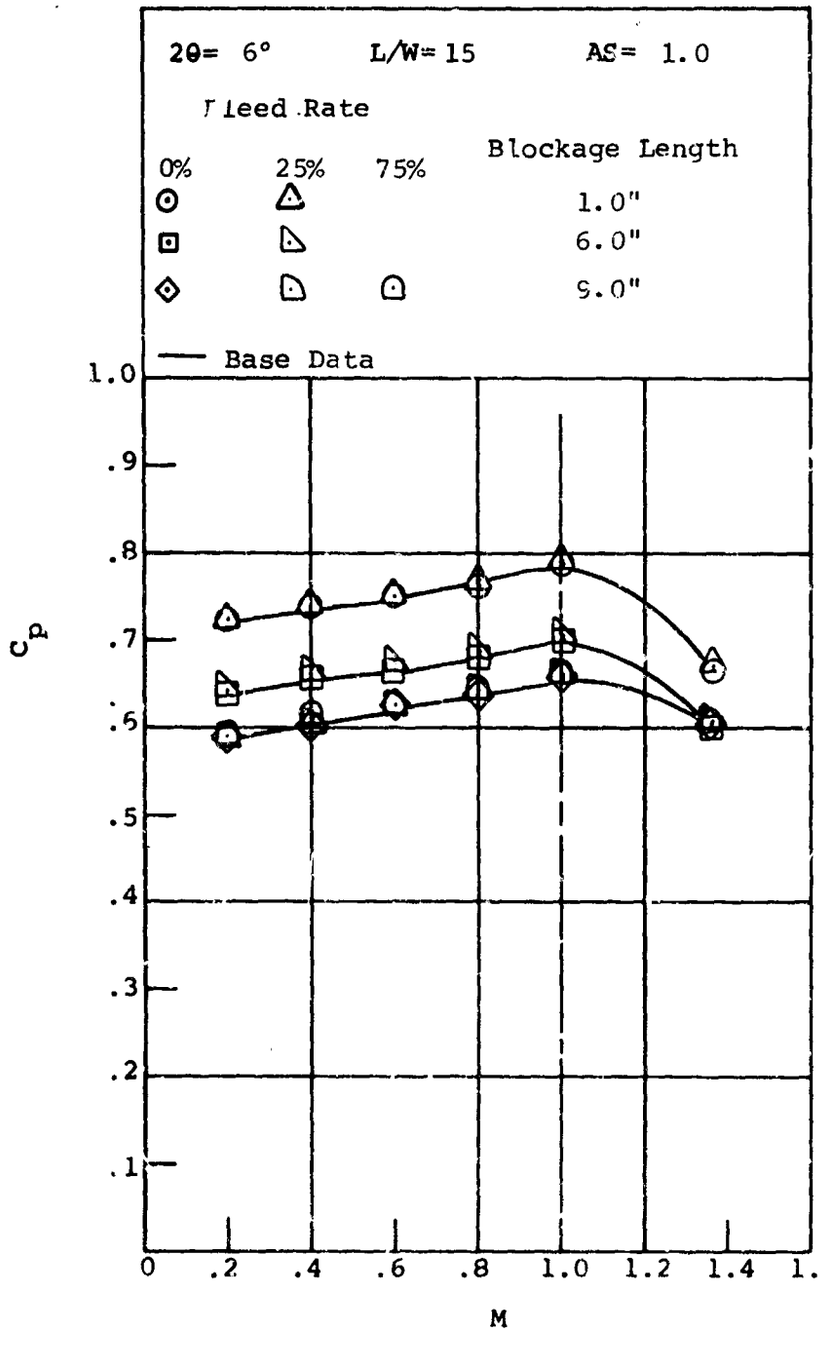

Figure 257. Pressure Recovery Versus Mach Number. Aspect Ratio = 1.0. Asymmetric Blockage Distribution Studies.

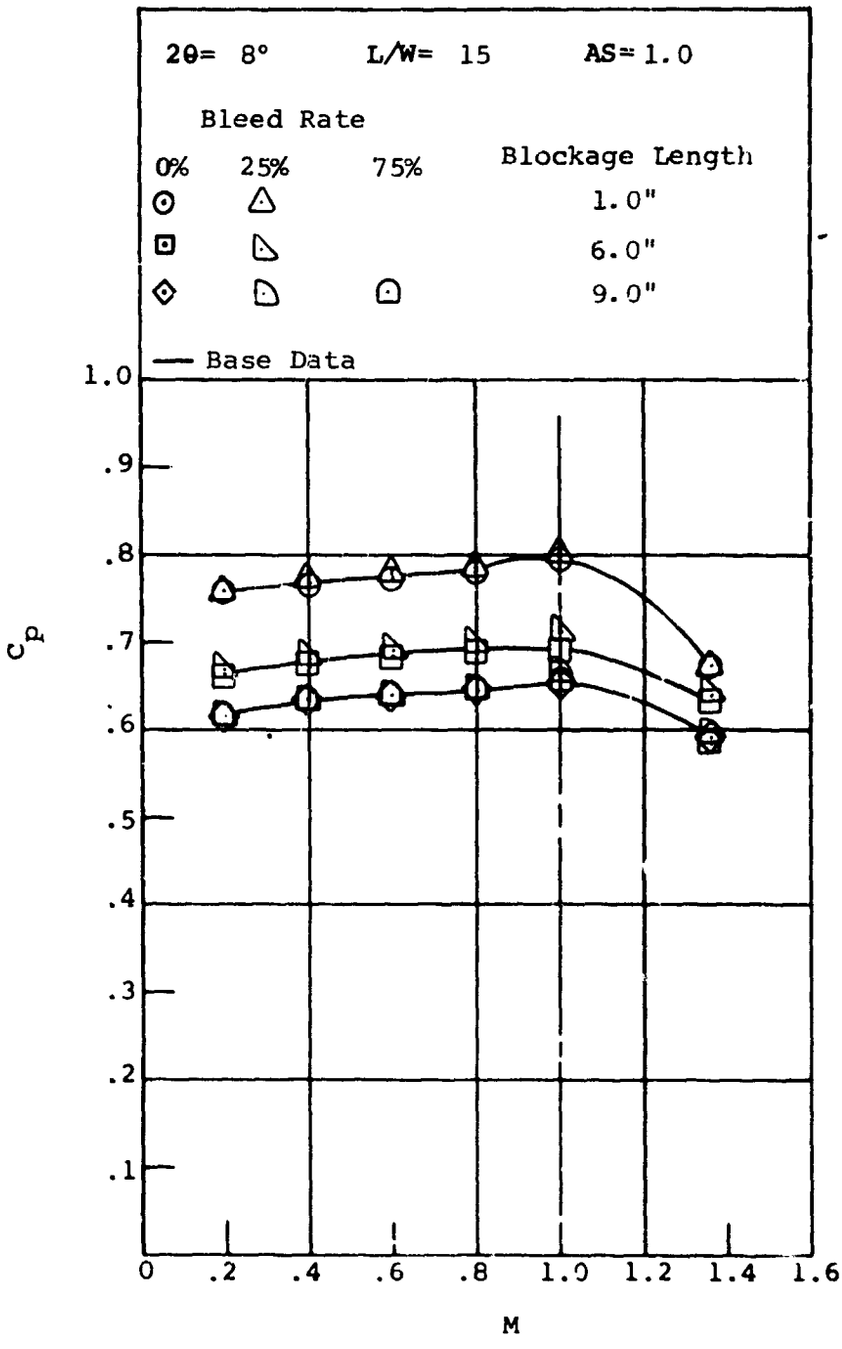

Figure 258. Pressure Recovery Versus Mach Number. Aspect Ratio = 1.0. Asymmetric Blockage Distribution Studies.

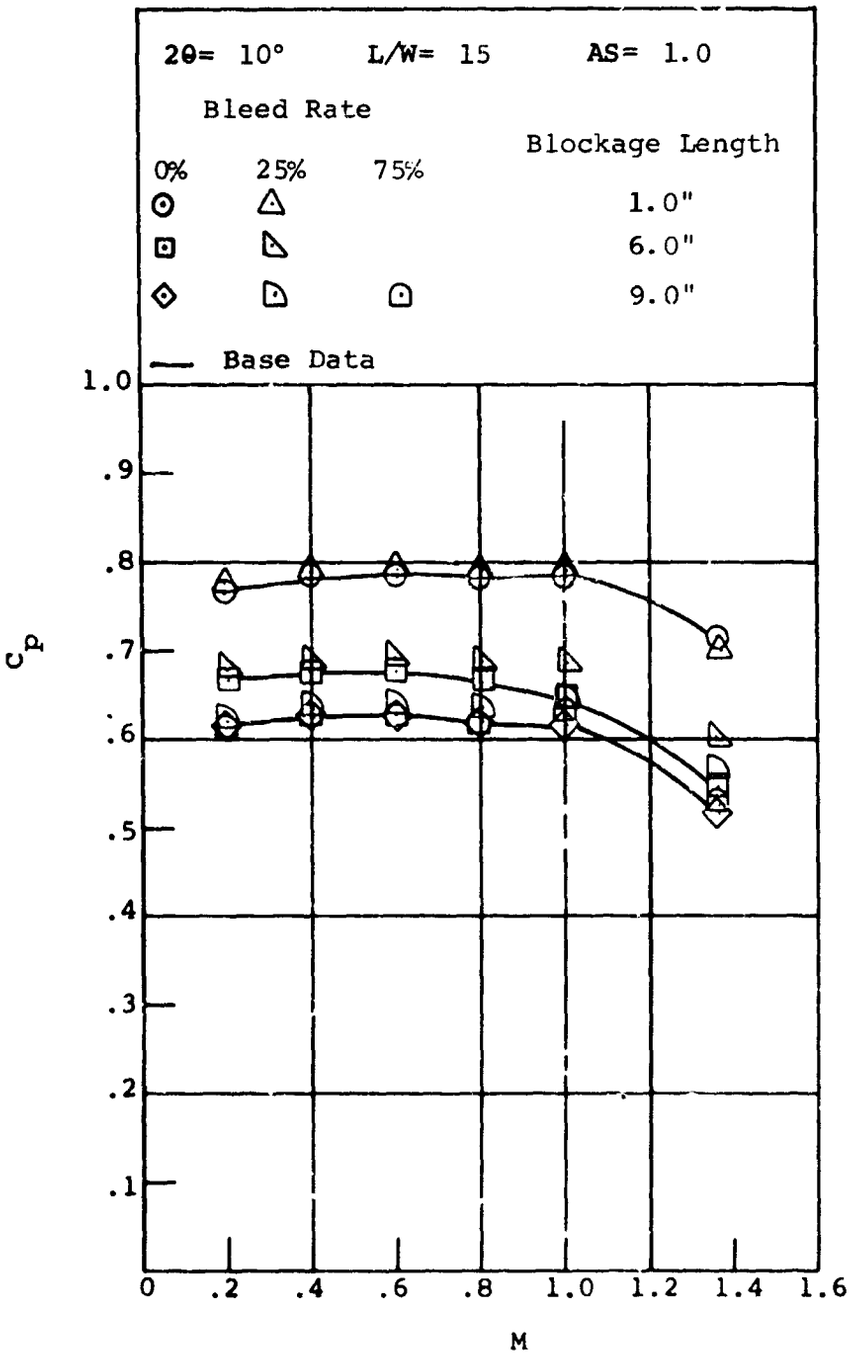

Figure 259. Pressure Recovery Versus Mach Number. Aspect Ratio = 1.0. Asymmetric Blockage Distribution Studies.

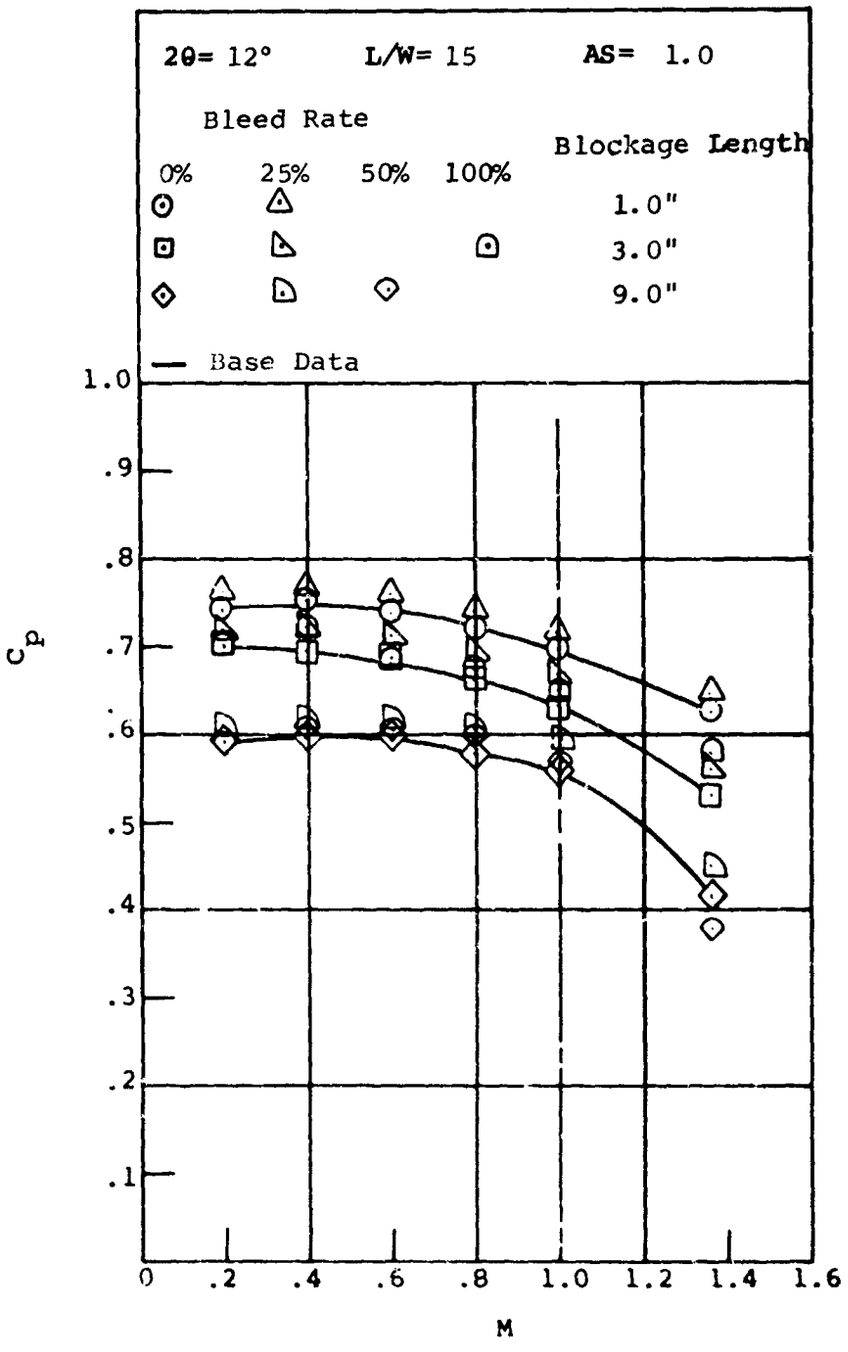

Figure 260. Pressure Recovery Versus Mach Number. Aspect Ratio = 1.0. Asymmetric Blockage Distribution Studies.

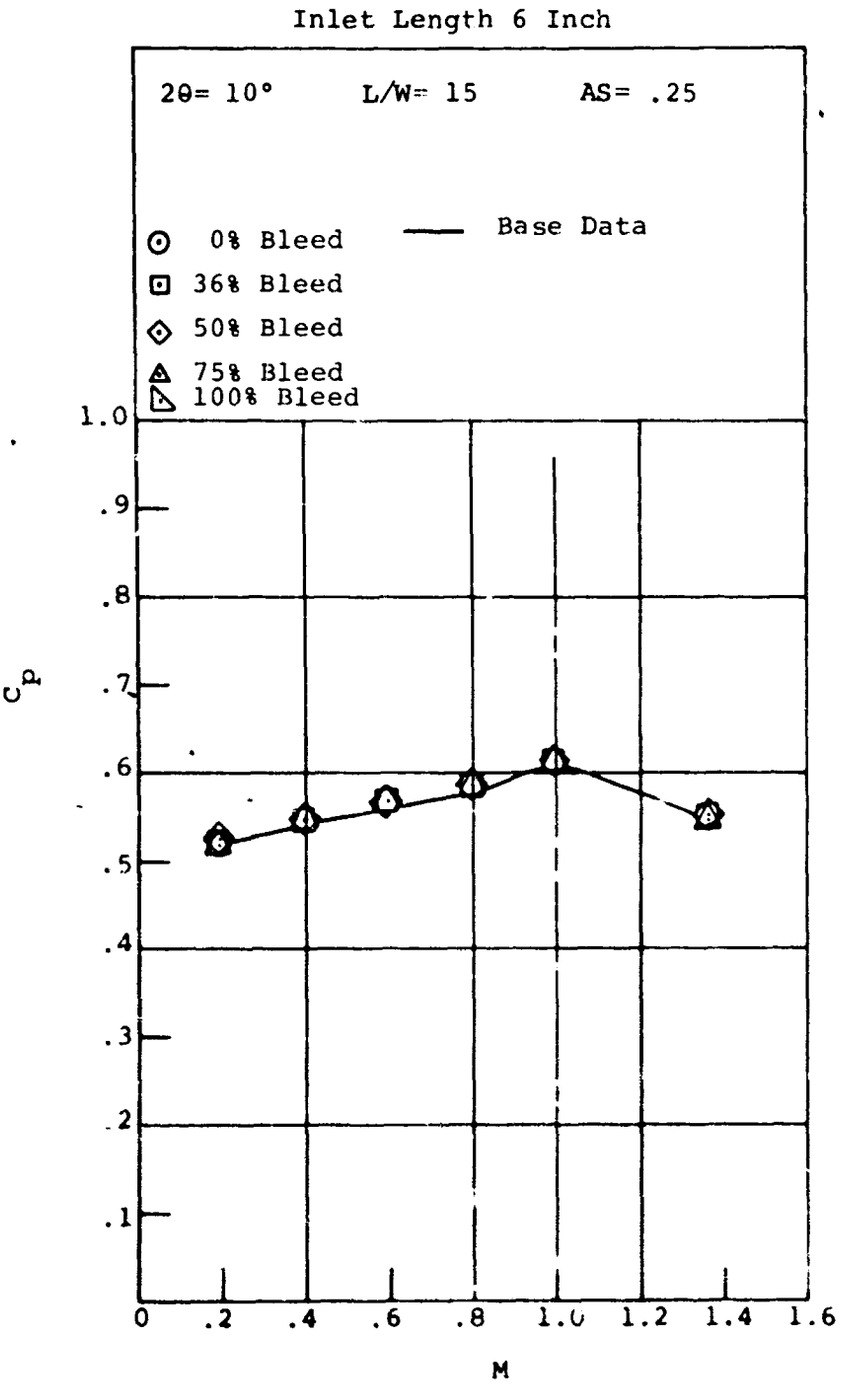

Figure 261. Pressure Recovery Versus Mach Number. Aspect Ratio = 0.25. Asymmetric Blockage Distribution Studies.

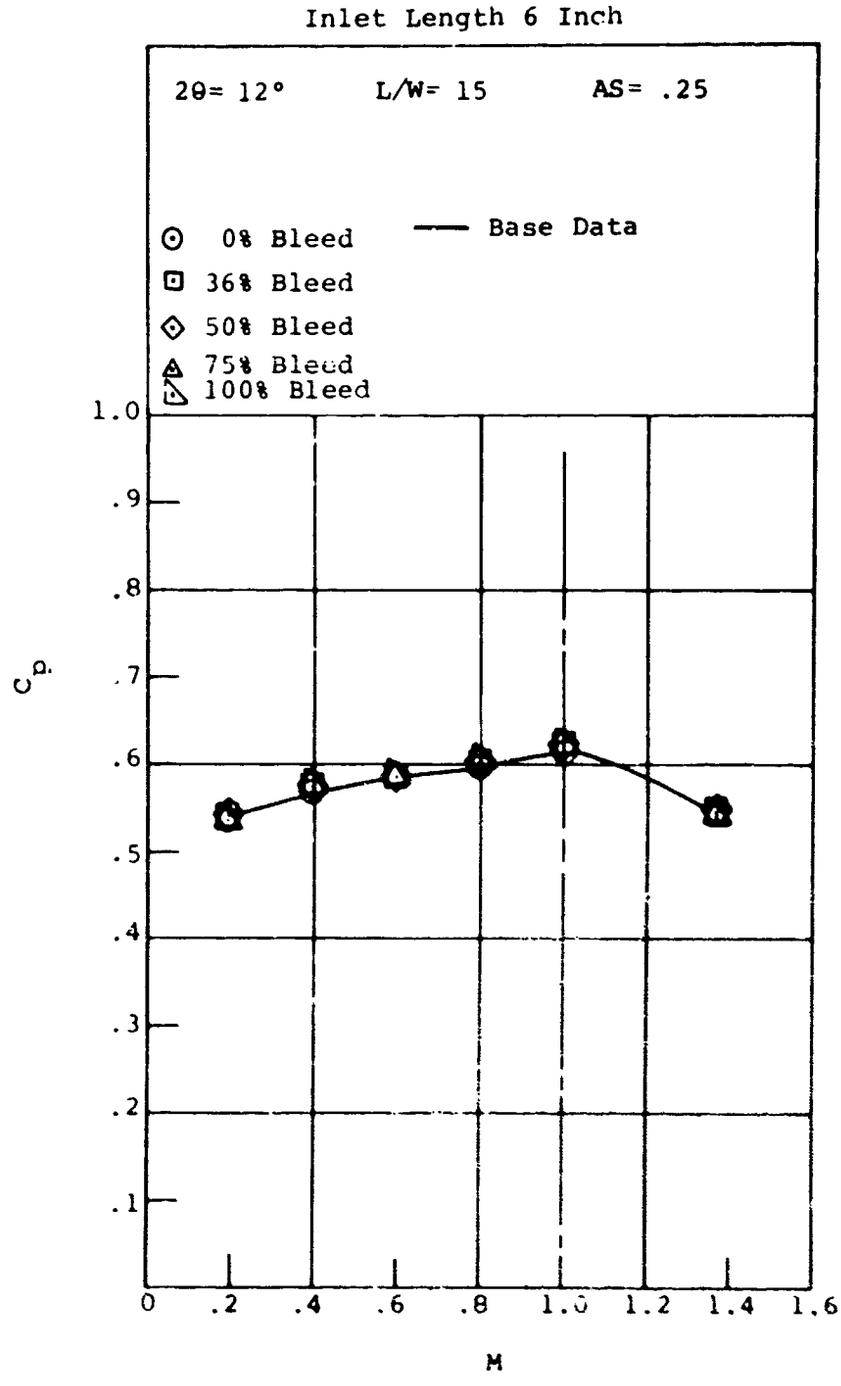

Figure 262. Pressure Recovery Versus Mach Number. Aspect Ratio = 0.25. Asymmetric Blockage Distribution Studies.

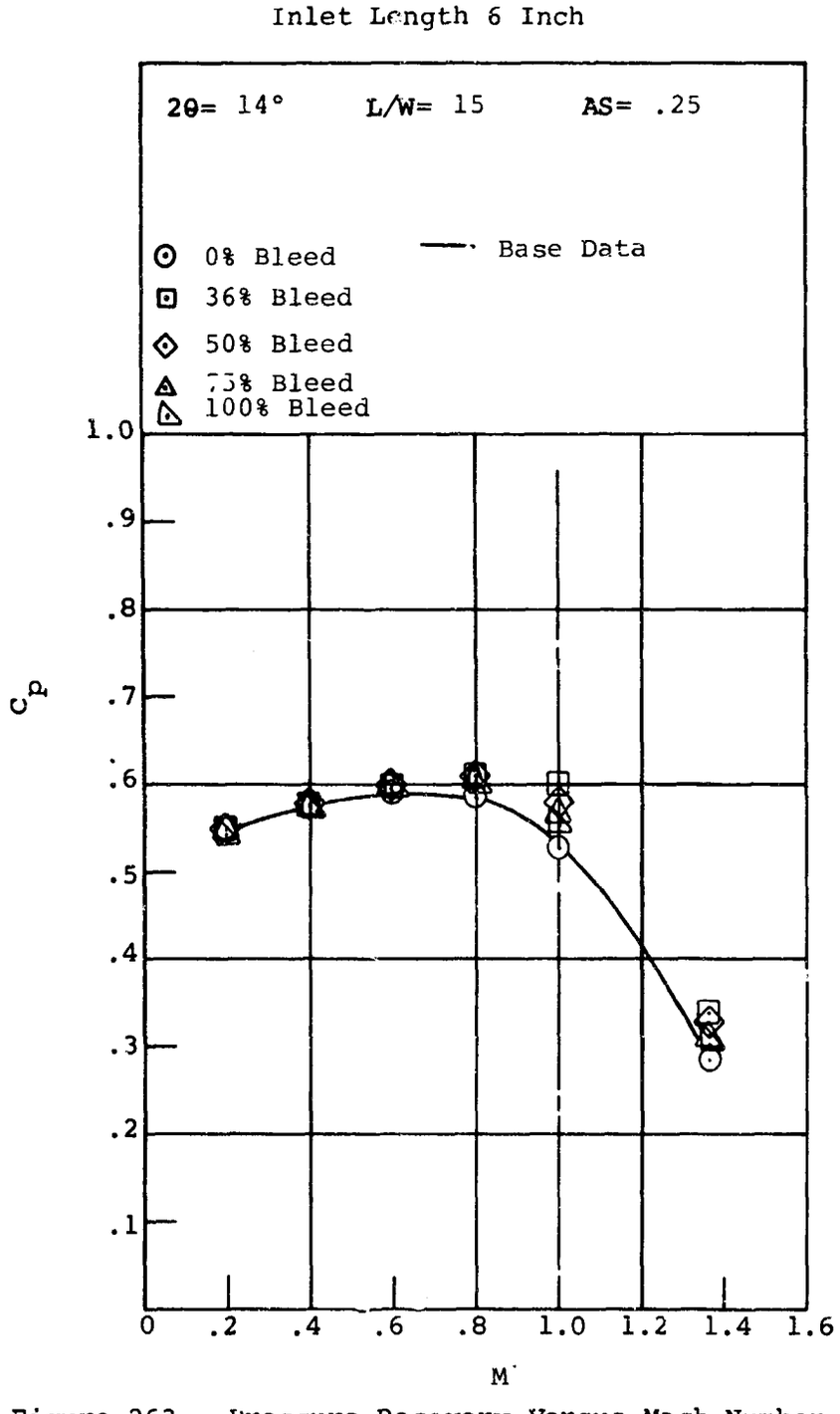

Figure 263. Pressure Recovery Versus Mach Number. Aspect Ratio = 0.25. Asymmetric Blockage Distribution Studies.

Inlet Length 6 Inch

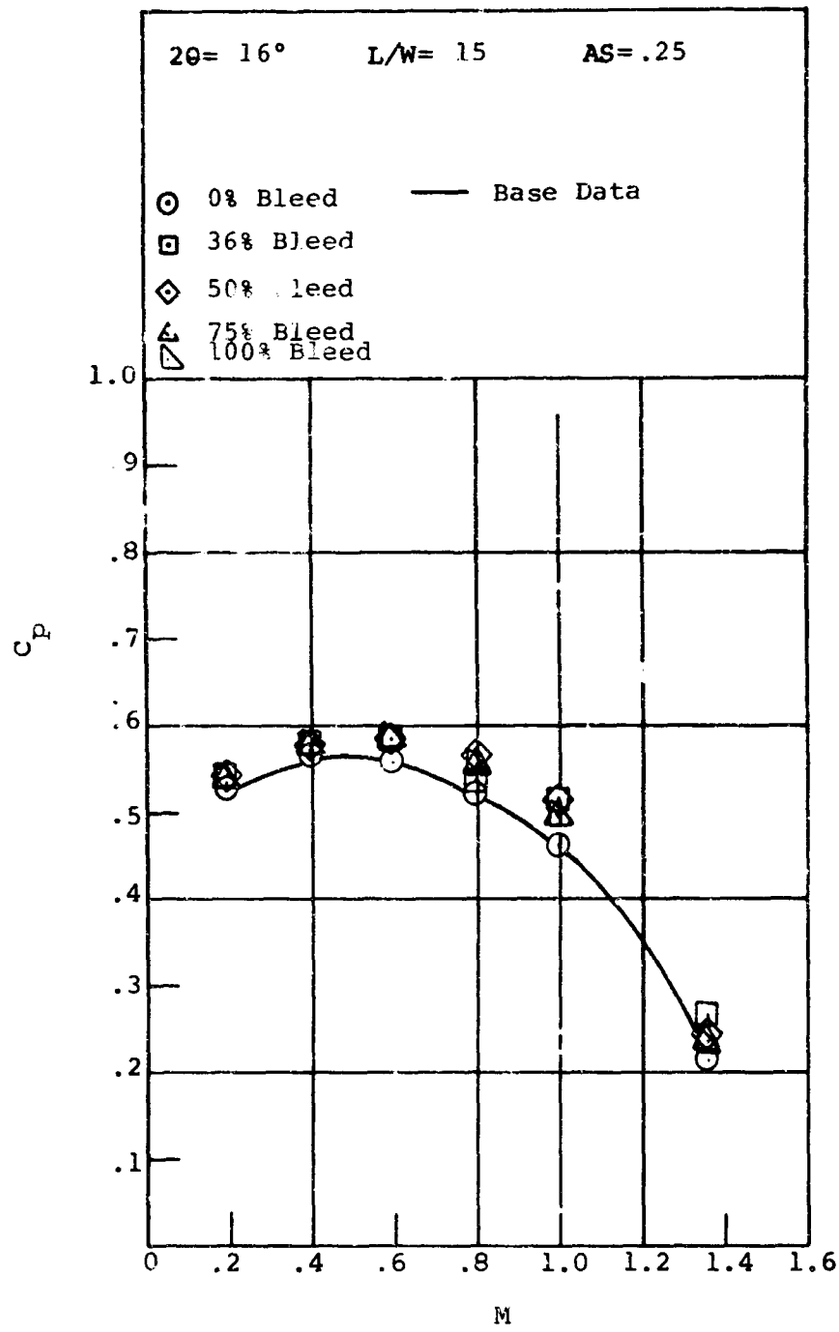

Figure 264. Pressure Recovery Versus Mach Number. Aspect Ratio = 0.25. Asymmetric Blockage Distribution Studies.

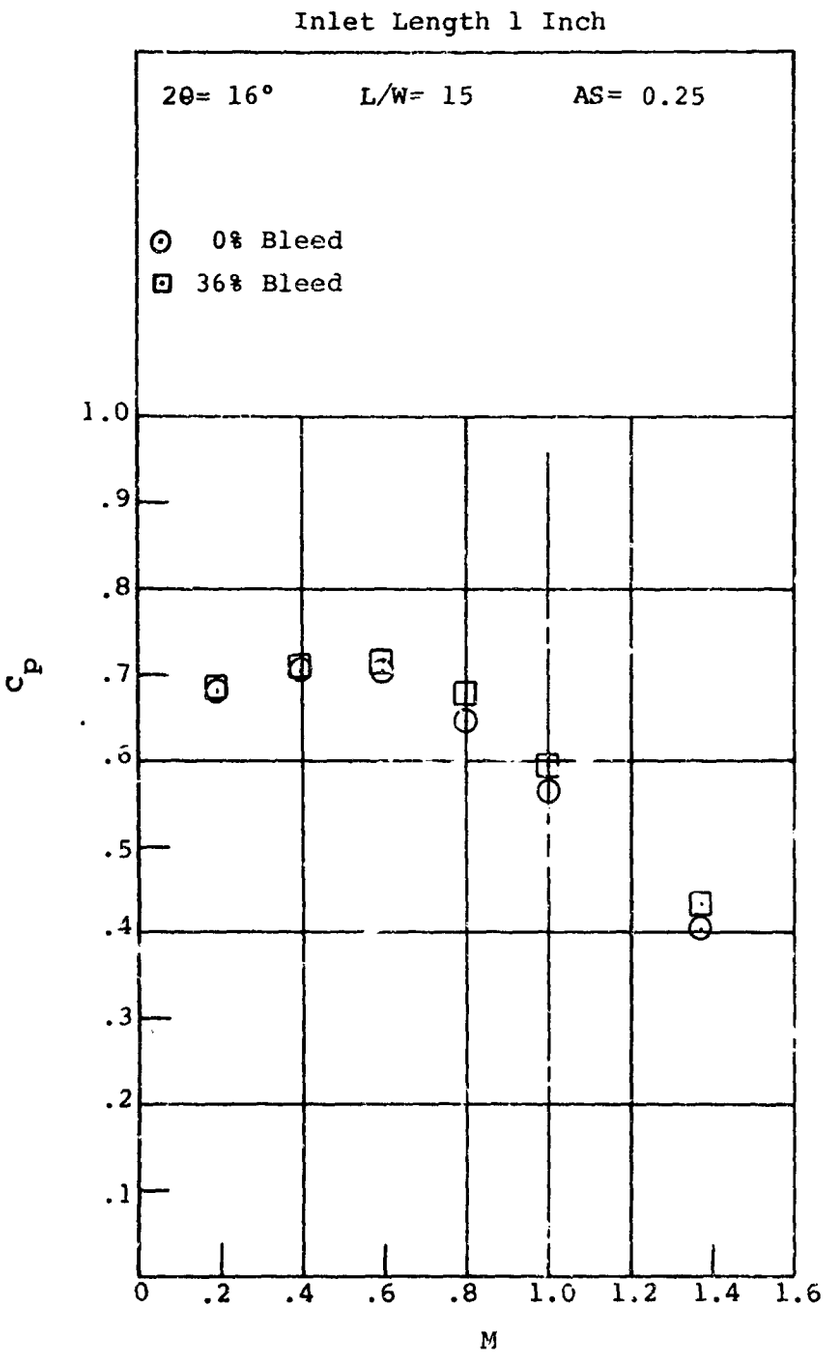

Figure 265. Pressure Recovery Versus Mach Number. Aspect Ratio = 0.25. Asymmetric Blockage Distribution Studies.

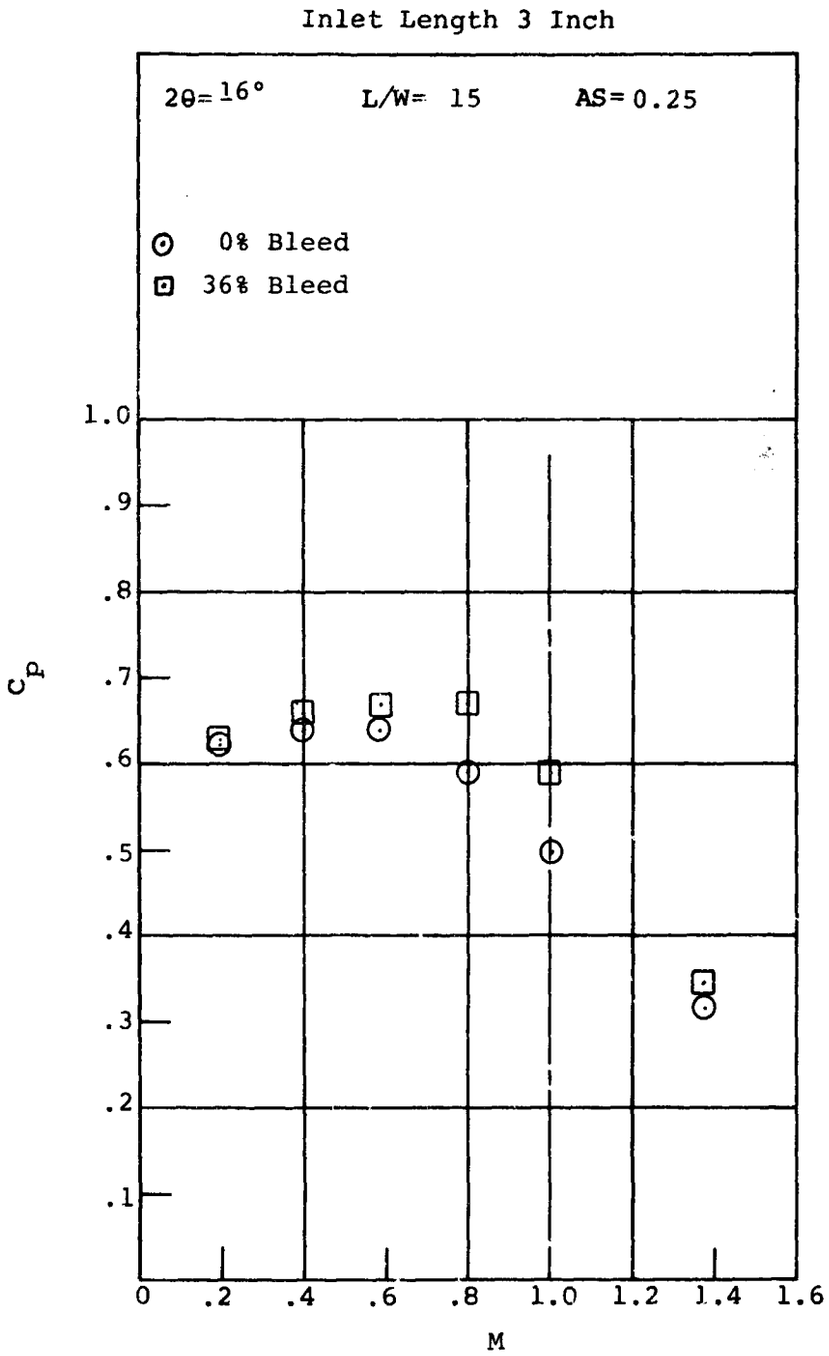

Figure 266. Pressure Recovery Versus Mach Number. Aspect Ratio = 0.25. Asymmetric Blockage Distribution Studies.

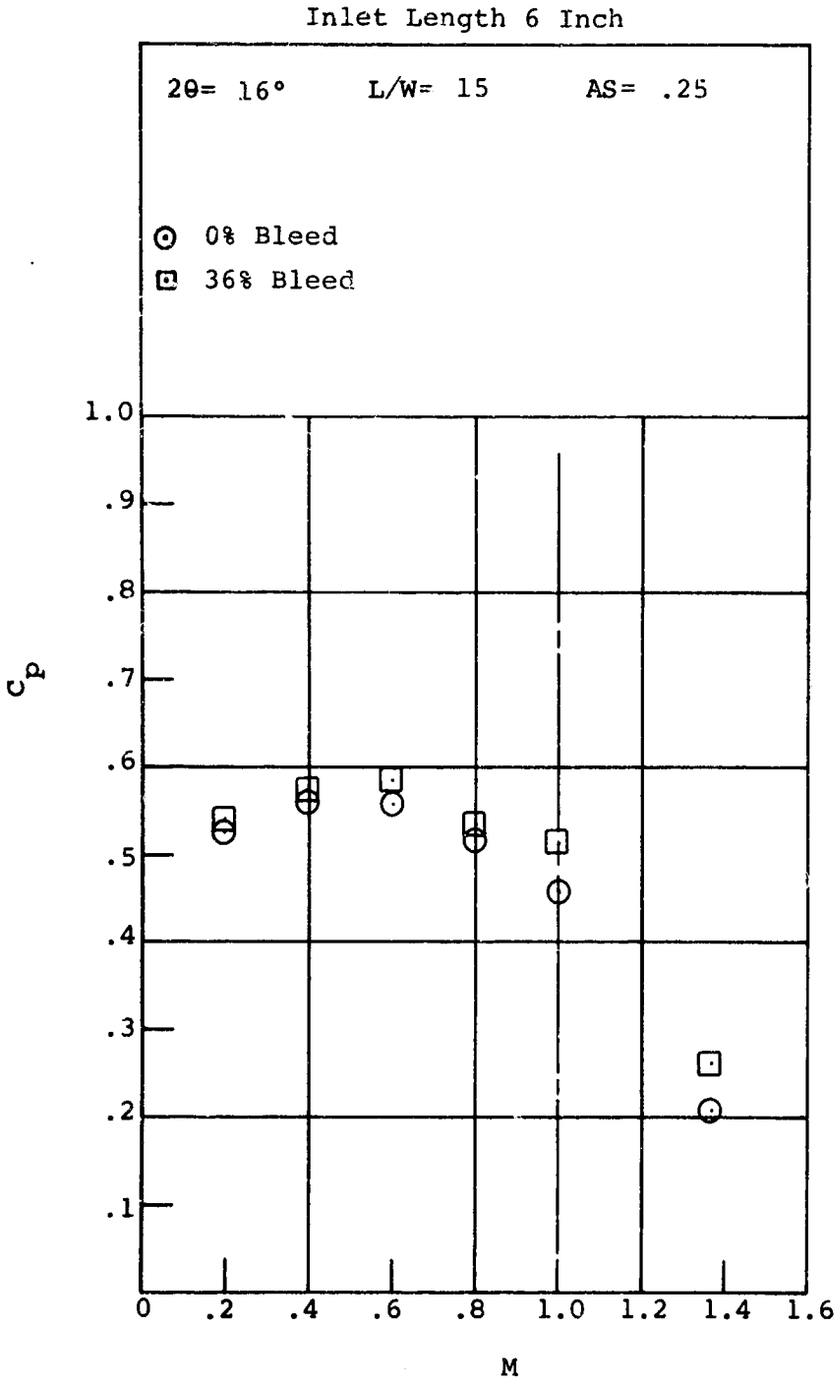

Figure 267. Pressure Recovery Versus Mach Number. Aspect Ratio = 0.25. Asymmetric Blockage Distribution Studies.

layer characteristic produced by suction, it would appear that a gross change in boundary layer velocity profile and distribution of turbulence throughout the boundary layer would be the parameters most affected that could have a strong bearing on pressure recovery.

One pronounced effect of applying strong bleed rates to a turbulent boundary layer is the possibility of relaminarizing the boundary layer flow. This effect is believed to be connected with the removal of the fluid very near the wall and with the production of fluid dynamic instabilities and turbulence within the boundary layer [see Kline, et al (1967)]. Relatively small suction flow rates will produce such an effect, particularly if the boundary layer is already operating or being produced in a favorable pressure gradient such as occurs in the inlet of the diffuser geometries. Once boundary layer suction ceases and the Reynolds number is sufficiently high, the boundary layer will again become turbulent. The higher the suction flow rate, the stronger the relaminarization effect. In the present studies, there is a 1/2" length of inlet (the 1/2" inlet length of the diffuser blocks) for which the boundary layer has a chance to reestablish itself before entering the diffuser. If it is postulated that a redistribution in boundary layer δ^* (and hence blockage) is not the primary effect responsible for altering the diffuser performance, the effect of bleed rate in terms of a relaminarization of the boundary layer may be explained as follows.

For very small bleed rates (up to but not exceeding approximately 25% bleed), the effect will be to remove low momentum fluid in the boundary layer near the wall and replace this with higher velocity fluid from the outer portions of the boundary layer. This is the usual effect desired in boundary layer control techniques wherein suction is applied. The fluid from the outer portions of the boundary layer acts to energize the boundary layer and enablesit to proceed further through an adverse pressure gradient before separation occurs. Such a boundary layer in a diffuser flow should help to increase diffuser performance by delaying separation. (It may be possible that even in these low suction flow rates the boundary layer is relaminarized but is able to reestablish its turbulent characteristics in the 1/2" length between the suction block and the diffuser throat before entering the diffuser.)

At large suction flow rates (greater than the 25% rate), the boundary layer may relaminarize and largely offset the effects of boundary layer energization found useful at the smaller suction rates. Thus, the performance of diffusers at these higher suction rates could decrease again toward the performance obtained with 0% bleed.

However, so little is known about the fundamental causes of turbulent boundary layer separation and how they are affected by changes in boundary layer profile, distribution of turbulent intensity across the boundary layer, etc., that the above arguments should be considered only as a hypothesis in explaining the observed behavior. It is possible that the observed change in diffuser performance is a function of all the above discussed effects including blockage redistribution.

It should be noted that in these suction experiments a pronounced difference in the amount of blockage redistribution is present between the aspect ratio = 0.25 and 1.0 geometries. In the aspect ratio = 0.25 geometry, the suction is applied over a very small portion of the perimeter of the inlet channel only. However, in the case of the aspect ratio = 1.0 geometry, the suction is applied to a full 1/4 of the inlet channel perimeter.

Regardless of the cause, the increased performance with the 25% suction rate is not large. The change in performance amounts to 3 to 4 points in recovery, which in terms of high pressure ratio (10 to 12 pressure ratio) centrifugal compressor performance might represent an increase in overall efficiency of about 1 point. The increased performance is probably a combination of effects, and a major redistribution in blockage at the throat produces only a minor change in diffuser pressure recovery compared to diffusers operating under the same inlet conditions but with symmetric blockage.

It is interesting to observe that in terms of compressor diffuser design, introducing a rough porous surface (the suction block) does produce a measurable change in pressure recovery performance at 0% bleed. Such an effect is probably associated with an increased "turbulence" level within the boundary layer flow entering the diffuser. It is interesting to speculate what effect would be produced in an actual

diffuser wherein the entire inlet flow periphery was "roughened". The results also indicate the importance of overall turbulence level in the inlet flow. No specific results have been obtained for high turbulence intensities purposely produced in the inlet flow, although the results of the porous surface tests indicate that this should have an effect on recovery. Actual compressor diffusers will have a high turbulence intensity in the inlet flow because of the wake-jet mixing off the impeller wheel; such an effect is worthy of study in future diffuser performance investigations.

4.8 ROUNDED THROAT CORNER STUDIES

Centrifugal compressor vane island diffuser designs often have rather sharp corners formed at the throat of the channel diffuser. A simple construction modification in such designs is the rounding of this sharp corner. To study the effect of what a throat rounding will do to diffuser performance, a series of tests were performed for a set of diffuser geometries at aspect ratio = 0.25 and 1.0. The rounded corner performance has been compared with the straight corner performance obtained in the first part of this investigation.

The corner rounding was performed according to the geometry laid out in Figure 268. Base study diffuser blocks were used, and the throat corner was rounded as indicated. The amount of rounding was determined by the 1/2" of inlet channel length preceding the sharp corner on the diffuser blocks.

The rounded corner geometry is no longer strictly a straight wall, symmetric, single-plane divergence straight wall diffuser. It is a trumpet-shaped diffuser which merges into a straight wall diffuser. However, the two diffusers have the same overall area ratio and inlet width W_1. The parameters on which to compare diffuser performance are, therefore, not exactly clear from a theoretical basis, since the diffuser could be classified as another type of two-dimensional diffuser. On the other hand, such a diffuser shape does represent a practical modification of a sharp corner diffuser that can easily be incorporated in an otherwise straight channel design in a piece of hardware. On this practical basis, it is not unreasonable to compare the performance of the rounded corner diffuser to that of the straight corner

diffuser. From a design standpoint, the rounded corner geometry represents either an added diffuser length as measured from the diffuser throat location or a modification of the diffuser throat region by extending the diffuser inlet upstream in the sharp corner configuration. We will return to a discussion of these points shortly.

As can be seen from Figure 268, very little rounding was actually made on most of the diffuser blocks (the amount of material removed from the sharp corner blocks is greatest for the largest divergence angle). The blocks were rough-cut approximately to shape and then hand-finished with a file and emery cloth to produce a smooth radius of curvature on the finished blocks. Particular care was maintained to provide a smooth and uniform junction between the radius of curvature and the straight section of the block (1) in the downstream divergence passage and (2) where the rounded corner joins the inlet blocks.

The performance data for the rounded corner tests is compared in Figures 269 through 278. The comparison basis is by treating the rounded corner geometry as an equivalent sharp corner geometry. Thus, in these figures no attempt is made to alter the length-to-width ratio in plotting the data.

In Figures 269 and 270, all the blockage data obtained on the rounded corner studies are compared with the blockage data of the base studies for the same inlet lengths and geometries. The blockage data are within the base data's estimated uncertainty. However, the blockage is grouped and falls slightly below the mean values for the base data. A comparison of the two sets of data has been made directly on the "raw" data format of C_p versus inlet Mach number M_t (so that the blockage B varies with Mach number M_t).

For low Mach numbers and low divergence angles 2θ, the pressure recovery performance is virtually identical between the two sets of data. If there is any trend in the data, it is to slightly higher pressure recovery at lo Mach numbers (usually less than 0.5 points in C_p) and a lower value of pressure recovery at the highest Mach number M_t of 1.365. At the highest divergence angles, however, the corner rounding produces an increase in recovery, particularly near sonic

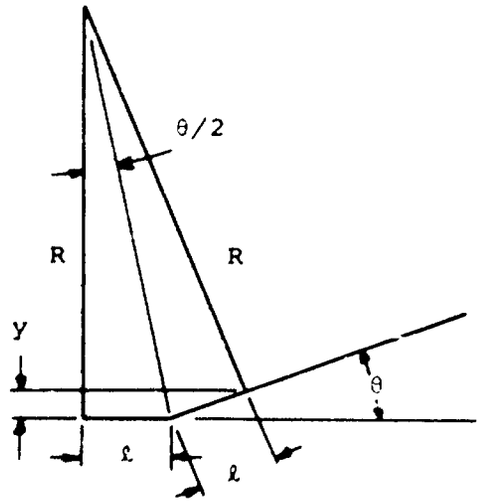

$\ell = 0.5"$

y/ℓ = sine

$\frac{\ell}{R} = \tan \theta/2$

hence $y = 0.5$ sine

$R = 0.5/\tan \theta/2$

θ degrees	Sin θ	θ/2 degrees	tan θ/2	R = 0.5/tan θ/2 inches	y = 0.5 sin θ inches
3	.05234	1.5	.02619	19.10	.0262
4	.06976	2	.03492	14.32	.0348
5	.08716	2.5	.04366	11.47	.0435
6	.10453	3	.05241	9.53	.0522
7	.12187	3.5	.06116	8.28	.0609
8	.13917	4	.06993	7.16	.0697

Figure 268. Rounded Throat Corner Geometry.

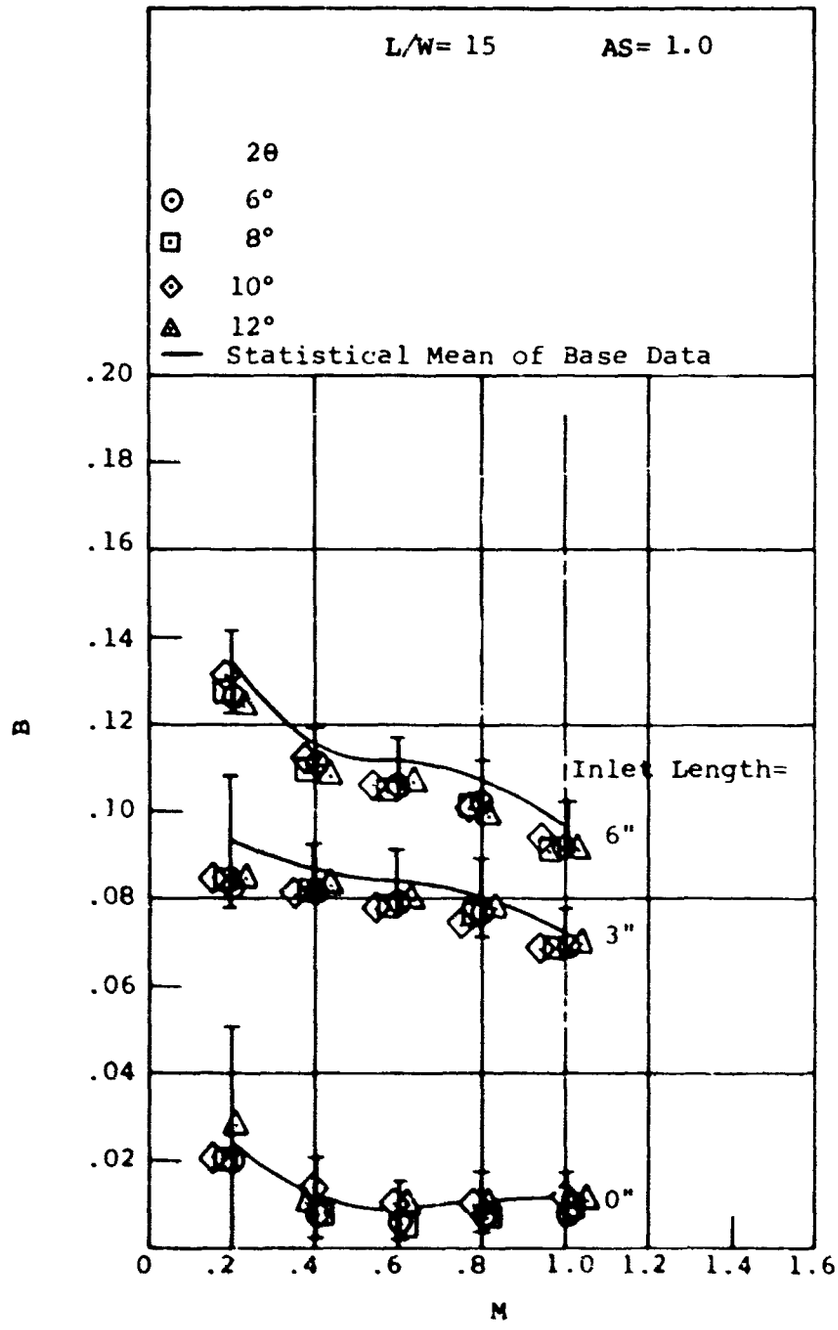

Figure 269. Blockage Versus Mach Number. Aspect Ratio = 1.0. "Rounded Corner" Studies.

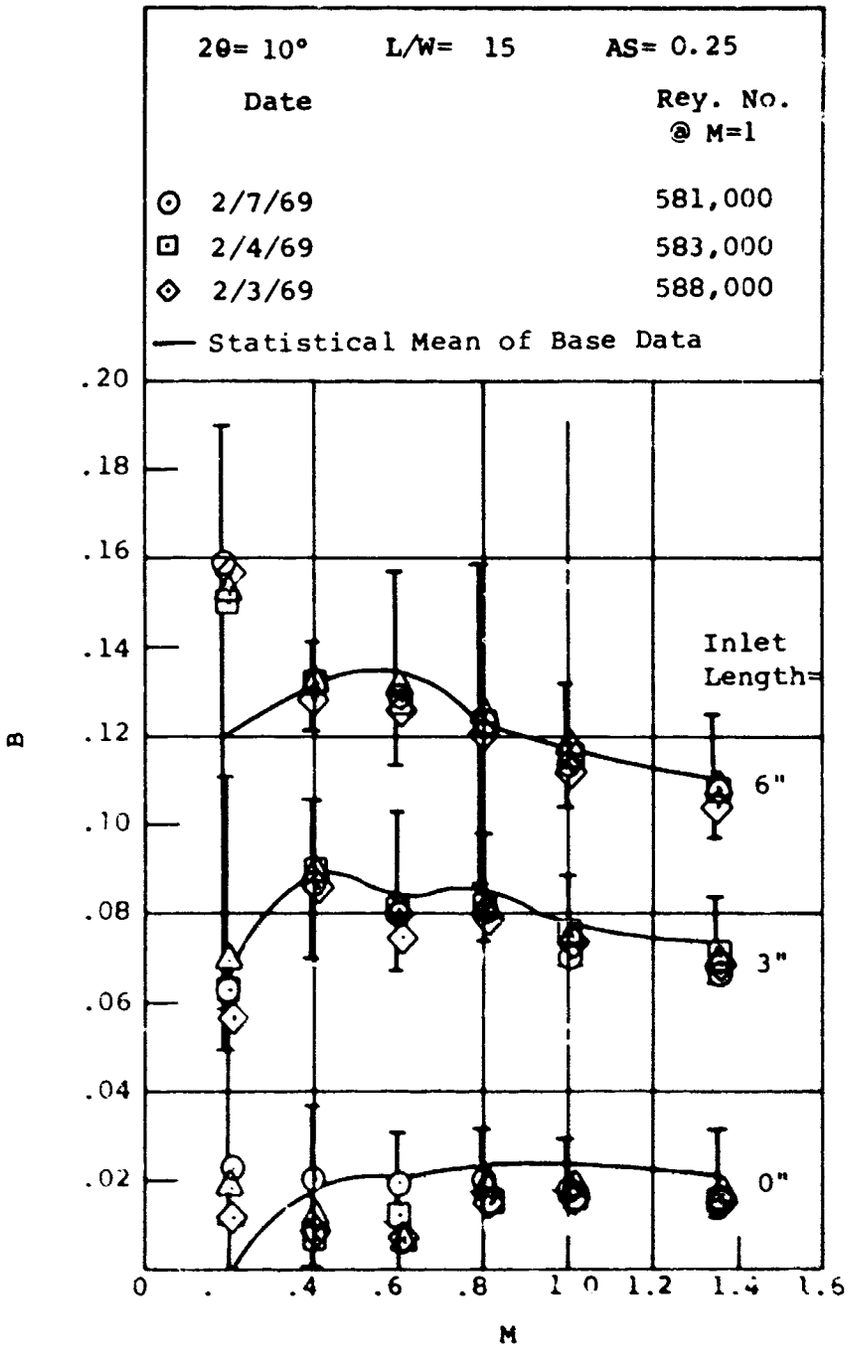

Figure 270. Blockage Versus Mach Number. Aspect Ratio = 0.25. "Rounded Corner" Studies.

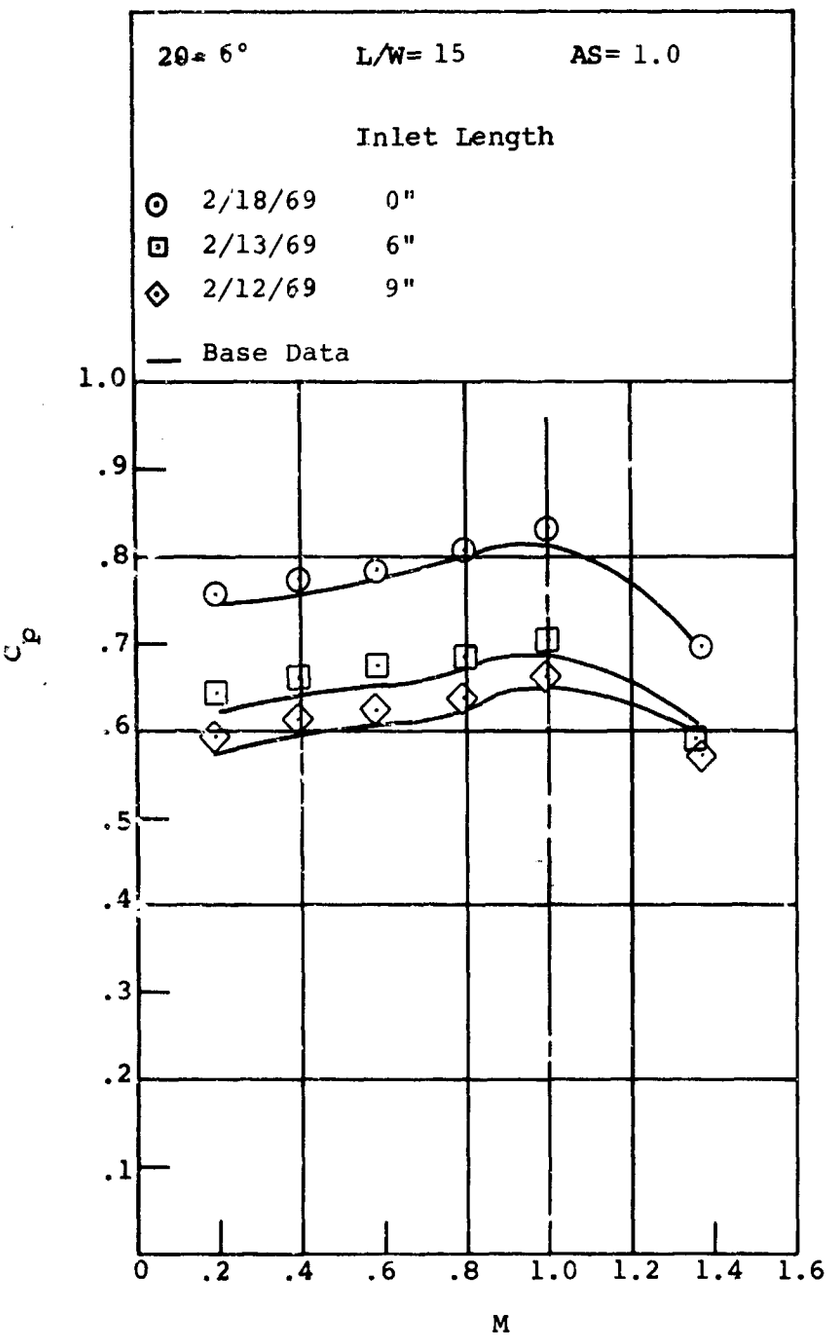

Figure 271. Pressure Recovery Versus Mach Number. Aspect Ratio = 1.0. "Rounded Corner" Studies.

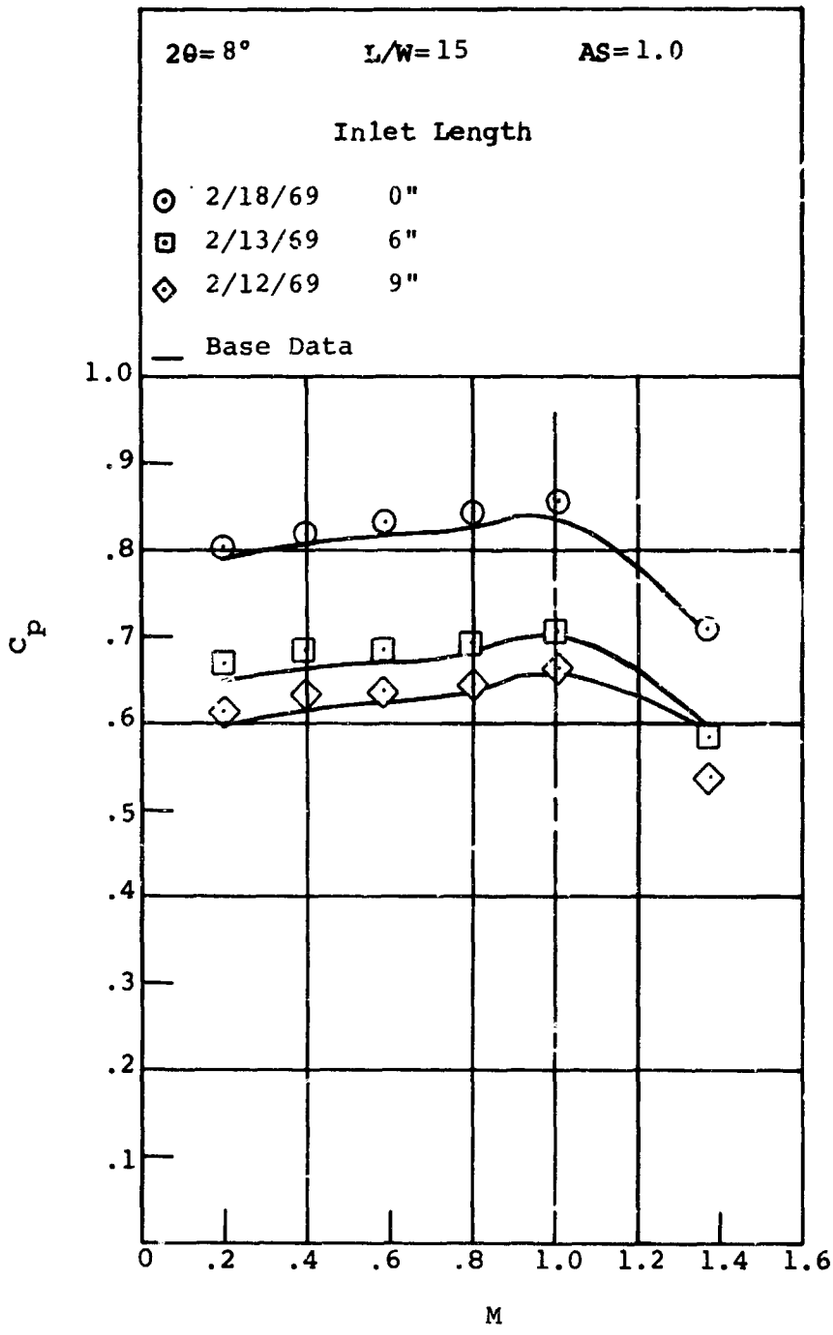

Figure 272. Pressure Recovery Versus Mach Number. Aspect Ratio = 1.0. "Rounded Corner" Studies.

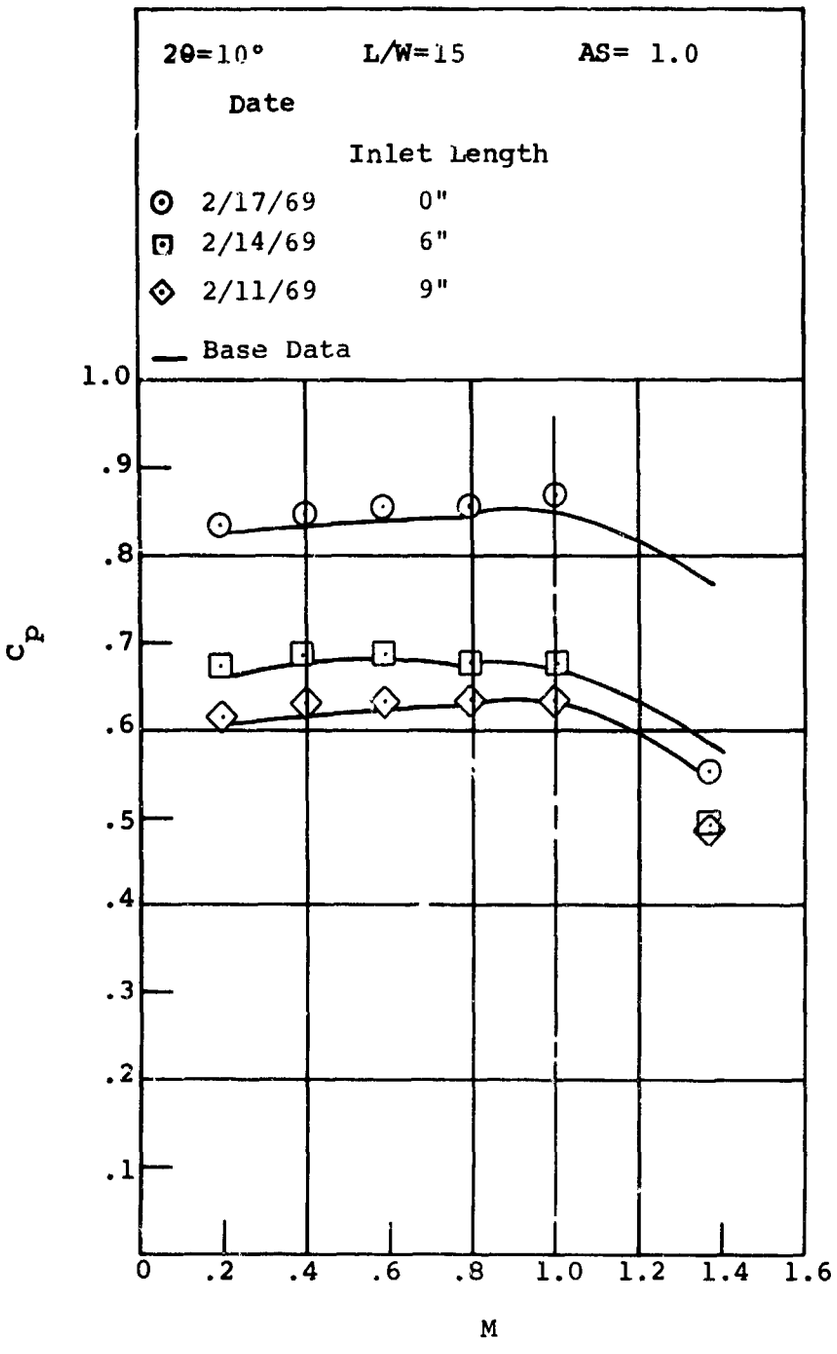

Figure 273. Pressure Recovery Versus Mach Number. Aspect Ratio = 1.0. "Rounded Corner" Studies.

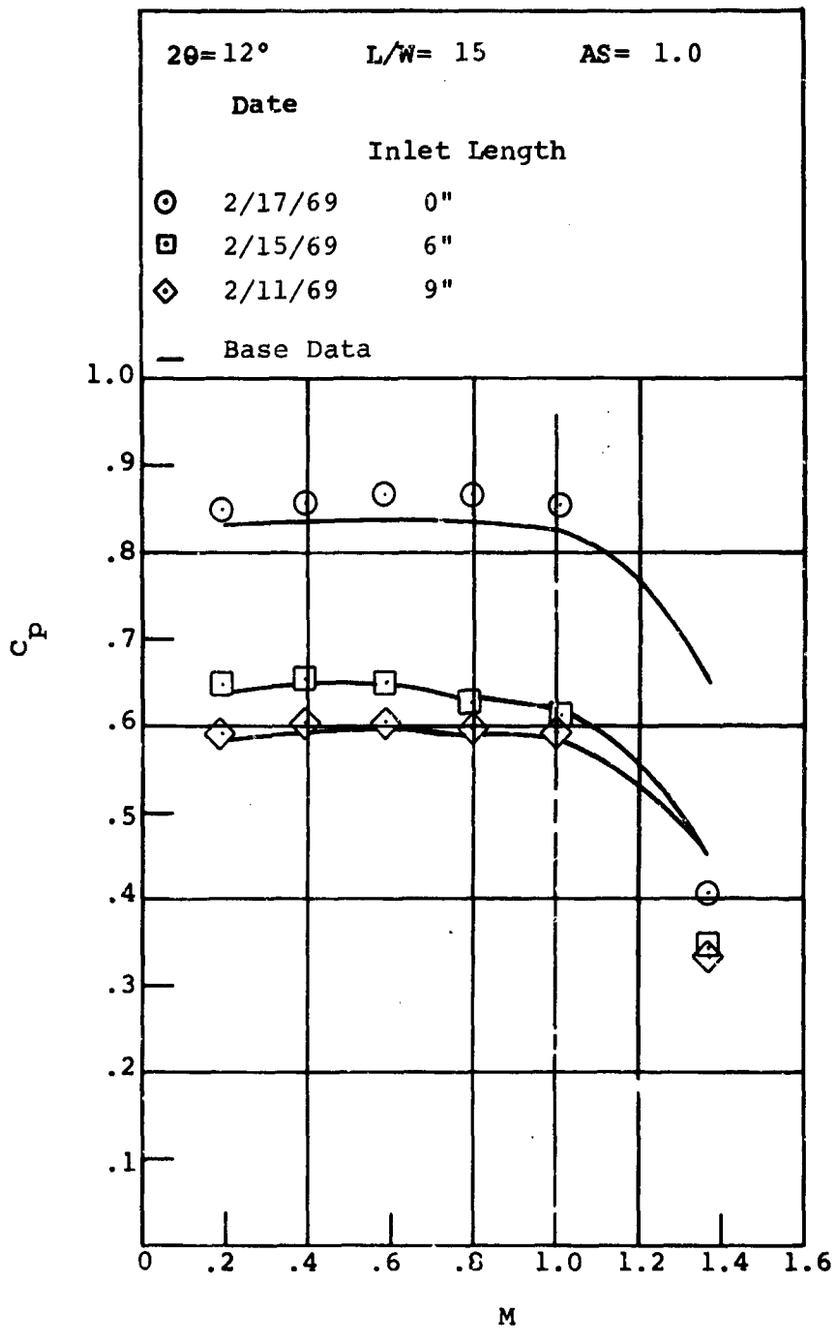

Figure 274. Pressure Recovery Versus Mach Number. Aspect Ratio = 1.0. "Rounded Corner" Studies.

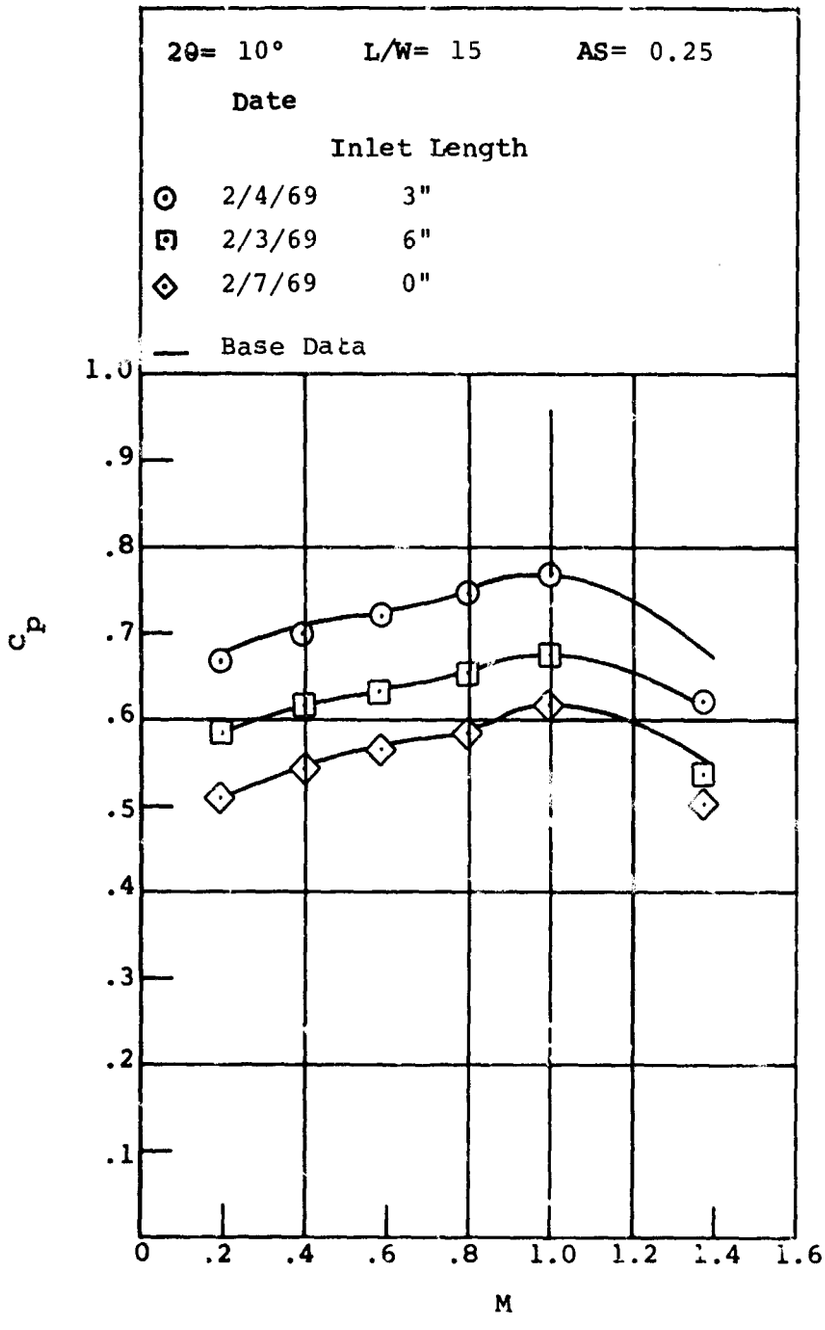

Figure 275. Pressure Recovery Versus Mach Number. Aspect Ratio = 0.25. "Rounded Corner" Studies.

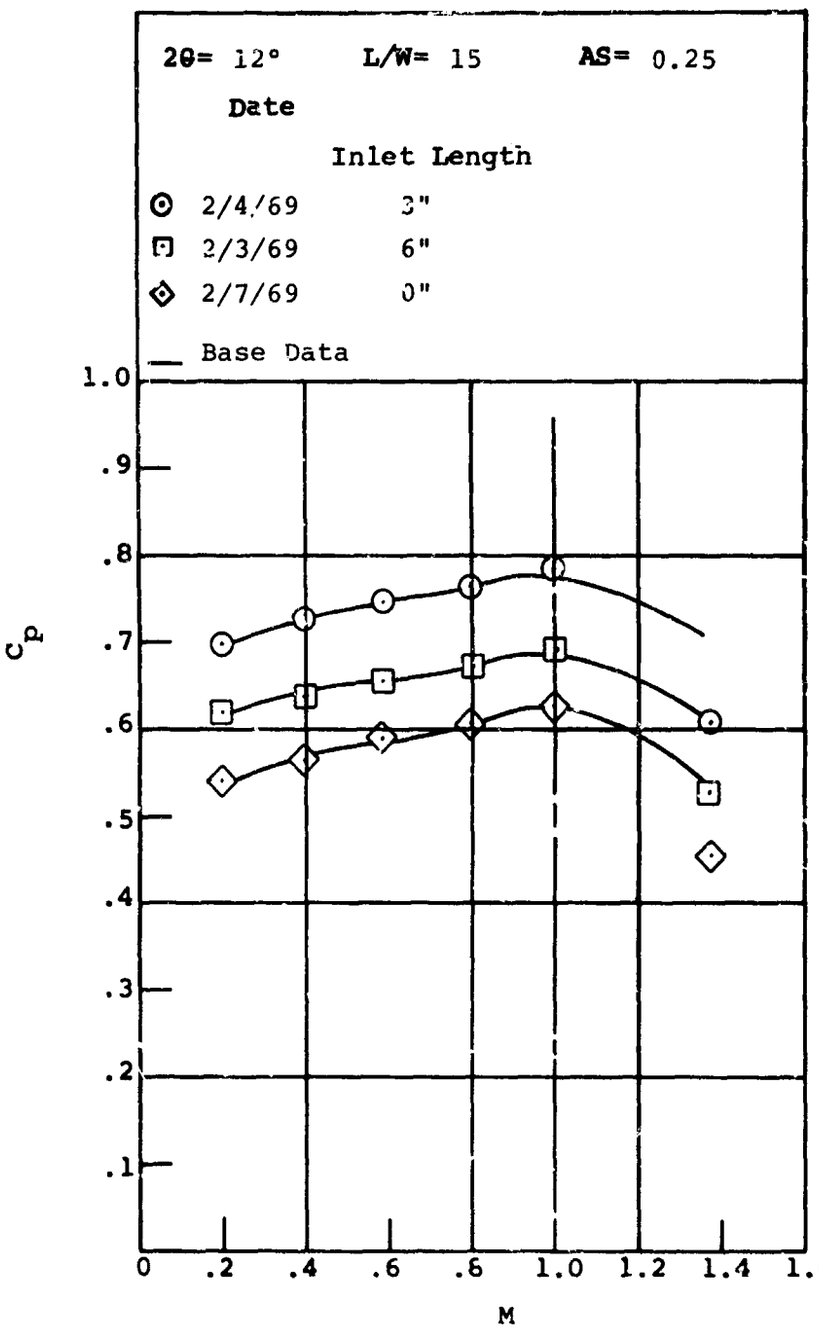

Figure 276. Pressure Recovery Versus Mach Number. Aspect Ratio = 0.25. "Rounded Corner" Studies.

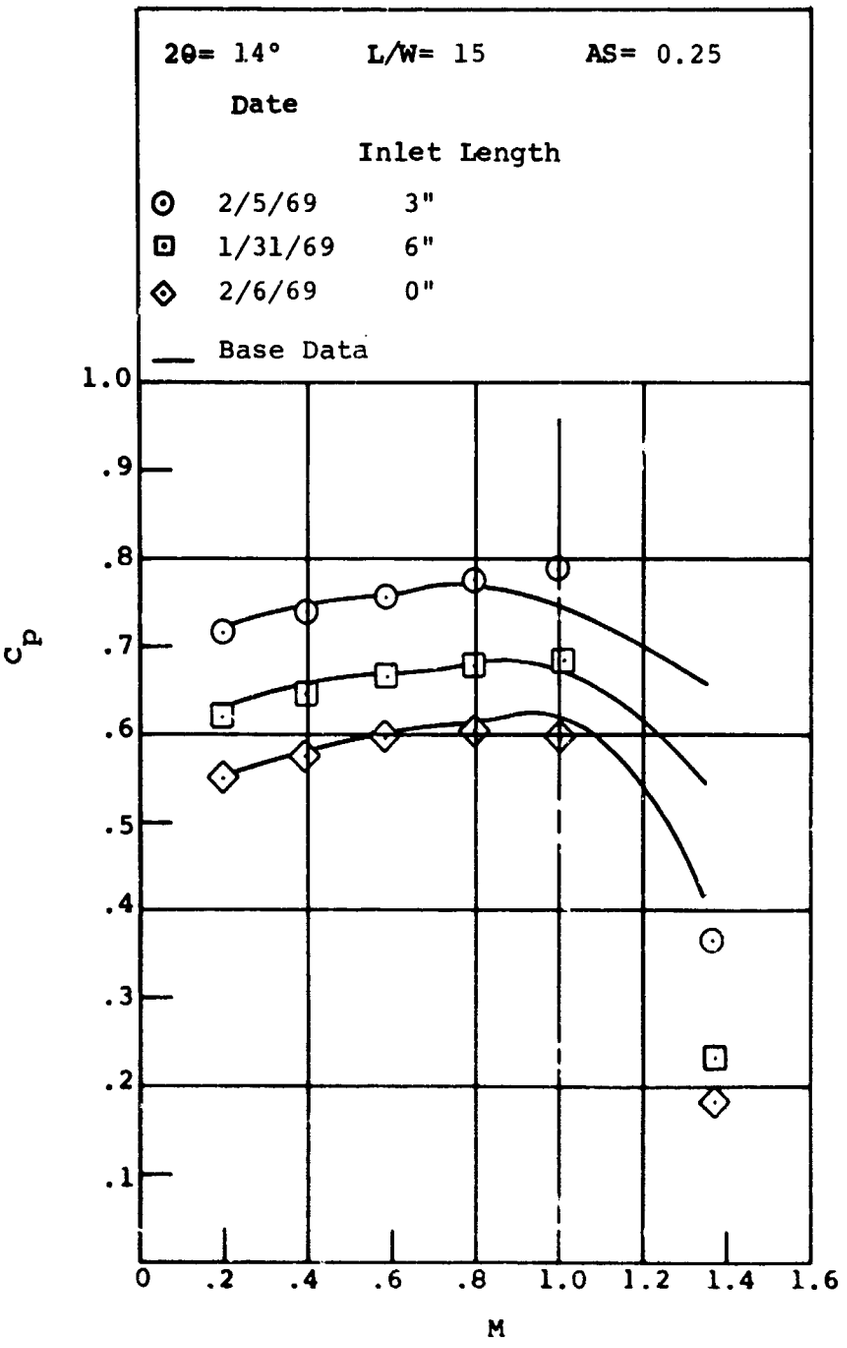

Figure 277. Pressure Recovery Versus Mach Number. Aspect Ratio = 0.25. "Rounded Corner" Studies.

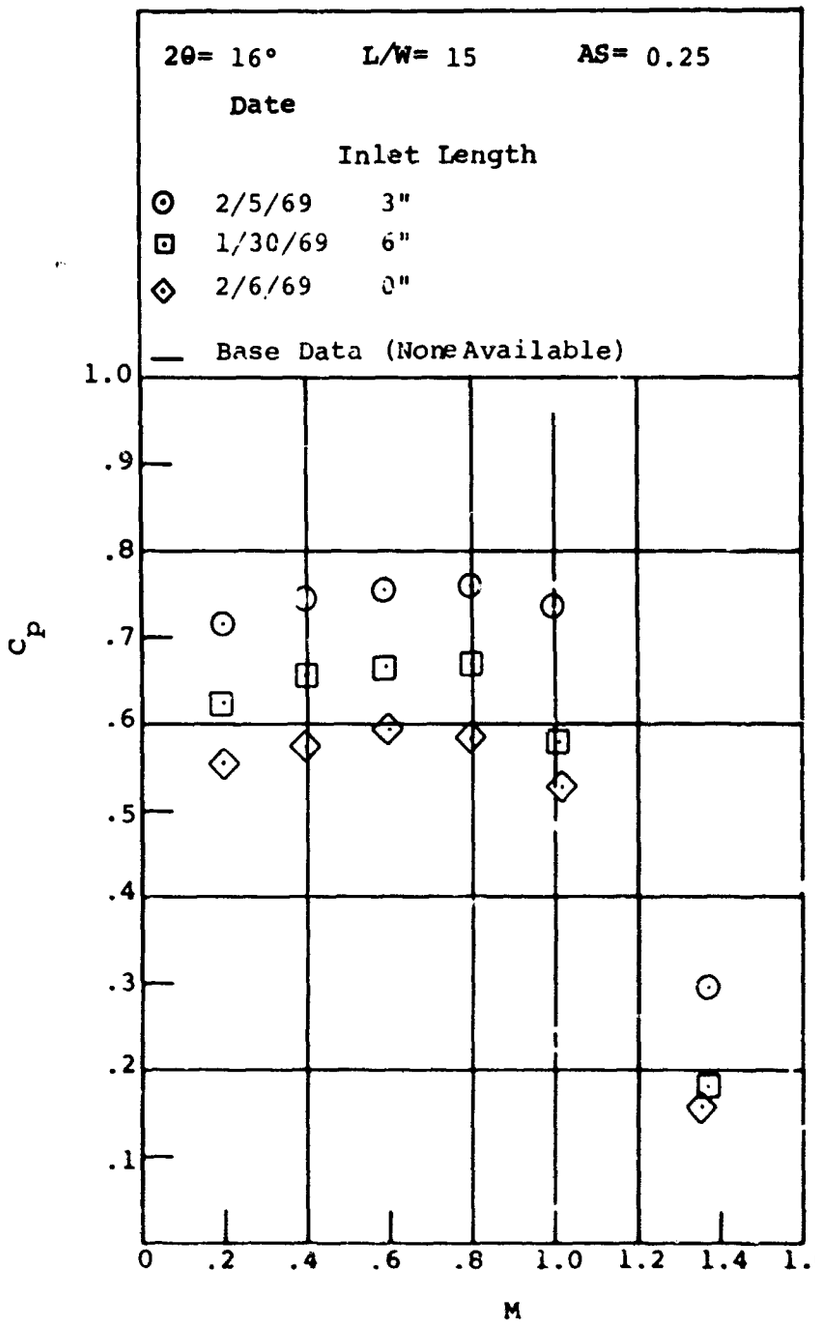

Figure 278. Pressure Recovery Versus Mach Number. Aspect Ratio = 0.25. "Rounded Corner" Studies.

conditions. In some cases, this is true for lower Mach numbers also. However, the same deterioration in performance, which is quite marked, is observed at the high (shock) Mach number of 1.365.

A way of looking at the rounded corner performance is to consider the rounded corner geometry as a sharp corner geometry with a longer diffuser length (higher L/W_1). On the basis of the performance maps for aspect ratio = 1.0, increasing the diffuser length-to-width ratio L/W_1 should lower diffuser recovery if the length-to-width ratio and area ratio are those of the peak recovery geometry. A study of the performance maps shows that the geometry of peak recovery changes with inlet Mach number and blockage. Since all of the rounded corner geometries were taken on L/W_1 = 15 configurations, only some of the test conditions correspond to those of peak recovery. Also, the additional 1/2" length on the aspect ratio = 1.0 configuration produces only a small increase in L/W_1 to an equivalent length-to-width ratio L/W_1 = 15.8. For the aspect ratio = 0.25 geometries, the increase is to a value of 15.55.

By examining the performance maps for aspect ratio = 0.25 in Figures 46 through 76, and for aspect ratio = 1.0 in Figures 77 through 106, it can be seen that these slight changes in aspect ratio L/W_1 hardly affect the magnitude of pressure recovery, since in both cases the length-to-width ratio L/W_1 is near the geometry for peak recovery at the angles tested. Here the slope of the pressure recovery hill is quite small; a small change in L/W_1 at constant area ratio does little to change the level of pressure recovery.

It had been felt previous to these tests that rounding of the sharp-edged corners might produce a significant increase in pressure recovery performance above the equivalent sharp-edged geometry through a reduction of the pressure dip which occurs locally around a sharp-edged corner at the throat. Such a local pressure dip for the sharp-edged geometry imposes a local pressure rise upon the boundary layer as it passes through the throat on the diverging wall. The local dip is the result of streamlined curvature in the main flow as the flow enters

the diverging passage. By rounding the throat corner, the magnitude of the local pressure dip should be relieved or eliminated entirely, depending upon the divergence angle. This should reduce the severity of the pressure rise imposed upon the boundary layer in the immediate vicinity of the diffuser throat.

Detailed pressure distributions on the diverging wall have not been made; thus it is not known to what extent the local pressure dip on the diverging wall is relieved. However, rounding the corner by the amounts produced in these studies has not produced a significant alteration in the shape of the performance hill on the pressure recovery map at the lower Mach numbers.

At sufficiently high Mach numbers (yet below sonic conditions), the local acceleration of the flow on the diverging wall at the throat can accelerate the core fluid immediately outside of the boundary layer to supersonic Mach number values. This can produce locally imbedded regions of supersonic flow around the sharp-edged throat corner. Although the situation is not fully understood, it is believed that if the supersonic values of Mach number are not too high, the core flow can isentropically decelerate again to a subsonic Mach number in the diverging passage. However, if the value of Mach number in the supersonic region is sufficiently high, the flow must decelerate through a local shock which terminates the supersonic imbedded region where it rejoins the subsonic flow in the diffusing passage. The termination of the flow by a normal shock imposes a much steeper pressure rise on the boundary layer flow immediately entering the diffuser than that which occurs when the flow outside the boundary layer decelerates isentropically. The behavior described here for the diffuser passage is analogous to the transonic flow in converging-diverging nozzles and is also related to the critical and supercritical flight regimes on airfoils at high subsonic Mach numbers [see Pearcey (1962)].

Thus the rounding of the sharp inlet throat corner should help delay the formation of imbedded supersonic regions and/or reduce the peak Mach number and consequent shock strength that occurs at the downstream end of the imbedded supersonic region. Depending upon the magnitude of the pressure gradient reduction achieved by rounding the corner, the pressure gradient performance of the diffuser should be increased slightly.

At Mach numbers 0.8 and higher, the rounded corner data show a definite increase in pressure recovery. This may perhaps be the result of the high Mach number effects discussed above.

Why the recovery deteriorates so badly for the rounded corner geometry when the Mach number ahead of the normal shock in the diffuser is 1.36 is not understood. Our understanding of the turbulent boundary layer is not sufficiently advanced to permit a very sound speculation upon what is actually occurring. Further understanding of the phenomena involved will depend upon more detailed fluid dynamic studies of the core and boundary layer flow in the vicinity of the diffuser throat.

Yet another way of looking at the slight recovery improvement with the rounded throat corner geometry is in terms of the small reduction in inlet throat blockage that can be achieved by a rounded diffuser corner.

An examination of Figures 268 and 269 shows that although the blockage data lie within the uncertainty bars of the base data, the values are consistently on the low side of the uncertainty limits. Since recovery is such a strong function of blockage, if the mean blockage of the rounded corner data is below the base data (and this is reasonable since the geometric throat is now 1/2" further upstream than for the base data), then the recovery values should be slightly higher, as is observed.

Centrifugal compressor diffuser designs sometimes incorporate channel diffusers with a short length of throat upstream of the inlet. Based on the studies of Welliver and Acurio (1967), it appears rational to eliminate this straight section of inlet throat [see Dean (1969)]. Assuming that the same overall radius for the diffuser exit and vane leading edge is maintained, changing the diffuser design to eliminate the straight section of inlet involves increasing the diffuser length-to-width ratio at constant area ratio. Such an alteration would not produce a significant change in channel diffuser pressure recovery if the comparison is based upon constant inlet blockage. Note, however, that from a design standpoint the elimination of the short, straight inlet may reduce the inlet throat blockage B to the new diffuser design. The performance

map data show how important blockage is to overall performance. Based upon the rounded corner tests, some improvement at high Mach numbers should therefore be possible by using a rounded corner, maintaining the same diffuser divergence angle 2θ and the same area ratio as in the sharp corner design.

In summary, some small improvement in pressure recovery can be gained by rounded throat corners as compared to sharp throat corner geometries. The main causes of the increased performance are probably (1) reduced local adverse pressure gradients on the diverging walls near the throat (particularly at high Mach numbers), and (2) slightly reduced throat blockage (the performance comparison has been based upon assuming that the rounded corner tests have the same blockage-Mach number relationship as was present in the base studies). Point (2) should not actually be a point of consideration, since the tests should be compared for the same throat blockage; the present data, however, does not permit a better evaluation of blockage for the rounded corner tests. However, from a designer's viewpoint, point (2) is an important consideration in overall diffuser design, as we will discuss in Section 5.

Although only a small increase in pressure recovery appears to be obtainable (and this over a limited Mach number range) with the rounded corner geometry, the cumulative effect of a series of minor changes such as this can permit the designer to achieve a significant improvement in diffuser pressure recovery in actual designs. To do so, however, the designer must be aware of the small recovery improvements possible and also of the possible trade-off in recovery between various design changes.

4.9 DISCUSSION

A number of physical phenomena that help to determine the pressure recovery performance of straight channel diffusers have already been discussed in preceding sections. However, other characteristics of the performance data that have not been discussed in detail are:

(1) At low diffuser angles, the base data shows a gradual rise in diffuser effectiveness with increasing throat Mach number.

(2) There is a gradual decrease in diffuser effectiveness with an increase in inlet Mach number at high diffuser angl s near and above the ridge of optimum recovery (C_p* and C_p**).

(3) There is a general decrease in diffuser performance of a few points in pressure recovery across the Mach number range with a reduction in inlet Reynolds number.

(4) There is a large change in recovery performance with a change in diffuser aspect ratio.

There are several physical phenomena which are involved in diffuser flow which may help to understand these observed pressure recovery characteristics.

Some diffuser characteristics can be related to the separation flow regime behavior observed to occur in the channel diffuser (at least under incompressible flow conditions). For example, some of the qualitative characteristics of the pressure recovery contour hills have already been discussed and related to the onset of transitory separation and fully separated flow within the diffuser channel. We will now analyze some of the characteristics related to the inlet Reynolds number, inlet Mach number, and channel geometry, and attempt to interpret these qualitatively in terms of the physical phenomena occurring around the diffuser throat and the boundary layer flow through the channel diffuser.

Inlet Mach Number

At low values of divergence angle 2θ, recovery increases with inlet Mach number up to choking conditions at the diffuser throat. When the throat is choked, the pressure recovery performance falls off appreciably when the Mach number ahead of the shock in the diffuser passage reaches a value of approximately 1.2 to 1.3. Visual observations indicate that the shock is essentially a normal shock. Shock wave - boundary layer interaction theory dictates that the rapid falloff in performance at diffuser shock Mach numbers of 1.2 to 1.3 is due to separation of the boundary layer by the rapid pressure rise imposed on the boundary layer passing under the foot of the shock.

As divergence angle 2θ is increased, the rate of rise of recovery with inlet Mach number becomes less, finally showing a decrease with inlet Mach number as the divergence angle 2θ becomes sufficiently large.

These trends with increases in divergence angle and inlet Mach number may be understood by discussing diffuser performance in terms of the diffuser effectiveness. Holding all diffuser conditions fixed except inlet Mach number, we might expect diffuser effectiveness to remain constant with an increase in throat Mach number. An examination of the effectiveness plots of Figures 167 through 178 illustrates that this does not occur and that effectiveness varies with inlet Mach number and divergence angle at constant aspect ratio, length-to-throat width ratio, and inlet blockage. For values of the divergence angle sufficiently below the ridge of optimum recovery (C_p* and C_p**), the effectiveness plots illustrate that the assumption of a relatively constant effectiveness diffuser with inlet Mach number may be approximately valid. At moderate divergence angles, however, an increase in effectiveness with inlet Mach number is observed.

At small values of divergence angle where the diffuser is essentially unstalled, the performance of the diffuser depends upon the rate of growth and separation behavior of the boundary layer passing through the diffusing passage. A simple and useful model has been used in the past to calculate the effect of boundary layer growth on pressure recovery for incompressible flow diffusers [see Reneau, et al (1964)]. For unstalled diffusers (small divergence angle and area ratio), the assumption is made that the boundary layers on the diffuser walls experience a pressure gradient and velocity distribution given by a one-dimensional flow diffusing through the area ratio expansion of the diffuser. Account is taken of the displacement effects of the boundary layer flow on the core flow pressure distribution. (In actual diffuser passages, of course, the flow is three-dimensional and has local variations in velocity and pressure, and it differs from the assumed one-dimensional, isentropic core flow.)

The boundary layer blockage in a cross section in the diffuser is defined by the equation

$$B = 1 - \frac{A_{effective}}{A_{geometrical}} \tag{47}$$

In terms of the diffuser dimensions and boundary layer displacement thickness δ^*, the blockage is

$$B = 1 - \frac{(W - 2\delta^*)(b - 2\delta^*)}{bW} \tag{48}$$

Under the assumptions given above, the pressure recovery performance of a small divergence angle, unstalled diffuser where a potential core flow still exists at the diffuser outlet is given by the pressure rise of the core flow through the diffuser. The area ratio for this core flow can be calculated from the area ratios at the inlet and exit of the diffuser minus the displacement effect (blockage effect) of the boundary layer. The incompressible pressure recovery performance for a straight wall diffuser in terms of the inlet and outlet blockage and the diffuser geometric area ratio is

$$C_p = 1 - \frac{1}{(1 - B_2)^2} \cdot \frac{(1 - B_1)^2}{(AR)^2} \tag{49}$$

where 1 = inlet
2 = outlet

For a fixed area ratio diffuser with given inlet conditions, the pressure recovery will thus decrease with increasing exit flow blockage B_2.

A change in diffuser effectiveness with inlet Mach number and divergence angle may be partially explained by changes in exit flow blockage B_2 as follows.

Local variations in pressure and velocity occur wherever there is a local curvature of the flow streamline through the diffuser. For single divergence, straight wall diffusers, there will be a static pressure reduction or dip in pressure at the junction of the diverging walls and the inlet throat passage. Here the streamlines experience a sharp change in direction,

since the streamlines very close to the wall must follow the wall contour. The static pressure will rise again to the one-dimensional pressure variation in the diverging passage soon after the flow moves around the corner of the throat and the streamlines again become straight. Near the throat corner, then, the boundary layer on the diverging walls sees a higher pressure gradient than do the boundary layers on the parallel sidewalls, whose streamlines experience no change in direction in a plane normal to the wall.

The growth and behavior of the sidewall and diverging wall boundary layers under the same applied pressure gradient in the diffuser determine the growth and thickening of the boundary layers and hence the pressure recovery and effectiveness of the diffuser as given by Equation 49.

Now as inlet Mach number is increased, the amount of reduction in pressure (pressure dip) at the diverging wall throat corner will become larger. This is a result predicted by compressibility pressure correction formulae such as the Prandtl-Glauert rule or the Karman-Tsien pressure correction formula [see Shapiro (1953)].

Assuming that all inlet boundary layer characteristics are held fixed as the diffuser inlet Mach number is raised, the reduction in local static pressure distribution near the throat on the diverging wall will become larger and impose a greater adverse pressure gradient on the boundary layer on the diverging wall immediately following the throat. This will result in an increased boundary layer thickening (larger blockage) at the diffuser exit and hence a lower pressure recovery as given by Equation 49. Thus, when all other diffuser parameters are held fixed, the diffuser effectiveness will appear to decrease with increasing inlet Mach number.

For large divergence angles (although for divergence angles still below the ridge of optimum C_p), the decrease in effectiveness with Mach number should become larger, since the pressure dip at the throat will be greater with a larger divergence angle.

Qualitatively, the following effects on effectiveness are observed: (1) an increase in Mach number at constant throat blockage and geometry and (2) an increase in divergence angle at

constant inlet length-to-throat width ratio, diffuser aspect ratio, inlet blockage, and Mach number.

Note also that another effect should appear at sufficiently high subsonic inlet Mach numbers. At high inlet Mach numbers, imbedded supersonic flow regions should occur as the flow is accelerated around the sharp corner on the diverging wall, as discussed in 4.8. It is quite likely that such regions of locally accelerated flow to supersonic velocities will be terminated by a normal shock. When this local shock becomes sufficiently strong, the rapid rise in pressure across the shock, which is imposed on the boundary layer passing under it, may be sufficient to separate the boundary layer flow.

Then, for a given high inlet Mach number, the acceleration of the flow and the strength of the local terminating shock can be expected to increase as 2θ is raised. Shock boundary layer interaction theory says that boundary layer separation may be expected when the shock Mach number reaches 1.2 to 1.3. A crude estimate of the divergence angle necessary to produce Mach numbers of 1.2 to 1.3 ahead of the terminating shock can be obtained by analogy to Prandtl-Meyer flow around a corner. For Prandtl-Meyer flow at inlet Mach number unity, a turning angle of 4° is sufficient to produce a Mach number of approximately 1.2, and a turning angle of 6° is sufficient to produce a Mach number of approximately 1.3. Thus divergence angles 2θ on the order of 8° to 12° may be sufficient to produce locally imbedded supersonic flow near the corner of the diverging wall and a terminating shock sufficient in strength to separate the boundary layer on this wall. The actual details of the flow at the throat will of course be different from those of the Prandtl-Meyer flow. However, both experimental and theoretical analyses have shown that such effects are indeed produced in nozzle flows [see Emmons (1944) and Oswatitsch (1962)]. Thus the supersonic imbedded region terminated by a local shock may explain the very rapid decrease in diffuser effectiveness as divergence angles become large at very high subsonic inlet Mach numbers.

In summary, the characteristics of the pressure recovery and the effectiveness performance versus inlet Mach number for a fixed geometry diffuser may be explained by the local two-dimensional flow effects at the throat corner where the diverging wall and inlet throat passage meet. The local flow

acceleration effects at the throat corner can account for a decrease in diffuser effectiveness as the inlet Mach number is raised. Further, if the inlet Mach number is sufficiently high, and the divergence angle is moderately large, regions of locally accelerated supersonic flow terminated by shocks can likely occur. If the strength of the terminating shock is sufficiently high, the shock may separate (or severely "damage") the boundary layer on the diverging wall as it passes through the shock. Such an effect should produce a rapid deterioration in diffuser effectiveness.

Inlet Reynolds Number

A prescribed condition for the Reynolds number tests has been that the boundary layers at the diffuser inlet have the same blockage effect for the two Reynolds number conditions tested. If we again assume a moderately low divergence angle diffuser situation where the pressure recovery performance is determined by the behavior and nature of the boundary layer growth in the diffuser passage, the observed trends in pressure recovery with inlet Reynolds number may be partially rationalized. For moderately low divergence angles where the core flow is maintained to the diffuser exit, the boundary layer growth through the diffuser will be a function of the length Reynolds number through the diffuser passage. At low inlet Reynolds numbers (it is recalled that the inlet Reynolds number R_D is defined in terms of the throat hydraulic diameter D), the inlet conditions between two Reynolds number tests must imply a lower core flow density for the lower Reynolds number conditions than for the high Reynolds number conditions. This lower density at low Reynolds numbers implies, therefore, a lower unit length Reynolds number for the flow through the diffuser.

If it is assumed, as a first approximation, that the boundary layer growth behavior is similar to that for incompressible flat plate flow, e.g.,

$$\delta^* = \text{constant} \cdot x \cdot (R_{e_x})^{-1/n} \qquad (50)$$

then the boundary layer displacement thickness grows as the reciprocal power of the unit length Reynolds number. At low

Reynolds number conditions where the unit length Reynolds number is small, the boundary layer growth will be larger relative to the high Reynolds number situation. A larger boundary layer growth will result in a larger blockage effect at the diffuser exit and hence a lower pressure recovery [see Equation (49)]. Qualitatively, this is the general behavior observed to occur for the results of the Reynolds number tests shown in Figures 185 through 212.

The effect of the inlet Reynolds number is also involved in the effectiveness/Mach number plots considered in the previous section. Because the base study tests were run with constant upstream stagnation pressure, the inlet Reynolds number varied with inlet Mach number (see Table XI). In fact, a variation of approximately a 5-to-1 reduction in Reynolds number occurs between the Mach number $M_t = 1.0$ and $M_t = 0.2$ tests. Thus, in addition to the Mach number effects discussed above, there is the additional effect of increasing throat Reynolds number with increasing Mach number in the effectiveness versus Mach number plots. This effect should be to counteract the Mach number effect discussed previously by increasing pressure recovery as Mach number, and hence Reynolds number is raised.

Another boundary layer effect is also present where inlet Mach number is varied. Compressible turbulent boundary layer calculation techniques predict a slightly smaller boundary layer growth (and hence displacement thickness growth) for a compressible boundary layer flow compared to an incompressible flow. At high inlet Mach numbers, the boundary layers in the initial portions of the diffuser passage will thus have an even smaller rate of boundary layer growth when compared to low Mach number tests because of this compressibility effect. The qualitative results should be a further increase in pressure recovery due to lower boundary layer blockage at the exit for the higher inlet Mach number data.

The combination of these boundary layer growth effects, one occasioned by Reynolds number changes and the other by boundary layer compressibility effects, may explain the increase in diffuser effectiveness observed in the aspect ratio 0.25 data at the low divergence angles (Figures 167,

168, and 169). Excluding these effects, it is difficult to see why diffuser effectiveness should be increased with increasing Mach number.

The relatively small reduction in recovery at low Reynolds numbers and at high Mach numbers may result from the slight increase in pressure recovery with increasing Reynolds number as throat Mach number is raised. This effect combined with the compressibility effect on the boundary layer characteristics may offset the adverse effect of inlet Mach number discussed above under "Inlet Mach Number Effects".

Aspect Ratio Effects

The qualitative explanations given in the preceding sections for diffuser flows which maintain a potential core and for the effects associated with the sharp throat corner on the diverging wall may partially explain the rather pronounced effects of aspect ratio observed in the base studies.

If a deterioration in the pressure recovery performance of a diffusing channel occurs primarily because of local acceleration effects on the diverging wall at the sharp throat corner, the amount of diverging wall at the throat in relation to the amount of parallel sidewalls should have an important relation to overall diffuser recovery. For low aspect ratio diffuser, the percentage of the throat periphery taken up by the diverging wall is small compared to high aspect ratio diffusers. Considering aspect ratio 1.0 diffusers as a reference, diffuser recovery should decrease with increasing aspect ratio (all other conditions described by the geometric and inlet variables held constant), and recovery should increase with decreasing aspect ratio. The general arguments are here again restricted to moderate divergence angle diffusers where the boundary layer remains unseparated and a core flow exists at the diffuser exit. This is the trend that is observed except for the sharp reduction in recovery at low aspect ratio.

However, we may expect a deterioration in performance as aspect ratio decreases to small values. For the straight wall, single divergence diffuser, the actual pressure recovery performance when only aspect ratio is changed must depend upon the diffuser effectiveness, which in turn depends upon

boundary layer behavior of the flow in the diffuser. In an attempt to understand the effect of aspect ratio on the boundary layer behavior, and hence on actual recovery performance, we will examine the low Mach number (incompressible flow) diffuser in the unstalled flow regime.

We will assume in the following that the pressure gradient and velocity distribution through the diffuser are based on an equivalent one-dimensional, incompressible, isentropic core flow. We will also assume that the boundary layer growth depends upon the streamline pressure gradient given by a potential core flow one-dimensional velocity distribution. In general, diffusers of low inlet blockage and moderately low divergence angle and area ratio correspond to such conditions. The area variation through the diffuser is

$$AR = 1 + \frac{x}{W_1} 2 \tan \theta \tag{51}$$

On a one-dimensional basis, the core flow velocity distribution through the diffuser will be

$$V = \frac{Q}{A} = \frac{Q}{b(W_1 + 2x \tan \theta)} \tag{52}$$

where Q = flow rate = VA

Using Bernolli's equation for the core flow, the pressure gradient distribution is

$$\frac{dp}{dx} = - \rho V \frac{dV}{dx} = \rho \frac{Q^2}{b^2} \frac{(2 \tan \theta)}{(W_1 + 2x \tan \theta)^3} \tag{53}$$

Now the momentum integral equation describing the turbulent boundary layer growth in the diffuser can be written

$$V^2 \frac{d\phi}{dx} + (2\phi + \delta^*) V \frac{dV}{dx} = \frac{\tau_o}{\rho} \tag{54}$$

where ϕ = momentum thickness

Using the expressions for the pressure and velocity distributions through the diffuser, the momentum integral equation can be rewritten as follows:

$$[2\emptyset + \delta^*]\left[-\frac{2\tan\theta}{\left(\frac{W_1}{L} + 2\bar{x}\tan\theta\right)}\right] = \frac{L\,\tau_o}{\rho V^2} - \frac{d\emptyset}{d\bar{x}} \qquad (55)$$

where $\bar{x} = x/L$

In order to solve this momentum integral equation for the boundary layer characteristics δ^* and $\emptyset$, the initial conditions at the diffuser inlet δ_1^* and $\emptyset_1$ must be prescribed. Also, an empirical equation for the variation of $\tau_o/\rho V(x)$ and an auxilliary equation for the shape parameter $H = \delta^*/\theta$ are usually assumed to be given.

To determine the influence of aspect ratio, we will now look at a special case where the aspect ratio is changed. In this special case, two diffusers will be compared having the same inlet boundary conditions (i.e., Reynolds number, δ^* and $\emptyset$) at the inlet and the same length-to-width ratio and divergence angle. For these two diffusers, the aspect ratio will be varied by interchanging the roles of the depth b and the width W_1 so that the inlet area for each diffuser is the same, i.e., $A_1 = bW_1$.

Since both diffusers are run at the same L/W_1 but different W_1, the diffuser length L will be different for each diffuser. We now write the pressure gradient and velocity distribution through both diffusers in terms of the reduced axial length $\bar{x} = x/L$:

$$\frac{dp(\bar{x})}{d\bar{x}} = \rho\,\frac{Q^2}{(L/W_1)^2(bW_1)^2}\cdot\frac{2\tan\theta}{(W_1/L + 2\bar{x}\tan\theta)^3} \qquad (56)$$

$$V(\bar{x}) = \frac{Q}{(L/W_1)(bW_1)(W_1/L + 2\,\bar{x}\tan\theta)} \qquad (57)$$

Since the inlet Reynolds number is based on hydraulic diameter and this is the same for each diffuser, both diffusers have the same flow rate Q.

We now assume, in addition to the special conditions described above, that the area ratio is sufficiently large that the pressure gradient term dominates over the shear stress term $\tau_o/\rho V^2$ in establishing the boundary layer growth characteristic in the diffuser.*

In terms of the reduced length $\bar{x}$, the boundary layer growth situation will then be the same in each diffuser, since the pressure gradient and the velocity distribution are identical for each diffuser, as can be seen from Equations 56 and 57. Given identical inlet conditions for the boundary layer in each diffuser, the differential equation for solving the boundary layer characteristics will also be identical for each diffuser yielding the same boundary layer displacement thickness at $\bar{x} = 1$; this can be seen from Equation 55. Thus the boundary layer displacement thickness in each diffuser will be identical at the outlet of the diffusers.

This result is now combined with the expression for recovery in terms of the effective through-flow area based on the geometric area and the flow blockage induced by the wall boundary layers given in Equation 48.

We now make one final assumption to the effect that the δ^{*2} term on the right of Equation 48 is much smaller than the other terms. This is true if the boundary layer displacement thickness δ^* is small compared to the diffuser exit dimensions. Thus

$$B_2 = 2\,\delta_2^* \frac{(b + W_2)}{bW_2} \tag{58}$$

Thus under the assumed conditions, the following quantities for each diffuser are constant:

---

*Reneau, et al (1964), has shown that this will occur for fixed L/W_1, at values of 2θ which are near maximum recovery. This is the region of primary interest.

$$L/W_1,\ 2\theta,\ bW_1,\ B_1,\ \text{and}\ \delta_2^*$$

and also for the special case under consideration where the roles of b and W_1 are interchanged between the two diffusers:

$$b_{1_L} = W_{1_S} \quad \text{and} \quad b_{1_S} = W_{1_L} \tag{59}$$

where L = large aspect ratio
S = small aspect ratio

Using these relations in Equation 48, the ratio of exit blockage of the large aspect ratio diffuser to that for the small aspect ratio diffuser is

$$\frac{B_{2_L}}{B_{2_S}} = \frac{(AS + AR)_L \, AS_S^{1/2}}{(AS + AR)_S \, AS_L^{1/2}} \tag{60}$$

By these arguments, small aspect ratio diffusers have larger exit blockage and therefore a lower pressure recovery than do large aspect ratio diffusers. Note that although the above arguments have been presented for the special case of two aspect ratio diffusers and for conditions where only inlet aspect ratio is changed, the arguments can be extended to pairs of diffusers throughout the entire aspect ratio range, and the inlet and geometric conditions correspond exactly to those desired for a comparison of diffuser performance maps. The prescribed conditions are, however, restricted to a consideration of geometries near or below the ridge of optimum recovery.

On the basis of the above arguments, two opposing effects thus occur with a change in diffuser aspect ratio:

1. A decrease in pressure recovery performance with increasing aspect ratio is caused by the adverse boundary layer effects brought on by the sharp throat corner on the diverging wall. As aspect ratio is increased, a greater percentage of the throat periphery is dominated by diverging wall boundary layers.

2. As aspect ratio is increased, the boundary layer growth characteristics through the diffuser are such as to produce a lower exit flow blockage and higher pressure recovery.

Because of the rather large boundary layer growth effect, this factor probably dominates over the sharp throat corner effect.

Since the above analysis holds only for pairs of diffusers whose aspect ratios are related by

$$AS_L = \frac{1}{AS_S} \tag{61}$$

it is possible to compare only pairs of diffusers on either side of the aspect ratio = 1.0. The pairs of diffusers are unique sets which together cover all aspect ratios between 0 and infinity. Thus, even though the above analysis tells us that under the assumed conditions a higher recovery may be expected for the high aspect ratio diffuser than for the low aspect ratio diffuser, and that there is a significant recovery difference between the low and high aspect ratios, the exact shape of the pressure recovery curve with aspect ratio cannot be determined.

Taking into account the tendencies for recovery to decrease with decreasing aspect ratio because of the sharp throat corner effect, a C_p vs. AS curve should look somewhat as shown in Figure 142. As aspect ratio becomes very large, the rate of change of pressure recovery with unit change in aspect ratio (e.g., the slope of the pressure recovery curve on the C_p vs. AS plot) should become small.

The above arguments are not presented as any quantitative means for calculating or predicting the changes in pressure recovery with aspect ratio (although calculations for aspect ratios 0.25 and 4.0 do yield reasonably accurate results for low divergence angles); the arguments are offered as a qualitative justification for the observed trends in pressure recovery with aspect ratio.

At very low aspect ratio, the diffuser performance should deteriorate badly. Various arguments may be presented to demonstrate why this should occur. These arguments depend upon the manner in which small aspect ratio is achieved.

In terms of practical diffuser design (i.e., centrifugal compressor design), small aspect ratio can be achieved by either increasing the throat width W_1 at constant depth b or decreasing the depth b and holding throat width W_1 constant. In either case, if the very low aspect ratio geometry is compared with higher aspect ratios, all other diffuser conditions (L/W_1, 2θ, B, M_t, and R_D) are to be held fixed.

Considering the case where the depth b is held constant, increasing the throat width W_1 to reduce aspect ratio increases the overall diffuser length L since L/W_1 is constant. If the aspect ratio is reduced sufficiently, the boundary layer at the inlet will grow in the diffuser, eventually merging in the centerline. If the aspect ratio is sufficiently small, a pipe-like fully developed flow condition can occur, causing a drop in static pressure with distance through the diffuser. This can be seen from the following arguments. The boundary layer displacement thickness will grow as a power of x:

$$\delta^* = \text{constant } x^n \tag{62}$$

where x = distance in stream direction
n = exponent greater than zero

The ratio of displacement thickness to diffuser width at the exit of the diffuser will therefore vary according to

$$\delta_2^* \propto L^n \propto W_1^n \tag{63}$$

since L/W_1 = constant and thus L varies directly as W_1.

Therefore the boundary layer displacement thickness relative to the throat depth varies as

$$\frac{\delta_2^*}{b} \propto \frac{W_1^n}{b} \tag{64}$$

If W_1 is increased sufficiently, δ_2^*/b can become large enough to cause boundary layer merger. Such a condition will produce a very poor diffuser pressure recovery.

The same case holds for the second possibility, that of holding W_1 constant and decreasing b. Referring to Equation 64, we again see that the ratio δ_2^*/b becomes sufficiently large as b is decreased holding W_1 constant.

On theoretical grounds, other arguments must be considered as well. Namely, the inlet Reynolds number R_D should be held constant to compare the influence of changes in aspect ratio.* From a practical standpoint, however, it appears that as aspect ratio is reduced to very low values, a sharp decrease in pressure recovery can be expected to occur, as has been observed in the pressure recovery/aspect ratio curves presented in this report. Johnston (1969b) has recently made measurements at aspect ratio 0.10 for incompressible flow at $L/W_1 = 6.0$. Depending upon Reynolds number, angle, and blockage, very low values of pressure recovery, and in some cases negative recovery, have been measured.

It therefore appears logical to conclude that in the case of centrifugal diffuser design, very low values of aspect ratio will result in very poor recovery performance. On the basis of the data uncovered in the present studies, aspect ratio should definitely be kept above 0.25.

---

*These points are discussed by Johnston (1969a) in a discussion on the paper by Runstadler and Dean (1968) and in the Author's Closure by Runstadler and Dean (1969).

5.0 APPLICATION OF CHANNEL DIFFUSER PRESSURE RECOVERY PERFORMANCE TO CENTRIFUGAL COMPRESSOR DIFFUSER DESIGN

5.1 RATING PARAMETERS

The purpose of the centrifugal compressor diffuser is to convert the flow kinetic energy leaving the impeller into a maximum rise in static pressure. In the modern, small, high performance gas turbine, it is the static pressure recovery of the diffuser that is of significance; the residual kinetic energy in the flow at the exit of the diffuser is usually dumped into a collector. The total-to-static stage isentropic efficiency is the performance parameter that is properly employed in evaluating overall compressor performance.

The performance data for the channel diffusers have been presented in the form of a diffuser static pressure recovery coefficient. Three other rating parameters are often used for evaluating diffuser performance. For the centrifugal compressor diffuser, the rating parameters are:

$$C_p = \text{pressure recovery coefficient} = (p_{coll}-p_2^*)/(p_{o_2}-p_2)^* \quad (65)$$

$$R_{Diffuser} = \text{Diffuser Recovery} \quad p_{coll}/p_{o_2}^* \quad (66)$$

$$\eta_D = \text{efficiency} = (h_{coll}-h_2^*)/(h_{o_2}-h_2)^* \quad (67)$$

$$C_D = \text{loss coefficient} = (p_{coll}-p_o^*)/(p_{o_2}-p_2)^* \quad (68)$$

where p = static pressure
h = static enthalpy
p_o = stagnation pressure
2 = impeller tip station
coll = collector station
* = after impeller discharge mixing process
h_o = stagnation enthalpy

Each of these parameters (for a given fluid) is a function of the inlet Mach number to the diffuser M_2^* and the pressure recovery coefficient C_p. It can be shown that

$$R_{diffuser} = 1 - (1-C_p)\left[1 - \frac{1}{\left(1 + \frac{k-1}{2} M_2^{*2}\right)^{\frac{k}{(k-1)}}}\right] \qquad (69)$$

$$\eta_D = \frac{R_{diffuser}^{k-1/k} - 1}{\left(\frac{k-1}{2} M_2^{*2}\right)} \qquad (70)$$

where M_2^* = flow Mach number at impeller tip after mixing of the impeller wake-jet flow

Any of the above rating parameters can therefore be used to describe the centrifugal compressor diffuser performance. We have chosen to use the static pressure recovery coefficient.

The relationship between overall compressor efficiency and diffuser performance is expressed as

$$\eta = \eta_i^* R_{diffuser}^{(k-1)/k} - \frac{1 - R_{diffuser}^{(k-1)/k}}{\mu_i (k-1)(\pi m_i)^2} \qquad (71)$$

where η = compressor total-to-static isentropic efficiency = $(h_{coll} - h_{o_i})/W_x$

η_i^* = impeller total-to-total (after mixing) isentropic efficiency

h_{o_i} = stage inlet stagnation enthalpy

h_{coll} = compressor collector enthalpy

W_x = work input/unit mass of fluid

μ_i = impeller work input coefficient = $(C_\theta/u)_2$

C_{θ_2} = mass flow averaged tangential velocity at impeller tip

u_2 = tip speed

πm_i = impeller tip Mach number based on u_2 and stage inlet stagnation speed of sound

Differentiating the above equation, we can obtain the leverage that diffuser performance has on overall compressor efficiency.

$$\frac{\partial \eta}{\partial C_p} = \left[\eta_i^* + \frac{1}{\mu_i (k01)(\pi m_i)^2}\right] \left(\frac{k-1}{k}\right) R_{diffuser}^{-1/k}$$

$$1-\left[1 + \frac{(k-1)}{2} M_2^{*2}\right]^{-k/(k-1)} \qquad (72)$$

For typical state-of-the-art air machines where PR is the pressure ratio:

PR	$\partial \eta / \partial C_p$
3	0.42
10	0.32

Thus for a high pressure ratio centrifugal compressor, about 1/3 of a point in overall compressor efficiency is gained for every point improvement in diffuser static pressure recovery. Next to the fluid dynamic optimization of the impeller, the diffuser plays a very critical role in achieving good overall performance.

5.2 FLUID MECHANICS OF THE CENTRIFUGAL COMPRESSOR DIFFUSER

Our discussion will be limited to vaned diffuser, as this appears to be the only design applicable to high performance, high pressure ratio centrifugal compressors. A sketch of the vane-island diffuser has been given in Figure 1. We define the centrifugal compressor diffuser as the combination of flow passages between the impeller tip radius and the diffuser collector where the static pressure rise has reached its maximum.

The design approach to be discussed is based upon separating the centrifugal diffuser into a series of flow elements rather than attempting to treat the pressure recovery performance of the overall diffuser as a single unit. The success of this approach is based upon having appropriate design techniques available to evaluate the fluid dynamic behavior in the flow regions ahead of the channel diffuser.

The justification for treating the overall diffuser as a series flow combination of a channel diffuser preceded by the flow in the vaneless and semivaneless regions is based largely on the studies of Welliver and Acurio (1967). Their work showed that over the range of impeller exit Mach numbers from subsonic to supersonic values, the flow adjusted itself in the vaneless and semivaneless regions of the diffuser to provide nearly a one-dimensional flow pattern entering the channel diffuser beyond the vane leading edge.

A typical pressure contour plot at a high impeller Mach number is shown in Figure 279. This figure was prepared from static pressure wall tap surveys made throughout the diffuser region in the Welliver and Acurio studies. The principal characteristic of this flow is a rapid adjustment to a near-constant pressure region ahead of the entrance to the channel diffuser. The flow appears to be nearly uniform and one-dimensional entering the channel diffuser. This is true whether the impeller exit Mach number is subsonic or supersonic. Also, little pressure rise occurs in the semivaneless space, since the flow streamlines run essentially parallel to lines of constant pressure.

For subsonic exit Mach numbers, the flow adjusts rather continually through the vaneless and semivaneless space to provide uniform channel diffuser inlet conditions. At supersonic impeller exit Mach numbers, the flow may remain supersonic until immediately ahead of the channel diffuser entry where it undergoes a rapid adjustment through a shock to establish the Mach number and flow conditions required to pass the flow through the channel diffuser throat.

Since most of the pressure rise ahead of the channel diffuser occurs in the vaneless space, the vane diffuser geometry (e.g., the vaneless space radius ratio, the number of vanes, vane spacing, vane shape, and depth) has an important bearing on the boundary layer growth that occurs on the sidewalls and suction surface in the vaneless and semivaneless space.

In high performance, high pressure ratio compressors, the streamline direction leaving the impeller is very close to tangential, and the flow follows a long streamline path before it arrives at the throat of the diffuser. This long path combined with the streamwise pressure gradient results in a

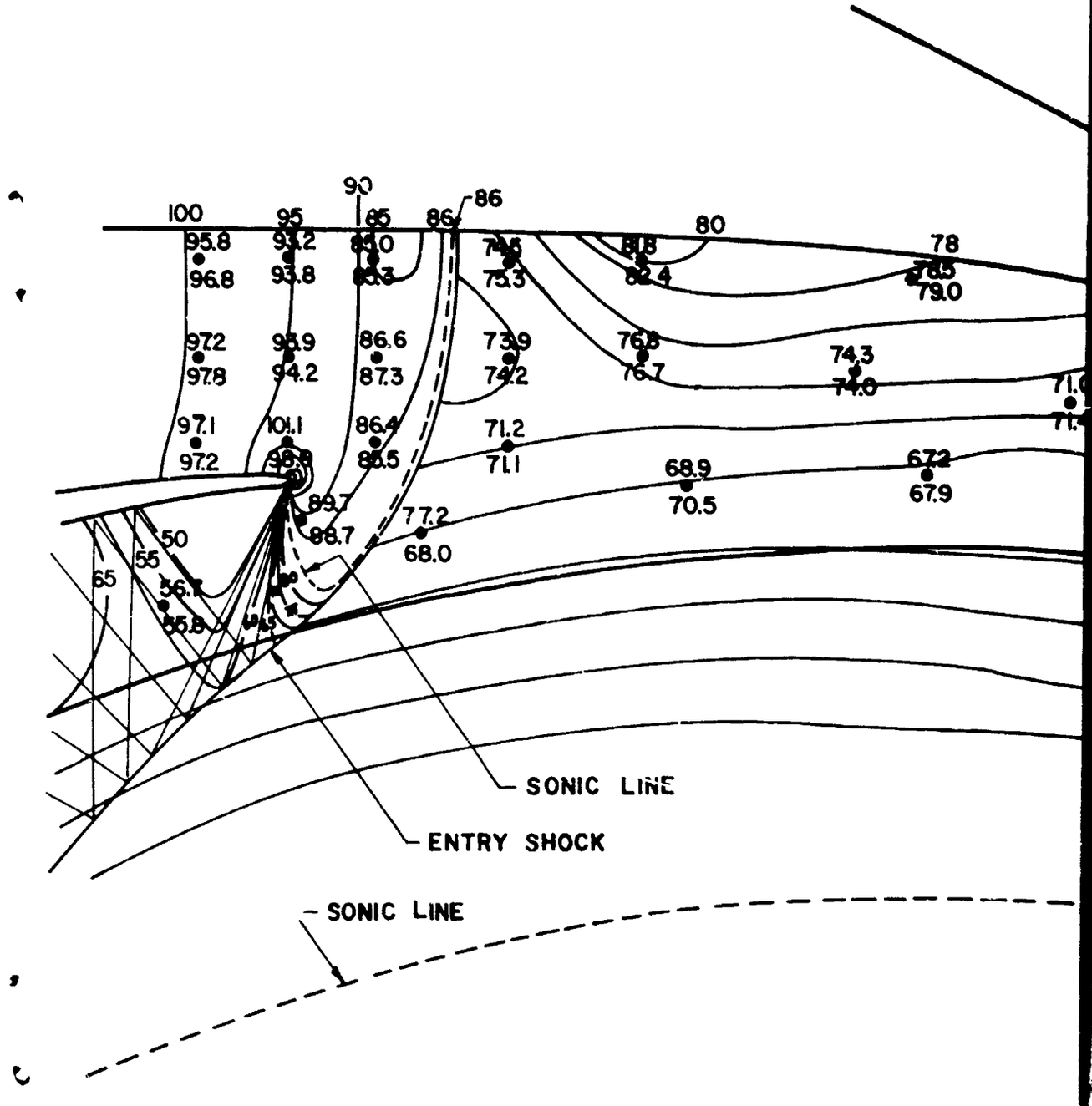

Figure 279. Vane-Island Diffuser Constant Pressure Contours (Welliver and Acurio, 1967).

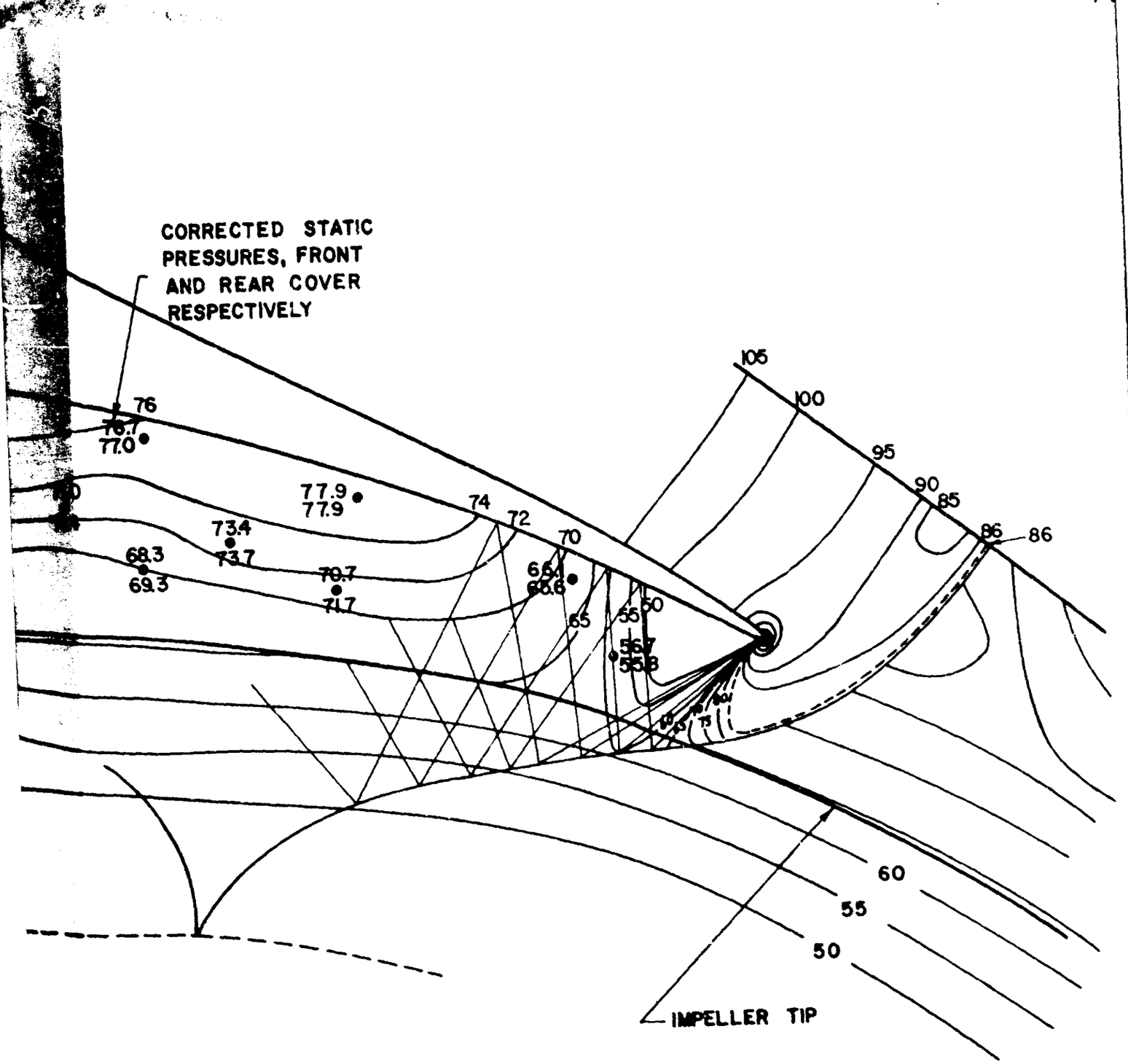
CORRECTED STATIC PRESSURES, FRONT AND REAR COVER RESPECTIVELY
105
100
95
90
85
86
86
76
76.1
77.0
77.9
77.9
74
72
70
73.4
73.7
68.3
69.3
70.7
71.7
66.1
66.6
65
55
50
56.7
55.8
60
55
50
IMPELLER TIP

boundary layer thickening between the impeller exit and the channel diffuser throat. If the depth of the vaneless space is not too small, the flow at the channel diffuser throat maintains a potential "core" surrounded by boundary layer fluid. The radial pressure gradient caused by the diffusing flow in the vaneless space produces not only an adverse pressure gradient in the streamwise direction but also a pressure gradient normal to the streamline direction; this component leads to secondary flow which bleeds the boundary layers on the sidewalls and suction surface, forcing boundary layer fluid back toward the tangential direction. If the secondary flow effects are sufficiently strong, the boundary layer flow may even reenter the impeller.

By treating the channel diffuser pressure recovery as a function of the geometric and throat inlet flow parameters, the performance of the channel diffuser can be predicted if the flow in the vaneless and semivaneless space can be predicted to give the inlet flow conditions at the channel throat.

The overall design of the centrifugal compressor diffuser obviously depends upon a proper analysis and modeling of the flow in the vaneless and semivaneless space. In particular, the diffusion and shock characteristics occurring in this region and their effect upon flow blockage must be understood. The success of the overall diffuser design will depend upon the proper analysis of this region in addition to optimizing the channel diffuser.

By altering the vaneless and semivaneless space geometry, the designer has the opportunity to adjust the inlet flow characteristics at the throat. In particular, by carefully controlling the vane leading edge radius (the vaneless space radius ratio), the flow depth, vane spacing, number of vanes, and vane angle of attack, the designer can obtain a trade-off between flow diffusion obtained in the vaneless and semivaneless space and that obtained in the channel diffuser.

A detailed description of the flow in the vaneless and semivaneless space and details of the flow around the vane leading edge are given by Dean (1969). The reader is referred to Dean's work for a discussion of the analysis of the vaneless and semivaneless flow.

5.3 CHANNEL DIFFUSER DESIGN

The vane-island geometry shown in Figure 1 has a straight wall, single-plane divergence channel diffuser. Other geometric shapes can be designed for the channel geometry. Whatever the geometry, however, if the designer has available pressure recovery performance maps for the channel diffuser, he is in a position to optimize the channel diffuser design.

For the single-plane, straight wall channel diffuser, the pressure recovery is a function of the geometric variables:

2θ = divergence angle
L/W_1 = length-to-throat width ratio
AS = aspect ratio

and the inlet variables:

B = throat blockage
M_t = throat Mach number
R_D = throat Reynolds number

and other secondary parameters such as inlet core flow turbulence intensity, blockage distribution, and boundary layer shape factor.

The designer's task is to optimize the vaneless and semi-vaneless space design with the design of the channel diffuser to obtain optimum overall pressure recovery and flow stability.

The channel diffuser design should produce the optimum peak recovery for the prescribed throat inlet conditions. The optimum peak geometry and recovery can be found from the performance maps of peak recovery as a function of aspect ratio presented in Figures 137 through 141.

Design Procedure

The diffuser design should proceed as follows

1. At the design point, the following are either known or prescribed:

$\dot{m}_T$ = total mass flow rate

p_o^* = impeller total pressure after mixing

T_o^* = impeller total temperature after mixing

M_2^* = flow Mach number at impeller exit

λ_2^* = swirl parameter (tangent of flow angle to radial)

$(b/r)_2$ = diffuser depth to impeller tip radius ratio

$R_{e_2}^*$ = impeller exit Reynolds number

r_c/r_2 = collector to impeller exit radius ratio

2. A vaneless and semivaneless geometry is assumed. This includes specification of:

N = number of diffuser vanes

b(r) = diffuser depth schedule

r_v/r_2 = vane leading edge to impeller exit radius ratio

α = vane leading edge mean angle to radial

and shape of vane suction surface up to location of channel diffuser throat.

3. Using the geometry specified in (2) with appropriate boundary layer and core flow analysis for the vaneless and semivaneless space, calculate the channel diffuser throat boundary layer displacement thickness on the suction, pressure, and sidewall surfaces, assuming a known value of M_t.

4. The channel mass flow rate is

$$\dot{m} = \frac{\dot{m}_T}{N} \tag{73}$$

and the effective channel throat flow area A_e is calculated from

$$A_e = \dot{m} \sqrt{\frac{R}{k}} \frac{\sqrt{T_o^*}}{p_o^*} F(M_t)/M_t = \frac{\dot{m}_T}{N} C_1 \tag{74}$$

$$F(M_t) = \left[1 + \frac{(k-1)}{2} M_t^2\right]^{k+1/2(k-1)} \tag{75}$$

where $$C_1 = \sqrt{\frac{R}{k}} \frac{\sqrt{T_o^*}}{p_o^*} F(M_t)/M_t$$

A_e is a minimum for $M_t = 1.0$.

If the impeller exit flow is at a high Mach number such as to require a rapid readjustment through a shock system upstream of the channel throat (high impeller exit Mach number M_2^*), the proper procedure is to design for a throat Mach number close to unity. [If the throat area is too large, the flow preceding the channel throat must readjust to meet the improved throat conditions of mass flow and flow area. This will produce a lower-than-design throat Mach number and a higher-than-design throat blockage (see Dean, 1969). Both factors will decrease the channel diffuser performance. The major factor will be the increase in throat blockage B.]

The design throat Mach number must be compromised with the design compressor range and other factors related to compressor application and manufacture. For a fixed area throat, the required effective throat area will alter with a change in mass flow, p_c^*, and T_o^* as the compressor moves along its operating line.

5. Knowing the throat Mach number, the effective throat area is calculated from (74) and the throat blockage is given by

$$B = 1 - \frac{A_e}{A_t} \tag{76}$$

or

$$B = 1 - \frac{\dot{m}_T C_1}{N A_t} \tag{77}$$

6. For a rectangular channel diffuser throat of aspect ratio AS, the blockage B is related to the boundary layer displacement thickness at the throat:

$$B \cong \frac{2\delta_t^*}{W_1} \left(1 + \frac{1}{AS}\right) \tag{78}$$

As a first approximation, assume that the calculated δ^* found in Step (3) is altered slightly by small changes in throat depth b.

Knowing the design throat Mach number M_t, the peak recovery/aspect ratio charts are entered to select the appropriate aspect ratio. (The present studies indicate that optimum

peak recovery is obtained near AS = 1.0. Until additional data is available, it is probably best to assume that the optimum peak geometry occurs for aspect ratio of unity. Further studies are necessary to refine our information on aspect ratio behavior near AS = 1.0; several points in efficiency may be gained by a more detailed knowledge of peak recovery as a function of AS, M_t, and B.)

An iteration procedure is required between the peak recovery/aspect ratio charts and Equation 78 to determine the optimum peak aspect ratio and throat blockage B for the prescribed depth b since

$$W_1 = \frac{b}{AS}$$

7. The throat area A_t is determined from

$$A_t = \frac{\dot{m}_T C_1}{N} \left(\frac{1}{1-B}\right) \tag{79}$$

Equations 77 and 78 provide two equations for throat blockage. Given the desired aspect ratio, it is necessary to adjust the throat depth b to determine the throat area.

Setting Equations 77 and 78 equal to each other,

$$1 - \frac{\dot{m}_T C_1}{N A_t} = 2\delta^*_t \frac{AS}{b}\left(1 + \frac{1}{AS}\right)$$

or

$$A_t = \frac{N}{\dot{m}_T C_1}\left[1 - 2\delta^*_t \frac{AS}{b}\left(1 + \frac{1}{AS}\right)\right] \tag{80}$$

where

$$C_1 = \sqrt{\frac{k}{R}} \frac{T_o^*}{p_o^*} \frac{F(M_t)}{M_t} \tag{81}$$

which must agree with the throat area calculated from

$$A_t = \frac{b^2}{AS} \tag{82}$$

8. The channel diffuser geometry for peak recovery is obtained from the peak recovery/aspect ratio charts and Table VI.

The diffuser length-to-width ratio must satisfy the collector-to-impeller exit radius ratio initially prescribed. If the optimum peak L/W_1 is too large, various options are available.

a) L/W_1 can be decreased. The amount of deterioration in diffuser recovery can be found from the diffuser performance maps. Since the ridge of optimum recovery lies essentially at a constant angle, and the slope of the recovery "hill" is small near peak recovery, L/W_1 can be decreased appreciably without a serious decrease in recovery.

b) Aspect ratio can be changed to give a smaller W_1 hence a smaller L. This will increase the aspect ratio slightly. The decrease in recovery will be small with a moderate change in aspect ratio, as seen from the peak recovery/aspect ratio charts.

c) The vaneless and semivaneless geometry can be changed to attempt to match the required L/W_1 within the allowable collector radius.

9. The throat Reynolds number is given by

$$R_D = \frac{V_t D}{\nu} = \frac{2}{\nu \rho_t C_1} \left(\frac{1-B}{1+AS}\right) b \qquad (83)$$

The present studies indicate that a high Reynolds number should be used for optimum recovery. The diffuser design should be optimized to obtain a high throat Reynolds number R_D.

10. The vaneless and semivaneless geometry should be adjusted as required by steps (4) to (10); steps (2) and (3) should then be repeated to adjust δ^*. The entire diffuser design should then be iterated until the channel diffuser recovery plus the vaneless and semivaneless space recovery is optimized to produce the optimum overall diffuser recovery C_{p_D}.

$$C_{p_D} = \left[\frac{g(M_2^*) - g(M_t)}{1 - g(M_t)} + C_p\right]\left[\frac{1 - g(M_t)}{1 - g(M_2^*)}\right] \qquad (84)$$

where

$$g(M) = \left[1 - \frac{(k-1)}{2} M^2\right]^{\frac{1-k}{k}} \qquad (85)$$

11. The overall diffuser design (in particular, the design of the vaneless and semivaneless space needed to adjust the channel throat conditions) must be optimized together with the impeller performance to obtain an overall optimum compressor performance. A detailed discussion of the design trade-offs required for optimizing the vaneless and semivaneless space and impeller design is given by Dean (1969).

Additional Considerations

From the foregoing outline, it is obvious that the total diffuser design is a lengthy iteration process. The design process depends upon our understanding the fluid dynamics throughout the entire compressor and our appreciation of the factors that influence the operating performance. Among the latter are the control of manufacturing tolerances, effect of operating conditions on design tolerances, and the operating conditions encountered along the compressor operating line.

Of primary importance to the designer is the pressure recovery and flow range between surge and choke along the compressor operating line. As discussed by Dean (1969), both of these factors are closely associated with the vaned diffuser performance.

One consideration evident from the channel diffuser performance maps obtained on the present study is the alteration in the shape of the recovery "hill" with changes in throat Mach number M_t and blockage B. For a fixed channel throat area, the designer must be aware of the change in location of the optimum channel diffuser geometry as M_t and B are altered as the compressor operating point moves along the operating line. Of particular importance is the possibility of the diffuser geometry moving to the unstable and low recovery portions of the performance map "hill" as Mach number and blockage are altered. (Actually the recovery "hill" moves under the fixed diffuser geometry location.) It is suspected that compressor surge in a vaned diffuser design is closely associated with channel diffuser flow stability.

A free parameter of some use to the designer is the number of vanes N. A large number of vanes is generally desired for flow stability. A small number of vanes will produce a high Reynolds number. The number of vanes must be compromised through the design procedures outlined previously.

As flow rate and impeller exit conditions change along the compressor operating line, the diffuser design must account for the alterations in throat Mach number and blockage. These changes will affect the channel and overall diffuser recovery and the flow range between choke and surge.

The design procedure outlined previously has been considered for a single design point. The actual diffuser design must compromise performance over the entire range of operation of the compressor. This involves a complicated procedure incorporating many parameters relative to the total compressor performance and to the characteristics of associated components such as a combustor or turbine. Some of these factors are discussed in further detail in the report by Dean (1969).

5.4 COMPARISON OF BASE DATA DIFFUSER RECOVERY WITH CENTRIFUGAL CHANNEL DIFFUSERS

Welliver and Acurio (1967) in a former exploratory development program under sponsorship of the U. S. Army Aviation Materiel Laboratories have made the only measurements available of pressure recovery in diffuser channels of a high-pressure-ratio centrifugal stage. Their rather extensive wall static pressure data and measurements of throat total pressures provide us with a set of performance data on straight channel diffuser geometries; the diffuser length-to-throat width ratios, diffuser divergence angles, aspect ratios, and inlet Mach numbers are bracketed by the range of data obtained on the present study.

Those measurements that can be compared to the present studies were all made on what is called the RF-2 stage. Measurements on the RF-2 stage permit calculation of the pressure recovery performance of the vane-island diffusers and of the inlet blockage and throat Mach number. This type of information is available for only a few of the tests, those for which stagnation pressure measurements were made in the throat. However, these data provide sufficient information to make a direct comparison of the measured recovery of the RF-2 diffusers with the recovery as measured by the data obtained on this contract.

A first examination of the data does not appear to show very good agreement between the pressure recovery performance of the RF-2 diffusers and the performance measured on this contract. However, in evaluating the data it is necessary to estimate the uncertainty in C_p, M, and B as measured on the RF-2 stage. When a proper evaluation of the uncertainty is made, all of the data agrees with the present data except for one point, Line 7, Run 3354A.

The uncertainty in C_p, B, and M arises from two primary sources: (1) the basic uncertainty in instrumentation accuracy, i.e., the uncertainty in the basic instrumentation used to obtain the pressure and temperature measurements; and (2) all other uncertainties introduced when evaluating C_p, M, and B, which arise in addition to the instrument uncertainties accounted for in Item (1).

Regarding Item (1), those who took the original data are in the best position to accurately evaluate this contribution to the uncertainty. However, these data do not appear in the Welliver and Acurio report. In the following analysis, it has been assumed that there is no contribution to the uncertainty from this source. Obviously this is not true, but it does give a conservative estimate of the uncertainty in the degree to which the RF-2 and present data agree.

To calculate the pressure recovery C_p, the blockage B, and the throat Mach number M, it is necessary to know the following parameters:

throat stagnation pressure, p_o
throat static pressure, p_t
throat stagnation temperature, T_{o_t}
throat geometric area, $Area_t$
exit pressure (collector pressure), p_e
diffuser channel mass flow rate, $\dot{m}_a$

where subscripts are:

t = throat
o = total conditions
e = exit
a = actual

These measurements appear in the RF-2 data.

The uncertainties in the calculated parameters using the RF-2 data have been calculated using the single sample uncertainty analysis described in Section 3.

The uncertainties in the p_t, p_e, and p_o are the result of either extrapolation or interpolation required in analyzing the RF-2 data and the probable uncertainty produced because of pressure fluctuations in the flow.

It has been assumed that the pressure recording system appropriately time-averages the static and total pressure measurements.

For the throat measurements it is necessary to interpolate between the static pressure measurements to accurately evaluate the pressures at the throat. For example, the "throat" wall static pressure data does not correspond to the true throat pressure since the "throat" static pressure taps were located 0.035 inch downstream of the geometric throat. In estimating the "throat" pressure, isobaric plots have been made from the RF-2 wall pressure measurements utilizing both front and back cover data. These plots have been used to interpolate the throat pressures.

To find the throat pressure it is necessary to estimate the shape of the static pressure distribution at the geometric throat. This must include the effect of acceleration of the flow between the vane leading edge and the geometric throat. The actual static pressure measurements obtained with the traverse probe in the present tests give, we feel, a reasonable idea of what this effect should be. However, the true nature of the static pressure distribution is unknown because of the effect of local shocks within the throat passage between the vane leading edge and the entrance to the diffuser. These shocks are not present in the present tests. We have estimated the uncertainty in throat pressure as $\pm$ 0.5 psia.

We have assumed that the throat total pressure may be uncertain to about $\pm$ 1 psia. This is based largely upon comparing the throat total pressure among the various runs.

The exit or collector pressure variation of $\pm$ 1 psia is based upon the observed scatter in the measured collector pressures and exit pressures reported.

The throat blockage is given in terms of the measured and theoretical mass flow rate for the diffuser geometrical throat area. The blockage uncertainty depends upon the uncertainty in the actual mass flow rate measurement and in the calculation of the theoretical mass flow rate.

The uncertainty in theoretical mass flow rate depends upon the uncertainties in stagnation pressure, throat area, stagnation temperature, and throat Mach number.

In the RF-2 tests, the throat area could vary between channel diffusers from the mean value reported for each geometry. Measurements at one point during the studies indicated that the throat dimensions might vary about the mean values given to about the following magnitudes because of manufacturing and assembly tolerances:

$$W = \pm 0.005 \text{ inch}$$

$$b = \pm 0.001 \text{ inch}$$

where area $A = bW$.

The uncertainty in the actual mass flow through a single channel diffuser arises because of the measurement uncertainty in the overall mass flow rate through the compressor and because of the uncertainty in the distribution of the total mass flow among the channel diffuser passages because of the throat area uncertainty.

In the following we have neglected the uncertainty in measuring the total mass flow and have contributed the uncertainty in actual mass flow entirely to the uncertainty in throat area.

The uncertainty in throat total temperature has been estimated as $\pm 10^\circ$ R.

It is necessary to cross-plot the present data in order to obtain plots of diffuser performance as a function of Mach number and blockage for the aspect ratios used in the RF-2 studies. Figures 280, 281, 282, and 283 show a cross plot of diffuser pressure recovery as a function of aspect ratio

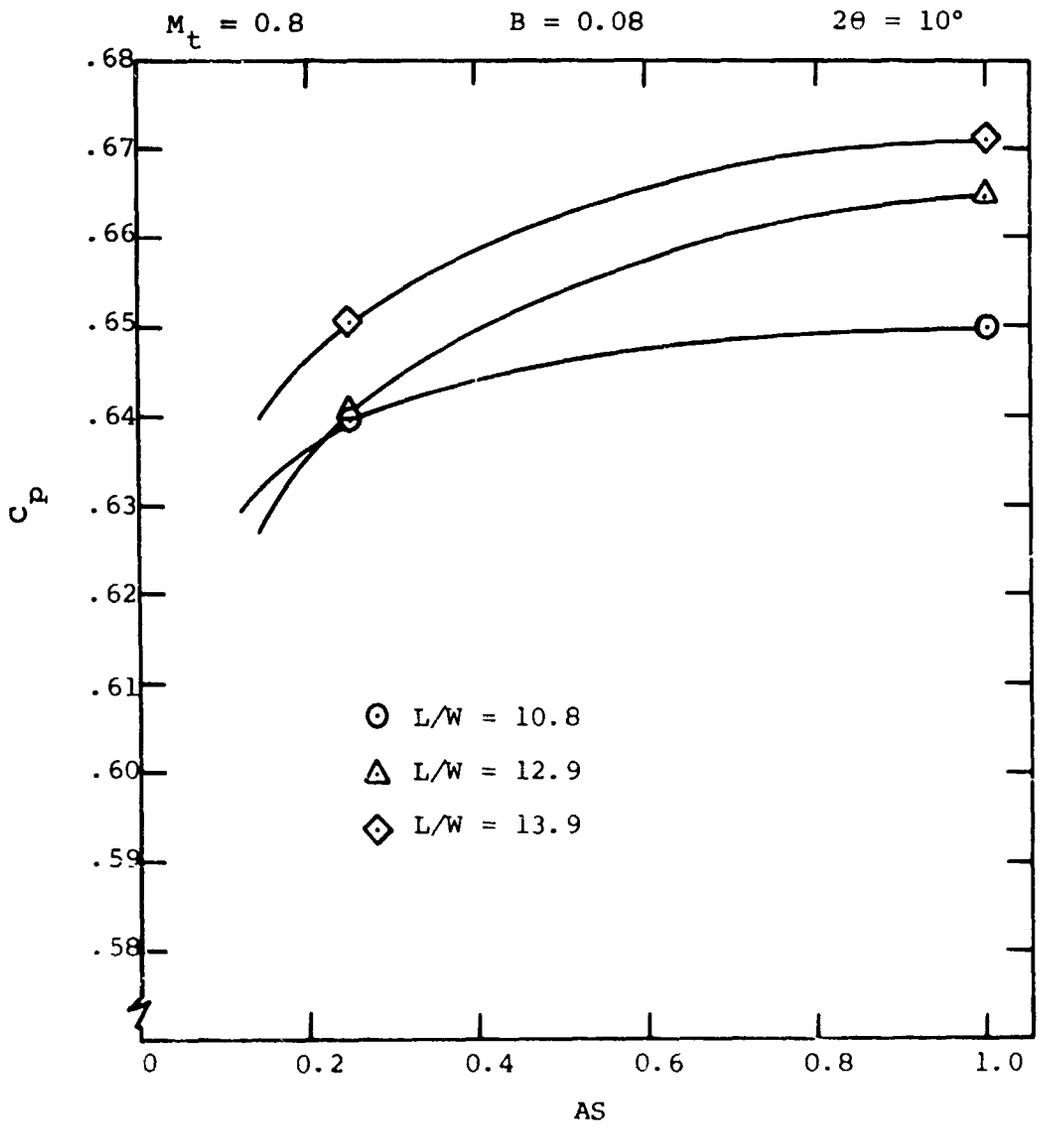

Figure 280. Pressure Recovery Versus Aspect Ratio. RF-2 Geometry.

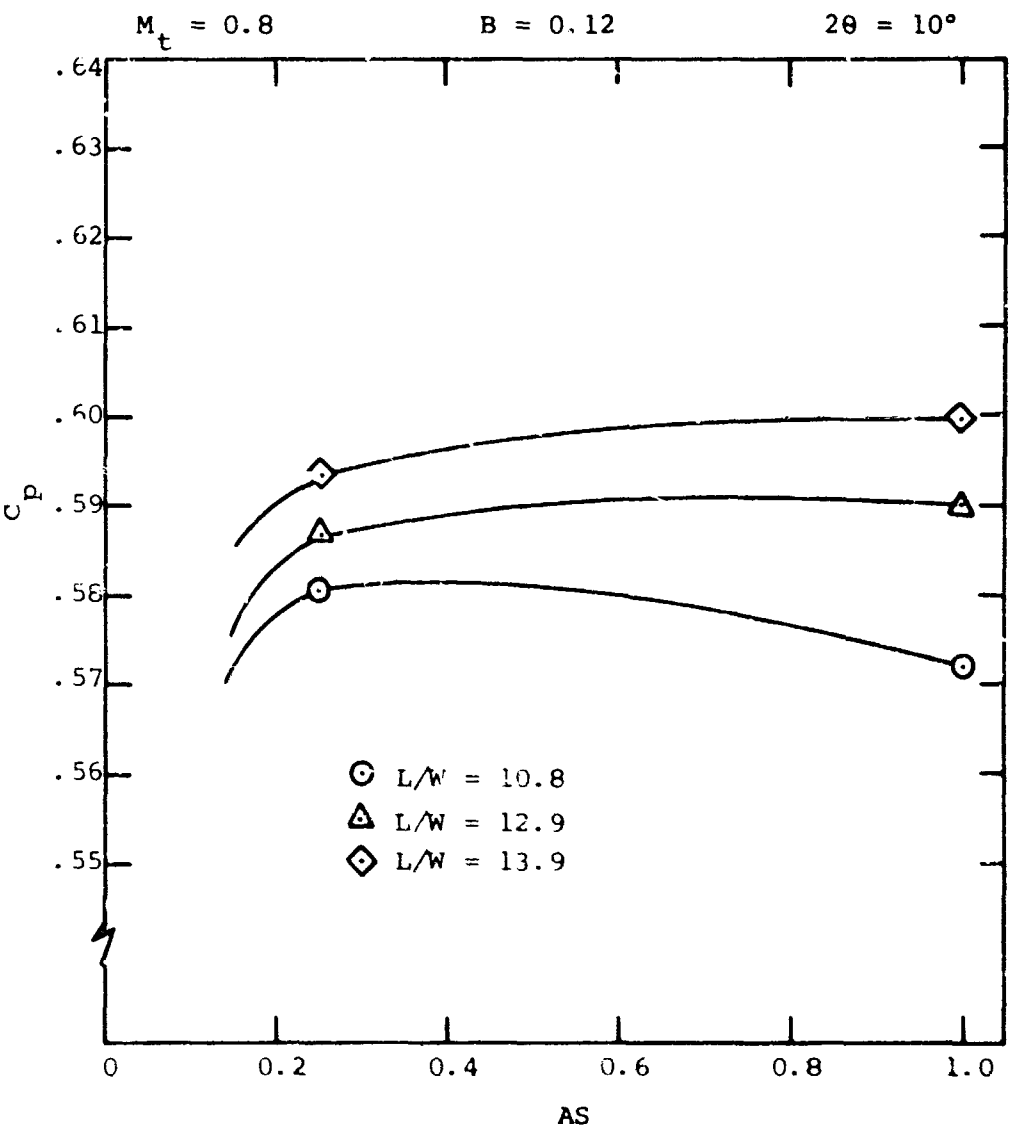

Figure 281. Pressure Recovery Versus Aspect Ratio. RF-2 Geometry.

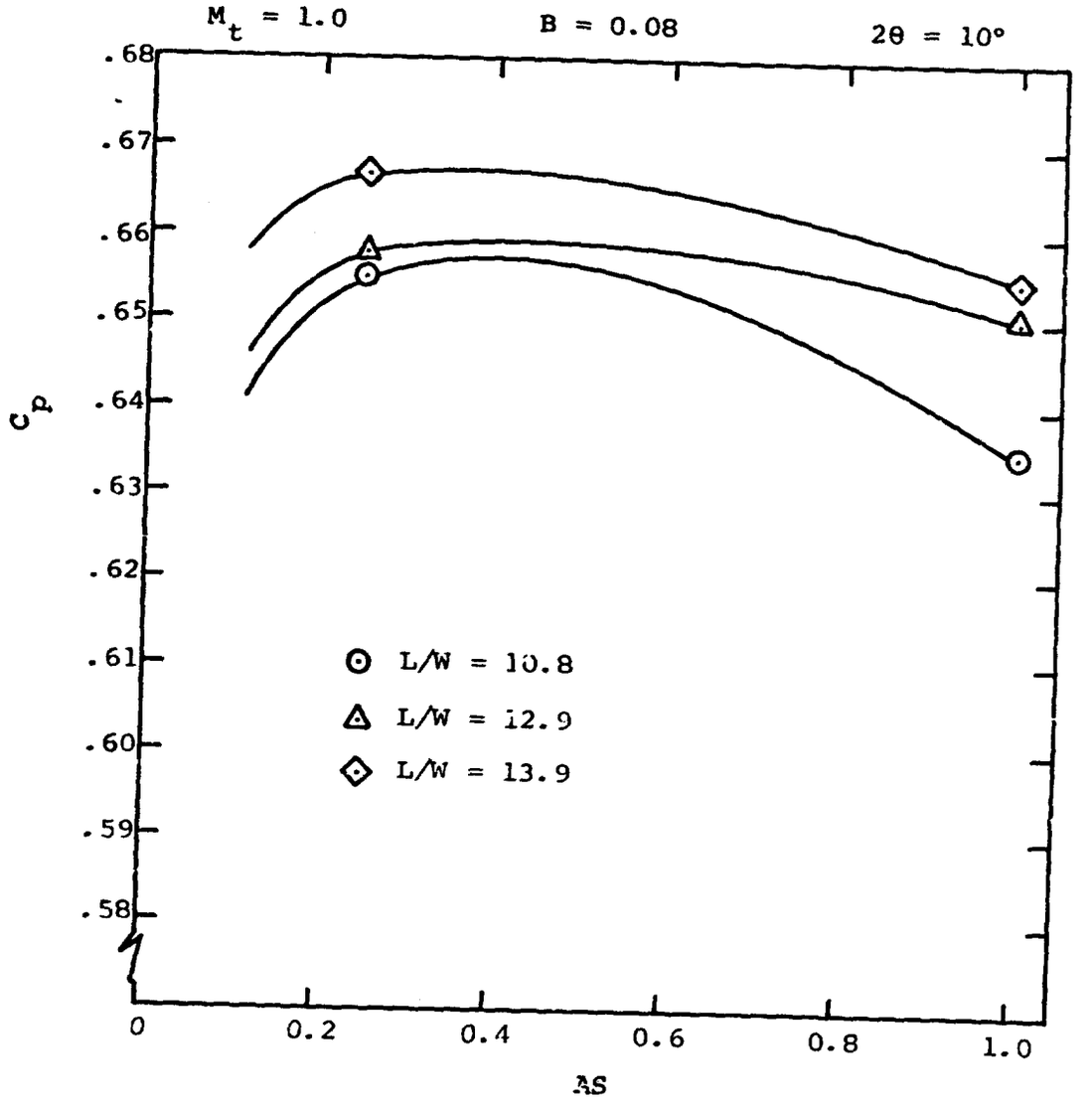

Figure 282. Pressure Recovery Versus Aspect Ratio. RF-2 Geometry.

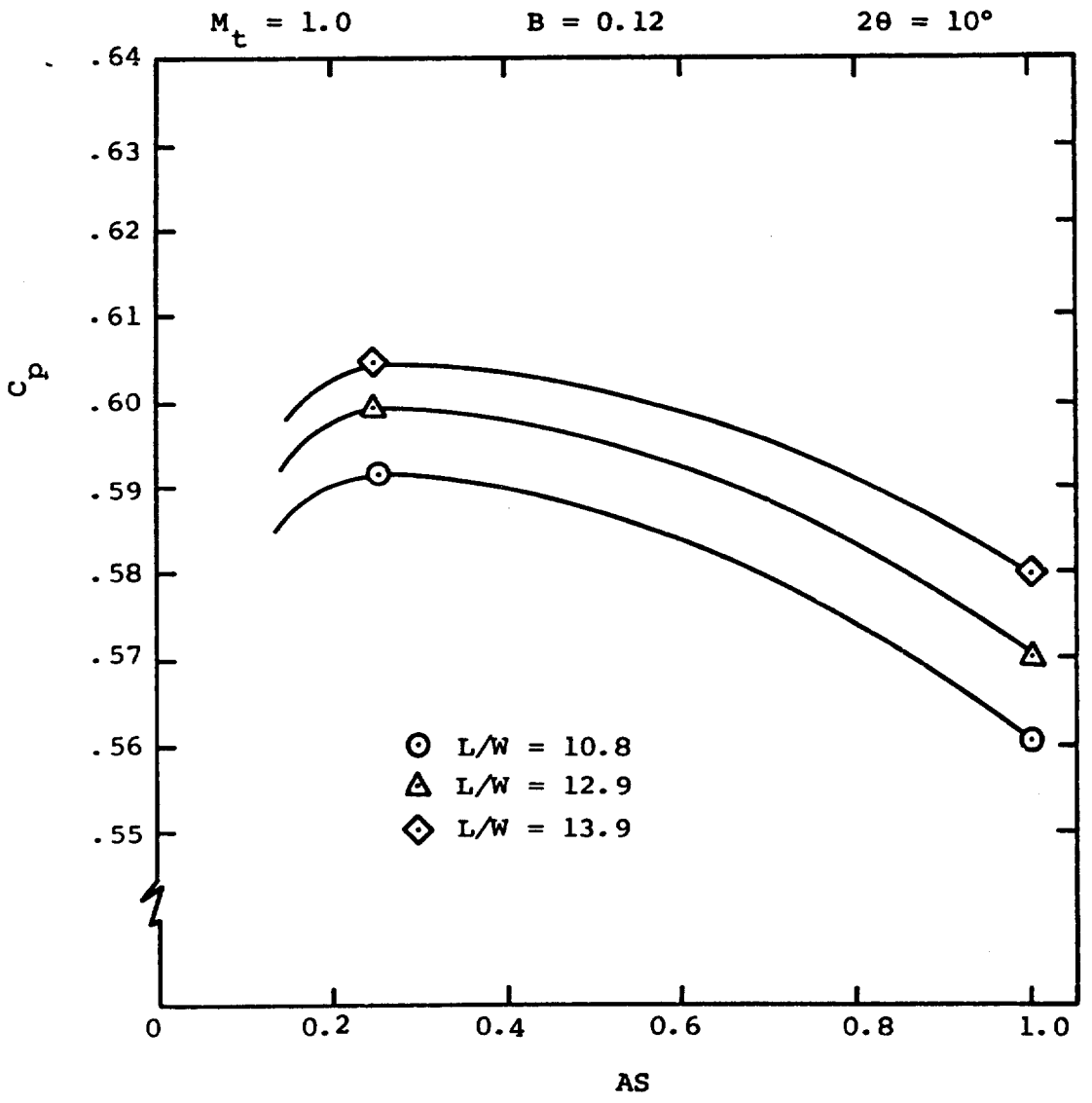

Figure 283. Pressure Recovery Versus Aspect Ratio. RF-2 Geometry.

for the 2θ = 10° diffuser at each of the L/W values used in the RF-2. These cover the range of Mach number and blockage used.

The curves shown on these figures can represent only approximately what may be expected for the intermediate values of C_p for aspect ratios between 0.25 and 1.0.

Over the range of aspect ratios covered by the RF-2 data (aspect ratio = 0.29, 0.39, and 0.46), it would appear that the pressure recovery performance should be quite close to the aspect ratio = 0.25 data.

In Figures 284, 285, and 286 the pressure recovery performance as a function of blockage for three values of Mach number is plotted for Run 3354A (2θ = 10°, L/W = 12.9, AS = 0.39), Run 3366 (2θ = 10°, L/W = 13.9, AS = 0.47), and Run 3369 (2θ = 10°, L/W = 10.8, AS = 0.29), respectively. The reduced RF-2 data is also shown. The uncertainty in the data is indicated on these figures.

A direct comparison can be made between the present diffuser pressure recovery performance as obtained for the base data and the measured diffuser recovery performance of the actual diffuser channels in the RF-2 investigations. In comparing the data it is important to keep two things in mind:

1) The calculated uncertainty in the RF-2 data.

2) The uncertainty in the present data (the present data is the solid lines drawn on these figures) that arises from two causes:
   a) The basic uncertainty in the measured data which is on the order of a half point in pressure recovery and blockage.
   b) The uncertainty in plotting these curves because of the variation of pressure recovery C_p with aspect ratio as given in Figures 280 through 283.

An examination of these figures shows that the RF-2 data agree with the base data except for the one point, Line 7, Run 3354A.

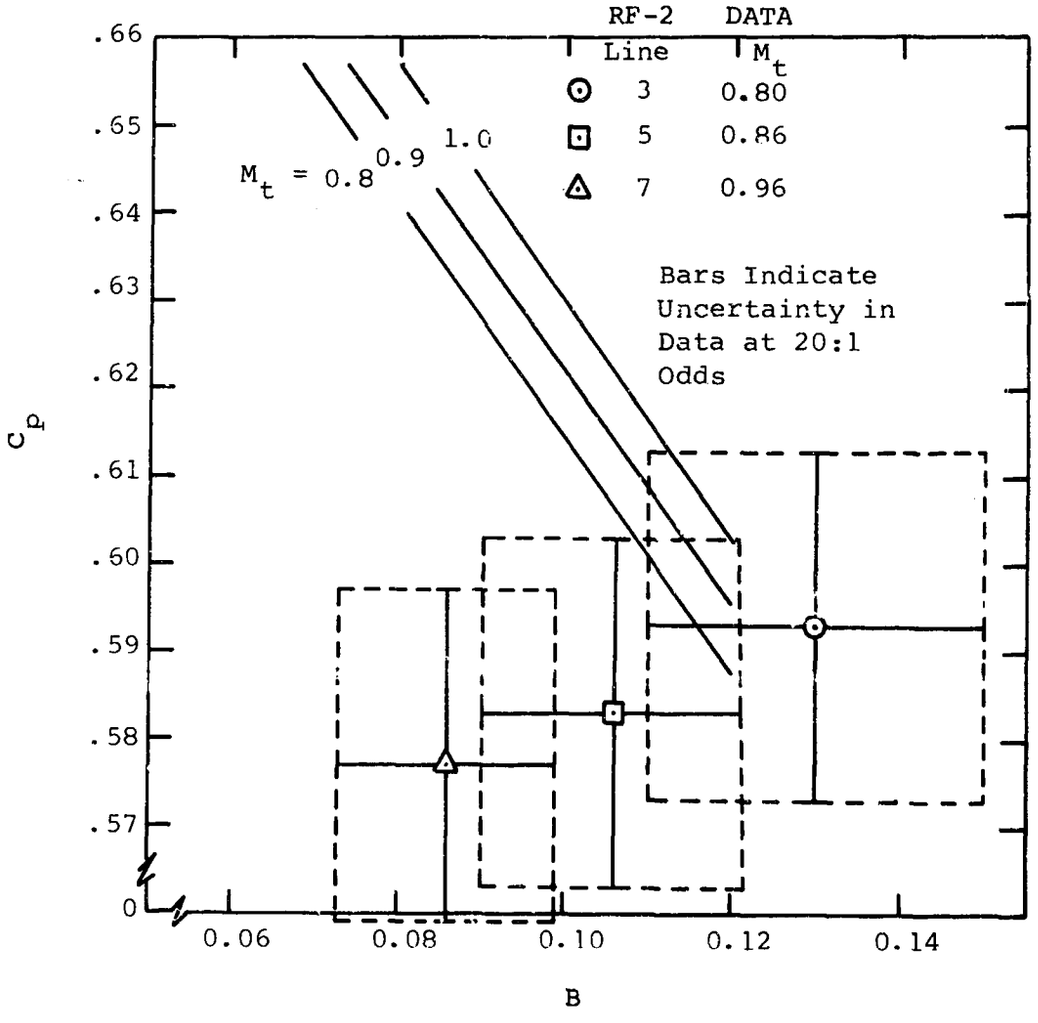

Figure 284. Comparison of Base Data and RF-2 Data. Run 3354.

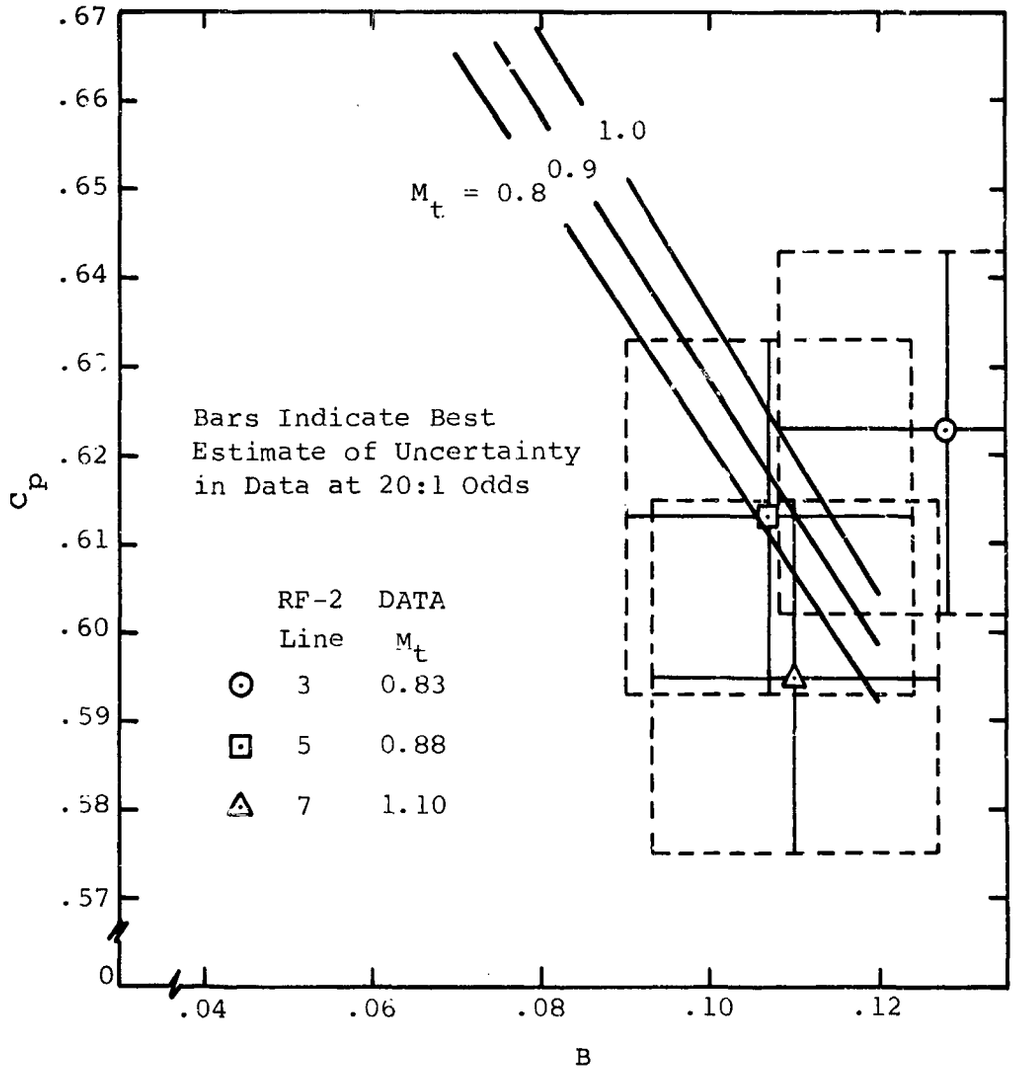

Figure 285. Comparison of Base Data and RF-2 Data. Run 3366.

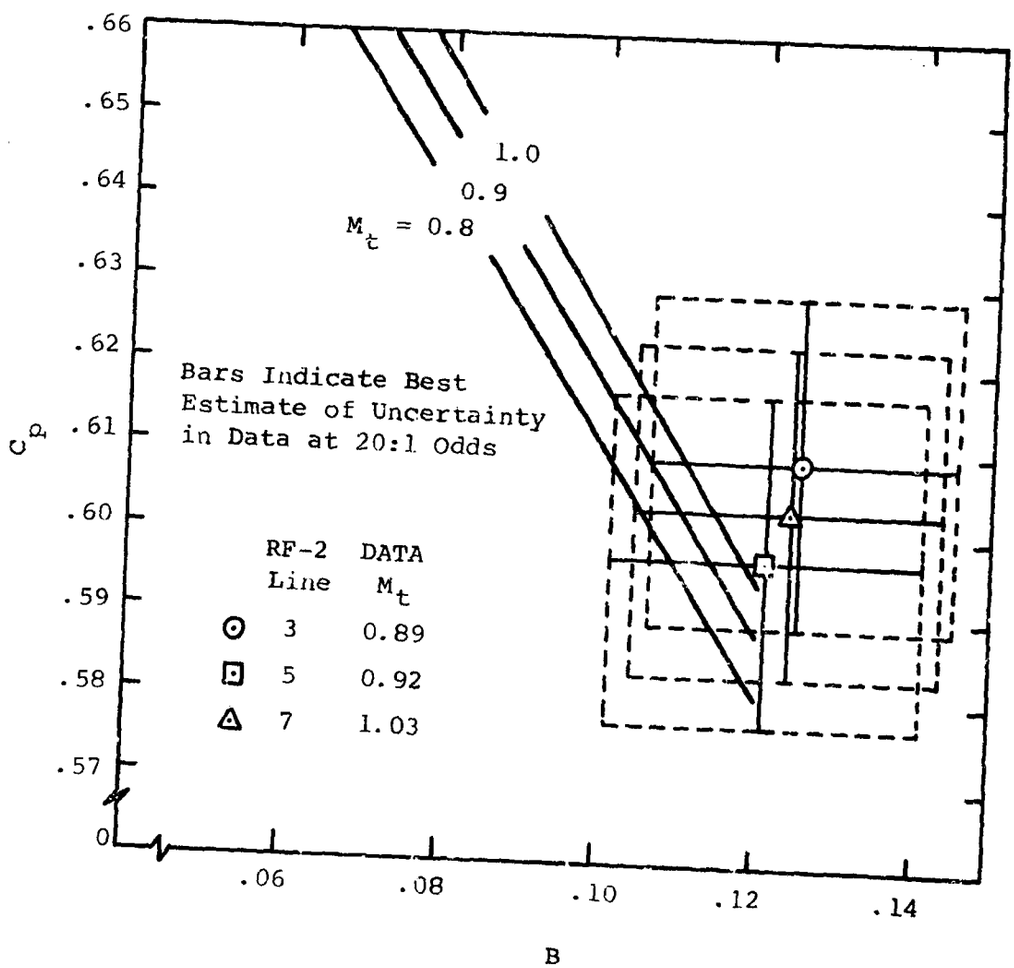

Figure 286. Comparison of Base Data and RF-2 Data. Run 3369.

There appears to be a trend in the RF-2 data to lower blockage and Mach number for each run as the speed is increased from Line 3 to Line 7. However if account is made of the uncertainty in the data, these trends are not necessarily meaningful.

The uncertainty shown on these figures is the minimal value expected. If the additional uncertainties due to instrumentation (basic instrument uncertainty, reading uncertainty, etc.) were included, the uncertainty limits shown would be increased. There may be an exception with regard to the uncertainty in stagnation temperature (which in the data reduction affects the uncertainty in blockage). If one assumes zero uncertainty in measured stagnation temperature, the blockage uncertainty is found to be $\pm$ 1 point in blockage instead of 2 points.

The data reduction has followed the format used by Welliver and Acurio (1967). Dean (1969) has calculated the channel diffuser performance by four different procedures in an attempt to determine true diffuser performance, taking into account the uncertainties in the RF-2 measurements. The various calculation procedures all produce a correlation of the RF-2 and present data of the same general agreement as shown in Figures 284, 285, and 286.

6.0 SUMMARY AND CONCLUSIONS

6.1 SUMMARY

Diffuser static pressure recovery performance has been measured as a function of diffuser geometry (L/W_1 and 2θ) for three aspect ratios (AS = 0.25, 1.0, and 5.0) around the region of peak diffuser recovery. These studies have investigated the influence of inlet flow parameters of throat blockage and throat Mach number.

Experiments have also been made to study the effect of inlet Reynolds number, boundary layer shape factor, asymmetric distribution of throat inlet blockage, and the effect of rounded throat corners.

This work has shown:

(1) Below the ridge of optimum recovery, good diffuser pressure recovery is maintained up to choked conditions and beyond until the shock in the diffusing passage reaches a Mach number of about 1.15. Above this Mach number it is presumed that the shock boundary layer interaction causes boundary layer separation in the diffusing passage with a resulting large degradation in diffuser performance.

(2) Throat blockage is a critical inlet parameter controlling diffuser performance. Increasing throat blockage results in decreasing diffuser pressure recovery, with all other conditions held constant.

(3) Aspect ratio is an important geometric parameter in establishing pressure recovery. Because recovery must deteriorate significantly for very small aspect ratios, aspect ratio becomes extremely important to pressure recovery behavior at low aspect ratios (below approximately 1.0). For fixed geometry and blockage, maximum recovery occurs at a low aspect ratio. For constant Mach number and blockage, maximum peak recovery occurs near aspect ratio 1.0.

(4) Diffuser maps in the form of contours of pressure recovery as a function of diffuser geometry have been established for aspect ratio = 0.25, 1.0, and 5.0 diffuser

geometries. A series of performance maps are presented as a function of inlet throat Mach number and throat blockage.

(5) Charts showing peak recovery for constant inlet Mach number and blockage are presented.

(6) Inlet Reynolds number appears to affect diffuser recovery, especially at diffuser geometries near and above the ridge of optimum recovery. In general, higher throat Reynolds numbers produce higher values of pressure recovery than low throat Reynolds numbers, with all other conditions held constant. Reynolds number appears to have a greater effect at low aspect ratio than at high aspect ratio.

(7) Other factors studied in this program such as inlet boundary layer shape factor, asymmetric blockage distribution, and rounding of the diffuser throat corners produce minor alterations in pressure recovery performance. However, the designer should be aware of these effects, since the cumulative effect of many small alterations in pressure recovery behavior is important to the achievement of the best diffuser design.

(8) A discussion of the application of the channel diffuser pressure recovery performance data presented in this report to the design of the centrifugal compressor diffuser is given. The importance of optimizing the channel diffuser design with the design of the overall diffuser and compressor impeller has been emphasized. The importance of understanding the total compressor fluid dynamic behavior in the achievement of the best compressor performance is discussed.

6.2 CONCLUSIONS

The good pressure recovery performance of single-plane, parallel wall, divergent diffusers at high Mach numbers has been established by these studies.

It has further been established that diffuser aspect ratio as well as throat inlet blockage is a governing diffuser performance

parameter for the types of diffusers encountered in many practical fluid machinery applications.

These studies have clarified the importance of throat Mach number and throat blockage in addition to diffuser aspect ratio in achieving optimum diffuser pressure recovery.

The importance of additional inlet parameters related to practical diffuser applications has been explored. While many of these parameters have a small effect on diffuser performance, the designer must recognize the cumulative effect of a large number of small changes in diffuser performance to achieving design optimization.

These studies have emphasized the critical importance of diffuser aspect ratio and have shown that peak recovery performance occurs at small aspect ratios in the vicinity of aspect ratio 1.0. Of critical interest to the designer is the detailed information on peak recovery behavior at small aspect ratio. Additional studies are needed and will hopefully be pursued in the future to clarify this question.

Data similar to that gathered on the present studies for the single-plane, symmetric divergence diffuser needs to be gathered for other practical channel diffuser geometries. A geometry of particular attractiveness is the conical diffuser. It is hoped that further studies aimed at the gathering of information on conical diffusers and the pressure recovery behavior at other aspect ratios between 0.25 and 1.0 will be undertaken.

LITERATURE CITED

Dean, Robert C., Jr. (1969). FLUID MECHANICS ANALYSIS OF HIGH-PRESSURE-RATIO CENTRIFUGAL COMPRESSOR DATA; to be published 1969.

Emmons, H. W. (1944); THE NUMERICAL SOLUTION OF COMPRESSIBLE FLUID FLOW PROBLEMS; NACA TN 932, 1944.

Fox, R. W. and Kline, S. J. (1962); FLOW REGIME DATA AND DESIGN METHODS FOR CURVED SUBSONIC DIFFUSERS; Journal of Basic Engineering, Transactions of ASME, Series D, Vol. 84, No. 3, September 1962, p. 303-312.

Fox, R. W. (1967); DISCUSSION ON ASME PAPER NO. 68-WA/FE-19 "STRAIGHT CHANNEL DIFFUSER PERFORMANCE AT HIGH INLET MACH NUMBERS" BY P. W. RUNSTADLER, JR. AND R. C. DEAN, JR.; Presented at the Winter Annual Meeting of the American Society of Mechanical Engineers, December 1968, Discussion to be published 1969.

Halleen, R. M., and Johnston, J. P. (1966); INLET MACH NUMBER EFFECTS ON SUBSONIC DIFFUSER PERFORMANCE; Creare Incorporated, Hanover, New Hampshire, Technical Note N-56, February 1966.

Johnston, J. P. (1960); ON THE THREE-DIMENSIONAL TURBULENT BOUNDARY LAYER GENERATED BY SECONDARY FLOW; Transactions ASME, Series D, Vol. 82, No. 1, March 1960.

Johnston, J. P., and Powars, C. A. (1967); EFFECTS OF ASPECT RATIO ON THE PERFORMANCE OF STRAIGHT-WALLED, TWO-DIMENSIONAL DIFFUSERS; Thermosciences Division, Department of Mechanical Engineering, Stanford University, August 1967.

Johnston, J. P. (1969a); DISCUSSION ON ASME PAPER NO. 68-WA/FE-19 "STRAIGHT CHANNEL DIFFUSER PERFORMANCE AT HIGH INLET MACH NUMBERS" BY P. W. RUNSTADLER, JR. and R. C. DEAN, JR.; Presented at the Winter Annual Meeting of the American Society of Mechanical Engineers, December 1968, Discussion to be published 1969.

Johnston, J. P. (1969b); Private Correspondence; Thermosciences Division, Department of Mechanical Engineering, Stanford University, 1969.

Kenny, D. P. (1968); A NOVEL LOW COST DIFFUSER FOR HIGH PERFORMANCE CENTRIFUGAL COMPRESSORS; ASME Paper 68-GT-38, 1968.

Kline, S. J., and McClintock, F. A. (1953); DESCRIBING UNCERTAINTIES IN SINGLE SAMPLE EXPERIMENTS; Mechanical Engineering, Stanford University, January 1953.

Kline, S. J., Reynolds, W. C., Schraub, F. A. and Runstadler, P. W., Jr. (1967); THE STRUCTURE OF TURBULENT BOUNDARY LAYERS; Journal of Fluid Mechanics, Vol. 30, December 1967.

Oswatitsch, K. (1962); SYMPOSIUM TRANSSONICUM; International Union of Theoretical and Applied Mechanics (IUTAM), Aachen, 1962, Proceedings published by Springer-Verlag, 1964.

Pearcey, H. H. (1961); SHOCK-INDUCED SEPARATION AND ITS PREVENTION BY DESIGN AND BOUNDARY LAYER CONTROL; In Vol. 2 of "Boundary Layer and Flow Control: by G. V. Lachmann, Pergamon Press, 1961, Pages 1166-1344.

Pearcey, H. H. (1962); THE AERODYNAMIC DESIGN OF SECTION SHAPES FOR SWEPT WINGS; Advances in Aeronautical Sciences, Vol. 3, p. 277, Pergamon Press, 1962.

Pearson, K. (1902); ON THE MATHEMATICAL THEORY OF ERRORS OF JUDGMENT; Philosophical Transactions of the Royal Society of London, Series A, Vol. 198, p. 235-299, 1902.

Reneau, L. R., Johnston, J. P., and Kline, S. J. (1964); PERFORMANCE AND DESIGN OF STRAIGHT, TWO-DIMENSIONAL DIFFUSERS; Thermosciences Division, Department of Mechanical Engineering, Stanford University, Report PD-8, September 1964.

Runstadler, P. W. (1966); STRAIGHT DIFFUSER PERFORMANCE AT HIGH INLET MACH NUMBERS; Creare Incorporated, Hanover, New Hampshire, Technical Note N-60, September 1966.

Runstadler, P. W., Jr., and Dean, R. C., Jr. (1968); STRAIGHT CHANNEL DIFFUSER PERFORMANCE AT HIGH INLET MACH NUMBERS; ASME Paper No. 68-WA/FE-19, presented at the Winter Annual Meeting of the ASME, December 1968.

Runstadler, P. W., Jr., and Dean, R. C., Jr. (1969); AUTHORS' CLOSURE TO ASME PAPER NO. 68-WA/FE-19; to be published 1969.

Sapiro, L. (1969); DISCUSSION ON ASME PAPER NO. 68-WA/FE-19 "STRAIGHT CHANNEL DIFFUSER PERFORMANCE AT HIGH INLET MACH NUMBERS" BY P. W. RUNSTADLER, JR. AND R. C. DEAN, JR.; Presented at the Winter Annual Meeting of the American Society of Mechanical Engineers, December 1968, Discussion to be published 1969.

Schlichting, H. (1962); BOUNDARY LAYER THEORY; McGraw-Hill Book Company, 1964.

Shapiro, A. H. (1953); THE DYNAMICS AND THERMODYNAMICS OF COMPRESSIBLE FLUID FLOW; The Ronald Press Company, New York, New York, 1953.

Sovran, G., and Klomp, E. D. (1965); EXPERIMENTALLY DETERMINED OPTIMUM GEOMETRIES FOR RECTILINEAR DIFFUSERS WITH RECTANGULAR, CONICAL, OR ANNULAR CROSS-SECTION; Fluid Mechanics of Internal Flow, Proceedings of Symposium on the Fluid Mechanics of Internal Flow, General Motors Research Laboratories, Warren, Michigan, 1965.

Sparks, C. R. (1961); ANALYTICAL AND EXPERIMENTAL INVESTIGATION ON THE RESPONSE OF ORIFICE METERS TO PULSATING COMPRESSIBLE FLOW; American Gas Association Project NO-15, Orifice Metering of Pulsating Gas Flow, Final Technical Report on SwRI Project No. 464-4, Southwest Research Institute, December 1961.

Van DeWoestine, R. V., and Fox, R. W. (1966); AN EXPERIMENTAL INVESTIGATION ON THE EFFECT OF SUBSONIC INLET MACH NUMBER ON THE PERFORMANCE OF CONICAL DIFFUSERS; Purdue University, Lafayette, Indiana, Fluid Mechanics Group, Technical Report FMTR-66-1, February 1966.

Welliver, A. D., and Acurio, J. (1967). DESIGN AND DEVELOPMENT OF SMALL, SINGLE-STAGE CENTRIFUGAL COMPRESSOR; USAAVLABS Technical Report 67-47, U. S. Army Aviation Materiel Laboratories, Fort Eustis, Virginia, September 1967, AD 385595L.

Unclassified

Security Classification

DOCUMENT CONTROL DATA - R & D

(Security classification of title, body of abstract and indexing annotation must be entered when the overall report is classified)

1. ORIGINATING ACTIVITY (Corporate author)	2a. REPORT SECURITY CLASSIFICATION
Creare, Incorporated Hanover, New Hampshire	Unclassified
	2b. GROUP

3. REPORT TITLE

PRESSURE RECOVERY PERFORMANCE OF STRAIGHT-CHANNEL, SINGLE-PLANE DIVERGENCE DIFFUSERS AT HIGH MACH NUMBERS

4. DESCRIPTIVE NOTES (Type of report and inclusive dates)

Final Report

5. AUTHOR(S) (First name, middle initial, last name)

Peter W. Runstadler

6. REPORT DATE	7a. TOTAL NO. OF PAGES	7b. NO. OF REFS
October 1969	486	27

8a. CONTRACT OR GRANT NO.	9a. ORIGINATOR'S REPORT NUMBER(S)
DAAJ02-67-C-0106 b. PROJECT NO. Task 1G162203D14413 c. d.	USAAVLABS Technical Report 69-56 9b. OTHER REPORT NO(S) (Any other numbers that may be assigned this report) Creare Technical Note No. N-88

10. DISTRIBUTION STATEMENT

This document is subject to special export controls, and each transmittal to foreign governments or foreign nationals may be made only with prior approval of US Army Aviation Materiel Laboratories, Fort Eustis, Virginia 23604.

11. SUPPLEMENTARY NOTES	12. SPONSORING MILITARY ACTIVITY
	US Army Aviation Materiel Laboratories Fort Eustis, Virginia

13. ABSTRACT

Measurements have been made of the pressure recovery of straight-channel, symmetric, single-plane divergence diffusers with inlet Mach numbers between 0.2 and 1.0. Three aspect ratios, 0.25, 1.0, and 5.0, have been studied for a range of length-to-throat width ratios and divergence angles of diffuser geometries near peak recovery.

Diffuser performance maps are given that show pressure recovery as a function of diffuser geometry for fixed values of throat Mach number, throat blockage, and aspect ratio for the range of variables tested. Of significant importance to the designer is the alteration in the shape of the pressure recovery contours on the performance maps with variations in Mach number, blockage, and aspect ratio.

Four subprograms have measured the effect of changes in diffuser inlet Reynolds number, boundary layer shape factor, asymmetric distribution of inlet blockage around the throat periphery, and the influence of rounded throat corners on the pressure recovery behavior of the straight-channel diffuser.

The importance to the designer of a knowledge of how diffuser performance depends upon the diffuser geometric and inlet parameters is discussed. The application of channel diffuser performance data to the design of centrifugal compressor diffusers is described. The channel diffuser performance measured in the present study is compared with recovery performance of the channel diffusers in centrifugal compressors.

DD FORM 1 NOV 68 1473 REPLACES DD FORM 1473, 1 JAN 64, WHICH IS OBSOLETE FOR ARMY USE.

Unclassified

Security Classification

Unclassified

Security Classification

14. KEY WORDS	LINK A		LINK B		LINK C	
	ROLE	WT	ROLE	WT	ROLE	WT
Diffuser						
Channel Diffusers						
Pressure Recovery						
Inlet Mach Number						
Centrifugal Compressor						
Inlet Blockage						
Diffuser Performance Maps						
Diffuser Aspect Ratio						

Unclassified

Security Classification

10722-69